Understanding the role of plant lipids in cold acclimation, a study of *Arabidopsis thaliana* and the extremophile *Eutrema salsugineum*

Susana Silvestre

Thesis submitted to the University of Nottingham for the Degree of Doctor of Philosophy

October 2019

I certify that everything presented in this thesis is my own original work, and any exception to this has been properly acknowledged. None of the presented here has been previously been submitted for the award of a degree in this or any other University.

This thesis will be available for library use on the understanding that it is subjected to copyright and no quotation from the thesis may be published without consent and proper acknowledgement.

Signature: 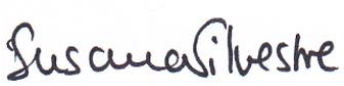

Date: 23rd October 2019

This project was funded by the BBSRC Doctoral Training Partnership (DTP) studentship programme in partnership with Rothamsted Research.

Abstract

Temperature fluctuations caused by the consequences of climate change and global warming will increase adaptive pressure on plants and crops, limiting their distribution and yield. Increasingly, with periods of unpredictable cold including unseasonal chilling and sub-zero temperatures, understanding the mechanisms of plant adaptation is of greater significance. Cold acclimation is the adaptive process that plants initiate to allow survival even under freezing temperatures. However, this is a multifactorial process involving molecular, metabolic and physiological adaptations, which remains to be fully understood. Lipid metabolism is a significant proportion of cellular activity, involving the breakdown or storage of fats for energy and the synthesis of structural (plasma- and endo-membranes) and functional (signalling and protective) lipids. The nature and diverse structures found in plant lipids provide a source of properties that, fully understood, could revolutionise the way crops are designed. This thesis was developed with the aim to further our understanding of the role of plant lipids in the cold acclimation process. The work was developed in the plant model *Arabidopsis thaliana* and utilised the extremophile *Eutrema salsugineum* as an exemplar. Cold-induced transcriptomic changes were analysed, which led to the identification of a phytyl ester synthase and a proton gradient regulator gene as key candidates for cold acclimation. The role of these genes was tested in a novel fluorescence-based screen and confirmed using lipidomic profiling. The capacity to remodel membrane composition and maintain structural integrity is a key adaptive strategy, therefore the role of the Eutrema long-chain base Δ^8-desaturase in sphingolipid remodelling during cold stress was determined. Lastly, a focus was given to Eutrema as an extremophile plant model where a germination, transformation and genome editing protocols were developed to produce mutants deficient in chloroplast-produced trienoic acids essential to cold acclimation.

Acknowledgements

First, I would like to acknowledge my Rothamsted supervisors, Louise V. Michaelson and Richard P. Haslam for their help and guidance through these four years of work. Thank you for all your support and motivation, especially with the mass spec and the endless needles you changed.

To my Nottingham supervisor, Erik Murchie and his group members, Lorna McAusland, CC and Dimitra for the help with the fluorescence screen and making my short stay in Nottingham a thousand times better.

To Cristina Barrero-Sicilia, for teaching me the molecular techniques anyone could wish for, and for being my very good friend from the start.

To Damiano Martignano for all the help setting up the gene editing protocol even in the busiest of times, and most importantly, and this includes Elisa (and little Davide) for being my very best friends!

To all the amazing people from the Lipid Group and the Lab 115, and all the friends I made along the way at Rothamsted for all the laughs, the help, and withstanding my innate grumpiness.

To my polyamorous duo Joana Ministro and Hernâni Ribeiro for always being there for me.

And last, but not least… Quero agradecer a toda a minha familia, em especial aos meus pais por todo o apoio e amor! E ao Tiago, o meu sobrinholas reguila mais favorito deste mundo!

To Tom, who has been by my side supporting, motivating and loving me.

Thank you to all.

Obrigada a todos 😊

Table of Contents

ABSTRACT I

ACKNOWLEDGEMENTS III

TABLE OF CONTENTS V

LIST OF ABBREVIATIONS XI

DEFINITIONS XIII

LIST OF FIGURES XIV

LIST OF TABLES XVI

CHAPTER 1. INTRODUCTION 1

1.1 *EUTREMA SALSUGINEUM*, A NEW PLANT MODEL 3

1.1.1 EUTREMA IS CLOSELY RELATED TO ARABIDOPSIS 4

1.1.2 HOW DOES EUTREMA RESPOND TO ABIOTIC STRESS? 5

1.2 COLD STRESS TRIGGERED RESPONSES 8

1.2.1 COLD RESPONSE IS MEDIATED BY TRANSCRIPTION FACTORS 10

1.2.2 METABOLIC ADAPTATION IS A MULTIFACTORIAL EQUATION 13

1.3 PLANT LIPIDS IN COLD ACCLIMATION 15

1.3.1 LIPIDS AS SIGNALLING MOLECULES 15

1.3.2 PLASMA MEMBRANES AS A FIRST DEFENCE MECHANISM 17

1.3.3 THE CHLOROPLAST IS A PRIMARY TARGET IN COLD STRESS 19

1.3.4 FATTY ACID DESATURATION IS A KEY RESPONSE TO COLD 20

1.3.5 WAXES ARE A FIRST BARRIER AGAINST COLD STRESS 21

1.4 LIPID METABOLISM IN PLANTS 22

1.4.1 FATTY ACID BIOSYNTHESIS 23

1.4.2 PHOSPHOLIPID METABOLISM 24

1.4.3 THYLAKOID MEMBRANE LIPID COMPOSITION 26

1.4.4 SPHINGOLIPID METABOLISM 28

1.5 PROJECT AIMS 33

CHAPTER 2. MATERIALS AND METHODS 36

2.1 PLANT MATERIAL 37
2.2 GERMINATION AND GROWTH 37
2.2.1 GERMINATION PROTOCOL 37
2.2.2 COMPOST COMPOSITION (ROTHAMSTED MIX) 39
2.2.3 CONTROL GROWTH CONDITIONS 39
2.2.4 COLD STRESS EXPERIMENTS 40
2.3 PLANT TRANSFORMATION 40
2.3.1 PLASMIDS AND EXPRESSION VECTORS 40
2.3.2 TRANSFORMATION OF AGROBACTERIUM TUMEFACIENS 41
2.3.3 GLYCERINE STOCK 42
2.3.4 AGROBACTERIUM – MEDIATED PLANT TRANSFORMATION 42
2.3.5 SELECTION OF TRANSFORMANTS 42
2.3.6 GENERATION SEGREGATION ANALYSIS 43
2.4 MOLECULAR BIOLOGY ANALYSIS 43
2.4.1 GENOMIC DNA EXTRACTION 43
2.4.2 PRIMER PAIRS 44
2.4.3 POLYMERASE CHAIN REACTION 45
2.4.4 ELECTROPHORESIS GEL 45
2.4.5 DNA SEQUENCING ANALYSIS 45
2.4.6 RNA EXTRACTION 49
2.4.7 CDNA SYNTHESIS 50
2.4.8 REVERSE TRANSCRIPTASE – QUANTITATIVE PCR 50
2.5 LIPID ANALYSIS 52
2.5.1 TOTAL LIPID EXTRACTION 52
2.5.2 TRIACYLGLYCEROL AND DIACYLGLYCEROL QUANTIFICATION 52
2.5.3 POLAR LIPID ASSESSMENT 53
2.5.4 FATTY ACID METHYL ESTERS 55
2.5.5 LONG-CHAIN BASE MEASUREMENT 56
2.5.6 SPHINGOLIPID ANALYSIS 57
2.5.7 ACYL-COA PROFILE 58
2.6 PLANT PHYSIOLOGY MEASUREMENTS 59
2.6.1 MORPHOLOGY ANALYSIS 59
2.6.2 ION LEAKAGE 60
2.6.3 CHLOROPHYLL FLUORESCENCE SCREEN 61
2.6.4 CHLOROPHYLL AND CAROTENOID ASSAY 63

2.7 GENOME EDITING BY CRISPR/CAS9 63
2.7.1 IDENTIFICATION OF EUTREMA FAD GENES 63
2.7.2 IDENTIFICATION OF THE CHLOROPLAST TRANSIT PEPTIDE 64
2.7.3 GUIDE RNA DESIGN 64
2.7.4 CAS9 VECTOR 66
2.7.5 ANZA™ RESTRICTION ANALYSIS 66
2.7.6 ASSEMBLY OF THE EXPRESSION VECTOR 67
2.7.7 TRANSFORMATION OF ESCHERICHIA COLI COMPETENT CELLS 70
2.7.8 TRANSFORMATION SUMMARY 71
2.7.9 IDENTIFICATION OF GENE EDITED T1 LINES 72
2.8 STATISTICAL ANALYSIS 72

CHAPTER 3. ARABIDOPSIS COLD ACCLIMATION RESPONSE ASSESSED BY CHLOROPHYLL FLUORESCENCE IMAGING.....74

3.1 INTRODUCTION 75
3.1.1 TRANSCRIPTOMIC ADAPTATION TO COLD STRESS 75
3.1.2 LINKING COLD, PHOTOSYNTHESIS AND LIPID METABOLISM 76
3.1.3 CHLOROPHYLL FLUORESCENCE ASSESSMENT OF COLD STRESS 79
3.1.4 CHAPTER AIMS 81
3.2 RESULTS 83
3.2.1 TRANSCRIPTOMIC ADAPTATION TO COLD STRESS IN ARABIDOPSIS 83
3.2.2 SELECTION OF THE CANDIDATE GENES 84
3.2.3 LIPID, PHOTOSYNTHESIS AND COLD RELATED GENES 85
3.2.4 COLD SCREEN DESIGN 93
3.2.5 TWO MUTANT LINES WERE SUSCEPTIBLE TO COLD STRESS 94
3.2.6 CHLOROPHYLL CONTENT WAS REDUCED BY COLD STRESS 97
3.2.7 ELECTROLYTE LEAKAGE UNDER COLD STRESS 98
3.2.8 NO VISIBLE MORPHOLOGICAL PHENOTYPE 102
3.3 DISCUSSION 104
3.3.1 THE TRANSCRIPTOME WINDOW INTO COLD ACCLIMATION 104
3.3.2 WHY A PHOTOSYNTHESIS RELATED METHOD TO SCREEN LIPID RELATED GENES? 107
3.3.3 CHLOROPHYLL FLUORESCENCE SHOWED PES1 AND PGR5L1A IMPAIRED CAPACITY FOR COLD ADAPTATION 109
3.4 CONCLUSION 111

CHAPTER 4. LIPID CHARACTERISATION OF THE COLD RESPONSIVE GENES *PES1, PGR5L1A* AND *IPCS3* 113

4.1 INTRODUCTION 114
4.1.1 PHYTYL ESTER SYNTHASE 115
4.1.2 PROTON GRADIENT REGULATION 5 – LIKE 1A 116
4.1.3 INOSITOL PHOSPHORYLCERAMIDE SYNTHASES 117
4.1.4 CHAPTER AIMS 119
4.2 RESULTS 120
4.2.1 PES1, PGR5L1A AND IPCS3 MOLECULAR DESCRIPTION 120
4.2.2 LIPIDOME REMODELLING IN RESPONSE TO COLD STRESS 125
4.2.3 IPCS3: A NEGATIVE CONTROL FOR CHLOROPLAST LIPID REMODELLING? 127
4.2.4 GALACTOLIPID COMPOSITION CHANGED IN THE MUTANT LINES 128
4.2.5 DAG AND TAG COMPOSITION WAS ALTERED IN PES1 134
4.2.6 PGR5L1A MUTANT SHOWED DISTURBED TAG AND FFA PROFILES 136
4.2.7 IPCS3 CHANGED THE CERAMIDE AND GIPC CONTENT 138
4.3 DISCUSSION 144
4.3.1 THE T-DNA INSERTION SALK LINES 144
4.3.2 GALACTOLIPIDS WERE AFFECTED IN THE MUTANT LINES 145
4.3.3 PES1 CHLOROPLAST LIPID COMPOSITION WAS AFFECTED BY TEMPERATURE 147
4.3.4 IPCS3 IS INVOLVED IN THE GIPC REMODELLING UNDER COLD 148
4.4 CONCLUSION 149

CHAPTER 5. SPHINGOLIPID LCB Δ^8-DESATURASE AS A MEDIATOR OF COLD STRESS RESPONSE IN ARABIDOPSIS 151

5.1 INTRODUCTION 152
5.1.1 LCB DESATURASES 152
5.1.2 STRESS RESPONSIVE SPHINGOLIPIDS 154
5.1.3 CHAPTER AIMS 155
5.2 RESULTS 157
5.2.1 IDENTIFICATION OF THE EUTREMA SLD GENES 157
5.2.2 PRODUCTION OF TRANSGENIC LINES 158
5.2.3 QUANTITATIVE ANALYSIS OF THSLD TRANSGENES OVEREXPRESSION 161
5.2.4 THSLD2 ALTERS THE CIS/TRANS RATIO IN THE T18:1 LCB 164

5.2.5 THE SPHINGOLIPID PROFILE CHANGED WITH THE GENOTYPE 169
5.2.6 THSLD1 AND THSLD2 RECOVERED THE GLUCOSYLCERAMIDE CONTENT IN THE SLD1SLD2 BACKGROUND 172
5.2.7 SLD1SLD2 SHOWED AN ACCUMULATION OF CERAMIDES.....180
5.2.8 THE HYDROXYCERAMIDE PROFILE CHANGED IN SLD1SLD2.....185
5.2.9 COL-0:THSLD1 AND COL-0:THSLD2 TOTAL SPHINGOLIPID CLASS CONTENT.....188
5.2.10 SLD OVEREXPRESSION SHOWED NO IMPACT ON ARABIDOPSIS GROWTH 189
5.2.11 SLD SHOWED NO EFFECT IN MEMBRANE DAMAGE UNDER COLD 193
5.2.12 ACYL-COA ACCUMULATED UNDER COLD STRESS 193
5.2.13 HIGHER RECOVERY RATE IN THE THSLD2 COMPLEMENTED LINES 197
5.3 DISCUSSION.....199
5.3.1 CONSERVED SLD1 AND SLD2 BETWEEN ARABIDOPSIS AND EUTREMA ..201
5.3.2 IS THERE A STEREOSPECIFICITY CORRELATED WITH EACH SLD GENE? 202
5.3.3 EXPECTED AND UNEXPECTED CHANGES IN SPHINGOLIPID PROFILE 204
5.3.4 THE SLD IMPACT IN THE COLD STRESS AND RECOVERY 205
5.4 CONCLUSION 208

CHAPTER 6. .CONTRIBUTION OF THE CHLOROPLASTIDIAL FATTY ACID DESATURASES TO *EUTREMA SALSUGINEUM* COLD ADAPTATION ...209

6.1 INTRODUCTION.....210
6.1.1 CHLOROPLAST FATTY ACID DESATURASES 211
6.1.2 THE ADVANTAGE OF GENOME EDITING TECHNOLOGIES 212
6.1.3 CHAPTER AIMS.....215
6.2 RESULTS 216
6.2.1 EFFICIENT GERMINATION ACHIEVED BY DIRECT SOW.....216
6.2.2 IDENTIFICATION OF EUTREMA FATTY ACID DESATURASE 220
6.2.3 EUTREMA SHOWED A HIGHER FATTY ACID RATIO OF 16:1/16:2 THAN ARABIDOPSIS 223
6.2.4 A MULTIPLEX APPROACH WAS USED FOR THE GENOME EDITING 224
6.2.5 GRNA:CAS9:DSRED EXPRESSION CLONE PRODUCTION.....232
6.2.6 EUTREMA SHOWED HIGH TRANSFORMATION EFFICIENCY WITH ONE FLOWER DIP 234
6.2.7 SIX EDITED CANDIDATES WERE IDENTIFIED BASED ON FRAGMENT SIZE .237
6.3 DISCUSSION.....243

6.3.1 Establishing Reliable Protocols for Eutrema 243
6.3.2 Off-Target Analysis of the gRNAs Designed 246
6.3.3 Investigating Screen Methods 249
6.3.4 The Contribution of FAD Genes to Cold Stress 250
6.4 Conclusion 251

CHAPTER 7. GENERAL DISCUSSION 253

REFERENCES 261

APPENDICES 296

List of Abbreviations

Abbreviation	Description
A	Adenosine
ABRC	Arabidopsis Biological Resource Centre
ACN	Acetonitrile, C_2H_3N
ACP	Acyl-Carrier Protein
AGI	Arabidopsis Gene Identifier
ATP	Adenosine Triphosphate
BLAST	Basic Local Alignment Search Tool
bp	base pair
BSA	Bovine Serum Albumin
C	Cytosine
CaMV	Cauliflower Mosaic Virus
Cas9	CRISPR associated protein 9
CDS	Coding Sequence
cDNA	complementary DNA
CEF	Cyclic Electron Flow
CI	Confidence Interval
CRBD	Complete Randomized Block Design
CRISPR	Clustered Regulatory Interspaced Short Palindromic Repeats
d18:0	Sphinganine
DAS	Days After Sowing
ΔpH	Proton (pH) Gradient
DEGs	Differentially Expressed Genes
DEPC	Diethyl Pyrocarbonate, $C_6H_{10}O_5$
DGAT	Diacylglycerol Acyltransferase
DGDG	Digalactosyldiacylglycerol
DNA	Deoxyribonucleic Acid
DSB	Double-Strand Break
EDTA	Ethylenediaminetetraacetic acid, $C_{10}H_{16}N_2O_8$
ELIP	EARLY INDUCED LIGHT PROTEIN
ELT	Esterase/Lipase/Thioesterase
EMS	Ethyl Methanesulfonate, $CH_3SO_3C_2H_5$
ER	Endoplasmic Reticulum
ESI	Electrospray Ionization
FA	Fatty Acid
FAD7 / 8	Fatty Acid Desaturase 7 / 8
FAMEs	Fatty Acid Methyl Esters
FID	Flame Ionisation Detector
G	Guanine
GC	Gas Chromatography
GIPC	Glycosylinositolphosphoryl Ceramides
GlcCer	Glucosylceramides
gDNA	genomic DNA
gRNA	guide RNA
HR	Homologous Recombination

(Continued on the next page)

Abbreviation	Description
indels	Insertion/deletion mutations
IPCS3	Inositol Phosphorylceramide Synthase 3
IPA	Isopropanol, C_3H_8O
K	Potassium, K
kbp	Kilo base pair
LCB	Long-Chain Base
LET	Linear Electron Flow
Lyso PC	Lysophosphatidylcoline
MeOH	Methanol, CH_3OH
MGDG	Monogalactosyldiacylglycerol
MRM	Multiple Reaction Monitoring
mRNA	messenger RNA
MS	Mass Spectrometry
MS/MS	Tandem Mass Spectrometry
MUSCLE	Multiple Sequence Comparison by Log-Expectation
MYA	Million Years Ago
N	Nitrogen, N
NaAC	Sodium Acetate, $C_2H_3NaO_2$
NaCl	Sodium Chloride, NaCl
NADP	Nicotinamide Adenine Dinucleotide Phosphate
NASC	Nottingham Arabidopsis Stock Centre
NCBI	National Centre for Biotechnology Information
NHEJ	Nonhomologous end-joining
NPQ	Non-Photochemical Quenching
nt	nucleotides
P	Phosphorous, P
PA	Phosphatidic Acid
PAM	Protospacer-Adjacent Motif
PC	Phosphatidylcholine
PCD	Programmed Cell Death
PE	Phosphatidylethanolamine
PG	Phosphatidylglycerol
PGR5	Proton Gradient Regulation 5
PGR5L1A	Proton Gradient Regulation 5 Like 1 A
PI	Phosphatidylinositol
PM	Plasma Membrane
Pol III	RNA polymerase III
PS	Phosphatidylserine
PSI / PSII	Photosystem I / II
ΦPSII	Effective Quantum Yield of Photosystem II
RNA	Ribonucleic Acid
RT-qPCR	Reverse Transcriptase-Quantitative PCR
RNA-Seq	RNA Sequencing
rpm	rotations per minute
s	Second(s)
SDS	Sodium Dodecyl Sulphate, $NaC_{12}H_{25}SO_4$
SIGnAL	Salk Institute Genome Analysis Laboratory

(Continued on the next page)

Abbreviation	Description
SLD	Sphingolipid ∆8 LCB desaturase
SQDG	Sulfolipid Sulfoquinovosyldiacylglycerol
SpCas9	Streptococcus pyogenes Cas9
T	Thymine
TALEN	TAL Effector Nucleases
t18:1$^{\Delta 8E}$	Δ8*trans*-4-hydroxysphingenine isomer ($^{\Delta 8E}$)
t18:1$^{\Delta 8Z}$	Δ8*cis*-4-hydroxysphingenine isomer ($^{\Delta 8Z}$)
TAG	Triacylglycerol
T-DNA	Agrobacterium tumefaciens transfer-DNA
TF	Transcription Factor
Tris-HCl	Tris(hydroxymethyl)aminomethane hydrochloride
UTR	Untranslated Region
VLCFA	Very Long Chain Fatty Acid
ZFN	Zinc Finger Nuclease

Definitions

Expression	Definition
Homologue	Two sequences that are related
Orthologous	A gene found in different species that evolved from a common ancestor through speciation
Paralogue	Genes found in the same species that share the same ancestral genes
Saturated	Absence of double bonds, causing a saturation of the hydrocarbon chains with hydrogen atoms
Transformation Event	One individual pot containing flowering plants transformed by *Agrobacterium*-mediated floral dip
Unsaturated	Presence of double bond(s) in the hydrocarbon chain

List of Figures

Figure 1.1 Eutrema salsugineum, Shandong ecotype....7
Figure 1.2 The CBF Regulation Pathway in Plants....12
Figure 1.3. Lipid Remodelling in Plasma Membrane During Cold Stress....19
Figure 1.4 Phospholipid Molecular Structure....26
Figure 1.5 Glycolipids and Phosphatidylglycerol Structure....27
Figure 1.6 Sphingolipid Structure....29
Figure 1.7 Sphingolipid Biosynthesis Pathway....31
Figure 1.8 Project Aims....35
Figure 2.1 Germination Optimization of Eutrema....40
Figure 2.2 Segregation Analysis of the Transformed Lines....43
Figure 2.3 Mass Spectrometry Based Lipid Analysis Methods....54
Figure 2.4 pDE-Cas9-proDsREDter vector....67
Figure 2.5 pDONR221™ vector....68
Figure 3.1 Chloroplast Structure....78
Figure 3.2 Chlorophyll Fluorescence Trace....80
Figure 3.3 Arabidopsis Cold Acclimation Workflow....82
Figure 3.4 Fold Change of the Genes with Aligned Reads....84
Figure 3.5. Cold Screen Design to Test the Mutant Lines....94
Figure 3.6. Maximum Quantum Efficiency of Photosystem II....96
Figure 3.7 Effective Quantum Yield of Photosystem II....99
Figure 3.8. (Non-)Photochemical Quenching under Cold Stress....100
Figure 3.9. Pigment Content of the Arabidopsis Mutant Lines....101
Figure 3.10. Injury Index of the Arabidopsis Lines under Cold Stress....102
Figure 3.11. Arabidopsis Mutant Lines under Control and Cold Stress....103
Figure 4.1 Arabidopsis Cold Acclimation Workflow – Lipidomic Profile....120
Figure 4.2 Gene Models for AtPES1, AtPGR5L1A, and AtIPCS3....122
Figure 4.3. Molecular Characterisation of the three T-DNA Lines....123
Figure 4.4 Expression Analysis of the three T-DNA Lines....126
Figure 4.5 Col-0, pes1, pgr5l1a and ipcs3 Growth Phenotype....128
Figure 4.6 Multivariate Analysis of Galactolipids....130
Figure 4.7 Galactolipid Composition of T-DNA Lines....132
Figure 4.8 Total Content of MGDG, DGDG, SQDG, and PG....133
Figure 4.9 Multivariate Analysis of pes1 Lipids....135
Figure 4.10 Multivariate Analysis for pgr5l1a Lipids....137
Figure 4.11 Long-Chain Base Profile of ipcs3....139
Figure 4.12 ipcs3 Ceramide and GIPC Multivariate Analysis....141
Figure 4.13 Ceramide and GIPC Profiles for ipcs3....143
Figure 5.1 Schematic Representation of the Chapter Aims....156

FIGURE 5.2 ARABIDOPSIS AND EUTREMA SLD SEQUENCE HOMOLOGY 159
FIGURE 5.3 SLD GENES AND OVEREXPRESSING LINES GENOTYPE 162
FIGURE 5.4 EXPRESSION ANALYSIS OF THE SLD GENES 165
FIGURE 5.5 LCB PROFILE FOR THE SLD LINES 168
FIGURE 5.6 SPHINGOLIPID MULTIVARIATE CANONICAL ANALYSIS 170
FIGURE 5.7 SPHINGOLIPID MULTIVARIATE ANALYSIS FOR COL-0:THSLD 173
FIGURE 5.8 GLUCOSYLCERAMIDE AND GIPC CONTENT OF THE SLD LINES 178
FIGURE 5.9 TOTAL GLUCOSYLCERAMIDE AND GIPC CONTENT 180
FIGURE 5.10 CERAMIDE PROFILE OF THE SLD LINES 183
FIGURE 5.11 CANONICAL VARIATES ANALYSIS OF CERAMIDE PROFILE OF SLD LINES 184
FIGURE 5.12 TOTAL CERAMIDE CONTENT IN THE SLD LINES 184
FIGURE 5.13 TOTAL HYDROXYCERAMIDE CONTENT FOR THE SLD LINES 186
FIGURE 5.14 HYDROXYCERAMIDE PROFILE FOR THE SLD LINES 187
FIGURE 5.15 TOTAL CONTENT OF SPHINGOLIPIDS IN COL-0:THSLD GENOTYPES 189
FIGURE 5.16 GROWTH PHENOTYPE OF THE SLD LINES 192
FIGURE 5.17 MEMBRANE DAMAGE IN THE SLD LINES UNDER COLD STRESS 194
FIGURE 5.18 ACYL-COA PROFILE UNDER CONTROL AND COLD TEMPERATURES 196
FIGURE 5.19 RECOVERY RATE OF THE SLD LINES AFTER FREEZING STRESS 198
FIGURE 5.20 SLD AMINO ACID PREDICTED DOMAINS 201
FIGURE 5.21 EXPECTED RESULTS FOR THE SLD OVEREXPRESSING LINES 207
FIGURE 6.1 COMPARISON BETWEEN ZFN, TALEN AND CRISPR SYSTEMS 214
FIGURE 6.2 WORKFLOW FOR EDITING THE GENOME OF EUTREMA 216
FIGURE 6.3 GERMINATION EFFICIENCY OF EUTREMA SALSUGINEUM 219
FIGURE 6.4 EUTREMA PLANTS DURING TRANSFORMATION 220
FIGURE 6.5 MULTIPLE SEQUENCE ALIGNMENT FOR THE FAD GENES 221
FIGURE 6.6 FATTY ACID PROFILE FOR EUTREMA AND ARABIDOPSIS 224
FIGURE 6.7 GENE STRUCTURES AND GRNAS OF THFAD7 AND THFAD8 231
FIGURE 6.8 ENTRY CLONES ANALYSIS 233
FIGURE 6.9 EXPRESSION CLONES ANALYSIS 235
FIGURE 6.10 EUTREMA TRANSFORMATION WITH THE CRISPR VECTOR 236
FIGURE 6.11 T1 CRISPR LINES GENOTYPE ANALYSIS 239
FIGURE 6.12 T1 CRISPR LINES SEQUENCING RESULTS 241
FIGURE 6.13 FATTY ACID PROFILE OF THE T1 CRISPR LINES 242
FIGURE 6.14 EUTREMA (SHA) AND ARABIDOPSIS (COL-0) FLOWERING PLANTS 245
FIGURE 7.1 SUMMARY OF THE RESULTS OBTAINED IN THIS PROJECT 255
FIGURE 7.2 OPEN QUESTIONS FOLLOWING THE WORK DEVELOPED IN THIS PROJECT 260

List of Tables

TABLE 1.1 PLANT LONG-CHAIN BASE COMMON STRUCTURES....32
TABLE 2.1 ARABIDOPSIS T-DNA ACCESSIONS....38
TABLE 2.2 ARABIDOPSIS TRANSGENIC LINES....41
TABLE 2.3 PRIMER PAIRS USED FOR GENOTYPING....46
TABLE 2.4 PRIMER PAIRS USED FOR GENE EXPRESSION ANALYSIS....51
TABLE 2.5 MRM PARAMETERS FOR LONG-CHAIN BASE ANALYSIS....57
TABLE 2.6 SOLVENT GRADIENT FOR SPHINGOLIPID ANALYSIS....58
TABLE 2.7 MRM PARAMETERS FOR ACYL-COA ANALYSIS....60
TABLE 2.8 FLUORESCENCE PARAMETERS....62
TABLE 2.9. PRIMER SEQUENCES USED FOR CLONING....70
TABLE 2.10 SUMMARY OF THE CLONING ASSOCIATED TRANSFORMATION....71
TABLE 2.11 PRIMER PAIRS USED FOR IDENTIFICATION OF GENE EDITED LINES....73
TABLE 3.1 GENES OF INTEREST SELECTED FROM TRANSCRIPTOMIC ANALYSIS....90
TABLE 6.1 PREDICTION FOR TARGETING PEPTIDE....222
TABLE 6.2 SUMMARY OF THE GRNA PROPERTIES....228
TABLE 6.3 OFF-TARGETS FOR THE DESIGNED GRNAS....229
TABLE 6.4 EUTREMA TRANSFORMATION SUMMARY....236

Chapter 1.

Introduction

Low temperatures have long been recognised as a major constraint that severely impair plant growth and development. The susceptibility of crops to cold temperatures limits the use of valuable varieties and lowers yields. The impact of temperature on food production is now, more than ever, a challenge for researchers (Dhankher and Foyer 2018), breeders and growers alike (van Etten *et al.* 2019). For example, the search for improvements in seed oil quality by reducing levels of fatty acid desaturation, may potentially expose crops to greater risk from colder growing seasons (Kaur *et al.* 2019). As climate change is driving greater temperature fluctuations, the frequency of unpredictably cold weather is expected to increase e.g. episodes such as the winter (January 2019) polar vortex that resulted in record low temperatures in the American mid-west and the unusually low UK temperatures (-14°C) in 2018. The importance of understanding the mechanisms underlying cold stress responses in plants is therefore more urgent, driving the need for enhanced resilience and climate-smart crops [(Zhang *et al.* 2019), https://csa.guide/]. However, the strategies involved in cold adaptation are complex and involve a multitude of molecular, metabolic and physiological adaptations. The cascade of molecular processes triggered by low temperatures is yet to be fully understood. Once the cold temperatures are sensed, it is typically followed by the activation of stress-related gene expression mediated by transcription factors (TFs) that modulate the plants response (Meshi and Iwabuchi 1995, Shinozaki *et al.* 2003, Chinnusamy *et al.* 2010). However, the response of plants to cold is not limited to the transcription network; an analogous series of associated metabolic and physiologic adaptations are initiated that allow survival. Cold temperature resilience is often defined by the ability of the cell membranes to adapt. As a major component of chloroplast, plasma and endo- membranes, lipids have a recognizable structural role in adaptation. The diverse and complex nature of lipid forms (e.g. desaturation, carbon chain length, head groups) provide the unique physical and chemical properties essential for metabolic adaptation to stress. Although sensitive to cold stress, *Arabidopsis thaliana* (herein Arabidopsis) serves as the classic plant model for the exploration of plant

chilling responses (Zuther *et al.* 2012, Zuther *et al.* 2018). There are plants (extremophiles) that thrive in extreme environments and offer a deeper understanding of the mechanisms of abiotic metabolic adaptation. Plants have evolved and adapted to their native surroundings, developing their own specific cold tolerance strategies (Kreyling *et al.* 2015). Extremophile species can endure extreme abiotic conditions and therefore provide resource to study resilience to severe environmental conditions (Amtmann *et al.* 2005). One such example is *Eutrema salsugineum* (Eutrema), a *Brassicaceae* commonly known as 'salt cress' due to its documented resilience to high levels of salinity. In addition to its halophytic properties, it also shows a high tolerance to drought and cold (Amtmann *et al.* 2005, Griffith *et al.* 2007, Amtmann 2009). Furthermore, Eutrema (formerly *Thellungiella halophila;* (Koch and German 2013),) has a close evolutionary relationship with Arabidopsis, featuring high genomic sequence identity and similar plant morphology (Wang *et al.* 2004, Amtmann 2009). Eutrema is now routinely referred to a model species for the study of plant stress tolerance as discussed below (Griffith *et al.* 2007, Zhu 2015).

1.1 *Eutrema salsugineum*, A NEW PLANT MODEL

As climate change is driving research towards stress tolerant traits in plants for the improvement of crops, researchers are focusing on understanding mechanisms of plant plasticity. Some examples include resurrection plants, a small group of approximately 300 species of vascular plants that can lose at least 90% of their water content upon drought, which can be restored once water is available (Liu *et al.* 2019). There are a few species closely related to Arabidopsis that fall into this category. One such example is the self-incompatible *Arabidopsis halleri*, known for its tolerance to toxic levels of heavy metals (Preite *et al.* 2019). Other examples include *Eutrema parvula* (*Schrenkiella parvula,* or *Thellungiella parvula*) and *Eutrema salsugineum*, which have both been described as tolerant to high salinity conditions (Inan *et al.* 2004, Orsini *et al.* 2010). However, *Eutrema salsugineum* has been extensively

studied for its additional tolerance to drought and cold/freezing conditions (Inan *et al.* 2004, MacLeod *et al.* 2015). In contrast to Arabidopsis, which even amongst the most resistant ecotypes (Zuther *et al.* 2012, Nagler *et al.* 2015, Zuther *et al.* 2015, Zuther *et al.* 2018) has limited tolerance to extreme environments, *Eutrema salsugineum* is an extremophile.

1.1.1 *Eutrema is Closely Related to Arabidopsis*

Eutrema salsugineum has several ecotypes found in China, Russia, Kazakhstan, Canada, and USA (Wang *et al.* 2015); with an accession also recently reported in Mexico (German and Koch 2017). It is classified as an extremophile resilient to different abiotic stresses, such as cold (Griffith *et al.* 2007, Wang *et al.* 2017), salt (Inan *et al.* 2004, Lee *et al.* 2016), and drought (Xu *et al.* 2007, MacLeod *et al.* 2015). Different accessions from Eutrema have been identified, at least 14 have been characterised with regard to their capacity for salinity and freezing tolerance, and it is clear that natural genetic variation exists amongst the accessions (Lee *et al.* 2012, Lee *et al.* 2016). From these, the Shandong and Yukon ecotypes are the most studied, originally found in the North Eastern coast of China and in the southwest of the Yukon territory in subarctic Canada, respectively (Wong *et al.* 2005, Wong *et al.* 2006, Amtmann 2009, Gao *et al.* 2009, Khanal *et al.* 2017). Based on chloroplastic (*ndhF – NADH DEHYDROGENASE F*) and nuclear (*PHYA – PHYTOCHROME A*) markers (Beilstein *et al.* 2008) the phylogenetic position of Eutrema in the *Brassicaceae* family was assessed, revealing that its separation from *Arabidopsis thaliana* and *Arabidopsis lyrata* occurred approximately 43.2 million years ago (MYA), and from *Eutrema parvula*, another close relative of *Brassica rapa* (Cheng *et al.* 2012), 38.4 MYA (Yang *et al.* 2013). The *Eutrema* (or *Thellungiella*) genus includes three other species closely related to *Eutrema salsugineum,* these are *E. halophila*, *E. parvula* and *E. botschantzevii.*

Eutrema salsugineum (from here on referred to as Eutrema) has a life cycle of two to two and half months and is similar in structure and size to Arabidopsis, although its leaf shape may change with the growth

conditions, as it can appear waxier and serrated [Figure 1.1, (Bressan *et al.* 2001)]. It requires a stratification or a period of vernalization to promote flowering, which, once started, extends for long periods producing copious amounts of seed by self-pollination. Despite similarities in the flower morphology between Arabidopsis and Eutrema these two species cannot be crossed successfully (Bressan *et al.* 2001). Recently, however, a protocol has been developed for grafting between Eutrema and Arabidopsis (Li *et al.* 2019), a technique especially useful for developmental and signalling studies. The genome of Eutrema (Wu *et al.* 2012, Yang *et al.* 2013), is approximately twice the size of Arabidopsis and shares approximately 95% sequence identity (Wang *et al.* 2004). Furthermore, it is noteworthy that the genome of *Eutrema salsugineum* is 100 Mb bigger than *Eutrema parvula* (Dassanayake *et al.* 2011). Many consider the increased genome size and gene duplication events contribute to the abiotic stress tolerance exhibited by Eutrema. The similarity level between genomes of Eutrema and Arabidopsis permit a direct comparison between genes and their function, rendering most of the experimental procedures developed for Arabidopsis highly adaptable to this extremophile. This constitutes a major advantage in stress related studies, opening the possibility of expressing genes of interest from the extremophile in Arabidopsis facilitating their characterization, and potential role in stress resilience.

1.1.2 *How does Eutrema respond to abiotic stress?*

The mechanisms responsible for Eutrema's tolerance to abiotic stress remain elusive, but proposed theories involve the genomic differences to Arabidopsis (Taji *et al.* 2004, Zhang *et al.* 2019), a highly regulated photosynthetic system (Khanal *et al.* 2017) and its leaf cuticular composition (Xu *et al.* 2014, Tang *et al.* 2018). The difference in genome size between Eutrema and Arabidopsis likely underpins the resilience mechanisms found in the extremophile. Gene duplication mechanisms and transposable elements, which increase genome size, are often involved in evolutionary stress coping mechanisms (Fedoroff 2000,

Hittinger and Carroll 2007, Oh *et al.* 2012, Yang *et al.* 2013). However, a comparison of gene copy number for stress-induced genes between Arabidopsis and Eutrema, found that most of the TF families were present in approximately the same copy number (Yang *et al.* 2013). In fact, only the *UBIQUITIN-DEPENDENT PROTEIN MODIFICATION* gene family was shown to have a statistically significant increase in gene copy number in Eutrema. This suggests that a highly stress-specific translational and transcriptional reprogramming occurs in Eutrema (Yang *et al.* 2013), which can lead to metabolic and signalling changes (Mucha *et al.* 2015). Furthermore, 21 gene families were identified to have significantly increased expression in Eutrema in comparison to Arabidopsis, suggesting an evolutionarily adaptation to extreme conditions in Eutrema (Yang *et al.* 2013). The hypothesis that cold tolerance in Eutrema is derived from a constitutive high level of expression of stress-responsive genes is corroborated in the response of Eutrema to salt stress (Taji *et al.* 2004). According to Taji *et al*. (Taji *et al.* 2004), only six Eutrema genes were differentially expressed under salt stress, which is indicative of a constitutive high level of expression of stress-responsive genes (Taji *et al.* 2004, Gong *et al.* 2005). Further work by Wong *et al.* reported that genes induced by cold stress are more similar between Eutrema and Arabidopsis, than either salt- or drought-induced sequences (Wong *et al.* 2005). A shared response to cold stress in Arabidopsis and Eutrema opens the possibility of combined approach in which gene functionality can be tested in Arabidopsis, for which molecular tools and resources are more advanced.

Extreme weather conditions in winter, such as high light intensity combined with low temperature (chilling or freezing) present plants with specific problems. Low temperatures reduce the rate of photosynthesis both directly and indirectly, by influencing the activity of photosynthetic enzymes involved in the Calvin cycle, such as Rubisco or by reducing stomatal conductance. Therefore, plants require photoprotective mechanisms e.g. alternative electron sinks to mitigate the damage. As with all plants, Eutrema carefully regulates its photosystems; e.g. 15% of

down-regulated transcripts under cold stress were photosynthesis related (Wong *et al.* 2006). Eutrema has increased photoinhibition protection mechanisms for the photosynthetic acclimation to low temperatures. In fact, the two most studied ecotypes Shandong and Yukon presented different strategies in their photosynthetic acclimation to cold. The first was found to have a stable and slower response with an energy partitioning towards photochemistry, whilst the latter was shown to adapt faster with a non-photochemical strategy (Khanal *et al.* 2017). Further differences were found between Arabidopsis and Eutrema adaptation to freezing stress through the analysis of the metabolite profile (Lee *et al.* 2012). Yukon ecotype showed the reduced (GSH) and oxidized (GSSG) forms of glutathione unchanged after three days of 4°C treatment, contrary to that observed in Arabidopsis (Benina *et al.* 2013). However, in common with Arabidopsis, sucrose, fructose and glucose were accumulated in response to cold stress (Benina *et al.* 2013).



Figure 1.1 Eutrema salsugineum, Shandong ecotype

Adult plant grown under control conditions in a growth chamber. (A) general view, (B) Top view, and (C) Detail of the inflorescence. Scale bar represents 2.0 cm.

1.2 COLD STRESS TRIGGERED RESPONSES

As sessile organisms, plants are unable to regulate their internal temperature and are therefore highly influenced by the surrounding environment. Low temperature is an important feature for the natural distribution of plant species, as a result the survival range of many agricultural crops is limited. The trait for low temperature tolerance shows a lot of natural variation. Eutrema, for example, can tolerate lower temperatures than those recorded for any Arabidopsis accessions (Zuther *et al.* 2012), with one-third of the studied 14 Eutrema accessions more freeze-tolerant (Lee *et al.* 2012). This natural variation is attributed to the different locations from which the different ecotypes originated (Lee *et al.* 2012, Khanal *et al.* 2017). Understanding how plants sense and cope with such stress is essential to explore features that would be potentially advantageous to winter crops. Low temperature stress can refer to chilling or freezing. Chilling stress is characterized by temperatures above 0ºC reaching to 15ºC or even 20ºC in some cases where plants are adapted to subtropical and tropical environments. Cold temperatures are often perceived as the adaptation period that allows survival under freezing temperatures, often referred to as cold acclimation (Thomashow *et al.* 1990). In Arabidopsis, for example, seven days have been demonstrated to be enough for the plant to reach maximal freezing tolerance (Livingston *et al.* 2007). Freezing stress is thus generally considered to begin when plants are exposed to temperatures below 0ºC and ice is formed, primarily in the intercellular spaces due to its lower freezing point and the activity of ice-nucleating agents (Steponkus 1984, Thomashow 1998) [further reviewed in references (Steponkus 1999, Wanner and Junttila 1999, Zhang *et al.* 2004, Reyes-Diaz *et al.* 2006)]. Chilling stress reduces plant growth and development, causes loss of vigour and surface lesions. Cold symptoms are caused by the altered physical and chemical composition of the membranes, electrolyte leakage, decreased protoplasmic streaming, and changes in cell metabolism. Cell metabolic responses involve changes in nucleic acid and protein synthesis, enzyme conformation and affinity,

water and nutrient balance and impairment of photosynthesis, with down-regulation and photo-damage of the photosystem II (PSII) (Wong *et al.* 2006, Johnova *et al.* 2016). Nonetheless, plants can endure low, non-freezing temperatures which increase their resilience to stress and extend their tolerated range of temperatures in a process called cold acclimation (Thomashow 1999). The regulatory network underlying cold acclimation is complex and involves molecular, transcriptomic, proteomic, and lipidomic reprogramming (Thomashow 2005, Guy *et al.* 2008, Thomashow and Thomashow 2010, Alcazar *et al.* 2011, Hincha and Zuther 2014). Some of the characteristics of cold acclimated plants include increased abscisic acid (ABA) and sugar levels, accumulation of osmoprotectants such as proline, accompanied by a modified lipid profile (Xin and Browse 2000, Janska *et al.* 2010, Zhang *et al.* 2013, Barrero-Sicilia *et al.* 2017). All these changes contribute to the activation of defence mechanisms against an immediate stress, but also underpin the priming of plant response in the case of repeated stress events [as reviewed in (Hilker and Schmulling 2019)). Gene expression can be activated by ABA-dependent or ABA-independent mechanisms (Thomashow 1999, Xue-Xuan *et al.* 2010), which can be distinguished by different recognition sites in the promoter of the induced gene (Baker *et al.* 1994, Uno *et al.* 2000). ABA-independent gene expression is regulated by the CBF/DREB1 (*C-REPEAT-BINDING FACTOR/ DEHYDRATION RESPONSIVE ELEMENT-BINDING FACTOR 1*) TF regulon which specifically binds to the CRT (*C-REPEAT/DRE*) element in cold-induced gene promoters (Baker *et al.* 1994, Yamaguchi-Shinozaki and Shinozaki 1994, Stockinger *et al.* 1997). Typically plants accumulate ABA in response to abiotic stress which mediates stress signal transduction, and gene expression (Xiong and Zhu 2003). However, the low temperature response pathway accumulates ABA transiently and to a lesser extent (Lang *et al.* 1994, Thomashow 1999, Xue-Xuan *et al.* 2010). ABA-dependent gene expression works through an *ABA RESPONSIVE ELEMENT* (*ABRE*) in the promoter region of the induced genes, to which ABF proteins (*ABRE-BINDING FACTORS*) bind and activate expression (Uno *et al.* 2000, Xue-Xuan *et al.* 2010). The role of

ABA in plant responses to cold stress may also result from its functions as a plant hormone, regulating growth, sugar content, leaf senescence, seed dormancy and germination, cell division and elongation (Walton 1980, Xue-Xuan *et al.* 2010, Yang *et al.* 2016). One contribution of ABA to cold acclimation is its role in promoting phospholipid [inositol 1,4,5-triphosphate, ($Ins(1,4,5)P_3$)] metabolism (Lee *et al.* 1996), generating second-messenger molecules involved in initiating cold related responses (Sanchez and Chua 2001, Xiong *et al.* 2002).

1.2.1 *Cold Response is Mediated by Transcription Factors*

Modulated responses to stress are regulated by stress-induced gene expression which can be classified as transient or long-term, in a complex regulatory gene network mediated by TF (Yamaguchi-Shinozaki and Shinozaki 1994, Fowler and Thomashow 2002, Vogel *et al.* 2005). Drought, salt and cold stress induced signalling pathways often intersect, which can result from crosslinked effects, as cold and freezing temperatures can cause water deficit that subsequently results in an osmotic stress (Shinozaki and Yamaguchi-Shinozaki 2000, Zhu 2001). Any discussion of the plant stress response to cold must consider the mechanisms by which gene expression is modulated, namely the cascade of TF. Although there are several families of stress induced TFs, a significant portion of the cold induced genes are activated by the ABA-independent CBF/DREB1 regulon in Arabidopsis (Yamaguchi-Shinozaki and Shinozaki 1994, Vogel *et al.* 2005). The regulation can be up- or downstream transcription, and it is activated by low temperatures through a complex network of positive and negative regulators and TFs (Figure 1.2). The characteristic CRT element is present in both cold and drought regulated genes, and by binding to it the CBF/DREB1 regulon TFs activate expression. *CBF1* and *CBF3* have a positive relationship with their downstream target genes and stress tolerance (Jaglo-Ottosen *et al.* 1998, Liu *et al.* 1998, Kasuga *et al.* 1999). CBF3 expression is induced by ICE1 (*INDUCER OF CBF EXPRESSION1*), a MYC-type bHLH (*basic HELIX-LOOP-HELIX*) TF (Chinnusamy *et al.* 2003, Lee *et al.* 2005),

although by directly interacting with MYB15 [R2R3-type MYB TF, (Dubos *et al.* 2010)], the *CBF* gene expression driven through ICE1 can be blocked (Shinwari *et al.* 1998, Agarwal *et al.* 2006). ICE2 has an identical bHLH domain to ICE1 and it is a positive regulator of *CBF1* (Fursova *et al.* 2009). Whilst, *CBF2* is positively modulated by *CAMTA3* (*CALMODULIN BINDING TRANSCRIPTION ACTIVATOR3*) (Doherty *et al.* 2009), but suppressed by *HOS1* (*HIGH EXPRESSION OF OSMOTICALLY RESPONSIVE1*) (Ishitani *et al.* 1998, Lee *et al.* 2001), in which case CBF2 acts as negative regulator of both *CBF1* and *CBF3* (Novillo *et al.* 2004). Post-transcriptionally, CBFs are regulated by their own product, as RNA metabolism can be involved in the post-transcriptional cold stress regulation. The *LOW EXPRESSION OF OSMOTICALLY RESPONSIVE GENES* (*LOS*) are also involved in cold responses. *LOS1* encodes a translation elongation factor 2 (eEF-2), which negatively regulates *CBF* expression through feedback regulation or by their downstream targets (Guo *et al.* 2002), while LOS2 positively regulates the cold-responsive gene expression of *COR/ LTI/ RD/ KIN* (*COLD-REGULATED*, *COLD-INDUCIBLE*, *LOW-TEMPERATURE-INDUCED*, and *RESPONSE TO DESSICATION*) (Ohta *et al.* 2001, Lee *et al.* 2002). Arabidopsis LOS4 is localized in both nucleus and cytoplasm and is proposed as regulator of mRNA transport between compartments (Aubourg *et al.* 1999, Gong *et al.* 2002, Gong *et al.* 2005). Low temperature-induced gene expression can be described as transient, often only detected within one to five hours upon cold exposure, whereas some genes can be induced and remain activated during the cold stress period (i.e. long-term) (Shinwari *et al.* 1998, Fowler and Thomashow 2002, Vogel *et al.* 2005). *CBF1* and *CBF3* were reported as transiently expressed, activated within 40 min of cold exposure, followed by the expression of their target genes within 2h to 5h after exposure to cold (Shinwari *et al.* 1998, Novillo *et al.* 2004).

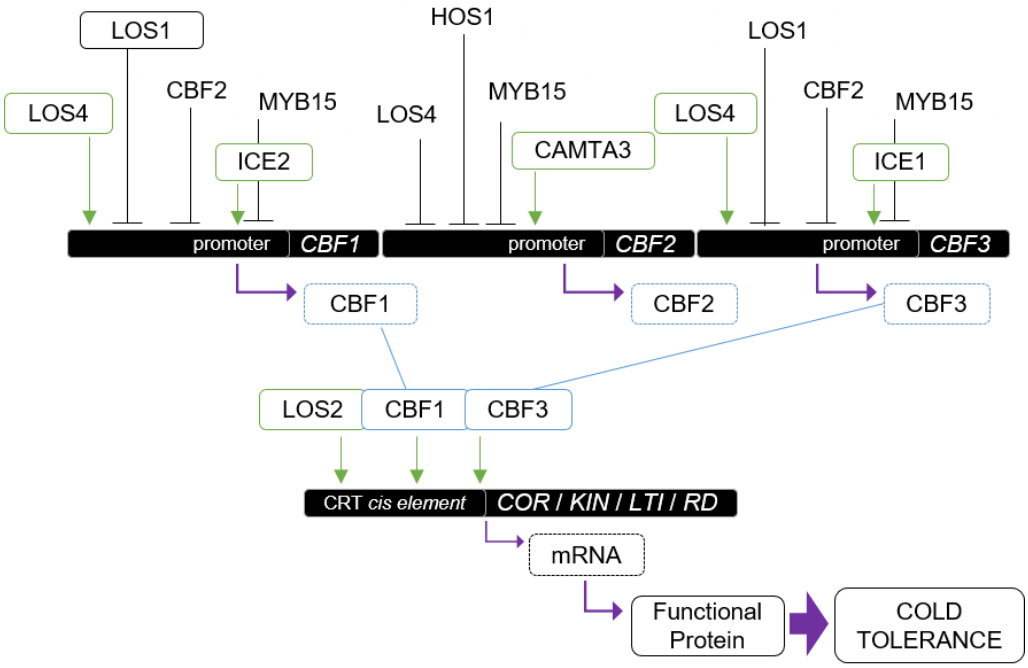

Figure 1.2 The CBF Regulation Pathway in Plants

Schematic representation of the ABA-independent CBF transcription regulation pathway. LOS, Low Expression of Osmotically Responsive Genes; CBF, C-Repeat-Binding Factor; ICE, *Inducer of CBF Expression*; HOS, *High Expression of Osmotically Responsive*; CAMTA3, *Calmodulin Binding Transcription Activator3*; COR, *Cold Responsive*; KIN, Cold-Inducible; LTI, Low-Temperature-Induced; RD, Response to Desiccation; mRNA, messenger RNA. Green (■) arrows illustrate positive regulation, black (■) arrows show negative regulation, purple (■) arrows represent induced transcription.

The transiently expressed genes also include genes coding for proteins involved in signal transduction or cellular communication (including response regulators, protein kinases, and phosphatases), and gene regulation (Fowler and Thomashow 2002). Examples of the long-term gene expression include cryoprotective polypeptides (COR/LEA proteins), sugar pathway enzymes and *EARLY LIGHT-INDUCED PROTEINS* (*ELIP*) (Fowler and Thomashow 2002, Kreps *et al.* 2002). This pattern may suggest a first fast acting stage in response to low temperatures, followed by a prolonged adaptive stage thought to be activated by multiple low temperature regulatory pathways (Fowler and Thomashow 2002, Kreps *et al.* 2002).

In plants, cold response mechanisms involve lipid modulation, reflecting both the structural and signalling functions of lipids. However, information

on lipid-related TFs with a role in cold stress is scarce, and yet to be explored. A survey of the Acyl Lipid Metabolism online database (http://aralip.plantbiology.msu.edu) found 27 TFs associated with plant lipid metabolism, however from these only eight were identified as differentially expressed in Arabidopsis, Eutrema or both in a comparative cold acclimation transcriptome analysis [(Barrero-Sicilia *et al.* 2017), see Appendix 26]. Included in this pool was *TT8* (*TRANSPARENT TESTA8*), which was found upregulated in both species after three days of cold conditions (Barrero-Sicilia *et al.* 2017). *TT8* and *TT2* are TFs localized in the nucleus that regulate proanthocyanidin and flavonoid synthesis in the seed coat (McGlew *et al.* 2015). *TT2* has an R2R3 MYB domain, and negatively regulates fatty acid accumulation in Arabidopsis seeds, although it has been shown to have a positive effect on environmental stress tolerance during seed germination and establishment (Chen *et al.* 2012). *TT8*, encodes a bHLH domain regulatory protein which indirectly inhibits the expression of a series genes in the FA biosynthesis pathway, including *FATTY ACID BIOSYNTHESIS* (*FAB2*), *FATTY ACID ELONGATION1* (*FAE1*), *FATTY ACID DESATURASE2* (*FAD2*), and *FAD3* (Chen *et al.* 2014) that are important mediators of lipid-related cold responses (Miquel *et al.* 1993, Shanklin and Cahoon 1998). In extremophiles such as Eutrema, only a few genes have been reported to be activated under abiotic stress conditions (Wong *et al.* 2006). The mechanism of upregulation of expression of these genes is still unknown. Wong *et al.* (Wong *et al.* 2005) reported a MYB family TF, MybSt1 was ubiquitously found in Eutrema cDNA libraries from cold, drought, and salt stress experiments, implying a role in regulating abiotic stress responses.

1.2.2 *Metabolic Adaptation is a Multifactorial Equation*

Once transcriptomic changes are activated, metabolic modifications to the cells metabolism and physiology further allow the plant to adapt to its surroundings. Sugars, amino acids, polyamines, ammonium compounds and proteins produced during cold acclimation have an active role in stabilizing both membrane proteins and phospholipids, conserving

membrane integrity (Janska *et al.* 2010, Rahman *et al.* 2010). Changes in protein and lipid membrane composition help to restore metabolite homeostasis and are proposed as one of the cell's cold sensors (De Palma *et al.* 2008, Chinnusamy *et al.* 2010). Other sensing mechanisms may involve calcium (Ca^{2+}) channels, kinases and G-protein associated receptors (Xiong *et al.* 2002, Janska *et al.* 2010). Cold sensors trigger a signalling cascade, including Ca^{2+} -flux and -dependent protein kinases (CDPKs), mitogen-activated protein-kinase (MAPK) mediated cascades, phospholipids, and TFs, which collectively regulate cold responsive gene expression (Xiong *et al.* 2002, Guy *et al.* 2008, Janska *et al.* 2010). An ever-increasing number of cold inducible genes known as *COR*, *KIN*, *LTI*, and *RD* result in regulatory and functional proteins that intervene in the cell's metabolism to adapt to low temperatures. Profound changes in the cell's proteome occurs mainly in the plastids, cytosol and nucleus, and these can be distinguished by their structural, regulatory and osmoprotection functions (Johnova *et al.* 2016). The identification of individual genes with a role in the plant's metabolism and adaptation to cold temperatures through the selection and characterisation of their mutant phenotypes has proven a powerful tool. COR15 proteins increase freezing tolerance in Arabidopsis by stabilizing chloroplast membranes (Artus *et al.* 1996, Uemura *et al.* 1996, Thalhammer *et al.* 2014). In Arabidopsis, COR15 is encoded by two genes, *COR15A* and *COR15B* that share 82% of sequence identity (Wilhelm and Thomashow 1993). The respective hydrophilic proteins are then targeted to the chloroplast stroma where they form amphipathic α-helices that interact specifically with monogalactosyldiacylglycerol (MGDG) (Thalhammer *et al.* 2010, Thalhammer *et al.* 2014). In addition, the Arabidopsis gene *SENSITIVE TO FREEZING 6* (*SFR6*) is thought to participate in the downstream regulation of the CBF pathway, activating the expression of COR genes as demonstrated in both Arabidopsis and rice (Knight *et al.* 2009, Wathugala *et al.* 2011).

1.3 PLANT LIPIDS IN COLD ACCLIMATION

Upon abiotic stress plants activate sensing mechanisms that are translated into downstream biological processes, often through the plasma membrane [PM, (Steponkus 1984)], and culminate into a modulated coping response. The multiplicity of abiotic stresses and their interlinking effects suggest shared sensors, and, hence, diverse signalling pathways. Low temperature damage, also associated with freezing injury, can arise from changes in the intercellular water temperature which affects water potential through the PM, affecting also its own conformation causing structural damage and hence increasing ion leakage (Steponkus 1984). Lipid signalling molecules are viewed as important mediators of stress, however, these molecules represent less than 1% of total plant lipids characterized, due to their transient accumulation and high turnover rate (Hou *et al.* 2016). A brief review of some of the lipid-related strategies against cold stress can be found throughout the following sections.

1.3.1 *Lipids as Signalling Molecules*

Signalling lipids have been shown to be derived from reactions involving phospholipases, lipid kinases or phosphatases, which produce phosphatidic acid (PA), phosphoinositides (PtdIns), sphingolipids, and free FA (FFAs). Phospholipase D (PLD) catalyses the hydrolysis of structural phospholipids, such as PC, PE, and PG to produce PA (Bargmann and Munnik 2006). A fast increase in PA was reported in Arabidopsis in response to cold stress (Ruelland *et al.* 2002), due to the previous activation of both PLD, and PLC/DGK (Diacylglycerol Kinases) (Vergnolle *et al.* 2005). PLDs have been reported to be involved in intracellular signalling events in response to external stimuli such as plant-pathogen interactions, dehydration, osmotic and freezing stresses (Wang 2000, Bargmann and Munnik 2006, Bargmann *et al.* 2009). The PA biosynthetic pathway is one of the lipid signalling cascades that is actively responsive to stresses, e.g. salt and cold. However, quantitative determinations of PA in samples remain an analytical challenge as

breakdown products from other phospholipids are hard to distinguish from the original extracted PA. Ruelland *et al.* proposed that under freezing conditions a fast induction occurs through the phosphorylation of PtdInsP to $PtdInsP_2$, which is then hydrolysed by PLC (Ruelland *et al.* 2002). PLC hydrolyses $PtdIns(4,5)P_2$ into the second messengers $Ins(1,4,5)P_3$, and DAG (Munnik 2001). The latter is then converted to PA by the action of DGK. However, there is evidence that $PtdIns(4,5)P_2$ may act as a stress signalling agent regulating cellular ion homeostasis (Xiong *et al.* 2002). The fast induction of the signalling molecules observed suggests a post-translational, rather than transcriptional, regulation of PLC (Ruelland *et al.* 2002). PA is thought to act as a second messenger by recruiting target proteins with varied stress functions such as TFs, protein and lipid kinases, phosphatases and also cytoskeletal rearrangements and trafficking (for further review (Testerink and Munnik 2005, Barbaglia and Hoffmann-Benning 2016)). PLD is also proposed to have a mechanical role as a membrane anchor (Bargmann and Munnik 2006). The δ class (PLDδ) bind microtubules and interact with the cytoskeleton stabilizing the membrane (Gardiner *et al.* 2001). In Arabidopsis, *pldδ* mutants showed impaired freezing tolerance and reduced PA levels, whereas overexpression of this gene has the contrary effect (Li *et al.* 2004). The *ACYL CoA-BINDING PROTEIN6* (*ACBP6*) seems to regulate both *PLDδ* and *PLDα* expression (Allen *et al.* 1999, Chen *et al.* 2008, Du *et al.* 2010) which controls PA production influencing the signalling cascade, and ultimately increasing freezing tolerance (Bargmann and Munnik 2006).

Sphingolipids have been recognized by their importance in plant cell signalling in cold transduction pathways by their membrane derivatives (Worrall *et al.* 2008, Ali *et al.* 2018, Huby *et al.* 2019). PA interacts with sphingosine kinases (Guo *et al.* 2011), that regulate the production of LCB-1-phosphates (LCBPs) which could have a signalling role on the ABA-mediated stomatal closure (Coursol *et al.* 2005). The mechanism by which PA regulates and interacts with its target proteins, and its specific role in cold stress, if any, is still not fully understood. The fast and

transient production of phyto-S1P by the LCB kinase isoform (LCBK2) has also been reported to have an effect in root growth and cold-responsive gene expression (Dutilleul *et al.* 2012). The ceramide-kinase ACD5 (*ACCELERATED CELL DEATH5*) in Arabidopsis is involved in the programmed cell death regulation, however it was also reported to be involved in cold tolerance (Liang *et al.* 2003, Donahue *et al.* 2010, Dutilleul *et al.* 2015). Phosphorylated ceramides (Cer-P) were found to be rapidly and transiently accumulated upon cold shock treatment, with a 70% decrease in its accumulation in the knockout mutant when compared to the wild-type (Dutilleul *et al.* 2015). However the resulting impact on the *acd5* mutant was reverted by treatment with gibberellic acid, even at cold temperatures (Dutilleul *et al.* 2015).

1.3.2 *Plasma Membranes as a First Defence Mechanism*

The fluidity of the PM is a structural and functional key asset, with an increased significance in sensing temperature stress as it transitions from a fluid state at high temperature to a rigid gel phase when low temperatures are present (Figure 1.3, (Chinnusamy *et al.* 2010)). The PM is mainly composed of phospholipids, which can constitute approximately 30% of the PM in tobacco cells (Cacas *et al.* 2016). Along with sphingolipids, which can be found in the detergent-resistant portions associated with sterols (Borner *et al.* 2005, Minami *et al.* 2009, Cacas *et al.* 2012), result in a molar ratio of 1 protein to 50-100 lipid molecules (Mamode Cassim *et al.* 2019). Formation of non-bilayer lipid structures in the membranes, such as the inverted hexagonal (H_{II})-type structures, can occur under cold temperatures causing lesions in the membrane (Uemura *et al.* 1995, Uemura and Steponkus 1997). The adaptation of the membranes against these effects is crucial to maintain cell and organelle homeostasis. Low temperature induced changes in the physical conformation of membranes are mainly due to the increased level of unsaturated lipids enhancing membrane fluidity and stabilization, allowing cells to mechanically adapt to cold (Miquel *et al.* 1993, Thomashow 1994, 1999). Under such conditions changes in the lipid

composition, and membrane repair systems are activated in order to maintain its structure, keeping membrane integrity and avoiding damage (Uemura *et al.* 1995). Stabilisation of the PM by decreased viscosity induced by the accumulation of unsaturated fatty acids is thus a key element of freezing stress resilience (Uemura *et al.* 1995, Steponkus 1999, Martiniere *et al.* 2011). Progress has been made in the characterisation of these pathways not only in Arabidopsis (Mamode Cassim *et al.* 2019), but also in economically important crops, such as peanut [full review in (Zhang *et al.* 2019)].

The essential role of sphingolipids in cell membrane organization and turnover makes them a key candidate for the plant response to cold or freezing response (Pata *et al.* 2010, Barrero-Sicilia *et al.* 2017). Glucosylceramides in particular, have been found to accumulate in chilling resistant plants (Cahoon and Lynch 1991, Imai *et al.* 1995), furthermore, the presence of certain long-chain base (LCB) forms in the ceramide moiety of the glucosylceramides might be a key feature of cold acclimation. The Δ^8-desaturation is the primary modification by desaturation of the LCB in plants and its configuration can take up the *cis* or *trans* configuration, and though it is not critical for plant development, it might be involved in the plants response to environmental stresses such as cold (Chen *et al.* 2012), or aluminium tolerance (Ryan *et al.* 2007). A higher content in the $^{\Delta 8}$*cis*-4-hydroxysphingenine isomer (t18:1$^{\Delta 8Z}$) relative to its *trans* isomer t18:1$^{\Delta 8E}$ was shown to be constant in chilling resistant species, such as lily-of-the valley (*Convallaria keiskei* Miq.), wheat (*Trititcum aestivum* L.), or oat [*Avena sativa* L., (Imai *et al.* 1997)]. In tomato (*Solanum lycopersicum* cv. Micro-Tom) a 4°C treatment increased the transcript levels of the sphingoid LCB Δ^8-desaturase (*SLD*) genes up to 23.4-fold in leaves (Zhou *et al.* 2016). In Arabidopsis, the mutated *SLD* genes showed an accumulation of glucosylceramides, accompanied by a higher sensitivity in the growth phenotype under chilling temperatures (Chen *et al.* 2012).

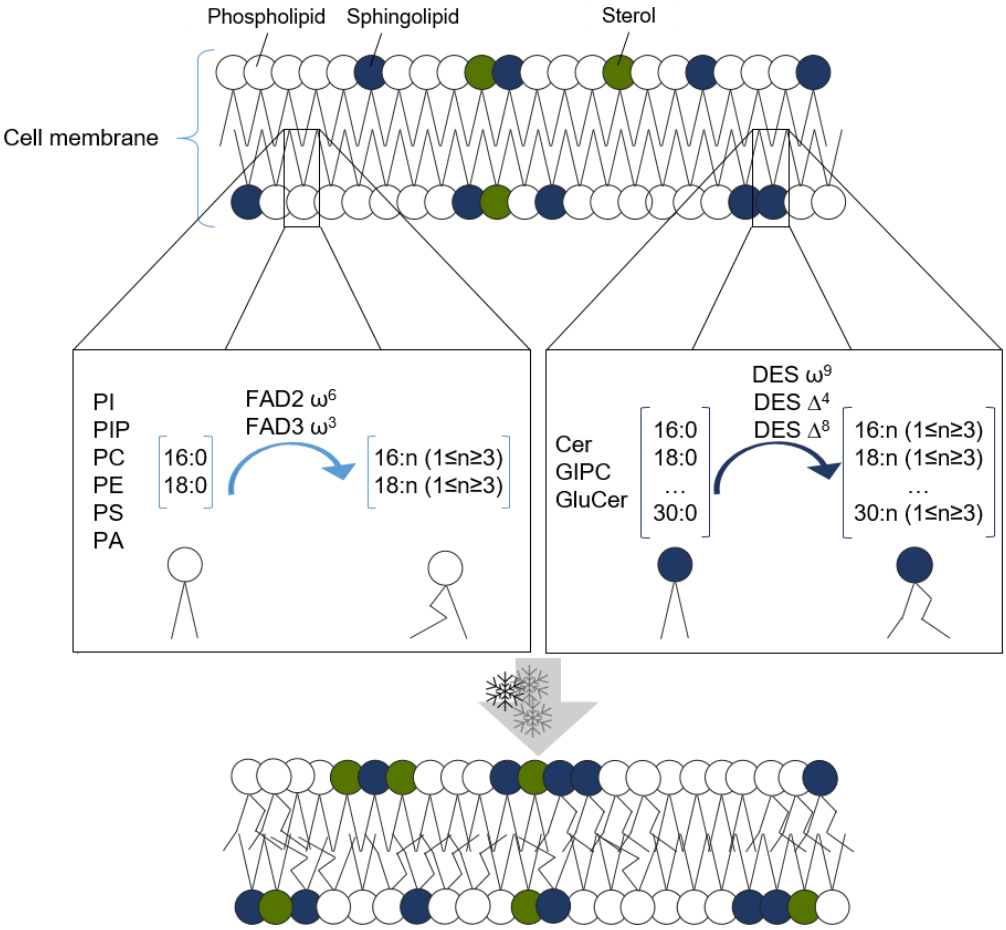

Figure 1.3. Lipid Remodelling in Plasma Membrane During Cold Stress

Schematic representation of the endoplasmic reticulum localised desaturation of phospholipids and sphingolipids species involved in the remodelling of the plasma membrane under cold stress. PI – phosphatidylinositol; PIP, phosphoinosites; PC, phosphatidylcholine; PE, phosphatidylethanolamine; PS, phosphatidylserine; PA, phosphatidic acid; FAD, Fatty Acid Desaturase; Cer, Ceramides; GIPC, glycosylinositolphosphoryl ceramide; GluCer, glucosylceramide; DES, desaturase. Adapted from (Barrero-Sicilia *et al.* 2017).

1.3.3 *The Chloroplast is a Primary Target in Cold Stress*

The specific composition of the inner and outer chloroplast membranes adapts in response to cold temperatures. The increased lipid spacing in the membranes when COR15 proteins are present suggests a parallel structure orientation to the inner chloroplast envelope membrane lipids, rich in the non-bilayer MGDG, this increases membrane protein stability (Artus *et al.* 1996, Uemura *et al.* 1996, Thalhammer *et al.* 2014). *SFR2* encodes a glycosyl-hydrolase with galactosyltransferase activity, which

combined with TAG-biosynthetic enzymes changes the chloroplast bilayer- to a non-bilayer-forming membrane lipid ratio, remodelling the outer chloroplast membrane and stabilizing it when under freezing conditions (Moellering *et al.* 2010). *ACYL LIPID DESATURASE1* (*ADS1*) encodes a soluble Δ^9-desaturase that catalyses the desaturation of stearic acid (MDGD(34)), which is thought to occur prior to the onset of the cytosolic Ca^{2+} signalling pathway indicating a role of the chloroplast membrane in cold acclimation (Chen and Thelen 2016). *SFR2* is predicted to encode a glycosyl hydrolase family 1 (GH-1) protein that changes the ratio of bilayer- to non-bilayer-forming membrane lipids in the chloroplast (Moellering *et al.* 2010). The *sfr2* mutants showed extensive intracellular damage after freezing recovery, with rupture in both chloroplasts and tonoplasts likely through the fusion of destabilized membranes in these organelles (Fourrier *et al.* 2008, Moellering *et al.* 2010). Recently it was reported that *SFR2* is activated by changes in the cytosolic pH and Mg^{2+} showing a possible role in cold stress sensing mechanisms (Barnes *et al.* 2016). The mechanical protection of biological membranes also has an important role in the production of stress responsive signalling lipids, which can be derived from membrane lipids, such as phospholipids or sphingolipids, through enzymatic reactions (Xiong *et al.* 2002).

1.3.4 *Fatty Acid Desaturation is a Key Response to Cold*

Increasing fatty acid unsaturation levels is a feature of cold stress adaptation of membranes (Figure 1.3), mediated by different Fatty Acid Desaturases (FAD) located in the chloroplast and endoplasmic reticulum [ER, (Wallis and Browse 2002, Upchurch 2008)]. Desaturation involves an enzymatic reaction in which a double bond is introduced to an acyl chain, and a molecule of dioxygen is reduced to water (Shanklin and Cahoon 1998). For desaturation two electrons are necessary for the formation of each double bond, where both plastid and ER electron transport systems supply the required electrons (or reducing equivalents) (Shanklin and Cahoon 1998). There are up to seven FAD enzymes in

plants with a significant role in the unsaturation level of membrane fatty acids (Miquel *et al.* 1993, Kodama *et al.* 1994, Matos *et al.* 2007, Chen and Thelen 2013, Chen and Thelen 2016), and some have been reported to play a role in cold tolerance. The ω-3 FATTY ACID DESATURASE 7 and 8 (FAD7 and FAD8) localised in the chloroplast are responsible for the production of trienoic acids essential for the cold stress response (Routaboul *et al.* 2000, Roman *et al.* 2015, Tovuu *et al.* 2016). FAD2 has ω^6-oleate desaturase activity, which when suppressed causes the Arabidopsis mutants to be chilling-sensitive at 12ºC, and to die when exposed to 6ºC (Miquel *et al.* 1993). And *FAD3*, when overexpressed, was reported to enrich the linoleic acid content of the mitochondria membranes, showing higher viscosity, and, hence, reduced rigidification with cold stress (Matos *et al.* 2007).

1.3.5 *Waxes are a First Barrier Against Cold Stress*

The first line of physical defence against abiotic stresses is the leaf cuticle which incorporates in its structure intra- and epi-cuticular waxes (Shepherd and Griffiths 2006). Reports show that cuticular wax is affected by cold (Gauvrit and Gaillardon 1991, Hietala *et al.* 1997, Amid *et al.* 2012), although the extent, severity and their specific role in cold stress is still unknown. In Arabidopsis the *sfr3* mutant resulted from a missense mutation in the *ACC1* gene that encodes the homomeric Acetyl-CoA Carboxylase (ACCase) which ultimately affects the leaf surface wax composition of these mutants (Amid *et al.* 2012). This enzyme is also involved in *de novo* fatty acid biosynthesis. It is required to produce malonyl-CoA essential for lipid biosynthesis (Baud *et al.* 2003, Amid *et al.* 2012). Of such importance that its mutation alters cuticle permeability, wax morphology and composition in the cold, and flower development (Amid *et al.* 2012). In Eutrema, leaf cuticular wax composition is thought to play a relevant part in the plant's stress strategies (Teusink *et al.* 2002, Amid *et al.* 2012, Tang *et al.* 2018). The analysis of the wax profile of Eutrema, not only revealed higher content than in Arabidopsis (Teusink *et al.* 2002), but different characteristics

between stem and rosette leaves. The latter showed 15% more total fatty acids than stem leaves, with total combined C16 and C18 fatty acids being 12% higher on rosette than stem leaves. The accumulation of these long-chain fatty acids precursors of both wax and cutin production did not translate, however, in higher content of such cuticle lipids in the rosette leaves (Tang *et al.* 2018). Stem leaves accumulated five-fold higher content of total surface cuticular wax than rosette leaves, showing irregular wax crystals (Tang *et al.* 2018). This translated into lower cuticle permeability when compared to the rosette leaves (Tang *et al.* 2018). As a primary hydrophobic barrier, cuticles are a prime defence against water loss (Xu *et al.* 2014), and due to their polymer matrix can also act against damage induced by mechanical or freezing stresses (Amid *et al.* 2012). The differences found in the cuticle structure and permeability in the stem leaves might contribute for the plant's and flower protection in the extreme weather conditions in their native regions, guaranteeing the completion of the life cycle and, hence, the next generation.

1.4 LIPID METABOLISM IN PLANTS

Plants balance the fatty acid production according to the cells' needs. In oilseeds, fatty acid production is driven for the synthesis of triacylglycerol (TAG) which account for 60% of the seed weight. Seed oils which are predominantly composed of TAGs are of major economic importance for food security and industrial applications (Barthole *et al.* 2012, Tocher *et al.* 2019). The accumulation of these compounds in seeds provides a carbon reserve for the germination and growth of the seedling until it becomes photosynthetically active. In vegetative tissues structural, signalling, and surface protection functions arise from the multitude of plant lipid forms and species with unique physical properties. Phospholipids combined with sphingolipids, sterols and proteins constitute the PM, interacting with and having an active role in the cells metabolism (Figure 1.3, (Cacas *et al.* 2012)). The chloroplast thylakoid membranes, on the other hand, has a unique composition of galactolipids (Dormann and Benning 2002). Lipid biosynthesis is a complex pathway

involving different cell compartments, thus involving lipid trafficking mechanisms. These are extensively studied, and extensive and updated reviews can be found (Benning 2008, Xu *et al.* 2008, Benning 2009, Hurlock *et al.* 2014, Lindquist and Aronsson 2018, Michaud and Jouhet 2019). Two main biosynthesis pathways exist which are referred as “prokaryotic” and “eukaryotic”. These are associated with their location within the cell, the prokaryotic pathway synthesizes lipids in the plastid, whilst the eukaryotic pathway involves the ER and cytosol (Ohlrogge and Browse 1995, Li-Beisson *et al.* 2013). The plastidial, or prokaryotic, pathway produces glycerolipids with a 16 carbon (C16) fatty acid in sn-2 position, whilst the eukaryotic pathway produces glycerolipids with a C18 at the sn-2 position (Li-Beisson *et al.* 2013).

1.4.1 *Fatty Acid Biosynthesis*

Fatty acid synthesis is regulated according to the supply and demand for acyl chains. It utilizes the carbon flux derived from photosynthesis in the form of pyruvate and it is localized in the plastid, after which the fatty acyl chains are then channelled for the production of more complex lipid molecules in the plastid, or transported to the cytosol and ER (Ohlrogge and Jaworski 1997). Briefly, in dicots, the plastid ACCase catalyses the formation of malonyl-CoA from acetyl-CoA, which is then transferred by the fatty acid synthase (FAS) to the Acyl Carrier Protein (ACP), where the C16 to C18 chains are assembled. The end product is usually a 16:0 to 18:0-ACP which is then utilized by a variety of enzymes in the plastid or after being exported in the ER or cytosol (for a complete review (Harwood 1996, Ohlrogge and Jaworski 1997, Nikolau *et al.* 2003, Li-Beisson *et al.* 2013)). Malonyl-CoA is made in the cytosolic pool by the homomeric ACCase and used for elongation of fatty acids into long- and very-long- chain fatty acids (VLCFA) required by phospholipids, surface waxes, or sphingolipids (Roesler *et al.* 1994). The regulation of fatty acid synthesis and further modifications have been extensively reviewed (Jaworski *et al.* 1990, Faergeman and Knudsen 1997, Ohlrogge and Jaworski 1997, Li-Beisson *et al.* 2013, McGlew *et al.* 2015) and are not

discussed here. Modifications in the ER include chain-length elongation by the Fatty Acid Elongase (FAE), and membrane bound desaturation (Shanklin and Cahoon 1998). VLCFA can be further modified into biologically active molecules required for the production of sphingolipids and waxes. The elongation process requires a functional protein complex (Denic and Weissman 2007) that mediates a series of four reactions in the presence of malonyl-CoA and NADPH which then releases its products as CoA thioesters (Lessire *et al.* 1985). Although extensively studied, there are still several questions regarding the significance of VLCFA in cell metabolism (further review of FAE in (Cassagne and Lessire 1978, Cassagne *et al.* 1994, Haslam and Kunst 2013, Morineau *et al.* 2016)).

The ability to adjust membrane fluidity according to temperature changes involves the regulation of the unsaturation and chain length of membrane fatty acids. The C16 to C18 acyl chains produced by the FAS complex are subsequently desaturated by chloroplast and ER membrane-bound desaturases (Browse and Somerville 1991, Wallis and Browse 2002). For each double bond two electrons are required, supplied by electron transport systems in both chloroplast and ER (Shanklin and Cahoon 1998). The characterization of the seven-different fatty acid desaturase (FAD) classes was made possible by studying fatty acid desaturase mutants. Mutations *fad2* and *fad3* affect extra-chloroplast lipid desaturation, whereas *fad4*, *fad5* (Kunst *et al.* 1989), *fad6*, *fad7*, and *fad8* gene mutations affect chloroplast desaturation (Browse and Somerville 1991, Wallis and Browse 2002, Upchurch 2008). Fatty acyl chains are further modified and remodelled to produce the plastid galactolipids, MDGD, DGDG and SQDG (Benning 2008), phospholipids and sphingolipids.

1.4.2 *Phospholipid Metabolism*

Phospholipids are formed by two fatty acids linked to a glycerol, which in is linked to a phosphate group. To this phosphate a highly polar head group is linked, causing phospholipids to have both hydrophilic and

hydrophobic properties (i.e. amphipathic). In photosynthetic tissues, phospholipids are the second most abundant lipid family (after the galactolipids), and in non-photosynthetic tissues are the most abundant lipid species (Cacas *et al.* 2012). The major structural phospholipids include phosphatidylinositol (PI), phosphatidylcholine (PC), phosphatidylethanolamine (PE), phosphatidylserine (PS), phosphatidylglycerol (PG), and phosphatidic acid (PA) (Figure 1.4, reviewed in (Nakamura 2017). Despite being only found in minor quantities, PA is the backbone for the synthesis of other phospholipids. PI is a precursor for phosphoinositides, by phosphorylation of the inositol head group, which have cell functions comprising exo- and endocytosis, signal transduction, or PM-cytoskeleton interactions (Di Paolo and De Camilli 2006, Xue *et al.* 2009). By specifically binding their head groups to cytosolic proteins or cytosolic domains of membrane proteins, phosphoinosites regulate protein functions and cellular localization (Di Paolo and De Camilli 2006). In plant cells there are up to six forms described so far, identified as phosphatidylinositol-3-phosphate [PtdIns(3)P], phosphatidylinositol-4-phosphate [PtdIns(4)P], phosphatidylinositol-5-phosphate [PtdIns(5)P], phosphatidylinositol-3,4-biphosphate [PtdIns(3,4)P_2], phosphatidylinositol-3,5-biphosphate [PtdIns(3,5)P_2], and phosphatidylinositol-4,5-biphosphate [PtdIns(4,5)P_2]. PtdIns(4,5)P_2 is localized in the PM (van Leeuwen *et al.* 2007), and although present at low concentration it has an essential role as a second messenger, and as a modulator of the activity of cytoskeletal-associated proteins and vesicle-trafficking proteins. It has also been associated with inositol 1,4,5-triphosphate [Ins(3)P] and Ca^{2+} mobilization in response to salt and osmotic stresses (DeWald *et al.* 2001, Xiong *et al.* 2002).

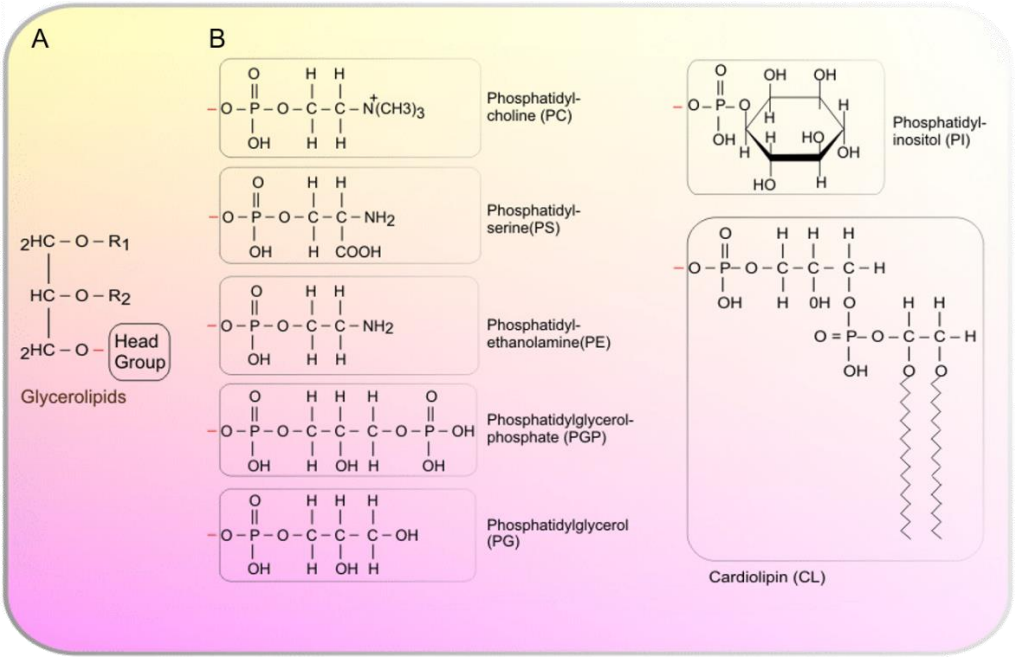

Figure 1.4 Phospholipid Molecular Structure

Phospholipids are formed by a common backbone (A) constituted by two acyl groups at *sn*-1 and *sn-2* positions (R1 and R2) linked to a glycerol residue, which in turn is linked to a phosphate group. To this phosphate a highly polar head group is linked (B) such as serine, choline, glycerol, or inositol forming the phosphatidylcholine (PC), phosphatidylserine (PS), phosphatidylethanolamine (PE), phosphatidylglycerol (PG, phosphatidylinositol (PI) or cardiolipin (CL) depending on the residue added. Adapted from (Li-Beisson *et al.* 2013).

1.4.3 *Thylakoid Membrane Lipid Composition*

Plastid membranes have a specific composition, and due to their structural and functional nature, chloroplast photosynthetic membranes have a major role in the plant metabolism (Section 1.3.3). Chlorophyll, proteins and lipids are the three major components of the thylakoid membranes (Koochak *et al.* 2019). These have a specific lipid composition that includes monogalactosyldiacylglycerol (MGDG), digalactosyldiacylglycerol (DGDG), phosphatidylglycerol (PG), and limited amounts of sulfoquinovosyldiacylglycerol (SQDG) (Andersson and Dormann 2009). The percentage content of these galactolipids varies between species (Kobayashi 2016). For example, spinach leaves showed MDGD to be predominant in the thylakoids, while DGDG showed to constitute 30% of the outer envelope membrane against 17% MGDG

(Block *et al.* 1983, Dorne *et al.* 1990). MGDG contains one galactose head group bound in a β-glycosidic bond to diacylglycerol backbone (Figure 1.5). DGDG contains a second galactose moiety bound in α-glycosidic bond to the first galactose, and SQDG is a sulphur-containing lipid (Dormann and Benning 2002, Andersson and Dormann 2009, Li-Beisson *et al.* 2013). The galactolipids are synthesized in the chloroplast envelope by either MGD1/DGD1- or MGD2/3 and DGD2- mediated pathways (Benning and Ohta 2005). In Arabidopsis the majority of MGDG is produced by MGDG Synthase 1 (MGD1) localised in the inner-envelope of the chloroplast (Awai *et al.* 2001) which composition resembles that of the thylakoids. In contrast, DGDG is mainly produced in the outer-envelope predominantly by DGDG Synthase 1 (DGD1), or DGD2 in phosphate-limited growth conditions (Kelly *et al.* 2003). SQDG is also synthesized in the stroma side of the chloroplast inner envelope (Tietje and Heinz 1998), mediated by the UDP-Sulfoquinovose Synthase encoded in Arabidopsis by *SQD1* [(Essigmann *et al.* 1998), further review in (Shimojima 2011)].

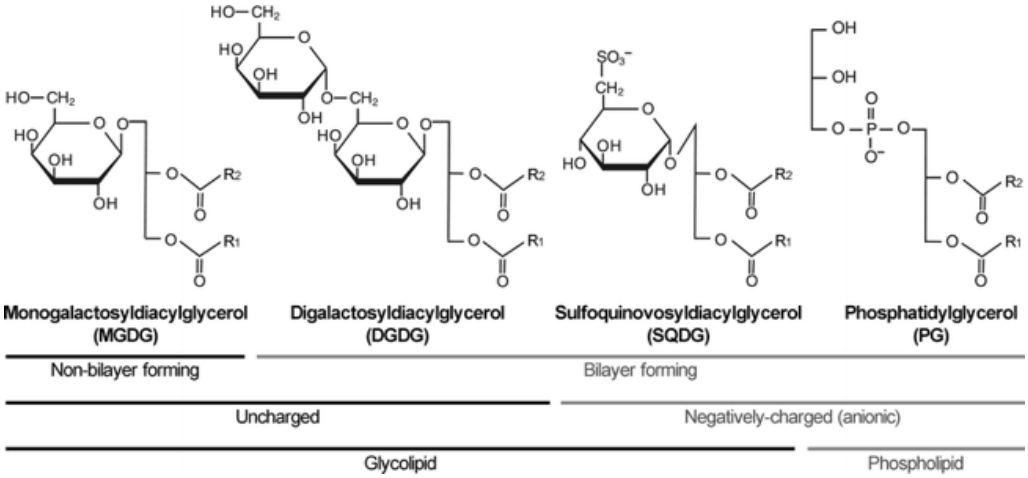

Figure 1.5 Glycolipids and Phosphatidylglycerol Structure

The thylakoid membranes have a specific lipid composition formed of monogalactosyldiacylglycerol (MGDG), digalactosyldiacylglycerol (DGDG), sulfoquinovosyldiacylglycerol (SQDG) glycolipids, and the phospholipid phosphatidylglycerol (PG). Figure adapted from (Kobayashi 2016).

1.4.4 *Sphingolipid Metabolism*

Sphingolipids are structurally diverse molecules, composed of a ceramide backbone and a hydrophilic head group [(Pata *et al.* 2010), Figure 1.6]. The ceramide backbone is composed of long- (C16 – C18) to very long-chain (C20 – C26) fatty acids (VLCFA) linked via an amide bond to a long-chain base (LCB), or sphingoid base (Figure 1.6). The first step of the sphingolipid biosynthesis pathway in the ER is catalysed by the serine palmitoyltransferase (SPT), using serine and palmitoyl-CoA to produce the precursor of the LCBs 3-ketosphinganine, which is then reduced to sphinganine [d18:0, Figure 1.7, (Hanada and Nishijima 2003, Chen *et al.* 2006)]. The acyl-CoA pool is directly involved in the sphingolipid pathway. In the first step a CoA ester of palmitic acid (16:0), palmitoyl-CoA is a substrate for the synthesis of 3-ketosphinganine (Chen *et al.* 2006). Acyl-CoA's are also involved in the acetylation of dihydroxy LCBs (d18:0[1]) by ceramide synthase I (CSI), which are then directed through the glucosylceramide synthesis pathway. Very-long chain fatty acyl-CoA can be integrated with trihydroxy LCBs by CSII, which are thought to be directed towards glucosylceramide and GIPC synthesis in the ER and in the Golgi compartment, respectively (Markham *et al.* 2013, Michaelson *et al.* 2016). The first product of this pathway is the sphinganine (d18:0), a saturated C1-, C3-dihydroxy C18 LCB, which can be further modified by hydroxylation or desaturation (Table 1.1).

LCB hydroxylation is catalysed by the C4-hydroxylase (Sperling *et al.* 2001), producing phytosphingosine (t18:0), whilst desaturation can occur by the action of the Δ^4- and Δ^8-desaturases (Michaelson *et al.* 2009), which add a double bond at acyl chain position C4 or C8 in the LCB, respectively. The Δ^8-desaturation is unique to plants, in contrast to yeast or animal cells that do not possess C8-desaturated LCBs (Imai *et al.* 1997). C4-hydroxylation and Δ^8-desaturation are the primary modifications found in plants (Chen *et al.* 2008, Markham *et al.* 2013).

[1] The denomination "d18:0" is interpreted as two (d, or three if "t") hydroxyl groups, an 18-carbon chain length (18), followed by the number of double bonds which in this example is zero (:0).

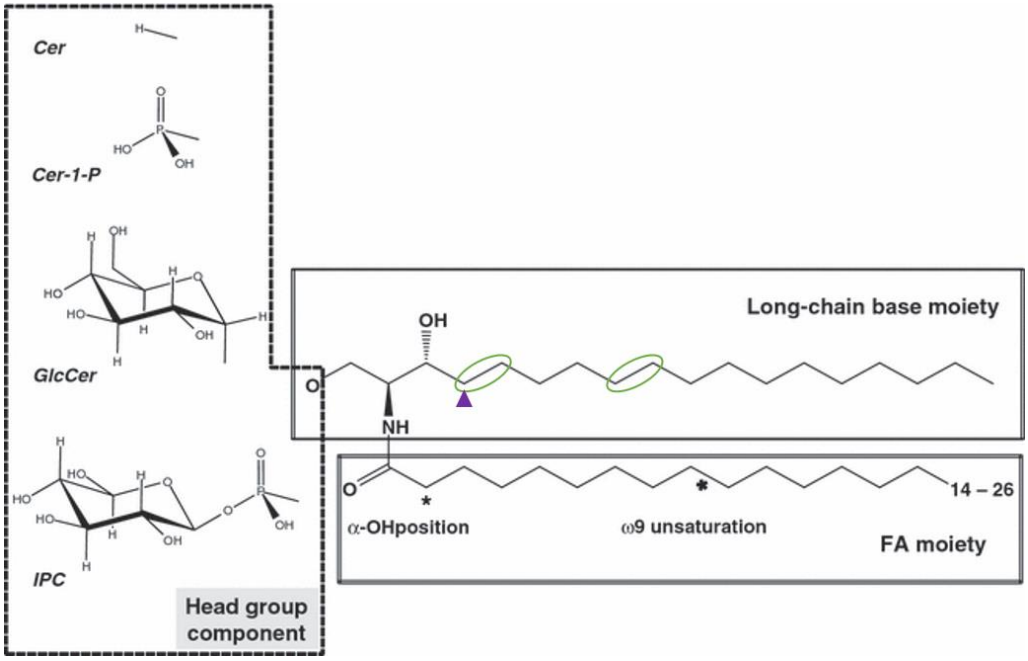

Figure 1.6 Sphingolipid Structure

Sphingolipids are composed of a long-chain base (LCB) and a fatty acid (FA) hydrophobic moiety, linked to a hydrophilic head group. LCB modifications are shown for Δ^4- and Δ^8-desaturation (■, circles) and C4-hydroxylation (▲, arrow), and in the FA as α-hydroxylation (α-OHposition,*) and ω9-desaturation (*****). Cer, ceramide; GlcCer, glucosylceramide; IPC, inositol phosphoryl ceramide which can be further glycosylated to the glycosylinositolphosphoryl ceramide (GIPC). Adapted from (Pata *et al.* 2010).

The C4-hydroxylase is encoded by two redundant genes in Arabidopsis (Sperling *et al.* 2001), *SBH1* and *SBH2* (for *SPHINGOID BASE HYDROXYLASE 1* and *2*), which suppression resulted in severe growth problems and lack of transition to reproductive growth showing how critical this modification can be in the plant's metabolism (Chen *et al.* 2008). Δ^8-desaturation might not be critical for the plant's development, but it has been suggested to be involved in responses to environmental stress such as cold (Chen *et al.* 2012). The enzyme generates double bonds in *cis* or *trans* position at the C8 position of the LCB chain (Sperling *et al.* 1998), using either t18:0 or d18:0 as substrates. The trihydroxylated LCB (t18:0) can thus be further desaturated by the LCB Δ^8-desaturase to produce (*E*)-4-hydroxysphing-8-enine (t18:1$^{\Delta 8E}$), or (*Z*)-4-hydroxysphing-8-enine (t18:1$^{\Delta 8Z}$, Table 1.1). Sphing-8-enine (d18:1) can be produced from sphinganine (d18:0), also in the *cis* (*Z*)- or *trans* (*E*)-sphing-8-enine isoforms (d18:1$^{\Delta 8Z}$ or d18:1$^{\Delta 8E}$, Table 1.1). Both Δ^8-desaturated LCBs 4-

hydroxysphing-8-enine (t18:1$^{\Delta 8}$) and sphing-8-enine (d18:1$^{\Delta 8}$) are considered the predominant LCB species found in leaves and roots of the genus *Brassica* (Imai *et al.* 2000). However, different *cis*/*trans* (*Z*/*E*) Δ^8-desaturation ratios can be found in other plant species [(Imai *et al.* 1997), previously discussed in Section 1.3.2]. In Arabidopsis direct alkaline hydrolysis of whole leaf extracts showed the prevalence of the *trans* t18:1$^{\Delta 8E}$ isomer (Sperling *et al.* 1998, Markham *et al.* 2006). The Δ^4-desaturation cannot occur simultaneously with the C4 hydroxylation, and it is only observed in the dihydroxy LCB species (d18). The Δ^4-desaturase adds a double bond in the C4 position of the LCB chain, in the *trans* position, using di-hydro-ceramide as a substrate (Figure 1.7) instead of the free dihydrosphingosine (d18:0) to produce the desaturated sphingosine (d18:1$^{\Delta 4E}$) (Michaelson *et al.* 2009, Michaelson *et al.* 2016). The predominant form of Δ^4-desaturation can be found as a second double bond introduced in either isoforms of sphing-8-enine (d18:1$^{\Delta 8Z}$ or d18:1$^{\Delta 8E}$), forming (4*E*,8*E*)-sphing-4,8-dienine (d18:2$^{\Delta 4E 8E}$) and (4*E*,8*Z*)-sphing-4,8-dienine (d18:2$^{\Delta 4E 8Z}$) (Imai *et al.* 1997, Imai *et al.* 2000, Sperling and Heinz 2003). The Δ^4-desaturated LCB containing ceramides are thought to be directed towards the synthesis of complex sphingolipids e.g. glucosylceramides (Michaelson *et al.* 2009).

Further diversity in the sphingolipids moiety can be achieved by modifications in the LCB amide-linked fatty acid chain, these can be incorporated as saturated or ω9-monounsaturated fatty acyl chains that can vary in length from long-chain (16 – 18 carbons) to VLCFA of up to 26 carbons (Imai *et al.* 2000, Konig *et al.* 2012). In addition to being precursors for more complex classes, ceramides also have an active role in plant metabolism (Lynch and Dunn 2004). However, together with hydroxyceramides, produced by the α-hydroxylation of the fatty acid moiety (Konig *et al.* 2012), these neutral sphingolipids only represent approximately 2% of the total sphingolipid content in Arabidopsis (Markham *et al.* 2006, Markham and Jaworski 2007).

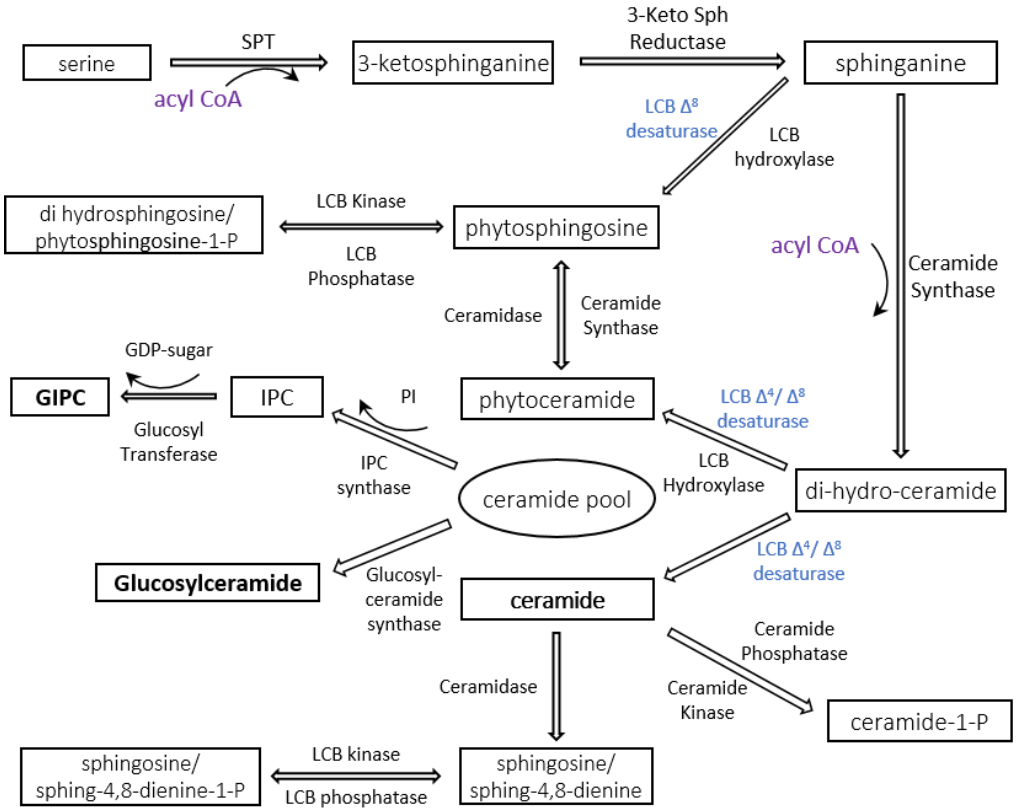

Figure 1.7 Sphingolipid Biosynthesis Pathway

Simplified schematic representation of the sphingolipid biosynthesis pathway, showing the key steps for the LCB Δ^4- and Δ^8-desaturases (■), and the acyl CoA pool (■) integrated in the biosynthesis process. SPT, Serine Palmitoyl-transferase; Sph, Sphingolipid; LCB, Long-chain base; PI, Phosphatidyl inositol; IPC, inositol phosphoryl ceramide; GIPC, glycosylinositolphosphoryl ceramide. Adapted from (Michaelson *et al.* 2016).

The predominant classes in plants are represented by the complex forms that arise from the addition of a hydrophilic head group to the ceramide backbone (Figure 1.6). The addition of glycosyl residues and other polar phosphate-containing head groups at the ceramide C1 position forms the glucosylceramides, also known as glucocerebrosides (Sperling *et al.* 2005). The production of this class is catalysed by the glucosylceramide synthase (GCS, Figure 1.7), coded by a single gene (*GCS*) in Arabidopsis which, when mutated, can severely impair the plant's development, failing to growth beyond seedling stage (Msanne *et al.* 2015), showing the importance of this complex sphingolipid in the plant's metabolism. The glucosylceramide class is composed of a wide variety of molecules in plants, in contrast to both fungi and mammals, that

present a less varied backbone structure (Warnecke and Heinz 2003). The addition of an inositol phosphate head group to the ceramide, to which sugar residues can be linked, form the glycosylinositolphosphoryl ceramide (GIPCs) or phytoglycolipid class (Lynch and Dunn 2004). GIPCs are the predominant class in plant tissues (Markham and Jaworski 2007), and in Arabidopsis three enzymes coded by the *INOSITOL PHOSPHORYLCERAMIDE SYNTHASE 1* to *3* (*IPCS1 – IPCS3*) are responsible for their production (Wang *et al.* 2008, Mina *et al.* 2010). The hydrophilic polar head properties of these complex structures impair their solubility in organic solvents, such as chloroform/methanol, which up until recently had a detrimental effect on the GIPC research (Markham *et al.* 2006, Markham and Jaworski 2007, Markham 2013). Bure *et al.* (Bure *et al.* 2014) reviewed available methods and compiled a dataset of structures found so far in both plants and fungi, illustrating the biodiversity of these molecules that lead to a multitude of functions in cell metabolism (Gronnier *et al.* 2016).

Table 1.1 Plant Long-Chain Base Common Structures

LCBs common name, chemical terms and abbreviations. d, dihydroxy; t, trihydroxy; Δ, desaturase; *E*, *trans* and *Z*, *cis* positions of the double bond added by the desaturase.

LCB	Chemical Term	Abbreviation
Sphinganine	Dihydrosphingosine	d18:0
Sphingosine	(*E*)-sphing-4-enine	d18:1$^{\Delta 4E}$
Sphing-8-enine	(*E*)-sphing-8-enine	d18:1$^{\Delta 8E}$
	(*Z*)-sphing-8-enine	d18:1$^{\Delta 8Z}$
Sphinga-4,8-dienine	(4*E*,8*E*)-sphinga-4,8-dienine	d18:2 $^{\Delta 4E8E}$
	(4*E*,8*Z*)-sphinga-4,8-dienine	d18:2 $^{\Delta 4E8Z}$
Phytosphingosine	4-hydroxysphinganine	t18:0
Phytosphingenine	(*E*)-4-hydroxysphing-8-enine	t18:1$^{\Delta 8E}$
	(*Z*)-4-hydroxysphing-8-enine	t18:1$^{\Delta 8Z}$

1.5 PROJECT AIMS

This thesis was developed with the aim to further understand the role of lipids in the process of plant adaptation to cold temperatures. To address this question experiments were planned to use the plant model Arabidopsis in parallel with the extremophile Eutrema as a source of cold adaptation strategies. The project established three objectives: (1) identify gene candidates to cold acclimation; (2) study the sphingolipid Δ^8-desaturase and (3) establish Eutrema as a model for abiotic stress research (summarised in Figure 1.5).

Cold acclimation comprises a complex cascade of processes that enable the plant to make the necessary adjustments for its survival to prolonged low temperatures or even freezing temperatures. To achieve this, the plant activates or reduces the transcription of certain genes, which modify metabolism according to environmental conditions. This led to the hypothesis that through transcriptome analysis under specific stress conditions the identification of essential genes to this adaptation is possible. The aim of the work described in Chapter 3 was thus to analyse the transcriptome changes recorded after a three-day cold acclimation period, allowing the identification of key gene candidates for cold acclimation in Arabidopsis. This was performed by the analysis of the differentially expressed gene pool, from which 19 genes were tested under cold conditions through the development of a high-throughput chlorophyll fluorescence screen. This allowed the identification of two genes with an impact on the plant's performance under cold stress. Moreover, this identified the pathways and networks that are crucial to cold temperature adaptation. To further understand the role of these genes in the context of lipid remodelling, a targeted lipidomic analysis was performed and the main results discussed in Chapter 4.

Cellular membranes are crucial to temperature adaptation. Sphingolipids are major components of the cell's plasma- and endo-membranes, with an impact on the membrane stability under cold stress and a potential role as stress signalling molecules. The unique LCB moiety of the

sphingolipids can be modified through hydroxylation and desaturation, which is thought to be a key element in the plant's cold stress adaptation. Previously, the role of the Arabidopsis LCB Δ^8-desaturase genes (*SLD*) was characterised, and preliminary experiments related these genes with cold stress. However, questions remained as to the functionality of each gene and their role in the cold stress. The aim of Chapter 5 was to investigate the potential of the LCB Δ^8-desaturation in sphingolipid remodelling using Eutrema *SLD* genes as mediators. These were identified *in silico*, cloned and expressed in two Arabidopsis backgrounds, the wild-type Col-0 and the double mutant for the endogenous *SLD* genes *sld1sld2.* The genotypes produced were analysed for changes in the LCB and sphingolipid profiles and their cold and freezing stresses response characterised.

Increased fatty acid desaturation is an established metabolic response to cold stress, and two chloroplast located fatty acid desaturases, FAD7 and FAD8, have been identified as responsible for the production of trienoic fatty acids essential to cold responses. Eutrema is often proposed as a plant model for abiotic stress studies, but its characteristic long-life cycle and stress resilience are still a challenge in the adaptation of protocols, limiting the amount of research. The work developed in Chapter 6 aimed to characterise Eutrema cold adaptation strategies in the absence of the chloroplastidial *ThFAD7* and *ThFAD8.* Targeting these genes will enable the assessment of Eutrema's coping strategies in the absence of polyunsaturated fatty acids. Moreover, the improvement of germination and transformation protocols, and the development of the first CRISPR/Cas9 genome editing protocol as applied to the chloroplast desaturases FAD7 and FAD8 allowed the validation of Eutrema as a plant model for abiotic stress.

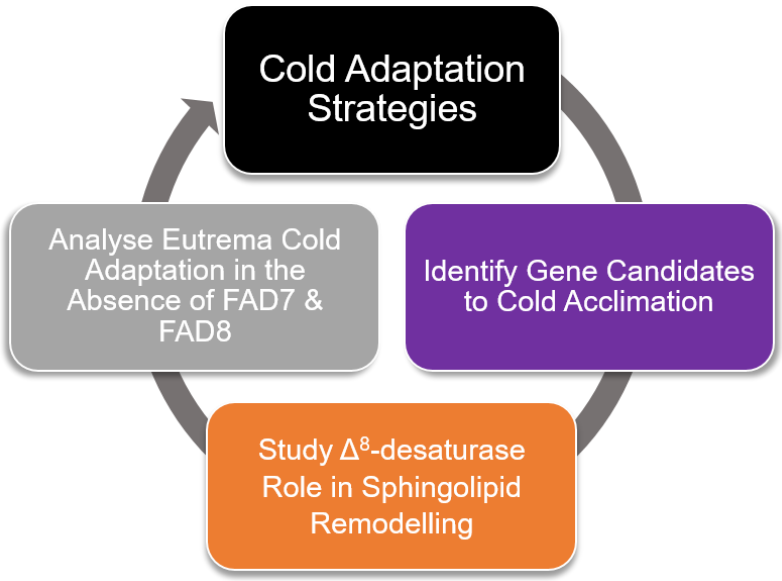

Figure 1.8 Project Aims

Three objectives were designed to further understand the role of lipids in the plant's cold acclimation strategy.

Chapter 2.

Materials and Methods

2.1 PLANT MATERIAL

The wild-type *Arabidopsis thaliana* L., ecotype Columbia-0 (Arabidopsis, Col-0) and *Eutrema salsugineum* ecotype Shandong (Eutrema, Sha) were used. The Arabidopsis T-DNA insertion mutant lines were all derived from the ecotype Col-0 and were obtained from the SALK insertion collection (Alonso 2003) (Table 2.1) except where otherwise specified. The lines were selected based on The Arabidopsis Information Resource (TAIR) website (https://www.arabidopsis.org/). The *EARLY INDUCED LIGHT PROTEIN* (*ELIP*) mutant lines, *elip1, elip2* and *elip1elip2* originated from the GABI-Kat project (Kleinboelting *et al.* 2012) (https://www.gabi-kat.de/). All lines were obtained from the Arabidopsis Biological Resource Centre, Nottingham Arabidopsis Stock Centre (NASC) (http://arabidopsis.info/), with the exception of the double mutant *sld1sld2*, derived from the accessions SALK_010384 and SALK_013243 and kindly provided by Dr Jonathan E. Markham (Chen *et al.* 2012).

2.2 GERMINATION AND GROWTH

2.2.1 *Germination Protocol*

2.2.1.1 Arabidopsis thaliana

Approximately 50 seeds per genotype were soaked for 15 min (min) in 800 µL of 70% ethanol (EtOH) with the aid of a rotator for a more efficient soak. The 70% ethanol was removed, 15 µL of 100% EtOH was added for one minute, removed and the tubes were left in a laminar flow hood until completely dry. Seeds were distributed into plates containing half-strength Murashige and Skoog (MS, Sigma®) basal salt medium supplemented with 2.0% sucrose, 0.5 g/L MES (2-[N-Morpholino]-ethanesulfonic Acid Hydrate, Sigma®), and 0.8% agar for jellification. A stratification period of five days at 4°C in the dark was used. After which, plates were transferred to continuous light (30 µmol/m^2/s) and 20°C conditions for up to six days to allow germination. Six germinated

seedlings per genotype and experiment were individually sown in pots (5 x 5 cm) with compost (Section 2.2.2).

Table 2.1 Arabidopsis T-DNA Accessions

Information for each of the mutant lines used in this project, with the respective gene, locus identifier (AGI), mutant name used, T-DNA insertion accession and site. UTR, untranslated region

Gene	AGI	Mutant	T-DNA Accession	Insertion Site
SLD1	At3g61580	*sld1*	SALK_010384	Exon 1
SLD2	At2g46210	*sld2*	SALK_013243	Exon 1
AZI1	At4g12470	*azi1*	SALK_085727C	Exon 1
ELIP2	At4g14690	*elip2*	GABI_252D03	Exon 3
ELIP1	At3g22840	*elip1*	GABI_369A04	Exon 1
ELIP1, ELIP2	-	*elip1elip2*	N2103098	Exon 1 (*ELIP1*) & Exon 3 (*ELIP2*)
COR15A	At2g42540	*cor15a*	SALK_033954C	Promoter
COR15B	At2g42530	*cor15b*	SALK_085398C	Exon 2
LTR	At4g30650	*ltr*	SALK_118610C	Promoter
FABO	At4g31810	*fabo*	SALK_084020C	5’ UTR
GSTU17	At1g10370	*gstu17*	SALK_139615C	Exon 2
PES1	At1g54570	*pes1*	SALK_076354C	5’ UTR
LTP3	At5g59320	*ltp3*	SALK_095248C	Exon 1
LTP4	At5g59310	*ltp 4*	SALK_000561C	Promoter
ADS4	At1g06350	*ads4*	SALK_043674C	Promoter
IPCS3	At2g29525	*ipcs3*	SALK_152650C	5’ UTR
SFR2	At3g06510	*sfr2*	SALK_112965C	Exon 6
PGR5-LIKE1A	At4g22890	*pgr5-l1a*	SALK_024747C	5’ UTR
PGR5-LIKE1B	At4g11960	*pgr5-l1b*	SALK_059238C	Exon 2
CYP74B2	At4g15440	*cyp74b2*	SALK_094392C	Exon 1
CSLA1	At4g16590	*csla1*	SALK_152629C	3’ UTR
FAD7	At3g11170	*fad7*	SALK_147096C	Intron 6 and Exon 7
FAD8	At5g05580	*fad8*	SALK_093590	Exon 1
FAD7, FAD8	-	*fad7-1fad8*	CS8036	Point Mutation in *FAD7* and *FAD8*

2.2.1.2 Eutrema salsugineum

Three different germination protocols were tested to obtain maximum efficiency of germination (Figure 2.1). The protocols were: (1) seed sterilization; (2) sowing the seeds directly in compost; and (3) sowing the seeds directly in compost following a sandpaper pre-treatment. The seed sterilization protocol was based on the current protocol used for Arabidopsis as described in Section 2.2.1.1. For the direct sowing protocol, seeds were placed directly into soil without any treatment, while in the sandpaper protocol, a pre-treatment was applied before sowing the seeds by gently scrubbing the seeds with a low-grade sandpaper and directly sowing in compost. For all the protocols two stratification periods of 4°C and dark conditions were tested. One week, as this was the recommended time for Arabidopsis, or three as previously recommended (Bressan *et al.* 2001). The most efficient protocol was assessed by the germination rate and used in the subsequent experiments. The germination rate was assessed as the percentage of germinated seeds in relation to the total number of seeds.

2.2.2 *Compost Composition (Rothamsted Mix)*

The compost mixture used was *Levington's FS2 + S*, a peat-based compost with silver sand to aid drainage. The nutrient composition was as follows: nitrogen (N) 144 mg/L, phosphorus (P) 73 mg/L, and potassium (K) 239 mg/L.

2.2.3 *Control Growth Conditions*

The control conditions for plant growth were 23/18°C day/night, 16h day photoperiod, 65% relative humidity (RH), and 200 µmol/m^2/s of light, watered regularly every other day. For the chlorophyll fluorescence screen described in Chapter 3, plants were grown for 18-20 days after sowing (DAS) under control conditions, but the light intensity was 150 µmol/m^2/s. For the freezing experiment described in Chapter 5 (Section 5.2.13, Figure 5.19 A), plants were grown for 19 DAS under the same control conditions as above, with light intensity of 50 µmol/m^2/s.

Protocol	Stratification	Growth Conditions
Germination Protocol 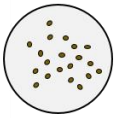	1W @4°C	1W @20°C > Soil > GR optimum conditions
	3W @4°C	1W @20°C > Soil > GR optimum conditions
Soil Directly 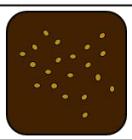	1W @4°C	GR optimum conditions
	3W @4°C	GR optimum conditions
Sandpaper & Soil 	1W @4°C	GR optimum conditions
	3W @4°C	GR optimum conditions

Figure 2.1 Germination Optimization of Eutrema

Three germination protocols were designed and tested to achieve a reproducible protocol for the germination of Eutrema. All three protocols were tested using Arabidopsis wild-type Col-0 as a control, and stratification periods of one (1W @4°C) or three (3W @4°C) weeks at 4°C and dark conditions. GR, growth

2.2.4 *Cold Stress Experiments*

Cold stress experiments were performed throughout this project and defined as a constant temperature of 4°C, with a 16h day photoperiod, 65% RH, and 200 µmol/m^2/s, except specified otherwise. The Chlorophyll fluorescence screen described in Chapter 3 was performed at 5°C with a 16h day photoperiod and 150 µmol/m^2/s. The freezing experiment described in Chapter 5 (Section 5.2.13,, Figure 5.19 A) was performed at 4°C and 50 µmol/m^2/s, the temperature was then reduced to -5°C for 24h (temperature decreased at a rate of 0.10°C/min). After the 24h period the temperature was recovered to 4°C for four days, and then the plants were moved back to the control temperature.

2.3 PLANT TRANSFORMATION

2.3.1 *Plasmids and Expression Vectors*

For the work developed in Chapter 5, the Eutrema *ThSLD1* and *ThSLD2* genes were overexpressed in two Arabidopsis backgrounds, the wild-

type Col-0 and the double mutant line *sld1sld2*. This was achieved using the cauliflower mosaic virus (CaMV) 35S promoter (Gronenborn *et al.* 1981, Benfey and Chua 1990), and the *Agrobacterium NOPALINE SYNTHASE* terminator sequence (*nos/ter*) (Depicker *et al.* 1982) resulting in the sequences *2x35S/prom-ThSLD1-nos/ter* and *2x35S/prom-ThSLD2-nos/ter.* These fragments were cloned into the binary vectors *pBINGlyRed* and *pBIN19* which possess DsRED (Baird *et al.* 2000, Jach *et al.* 2001) and kanamycin (Errampalli *et al.* 1991, de Vries and Wackernagel 1998) resistance genes, respectively. These vectors were synthetized by Genscript® and used for the *Agrobacterium tumefaciens* transformation as described in Section 2.3.2*.* The DsRED vectors were used to transform Arabidopsis double mutant *sld1sld2*, and the kanamycin vectors used for Arabidopsis wild-type Col-0 transformation by the floral dip method described in Section 2.3.4 (Table 2.2).

Table 2.2 Arabidopsis Transgenic lines

The transgenic lines and respective vectors used for transformation, background at T0 generation and the selectable marker used.

Transgenic line	**T0 Background**	**Plant Selection Marker**
sld1sld2	Arabidopsis Col-0	Kanamycin (50 mg/mL)
sld1sldl2:*ThSLD1*	Arabidopsis *sld1sld2*	DsRED fluorescence
sld1sdl2:*ThSLD2*	Arabidopsis *sld1sld2*	DsRED fluorescence
Col-0:*ThSLD1*	Arabidopsis Col-0	Kanamycin (50 mg/mL)
Col-0:*ThSLD2*	Arabidopsis Col-0	Kanamycin (50 mg/mL)

2.3.2 *Transformation of Agrobacterium tumefaciens*

The expression vectors produced were transformed into competent *Agrobacterium tumefaciens* cells strain AGL-1 (Lazo *et al.* 1991) by electroporation (Shaw 1996) as follows. Agrobacterium cells (40 µL) were thawed on ice, the expression vectors (2 µL) were added and the reaction

was kept on ice for one minute. The reactions were then transferred to a pre-chilled cuvette, which was then placed in the electroporator slide (kept at -20°C). The electroporator was set to 2.2 kV, 25 μFD for capacitance and 400 Ω for pulse controller. After electroporation, 1 mL of SOC medium (Formedium™) was added to the reactions, transferred to a test tube and incubated at 28°C for 3h. After incubation, reactions were plated in 2xYT Broth medium (Formedium™) agar plates supplemented with the antibiotics carbenicillin (50 mg/L), spectinomycin (100 mg/L), streptomycin (100 mg/L), and rifampicin (50 mg/L) and incubated at 28°C for two days. All antibiotics supplied from MELFORD Laboratories, Ltd.

2.3.3 *Glycerine Stock*

The Agrobacterium cells with the expression vector were preserved in glycerol, by adding 0.5 mL of each sample to 0.5 mL of glycerol 50% (v/v), immediately frozen in liquid nitrogen (N_2) and stored at -80°C.

2.3.4 *Agrobacterium – Mediated Plant Transformation*

The floral dip method (Clough and Bent 1998) was used for the *Agrobacterium*-mediated transformation of flowering plants. Floral dipping solution comprised of 5% sucrose complemented with 0.05% Silwet L-77 (Vac-In-Stuff, distributed by ©Lehle Seeds). The transformed plants were kept in the dark at high humidity for 24h, after which they were restored to control conditions, watered regularly and allowed to set seed.

2.3.5 *Selection of Transformants*

The transformed seeds selected via the DsRED fluorescence marker, which is expressed in the seed coating and emits a red fluorescence glow under a DsRED filter. The selection was performed with a light microscope Leica® M205 FA Stereomicroscope with a DsRED fluorescence filter, by comparing not transformed no fluorescence control seeds with the seeds from the transformed plants. The selection with

kanamycin was performed according to Harrison *et al.* (Harrison *et al.* 2006). Kanamycin (50 mg/L, MELFORD Laboratories Ltd., UK) was added to the growth medium for both wild-type and transformed lines, which were placed in dark for two days, after which a 24h exposure to light conditions was enough to distinguish the resistant seedlings. These had green cotyledons, as opposed to the wild-type and non-resistant seedlings which did not develop.

2.3.6 *Generation Segregation Analysis*

Homozygous lines were selected through the segregation analysis of each generation of the transformed lines following a Mendelian trend (

Figure 2.2). At the T1 generation, the lines with a 3:1 ratio of transformed to non-transformed seeds were selected. The transformed seeds were then selected and used to obtain homozygous lines.

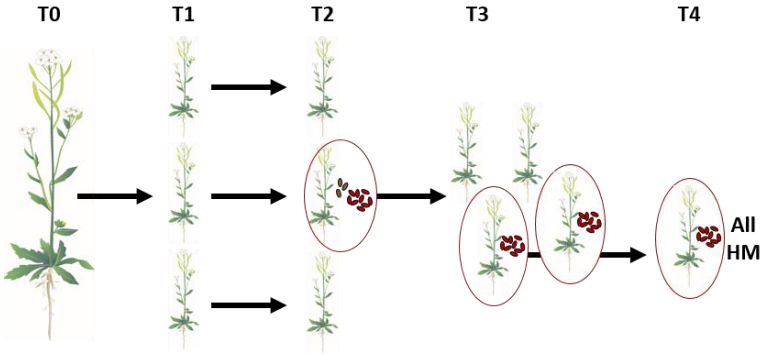

Figure 2.2 Segregation Analysis of the Transformed Lines

The selection of the transformed lines, was performed from T0 through T4 to obtain homozygous (HM) lines based on the analysis of the DsRED positive seeds, showed by the red seeds (●) in contrast with the not transformed seeds as showed in T2 (●).

2.4 MOLECULAR BIOLOGY ANALYSIS

2.4.1 *Genomic DNA Extraction*

Two methods of genomic DNA (gDNA) extraction from vegetative tissue were used. The DNeasy® Plant Minikit (Quiagen® 2011) was used

according to manufacturer's instructions. A second protocol was as described in Klimyuk *et al.* (Klimyuk *et al.* 1993). Briefly, leaf samples were crushed in 0.25 M sodium hydroxide (NaOH), incubated at 96°C for 30 seconds (s). After which, 0.25 M hydrochloric acid (HCl) and 0.5 M Tris-HCl (pH 8.00) / 0.25% IGEPAL CA-630 (Sigma-Aldrich®) were added, and samples were incubated at 96°C for two min. In both methods, rosette leaves were used (three replicates per genotype). Quantification was performed with a NanoDrop® ND–1000 Spectrophotometer (Labtech International, UK).

2.4.2 *Primer Pairs*

The primers used to amplify genes of interest were designed following Bustin and Huggett (Bustin and Huggett 2017) recommendations with the NCBI Primer Designing tool which uses Primer3 and BLAST (https://www.ncbi.nlm.nih.gov/tools/primer-blast/, Table 2.3). The SALK lines primers were designed using the T-DNA Primer Design tool (http://signal.salk.edu/tdnaprimers.2.html). The Arabidopsis mutant lines SALK and GABI-Kat gDNA was extracted [as above]. To identify homozygous lines for each genotype, the absence of the wild-type sequence and the presence of the T-DNA insertion were confirmed. T-DNA insertion was confirmed using the right primer (RP) of each gene paired with the T-DNA left border primer (LBa1, 5'-TGGTTCACGTAGTGGGCCATCG-3'). Lines *elip1*, *elip2*, and *elip1elip2* (Bolle *et al.* 2013) were confirmed using specific primers for the T-DNA (LB_o8474 5'-ATAATAACGCTGCGGACATCTACATTTT-3' and RB_o3144 5'-GTGGATTGATGTGATATCTCC-3'). The confirmed homozygous lines for each genotype set seed, which was bulked and used for all subsequent experiments. For any reaction, Arabidopsis wild-type Col-0 was used as control. All primers were obtained from Sigma-Aldrich®.

2.4.3 *Polymerase Chain Reaction*

For genotyping purposes, the Thermo Scientific™ DreamTaq Green PCR Master Mix was used following the manufacturer's protocol. The PCR program consisted of a first step of denaturation of 94°C for 5 min, followed by 36 cycles of denaturation for 30s at 94°C, annealing at appropriate Tm (melting temperature) for each of the primer pairs, and an extension step of one minute per kbp at 72°C, after which a final extension step was performed at 72°C for 5 min. When using the Q5® High-Fidelity DNA Polymerase (New England Biolabs® Inc) the PCR program was an initial denaturation 98°C for 30s, followed by 30 cycles of denaturation 98°C for 10s, annealing at 65°C for 30s, extension at 72°C for 4 min (1 min/kb), and final extension at 72°C for 10 min.

2.4.4 *Electrophoresis Gel*

gDNA samples were visualised in a 1% agarose (w/v, Agarose Genetic Analysis Grade, Fisher Bioreagents) 0.002% ethidium bromide (v/v, Sigma-Aldrich®) electrophoresis gel. The band sizes measured with GeneRuler™ DNA ladder 1 kb, 100 bp, 50 bp (Thermo Fisher Scientific).

2.4.5 *DNA Sequencing Analysis*

DNA sequencing (Sanger *et al.* 1977, Swerdlow *et al.* 1990, Hunkapiller *et al.* 1991) was provided by Eurofins Genomics, according to the respective guidelines (https://www.eurofinsgenomics.eu/en/custom-dna-sequencing/eurofins-services/tubeseq-service/). Either the standard primer pair M13uni-21 and M13rev-29 was used, or specific primer pairs were pre-mixed in the sample tubes (Table 2.9). The specific primer pairs were designed for sequencing purposes, followed the Eurofins Genomics guidelines to achieve optimum conditions; and were obtained from Sigma-Aldrich®. Sequencing results were obtained, and pairwise or multiple alignments were performed with Geneious® 10.2.3 (©Biomatters Ltd.).

Table 2.3 Primer Pairs used for Genotyping

Left (LP) and right (RP) primer sequences (5' to 3') used for the amplification of the T-DNA insertion flanking sequence for each gene. AGI, locus identifier; TM, melting temperature and GC, content of guanine (G) and cytosine (C) for each primer according to the T-DNA Primer Design tool; Size, fragment size produced.

Gene	AGI	T-DNA Accession		Sequence 5' … 3'	TM (°C)	GC (%)	Size (bp)
AtACT2	At3g18780	-	LP	TTCCCTCAGCACATTCCAGCAGGT	66.3	54.2	156
			RP	AACGATTCCTGGACCTGCCTCATC	64.5	54.2	
AtADS4	At1g06350	SALK_043674C	LP	AAAATGTTGGGATTTTCAGCC	60.2	38.1	1241
			RP	CCTTCTTTAGGGCTATGTGGG	60.0	52.4	
AtAZI1	At4g12470	SALK_085727C	LP	AAACACGTCTTTGAGCTCAGC	59.7	47.6	1889
			RP	AAGCACATTGGAAACCAGATG	60.0	42.9	
AtCOR15A	At2g42540	SALK_033954C	LP	TAGACTTACGTGGCCTCGTTG	60.3	52.4	1087
			RP	AGGAGATGTTACTGTCCGTCAG	58.3	50.0	
AtCOR15B	At2g42530	SALK_085398C	LP	CGTGACTTTAGAAGGGAAGGG	60.1	52.4	962
			RP	TAATGGCCTTGTTGAGGATTG	60.0	42.9	
AtCSLA1	At4g16590	SALK_152629C	LP	ATAGTTGTGACTGGCCAGTGG	60.0	52.4	1201
			RP	GTAAACGAATGGGTTGTGACC	59.2	47.6	
AtCYP74B2	At4g15440	SALK_094392C	LP	GAGCCATCGCACAAATTTATTAC	59.9	39.1	1128
			RP	CCACTGCTAAACTTGGCGTAG	60.0	52.4	

(Continued on the next page)

Gene	AGI	T-DNA Accession		Sequence 5' … 3'	TM (°C)	GC (%)	Size (bp)
AtELIP1	At3g22840	GABI_369A04	LP	CATTTCTGATCACCCGTCCTATAA	61.4	41.7	1078
			RP	AACACACAGTAGGCCTAACACAGA	60.2	45.8	
AtELIP2	At4g14690	GABI_252D03	LP	GTCCTTCCACTTCCCTACGTTACT	61.2	50.0	1239
			RP	AACGAAATGATGCTACTCAAAACG	61.6	37.5	
AtFABO	At4g31810	SALK_084020C	LP	TCTACTTTGAGCAGCTCCGAG	59.9	52.4	953
			RP	GGTCTTCGAAATCTGCATCTG	59.8	47.6	
AtGSTU17	At1g10370	SALK_139615C	LP	AACGCTTCAACGTGTCAAAAC	60.2	42.9	1210
			RP	ACGTAACGTTTAACGTACGCC	59.1	47.6	
AtIPCS3	At2g29525	SALK_152650C	LP	AATAAAGACCACCGTGGAACC	60.1	47.6	1005
			RP	ACAAAACCATGGACGCATAAC	59.7	42.9	
AtLTP3	At5g59320	SALK_095248C	LP	TCGATGCATAATCAAATCGTG	59.5	38.1	1025
			RP	GTTCAAACACAATGGCTTTCG	60.5	42.9	
AtLTP4	At5g59310	SALK_000561C	LP	TAAGCATCTGCATGCTTGTTG	60.0	42.9	1172
			RP	TCGTGTATTTATTCCCGCTTG	60.0	42.9	
AtLTR	At4g30650	SALK_118610C	LP	CGTAGCCTGACTTTGCAAAAG	60.1	47.6	1157
			RP	TGTTGACCGGTTTTTATGCTC	60.0	42.9	

(Continued on the next page)

Gene	AGI	SALK		5’ … 3’ Sequence	TM (°C)	GC (%)	Size (bp)
AtPES1	At1g54570	SALK_076354C	LP	GCGACTAGTGAATTAACTGCG	57.8	47.6	1120
			RP	TTTCCCATTCACTTCATTTGC	59.9	38.1	
AtPGR5-LIKE A	At4g22890	SALK_024747C	LP	AGCCATTGAATCAATCAAACC	58.9	38.1	1119
			RP	GTGCTTTAAGCGTGTCTCCAC	59.9	52.4	
AtPGRL1B	At4g11960	SALK_059238C	LP	TGCATAATCAAGGAGGTCCAC	60.0	47.6	1216
			RP	TCTGATCTTTCTTTGGGAACG	59.3	42.9	
AtSFR2	At3g06510	SALK_112965C	LP	GAGCCCACCAAAGGAATTAAG	60.0	47.6	1154
			RP	AAGGTCGTCGAATCACATCTG	60.1	47.6	
AtSLD1	At3g61580	SALK_010384	LP	GCTTGATACCCATCTTAGCCC	59.9	52.4	1129
			RP	AACTCACGTTTGATCCAGTCG	60.2	47.6	
ThSLD1	Thhalv10005967m.g	-	LP	CGCCTGGAACCACCTGGGAAAT	65.1	59.1	300
			RP	ATGATGACGTAATGGCCCGAG	60.3	52.4	
AtSLD2	At2g46210	SALK_013243	LP	ACCGGTATACACATCTGCTGC	60.0	52.4	1036
			RP	TTTCTCTGGTTCATCAATGGC	60.1	42.9	
ThSLD2	Thhalv10001443m.g	-	LP	ACGGCTACCACGTGAGAGACTT	63.3	54.5	299
			RP	GACGATTTTGTTACACGGCTTC	58.5	45.5	
AtUBC21	At5g25760	-	LP	GCTCTTATCAAAGGACCTTCGG	58.8	50.0	101
			RP	CGAACTTGAGGAGGTTGCAAAG	60.0	50.0	

2.4.6 *RNA Extraction*

Total RNA was extracted according to the vegetative tissues protocol as previously described (Onate-Sanchez and Vicente-Carbajosa 2008). Each sample was ground in liquid N_2 to which 300 µL of cell lysis solution (2% SDS, 68 Mm Sodium Citrate, 132 mM Citric Acid, 1 mM EDTA) was added and homogenized quickly by vortex. To this, 100 µL of protein-DNA precipitation solution (4 M sodium chloride, NaCl, 16 mM Sodium Citrate, 32 mM Citric Acid) was added, and incubated at 4°C for 10 min, then centrifuged at 4°C for 15 min. The supernatant was transferred to a new tube, 300 µL of 100% isopropanol (C_3H_8O) were added and centrifuged for 4 min. The supernatant was decanted, and the pellet was washed with 500 µL of ethanol 70% (v/v), centrifuged twice for 5 min, air-dried for 10 min and re-suspended in 25 µL DEPC (diethyl pyrocarbonate) water. RQ1 DNase (2 µL, PROMEGA, USA) was added to each tube and incubated for 30 min at 37°C for DNA digestion. After the DNase treatment, a PCR confirmation step was performed using the *AtUBC21* or *AtFAD8* primer pairs to confirm the complete DNA digestion of each sample. A water sample and a gDNA Col-0 sample were included as negative and positive control. The PCR program and electrophoresis gel used as described in Sections 2.4.3 – 2.4.4. Samples that showed a smeared result and no distinct band of 101 bp for *AtUBC21* or 505 bp for *AtFAD8* were considered negative for gDNA and selected to complete the RNA extraction, as follows. DEPC water (70 µL), 3 mM NaAC pH 5.2 (10 µL), and 100% ethanol (220 µL) were added and tubes incubated at -20°C for 1h. After the incubation, tubes were centrifuged for 30 min at 4°C, the supernatant was discarded, and the pellet was re-suspended in 25 µL of DEPC water. All centrifugation steps were performed at 14000 rpm. RNA was quantified with NanoDrop® ND–1000 Spectrophotometer (Labtech International, UK), and RNA integrity was confirmed by a 1.5% agarose (w/v) gel electrophoresis. One to two rosette leaves per plant were collected from three four-week-old plants per line.

2.4.7 *cDNA Synthesis*

First-strand complementary DNA (cDNA) was synthesized from 0.5 µg/µL of total RNA according to the standard procedure protocol of the Transcriptor First Strand cDNA synthesis kit (Roche, Version 6.0, Chapter 2.2, p 9-10; © 2011 Roche Diagnostics International Ltd). Briefly, 2.0 µg of each RNA sample was mixed with the anchored-oligo(dT)18 primer, to generate full-length cDNA, incubated for 10 min at 65°C for the denaturation of the template-primer mix. The Transcriptor RT reaction buffer, Protector RNase inhibitor, dNTP mix (10 mM each) and the Transcriptor Reverse Transcriptase were added. This final reaction was incubated for 30 min at 55°C, 10 min at 25°C, and 30 min at 55°C. cDNA samples were kept at -20°C until further use.

2.4.8 *Reverse Transcriptase – Quantitative PCR*

Reverse Transcriptase – quantitative PCR (RT-qPCR) used cDNA in a Lightcycler® 96 System (©2011 Roche Diagnostics International Ltd). The FastStart Essential DNA SYBR Green Master Mix (Roche Diagnostics) was used according to the manufacture instructions. The RT-qPCR programme: pre-incubation at 95ºC for 600s, 35 cycles of a three-step amplification at 95ºC for 20s, 60ºC for 15s, and 72ºC for 15s; followed by a melting step at 95ºC for 5s, 70°C for 60s, and 95ºC for 1s, and a final cooling step (40ºC for 30s). RT-qPCR results were analysed with the Lightcycler® 96 System Software (Version 1.1.0.1320, © 2011 Roche Diagnostics). Specific primers were designed with the NCBI Primer Designing tool and used to amplify coding regions of interest spanning an exon-exon junction (Table 2.4). Two Arabidopsis genes *UBIQUITIN-CONJUGATING ENZYME 21* (At5g25760, *AtUBC21*) and *ACTIN 2* (At3g18780, *AtACT2*) were used as reference genes (Table 2.4). The expression levels were expressed against the reference genes using the $2^{-\Delta\Delta Ct}$ method (Livak and Schmittgen 2001). Three replicates per line, and two technical replicas were used. cDNA dilution series were used to test the sensitivity of each primer pair.

Table 2.4 Primer Pairs used for Gene Expression Analysis

At corresponds to *Arabidopsis thaliana* genes, and Th to *Eutrema salsugineum* genes, respectively. The AGI codes are linked to the TAIR (https://www.arabidopsis.org/) or Phytozome (https://phytozome.jgi.doe.gov/pz/portal.html) pages for each of the respective genes. AS, Amplicon size.

Gene	Exon	AGI	Forward Primer 5' … 3'	Reverse Primer 5' … 3'	Size (bp)
AtACT2	Exon 3	At3g18780	TTCCCTCAGCACATTCCAGCAGAT	AACGATTCCTGGACCTGCCTCATC	70
AtIPCS3	Exon 9	At2g29525	GGCACACGAAGGTGGATCA	AGCCAACTTACCTGGCAGTTT	165
	Exon 10	At2g29525	CACGAAGGTGGATCAAGCACT	TGAGCCAACTTACCTGGCAGT	163
AtPES1	Exon 2	At1g54570	CCTCCACGGTGGTTTAGTCC	CGAGACATGAAAAGCCTTGCC	141
	Exon 10	At1g54570	CTCTTTCGTGGAATGGCCC	GTTCACCCCGGTTATGGAGAG	197
AtPGR5L1A	Exon 9	At4g22890	GTCAAATGCACCAACTGCGG	CTCACAGGGTTTAAGCTTGGCT	94
ThSLD1	Exon 1	Thhalv10005967m.g	GCACATCCAATTCACGCTAA	GTCGTTACCTGTGGGTGGAC	67
ThSLD2	Exon 1	Thhalv10001443m.g	CCATCTCCGGCGAGTATCT	GACTCCTGTACGGAAGATTATGC	68
AtUBC21	Exon 2	At5g25760	GCTCTTATCAAAGGACCTTCGG	CGAACTTGAGGAGGTTGCAAAG	101

2.5 LIPID ANALYSIS

2.5.1 *Total Lipid Extraction*

Total lipids were extracted using a modified Bligh and Dyer method (Bligh and Dyer 1959). Briefly, 100 mg of freeze-dried rosette leaf material (18 DAS grown under control conditions as in Section 2.2.3) were crushed, transferred to 1 mL of isopropanol and incubated for 20 min at 75°C to denature lipase activity, combined with 2.7 mL of Chloroform/Methanol/Water (1:1:0.7 v/v/v), vortexed, and 2 mL of Chloroform/Water (1:1 v/v) was added. The samples were then centrifuged, the chloroform phase extracted (Krank *et al.* 2007, Lee *et al.* 2011, Usher *et al.* 2017). Samples were re-extracted with 1 mL of chloroform, the two lipid extractions were then combined and dried with a continuous N_2 flow. The total lipid extract was re-suspended in 200 µL of chloroform and used for the analysis of di- (DAG) and triacylglycerol (TAG), phospholipids, free fatty acids (FFA), monogalactosyldiglycerol (MGDG), digalactosyldiglycerol (DGDG) and sulfoquinovosyldiacylglycerol (SQDG), as described below.

2.5.2 *Triacylglycerol and Diacylglycerol Quantification*

TAG and DAG analysis combined 20 µL of total lipid extract with 980 µL of Isopropanol/Methanol/50mM Ammonium Acetate/Dichloromethane (4:3:2:1 v/v/v/v) spray solution. To which 0.857 nmol/mL of either internal standard 45:0-TAG (15:0-15:0-15:0) or 38:4-DAG (18:0-20:4, Nu-Chek Prep, Elysian, MN, USA) were added. The molecular species were analysed by electrospray ionisation tandem triple-quadrupole mass spectrometry (ESI-MS/MS, Q-TRAP® 4000, AB SCIEX™, Figure 2.3). Samples were infused at 15 µL/minute with an auto sampler (LC mini PAL, CTC Analytics, Switzerland). The scan speed was of 100 µ/s. The collision energy, with nitrogen in the collision cell, was +25 V, declustering potential of +100 V, entrance potential of +14 V; and exit potential of +14 V. Sixty continuum scans were averaged in the multiple

channel analyser mode. For product ion analysis (neutral loss survey scan), the first quadrupole mass spectrometer (Q1) was set to select the mass and Q3 for the detection of fragments fragmented by collision induced dissociation. Molecular species were detected as $[M+NH_4]^+$ ions by a series of neutral loss scans which targeted losses of fatty acids. For all analyses gas pressure was set on 'low', and the mass analysers were adjusted to a resolution of 0.7 μ full width height. The source temperature was of 100°C; the interface heater on, +5.5 kV was applied to the electrospray capillary; the curtain gas set at 20 (arbitrary units); and the two ion source gases set at 45 (arbitrary units). TAG molecular species were quantified after background subtraction, smoothing, integration, isotope deconvolution and comparison of sample peaks with those of the internal standard using LipidView™ Softwarer v1.2 [AB SCIEX™, USA, (Ejsing *et al.* 2006)]. The peak area of each lipid was normalized to each respective internal standard and further normalized to the dry weight of the initial sample. The mass spectral responses of various molecular species were variable, due to differential ionisation of individual acyl glycerol molecular species, to which no response factors for individual species were determined. Thus, values presented could not be directly correlated to the lipid content of each genotype, however it still allowed the comparison of the molecular species across samples studied.

2.5.3 *Polar Lipid Assessment*

The analyses of phosphatidylcholine (PC), lyso phosphatidylcholine (LPC), phosphatidylethanolamine (PE), phosphatidylinositol (PI), phosphatidylglycerol (PG), FFA, MGDG, DGDG and SQDG were as follows. 20 μL of lipid extract were added to Chloroform/Methanol/300 mM ammonium acetate (300/665/35 v/v/v) with internal standards added. These were incorporated as 0.857 nmol/mL of 48:2-PC (24:1-24:1), 0.50 nmol/mL of 13:0-LPC, 0.40 nmol/mL of 28:0-PE (14:0-14:0), 0.50 nmol/mL of 38:4-PI (18:0-24:0), 0.080 nmol of 28:0-PG (14:0-14:0), and 0.607 nmol/mL of 15:0-FFA. All internal standards were supplied by Avanti (Alabaster, AL, USA) and quantified as previously described

(Devaiah *et al.* 2006). Samples were directly infused at 15 µL/minute with an auto sampler (HTS-xt PAL, CTC-PAL Analytics AG, Switzerland). Data acquisition and acyl group identification of the polar lipids based on previously described work (Ruiz-Lopez *et al.* 2014). The analysis was performed by ESI-MS/MS on a Q-TRAP® 4000 (AB SCIEX™, Figure 2.3). Data was processed using LipidView™ Software v1.2 [AB SCIEX™, USA, (Ejsing *et al.* 2006)] where isotope corrections were applied. Lipid classes were identified, and the respective molecular species analysed as total acyl carbon chain (C) and total number of double bonds (C:X). The peak area of each lipid was normalized to each respective internal standard and further normalized to the dry weight of the initial sample.

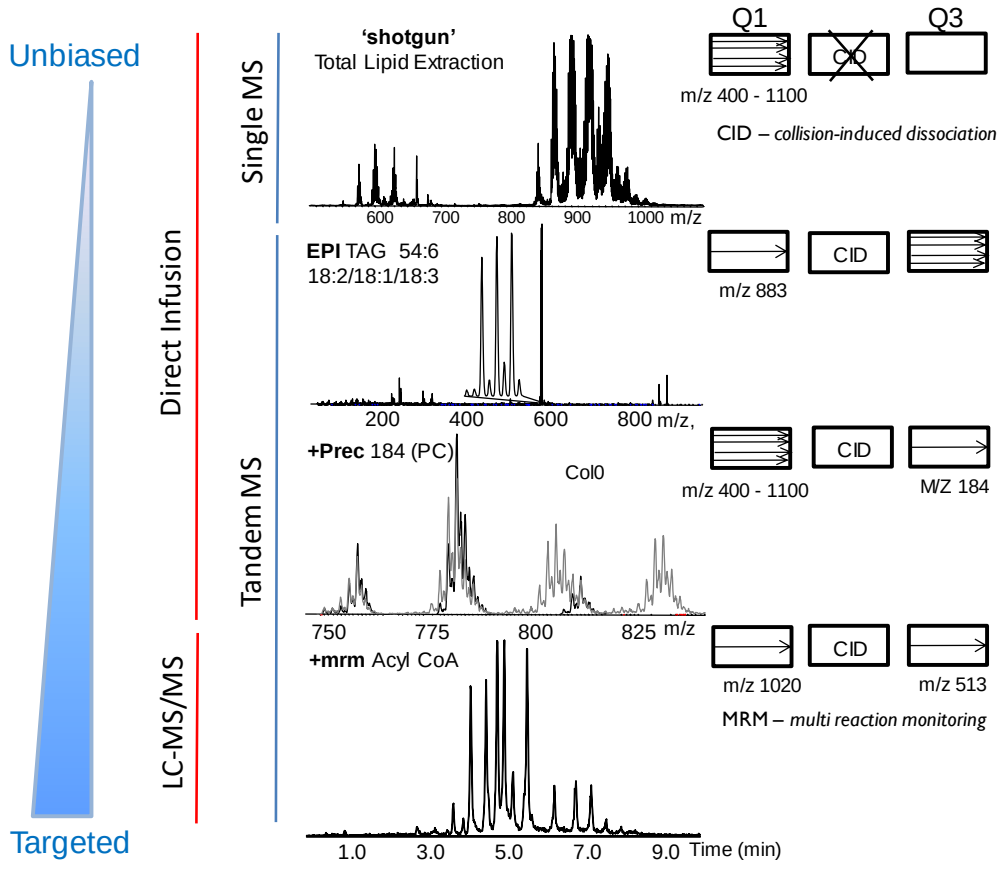

Figure 2.3 Mass Spectrometry Based Lipid Analysis Methods

Different mass spectrometry (MS) methods can be used for targeted to "shotgun" lipid analysis. LC-MS/MS, liquid chromatography tandem MS; Q1/Q3, tandem triple-quadrupole; CID, collision induced dissociation; MRM, multiple reaction monitoring. Figure kindly provided by Dr. Richard P. Haslam.

2.5.4 *Fatty Acid Methyl Esters*

A two-step direct methylation protocol was used for the extraction of 20 mg of fresh 14 DAS rosette leaf tissue grown under control conditions (see Section 2.2.3), with one leaf per plant and one plant per replicate used. Samples were placed in glass vials and 50 µg/mL of heptadecanoic acid (C17:0, Sigma-Aldrich®) was added to samples as an internal standard. Lipids were extracted and directly methylated as follows. 1 mL of methylation mix comprising of 85% methanol (MeOH), 10% hydrochloric acid (HCl), and 5% 2,2-dimethoxypropane was added. The capped vials were heated to 80 – 85ºC for 1h (pilot experiments were undertaken to ensure one hour was sufficient to ensure full methylation), allowed to cool to room temperature, and 1 mL of 1% NaCl was added. The samples were mixed, and lipids extracted into 1 mL hexane. Following methylation, the hexane fraction was dried under continuous N_2 flow and re-suspended in 50 µL of hexane. Methyl ester derivatives of total fatty acids (FAMEs) were analysed by Gas Chromatography (GC) (Agilent 7890A, Agilent Technologies) using an Agilent DB-225 column (30 m × 0.32 mm × 0.3 µm, Agilent Technologies). Inlet and detector temperature was set to 250°C and 1 µL of each sample was analysed using splitless injection and a constant flow rate of 2 mL/minute. The oven temperature cycle as start temperature of 50°C held for 1 minute to allow vaporised samples and the solvent (hexane) to condensate at the front of the column. Oven temperature was then increased to 190°C at 40°C/minute followed by a slower increase to 220°C at a rate of 1.5°C/minute. The final temperature of 220°C was held for one minute giving a total run time of 25 min and 50s per sample. FAMEs were detected using a Flame Ionisation Detector (FID). Chromatograms were analysed using the offline session of the Agilent ChemStation software (Agilent Technologies, USA). The peak area of each FAME was normalized to the internal standard and further normalized to the fresh weight of the initial sample. The retention time and identity of each peak was calibrated using the Supelco® 37 Component FAME Mix (certified reference material TraceCERT®, Sigma-Aldrich®).

2.5.5 *Long-Chain Base Measurement*

The extraction and analysis of the sphingolipid long-chain base (LCB) were based in methods previously described (Sperling *et al.* 1998). Briefly, 20 – 30 mg of 18 DAS fresh leaf tissue were subject to alkaline hydrolysis to release the LCBs from the leaf sphingolipid pool, whilst also removing phospholipids (which subsequently interfere with MS analysis). For this, 10% barium hydroxide ($BaOH_2$), 1,4-dioxane 1:1 (v/v), and 2.0 µL of internal standard (D-erythro-Sphingosine C17 base, 1 mg/mL, Avanti® Polar Lipids Inc.) were applied to the leaf samples and incubated at 110°C overnight. Tubes were cooled down, and the LCB phase was extracted with Chloroform/Water 2.66/1.66 (v/v). The LCBs were then converted to dinitrophenyl derivatives using 0.5% (v/v) methanolic 1-fluoro-2,4-dinitrobenzene and 0.8 mL of 2 M boric acid (dissolved in potassium hydroxide (KOH), and incubated at 60°C for 30 min. LCBs were then extracted by phase partitioning (Chloroform/Methanol/Water 2/1/1 v/v/v), washed and re-suspended in 500 µl of Methanol (MeOH) for analysis. One leaf per plant was collected, and independent plants were used as independent replicates. Extraction and analysis were performed in a random order to minimise bias. The extract was analysed by reverse-phase high-performance liquid chromatography (HPLC), in combination with tandem mass spectrometry (ESI-MS/MS) in multiple reaction monitoring (MRM) mode (Table 2.5), allowing the identification of specific LCB species. Elution was performed with a Hichrom 5 C18 column (4 × 250 mm, Hichrom Ltd.) with a flow rate of 1 mL/minute and an increasing concave gradient from 80 to 100% of Methanol/Acetonitrile/Isopropanol (10/3/1, v/v/v), against water in 45 min. The elution was monitored with ESI-MS/MS MRM on a Q-TRAP® 4000 (AB SCIEX™) and at a wavelength of 350 nm on an Agilent 1200 HPLC. The peak areas of the LCB molecular species were normalized to the internal standard using Analyst® v1.6.2 Software (AB SCIEX™), and further normalized to the fresh weight of the initial sample.

Table 2.5 MRM Parameters for Long-Chain Base Analysis

The Multiple Reaction Monitoring (MRM) pairs used for the selected acyl-CoA molecular species analysis is shown, with the respective parent (Q1) and product ion (Q3) masses, declustering potential (DP) and collision energy (CE).

Molecular Species	Q1 Mass (Da)	Q3 Mass (Da)
d18:2	462.0	161.8
d18:1	464.0	161.8
d18:0	466.0	161.8
t18:1	480.0	161.8
t18:0	482.0	161.8

2.5.6 *Sphingolipid Analysis*

Sphingolipids were extracted from 30 mg of freeze-dried 19 DAS whole plant tissue grown under control conditions (see Section 2.2.3), following the extraction protocol previously described (Markham 2013). The freeze-dried samples were disrupted in the extraction solvent composed of Isopropanol/Water/Hexane (5.5/2/2.5 v/v/v, only lower phase used) with 10 µL of internal standard mix and incubated for 30 min at 60°C. Samples were centrifuged, the supernatant collected to a new tube and the previous step was repeated for the pellet. The total extract was dried under a continuous N_2 gas flow, methylamine reagent was added, and samples incubated for 90 min at 50°C. Samples were dried under N_2 flow and dissolved in sample solvent Tetrahydrofuran/Methanol/Water (4/2/4 v/v/v) with added 0.1% Formic Acid. The internal standard mix was composed of GM1 (2 nmol) for the quantification of the glycosylinositolphosphoryl ceramides (GIPCs), Glucosyl-C12-Ceramide (1 nmol) for glucosylceramides, C12-ceramides (0.1 nmol) for ceramides and hydroxyceramides, and the C17-sphingosine (0.1 nmol) for free LCBs (Markham 2013). All internal standards were supplied from Avanti® Polar Lipids Inc. The analysis was performed by HPLC followed by ESI-MS/MS in MRM mode according to previously described [(Markham 2013), Figure 2.3]. The extract was eluted using an Eclipse XDB-C18 column (3.5 µm particle size, 3.0 × 100 mm, Agilent Technologies), and two solvents A and B were used for the elution of the different

sphingolipid classes as described in Table 2.6. Both solvents were composed of Tetrahydrofuran/Methanol/5 mM Ammonium Formate (v/v/v) in different proportions for A (30/20/50) and B (70/20/10), both complemented with 0.1% Formic Acid. A flow rate of 1 mL/minute, oven temperature of 40°C, and a post-run equilibration of 20s were used. The ESI-MS/MS in MRM modes was performed in Q-TRAP® 4000 (AB SCIEX™). The MRM parameters allowed to distinguish each of the four main LCBs t18:0, t18:1, d18:0 and d18:1 in combination with each fatty acyl chain (16:0, 18:0, 20:0, 20:1, 22:0, 22:1, 24:0, 24:1, 26:0, and 26:1) for each class, and the full description can be found in (Markham 2013). Ceramides and hydroxyceramides used the same HPLC gradient but different MRM parameters. The peak areas were normalized to the internal standard using Analyst® v1.6.2 Software (AB SCIEX™), and further normalized to the dry weight of the initial sample.

Table 2.6 Solvent Gradient for Sphingolipid Analysis

Gradient of solvent B used for the elution of each sphingolipid class. Cer, Ceramides; HCer, hydroxyceramide; GlucCer, Glucosylceramide; GIPC, glycosylinositolphosphoryl ceramide; LCB, Long-chain base; min, min Adapted from (Markham 2013).

	Cer & HCer	GlucCer	GIPC	LCB
Start	55%, 1 min	55%, 1 min	26%, 1 min	10%, 1 min
Gradient	85%, 7 min	80%, 5 min	58%, 5 min	20%, 3.5 min
	100%, 7.2 min	100%, 5.2 min	100%, 5.2 min	100%, 4 min
End	8 min	6 min	6 min	5 min

2.5.7 *Acyl-CoA Profile*

Acyl-CoAs were extracted from 15 – 20 mg of freshly harvested, and immediately frozen in liquid N_2, 15 DAS rosette leaf tissue grown under control conditions (see Section 2.2.3). The method was based in previously described work (Larson and Graham 2001). Briefly, the frozen leaf samples were ground to a fine powder with the aid of liquid N_2, 200 µL of extraction buffer composed of 100% isopropanol, 50 mM potassium

phosphate (KH_2PO_4) buffer pH 7.2, glacial acetic acid (CH_3COOH) and 50 mg/mL of bovine serum albumin (BSA), were added. After which, three washes with isopropanol/saturated petroleum ether at 50°C were performed to remove lipids. Saturated ammonium sulphate ($(NH_4)_2SO_4$) and Methanol/Chloroform (2/1, v/v) were added to the aqueous phase, and the samples incubated for 20 min at room temperature. Samples were then centrifuged at 13500 rpm for three min, and the supernatant transferred to tapered vials, dried under a N_2 gas flow and the extract re-suspended in 40 µL of 90% Acetonitrile (C_2H_3N). These were analysed using liquid chromatography tandem mass spectrophotometry (LC-MS/MS) with MRM in positive ion mode using a Q-TRAP® 4000 (AB SCIEX™, Figure 2.3). An Eclipse XDB-C18 column (3.5 µm particle size, 3.0 × 100 mm, Agilent Technologies), and the solvents A (100% Acetonitrile, 15 mM Ammonium Hydroxide), B (10% Acetonitrile, 15 mM Ammonium Hydroxide), and C (70% Acetonitrile, 0.1% Formic Acid) were used for the elution of the components. The analysis performed through MRM mode ranged acyl-CoA molecular species from 14:0 to 32:0 (number of carbons in the acyl chain:number of double bonds), and the MRM parameters for the selected molecular species specified in Table 2.7. The peak areas were obtained with Analyst® v1.6.2 Software (AB SCIEX™), normalized to the standard curve and fresh weight of the initial sample as:

$$((Peak\ Area\ \times 0.000007)/Sample\ Weight) \times 1000.$$

2.6 PLANT PHYSIOLOGY MEASUREMENTS

2.6.1 *Morphology Analysis*

Plants were assessed for any visible changes in the growth morphology, number of green leaves, rosette diameter (cm), presence and height (cm) of main shoot were assessed together with photos to illustrate any effects derived from the T-DNA insertion and/or the tested temperatures.

Table 2.7 MRM Parameters for Acyl-CoA Analysis

The Multiple Reaction Monitoring (MRM) pairs used for the selected acyl-CoA molecular species analysis is shown, with the respective parent (Q1) and product ion (Q3) masses, declustering potential (DP) and collision energy (CE).

Molecular Species	Q1 Mass (Da)	Q3 Mass (Da)	DP (volts)	CE (volts)
14:0	978.3	471.3	180	50
16:0	1006.4	499.4	180	50
16:1	1004.4	497.4	180	50
16:3	1000.4	493.4	180	50
18:0	1034.4	527.4	190	52
18:1	1032.4	525.4	185	52
18:2	1030.4	523.4	180	52
18:3	1028.4	521.4	180	52
20:0	1062.4	555.4	190	52
20:1	1060.4	553.4	190	52
22:0	1088.4	581.4	190	53
24:0	1118.5	611.5	210	57
24:1	1116.5	609.5	208	57
26:0	1146.4	639.5	220	58
26:1	1144.4	637.5	218	58
28:0	1174.4	667.5	220	58
28:1	1172.4	665.5	120	53

2.6.2 *Ion Leakage*

Ion leakage was measured by assessing water conductivity. Each sample comprised five leaf discs of 3 mm diameter per plant, and a sample per plant were analysed. The leaf discs were immersed in deionized water for 24h, and the water conductivity of each sample was measured ($Cond_{24h}$) with an ECCON603PLUSK (Eutech Instruments, The Netherlands). Samples were then incubated at 90°C for 90 min, allowed to cool down and total conductivity was measured ($Cond_{Total}$). The relative conductivity (RC, %) of each sample was calculated as $(Cond24h/CondTotal) \times 100$. Injury index ($I_d$, %) was calculated as a measure of cold stress, with the formula $Id = (Rs - Rc/1 - Rc) \times 100$,

where R_s is the RC of the stressed tissue, and R_c is the RC of control (Whitlow *et al.* 1992).

2.6.3 *Chlorophyll Fluorescence Screen*

A cold acclimation test was performed to screen candidate genes selected from an Arabidopsis RNA-Sequencing (RNA-Seq) experiment as described in Chapter 3 using an imaged chlorophyll *a* fluorescence technique (McAusland *et al.* 2019). The 19 T-DNA insertion homozygous lines and Col-0 were grown under control conditions (at 150 µmol/m^2/s, see Section 2.2.3) for 18 - 20 DAS. At the last day of control conditions, a control measurement was performed, and the trays moved to a 5°C (at 150 µmol/m^2/s, see Section 2.2.4) controlled environment room. The fluorescence measurements were taken every day during the eight days of stress (except for day six). The experiment was designed using a Complete Randomized Block Design (CRBD) with three blocks of two trays (35 x 24.5 cm), and within each block two replicates per genotype were randomly distributed, adding up to a total of six replicates per genotype. The fluorescence measurements were performed at 18 - 20°C with a PSI© FluorCam CF imager (FC800-222, Photon Systems Instruments, Czech Republic) with an imaged area of approximately 1 x 1.5 m accommodating two trays (35 x 24.5 cm) in a total of 48 Arabidopsis plants, allowing each block to be measured at the same time. The measurements were set up through the respective FluorCam® 7.0 Software. The dark adaptation times were tested and based on previous experience 30, 45, and 60 min were tested to allow for the wild-type Arabidopsis Col-0 to reach a maximum quantum efficiency of the PSII (F_v/F_m) value of a minimum of approximately 0.83 (Bjorkman and Demmig 1987), this was achieved with a 60 min dark adaption time (results not shown) which was then used throughout. Following dark adaptation and before actinic, a saturation pulse of 820 µmol/m^2/s and duration 0.8s was applied, which allowed for the measurement of the F_v/F_m. An initial induction actinic light of 700 µmol/m^2/s was then applied after which key parameters such as the quantum yield of the PSII in light

adapted steady-state (ϕPSII) and the coefficient of photochemical quenching in steady-state (qP) could be measured (Table 2.8). This protocol therefore also included the measurement of other parameters such as the non-photochemical quenching (NPQ) which can be useful for further exploration of the photoprotective properties of the mutants under cold stress (Ruban *et al.* 2012). The temperature conditions in which to perform the dark adaption was also tested at control and cold conditions as 1 h was considered significant in any adaption event that might occur by changing the temperature during this period, so to avoid this each block was dark adapted for 1h in the respective growing conditions and taken to the FluorCam in dark for the measurement. The FluorCam 7.0® software was used for the processing of the chlorophyll *a* fluorescence image data, as the data was collected by the camera on top of the chamber and recorded for each pixel of the image the areas for each plant were individually selected post-measurement, and the parameters calculated as shown in Table 2.8.

Table 2.8 Fluorescence parameters

Chlorophyll *a* fluorescence parameters (P) measured and calculated by the FluorCam® 7.0 software for the cold stress conditions screen of the T-DNA insertion lines. PSII, photosystem II; F, fluorescence.

P	Description	Formula
F_o	Minimum fluorescence in dark-adapted state	Measured
F_m	Maximum fluorescence in dark-adapted state	Measured
F_s	Steady-state minimum fluorescence in light	Measured
F_m'	Steady-state maximum fluorescence in light	Measured
F_v/F_m	Maximum PSII quantum yield in dark-adapted state	$(Fm - Fo)/Fm$
ΦPSII	PSII quantum yield in light-adapted steady-state	$(Fm' - Fs)/Fm'$
NPQ	Steady-state non-photochemical quenching in light	$(Fm - Fm')/Fm'$
qP	Coefficient of photochemical quenching in steady-state	$\frac{(Fm' - Ft')}{(Fm' - Fo')}$

2.6.4 *Chlorophyll and Carotenoid Assay*

Fresh 20 DAS rosette leaves were harvested and the fresh weight (g) recorded. Tissue was transferred to 80% acetone, ground with a glass rod and the tubes were centrifuged to remove debris. The pigment concentration was determined spectrophotometrically using the wavelengths 646.6 nm and 663.6 nm for chlorophyll (Chl) *b* and *a*, respectively, 470 nm for total carotenoids, and 750 nm to enable a turbidity correction, with an 80% acetone blank. The pigment content was calculated as:

Chl *a* (mg/g FW) =

$$\left[\left(\left(12.25 \times (A_{663.6} - A_{750})\right) - \left(2.55 \times (A_{646.6} - A_{750})\right)\right) \times V\right] / 1000 \times W$$

Chl *b* (mg/g FW) =

$$\left[\left(\left(20.31 \times (A_{646.6} - A_{750})\right) - \left(4.91 \times (A_{663.6} - A_{750})\right)\right) \times V\right] / 1000 \times W$$

Total Carotenoids (mg/g FW) =

a) $((1000 \times A_{470}) - (3.27 \times Chl\ a) - (104 \times Chl\ b))/229$

b) $(Answer\ a \times V)/(1000 \times W)$

Where A is the absorption value, V is the volume of the extract (mL) and W is the fresh weight of the sample (g) (Porra *et al.* 1989).

2.7 GENOME EDITING BY CRISPR/CAS9

2.7.1 *Identification of Eutrema FAD Genes*

The Eutrema *FATTY ACID DESATURASE 7* (*ThFAD7*) and *8* (*ThFAD8*) sequences were identified in the online database *Eutrema salsugineum V1.0* in Phytozome 12. The respective entries were identified as Thhalv10020755m.g (scaffold_13:5843498…5846134, reverse) for *ThFAD7* and Thhalv10013625m.g (scaffold_2:1617400...1619938 forward) for *ThFAD8*. The protein alignment between the Arabidopsis and Eutrema FAD7 and FAD8 sequences was produced by Multiple Sequence Comparison by Log-Expectation (MUSCLE) using the online

tool CLUSTAL MUSCLE 3.8 (Madeira *et al.* 2019) The alignment of the genomic sequences of *ThFAD7* and *ThFAD8* genes was performed using Geneious® 10.0.9 (Biomatters Ltd, New Zealand) to identify the conserved regions allowing the gRNA design.

2.7.2 *Identification of the Chloroplast Transit Peptide*

The identification of the chloroplast transit peptide in the amino acid sequences of ThFAD7 (V4NQN1) and ThFAD8 (V4KR96) used the online tool TargetP 1.1 Server (Technical University of Denmark, Denmark). First, the UniProt database identified two domains in each of the genes. A first domain from residues 1-132 (ThFAD7) and 1-123 (ThFAD8) with no known function, and a second described as fatty acid desaturase in both genes from residues 140-394 (ThFAD7) and 131 to 385 (ThFAD8). The FASTA sequence for the first unknown domain for both genes was obtained as below and used for the identification of the chloroplast transit peptide sequence, both searches were performed by selecting *Plant* as *Organism Group* and *No-Cutoffs*.

>tr|V4NQN1|1-132

MANLVLSECGIRPLPRIYTTPRSNPLSNINKPIFNFRPSPSSSTTSSSLA
FRLNSRDAFFTRNWALNVSTPLTVETPIEEEHETQRFDPGAPPPFNLA
DIRAAIPKHCWVKNPWKSMSYVVRDVAIVFALAA

>tr|V4KR96|1-123

MASWVLSECGIKPLSRFYPKPTTSFISNPTPTFRFNPSPSSLKPRNGF
FPKARNWALNVATPLTTLEPPSEEEHTKRFDPGAPPPFNLADIRAAIP
KHCWVKNPWKSMSYVVRDVAIVFGLAA

2.7.3 *Guide RNA Design*

Four single guide RNAs (gRNA) were designed to target the two genes *ThFAD7* and *ThFAD8* to increase the probability of producing mutations. Two gRNA were designed to target simultaneously the conserved regions of *ThFAD7* and *ThFAD8* in exon 1 (gRNA1) and exon 7 (gRNA2),

and other two independent gRNAs were designed to target exon 1 of *ThFAD7* (gRNA3) and exon 1 of *ThFAD8* (gRNA4). The gRNA design targeted the genomic sequences for *ThFAD7* and *ThFAD8* according to the database Phytozome 12. The gRNAs were designed using the *Find CRISPR Sites* tool in Geneious® 10.0.9 (Biomatters Ltd, New Zealand) by selecting a target of 20 nucleotides plus a *NGG* protospacer-adjacent motif (PAM) site. The specificity score, off-target score, mismatch count and position, and the out-of-frame score were then considered to be suitable using the guide RNA selection tool CRISPOR (v4.3, February 2018) available online [www.crispor.tefor.net (Haeussler *et al.* 2016, Concordet and Haeussler 2018)]. CRISPOR website only searched up to four mismatches between the gRNA sequence and potential off-targets in Eutrema genome, including all the sequences flanked by one of the motifs NGG, NAG, NGA. A comparison to the Eutrema (taxid:72664) genome in the database of National Centre for Biotechnology Information (https://blast.ncbi.nlm.nih.gov/Blast.cgi, NCBI) was performed to confirm no sequence similarity with other genes in the database (Appendix 1). The two selected conserved gRNAs were gRNA1 (5' AACAAAGAGAGCCCAGAACA**TGG** 3') and gRNA2 (5' GCTTCTACTAGATGATAATG**TGG** 3'). The two specific gRNAs (one for each gene) targeted the first exon and were localised at a distance of at least 160 bp upstream the conserved gRNA1 and gRNA2 to avoid any potential positional competition of the gRNA/Cas9/DNA complex onto the target loci. The unique gRNA for *ThFAD7* was identified as gRNA3 (5' GTGAACGGAGGAGGCGCGCCT**GGG** 3'), and for *ThFAD8* as gRNA4 (5' GTTGAAGGGAGGGGGCGCACC**TGG** 3'). The three-nucleotide sequence marked in bold at the end of each gRNA sequences represents the PAM site. Each of the gRNAs was designed to be transcribed from a different RNA polymerase III (Pol III) promoter, hence four Arabidopsis small RNA promoters were selected from the literature (Ma *et al.* 2015, Morineau *et al.* 2016). gRNA1 was preceded by AtpU3B (X52629), gRNA2 by AtpU6-29 (X52529), gRNA3 by AtpU6-1 (X52527), and gRNA4 was preceded by AtpU6-26 (X52528), the promoter sequences can be found in Appendix 2. The requirement for a specific nucleotide "A"

for AtpU3, and of a “G” for AtpU6 were met, adding the respective nucleotide to the 5’ end of the gRNA sequence when necessary (Belhaj *et al.* 2015). Following the gRNAs, was a Cas9 binding hairpin 5’ GTTTTAGAGCTATGCTGAAAAGCATAGCAAGTTAAAATAAGGCTAG TCCGTTATCAACTTGAAAAAGTGGCACCGAGTCGGTGC 3’, according to (Chen *et al.* 2013). The structure *promoter – gRNA – hairpin – Terminator* was designed to include the four gRNA and flanked by Gateway™ (Invitrogen®) *attB1* and *attB2* recombination sites. The final *attB* flanked cassette with the four gRNAs, and respective promoters, hairpins and terminator (polyT), were sourced from Genscript® in the vector *pUC19* (3870 bp).

2.7.4 *Cas9 Vector*

The vector containing the *Streptococcus pyogenes* Cas9 (SpCas9), pDE-Cas9-proDsREDter (Figure 2.4 A) was kindly donated by Professor Jean-Denis Faure [INRA, Paris, (Fauser *et al.* 2014, Morineau *et al.* 2016)]. This vector was selected because it includes a DsRED expression *cassette* which was fundamental for the work with Eutrema, it also include the *attR1* and *attR2* recombination sites for the Gateway® cloning technology. The pDE-Cas9-proDsREDter vector was checked by restriction digestion with the enzyme Invitrogen™ Anza™ *NotI* with the recognition site 5’ GC|GGCCGC 3’ (Figure 2.4 A). The total size of the vector was 15,821 bp, with four recognition sites producing fragments of sizes 8815 bp, 4184 bp, 1532 bp, and 1290 bp respectively, as shown in the 1% agarose gel Figure 2.4 B.

2.7.5 *Anza™ Restriction Analysis*

The restriction analysis protocol was followed according to the Invitrogen™ Anza™ instructions. Briefly 2.0 µL of Anza™ Red Buffer (10X), up to 1 µg of sample, and 1.0 µL of Anza™ restriction enzyme was added for a final volume of 20.0 µL. The reaction was incubated at 37°C for 15 min, after which each restriction reaction was verified by electrophoresis in a 1% agarose gel (according to Section 2.4.4).

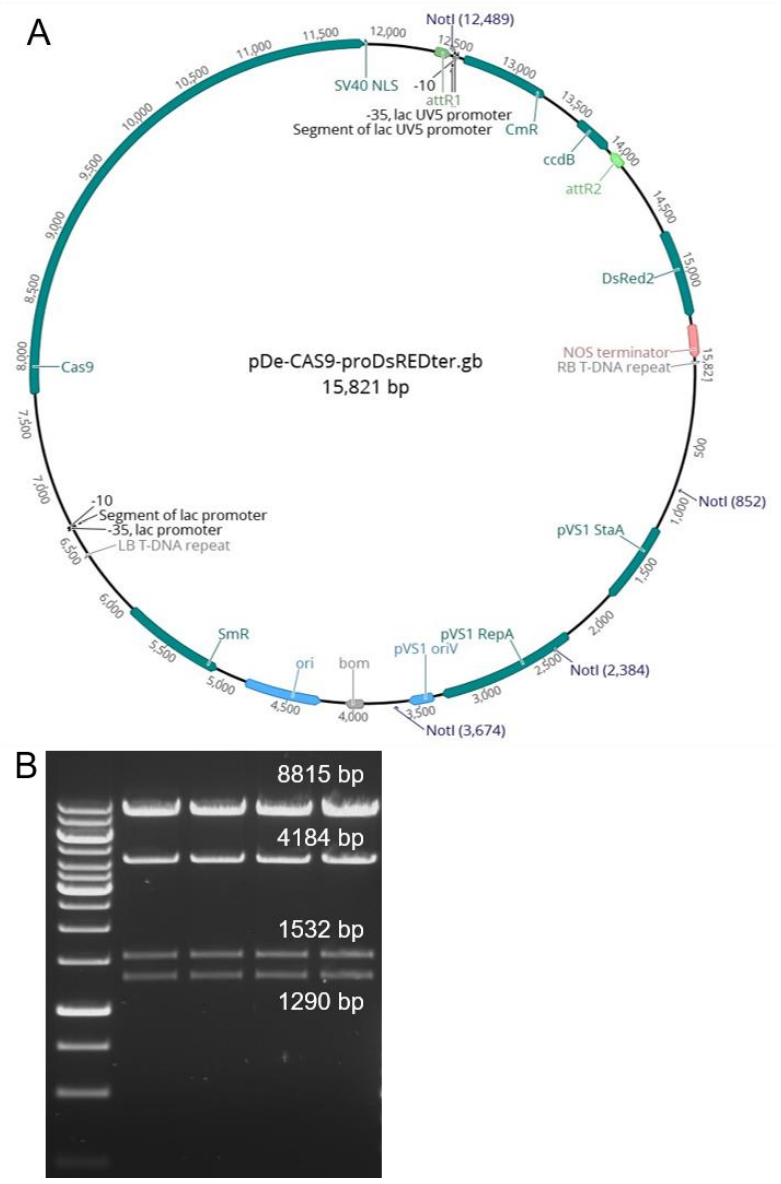

Figure 2.4 pDE-Cas9-proDsREDter vector

(A) pDE-Cas9-proDsREDter vector with the Cas9 sequence, the DsRED selection marker, the *attR1* and *attR2* cloning sites, and the *NotI* restriction sites. (B) Restriction analysis results using *NotI* in a 1% agarose gel and Thermo Scientific™ GeneRuler 1 kb DNA ladder for fragments size reference. The fragment sizes from the restriction analysis were expected to be 8815 bp, 4184 bp, 1532 bp, and 1290 bp.

2.7.6 *Assembly of the Expression Vector*

The *pUC19* vector containing the gRNA cassette and the pDE-Cas9-proDsREDter vector were assembled together using the Gateway® Cloning Protocol (Invitrogen™). First, a PCR was performed to isolate

the gRNA cassette from the *pUC19* vector, using the Q5® High-Fidelity DNA Polymerase (NEB) with the respective protocol, PCR program as in Section 2.4.3, and the primers used for *attB1* and *attB2* were as described in Table 2.9. All primers were obtained from Sigma-Aldrich®. Results ran in 1% agarose gel and 3870 bp fragments (approximately 4 kbp) were observed (results not shown). The bands were then extracted and purified with QIAquick® Gel Extraction Kit (QIAGEN®), following the respective protocol, and quantified with NanoDrop® ND–1000 Spectrophotometer (Labtech International).

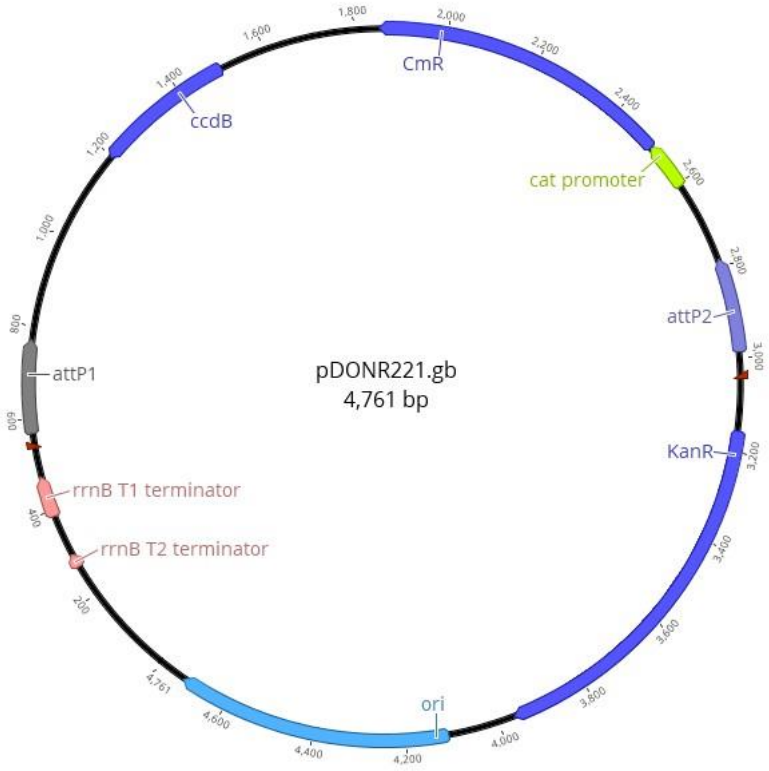

Figure 2.5 pDONR221™ vector

The vector contains the *attP1* and *attP2* recombination sites and the M13 primer pair (●); CmR, chloramphenicol acetyltransferase resistance gene; cat promoter, CmR promoter; ccdB, bacterial toxin gene; rrnB T1 and T2 terminators, transcription terminators; ori, origin of replication; KanR, kanamycin resistance gene.

2.7.6.1 BP Reaction

Once the *att*B PCR product containing the gRNA cassette was isolated, the BP reaction was performed using 127.7 ng of the *att*B PCR Product, 150 ng/L of the pDONR221™ as the *attP*-containing donor vector (Figure 2.5), and 1 µL of the BP Clonase™ II enzyme. The reactions were incubated for 2h at 25°C, after which 2 µg/µL of Proteinase K was added and the reaction incubated at 37°C for 10 min. The BP reaction was performed in three replicates plus a negative control where the *attB* PCR product was replaced with nuclease-free water. These four BP reactions were transformed into One Shot® TOP10 *E. coli* Competent Cells as described below in Section 0. Three colonies for each of the three entry clones were used to confirm the results of the BP reaction by restriction analysis (Section 2.7.5) and Sanger sequencing (Section 2.4.5). The restriction analysis was performed with *Hind*III (Invitrogen™ Anza™) which recognition site 5' A|AGCTT 3'. Sequencing analysis used the primer pair M13uni-21/M13rev-29 (Table 2.9).

2.7.6.2 LR Reaction

The entry clones (up to 257.1 ng per reaction) were used for the LR reaction with the destination vector pDE-Cas9-proDsREDter (300 ng per reaction), the LR Clonase™ reaction buffer (5X, 4µL per reaction), and TE buffer, pH 8.0, up to a final volume of 16 µL. Reactions were incubated at 25°C for 5h due to the large size of the plasmid (15 kb), after which proteinase K was added and incubated further 10 min at 37°C. Eight reactions were performed, which included a negative control without the entry clone, and a positive control with the pENTR™ vector instead of the entry clone. The LR reactions were transformed into One Shot® TOP10 *E. coli* Competent Cells (Section 0). One colony for each of the six expression clones was used to confirm the results of the LR reaction, via restriction analysis (Section 2.7.5) and Sanger sequencing (Section 2.4.5). The restriction analysis was performed with *NotI* and *NheI* (Invitrogen™ Anza™) with the recognition sites 5' GC|GGCCGC 3' and

5’ G|CTAGC 3’, respectively. Sequencing analysis used the primer pairs for AtpU3, AtpU6-29, AtpU6-1, and AtpU6-26 described in Table 2.9.

Table 2.9. Primer sequences used for cloning

Primer pairs and sequences used with during cloning with the corresponding reaction information. Fw, forward; Rev, reverse.

Primer		**Primer Sequence 5’ … 3’**	**Reaction**
attB1	Fw	TCCACAAGTTTGTACAAAAAAGCAGGCT	Extract gRNA *cassette*
attB2	Rev	TAACCACTTTGTACAAGAAAGCTGGGTACC	
M13uni-21	Fw	GTAAAACGACGGCCAGT	Sequencing entry clone
M13rev-29	Rev	CAGGAAACAGCTATGACC	
AtpU3	Fw	GTACAGTATAGGCTTGAGCTC	Sequencing expression clone
	Rev	AGCCCTCTTCTTTCGATC	
AtpU6-29	Fw	TCTCTCTGGTGCACCAAC	
	Rev	AAGGCCTATCCCTCGCTT	
AtpU6-1	Fw	ACGCTGAGTGTGAGTGAG	
	Rev	TTCTTGAAGGTTCGATGCC	
AtpU6-26	Fw	TAACCATGGACGCGTCC	
	Rev	TCGGCGTTCAATTTCTGG	

2.7.7 *Transformation of Escherichia coli Competent Cells*

The entry and expression clones were transformed into Invitrogen™ One Shot™ TOP10 Chemically Competent *Escherichia coli* (*E. coli*) (ThermoFisher Scientific), using the respective protocol. The BP recombination reaction (1 µL) was added to a vial containing One Shot™ TOP10 Chemically Competent *E. coli* cells and incubated in ice for 10min, heat-shocked for 30s at 42°C and immediately transferred to ice. Room temperature SOC medium (250 µL, Formedium™) was added, and the vials were incubated for 1h at 37°C (w/ shaker 200 rpm). The transformed *E. coli* were then plated in 2xYT Broth medium (Formedium™) agar plates supplemented with 50 mg/L of kanamycin for the BP reaction, or 100 mg/L of spectinomycin and 100 mg/L of streptomycin for the LR reaction (all obtained from Sigma-Aldrich®). For

both the BP and LR reactions two plates were prepared in which 10 and 100 µL of each reaction were plated. The plated reactions were incubated overnight at 37°C, after which the number of colonies was counted, and transferred to SOC medium (Formedium™) supplemented with the respective antibiotics for either BP or LR reactions (Table 2.10). Independent colonies per reaction as described in Table 2.10.

Table 2.10 Summary of the Cloning Associated Transformation

Antibiotics used with stock and working concentrations, number of colonies carried on to the next step of the Gateway® Cloning protocol, and for the *Agrobacterium* transformation. For BP and LP reactions One Shot™ Competent *E. coli* were used.

Reaction	Antibiotic	Stock	Work	Colonies
BP	Kanamycin	50 mg/L	50 µg/mL	Three independent colonies per replicate
LR	Spectinomycin	100 mg/L	100 µg/mL	One independent colony per replicate
	Streptomycin	100 mg/L	100 µg/mL	
Agrobacterium Transformation	Spectinomycin	100 mg/L	100 µg/mL	Four independent colonies per replicate
	Streptomycin	100 mg/L	100 µg/mL	
	Rifampicin	50 mg/L	50 µg/mL	
	Carbenicillin	50 mg/L	50 µg/mL	

2.7.8 *Transformation Summary*

The expression vectors produced from the LR reaction were transformed into competent *Agrobacterium tumefaciens* cells strain AGL-1 (Section 2.3.2). Two expression vectors were used to transform *Agrobacterium*, and four independent colonies were transferred to SOC medium (Formedium™) after two incubation days (Table 2.10). Two independent lots of Eutrema plants were transformed, lot A was subjected to three repeated flower dip events (http://thellungiella.org/protocols.htm) each separated by fifteen days according to the recovery rate of the plants from the previous dipping. Lot B was transformed only once at the onset of the first flowering buds. Within each batch five to six pots per clone were transformed, each pot (9 x 9 cm), with nine plants in, corresponded to an

independent transformation event in a total of 11 for lot A and 10 for lot B. The transformed plants were kept in the dark at high humidity for 24h, after which they were restored to controlled conditions, watered regularly and maintained until seed set. After the transformed Eutrema seeds were harvested, a post-harvest treatment was necessary to complete seed dormancy. After cleaning the seeds, these were placed at -80°C for eight days and then stored at room temperature.

2.7.9 *Identification of Gene Edited T1 Lines*

The identification of gene edited lines was performed in the T1 generation, firstly by amplifying specific genic regions in *ThFAD7* and *ThFAD8* targeted by the gRNAs *via* PCR (described in Sections 2.4.1 – 2.4.4). Followed by Sanger sequencing (Section 2.4.5) of the amplified gDNA fragments. The primer pairs used are shown in Table 2.11, which were confirmed by BLAST in NCBI to guarantee their specificity.

2.8 STATISTICAL ANALYSIS

In Chapter 3, statistical analysis of the chlorophyll fluorescence cold screen parameter F_v/F_m was performed by comparing F_v/F_m values of wild-type Col-0 and each of the mutant lines using a two-sample unpaired T-test ($p<0.05$) for both control and cold conditions. Otherwise in Chapter 3, results for the individual T-DNA lines were compared to the wild-type Col-0 through the analysis of the respective confidence intervals to avoid a biased analysis resulting of the use of a T-test for multiple comparisons. In Chapter 4, RT-qPCR results for the relative expression of the genes of interest were analysed using an analysis of variance (ANOVA) with the treatment structure “Genotype*Amplicon”. Lipid data for TAG, DAG, phospholipids, galactolipids and SQDG were analysed using canonical variate analyses (CVA). Differences in the LCB profile were assessed by an ANOVA with the treatment structure “Genotype*Temperature”. Each sphingolipid class profile was analysed through a principal component analysis (PCA) to three dimensions. In Chapter 5, differences between

genotypes and lines within genotypes were analysed with an ANOVA treatment structure “Genotype/Line”, or in the case of the relative conductivity “Genotype/Line/Temperature”. The complete sphingolipid profile was analysed using a CVA, which was then broken down into each sphingolipid class where glucosylceramides and GIPCs were analysed using a PCA with three dimensions, whilst ceramide used a CVA. All CVAs are presented with two dimensions using “Genotype” as the treatment factor. When necessary, data sets were transformed to achieve a balanced distribution of the residuals. When appropriate, the multiple comparison Bonferroni test was used. All statistical analyses were performed in GenStat® 19th Edition (VSN International Ltd, 2018).

Table 2.11 Primer Pairs used for Identification of Gene Edited Lines

Tm, Melting temperature; GC, content of guanine (G) and cytosine (C) in the primer sequence.

Target Gene	Target gRNA	Exon		Oligonucleotide 5’ … 3’	Tm (°C)	GC %
ThFAD7	1 & 3	1st	LP	TTGAATGTGAGCACGCCTCT	60.0	50.0
			RP	GTTGCCAATTGGGTTGGTCTAC	60.0	50.0
ThFAD7	2	7th	LP	TGGATCGTGACTACGGGTTG	59.5	55.0
			RP	CGGGCTCCCTGTAATACTTCC	59.9	57.1
ThFAD8	1 & 4	1st	LP	CCCTAAAGCCAGGAACTGGG	60.0	60.0
			RP	AGAAGCTACCATGTCCACTGC	60.1	52.4
ThFAD8	2	7th	LP	TACCTGAGAGGAGGGCTCAC	60.0	60.0
			RP	TCAAAGCAAGTCCATGCCAGA	60.2	47.6

Chapter 3.
Arabidopsis Cold Acclimation Response Assessed by Chlorophyll Fluorescence Imaging

3.1 INTRODUCTION

3.1.1 *Transcriptomic Adaptation to Cold Stress*

As sessile organisms, plants must adapt their metabolism and physiology in response to the surrounding environment. Exposure to cold temperatures, above 0°C, enables the plant to become more tolerant to freezing temperatures, in a process called cold acclimation [Chapter 1, Section 1.2; (Gilmour *et al.* 1988, Thomashow *et al.* 1990)]. The range of temperatures at which adaption occurs, however, varies depending on the plant species. For Arabidopsis, cold acclimation occurs at temperatures ranging between 10 and 0°C, enabling the plant to survive down to -10°C (Gilmour *et al.* 1988, Thomashow 1994). For the extremophile Eutrema, these temperatures can be as low as -16°C (Lee *et al.* 2012). Cold-induced transcriptomic regulation leads to the remodelling of the plant's metabolism, essential to survival (Thomashow 1999, Thomashow and Thomashow 2010). Thus, through the analysis of these transcriptomic responses, a global analysis of cold acclimation can be performed. As transcriptomic techniques have evolved, detailed information on the complex regulatory networks of gene expression has been revealed (Yamaguchi-Shinozaki and Shinozaki 2006). As discussed in Chapter 1, in Arabidopsis a significant portion of the cold induced genes are activated by the ABA-independent CBF/DREB1 regulon through a complex network regulated by transcription factors (TFs) (Yamaguchi-Shinozaki and Shinozaki 1994, Vogel *et al.* 2005). The immediate, or transient, cold-induced gene expression only detected within 1 to 5h upon cold exposure is mediated by TFs, which induce gene expression that can be active for longer periods (>5h) (Shinwari *et al.* 1998, Fowler and Thomashow 2002, Vogel *et al.* 2005). Examples include cryoprotective polypeptides (COR/LEA proteins), sugar pathway enzymes or *EARLY LIGHT-INDUCED PROTEINS* (Thomashow *et al.* 1996, Uemura *et al.* 1996, Fowler and Thomashow 2002, Kreps *et al.* 2002). These responses suggest a pattern in which the transcription

factor mediated first stage leads to a more prolonged adaptive stage, often associated with metabolic changes (Raju *et al.* 2018). These metabolic changes involve a myriad of processes such as accumulation of carbohydrates (Zuther *et al.* 2004, Lee *et al.* 2012, Nagele *et al.* 2012), down-regulation of photosynthesis (Wong *et al.* 2006), and increased desaturation of fatty acids (Miquel *et al.* 1993). DNA microarrays served traditionally as a method of surveying gene expression (Tarca *et al.* 2006, Wong *et al.* 2006), however new technologies such as RNA-Sequencing (RNA-Seq) are transforming the way transcriptomics are analysed. RNA-Seq is based on deep-sequencing techniques, where small 30–400 bp cDNA fragments converted from RNA are sequenced, down to one bp resolution (Wang *et al.* 2009). Several advantages arise from the use of this method, as it can reveal transcript sequence variations, or the precise location of transcript borders (Wang *et al.* 2009). Non-model organisms whose genome have not yet been sequenced can be analysed by RNA-Seq, as it does not depend on a genomic sequence template (Wang *et al.* 2009, Balakrishnan *et al.* 2012). In comparison to previous methods, e.g. microarrays, RNA-Seq provides an accurate method to assess the response of the entire transcriptome in any given condition, tissue, time or species (Giorgi *et al.* 2013, Lee *et al.* 2013, Calixto *et al.* 2018, Contreras-Lopez *et al.* 2018), thus, enabling the discovery of novel pathways and mechanisms that reflect the cellular response to stress in an unbiased approach (Calixto *et al.* 2018).

3.1.2 *Linking Cold, Photosynthesis and Lipid Metabolism*

Low temperature slows down the plant's metabolism by reducing the activity of enzymes, which can severely impair photosynthesis, with an observed impact on the Calvin Benson cycle, or photoinhibition of the photosystem II (PSII) (Goulas *et al.* 2006, Murata *et al.* 2007). Furthermore, adaption to cold environments can affect the stability and leakiness of the chloroplast thylakoid membranes, destabilising the structural organisation of the complex network of proteins associated with the photosystems, and ultimately photosynthesis (Eberhard *et al.* 2008).

The chloroplast is composed of an intricate system of internal thylakoid membranes (Figure 3.1), which are the site of the photosynthetic electron transport chain. Together with chlorophyll and proteins, lipids are the major components of thylakoids (Schaller *et al.* 2011, Kobayashi 2016), comprising 64% of the membrane composition (Koochak *et al.* 2019). The characteristic chloroplast lipid composition is based on the galactolipids MGDG and DGDG, the sulfolipid SQDG, and the phospholipid PG (Dormann and Benning 2002). These lipids are of such importance that galactolipid deficiency can have a detrimental effect on chloroplast development (Jarvis *et al.* 2000, Fujii *et al.* 2018). The thylakoids membranes are stacked to form the grana (grana core or stacked membranes) and connected by the stroma lamellae (Figure 3.1). In plants, glycerolipids are produced via the prokaryotic (plastidial) and the eukaryotic pathways, whilst the *de novo* synthesis of fatty acids in plants occurs in the chloroplast stroma [(Ohlrogge and Jaworski 1997), reviewed in Chapter 1]. In Arabidopsis, for example, glycerolipids synthetized through the eukaryotic pathway were found to be correlated with the development of functional guard cell chloroplasts with an impact on the guard cells responses to light (Negi *et al.* 2018). The double-envelope membrane is the chloroplast's interface with the cytosol, and it is involved not only in the synthesis of galactolipids, but also has an active role in the lipid trafficking to the ER (Dormann and Benning 2002, Benning 2008, 2009). However, different compositions can be found with the inner-envelope lipid profile being much like that of the thylakoid membranes, whilst the outer-envelop is almost exclusively composed of phosphatidylcholine (PC) [reviewed in (Botella *et al.* 2017)]. The lipid composition of the thylakoids, has also been proposed as mechanism that determines the distribution of the photosynthesis apparatus (Koochak *et al.* 2019), moreover, this could form part of a wider photoprotective role (Siegenthaler and Murata 1998). PSII and light-harvesting complex II (LHCII) are associated with the grana, whilst PSI and LHCI are usually associated with the connective stroma lamellae (Koochak *et al.* 2019). Evidence suggests that the lipid to photosynthesis-related protein ratio is thought to strongly influence the fluorescence

emission from LHCII (Akhtar *et al.* 2019). While the lipid environment *per se* might not be a determinant in the fluorescence quenching mechanisms, is it certainly a factor to consider as higher protein-to-lipid ratios showed stronger fluorescence quenching (Natali *et al.* 2016, Akhtar *et al.* 2019). Evidence for the relationship between temperature, photochemical performance and thylakoid membranes using mutant lines for the fatty acid desaturase *FAD7* and *FAD8* genes showed that a heat-induced rise of the chlorophyll fluorescence was correlated to the fluidity of the chloroplast thylakoid membranes (Tovuu *et al.* 2013). Another example is the *Chlamydomonas reinhardtii* mutant for MGDG-specific lipase PLASTID GALACTOGLYCEROLIPID DEGRADATION1 (PGD1) *pgd1* showed an altered ratio of proteins associated with the photosystems, and the accumulation of reactive oxygen species (ROS) increasing photodamage with environmental stresses (Du *et al.* 2018). As a consequence of stress-induced damage lipid peroxidation occurs, which concomitantly with the reduced activity of antioxidant enzymes can cause membrane damage (Djanaguiraman *et al.* 2010, Djanaguiraman *et al.* 2018)

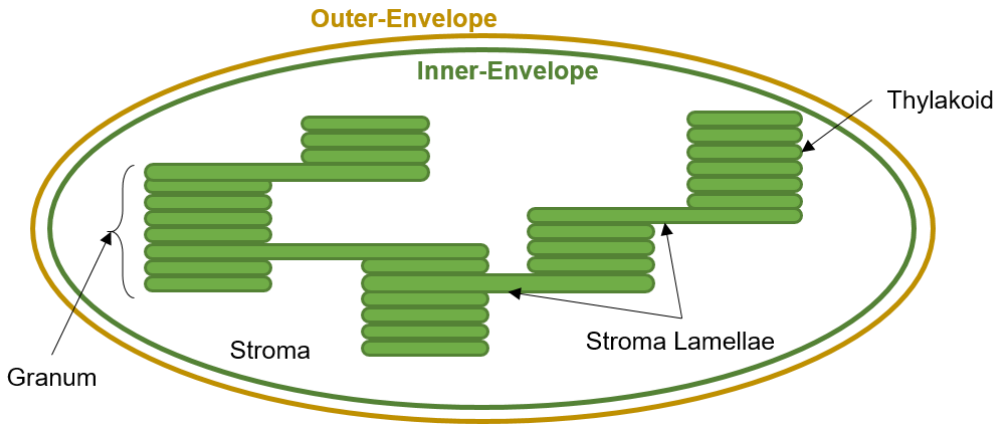

Figure 3.1 Chloroplast Structure

The chloroplast is enclosed by a double membrane denominated inner- and outer-envelope. In the chloroplast stroma, the thylakoids form appressed (granum) regions interconnected by non-appressed regions (stroma lamellae).

3.1.3 *Chlorophyll Fluorescence Assessment of Cold Stress*

Chlorophyll located in the thylakoid membranes of the chloroplast absorbs light energy and is associated with PSI and PSII forming protein-pigment reaction centres (Horton *et al.* 1996). The excitation energy within chlorophyll can then be directed to photosynthesis (photochemistry), dissipated as heat (non-photochemical quenching, NPQ) or re-emitted as a longer wavelength photon (fluorescence) (Maxwell and Johnson 2000, Murchie and Lawson 2013). To reduce the risk of damage of the photosystems, plants have several coping mechanisms that are activated, as thermal energy dissipation by NPQ, the xanthophyll cycle, and ROS production (Demmig-Adams 1990, Murata *et al.* 2007, Eberhard *et al.* 2008). NPQ is a photoprotective process ensuring the reduction of excess energy from the chlorophyll, reducing the probability of ROS production. NPQ is a multifactorial process, involving different components with specific regulation (Horton *et al.* 1994). Its dominant component is the energy-dependent non-photochemical quenching qE which is induced by an increase in the proton gradient (∆pH) across the thylakoid membrane (Wang *et al.* 2017). The ∆pH can be produced by the cyclic electron flow (CEF) around PSI regulated by the PGR5-PGR5L1 complex (PROTON GRADIENT REGULATION 5 – PGR5 LIKE1) and, in a minor proportion the NAD(P)H DEHYDROGENASE-LIKE (NDH) complex [(Munekage *et al.* 2002, Li *et al.* 2004, Yamori *et al.* 2011), for review (Yamori and Shikanai 2016)]. Other energy-dependent NPQ can be found in the conversion of violaxanthin to zeaxanthin (Demmig-Adams 1990, Zhang *et al.* 2012), or involving a PSII-associated protein PsbS, that can lead to conformational changes in the membrane. The hypothesis that the recovery of photoinhibition under low-temperature stresses might be accelerated by membrane lipids has also been proposed (Gombos *et al.* 1994, Vijayan and Browse 2002).

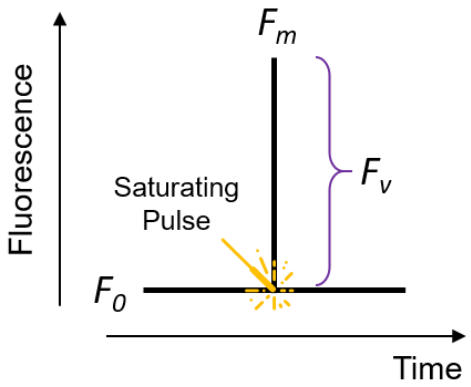

Figure 3.2 Chlorophyll Fluorescence Trace

Fluorescence trace in a dark-adapted leaf, the minimal fluorescence (F_0) is measured when the reaction centres are opened, which with the introduction of a saturating light pulse (■) close and the maximal yield of fluorescence (F_m) is obtained. The variable fluorescence (F_v) can then be calculated through $F_m - F_0$, and the maximum quantum efficiency of the PSII calculated as F_v/F_m.

Chlorophyll fluorescence analysis is based on the principle that photosynthesis (photochemistry), NPQ and fluorescence are competing processes. Thus, their responses to *stimuli* will be proportional to each other allowing extrapolations in the assessment of the metabolic state of the plant (Maxwell and Johnson 2000, Oxborough 2004, Ruhle *et al.* 2018). Critically, the yield of the chlorophyll *a* fluorescence from PSII can be easily measured and allows separation of non-photochemical (re-emitted heat) and photochemical (photosynthesis) or quenching (dissipation) processes, allowing an accurate indication of how much absorbed light energy is partitioned to photoprotection and how much is used for photosynthesis (Schreiber *et al.* 1986, Maxwell and Johnson 2000, Baker and Rosenqvist 2004, Murchie and Lawson 2013). This technique measures chlorophyll fluorescence readily as re-emitted light, and provides a rapid and non-invasive screening technique, which yields a high number of parameters from both single and complex measurements (Murchie and Lawson 2013). The chlorophyll fluorescence analysis is based on the transient rise in the chlorophyll fluorescence (F_v) when a saturating light pulse is applied (Figure 3.2). The dark adaptation period leads to the maximal plastoquinone A (Q_A) oxidation (or opened reaction centres) at which point the minimum

fluorescence (F_0) can be assessed. The light pulse is then applied, which saturates Q_A (saturating the reaction centres) and maximum chlorophyll fluorescence (F_m) is obtained [further review in (Murchie and Lawson 2013)]. Environmental stresses are a constraint to the photosynthetic performance, with an impact on the plant's health that can be observed by the number of mechanisms evolved to avoid damage. Chlorophyll fluorescence is thus capable of sensitively identifying differing responses to stress, as a measure of plant performance and health (Barbagallo *et al.* 2003, Murchie and Lawson 2013, Silvestre *et al.* 2014).

3.1.4 *Chapter Aims*

Arabidopsis and Eutrema transcriptome changes in response to three days of cold acclimation were assessed by RNA-Seq[2]. As a valuable pool of information on the specific response of the plants to the cold acclimation process, the significantly responding transcripts were analysed with the aim of identifying new lipid-related players in the plant's response to cold stress. As the agreed plant model, Arabidopsis has resources available that allow rapid gene identification, these resources are not as well developed for other plant models such as Eutrema. The T-DNA insertional mutants in the SALK or GABI-Kat collections are such examples of Arabidopsis resources (Alonso 2003, Kleinboelting *et al.* 2012, Bolle *et al.* 2013). Thus, in the present chapter (see Figure 3.3 for experimental workflow) the Arabidopsis transcriptome changes were used as a resource for the identification of genes with a novel lipid-related function in the plant's acclimation process. For this, a list of candidate genes was produced with a focus on lipid-related functions. However, whenever possible a parallel will be established with the Eutrema RNA-Seq results (Appendix 3). As a holistic approach to analyse the impact of the selected genes in the plant's health state, an imaged chlorophyll *a* fluorescence technique was used as a cold stress screen.

[2] The RNA-Seq analysis was performed previously by Cristina Barrero-Sicilia, Louise V. Michaelson, and Richard P. Haslam, and the results were kindly shared with Susana Silvestre for analysis and interpretation.

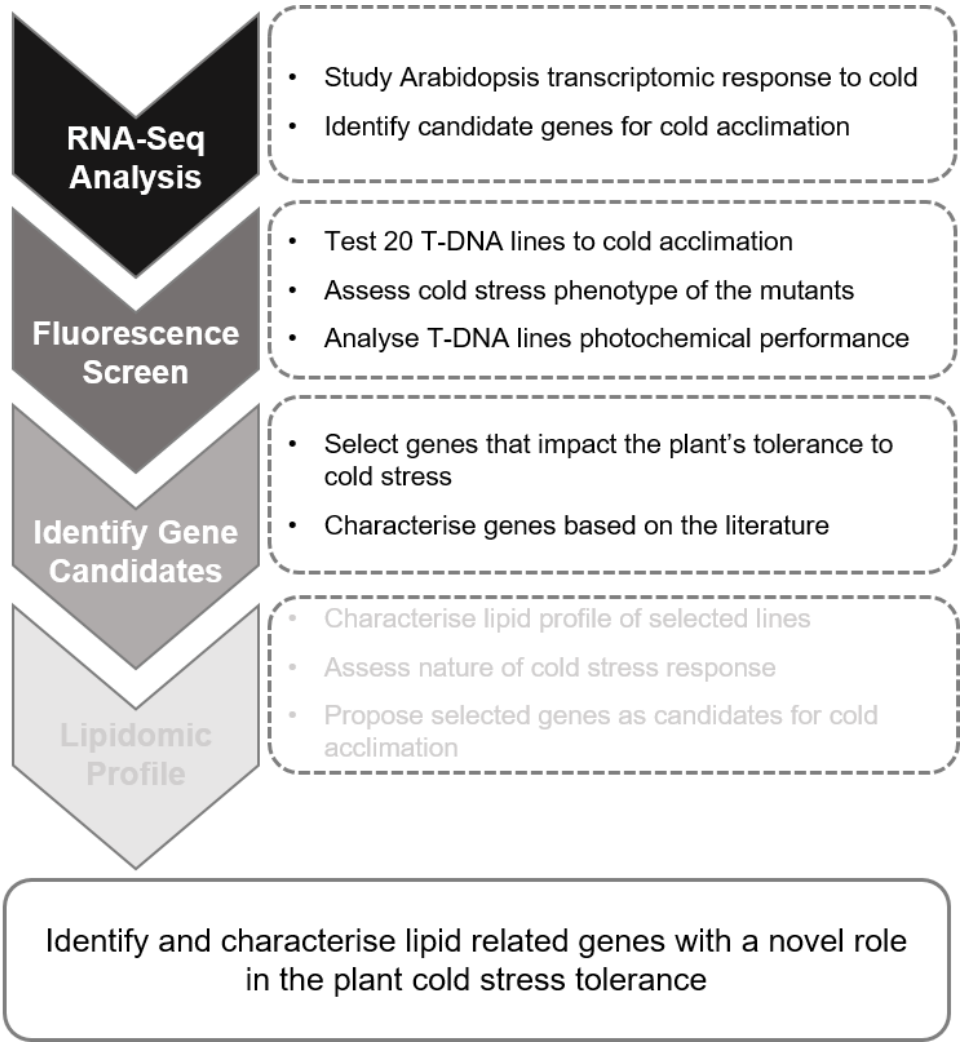

Figure 3.3 Arabidopsis Cold Acclimation Workflow

The figure shows the workflow planned to achieve the aims proposed for this chapter which culminates into the identification of cold responsive gene candidates ("Identify Gene Candidates"). Whilst the Lipidomic profile section is developed in Chapter 4.

To test the technique and complement the screen, known cold responsive and photosynthesis related genes were included as positive controls. The homozygous T-DNA lines were obtained and confirmed by PCR, and their phenotype under low temperature was assessed. The screen was performed in randomized block design to allow the measurement of the chlorophyll fluorescence quenching, which produced data on the photochemical and non-photochemical quenching response to cold stress of the candidate lines in comparison with wild-type Arabidopsis Col-0. In addition, quantification of chlorophyll, total carotenoids, and ion leakage measurements were performed to

complement the fluorescence screen data. The fluorescence technique enabled the quantitative and qualitative assessment of the impact of cold stress in the T-DNA lines, from which two gene candidates were identified as a having a significant impact on plant photosynthetic capacity, *PES1* and *PGR5L1A.*

3.2 RESULTS

3.2.1 *Transcriptomic Adaptation to Cold Stress in Arabidopsis*

The analysis of Arabidopsis transcriptomic changes with exposure to cold stress used RNA-Seq. The analysis was previously performed by Cristina Barrero-Sicilia, Richard P. Haslam, and Louise V. Michaelson (results not published), and kindly provided as a unique database. For this experiment, plants were grown under control conditions (Section 2.2.3) and exposed to cold temperatures at 4°C (Section 2.2.4) for three days. Leaves of 22 DAS plants were harvested for total RNA extraction from both control and cold stress, and RNA-Seq analysis performed. TruSeq RNA libraries were made and run of four lanes of 100 bp paired end Illumina Hi-Seq 2500 in Rapid run mode, generating 41-83 million reads per sample. Data was analysed by differential changes in the fold change with cold stress [Figure 3.4, (Love *et al.* 2014)].

The analysis of the cold stress transcriptome yielded approximately 25000 genes with aligned reads to Arabidopsis (Figure 3.4), revealing its tendency to upregulate more genes with higher fold change, than the downregulated ones. With the upregulated pool reaching $\log_2$ fold change values higher than +8, whilst in the downregulated pool only one read showed a fold change lower than -4. This could be interpreted as the plant's strategy to activate genes that would actively contribute to its tolerance response. This analysis was the source of lipid related genes of interest with a possible role in the plant's ability to cope with cold stress. These were firstly chosen from the differentially expressed genes (DEGs) pool with fold change values higher or lower than +2.0 or -2.0, respectively, representing a significant effect caused by cold stress.

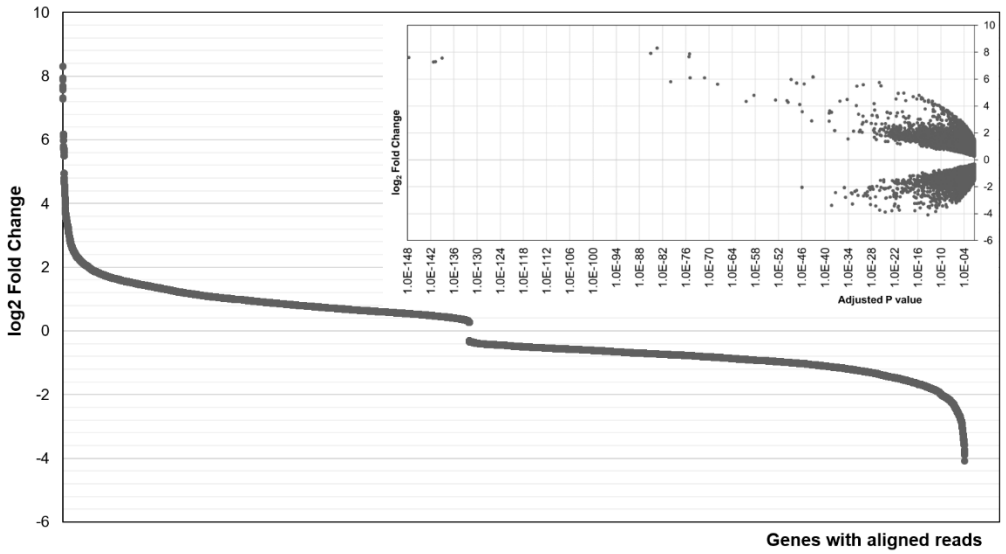

Figure 3.4 Fold Change of the Genes with Aligned Reads

Log_2 fold change distribution of the genes with aligned reads in Arabidopsis Col-0 after three days cold acclimation. The insert shows the distribution of the *p* value with the log_2 fold change. Measurements were performed in 22 DAS rosette leaves, N=5, under control conditions (23°C) and cold (4°C, details in Sections 2.2.3-2.2.4).

3.2.2 *Selection of the Candidate Genes*

The starting point for the selection of candidate genes of interest were the DEG pools higher or lower than +2 or -2 log_2 fold change (Figure 3.4). Lipids have a crucial role in cold stress adaptation strategies (Li *et al.* 2004, Li *et al.* 2008, Du *et al.* 2010, Moellering *et al.* 2010, Li *et al.* 2019), so it was decisive that the DEGs selected had a related lipid function. An extensive *in silico* analysis was undertaken to confirm the function of selected candidate genes, including searches in the databases TAIR (https://www.arabidopsis.org/), UniProt (https://www.uniprot.org/), and published literature (https://www.ncbi.nlm.nih.gov/). A list of lipid-related gene candidates was formulated from these criteria as potentially associated with cold acclimation. A myriad of functions within lipid metabolism arose, e.g., lipid transfer proteins, lignin biosynthesis or chloroplast associated. To screen these genes for a real impact in the plant's ability to cope with stress, which often translates in the plant's health state, chlorophyll *a* fluorescence imaging technique was chosen as a screen method. To avoid a biased analysis of the screen results,

photosynthesis related genes of interest were included from the original pools of DEGs. The final list included in the screen comprised the genes *ELIP1*, *ELIP2*, *ELIP1ELIP2*, *GSTU17*, *PGR5-LIKE1A*, and *PGR5-L1B*. Furthermore, as the aim was to characterise the phenotype under cold stress, the same was done for DEGs with a cold-related function. *AZI1, COR15A, COR15B,* and *LTR* were included as a control for the cold stress response. Table 3.1 shows the 18 genes resulting from this selection ordered by the $\log_2$ fold change, with a summary of the respective function. As individual gene activity can be identified by its mutant phenotype, the respective T-DNA insertion lines were obtained (Section 2.1), and grown together under the same control conditions, allowing the identification of homozygous T-DNA lines (Appendix 4). The resulting seeds were bulked together per T-DNA line and used for the subsequent experiments. This enabled higher uniformity within and between lines, reducing potential priming effects from previous unknown growth conditions (Bruce *et al.* 2007).

3.2.3 *Lipid, Photosynthesis and Cold Related Genes*

The lipid related DEGs from the upregulated pool and included in the cold screen were *PES1* (*PHYTYL ESTER SYNTHASE 1*), two *LIPID TRANSFER PROTEIN 3* and *4* (*LTP3* and *LTP4*), an *ACYL-CoA DESATURASE-LIKE 4* (*ADS4*), a sphingolipid metabolism gene *IPCS3* (*INOSITOL PHOSPHORYLCERAMMIDE SYNTHASE 3*), and a 3-hydroxyisobutyryl-CoA hydrolase-like protein referred here as *FABO* (Table 3.1). *PES1* is a chloroplast enzyme involved in the chlorophyll degradation process by channelling the resulting free phytol, an isoprenoid alcohol highly toxic to membranes and proteins, for the production of phytyl esters (Ischebeck *et al.* 2006, Lippold *et al.* 2012). This function has been reported to be important under stresses that lead to the chlorophyll degradation, such as senescence or nitrogen deficiency (Gaude *et al.* 2007). The lipid transfer proteins differentially expressed *LTP3* and *LTP4* shared 81.9% sequence similarity between their 115 and 112 amino acid proteins, respectively. These proteins

belong to a 100-member family in Arabidopsis, distributed into four major groups (Chae *et al.* 2009), and can exchange lipids between membranes. Several functional roles have been described in the literature for these two homologues, indicating their importance for plant lipid metabolism (Molina and GarciaOlmedo 1997, Pagnussat *et al.* 2015, Gao *et al.* 2016). Of interest, LTP3 was shown to be positively regulated by the transcription factor MYB96, and has been associated with abiotic stress responses, such as drought, and when overexpressed led to enhanced freezing tolerance in Arabidopsis (Seo *et al.* 2011, Guo *et al.* 2013). Whilst LTP4 was first described in barley as involved in pathogen resistance (Molina and Garcia-Olmedo 1993). *ADS4* is from a predicted annotation of *ACYL-COA DESATURASE LIKE*4 (Harris *et al.* 2004, Harris *et al.* 2006, Gaudet *et al.* 2011), comprising five exons coding for a 300-amino acid peptide localised in the ER membrane. In rice, *LTP7* and *LTP10* were found to be upregulated under cold temperatures in two tolerant varieties (de Freitas *et al.* 2019). The acyl-CoA desaturase-like (ADS) family in Arabidopsis has nine members involved in diverse metabolic functions with ADS1 involved in the cold acclimation of Arabidopsis (Smith *et al.* 2013, Chen and Thelen 2016, Yang *et al.* 2017). ADS4 was associated with *n*-6 (site of introduction of the double bond relative to the end of the molecule) fatty acids, with the VLCFAs 24:1(*n*-6) and 26:1(*n*-6) found in yeast cells when expressing *AtADS4* (Smith *et al.* 2013). Recently, *ADS4* was identified as the previously described mutant *cer17* that displayed a thick and irregular cuticle, with increased content of cutin monomers showing its involvement in wax synthesis (Yang *et al.* 2017). *FABO* (At4g31810) was described as a 3-hydroxyisobutyryl-CoA hydrolase, with a Gene Ontology (GO) biological process of fatty acid beta-oxidation (Harris *et al.* 2004, Harris *et al.* 2006, Gaudet *et al.* 2011). It has a gene structure consisting of 14 exons coding for a peptide of 409 amino acids, which includes a mitochondrion transit peptide in the first 26 amino acids. *IPCS3* was the last of the upregulated pool of DEGs to be added to the list, its fold change value was lower than the defined +2 threshold (Table 3.1), however, due to its nature as a functionally uncharacterised sphingolipid related gene it was included in

our screen. Three isoforms of the inositol phosphorylceramide synthases (IPCS) catalyze a crucial step in sphingolipid biosynthesis by transferring a phosphorylinositol group from phosphatidylinositol (PI) to phytoceramide [(Wang *et al.* 2008, Mina *et al.* 2010), Chapter 1]. *IPCS3* was previously shown to be highly expressed in stems and flowers of Arabidopsis, whilst *IPCS2* was shown to be ubiquitous (Mina *et al.* 2010). Recently, a study of the transcriptome of Arabidopsis lines overexpressing the *IPCS* genes revealed their potential role in the plant's ability to cope with biotic and abiotic stress (Pinneh *et al.* 2019, Pinneh *et al.* 2019). In the analysis of the RNA-Seq data, however, only *IPCS3* was shown to be upregulated after three days of cold stress, as both isoforms *IPCS1* and *IPCS2* were downregulated with a fold change value of -1.40 and -0.94, respectively. This result was unexpected and contributed to the inclusion of this gene in the selected DEGs to be screened.

From the downregulated pool three lipid related genes were selected, *CYP74B2* (or *HPL1*, *HYDROPEROXIDE LYASE 1*), the *CELLULOSE SYNTHASE-LIKE 1 CSLA1*, and *SFR2* (*SENSITIVE TO FREEZING 2*) (Table 3.1). *CYP74B2* or *HPL1* is a hydroperoxide lyase that uses lipid hydroperoxides for volatile production essential for signalling in biotic and mechanical stresses (Bate *et al.* 1998). Recently found to be a key regulator in oxylipin biosynthesis, which play a signalling role for different stresses, such as low temperatures (Vu *et al.* 2012, Vu *et al.* 2014, Nilsson *et al.* 2016). *CSLA1* belongs to one of six families structurally related to the cellulose synthase superfamily in Arabidopsis (Richmond and Somerville 2000). CSLA glycosyltransferases are thought to be involved in the synthesis of mannan and glucomannan essential in cell wall composition (Liepman *et al.* 2005, Goubet *et al.* 2009). *AtCSLA1* has a glycosyltransferase-like family 2 functional annotation (PF13641) for its 401-amino acid peptide with a transmembrane helix domain. However, no published functional analysis on the specific role of *AtCSLA1* in plant metabolism was found. The downregulation of this gene is an interesting response to cold by the plant, as the plant cell wall participates in the

plants response to cold by attenuating physical deformations caused by freezing. The *SENSITIVE TO FREEZING 2* gene was firstly discovered to be a β-glucosidase, essential for freezing tolerance in Arabidopsis (Thorlby *et al.* 2004). *SFR2* seems to be activated by changes in the cytosolic pH and Mg^{2+} concentration, which are proposed to act as a signalling mechanism for freezing stress (Barnes *et al.* 2016). SFR2 is then targeted to the chloroplast envelop (Fourrier *et al.* 2008) where it sequentially transfers galactosyl residues forming oligo-galactolipids, which are further converted into TAG (Moellering *et al.* 2010, Vu *et al.* 2014). This change in the lipid content alters the galactolipid ratio leading to a remodelling of the outer chloroplast membrane (Moellering *et al.* 2010). Interestingly, in the present RNA-Seq analysis *SFR2* was shown to be downregulated after three days in the cold. Still, *SFR2* was included in the cold stress screen, despite showing a fold change value outside the stipulated threshold i.e. lower than -2 for the downregulated pool.

All the photosynthesis related DEGs selected were upregulated with cold stress (Table 3.1), apart from *PROTON GRADIENT REGULATOR 5 - LIKE A* and *B* (*PGR5L1A* and *PGR5L1B*). Interestingly, these were expected to be upregulated as they were previously described as crucial to the efficient CEF around PSI (DalCorso *et al.* 2008, Hertle *et al.* 2013). This flow is essential for the induction of photosynthesis under stress conditions where metabolic sinks for electrons are limited such as drought, high light or low carbon dioxide (CO_2) (Clarke and Johnson 2001, Munekaga *et al.* 2004). These two genes were then included in the screen to ascertain their role in cold acclimation. The *EARLY-LIGHT INDUCIBLE PROTEINS 1* and *2* (*ELIP1* and *ELIP2*) showed quite high level of upregulation, in accordance with previous reports of accumulation of both proteins under 4°C, and a higher transcription level of *ELIP2* (Casazza *et al.* 2005), including in the extremophile Eutrema (Benina *et al.* 2013). The *GLUTATHIONE S-TRANSFERASE U17* (*GSTU17*) was also found to be upregulated after three days of cold stress, it has been described as involved in light signalling, and as a

negative component in salinity and drought stress signalling (Chen *et al.* 2012).

The selected cold related genes followed the same upregulated pattern as the photosynthesis DEGs (Table 3.1). The highest expression levels were shown by *AZI1* (*AZELAIC ACID INDUCED 1*), followed by the *COLD-REGULATED15, COR15A* and *COR15B*. *AZI1* is involved in systemic acquired resistance mechanisms in Arabidopsis (Cecchini *et al.* 2015), thought to be a key component of the plant's response to cold stress and the increased freezing tolerance in the yeast *Saccharomyces cerevisiae* (for details see (Xu *et al.* 2011)). The cold-regulated genes *COR15A* and *COR15B* are established in the literature (Wilhelm and Thomashow 1993, Baker *et al.* 1994, Artus *et al.* 1996, Thomashow *et al.* 1996, Uemura *et al.* 1996, Steponkus *et al.* 1998, Liu *et al.* 2014, Thalhammer *et al.* 2014). Both genes are encoded in the nucleus sharing 82% sequence identity and localised in the chloroplast where they interact with the inner envelope membrane maintaining its structure (Wilhelm and Thomashow 1993, Uemura *et al.* 1996, Thalhammer *et al.* 2014). The gene referred to here as *LTR* was identified as a member of a low temperature and salt responsive protein family in the TAIR database and according to Araport11 (Lamesch *et al.* 2012, Cheng *et al.* 2017). Whilst also being reviewed as a proteolipid membrane potential modulator due to its PFAM PF01679 annotation. The *LTR* (At4g30650) coding sequence (CDS) consists of 222 nucleotides, corresponding to two exons that code for a, small, 73-amino acids peptide. In the presented transcriptomic analysis showed a $\log_2$ fold change value of 2.904 (Table 3.1). This was considered a significant effect, and together with its annotation for low temperature response and membrane domain, was considered an interesting addition to the candidate DEGs of interest.

Table 3.1 Genes of Interest Selected from Transcriptomic Analysis

Log_2 FC, logarithmic fold change of each gene after three days of cold acclimation compared to control conditions; *P* value, adjusted *p* value for each log_2 fold change; AGI, Arabidopsis locus identifier; Colour code represent genes with a related function to lipids (■), photosynthesis (■), and cold (■).

Log_2 FC	*P* value	AGI	Gene	Protein	Function
8.305	3.58^{e-84}	At4g12470	*AZI1*	AZELAIC ACID INDUCED 1	Key role in Arabidopsis response to low temperature, and enhanced freezing tolerance of *S. cerevisiae* (Xu *et al.* 2011). Also involved in systemic immunity (Jung *et al.* 2009, Cecchini *et al.* 2015)
7.609	2.18^{e-148}	At4g14690	*ELIP2*	EARLY LIGHT-INDUCIBLE PROTEIN 2	Biogenesis of chlorophyll-binding complexes (Casazza *et al.* 2005, Rizza *et al.* 2011)
6.096	6.68^{e-72}	At3g22840	*ELIP1*	EARLY LIGHT-INDUCIBLE PROTEIN 1	Inhibits the chlorophyll biosynthesis pathway for photoprotection (Casazza *et al.* 2005, Rizza *et al.* 2011)
5.809	1.19^{e-80}	At2g42540	*COR15A*	COLD-REGULATED 15A	Targeted to the chloroplast, and suggested to be involved in the shift of the melting curves of phospholipids containing membranes to low temperature (Baker *et al.* 1994, Artus *et al.* 1996, Steponkus *et al.* 1998)
4.417	1.52^{e-50}	At2g42530	*COR15B*	COLD-REGULATED 15B	Chloroplast protection during freezing, prevents protein aggregation and attenuates enzyme activation (Wilhelm and Thomashow 1993, Liu *et al.* 2014)
2.904	3.66^{e-44}	At4g30650	*LTR*	LOW TEMPERATURE & SALT RESPONSIVE	Low temperature and salt responsive protein family
2.501	3.53^{e-23}	At4g31810	*FABO*	3-HYDROXYISOBUTYRYL-COA HYDROLASE-LIKE PROTEIN 2	ATP-dependent caseinolytic protease family protein. Involved in valine degradation pathway (Gipson *et al.* 2017)

(Continued on the next page)

Log_2 FC	*P* value	AGI	Gene	Protein	Function
2.311	1.96^{e-12}	At1g10370	*GSTU17*	GLUTATHIONE S-TRANSFERASE U17	Light signalling, de-etiolation, response to salt and drought (Chen *et al.* 2012)
2.286	8.19^{e-16}	At1g54570	*PES1*	PHYTYL ESTER SYNTHASE 1	Phytyl ester synthesis and diacylglycerol acyltransferase activities involved in the maintenance of integrity of photosynthetic membrane during abiotic stress (Gaude *et al.* 2007, Lippold *et al.* 2012)
2.236	1.39^{e-03}	At5g59320	*LTP3*	LIPID TRANSFER PROTEIN 3	Transfer phospholipids and galactolipids across membranes. Mediates freezing tolerance as a target of MYB96 (Seo *et al.* 2011, Guo *et al.* 2013)
2.129	7.94^{e-05}	At5g59310	*LTP4*	LIPID TRANSFER PROTEIN 4	Transfer phospholipids and galactolipids across membranes. May act in a redundant way with LTP3 regulating ABA signalling (Molina and Garcia-Olmedo 1993, Gao *et al.* 2016)
2.056	2.83^{e-03}	At1g06350	*ADS4*	ACYL-COA DESATURASE LIKE 4	Fatty acid desaturation on the n-6 position of the VLCFAs (Smith *et al.* 2013, Yang *et al.* 2017)
1.070	6.67^{e-09}	At2g29525	*IPCS3*	INOSITOL PHOSPHORYLCERAMIDE SYNTHASE 3	Transfer of a phosphorylinositol group from PI to phytoceramide, involved in response to stress (Mina *et al.* 2010, Pinneh *et al.* 2019, Pinneh *et al.* 2019)
-0.421	3.00^{e-03}	At3g06510	*SFR2*	SENSITIVE TO FREEZING 2	Beta-glucosidase and galactosyltransferase activity. Mutants are sensitive to freezing. (Thorlby *et al.* 2004, Fourrier *et al.* 2008, Moellering *et al.* 2010, Barnes *et al.* 2016)

(Continued on the next page)

Log_2 FC	*P* value	AGI	Gene	Protein	Function
-1.10	8.84^{e-09}	At4g22890	*PGR5L1A*	PROTON GRADIENT REGULATION 5-LIKE 1A	Thylakoid transmembrane protein, similarly to PGR5 it is involved in the cyclic electron transport in PSI. Homologous isoform to *PGR5L1B* (DalCorso *et al.* 2008, Hertle *et al.* 2013)
-1.79	4.73^{e-11}	At4g11960	*PGR5L1B*	PROTON GRADIENT REGULATION 5-LIKE 1B	Homologous isoform to *PGR5L1A* (DalCorso *et al.* 2008, Hertle *et al.* 2013)
-2.086	9.08^{e-11}	At4g15440	*CYP74B2 (HPL1)*	HYDROPEROXIDE LYASE 1	Hydroperoxide lyase that produces oxylipins, stress signalling molecules (Bate *et al.* 1998, Vu *et al.* 2012, Vu *et al.* 2014, Nilsson *et al.* 2016)
-3.729	1.61^{e-21}	At4g16590	*CSLA1*	CELLULOSE SYNTHASE-LIKE A1	Mannan and glucomannan biosynthesis in the cell wall (Liepman *et al.* 2005, Goubet *et al.* 2009)

3.2.4 *Cold Screen Design*

To account for the variety of functions of the selected genes of interest, a holistic approach to test the selected genes with an impact in the plant performance was required. Thus, an imaged chlorophyll *a* fluorescence test was setup using a PSI© FluorCam (Figure 3.5 B). As the imaged area of the FluorCam chamber was of approximately 1 x 1.5 m it allowed for 48 potted Arabidopsis plants to be imaged at any given time, which translated in two trays each fitting up to 24 plants (35 x 25 cm tray).

A complete randomised block design (CRBD) was applied to minimise any effects of localisation of the plants in the tray, the position of the tray in the growth chamber, or measurement bias caused by the imaged area of the PSI© FluorCam (Figure 3.5 B). The CRBD consisted of three blocks of two trays each, and within each block two replicates per genotype were randomly distributed, a total of six replicates per genotype (one replicate equals one plant, six plants per genotype in total, Figure 3.5 A). This design allowed for each block (two trays) to be measured at the same time. The 19 T-DNA insertion lines for the final selected genes were grown together with the wild-type Col-0 under control conditions at 23°C (Section 2.2.3) for 18 to 20 days. For the cold stress period the trays were moved to 5°C (Section 2.2.4) for eight days, after which they were recovered to control temperature for three days. A control measurement was performed before plants were moved to 5°C (on the last day of control temperature), and cold stress measurements were performed each day of the eight days of stress. The RNA-Seq experiment was performed after three days of cold acclimation (Section 3.2.1), however eight days were found to suit the identification of two genotypes with a significantly reduced performance under cold stress as assessed and discussed below.

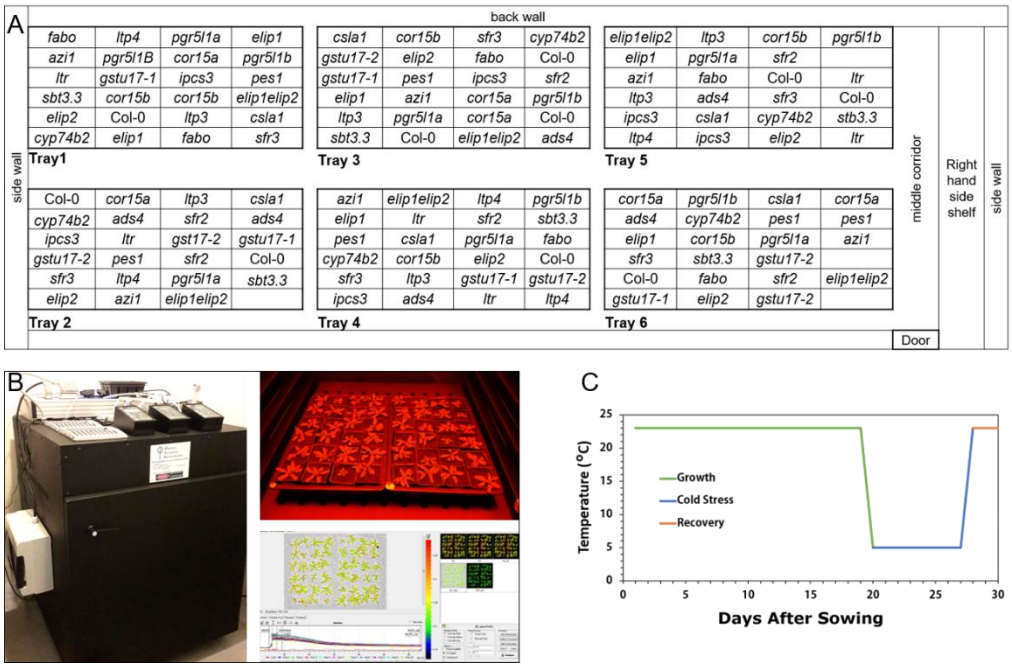

Figure 3.5. Cold Screen Design to Test the Mutant Lines

(A) Trays map for the Arabidopsis T-DNA genotypes and the wild-type Col-0 distributed according to a CRBD in three blocks of two trays each, with six replicates per line. Each tray was moved every other day to homogenise growth environment. (B) PSI© FluorCam (left), imaged area showing two trays fitted (top right), and FluorCam 7.0® software used to analyse data (bottom right). (C) Graphical representation of the experimental design where plants were grown for 18-20 DAS under control temperature (23°C, —), followed by eight days of cold stress (5°C, —), and recovered to control temperature (23°C, —).

3.2.5 *Two Mutant Lines were Susceptible to Cold Stress*

The cold stress screen of the selected lines was performed using the PSI© FluorCam quenching protocol (details in Section 2.6.3) to monitor the dynamics of the chlorophyll *a* fluorescence, and in particular the maximum quantum efficiency of the PSII (F_v/F_m). F_v/F_m was used to discriminate the mutant lines that showed decreased photochemical performance after eight days of cold, when compared to the wild-type Col-0 (Figure 3.6). F_v/F_m is a widely-used parameter, and as a ratio any reduction reflects the impaired capacity of the plant to cope with stress (de Freitas *et al.* 2019). The observed decreases can be explained by photodamage to the PSII reaction centres, along with the development of quenching processes (Barbagallo *et al.* 2003, Baker and Rosenqvist 2004, Murchie and Lawson 2013). Fluorescence was measured at 19

DAS at control temperature of 23°C, and every day of the eight days of 5°C cold stress. Figure 3.6 shows the results obtained for F_v/F_m in a quantitative (panel A) and qualitative (panel B) manner. Eight days of exposure to cold were necessary for a significant effect on the plants' acclimation (Figure 3.6 A). However, the qualitative panel allowed to visually analyse the evolution of individual plants performance with the continued exposure to cold temperature (Figure 3.6 B). A F_v/F_m value in control conditions of ~0.830 was previously established for all C3 plants (Bjorkman and Demmig 1987). In this screening experiment F_v/F_m was shown to gradually decrease, and a minimum of 0.765 was observed after the eight days of cold stress. While all the mutant lines tested in this screen showed a decrease in F_v/F_m with cold stress, only *pes1* and *pgr5l1a* showed a significant decrease compared to the wild-type Col-0 under the same conditions ($p<0.05$ and $p<0.001$, respectively; Figure 3.6 A). The response of F_v/F_m in *pes1* and *pgr5l1a* to cold stress was quite interesting, as PES1 is a chloroplastidial enzyme involved in the chlorophyll degradation pathway, also associated with stress (Ischebeck *et al.* 2006, Gaude *et al.* 2007, Lippold *et al.* 2012). While *PGR5L1A* is involved in the CEF around PSI as an energy dissipation mechanism (DalCorso *et al.* 2008, Hertle *et al.* 2013), which was originally found to be downregulated in the RNA-Seq experiment (Section 3.2.3). The fact that two lines with a mutation in a chloroplast related gene were found to underperform in a screen that measures chlorophyll fluorescence could suggest a biased screen technique. Nevertheless, other lines with a T-DNA insertion in chloroplast targeting genes were included in the screen, as for example the three *ELIP* mutants, *sfr2* or *pgr5l1b*, the isoform to *pgr5l1a*, without demonstrating a significant impact on their performance compared to the wild-type.

The quenching protocol used for the analysis of the cold acclimation of the T-DNA lines allowed for the calculation of other parameters (Section 2.6.3). The effective quantum yield of PSII (ΦPSII) was thus obtained and results are presented in Figure 3.7. This parameter can be calculated using the measured steady-state fluorescence parameters under light,

reflecting the proportion of light energy that is effectively used by the PSII (Genty *et al.* 1989). In this experiment, ΦPSII was more variable than the F_v/F_m under control conditions with an observed decrease of ΦPSII in the T-DNA lines *cor15a*, *csla1* and *ipcs3*. However, under stress conditions only *pes1* and *pgr5l1a* showed a decreased ΦPSII, with an average lower than Col-0 95% confidence interval (CI). Observed changes in F_v/F_m,

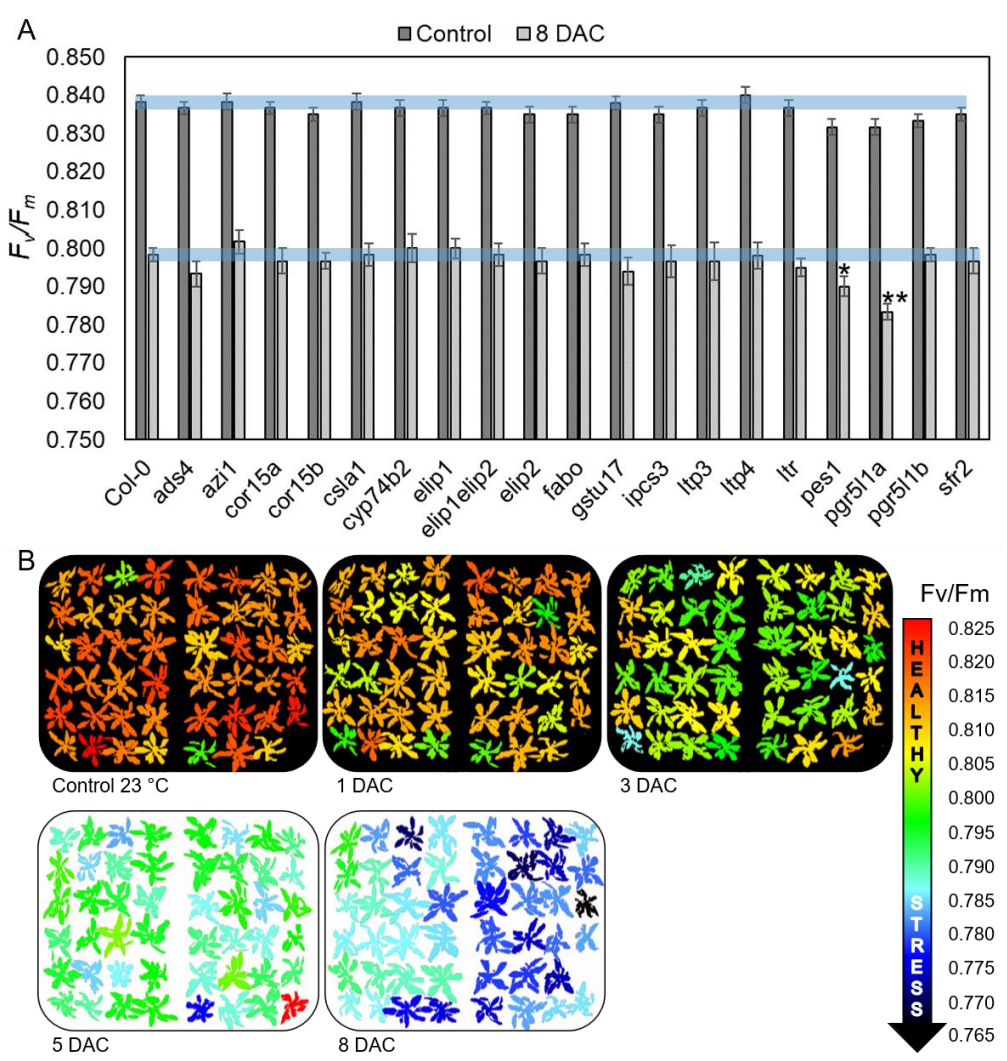

Figure 3.6. Maximum Quantum Efficiency of Photosystem II

(A) Quantitative assessment of the maximum quantum efficiency of photosystem II (F_v/F_m) for the Arabidopsis mutants against the wild-type Col-0 under control 23°C (■) and after eight days of cold stress at 5°C (8 DAC, ■). Bars represent mean ± standard error for six replicates per genotype. The mutant lines were tested against Col-0 using a two-sample unpaired t-test, (*) p<0.05, (**) p<0.001; (■) Col-0 standard error for each of the conditions. (B) Qualitative assessment of the F_v/F_m for the mutant lines at control 23°C, and at one, three, five and eight DAC at 5°C. Artificial colours illustrate F_v/F_m values for representative plants.

reflected an impact of cold stress on effective PSII efficiency in the T-DNA insertion lines. NPQ is a measure of the excess energy dissipation through heat, a photoprotective mechanism employed by plants when the absorbed light energy exceeds the capacity of photosynthesis to use it (Ruban *et al.* 2012). It is calculated by the ratio change of the maximum fluorescence under light and dark conditions [(Bilger and Bjorkman 1990), equations in Section 2.6.3]. NPQ showed a small increase with stress in all the lines, including the wild-type (Figure 3.8 A). Interestingly, some of the lines showed lower NPQ values than Col-0 under control conditions, for example *cor15b*, *ltr* and *pgr5l1a*. However, this relationship was only maintained for *pgr5l1a* after eight days of cold stress, which still showed an NPQ lower than Col-0. Suggesting the impairment of dissipation of energy by heat in this mutant, due to the contribution of PGR5L1A to the ∆pH through CEF required to trigger NPQ (Munekage *et al.* 2002, Ruban *et al.* 2012). In the same cold conditions, however, the mutant lines *csla1*, *elip1* and especially *ipcs3* showed higher levels of NPQ than the wild-type Col-0 (Figure 3.8 A).When the photosynthetic electron flow is saturated the yield of fluorescence rises, which translates into the redox state of the PSII determined by the photochemical quenching [qP, (Horton *et al.* 1994, 1996)]. The qP and the fraction of open reaction centres in PSII (qL) were also calculated, adding to the characterisation of the photochemical behaviour of the mutant lines. The qP decreased to an average of 55.8% after the eight days of cold stress, where Col-0 showed the lowest decrease of 53.3% whilst *ipcs3* showed the highest with 58.6% (Figure 3.8 B). The open reaction centres in the PSII reflected the results for qP, with an average decrease of 58.3%, only this time the mutant *pgr5l1a* showed the largest decrease of 61.4% (Figure 3.8 C).

3.2.6 *Chlorophyll Content was Reduced by Cold Stress*

Pigment content was measured to assess the effect of cold, and determine if any of the changes observed in the fluorescence results could be correlated to an impact on the chlorophyll or carotenoid

production caused by cold (Demmig-Adams 1990). Chlorophyll content was indeed affected by the eight days of stress imposed, reduced on average by a total of 25% (Figure 3.9 A-C). The mutant *pes1* was the one expected to show an increased accumulation of chlorophyll, especially under stress due to its role in the chlorophyll degradation pathway (Lippold *et al.* 2012). This was verified, with an accumulation of chlorophyll in *pes1* after eight DAC compared to Col-0, however not to such an extent that might be considered significant, i.e. *cor15a*, *csla1* or *sfr2* showed higher chlorophyll content that either *pes1* or Col-0. Carotenoids, especially the xanthophyll cycle components zeaxanthin, violaxanthin and antheraxanthin are known to be involved in the NPQ mechanism of energy dissipation (Bilger and Bjorkman 1990, Demmig-Adams 1990). Synthesis of zeaxanthin can be activated as a photoprotective mechanism increasing qE, the fast energy-dependent NPQ component induced by the increased ∆pH across the thylakoid membrane under stress conditions (Wang *et al.* 2017, Pinnola and Bassi 2018). The analysis of the T-DNA lines showed small changes in the total carotenoid content with a general tendency to be reduced by cold stress (Figure 3.9 D). This may reflect a general metabolic slowdown under such conditions, with the down-regulation of the photosynthesis. On the contrary, the mutant lines *sfr2* and *pes1* showed an accumulation of carotenoids with stress, which may suggest the activation of the xanthophyll cycle related to the reduced NPQ observed in *sfr2*, but not as pronounced as that measured in *pes1.*

3.2.7 *Electrolyte Leakage under Cold Stress*

Low temperature affects the flexibility of lipid membranes, they become rigid, which can lead to damage and electrolyte leakage. Electrolyte leakage is commonly used in the literature to assess the plant's ability to cope with stress (Murray *et al.* 1989, Artus *et al.* 1996, Bajji *et al.* 2002, Campos *et al.* 2003, Hnilickova *et al.* 2019). By measuring the electrolytes that are leaked through the plant tissue it is possible to assess the membrane permeability. As membranes are a primary point

of defence against cold, and freezing stresses, measuring electrolyte leakage allows the extrapolation of the stress-related damage to the membranes. To avoid a biased analysis, it is expressed as a percentage of the total conductivity, obtained by boiling the tissue, and defined as the relative conductivity. The injury index is calculated using the relative conductivity of control and of eight days of cold stress. The analysis showed variable results depicted by the range of standard error (Figure 3.10). Despite this, a general increase of the injury index was observed, where higher percentages reflect increased damage to the membranes in the mutant lines compared to the wild-type Col-0. Of note, the *ELIP* mutants, *ltp4* and *pes1* showed higher average injury index than the threshold standard error of Col-0, whilst *ltr* showed to be the least affected of the mutants

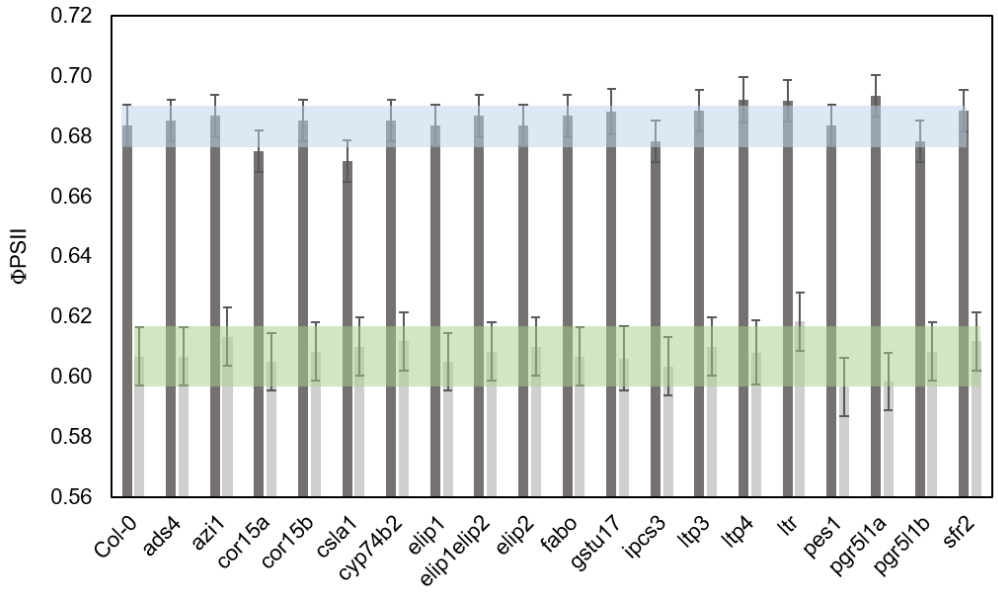

Figure 3.7 Effective Quantum Yield of Photosystem II

Effective quantum yield of photosystem II (ΦPSII) for the Arabidopsis mutant lines and the wild-type Col-0 under control 23°C (■) and after eight days of cold stress at 5°C (8 DAC, ■). Bars represent mean ± 95% Confidence Interval (CI) for six replicates per genotype. Blue (■) and green (■) bars represent the wild-type Col-0 CI at control and 8 DAC, respectively.

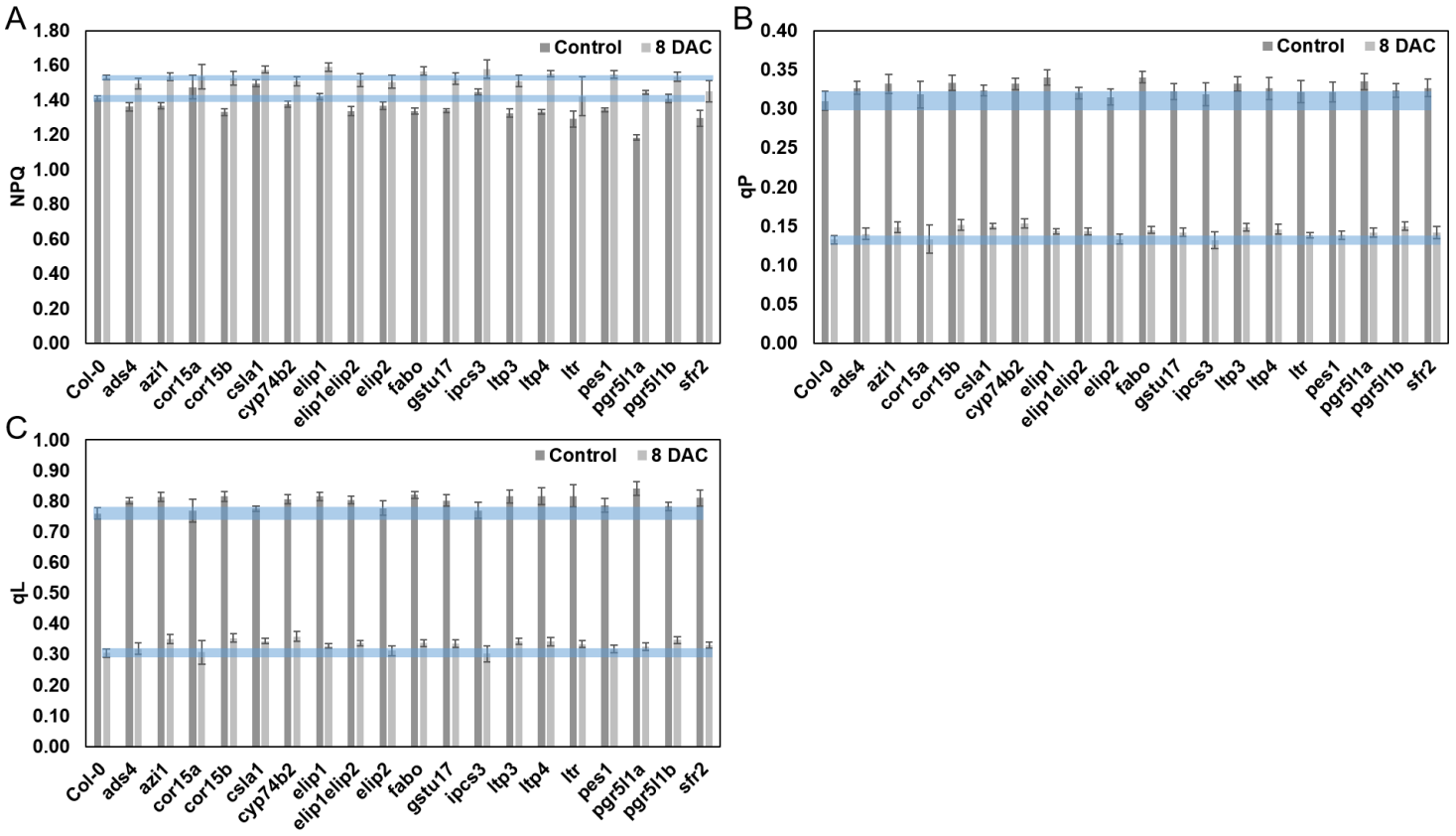

Figure 3.8. (Non-)Photochemical Quenching under Cold Stress

(A) Non- (NPQ) and (B) Photochemical quenching (qP); (C) Fraction of open reaction centres in PSII (qL) for the Arabidopsis mutant lines under control 23°C (■) and after eight days of cold 5°C stress (8 DAC, ■). Average ± standard error for six replicates per genotype, (■) Col-0 standard error for each of the conditions.

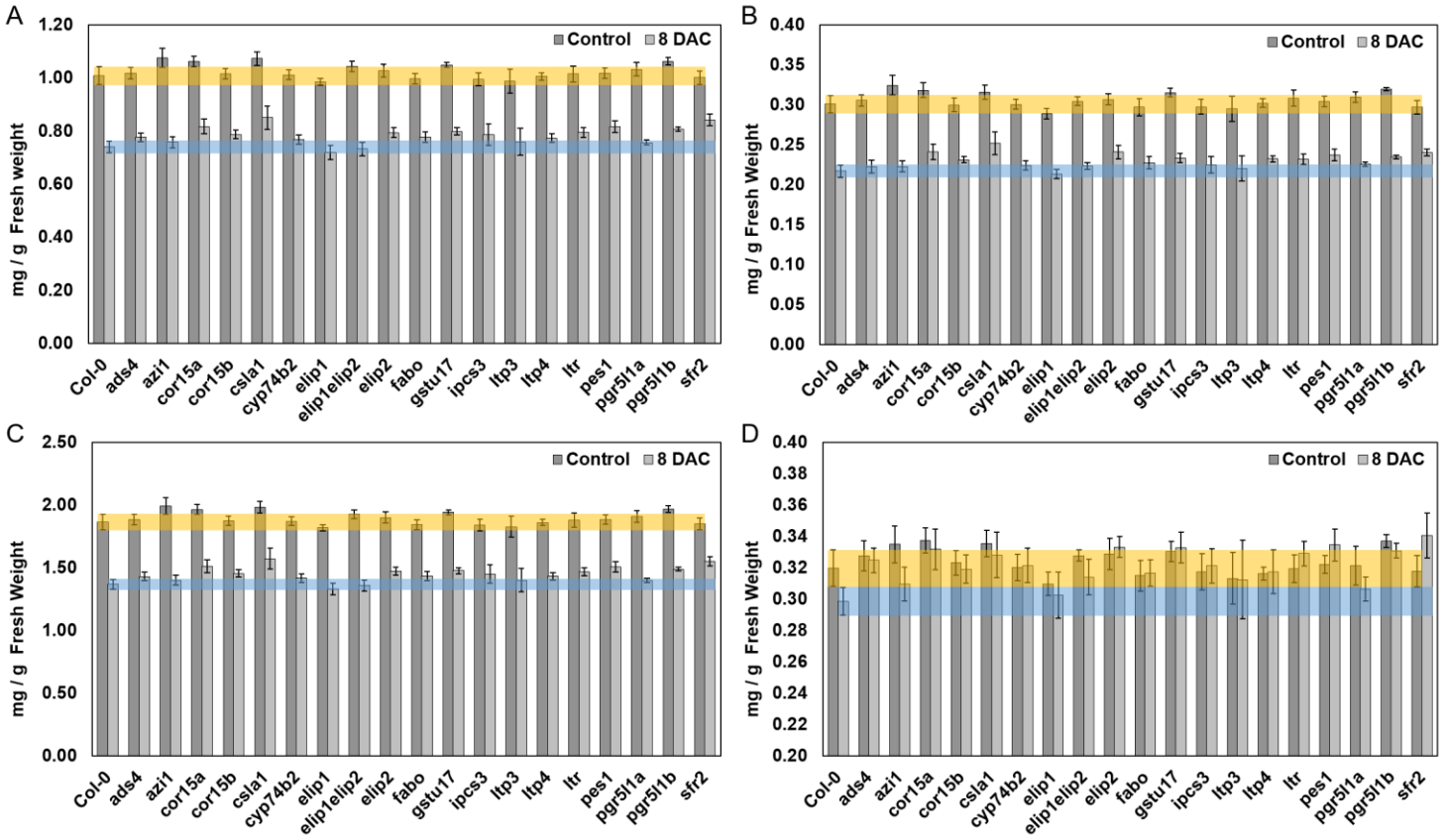

Figure 3.9. Pigment Content of the Arabidopsis Mutant Lines

Chlorophyll *a* (A), *b* (B), and total (C), total carotenoids (D) for the Arabidopsis mutant lines and the wild-type Col-0 under control 23°C (■) and after eight days of cold exposure (DAC, ■) at 5°C. Average ± standard error for six replicates per genotype; Col-0 standard error for control (■) and 8 DAC (■).

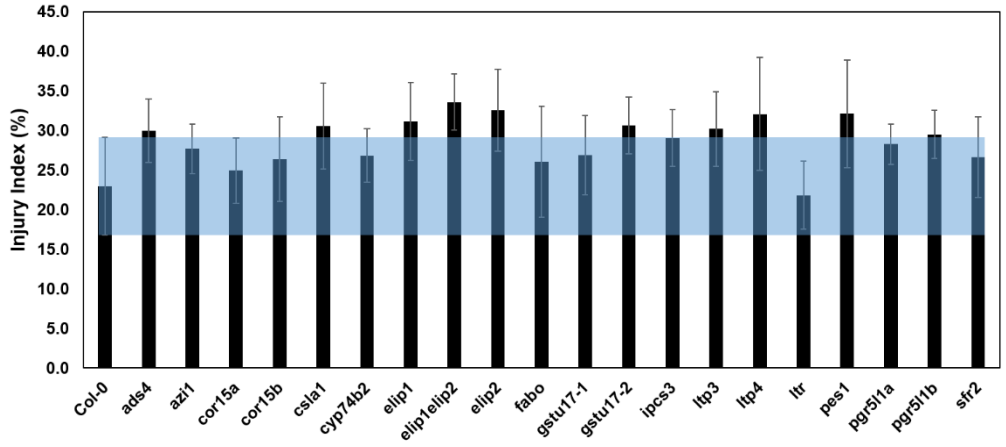

Figure 3.10. Injury Index of the Arabidopsis Lines under Cold Stress

The injury index of the Arabidopsis mutant lines and the wild-type Col-0 was analysed through electrolyte leakage of five leaf discs per replicate, and six replicates per genotype. The injury index was calculated from the relative conductivity at 19 DAS under control 23°C and at eight DAC at 5°C temperatures. Average ± standard error; (■) Col-0 standard error.

3.2.8 *No Visible Morphological Phenotype*

Adding to the characterisation of the mutant lines selected for the presented fluorescence screen, photos of the CRBD trays used were taken before the control measurement at 19 DAS, and throughout the cold stress treatment. No obvious changes in visible morphological traits, e.g. rosette diameter, leaf number and size, discoloration, or developmental time, were detected for any of the mutant lines, even after eight days of cold stress (Figure 3.11, it was not possible to photograph the plants on the eighth day of stress, this figure shows the plants after seven days of stress). This opens the discussion that any of the selected and tested genes were crucial for the plants' development, even under stress conditions. Perhaps testing the mutant lines with more severe conditions such as freezing temperatures, with or without a cold acclimation pre-treatment might have exaggerated or even forced a more accentuated phenotype.

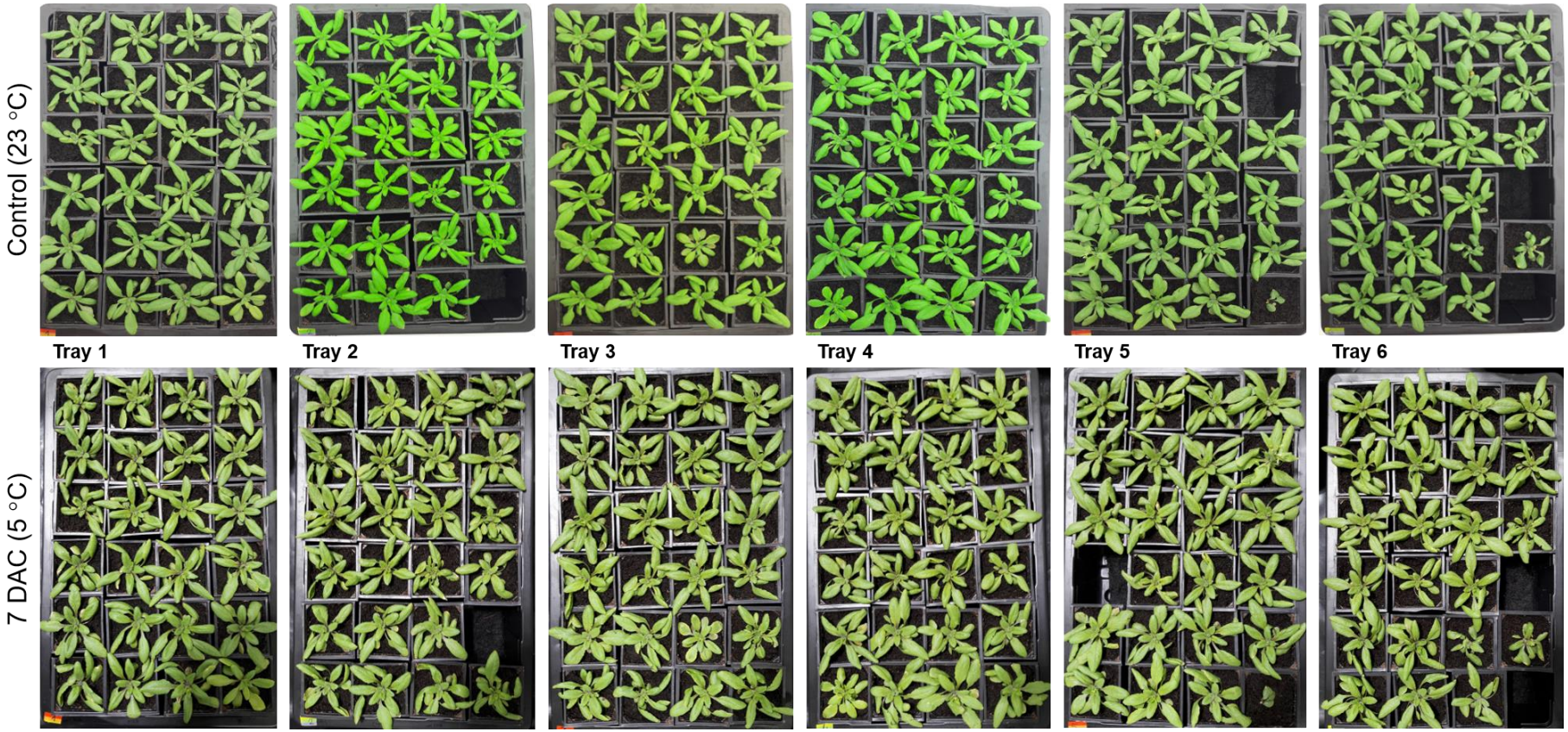

Figure 3.11. Arabidopsis Mutant Lines under Control and Cold Stress

The Arabidopsis mutant lines and Col-0 used for the cold stress screen are shown 19 DAS at control 23°C (top panel), and after seven days of cold stress at 5°C (7 DAC). Six replicates per genotype, distributed in a CRBD of three blocks of two trays each.

3.3 DISCUSSION

3.3.1 *The Transcriptome Window into Cold Acclimation*

Cold acclimation is the process that plants undertake under low, non-freezing temperatures as an adaptation strategy for winter survival (Gilmour *et al.* 1988, Thomashow *et al.* 1990). Cold stress might not induce noticeable phenotypical responses, as it refers to temperatures that are above the 0°C freezing threshold. However, it represents an important adaptation period for the plant to guarantee survival to the next generation in the event of more extreme conditions to come. The Arabidopsis cold acclimation response was investigated in this chapter through the analysis of the transcriptomic changes after three days at 4°C. This analysis revealed a higher tendency of Arabidopsis to upregulate, i.e. activate expression of genes in response to stress, as this pool of DEGs showed higher range of fold change values that reached a $\log_2$ of +8. This data is in accordance with previously described data, where 70% of the cold-regulated genes were upregulated in Arabidopsis (Lee *et al.* 2005). This trend appears to be conserved in other species, including the extremophile Eutrema, where 60% of the DEGs were up-regulated in leaves (Wang *et al.* 2017). As key modulators of the cell's response to stimuli, transcription factors are characteristic of an early response, whilst metabolism related genes are found to be upregulated in later stages (Lee *et al.* 2005, Raju *et al.* 2018). Changes in the metabolism of the plant during cold are essential for the physiological adaption of the plant. Plant lipids are a key component of the metabolic changes the plant undertakes. Increased polyunsaturated fatty acid content, for instance, results in higher flexibility of the membrane lipid bilayer, which allows the plant to withstand freezing damage (Sakamoto and Murata 2002, Upchurch 2008, Mironov *et al.* 2012). Trienoic acids produced in the chloroplast by the fatty acid desaturases FAD7 and FAD8 are such an example. Rice lines with a mutation in the *FAD8* gene fail to cold acclimate, or alternatively the overexpression of *FAD7* in tobacco

led to increased cold tolerance (Khodakovskaya *et al.* 2006, Tovuu *et al.* 2016). Interestingly, the results obtained from the RNA-Seq in Arabidopsis did not identify any of these FADs in the DEGs pool, however, in the Eutrema RNA-Seq dataset both enzymes were found to be upregulated pool (Appendix 3), suggesting a more significant participation of these enzymes in the cold resilience of this extremophile. Combining functional genomic approaches, such as transcriptomics with the analysis of lipidomics has proven to elucidate this relationship, not only in Arabidopsis, but also in crops such as sorghum or corn (Gu *et al.* 2017, Marla *et al.* 2017, Raju *et al.* 2018).

The *COLD REGULTAED15* genes *COR15A* and *COR15B* were amongst the most up-regulated ones. These genes are well described in the literature (Wilhelm and Thomashow 1993, Baker *et al.* 1994, Artus *et al.* 1996, Thomashow *et al.* 1996, Steponkus *et al.* 1998, Liu *et al.* 2014), particularly *COR15A,* which has been previously described as being significantly induced by cold stress in Arabidopsis (Benina *et al.* 2013). In Eutrema, *COR15B* was previously described to be upregulated under both cold and drought stresses, with four-fold higher expression under cold (Wong *et al.* 2006). Their expression under cold stabilises the chloroplast membrane by binding to the thylakoid membrane galactolipids, where more unsaturation seems to facilitate an efficient binding (Navarro-Retamal *et al.* 2018). As the prime site of photosynthesis, maintenance of the thylakoid membrane would seem a key aspect to a more efficient photosynthetic performance of the plant. However, the mutant lines for each of these genes did not show a perturbed photochemical performance under cold stress in comparison with the wild-type Col-0. Conceivably, a double mutant line for both *COR15A* and *COR15B* would present increased damage under stress conditions, as these homologues are thought to work together (Thalhammer *et al.* 2010, Thalhammer *et al.* 2014). Other upregulated lipid genes included two lipid transfer proteins *LTP3* and *LTP4*, the first has been previously related to freezing stress as a target of the transcription factor MYB96 (Guo *et al.* 2013). Whilst *LTP4* has been

found to be upregulated in Eutrema with cold stress, however drought stress seemed to have a higher impact in the upregulation of this genes (Wong *et al.* 2006). MYB96 by itself was not found in neither of the Arabidopsis nor Eutrema RNA-Seq data produced by our group, as expected after three days of cold acclimation. However, the upregulation of the *LTP* genes might be extrapolated from its action, as after three days of cold acclimation a metabolic response is more likely to be observed. The gene here identified as *FABO* was not characterised at the time of the selection, and it was included due to its fatty acid β-oxidation gene ontology (Harris *et al.* 2004, Harris *et al.* 2006, Gaudet *et al.* 2011). However, since then it has been characterised, and renamed *CHY4* as involved in the branched-chain amino acid valine degradation, essential to seed development and germination of Arabidopsis as an alternative energy source (Gipson *et al.* 2017).

ADS4 showed the same level of upregulation in both Arabidopsis and Eutrema (Appendix 3) datasets produced by our group. Involved in wax biosynthesis, this result was not a surprise as cuticles are an important barrier to freezing stress (Amid *et al.* 2012). Eutrema is characterised by high wax content (Teusink *et al.* 2002). Yet, the *SENSITIVE TO FREEZING3* gene that codes for an acetyl-CoA carboxylase that modulates the wax composition and cuticle permeability under freezing stress (Amid *et al.* 2012) was not found in the RNA-Seq presented here. Only *SFR2*, which is involved in the remodelling of the chloroplast membrane under freezing stress, was found in the RNA-Seq analysis, but in the downregulated pool of DEGs. This might suggest a very specific role for these enzymes in freezing below 0°C, as it occurs with other members of the *SFR* family (Amid *et al.* 2012). The sphingolipid gene *IPCS3* was also included in the screen despite falling below the $\log_2$ fold change threshold of +2. Through the regulation of the membrane permeability, a key feature of the cell that allows higher plasticity to cope with cold and potentially freezing stresses, sphingolipids are an important factor to consider in cold acclimation strategies.

3.3.2 *Why a Photosynthesis Related Method to Screen Lipid Related Genes?*

The work developed in this chapter used RNA-Seq analysis as a source of DEGs with a potential role in the lipid adaptive processes that modulates cold acclimation in Arabidopsis. To functionally analyse such genes, a reverse genetics approach was used where the respective mutant lines were obtained and tested using cold stress as a screen. Different approaches have been employed to produce mutations that ease the functional characterisation of genes of interest (Thorneycroft *et al.* 2001, O'Malley and Ecker 2010). Methods that range from ethyl methanesulfonate (EMS) induced mutations (Kim *et al.* 2006), the *Agrobacterium*-transferred DNA (T-DNA) insertion mutations (Alonso 2003) or the newly developed clustered regularly interspaced short palindromic repeats (CRISPR) which allow efficiently targeted mutations (Belhaj *et al.* 2015). Due to the pool size of candidate genes to be analysed in the cold screen, the T-DNA insertion mutants from the collections SALK (Alonso 2003) and GABI-Kat (Kleinboelting *et al.* 2012) were used. Some disadvantages are associated with the use of T-DNA insertion mutants this includes possible neglected pleiotropic effects or not detected untargeted mutations (Thorneycroft *et al.* 2001). However, the library of mutated genes in these collections with the associated database of information, plus the ease of obtaining seeds through the Nottingham Arabidopsis Stock Centre (NASC, http://arabidopsis.info/) were an advantage for the present work that included 18 genes of interest.

As the number of genes of interest resulted in 19 T-DNA insertion lines, plus the wild-type Arabidopsis Col-0, a high throughput phenotypic profiling technique was desirable to easily and reliably assess their function. Traditional lipidomic techniques, such as thin layer chromatography (Li *et al.* 2015), liquid chromatography coupled with mass spectrometry (LC-MS, (Markham 2013), or gas chromatography (Browse *et al.* 1985) have been used to analyse the contribution of lipid metabolism in the plant's adaptation to cold stress. However, these

approaches are centred in the analysis of selected lipid species and abundance. The aim of this work involved a holistic view of the lipid metabolism in the plant's capacity to withstand and adapt to cold conditions. Thus, it was necessary to find a screening method that assessed the status of the plant, whilst also having the potential for high-throughput and non-destructive analysis. As one of the major components of plant's metabolism, photosynthesis is highly affected by cold stress (Eberhard *et al.* 2008), with an observed reduction in the photosynthetic related transcripts in several plant species e.g. Arabidopsis, barley (Yamaguchi-Shinozaki and Shinozaki 2006) and sorghum (Marla *et al.* 2017). As a strategy to avoid detrimental effects to the photosystems, genes involved in the quenching mechanism are often activated (Li *et al.* 2000, Marla *et al.* 2017). Furthermore, assessment of photosynthetic performance can be achieved by the analysis of the chlorophyll fluorescence kinetics (Genty *et al.* 1989, Maxwell and Johnson 2000). The relative contribution of pigment-protein complexes of PSII and PSI in the thylakoid membranes to the fluorescence changes with leaf temperature, make it a temperature sensitive method (Djanaguiraman *et al.* 2018). Thus, as the photochemical performance is assessed it allows inferences to be made on the photosynthetic health of the plant. The method used in the screen was an imaged chlorophyll *a* fluorescence technique using the PSI FluorCam (McAusland *et al.* 2019). Measurements were performed through a camera on the top of the chamber that delivers and collects the fluorescence signal which enabled the non-invasive measurement of cold adaptation in the mutant lines throughout eight days of exposure to 5°C temperatures. The PSI FluorCam chamber size allowed 48 Arabidopsis adult whole plants to be analysed in one measurement showing its high-throughput applicability. The same chamber has been recently used in a wheat phenotyping experiment that characterised photosynthetic and photochemical parameters of at least 500 wheat samples per day under fluctuating light conditions (McAusland *et al.* 2019). To determine the screen sensitivity, photosynthesis related genes that could affect photochemical performance from the RNA-Seq DEG pools were selected and added to

the screen. At the end of the eight days of cold conditions two mutant lines were shown to be significantly perturbed in their photochemical performance when compared to the wild-type Col-0. These lines were *pes1* and *pgr5l1a,* discussed in the section below. Genes such as *COR15A* and *COR15B* are known to be have a targeted effect in the chloroplast under cold stress (Wilhelm and Thomashow 1993, Baker *et al.* 1994, Artus *et al.* 1996, Steponkus *et al.* 1998, Liu *et al.* 2014), however the mutated lines for these genes did not present significant impact in the fluorescence screen performed. This same response was found in other photosynthesis related genes, such as the *ELIP* mutants (Casazza *et al.* 2005), or the *PGR5L1A* homologous *PGR5L1B* (DalCorso *et al.* 2008). Nevertheless, the chlorophyll fluorescence technique used here identified two genes that pose as candidates in the cold acclimation response in Arabidopsis, validating the cold stress screen used here. Furthermore, this technique has been previously applied as an effective screen method in various settings and species. In Arabidopsis nine accessions were characterised as to their cold tolerance, which found F_v/F_m to be highly correlated with membrane damage measured by electrolyte leakage (Mishra *et al.* 2011). Two wheat cultivars were selected through their F_v/F_m response of maintaining high photosynthetic capacity under heat stress (Sharma *et al.* 2015), or used to characterise different varieties of the legume genus *Lathyrus* to drought conditions (Silvestre *et al.* 2014).

3.3.3 *Chlorophyll Fluorescence Showed pes1 and pgr5l1a Impaired Capacity for Cold Adaptation*

The cold stress screen showed T-DNA lines *pes1* and *pgr5l1a* to have significantly underperformed in the photochemistry assessment after eight days of stress (Figure 3.6). Both genes were previously described in the literature and referred to as stress-related genes (DalCorso *et al.* 2008, Lippold *et al.* 2012). *PES1* as a member of the esterase/ lipase/ thioesterase family of acyltransferases and is involved in the synthesis of fatty acid phytyl esters in the chlorophyll degradation pathway (Lippold *et*

al. 2012). As chlorophyll degradation occurs under stress conditions (Hortensteiner 2006, vom Dorp *et al.* 2015), it seemed plausible that this gene would intervene in the cold adaption of Arabidopsis. The same applied to *PGR5L1A,* which is involved in the CEF around PSI, a key element for excess energy dissipation (Munekage *et al.* 2002, DalCorso *et al.* 2008). However, the mutated line for its homologue *PGR5L1B* did not show any photochemical impairment, indicating perhaps a functional predominance of the *PGR5L1A* isoform. In Arabidopsis, two genes encode for phytyl ester synthases *PES1* and *PES2*, the latter was previously considered to be predominant for the phytyl ester synthesis including during responses to nitrogen deficiency (Lippold *et al.* 2012). In the present study, however, only *PES1* was found in the DEGs pool over the imposed thresholds and hence included in the screen, only later in a specific search for *PES2* was it revealed in the DEGs pool. Unexpectedly, this gene was found to be downregulated (log_2 fold change of -0.63) in Arabidopsis after three days of cold temperature, opening the possibility of a specific role of *PES1* under cold acclimation. Recently, PES1 was shown to be cold-induced in the oil-producing crop jojoba (*Simmondsia chinensis*) further anticipating a role in cold stress response (Gao *et al.* 2019).

Growth phenotype, and overall morphology under cold stress was not shown to be affected by the lack of either *PES1* or *PGR5L1A*, as previously observed for *pes1* (Lippold *et al.* 2012). Despite this, both *pgr5l1a* and *pes1* showed an impairment in the photochemical performance of the PSII. A maximum of eight days of cold stress were used for the fluorescence screen to allow the mutant lines to show a cold stress related phenotype. However, measurements were taken daily to assure a complete profile of the mutant lines. A detailed analysis of the F_v/F_m over the eight days of stress (Appendix 5) revealed that *pgr5l1a* was affected after only three days of exposure to 5°C. The mutant *pes1* was susceptible after a longer period of stress (eight days), the same time had been previously reported with the mutant *sfr2-1* (Thorlby *et al.* 2004). After the eight days of stress both lines *pgr5l1a* and *pes1* showed

a significant decrease in the F_v/F_m together with a decreased ΦPSII compared to the wild-type Col-0, demonstrating cold-induced photoinhibition of the PSII. A decrease in F_v/F_m may be caused by impaired repair and reinsertion of the D1 protein (Takahashi and Murata 2005). *pes1* did not show any significant changes in the quenching parameters measured, however it showed accumulated levels of chlorophyll and a 10.7% increased accumulation of total carotenoids under cold stress. This was only surpassed in *sfr2* which showed a 12% increased carotenoid accumulation with eight days of stress. *pgr5l1a* showed a contrary tendency, with a reduced NPQ under both control and cold stress, compared to Col-0 values. This was accompanied by an increased photochemical quenching qP, and higher ratio of open reaction centres in PSII, especially under control conditions. These results suggest different strategies of each mutant line to cope with cold stress, indicating the influence of these two genes in the plant's cold acclimation. However further testing is necessary to investigate the underlying mechanisms of this relationship. As the plant lipid adaptation to cold stress was the drive for this study, a lipidomics approach was then developed to analyse the lipid changes observed in the mutant lines identified by the screen. The mutant line *ipcs3* was included in the lipidomic analysis, alongside *pes1* and *pgr5l1a*, to identify disturbances in the galactolipids that composed the thylakoid membranes. As *ipcs3* showed no difference to Col-0 in the F_v/F_m and its involvement in sphingolipid metabolism did not anticipate a modified galactolipid profile (Wang *et al.* 2008, Mina *et al.* 2010). The targeted lipid analysis results are shown and discussed in Chapter 4.

3.4 CONCLUSION

This chapter started by the analysis of the Arabidopsis transcriptomic changes under cold acclimation, a process that enables the plant to tolerate cold or even freezing temperatures. As lipids have a crucial role in the plant's metabolism, which is ultimately slowed down with cold, related genes were identified in the up- and downregulated pools of

DEGs with the aim of identifying novel candidate genes. To ascertain the impact of these genes in the plant's ability to cope with cold, a high-throughput cold screen was designed using an imaged chlorophyll fluorescence technique. With this test it was possible to distinguish two mutant lines that did not perform as the wild-type after eight days of exposure to cold. These lines, *pes1* and *pgr5l1a* had a T-DNA insertion that affected the chlorophyll degradation pathway, and the CEF of the PSI, respectively. Due to their close relationship with chloroplast and photosynthesis metabolism, it was discussed if the method used caused a biased interpretation of the results. Further analysis into the energy quenching processes, showed *pgr5l1a* to have an impairment in the non-photochemical quenching of the excess energy. *PES1* and *PGR5L1A* were thus considered as candidates for the cold acclimation process in Arabidopsis. This led to the results discussed in the next chapter where a targeted lipid profile of the mutated lines for these two genes was assessed. A third mutant, *ipcs3* was added to the lipidomic characterisation and considered as a control as no significant photochemical phenotype was observed.

Chapter 4.

Lipid Characterisation of the Cold Responsive Genes *pes1, pgr5l1a* and *ipcs3*

4.1 INTRODUCTION

The work developed in the previous chapter identified cold responsive candidate genes through a cold stress high-throughput screen using the fluorescence of the chlorophyll *a* as a measure of the plant's health. As described in Chapter 3, a diverse panel of candidate genes were selected from the up- and down-regulated pools of DEGs resulting from an RNA-Seq study on the Arabidopsis cold acclimation. The fluorescence screen performed showed *PES1* and *PGR5L1A* to be involved in the photochemical performance of Arabidopsis under cold stress (Section 3.2.5). *PES1* and *PGR5L1A* have, however, distinct functions in the plant participating in the lipid and photochemical chloroplast metabolism, respectively. The chloroplast is a complex organelle that integrates diverse metabolic activities from photosynthesis to *de novo* fatty acid production. Furthermore, and as described in Section 3.1.2, chloroplasts have a complex membrane system, composed of an outer double membrane (chloroplast envelope) and internal interconnecting flattened membrane compartments called thylakoids where light-dependent photosynthesis occurs. Thylakoids comprise a unique blend of galactolipids MGDG, DGDG, sulfolipid SQDG and the phospholipid PG (Dormann and Benning 2002). As galactolipids are synthesized in the inner- and outer-envelope membranes of chloroplasts [(Benning and Ohta 2005, Kelly *et al.* 2016); see also Chapter 1], the lipid molecules have to be transported to different membranes and organelles. The ATP-Binding cassette (ABC) transporter allows the transfer of lipid precursors from the ER to the chloroplast is composed of three subunits trigalactosyldiacylglycerol1 (TGD1), TGD2 and TGD3 (Benning 2008, 2009). MGDG and DGDG are predominant in thylakoid membranes of chloroplasts, where together with PG are integral components of PSI and PSII, LHCII and are essential for photosynthesis and growth (Wada and Murata 2007). The spatial organisation of these lipids defines the thylakoid, differentiating appressed (granum) and non-appressed regions (stroma lamellae, Figure 3.1). Thus, establishing a unique relationship

between photosynthetic performance and lipid metabolism which can be crucial for the plant's adaptation and/or resilience to abiotic stress conditions. Thylakoid lipids have an established response to phosphate deprivation, cold (Li and Yu 2018) and heat stress (Higashi and Saito 2019). To explore the relationship with cold stress, the lipid metabolism of the T-DNA insertion lines for *PES1* and *PGR5L1A* was analysed. Alongside the wild-type Col-0, a third gene, *IPCS3*, was added to the analysis as a negative chloroplast lipid control.

4.1.1 *PHYTYL ESTER SYNTHASE*

During senescence the thylakoid membranes are disassembled, activating specific pathways for the degradation of galactolipids, photosystem-associated proteins and chlorophyll (Hendry *et al.* 1987). Abiotic stress can also be a cause of chlorophyll degradation, 15 days of high light stress in Arabidopsis resulted in a 50% loss of chlorophyll (Collakova and DellaPenna 2003). Chlorophyll is composed of a magnesium cation in the centre of a tetrapyrrole ring and an ester-linked phytol (hydrophobic) side chain (Fleming 1967). The first steps of its degradation pathway are thought to be common to all plants, in which chlorophyll is dephytylated by the enzyme chlorophyllase and thus yielding phytol and chlorophyllide (Ben-Yaakov *et al.* 2006, Hortensteiner 2006). The chlorophyll degradation pathway is well studied, due to its significance to photosynthesis and plant productivity. Briefly, the chlorophyllide product is degraded into a colourless intermediate, which is then transported and finally stored in the vacuole (Hortensteiner 2006). The resulting free phytol, released from chlorophyll in a 1:1 molar ratio (Gutbrod *et al.* 2019), is accumulated in high quantities, but as a C20 (with one double bond) isoprenoid alcohol it can become toxic to the plant cells. Such a potentially harmful process requires coordinated metabolic processing of free phytol. Arabidopsis has been shown to metabolise its free phytol pool by redirecting the phosphorylated versions into tocopherol biosynthesis or in parallel, via a specific enzymatic pathway, into the synthesis of fatty acid phytyl esters (Ischebeck *et al.* 2006,

Lippold *et al.* 2012, vom Dorp *et al.* 2015). A common step is the phosphorylation of phytol into phytyl-phosphate (phytyl-P) and phytyl-diphosphate (phytyl-PP) by the membrane-bound kinases VTE5 and VTE6, respectively (Valentin *et al.* 2006, vom Dorp *et al.* 2015). Fatty acid phytyl esters have been reported to accumulate during senescence, as predicted, but also during nitrogen deficiency and cold stress (Gaude *et al.* 2007). In Arabidopsis two phytyl ester synthase (PES) genes were identified, *AtPES1* (At1g54570) and *AtPES2* (At3g26840), the latter was suggested as the gene responsible for the predominant phytyl ester synthase activity (Lippold *et al.* 2012). Both genes contain acyltransferase and hydrolase domains, associated with the Esterase/Lipase/Thioesterase (ELT) family of proteins. PES enzymes are present in the chloroplast (Lippold *et al.* 2012) and their role in the adaptation to stress conditions has been explored; in particular nitrogen deprivation and senescence in which the double mutant showed an effect on TAG in leaves (Lippold *et al.* 2012). Recently, *PES1* has been associated with the cold stress response of jojoba (*Simmondsia chinensis*) seedlings (Gao *et al.* 2019).

4.1.2 *PROTON GRADIENT REGULATION 5 – LIKE 1A*

In chloroplast thylakoids, two photosystems (PSI and PSII) function in series to produce the electron flow for $NADP^+$ reduction to NADPH, in a process called linear electron transport (LET) (Shikanai 2007). Together with ATP, NADPH is mostly used for the fixation of carbon in photosynthesis (Eberhard *et al.* 2008). ATP can be produced through the generation of a ΔpH across the thylakoid membrane derived from cytochrome b_6f electron transport. However, an alternative pathway results from the CEF around PSI (Arnon *et al.* 1954). However, in C3 plants this process seems to have a limited role in ATP production (Joet *et al.* 2002), rather its function is more closely linked to photoprotection mechanisms (Clarke and Johnson 2001, Munekage *et al.* 2002). In Arabidopsis, the *PROTON GRADIENT REGULATION 5* (*PGR5,* AT2G05620) gene was shown to be involved in CEF around PSI, draining

electrons from PSI and thus inducing thermal dissipation, enabling the photoprotection of PSI (Munekage *et al.* 2002) in high light. A thylakoid transmembrane protein PGR5L1 was later identified due to its *pgr5*-like photosynthetic phenotype, with no homology between genes (DalCorso *et al.* 2008). In Arabidopsis, PGR5L1 is encoded by two homologous genes *PGR5L1A* (At4g22890) and *PGR5L1B* (At4g11960). PGR5L1 is thought to be essential for the recruitment of PGR5 thus forming a PGR5-PGR5L1 complex, despite not being essential for the PSI correct assembly, it intervenes in the regulation of CEF (DalCorso *et al.* 2008), by which mechanism it is still uncertain (Yamori and Shikanai 2016, Nawrocki *et al.* 2019). However, CEF maintains the ∆pH across the thylakoid membranes allowing NPQ, essential to the protection of the photosystems in stress conditions (Johnson 2011, Pinnola and Bassi 2018). Thus, the PGR5-PGR5L1 complex is thought to be a key component in the protection of the photosystem against stresses, such as heat (Zhang and Sharkey 2009), high light (DalCorso *et al.* 2008, Wang *et al.* 2014) or drought (Long *et al.* 2008). A previous report was found to link the PGR5L1-PGR5 complex to cold stress in tomato (*Solanum lycopersicum*), showing the upregulation of both *PGR5L1A* and *PGR5* with a consequent underperformance of the mutated lines under cold stress (Wang *et al.* 2017). However, it was also correlated with an alternative regulatory complex NAD(P)H dehydrogenase-like (NDH) as described in previous reports [(Li *et al.* 2004, Yamori *et al.* 2011); reviewed in (Yamori and Shikanai 2016)].

4.1.3 *INOSITOL PHOSPHORYLCERAMIDE SYNTHASES*

Sphingolipids are a unique and complex lipid class, formed by a ceramide backbone produced in the ER, to which a series of head groups can be added originating a varied group of lipids [(Michaelson *et al.* 2016), Chapter 1]. The ceramide backbone is composed by the unique LCB linked to a long- or very long-chain fatty acid (VLCFA) through an amide linkage. Both LCB and VLCFA add to the varied forms found in this lipid classes, as they can have up to 26 carbons and be modified by specific

hydrolases and desaturases (reviewed in Chapter 1). The most abundant sphingolipids in plant tissues are the GIPCs and the glucosylceramides, which are also the most complex forms (Markham *et al.* 2006, Markham and Jaworski 2007, Markham 2013). Glucosylceramides have a glycosyl group linked to the C1 position, whilst in GIPCs the ceramide backbone is linked through an inositol phosphate to a myriad of sugar residues forming its head group (Warnecke and Heinz 2003, Lynch and Dunn 2004, Gronnier *et al.* 2016). GIPCs are synthesized in the Golgi compartment, after transport of the ceramide backbone usually composed of VLCFA linked, predominantly, to desaturated trihydroxy LCB t18:1 (Markham *et al.* 2013). In the Golgi, the first committed step of GIPC synthesis is catalyzed by INOSITOL PHOSPHORYLCERAMIDE SYNTHASE (IPCS) which transfers an inositol phosphate head group from PI to the ceramide backbone forming inositol phosphorylceramide [IPC, (Bromley *et al.* 2003)]. IPC can then be further modified by the addition of many different saccharides (Gronnier *et al.* 2016). In Arabidopsis, three homologous coding sequences code for IPCS, *AtIPCS1* (At3g54020), *AtIPCS2* (At2g37940) and *AtIPCS3* (At2g29525) (Mina *et al.* 2010). Previously, *AtIPCS2* was characterised through the mutant T-DNA insertion line *erh1* leading to the accumulation of ceramides and hydroxyceramides (Wang *et al.* 2008). This isoform has been suggested to be the most significant due to the observed higher turnover rate and enzyme activity in the presence of the substrate PI, when expressed in yeast (Mina *et al.* 2010). With further analysis showing ubiquitously higher expression levels of *AtIPCS2* in Arabidopsis Col-0, where *AtIPCS3* showed a comparable expression in stem and flower tissues (Mina *et al.* 2010). *AtIPCS2* has been also reported to be involved in the regulation of plant programmed cell death [PCD, (Liang *et al.* 2003, Wang *et al.* 2008)].

4.1.4 *Chapter Aims*

Following on from the work developed in Chapter 3, which revealed *pes1* and *pgr5l1a* to be sensitive to the cold stress, the impact of these mutations on lipid metabolism during cold stress was investigated (Figure 4.1). *PES1* and *PGR5L1A* have distinct functions, however both genes are located and involved in chloroplast metabolic maintenance. The chloroplast is the unique site of photosynthesis, which is primarily affected under stress. In an effort to understand the importance of lipid composition in the chloroplast and the cold-related function of the identified genes, these lines were analysed as to their thylakoid lipid content. The profile changes and accumulation of the galactolipids MGDG, DGDG, SQDG, and the phospholipid PG were assessed in *pes1, pgr5l1a,* and *ipcs3*. *IPCS3* is involved in the production of complex sphingolipids in the Golgi compartment (Mina *et al.* 2010), and no impact in the photochemical performance of *ipcs3* was previously observed (Chapter 3). These observations suggested that its stress involvement was not related to the chloroplast metabolism, in contrast to *PES1* and *PGR5L1A*, and therefore was used as a control.

To further investigate the role of *PES1* and *PGR5L1A* in the cold acclimation ability of Arabidopsis, targeted lipidomic analyses were performed under both control and after eight days of cold stress. These allowed an overview of the TAG, phospholipid and FFA profiles in the mutated lines. No impact on the photochemical performance was observed in *ipcs3*, however its presence in the up-regulated DEGs pool (Section 3.2.3) suggested a role in the cold adaptation of Arabidopsis. As such, lipidomic investigation into the cold response of *IPCS3* will also be shown. The present chapter therefore provides a description of chloroplast lipid metabolism of these genes and their interaction with cold stress adaptation. This analysis was followed by the characterisation of the main lipid classes in each T-DNA line, which was adapted to each specific metabolic context.

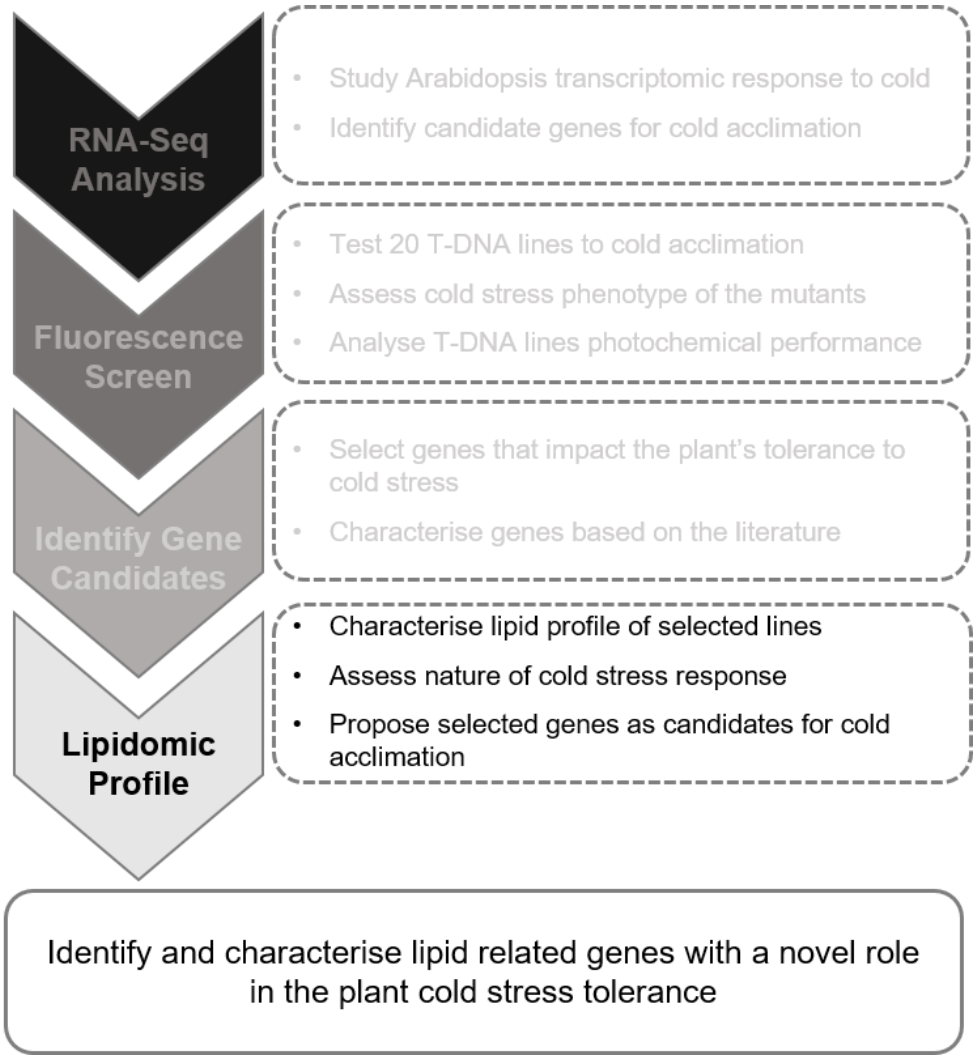

Figure 4.1 Arabidopsis Cold Acclimation Workflow – Lipidomic Profile

The figure follows the workflow which culminated with the identification of cold responsive gene candidates in Chapter 3 This chapter presents the lipid profile of the identified genes in their relationship with cold stress.

4.2 RESULTS

4.2.1 *PES1, PGR5L1A and IPCS3 Molecular Description*

The gene models for *AtPES1* (At1g54570), *AtPGR5L1A* (At4g22890) and *AtIPCS3* (At2g29525) showed multiple exons, 13, 10, and 11 respectively (Figure 4.2). The position of the left border of the T-DNA insertion is shown for each SALK line, which in all cases was localised upstream of the start codon. The gDNA was extracted, and PCR analysis

confirmed the presence of the T-DNA insertion in each of the SALK lines (Figure 4.3 A). The fragments amplified to test for the presence of the T-DNA were of 1,120 bp for *AtPES1*, 1,119 bp for *AtPGR5L1A*, and 1,005 bp for *AtIPCS3* respectively (Figure 4.2). Sanger sequencing of gDNA was used to confirm the location of the insertion of the T-DNA left border in each mutant line. The mutant line *pes1* (SALK_076354C) showed the T-DNA left border inserted at 303 bp upstream of *AtPES1* first exon in the 5' UTR (Figure 4.3 B). The other two lines, *pgr5l1a* (SALK_024747C) and *ipcs3* (SALK_152650C) had the T-DNA left border insertion 238 bp and 190 bp upstream of their first exon, and at 17 bp and at 11 bp upstream of each respective 5'UTR (Figure 4.3 C-D). According to TAIR database, *AtIPCS3* has five splice variants, for which the polymorphism SALK_152650.31.00.X (corresponding to the line SALK_152650C) would only affect splice variants 2 through 5 (At2g29525.2, At2g29525.3, At2g29525.4, and At2g29525.5). The first two are described with the polymorphism site in the exon region, whilst alleles 4 and 5 would be affected in the 5' UTR. Only one other germplasm entry with T-DNA localised in an exon region of the splice variants 1 to 3 (4 and 5 with T-DNA in the 5' UTR) was found to be SALK_152652. *AtPES1* had 12 listed germplasm entries, where only one showed the T-DNA positioned in mid-sequence in the seventh exon, however no homozygous seeds were available for this. *AtPGR5L1A*, as *AtIPCS3*, also showed five splice variants in TAIR database, with three germplasm entries. A fourth and homozygous entry SALK_024747C (SALK_024747.35.75.x) was found through the European Arabidopsis Stock Centre (NASC). Despite the *AtPGR5L1A* polymorphism was not found in the TAIR database, it was identified in the Sequence Viewer database, which confirmed it to be present in the 5' UTR of *AtPGR5L1A.*

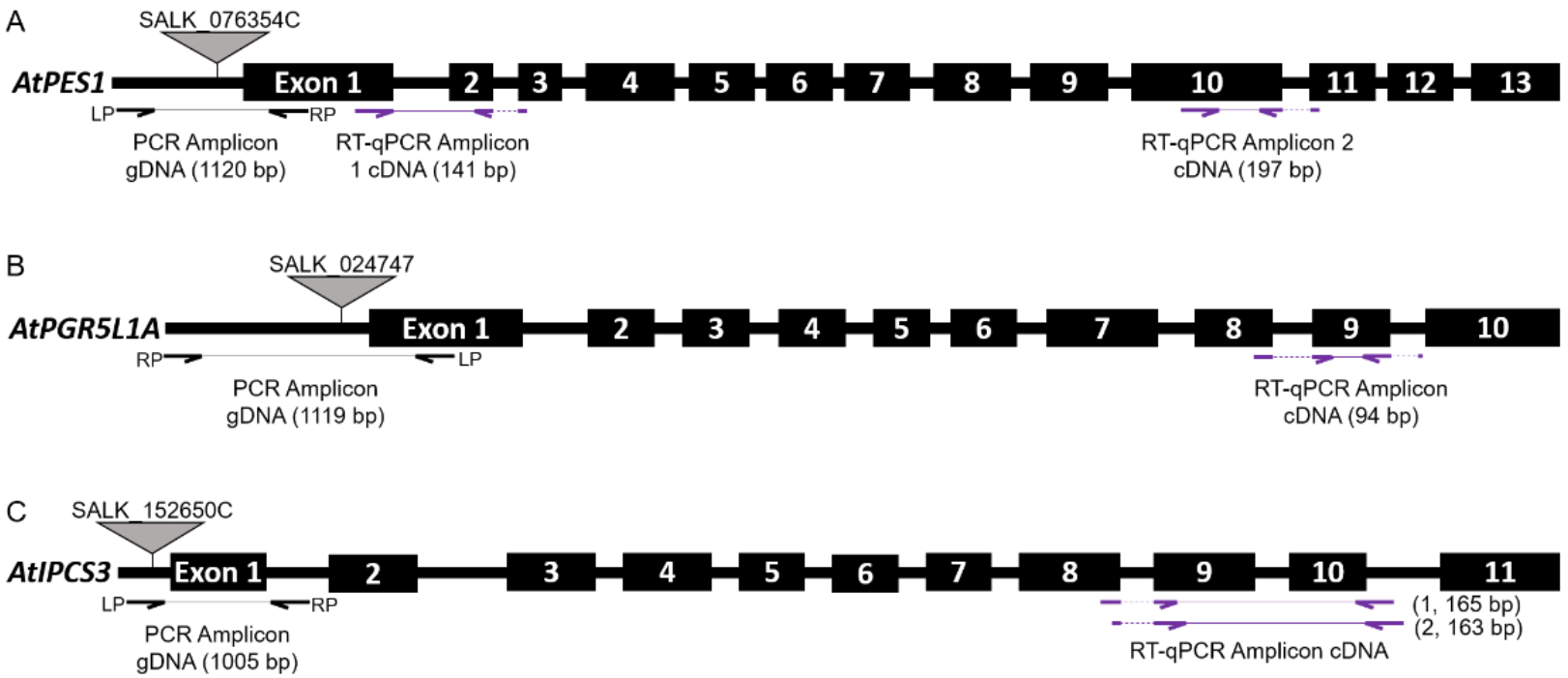

Figure 4.2 Gene Models for AtPES1, AtPGR5L1A, and AtIPCS3

(A) *AtPES1*, (B) *AtPGR5L1A*, and (C) *AtIPCS3* genes model with the respective T-DNA insertion sites of the SALK mutant lines (▼), primer binding sites marked by half arrows. LP, Left Primer; RP, Right Primer; gDNA, genomic DNA; cDNA, complementary DNA.

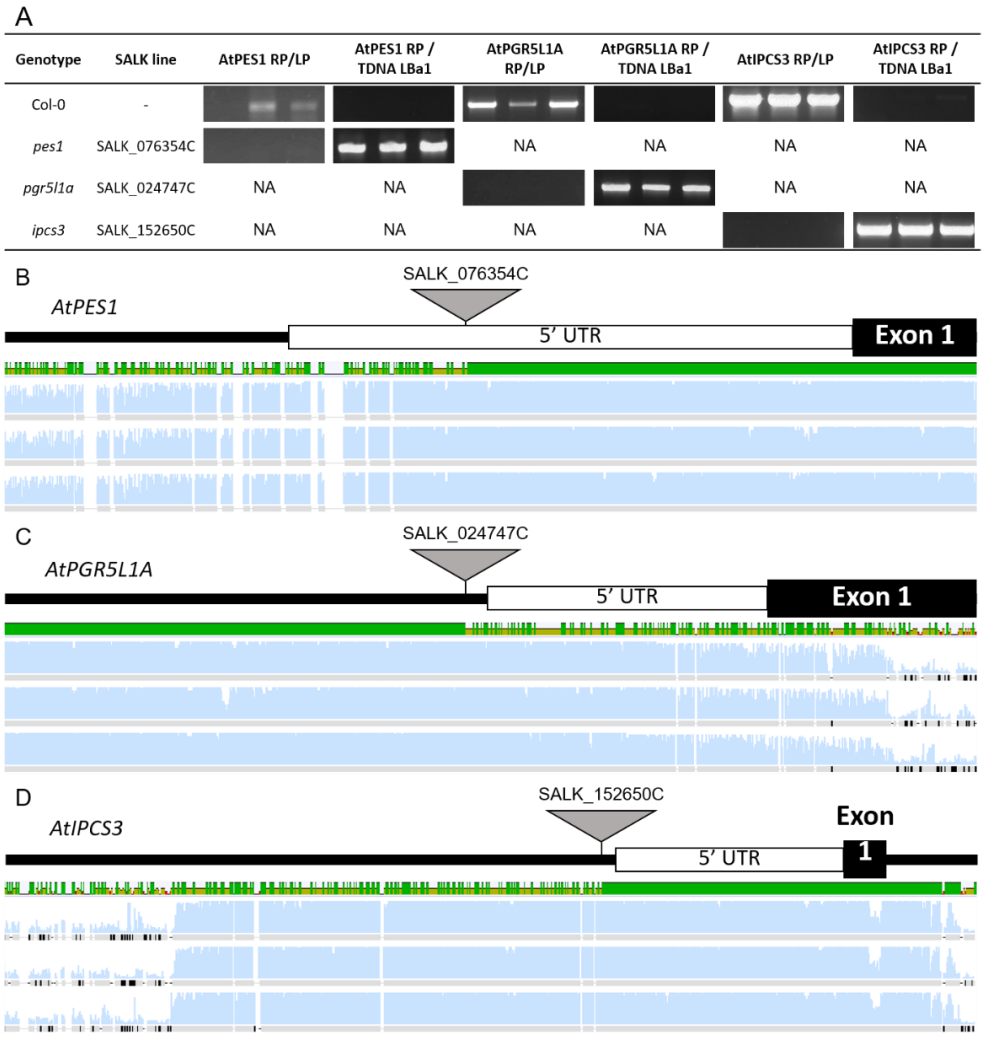

Figure 4.3. Molecular Characterisation of the three T-DNA Lines

(A) PCR analysis of *AtPES1*, *AtPGR5L1A*, and *AtIPCS3* to confirm the presence of the T-DNA insertion and absence of each respective wild-type gene, Arabidopsis Col-0 was used as control. LP, Left Primer; RP, Right Primer; LBa1, Left Border Primer of T-DNA; NA, Non-Applicable. (B) *pes1*, (C) *pgr5l1a*, (D) *ipcs3* gDNA Sanger sequencing, showing each respective T-DNA insertion location (▼) and first exon. Sequence alignment was performed with Geneious® against the database FASTA sequences. Green bar (■) on top of each panel represents sequence identity; blue bar (■) in each trace show sequence quality. All analyses were performed in 18 DAS adult leaves, N=3.

The results described above confirm the presence and the location of the T-DNA left border in the gene sequence of each line. Furthermore, the expression levels of the target genes in each T-DNA line were assessed by testing the expression of its own mutated gene and of two reference genes *AtUBC21* and *AtACT2*. For this, primer pairs were designed to span exon-exon junctions and to amplify regions of approximately 80 to 150 bp, as previously recommended [(Bustin and Huggett 2017), Figure

4.2]. Two sets of primer pairs were designed to test *pes1* and *ipcs3*, whilst for *pgr5l1a* only one pair was considered enough. Thus, two distinct regions were amplified for *AtPES1*, “Amplicon 1” of 141 bp spanning the 3’ end of exon 1 up to 5’ end of exon 3; whilst “Amplicon 2” targeted the tenth exon, with the right primer designed across exons 10 and 11 (Figure 4.2 A). The two amplicons of *AtIPCS3* were similar, as any other primer options showed very high self-complementary scores, increasing the probability of errors during the RT-qPCR reaction. Thus, amplicons 1 (163 bp) and 2 (165 bp) of *AtIPCS3* targeted exons 9 and 10, with the left primer designed across exons 8 and 9 in both cases (Figure 4.2 C). In *AtPGR5L1A,* one primer pair was designed to amplify a 94 bp region in exon 9, where the left primer spanned exons 8 and 9 whilst the right primer was designed across exons 9 and 10 (Figure 4.2 B). The expression analysis for each T-DNA line was individually compared to the wild-type Col-0, in which differences between genotypes (“Genotype”) and between amplicons within genotype (“Amplicon”) were assessed (Figure 4.4). Different results were obtained for the relative expression values of each amplicon when using *AtUBC21* or *AtACT2.* However, the relationships observed between the wild-type and the mutated lines were maintained using either reference, as can be observed by the statistical results obtained. *AtPGR5L1A* expression showed to be significantly reduced in *pgr5l1a* (Figure 4.4 B), as suggested by the position of the T-DNA left border (Figure 4.3 C). No differences were found between the expression levels of the two amplicons tested in each *pes1* and *ipcs3*. However, *pes1* showed an increased expression of both amplicons of *AtPES1* compared to Col-0, despite sequencing showing the T-DNA left border spanned the 5’ end of the promoter region (Figure 4.3 B). The primer pairs were tested *in silico* against the cDNA sequence of *AtPES2* which did not show any compatibility. The T-DNA left border in the *pes1* line was shown to be inserted in a regulatory region of *AtPES1* which could have had an unexpected effect of upregulating gene expression. Such effect has been previously reported, e.g. the Arabidopsis gene *ALDH3H1* (*ALDEHYDE DEHYDROGENASE 3H1*) where the T-DNA insertion mutant shown

higher levels of alternative transcripts than the wild-type plants (Missihoun *et al.* 2012). However, the cause of such effect was not further explored here, instead the lipid profile of *pes1* line was assessed and is discussed in the sections below. The line *ipcs3* showed no difference in the expression of both amplicons of *AtIPCS3* compared to Col-0 (Figure 4.4 C), suggesting that the presence of the T-DNA insertion did not influence the transcription of its coding sequence. The expression analysis of *AtPES1* and *AtIPCS3* in their respective mutant lines was thus not conclusive, and in the case of *pes1* contrary to the fluorescence phenotype described in Chapter 3 (Section 3.2.5). In this instance it might be anticipated that the transcription of the coding sequencing may not necessarily translate into a fully functional protein. To confirm this hypothesis further analysis into protein expression would be necessary, where a size difference or absence of PES1 protein could indicate a non-functional protein.

4.2.2 *Lipidome Remodelling in Response to Cold Stress*

An experiment was designed to assess the lipid changes driven by each genotype, and the impact of any loss of function on the plant's capacity to remodel the cellular lipidome in response to cold stress was investigated. To mimic the conditions used for the chlorophyll fluorescence analysis, six plants per genotype including Col-0 were grown in duplicate under control conditions for 19 DAS. At this age, one set of plants was moved to a 4°C cabinet (Section 2.2.4) for eight days (DAC). As seen previously in Chapter 3 no distinguishable phenotypic features were found in any of the mutated lines under either temperature, despite the visible effect of the cold stress in the plants (Figure 4.5). On the eighth day of stress (27 DAS for the control plants), the aerial tissue (rosette) of all plants was collected and freeze dried for further analysis. Following lipid extraction, lipid profiling was performed to characterise each T-DNA line. Due to the different proposed roles of *PES1* (Lippold *et al.* 2012)*, PGR5L1A* (DalCorso *et al.* 2008, Hertle *et al.* 2013), and *IPCS3* (Mina *et al.* 2010) analysis was adapted to the most relevant classes.

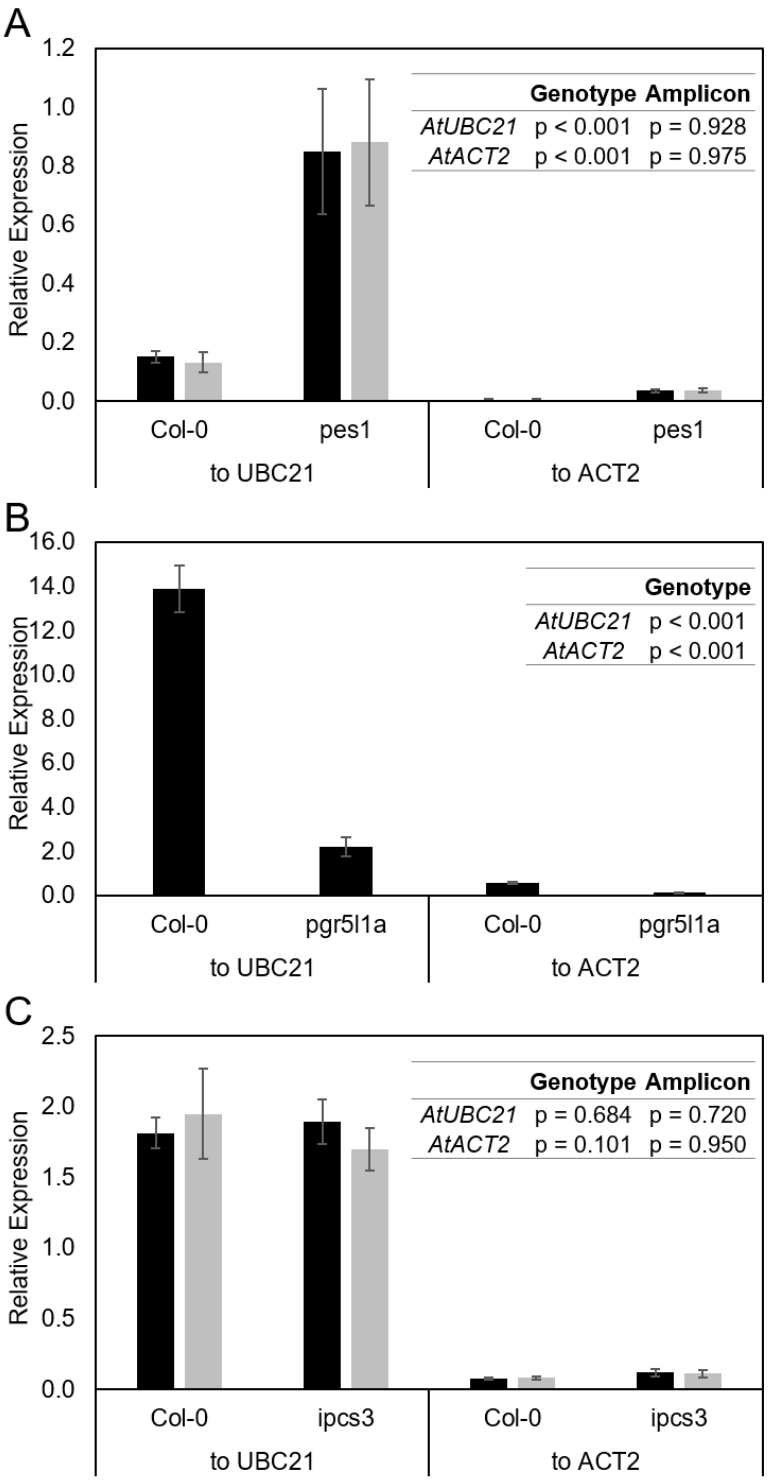

Figure 4.4 Expression Analysis of the three T-DNA Lines

Expression analysis of the mutant lines (A) *pes1* amplicons 1 (■) and 2 (■), (B) *pgr5l1a* amplicon 1 (■), (C) *ipcs3* amplicon 1 (■) and 2 (■). The wild-type Col-0 was used as positive control, the expression of each gene was calculated against the reference genes *AtUBC21* and *AtACT2*. Insert shows ANOVA results for differences between genotypes and amplicon within genotype. RNA was extracted from 18 DAS leaves from three different plants, and the RT-qPCR was performed with two technical replicates.

Due to the link between the photosynthetic apparatus in the thylakoid membranes, which incorporate MGDG, DGDG, SQDG, and PG, these lipids were thus analysed in the T-DNA lines under control and cold temperatures, except for *ipcs3.* In *ipcs3*, the galactolipid content was only analysed under control, as the limited aerial tissue collected at eight DAC was just enough for the analysis of its sphingolipid profile, and due to *IPCS3* function (Mina *et al.* 2010), the complex sphingolipids analysis was prioritised in the *ipcs3* mutant. Altogether lipid classes analysed also included TAG, phospholipids phosphatidylcholine (PC), phosphatidylethanolamine (PE), phosphatidylglycerol (PG), lyso phosphatidylcholine (LPC or lyso-PC), phosphatidylserine (PS), and FFA for *pes1* and *pgr5l1a*, and DAG only assessed for *pes1*.

4.2.3 *IPCS3: A Negative Control for Chloroplast Lipid Remodelling?*

IPCS3 was included in the experimental design as a negative control for chloroplast lipid composition. To confirm the suitability of *IPCS3* as such a control, galactolipids were profiled in plants grown at control temperature of 23°C (Figure 4.6 A). Unexpectedly, changes occurred in the chloroplast lipid profile of *ipcs3*, specifically molecular species of MGDG e.g. 34:6 and DGDG e.g. 36:6 (Figure 4.7). Given the known function of IPCS3 in sphingolipid synthesis ((Bromley *et al.* 2003, Mina *et al.* 2010), see Section 4.1.3), it was not anticipated that *ipcs3* show changes in chloroplast lipids. Indeed, both PG and SQDG compositions remain comparable to the wild-type Col-0. However, the observed changes in MGDG and DGDG composition at control temperature indicated a metabolic response to the perturbed sphingolipid metabolism in *ipcs3.* This association has not been previously reported and it requires further investigation to any links with the perturbed sphingolipid metabolism described in Section 4.2.7.



Figure 4.5 Col-0, pes1, pgr5l1a and ipcs3 Growth Phenotype

Growth phenotype of the T-DNA lines *pes1, pgr5l1a, ipcs3* and the wild-type Col-0 after 26 DAS of control 23°C day (top pots) and after eight days of cold stress at 4°C (8 DAC, bottom pots). One representative plant per genotype and temperature is shown.

4.2.4 *Galactolipid Composition Changed in the Mutant Lines*

The galactolipid (MGDG, DGDG, SQDG) and phospholipid (PG) composition characteristic to the chloroplast thylakoids showed differences in the T-DNA lines compared to the wild-type Col-0. Canonical multivariate (CV) analyses were performed for the results obtained under control (23°C, Figure 4.6 A) and after eight days of cold stress (4°C, Figure 4.6 B) to ascertain the differences between the T-DNA lines and Col-0 (CV loadings in Appendix 6). In either temperature, two dimensions were used to explain the compositional variation of the lipid pools shown in Figure 4.7. Under control conditions, CV1 explained 76.6% of the data variability which distinguished *pes1* profile (Figure 4.6 A). This response of *pes1* was influenced by MGDG 36:6, and the PG molecular species 34:3 and 34:1, whilst SQDG 36:5, 34:4, 34:2 and 34:1 also contributed for this result however with less weight in the positive loadings of CV1. In contrast, the 95% confidence intervals (CI) of each Col-0, *pgr5l1a* and *ipcs3* showed an overlap, but nevertheless each respective mean (represented by "×" in Figure 4.6 A) showed different responses in CV2 accounting for 18.8% of the data variability. Col-0 was

distinguished by the molecular species PG 34:1 and MGDG 34:6, which showed the most weight in the negative loading of CV2. In contrast, MGDG 36:6, 36:4 and SQDG 34:3 showed to mostly influence CV2 positive loadings where *ipcs3* and *pgr5l1a* were positioned. No analysis of the galactolipid profile of *ipcs3* was performed under cold conditions due to the limited availability of rosette tissue (Section 4.2.2).

Under chilling conditions (Figure 4.6 B), more than 90% of the galactolipid data variability distinguished *pes1* from Col-0 (CV1). CV1 was positively influenced by 34 carbon acyl chain species of DGDG 34:3, SQDG 34:3 and PG 34:4 and 34:1 characterised Col-0 profile. Whilst *pes1*, sitting in the negative CV1 was influenced mainly by the molecular species profiles of MGDG 36:6, 34:5 and 34:4, PG 34:3 and DGDG 34:1. PG molecular species were equally distributed through both CVs, with 34:4, 34:2 and 34:1 (mainly 16:X-18:X) characterising Col-0 and PG 34:3 (also 32:0 and 32:1, but to a lesser extent) weighting the negative loadings where *pes1* is situated. *pgr5l1a* showed an intermediate profile localised between Col-0 and *pes1* which loading showed influence of SQDG 36:5 and DGDG 36:5. The differences found in the individual lipid classes profile in the T-DNA lines did not translate into significant differences in the total lipid content amongst genotypes (Figure 4.8). The reduced temperature showed a significant ($p<0.001$) impact in the total content of MGDG, PG and SQDG lipid pools which showed at least 50% reduction in the total content, reaching up to a 73.0% reduction in the SQDG content in *pgr5l1a.* MGDG, together with PG showed to be the predominant classes ($p<0.001$), whilst SQDG was only found in minor quantities as expected.

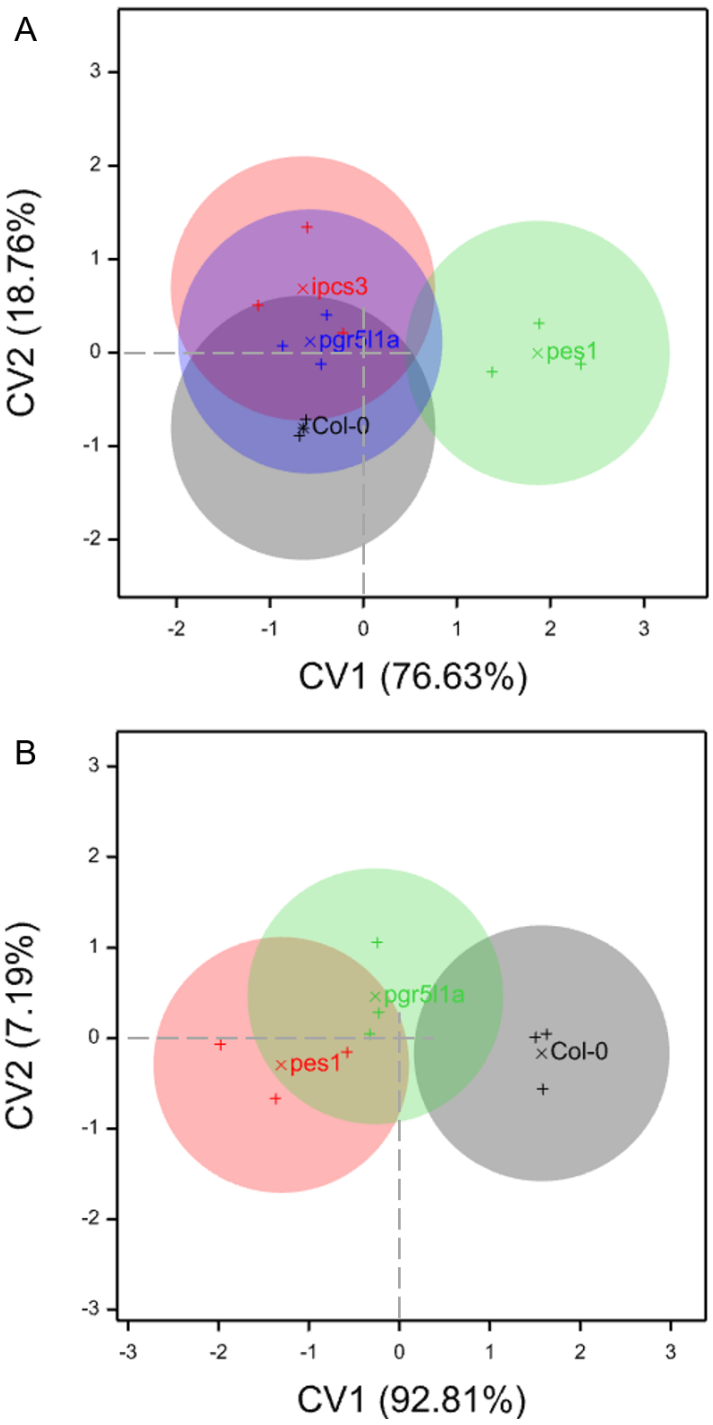

Figure 4.6 Multivariate Analysis of Galactolipids

Canonical variate (CV) analyses of the pool of the galactolipids for (A) Col-0 (■), *pes1* (■), *pgr5l1a* (■), and *ipcs3* (■) under control 23°C; and (B) Col-0 (■), *pes1* (■), *pgr5l1a* (■) after eight days under cold stress at 4°C. Two dimensions (CV1, CV2) were found to explain the variability of the data. Circles around means (×) represent 95% confidence intervals, individual points are represented by "+". Dashed lines represent zero in both CV1 and CV2. Loadings shown in Appendix 6.

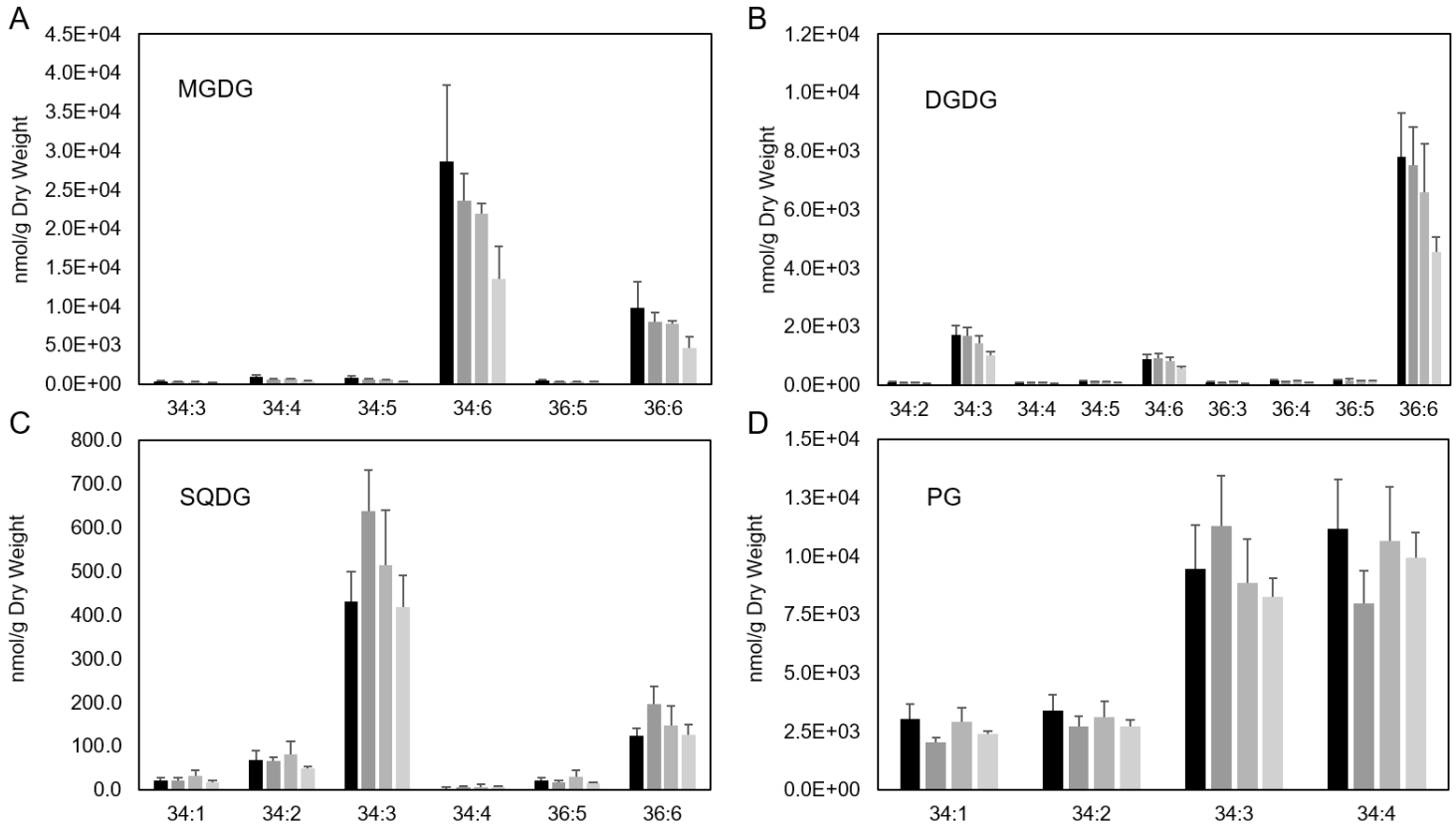

(Continued on the next page)

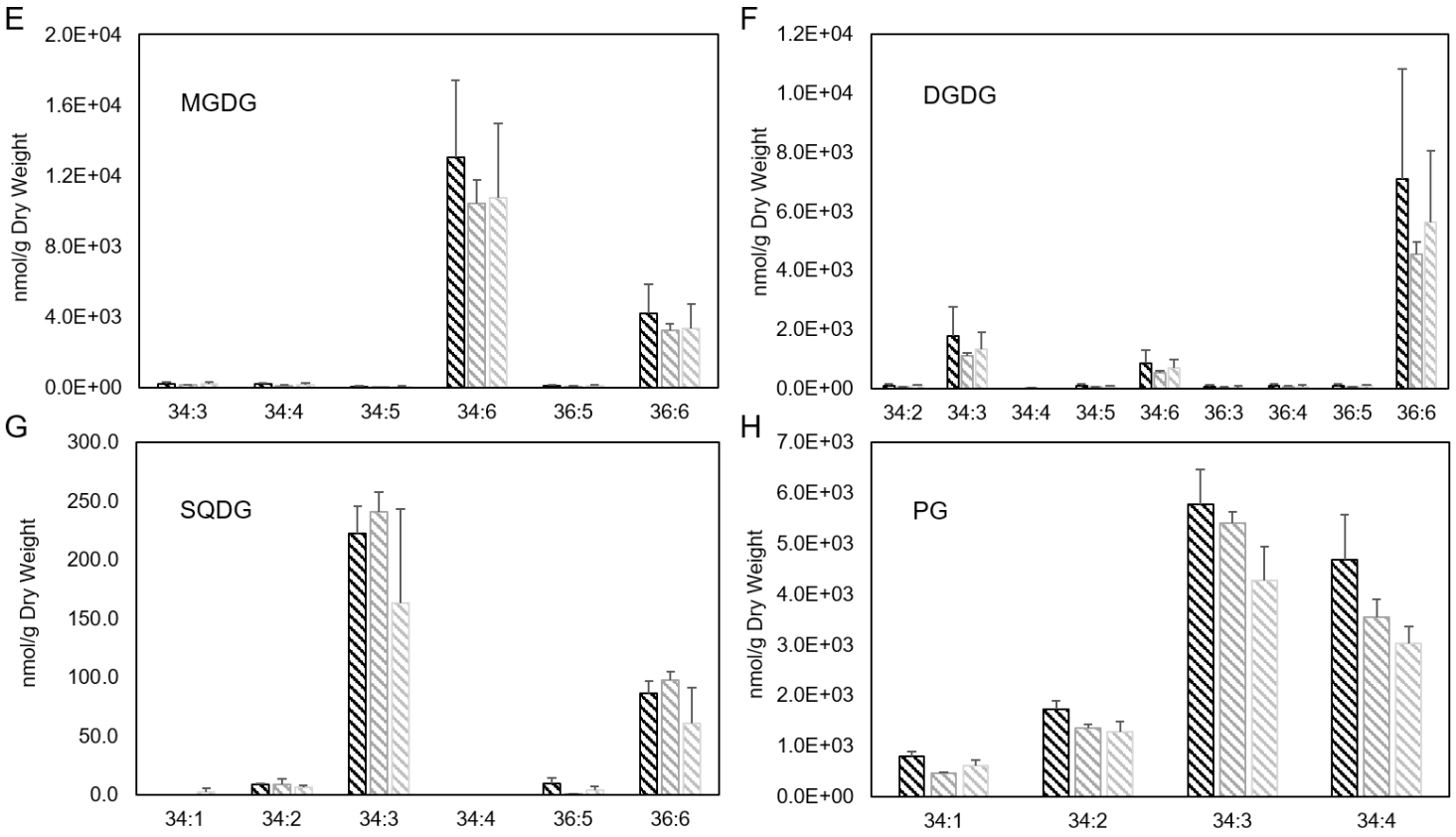

Figure 4.7 Galactolipid Composition of T-DNA Lines

Chloroplast lipids MGDG (A, E), DGDG (B, F), SQDG (C, G), and PG (D, H), under control 23°C (A-D, block colour) and eight days after cold stress at 4°C (E-H, patterned) for Col-0 (■), *pes1* (■), *pgr5l1a* (■), and ipcs3 (■). Bars represent mean + standard error, N=3.

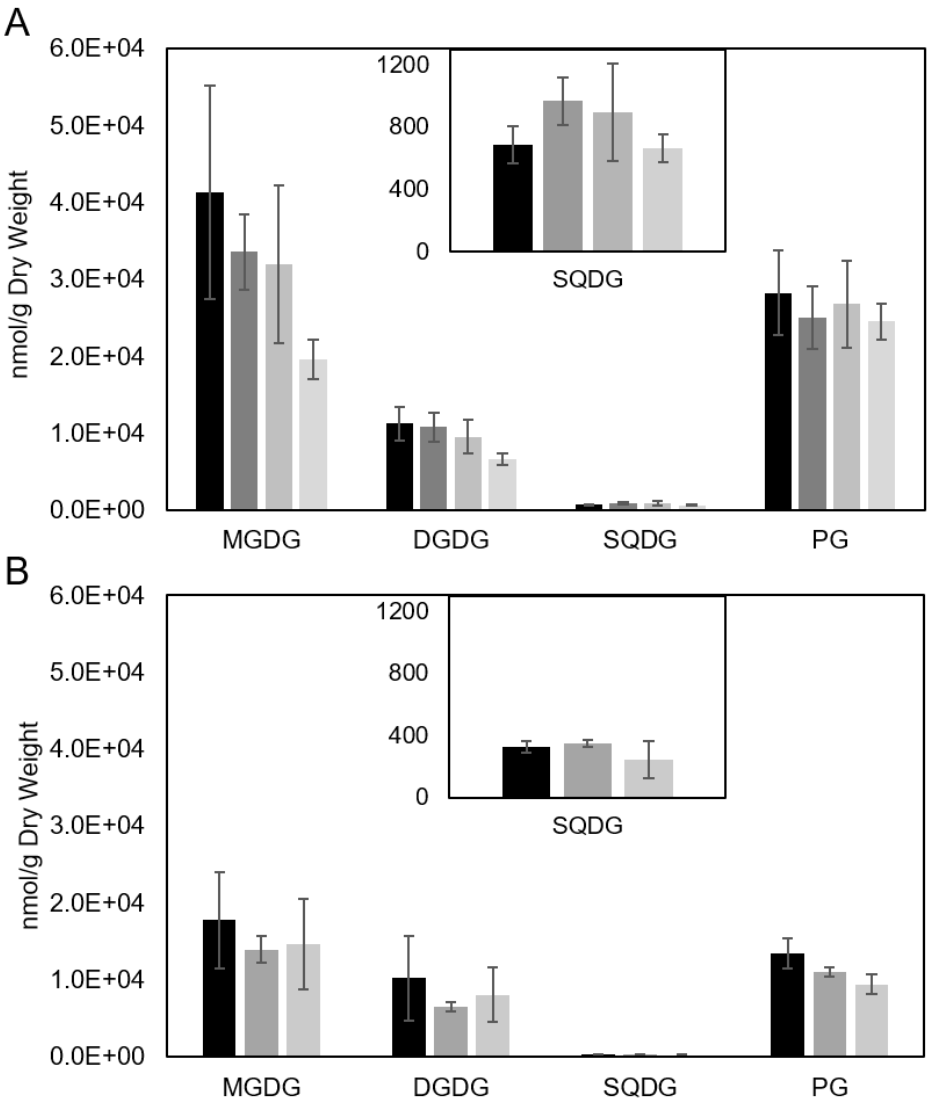

C

Treatment	P value (log_{10})
Genotype	p = 0.050
Temperature	p < 0.001
Genotype * Temperature	p = 0.537
Genotype * Temperature / Lipid Class	p < 0.001

Figure 4.8 Total Content of MGDG, DGDG, SQDG, and PG

Total content of MGDG, DGDG, SQDG, and PG for Col-0 (■), *pes1* (■), *pgr5l1a* (■), and ipcs3 (■), under control 23°C (A) and at eight days after cold 4°C (8 DAC, B). The insert shows the detail for SQDG content. Bars represent mean + standard error, N=3. (C) ANOVA results table showed results for the tested genotypes ("Genotype"), temperatures ("Temperature"), interaction between both ("Genotype * Temperature"), and lipid class within this interaction ("Genotype * Temperature / Lipid Class").

4.2.5 *DAG and TAG Composition was Altered in pes1*

PES is involved in the allocation of chlorophyll derived phytol into phytyl esters, however it also shows acyltransferase activity with broad substrate specificities (Lippold *et al.* 2012). Hence, and as previously shown, both *PES1* and *PES2* produce TAG from its DAG precursor, whilst also being able to mobilise acyl groups from MGDG to DAG (Lippold *et al.* 2012). With senescence or abiotic stresses, the chloroplast lipid composition changes. Degradation of chlorophyll and galactolipids from the thylakoid membranes results in the accumulation of fatty acid phytyl esters, tocopherol and TAG (Ischebeck *et al.* 2006, Gaude *et al.* 2007). The analysis of *pes1* mutant line showed a perturbed profile of the chloroplast galactolipids compared to Col-0, characterised by MGDG e.g. 36:6 and PG e.g. 34:3. In an effort to further investigate the impact of *PES1* in the cellular cold response, TAG, DAG, FFA and phospholipids were analysed in *pes1* alongside Col-0 at temperatures of 23°C and 4°C by multivariate analysis. This analysis reflected the respective compositional profiles of each class shown in Appendix 9 through Appendix 11. Two dimensions were so used to describe the lipid profile of dataset (Figure 4.9). In all the analyses, the first dimension (CV1) confirmed the impact of the cold stress in both Col-0 and *pes1*, being responsible for 75.3% to 95.3% of the variation observed. Whilst CV2 allowed to distinguish differences in the lipid profile amongst genotypes.

Under control temperatures, *pes1* showed a total overlap in its TAG profile with the wild-type, however some divergence between the genotypes was shown at eight DAC (Figure 4.9 A). This was mostly due to the presence of TAG molecular species with a sum of acyl chains of 48:X, 54:X and 60:X carbons in Col-0. This is in accordance with reports showing *PES1*- or *PES2*-expressing yeast are rich in 48:X, 50:X, 52:X, and 54:X TAG (Lippold *et al.* 2012). As a precursor for TAG synthesis and a substrate for PES1, an understanding of DAG content and composition is important. The DAG profile was measured and showed a distinction in its composition between temperature treatments (shown by CV1) and genotypes (shown by CV2, Figure 4.9 B).

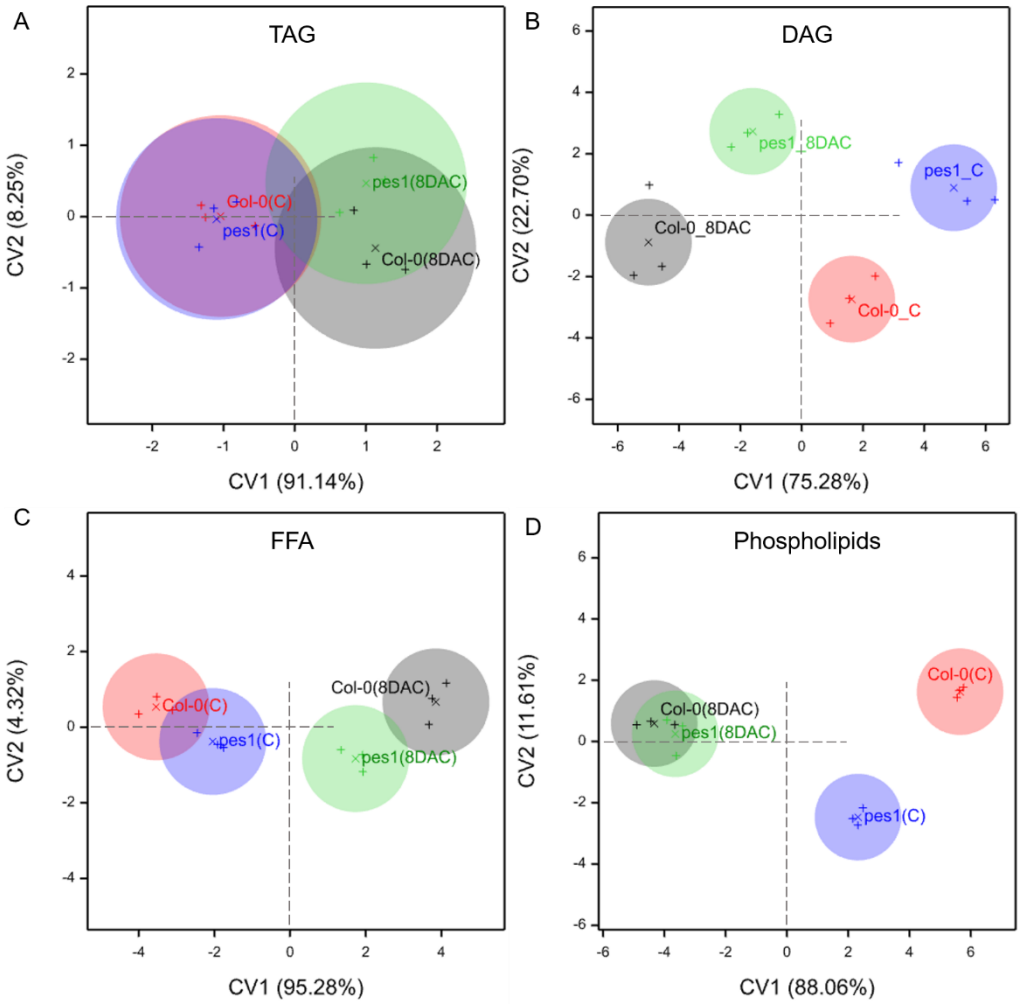

Figure 4.9 Multivariate Analysis of pes1 Lipids

Canonical multivariate (CV) analysis of (A) TAG, (B) DAG, (C) FFA, and (D) phospholipids measurements for the wild-type Arabidopsis (Col-0) and *pes1* (pes1) under control 23°C (■ Col-0_C, ■ pes1_C) and at eight days after cold stress at 4°C (■ Col-0_8DAC, ■ pes1_8DAC). Each analysis had two components assigned with the respective variability of the data (in percentage, %). Circles around means (×) represent 95% confidence intervals, individual points are represented by "+". Dashed lines represent zero in either axis. CV loadings shown in Appendix 7.

Compositional change did not translate into a significant difference in the size of the DAG total pool (Appendix 10). Differences between *pes1* and Col-0 in the FFA and phospholipid profiles were also found. FFA composition differed in the carbon acyl chain length, with control conditions having 18:X and 20:X carbons (Figure 4.9 C). Significant changes were observed in the major phospholipid pools in genotypes grown in control conditions. PE and PC showed changes between the genotypes under control conditions. The CV2 positive loadings showed

Col-0 deviated from *pes1* due to changes in PS content (Figure 4.9 D). Cold-induced phospholipid remodelling resulted in a shift towards LPC and PS (Figure 4.9 D). The fatty acid phytyl ester profile was not measured, as it has been published and established to accumulate under control conditions in the absence of *PES* genes, and under stress conditions. Despite the predicted redundancy between PES1 and PES2 (Lippold *et al.* 2012), it was clear that *PES1* did influence cold stress lipid remodelling

4.2.6 *pgr5l1a Mutant Showed Disturbed TAG and FFA Profiles*

PGR5L1 has been identified in Arabidopsis as part of the PGR5-PGR5L1 complex, which is thought to transiently interact with the PSI and the cytochrome b_6/f for the efficient CEF around PSI (DalCorso *et al.* 2008). The designation comes from its similar phenotype to the *PROTON GRADIENT REGULATOR 5* (*PGR5*), and in Arabidopsis PGR5L1 is encoded by two genes *AtPGR5L1A* and *AtPGR5L1B.* In Arabidopsis, these two genes share 58.8% sequence identity for the genomic sequence, however, their proteins have 80.1% similarity. In the fluorescence screen, only the T-DNA insertion line for *AtPGR5L1A* showed a significant impact with cold stress, which together with its expression pattern might suggest a role of this gene in the Arabidopsis cold stress response. No variation in the lipid profile was expected in the *pgr5l1a* mutant, as the *AtPGR5L1A* gene is related to the CEF around PSI and, so far, no reports were found of a relationship between electron flow and the plant's lipid metabolism. However, TAG, phospholipids and FFAs were analysed and compared with the wild-type Col-0 (as described for *pes1*).

Multivariate statistics were then applied to elucidate the data through a canonical multivariate test, which reflected the respective profiles of each class shown in Appendix 9 and Appendix 11. The multivariate analysis in each of these classes found that temperature explained 87.5% to 93.0% of the variability in the dataset shown by CV1 (Figure 4.10). The variation

between genotypes was found in CV2, (a maximum of 7.6% in the FFA profile; Figure 4.10 B). Together with TAG (Figure 4.10 A), FFA showed a significant difference in the cold dataset of *pgr5l1a* compared to Col-0. Primarily this was due to the impact of 16:X, 20:X and 24:X in the CV2 positive loadings of FFA. Concomitantly, TAG analysis showed a tendency for shorter acyl chains, in *pgr5l1a* e.g. 48:X to 52:X, whereas Col-0 was characterised by 54:X and 60:X.

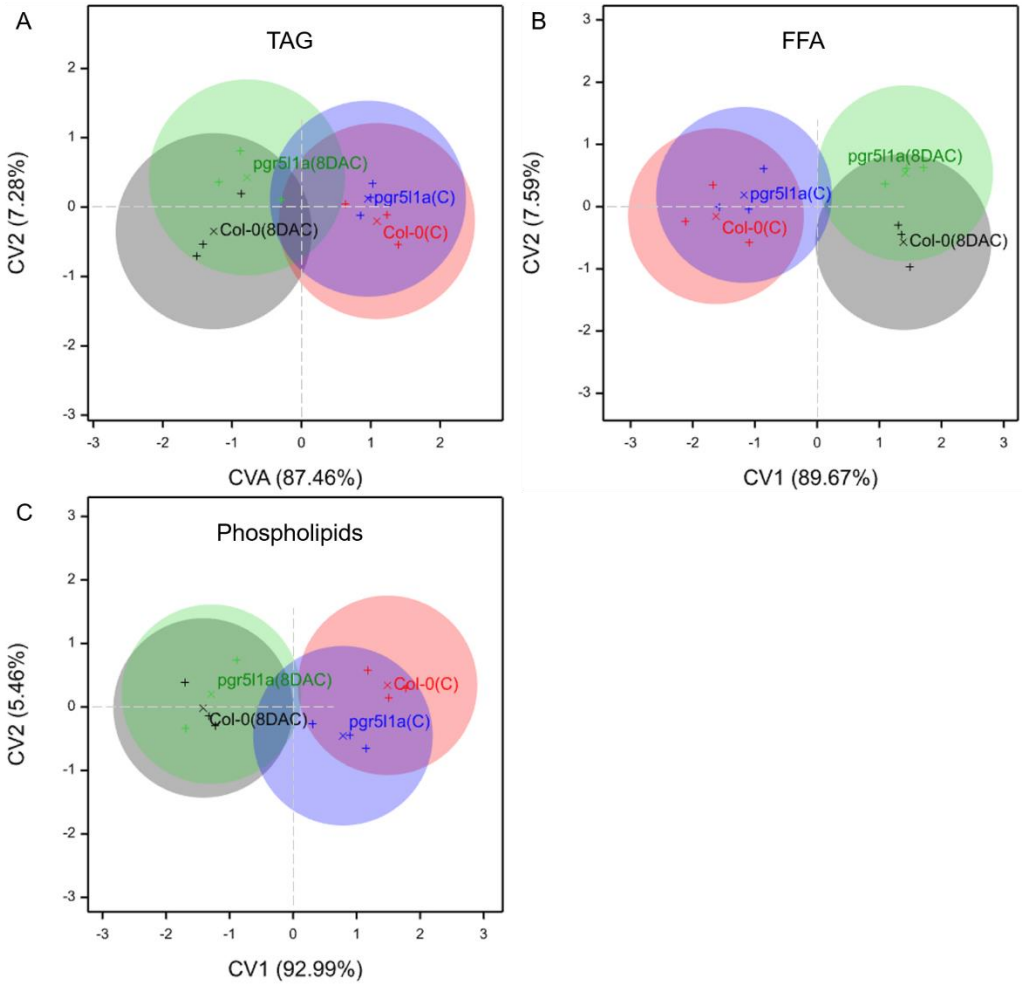

Figure 4.10 Multivariate Analysis for pgr5l1a Lipids

Canonical multivariate (CV) analysis of (A) TAG, (B) FFA, and (D) phospholipids for the wild-type Arabidopsis (Col-0) and *pgr5l1a* (pgr5l1a) under control 23°C (■ Col-0_C, ■ pgr5l1a_C) and at eight days after cold stress at 4°C (■ Col-0_8DAC, ■ pgr5l1a_8DAC). Each analysis had two components assigned with the respective variability of the data (in percentage, %). Circles around means (×) represent 95% confidence intervals, individual points are represented by "+". Dashed lines represent zero in either axis. CV loadings shown in Appendix 8.

4.2.7 *IPCS3 Changed the Ceramide and GIPC Content*

As previously described (Section 4.1.3), *IPCS3* catalyzes the production of GIPCs, and it is hypothesized that this lipid class plays a significant role in the cold acclimation process. Furthermore, RNA-Seq analysis (Chapter 3) showed *IPCS3* to be upregulated under cold stress (log_2 fold change of 1.07), while both *IPCS1* and *IPCS2* were downregulated (log_2 fold change of –0.94 in both cases), suggesting a specific role of this gene in cold acclimation. The LCB is a unique component of the sphingolipid class, which linked to a VLCFA forms the ceramide backbone of sphingolipids (further review in Chapter 1). To assess metabolic changes related to *IPCS3*, the sphingolipid profile of its T-DNA line was analyzed under both control (23°C) and 8 DAC (4°C) conditions. The LCB profile was also assessed showing a significant reduction of the isomers t18:1$^{\Delta 8Z}$ (*cis*) and t18:1$^{\Delta 8E}$ (*trans*) in *ipcs3* (Figure 4.11 A). This reduction did not affect the *cis*/*trans* ratio (Figure 4.11 C), but was reflected in the significant 26.4% reduction of the LCB content in *ipcs3* (Figure 4.11 B). Temperature did not seem to greatly affect the LCB pool, except for a reduction in saturated species d18:0 and t18:0 which could reflect the demand for desaturated species under cold stress.

The GIPCs are the most abundant sphingolipid in plant tissues, and are a key component of the plasma and endo-membranes [(Gronnier *et al.* 2016), further review in Chapter 1]. In the sphingolipid analyses performed, ceramides and GIPCs showed the most intricate pattern in *ipcs3*. To differentiate this response principal components multivariate analyses were used (Figure 4.12), which reflected the profiles shown in Figure 4.13. The first dimension (PC1) identified an outlier in the wild-type dataset. Plotting the second (PC2) and third (PC3) dimensions showed a separation between *ipcs3* and Col-0 profiles. The ceramide profile could be distinguished from Col-0 by PC2 where positive loadings were characterized by trihydroxy LCBs associated with very long-chain fatty acids (VLCFA, Figure 4.12 A). The full ceramide profile in Figure 4.13 A-D further reflected this, with an increased content of the t18:0 and t18:1 ceramides in tandem with a decrease in dihydroxy LCBs.

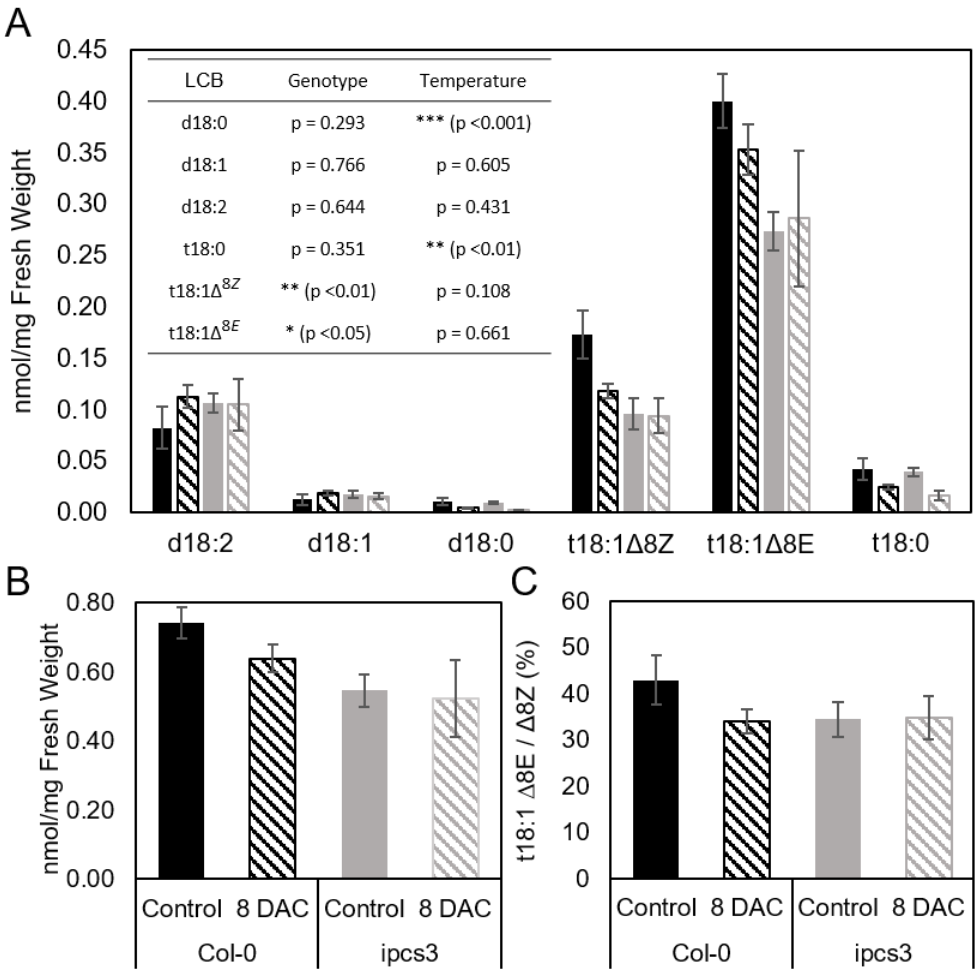

Figure 4.11 Long-Chain Base Profile of ipcs3

(A) Long-chain base (LCB) profile, (B) total LCB content, and (C) t18:1$^{\Delta 8Z}$ (*cis*) to t18:1$^{\Delta 8E}$ (*trans*) ratio for the T-DNA line *ipcs3* (■) and the wild-type Col-0 (■), analysed under control 23°C (block colour) and after eight days of cold 4°C (8 DAC, pattern). Bars represent mean ± standard error, N=6. ANOVA was used for analysis of differences amongst genotypes (A, results in insert; B, p <0.05; C, p =0.367), or temperature (A, results in insert; B, p =0.353; C, p =0.314).

In contrast, GIPC composition was similar in *ipcs3* and Col-0 under control temperatures. However, with cold stress *ipcs3* separated from Col-0 as shown by PC2 in Figure 4.12 B. This effect was mainly influenced by the acyl chain length in the FA of the ceramide backbone, which showed VLCFA in the positive loadings corresponding to the cold-induced *ipcs3* profile. Differences in the control temperature profile between the T-DNA line and the wild-type could be identified by the third dimension (PC3), which accounted for 15.5% of the variability (Figure 4.12 B). The resulting distinction between Col-0, with greater quantities

of trihydroxy LCBs t18:0 and t18:1, and *ipcs3* with d18:0 and d18:1 confirm the results obtained from the LCB measurements (Figure 4.11). However, there was no change in the total content of the GIPC pool (Appendix 14). As one of the main enzymes in the production of GIPC, the T-DNA line for IPCS would be expected to show a decreased production of this complex sphingolipid. Such an outcome might result from the tissue-specific expression of IPCS transcripts i.e. *IPCS2* has an ubiquitous expression in the whole plant, while *IPCS3* is localized to the stem and flower tissues (Mina *et al.* 2010). The hydroxyceramide and glucosylceramide profiles were also obtained, with minor changes in *ipcs3* profile to Col-0, as presented in Appendix 13.

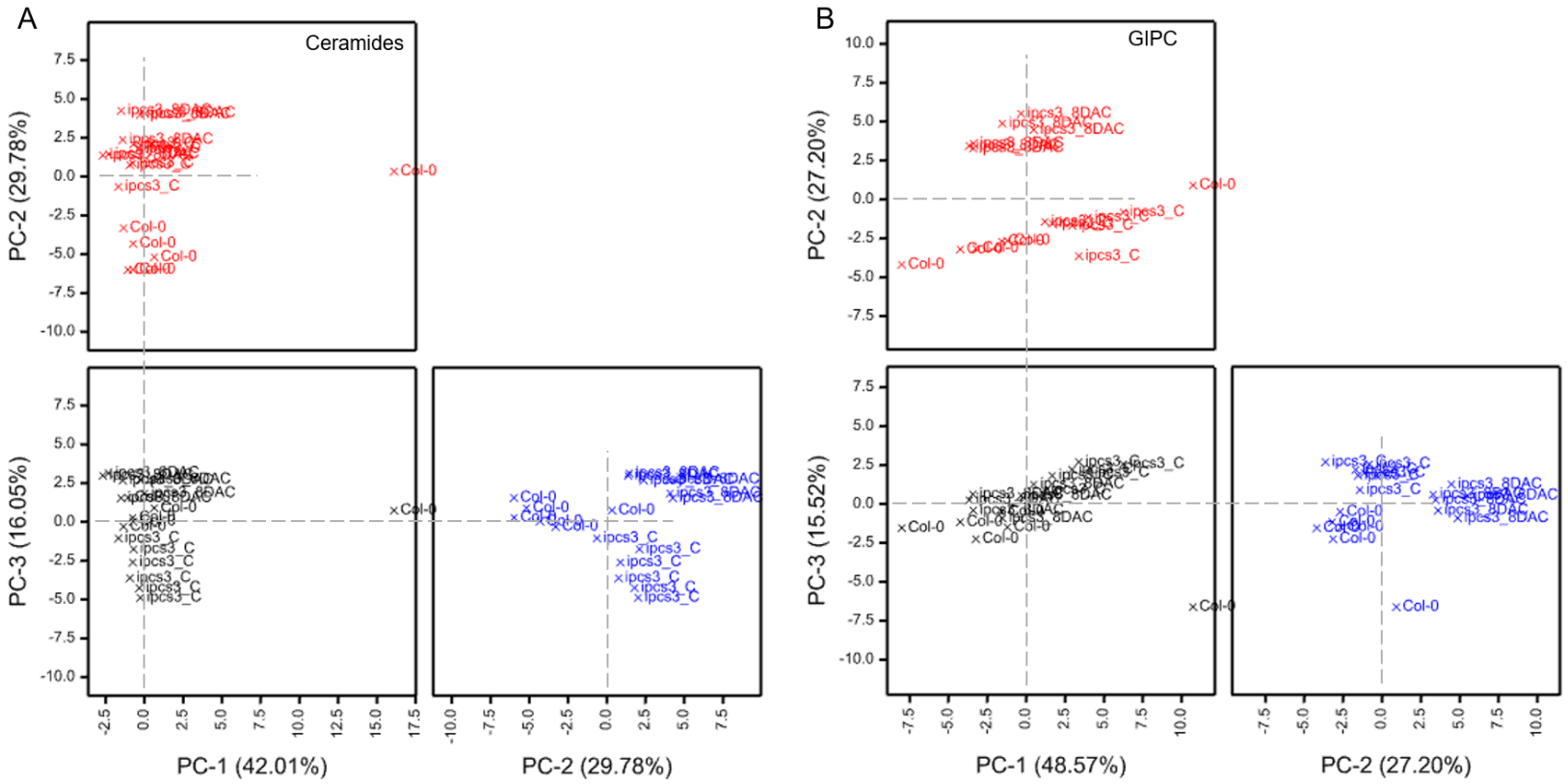

Figure 4.12 ipcs3 Ceramide and GIPC Multivariate Analysis

Principal component (PC) analysis for (A) ceramides and (B) GIPCs profile in the wild-type Col-0 at control conditions, and ipcs3 under control 23°C (ipcs3_C) and after eight days of cold 4°C (ipcs3_8DAC) conditions. Three PC explained 75.61% (A) and 91.29% (B) of the variability in the dataset. Individual replicas are represented by "×", N=6, dashed lines represent zero in each axis. PC loadings shown in Appendix 12.

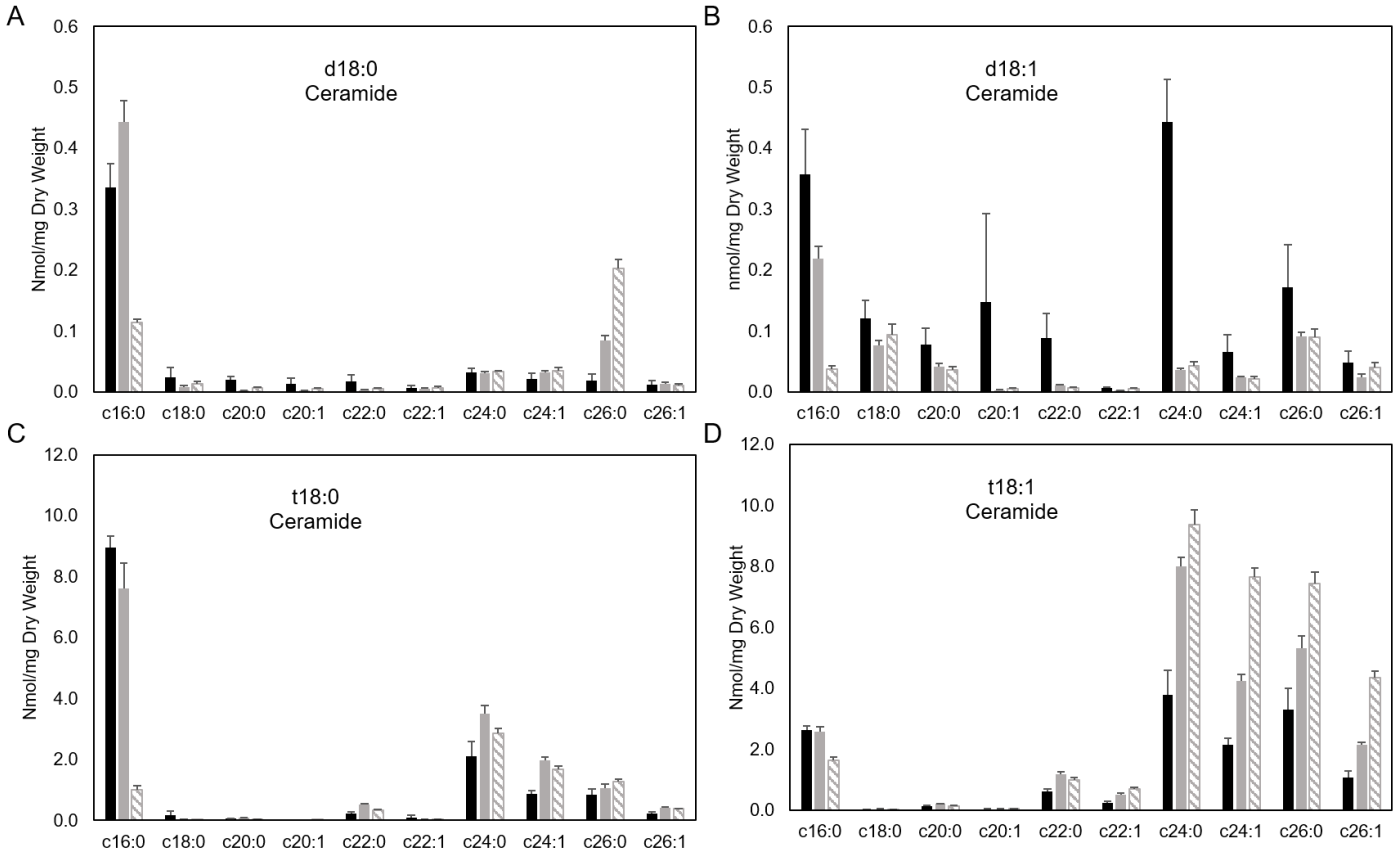

(Continued on the next page)

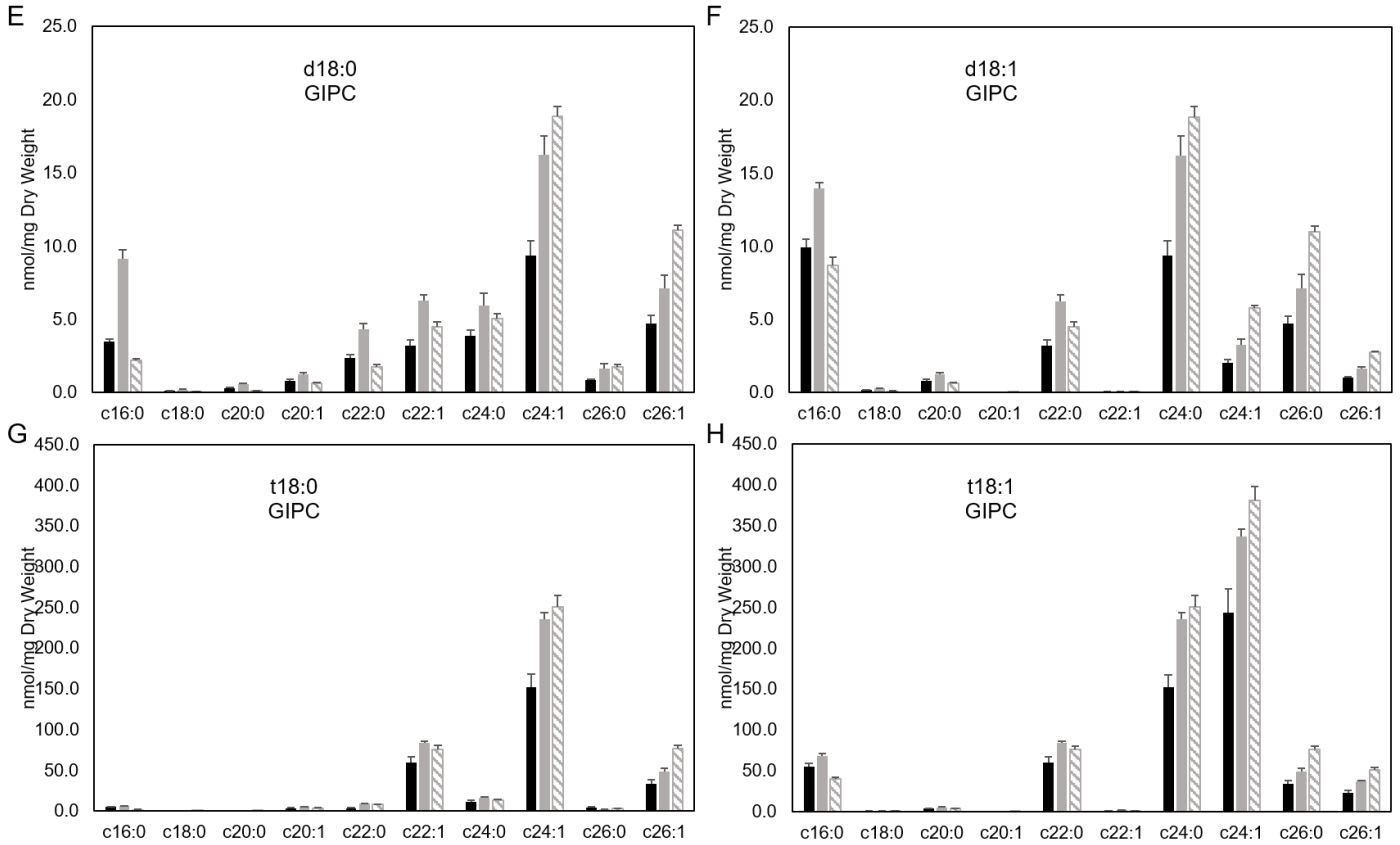

Figure 4.13 Ceramide and GIPC Profiles for ipcs3

Ceramide (A-D) and GIPC (E-H) fatty acid profile for the LCBs d18:0 (A, E), d18:1 (B, F), t18:0 (C, G), and t18:1 (D, H) profiles for Col-0 under control (■), *ipcs3* under control (■) and after eight days of cold (■ patterned) conditions. Bars represent mean + standard error, N=6

4.3 DISCUSSION

This chapter examined the changes in the lipidome associated with the candidate genes identified through the chlorophyll fluorescence cold-induced screen in Chapter 3. The three T-DNA insertion lines were genotyped, to confirm the presence and localisation of the T-DNA left border for each target gene. Gene expression analysis showed a reduction in *pgr5l1a* target gene expression, in contrast to the *pes1* and *ipcs3* T-DNA lines. These lines were then assessed using targeted lipid analysis as a preliminary assessment of the link between gene activity, chloroplast fluorescence and lipid remodelling in response to cold stress (as discussed in Chapter 1). The T-DNA line *pes1* showed a significantly different profile to Col-0, characterised by PG 34:3 and MGDG 36:6. Minor differences were found between *pgr5l1a* and the Col-0 lipid profiles. Despite the inclusion of *ipcs3* as a negative control for the galactolipid profile, changes in the MGDG and DGDG profiles were observed under control conditions. Further lipidomic characterisation of the lines was performed. *pes1* had a perturbed phenotype in TAG, DAG, FFA and phospholipids, whilst *pgr5l1a* demonstrated a shift in the TAG and FFA profiles compared to Col-0 under cold conditions. Profiling of *ipcs3,* identified a reduction in the trihydroxy LCB concomitant with a corresponding shift in the GIPC profile (characterised by d18:0 and d18:1).

4.3.1 *The T-DNA Insertion SALK lines*

The complete molecular characterisation of the T-DNA lines was only performed in the candidate lines chosen after the cold screen, due to the volume of lines initially obtained and included in the screen. Nonetheless, all lines used in the cold screen were previously confirmed to be homozygous for the presence of the T-DNA, and disruption of the respective wild-type sequence. Based on the gDNA sequencing data and the target gene expression analysis performed, *pgr5l1a* was shown to be disrupted with a subsequent reduction in its gene expression. Ambiguous

results were obtained for the lines *pes1* and *ipcs3*, which despite showing the presence of the T-DNA the gene expression analysis suggested the continued transcription of the targeted sequences. Despite this, the differences found in the lipid profile of these lines suggested a true disruption of the gene function at the protein level. Examples like this can be found in the literature, as the *mgd1* SALK line that allowed the identification and characterisation of the Arabidopsis *MGD SYNTHASE1,* in which T-DNA insertion was found 148 bp upstream of the start codon (Jarvis *et al.* 2000). As the preliminary lipid phenotype of the mutant lines showed significant results, future work should focus on obtaining further disrupted lines. This could be achieved by searching repositories like the SALK collection for mutants in which the T-DNA disrupts the coding sequence, or that present more than one T-DNA insertion (Alonso 2003, Rhee and Mutwil 2014). As an alternative, the application of genome editing CRISPR/Cas9 system could be explored, which would allow targeted editing of the different domains found in the PES to ascertain the different contributions of this enzyme to the chloroplast lipid metabolism. Creating single and double mutants for *PGR5L1(A/B)* or *IPCS(1-3)* to elucidate the relative contribution of these genes to the plant cold acclimation process would also be of value.

4.3.2 *Galactolipids were Affected in the Mutant Lines*

The galactolipid content was assessed in the T-DNA lines, in an effort to explore the potential connection between the perturbed photochemical performance observed under cold stress with the lipid metabolism of the chloroplast. As the main site of photosynthesis, the thylakoid membranes are constituted almost exclusively by MGDG, DGDG, PG and in minor quantities by SQDG (Andersson and Dormann 2009). The analysis presented here confirmed the typical distribution of galactolipids in the wild-type, which showed no alteration in any of the mutant lines. Moreover, exposure to cold temperatures for eight days showed an overall reduction in the content of these lipids, which could be associated with the reduced metabolism of the plant, associated with the defence

response to the applied stress conditions. Sphingolipids have been established to have an important part of plant cellular membranes, such as the plasma membrane, tonoplast and Golgi compartment, however are not found in the chloroplast (Andersson and Dormann 2009). Thus, no impact in the galactolipid composition of *ipcs3* was expected, rendering its use as a negative control. Nevertheless, *ipcs3* showed changes in its galactolipid profile which could possibly result from the disturbed sphingolipid metabolism as described in Section 4.2.7. A few cases in the literature were found that show similarities. The tomato (*Solanum lycopersicum*) sphingolipid LCB Δ^8-desaturase *SlSLD* knockdown, for example, showed severely damaged chloroplasts with chilling temperatures resulting in swollen thylakoids, reduced stacking of the grana and disruption of the thylakoid membranes (Zhou *et al.* 2016). The disruption of the Enoyl-CoA Reductase (*ECR*) gene required for the synthesis of VLCFA essential to the ceramide backbone of sphingolipids (reviewed in Chapter 1), in tobacco (*Nicotiana benthamiana*) plants also revealed poorly developed thylakoids (Park *et al.* 2005). However, no direct link between sphingolipid-related genes and galactolipids was found in the literature. Thus, further investigations are due to understand the observed relationship between sphingolipid and chloroplast metabolism. The changes observed in the galactolipid profile in *pgr5l1a* when compared to Col-0 were not expected, as this is a gene related to the CEF in the PSI and no previous relation to lipid metabolism was found. However, the observed changes could result from the oxidative damage to the photosystems caused by the lack of PGR5L1-PGR5 complex. As PGR5L1 is thought to be the thylakoid anchored protein that along with PGR5 form a CEF regulatory complex (Yamori and Shikanai 2016). The chlorophyll fluorescence results obtained in Chapter 3 suggested that the isoform *PGR5L1A* is the predominant coding sequence to the PGR5L1 protein. It would be of interest to explore the alternative CEF regulatory complex mediated by NDH to ascertain the relative contributions of each complex in the Arabidopsis cold stress adaptation, as this complex has been described to be of significance in species including tobacco or rice (Li *et al.* 2004, Yamori *et al.* 2011).

4.3.3 *pes1 Chloroplast Lipid Composition was Affected by Temperature*

The T-DNA line *pes1* showed the most altered lipid profile compared to the wild-type Col-0. *PES1* was upregulated in Arabidopsis in response to cold stress (Chapter 3), whereas *PES2* was downregulated (log_2 fold change of -0.63, Appendix 3). Furthermore, RNA-Seq confirmed the upregulation of *PES1* in Eutrema (log_2 fold change of 2.26, Appendix 3). Recently *PES1* was also found to be upregulated in jojoba seedlings under cold stress treatment (Gao *et al.* 2019), strengthening the results obtained in this work and suggesting the hypothesis of a specific role of *PES1* under cold stress conditions. The relationship between *PES1* and the resulting decrease in the F_v/F_m was then explored by firstly analysing the lipid classes associated with the thylakoid membranes. This revealed a distinct profile characterised by MGDG 36:6, PG 34:3, 34:1; and to a more minor extent by SQDG 36:5, 34:4, 34:2, 34:1 under control conditions. The cold stress imposed shifted profile characterised by MGDG 36:6, 34:5, 34:4, PG 34:3, and DGDG 34:1. Such differences were not, however, reflected in the total content of the galactolipids which showed no differences to the wild-type. This was of no surprise, as the proposed dominant coding sequence *PES2* was still present in the *pes1* line. However, these results indicate the specific enzymatic preferences of PES1. The differences found in the profile under cold stress, with the presence in the *pes1* profile of MGDG molecular species 36:6, 34:5, 34:4 could also highlight this affinity under stress conditions. As galactolipid degradation occurs under stress, TAG, tocopherol and fatty acid phytyl esters (FAPEs) accumulate. The PES enzyme is thought to have an essential role in this pathway, not only by allocating free phytol into FAPEs, but also by integrating MGDG-derived acyl chains into the production of TAG (Lippold *et al.* 2012). The TAG profile of *pes1* under control temperatures did not show differences to the wild-type, again as expected probably due to the presence of *PES2*. However, TAG accumulation with cold stress revealed a slight distinction between the profiles with the contribution of acyl carbon chains that varied in length

between 44:X, 46:X, 52:X and 56:X, despite reports of the PES enzyme preference for medium-chain (C10-C14) fatty acids (Lippold *et al.* 2012, Aslan *et al.* 2014). MGDG, DGDG, SQDG, and PG compose the thylakoid membranes and are associated with PSI and PSII (Mizusawa and Wada 2012). Where, for example, SQDG is thought to be connected to the functional and structural efficiency of the PSII in both Arabidopsis and the green algae *Chlamydomonas reinhardtii* (Sato 2004). The profile changes observed in *pes1* and the specific contribution of MGDG profile may have contributed to the significant reduction in F_v/F_m observed during the cold screen. As a preliminary assessment, this chapter identifies a possible relationship between *PHYTYL ESTER SYNTHASE* and chloroplast metabolism under cold stress, specifically the production of fatty acid phytyl esters. However, the approach taken here was limited by the extraction of the total lipid pool from the whole aerial tissue of the Arabidopsis mutants. As an active metabolism in the plant, lipids are in constant turnover varying with stages of development, time of the day, rate of growth and cell compartmentation. The changes noted here should take in consideration of all these factors.

4.3.4 *IPCS3 is Involved in the GIPC Remodelling under Cold*

As an inositol phosphorylceramide synthase, IPCS is involved in the first committed step of the GIPCs synthesis in the Golgi compartment. GIPCs are a key element of the plasma membrane, and the most abundant sphingolipid in vegetative tissues (Markham and Jaworski 2007, Markham 2013, Gronnier *et al.* 2016). However, and partially due to their complexity, knowledge about GIPC synthesis, location in the plasma membrane and physiological role in the plant is still limited. In the RNA-Seq analysis of the Arabidopsis cold acclimation remodelling, *IPCS3* was found to be upregulated in contrast to its other two isoforms *IPCS1* and *IPCS2* (Appendix 3). The role and specific substrate of IPCS3 is still unclear, whilst IPCS2 was suggested to have a broad substrate specificity, independent of the hydroxylation status of the ceramide (Wang *et al.* 2008). The results reported here show a preliminary

characterisation of the contribution of the *IPCS3* encoded enzyme to sphingolipid remodelling during cold stress in Arabidopsis. The LCBs t18:1$^{\Delta 8E}$ (*cis*) and t18:1$^{\Delta 8Z}$ (*trans*) were both reduced in *ipcs3*, reflecting a reduce*d cis*/*trans* ratio, which was not however affected by cold stress. The trihydroxylated and desaturated LCB t18:1, that compose the ceramide backbone, and specifically the ratio between its *cis*/*trans* isomers are thought to be preferentially directed to the Golgi compartment (from the ER, where they are produced) for the assembly of GIPCs (Chen *et al.* 2012). If so, the reduced ratio observed by the absence of *IPCS3* would show an impact on GIPC production. The increased accumulation of GIPC observed in the mutant showed the importance of this sphingolipid class in the plant's adaptation to cold stress, suggesting the involvement of the *IPCS2* encoded enzyme, as this is thought to be the chief isoform (Mina *et al.* 2010). The predominance of d18:1 and d18:0 moiety in the GIPC profile of *ipcs3*, may also suggest the broad substrate specificity of IPCS2, whilst allocating the synthesis of t18 containing GIPC to IPCS3. This is supported by the ceramide profile in *ipcs3* showing a distinct composition of t18:0 and t18:1 to the wild-type. These are preliminary conclusions which would need further confirmation and raise several questions including establishing substrate affinity, the importance of the LCB t18:1 *cis*/*trans* ratio, and ultimately their role in the Arabidopsis cold adaptation strategies.

4.4 CONCLUSION

The present chapter provides a characterisation of the lipid context of each of the T-DNA lines selected by the chlorophyll fluorescence based cold screen. The connection between each of the identified genes and the galactolipids was established. *PES1* showed a perturbed SQDG and PG profile under control conditions, which changed with cold stress to modify MGDG composition. This suggests the involvement of this galactolipid in the stabilisation of the PSII in the thylakoid membrane. *PGR5L1A* registered some lipid changes with cold stress that so far could

not have been distinguished to be a direct result of its mutation or indirectly as a result of the damage caused to the photosystems and thylakoids by the low temperatures enhanced by the lack of PGR5L1-PGR5 complex. Finally, *IPSC3* role in the complex sphingolipids GIPCs biosynthetic pathway, and its relationship to the LCB t18:1 *cis*/*trans* partition was also analysed. The results presented here represent only a preliminary characterisation of the functions of each gene. Neither of these genes has been thoroughly covered in the literature, opening up the possibility of future work to be developed to establish their relative contribution to the Arabidopsis cold adaptation.

Chapter 5.
Sphingolipid LCB Δ^8-Desaturase as a Mediator of Cold Stress Response in Arabidopsis

5.1 INTRODUCTION

Sphingolipids are complex structural lipids which are formed from a ceramide backbone that can be linked to complex sugar residues and undergo a series of modifications leading to numerous diverse forms (reviewed in Chapter 1). The array of physical properties that sphingolipids exhibit is enabled by the many different structural changes (Michaelson *et al.* 2016). This range of classes produces several different physical and functional properties that can influence cell metabolism (Michaelson *et al.* 2016). As ubiquitous components of the plasma membrane sphingolipids contribute to its physical structure (Yoshida and Uemura 1986, Sperling *et al.* 2005). They have also been shown to play a role in trafficking, as the heterogeneous distribution of sphingolipids and sterols forming detergent-resistant domains has been linked to the movement of specific proteins in the PM (Mongrand *et al.* 2004, Minami *et al.* 2010). Sphingolipids have also been proposed as signalling molecules, e.g. sphingosine-1-phosphate and phytosphingosine-1-phosphate which regulates stomatal aperture [(Coursol *et al.* 2003, Coursol *et al.* 2005), and further reviewed in (Ali *et al.* 2018)]. Their role in cell metabolism spans a multitude of processes, which have not yet been fully studied. These include PCD (Liang *et al.* 2003, Donahue *et al.* 2010), ABA-mediated stomatal guard cell closure (Ng *et al.* 2001, Coursol *et al.* 2003), and plant defence against biotic (Magnin-Robert *et al.* 2015, Sanchez-Rangel *et al.* 2015) and abiotic stresses (Dutilleul *et al.* 2012, Dutilleul *et al.* 2015), as some reported examples.

5.1.1 *LCB Desaturases*

The four enzymes responsible for the modifications of the hydrophobic ceramide moiety, namely the Δ^4- and Δ^8-desaturases, the C4-hydroxylase and the acyl amide α-hydroxylase, all belong to a membrane bound, oxygen-dependent, enzyme family. This family also includes the fatty acid desaturases (FAD) involved in the biosynthesis of polyunsaturated fatty acids (Shanklin and Cahoon 1998). FADs catalyse

the introduction of a double bond into an acyl chain and can be soluble or membrane-bound (Shanklin and Cahoon 1998). The latter show a significant conservation amongst amino acid sequences of mammals, fungi, plants or cyanobacteria, with three conserved histidine motifs (Shanklin *et al.* 1994, Hashimoto *et al.* 2008). These are identified through the motif H $X_{(3-4)}$ H $X_{(7-41)}$ H $X_{(2-3)}$ HH $X_{(61-189)}$ (H/Q) $X_{(2-3)}$ HH, where the amino acid residues H (histidine) are spaced by the specified amount in parenthesis of any other residues (X) (Shanklin and Cahoon 1998). The variation of a glutamine (Q) residue in the final histidine box was originally found in the Δ^6-desaturase in *Anabaena* (Reddy *et al.* 1993) and borage [*Borago officinalis*, (Sayanova *et al.* 1997)], and was also identified in the first report of Δ^8-desaturase (Sperling *et al.* 1995). Two groups can be found within the membrane-bound desaturase family that differ in the spacing between the first and third histidine motif, with the LCB C4-hydroxylase belonging to the “short” space group whilst the LCB desaturases are found in the “larger” spacing group (Sperling *et al.* 2003). Similar to the soluble fatty acid desaturases, the membrane-bound group also possess a di-iron cluster for catalysis (Shanklin and Cahoon 1998), requiring molecular oxygen and reducing equivalents delivered by cytochrome b_5 or by ferredoxin (Sperling *et al.* 2003).

Animal and yeast Δ^4-desaturases were firstly identified by Ternes *et al.* (Ternes *et al.* 2002). In Arabidopsis they were shown to be encoded by one gene localised in a tissue-specific manner to pollen and flowers (Michaelson *et al.* 2009). As with Δ^8-desaturase, the ablation of Δ^4-desaturase did not show any impairment in the plant’s physiology (Michaelson *et al.* 2009, Chen *et al.* 2012). The LCB Δ^8-desaturase was first described as an N-terminal cytochrome b_5 domain polypeptide with the characteristic domain of fatty acid desaturases in sunflower with di-iron-oxo motifs characteristic of fatty acid desaturases (Sperling *et al.* 1995). This latter led to its identification as a stereounselective sphingolipid desaturase through the expression of the identified Arabidopsis and *B. napus* cDNAs in yeast [*S. cerevisiae*, (Sperling *et al.* 1998)]. The specific nature of the stereounselective properties is still

uncertain, and possibly resulting from the different positioning of the substrates in the active site of the enzyme (Habel *et al.* 2010). Studies in Arabidopsis revealed that two genes encode the LCB Δ^8-desaturase (*SLD*) enzyme, both shown to have Δ^8-desaturase activity and identified as *AtSLD1* and *AtSLD2* (Sperling *et al.* 2001, Sperling and Heinz 2003, Chen *et al.* 2012). Both sequences are composed of a single exon and share 79% of genomic DNA identity, encoding a 449-amino acid protein each co-localizing in the ER (Chen *et al.* 2012). *AtSLD1* is ubiquitously expressed in the plant's aerial tissue, whilst *AtSLD2* appears to be mainly expressed in flowers and siliques (Chen *et al.* 2012). The double and single mutants for the Arabidopsis *SLD* genes were characterised by Chen *et al.* (Chen *et al.* 2012), who suggested that *AtSLD1* was the main contributor to the Δ^8-desaturation of the total LCBs. The impact of the mutated SLD led to a perturbed glucosylceramide to GIPC ratio (Chen *et al.* 2012). Despite these results, an explanation for this partitioning is still uncertain; as is the susceptibility of the mutants to chilling temperatures. Furthermore, the reduced impact in the sphingolipid profile caused by the absence of *AtSLD2* in the single mutant *sld2* could be suggested as a result of its low expression in the leaves. Suggesting that the role of *AtSLD2* in the sphingolipid biosynthesis pathway has not completely been elucidated.

5.1.2 *Stress Responsive Sphingolipids*

The essential role of sphingolipids in cell membrane organization and turnover suggests they have a significant role in plant response to cold or freezing [(Pata *et al.* 2010, Barrero-Sicilia *et al.* 2017), Chapter 1]. It has been previously reported that the *cis* to *trans* ratio of the t18:1 LCB isomers varies with species resistance to freezing temperatures, where resistance was associated with a predominance of the *cis* isomer (Imai *et al.* 1997). Glucosylceramides in particular, have been found to accumulate in chilling resistant plants (Cahoon and Lynch 1991, Imai *et al.* 1995). The Δ^8-desaturation is the primary structural modification by desaturation of the LCB pool in plants and it can take up the *cis* or *trans*

configuration, as mentioned above. Though it is not critical for plant development, Δ^8-desaturation is proposed to have a role in the plants response to abiotic stress, e.g. cold (Chen *et al.* 2012) or aluminium toxicity (Ryan *et al.* 2007). A higher content in the Δ^8*cis*-4-hydroxysphingenine isomer (t18:1$^{\Delta 8Z}$) relative to its *trans* isomer t18:1$^{\Delta 8E}$ has been shown to be a constant in chilling resistant species, such as lily-of-the valley (*Convallaria keiskei* Miq.), wheat (*Trititcum aestivum* L.) and oat (*Avena sativa* L.) (Imai *et al.* 1997). In tomato (*Solanum lycopersicum* cv. Micro-Tom) a 4°C treatment increased the transcript levels of the *SlSLD* genes up to 23.4-fold in leaves (Zhou *et al.* 2016). In Arabidopsis, the absence of the *SLD* genes showed an accumulation of glucosylceramides, accompanied by a higher sensitivity in the growth phenotype under chilling temperatures (Chen *et al.* 2012). The study of the *SLD* mutants in Arabidopsis suggested that *AtSLD1* is the main contributor to the Δ^8-desaturation of the total LCBs, leading to a perturbed ratio of glucosylceramides to GIPCs (Chen *et al.* 2012). However, an explanation for this partitioning is still uncertain, as is the susceptibility of the mutants to chilling temperatures.

5.1.3 *Chapter Aims*

The extremophile Eutrema is described as drought, salt and cold tolerant, and despite this remarkable capacity to adapt to different abiotic stresses, its underlying processes are not fully understood [(Wang *et al.* 2004, Griffith *et al.* 2007, MacLeod *et al.* 2015), reviewed in Chapter 1]. Eutrema is viewed as a potential source of information on the plasticity to adapt to abiotic stresses. However, reproducible molecular techniques, fully established in Arabidopsis as a plant model, are yet to be improved and applied to Eutrema (further discussed in Chapter 6). The proximity of the two Brassicaceae genomes, allows the exploration of gene function by expressing genes of interest from the extremophile into Arabidopsis facilitating their characterization, and more importantly, their potential role in stress resilience (Chen *et al.* 2018).

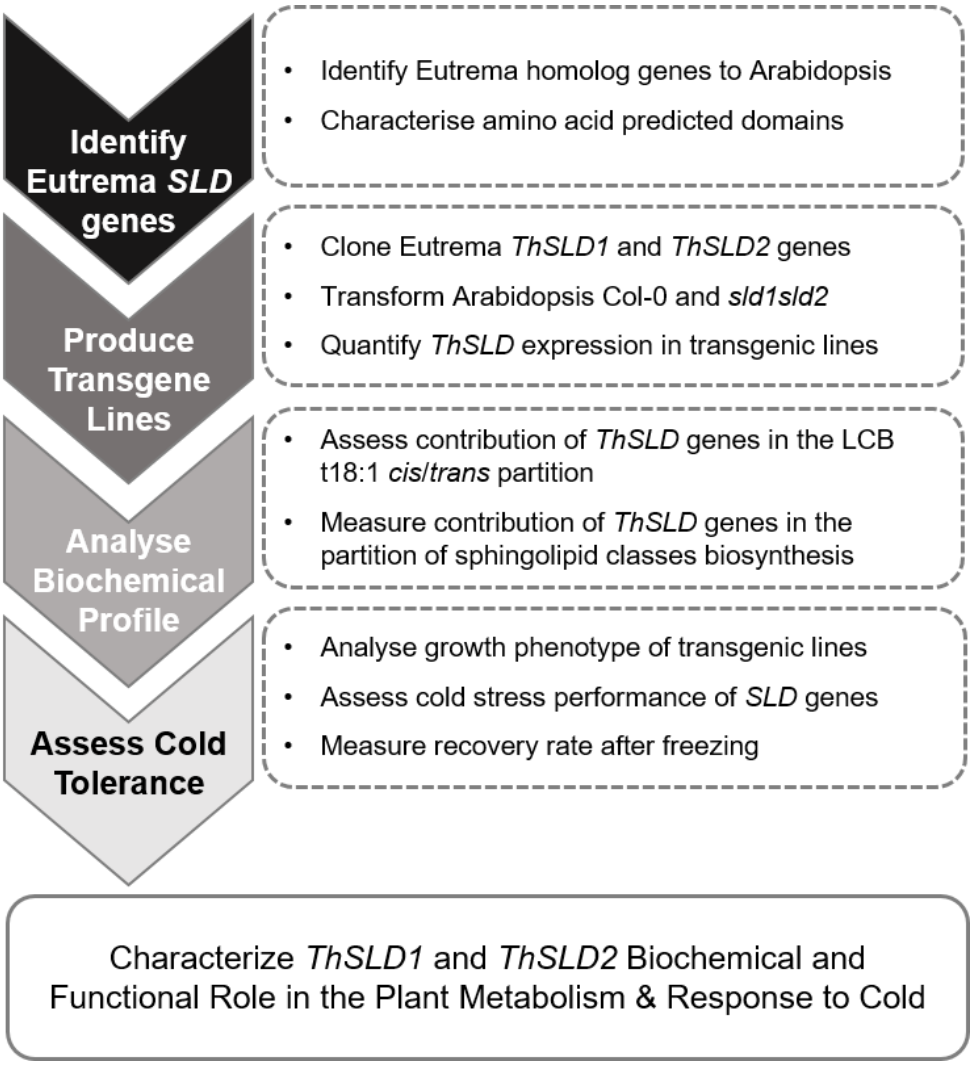

Figure 5.1 Schematic Representation of the Chapter Aims

The potential of the sphingolipid Δ^8-desaturation as a mediator of the cold stress response was investigated in the present chapter (Figure 5.1). In Arabidopsis *AtSLD1* (At3g61580) and *AtSLD2* (At2g46210) are thought to be involved in the plant's cold stress adaptation (Chen *et al.* 2012). In the RNA-Seq analysis performed in Arabidopsis and Eutrema after three days of exposure to cold, the *SLD1* gene was found to be upregulated in both species with higher expression level in Eutrema rather than in Arabidopsis (Appendix 3). The aim of this section was focused on the characterisation of the Eutrema *ThSLD* genes, by dissecting the impact of each gene in the sphingolipid biosynthesis pathway, followed by the investigation of its potential function under cold stress (Figure 5.1). This

was achieved by overexpressing both *ThSLD1* and *ThSLD2* in Arabidopsis wild-type Col-0 and the double mutant *sld1sld2*. The genotypes produced were identified as Col-0:*ThSLD1* and Col-0:*ThSLD2* for the vectors expressed in the wild-type Col-0, or as *sld1sld2*:*ThSLD1* and *sld1sld2*:*ThSLD2* for the lines overexpressing the *ThSLD* genes in the double mutant *sld1sld2* background. *ThSLD2* was overexpressed in the double mutant *sld1sld2* using the ubiquitous CaMV35S promoter with the aim of dissecting its role in the sphingolipid metabolism. Finally, the hypothesis that the overexpression of the *ThSLD* genes originating from an extremophile plant could enhance the plant's response to chilling temperatures was also be tested. As it was anticipated that overexpression would increase resilience and increase the t18:$1^{\Delta 8Z}$ to t18: $1^{\Delta 8E}$ ratio (*cis*/*trans*, Figure 5.1).

5.2 RESULTS

5.2.1 *Identification of the Eutrema SLD genes*

The Eutrema ThSLD sequences were identified through sequence similarity to the amino acid sequences of the Arabidopsis LCB Δ^8-desaturases. These were identified as Thhalv10005967m.g (EUTSA_v10005967mg, located in the scaffold 19:690832..692730 reverse, herein referred as *ThSLD1*) and Thhalv10001443m.g (EUTSA_v10001443mg, located in the scaffold 22:1122955..1124669 forward, herein referred as *ThSLD2*). Both proteins were also identified in the UniProt online database and described as *uncharacterized*. The Arabidopsis and Eutrema amino acid sequences (Appendix 15) showed a 94.4% of homology between the 449 amino acids of *AtSLD1* and *ThSLD1*, and a 94.0% homology between *AtSLD2* and *ThSLD2* (Figure 5.2 A). The paralogues *SLD1* and *SLD2* seemed to share lower sequence identity of 79.7% in Arabidopsis and 81.7% in Eutrema. The coding sequences (CDS) derived from the only exon in any of the sequences followed the same trend (Figure 5.2 A). The detailed alignment of the amino acid SLD sequences between the two species

was performed with MUSCLE 3.8 [(Madeira *et al.* 2019), Figure 5.2 B]. A domain search performed with SMART online software (Letunic and Bork 2018) identified three domains in all sequences, a cytochrome b_5-like Heme/Steroid binding domain (Ozols 1989) localised in amino acids 10 to 82, a transmembrane helix region in amino acid residues 112 to 134, followed by a fatty acid desaturase 273 amino acids long [identified from Pfam; (El-Gebali *et al.* 2019)]. The three characteristic histidine regions (Sperling *et al.* 1995, Shanklin and Cahoon 1998) were also identified (yellow box in Figure 5.2), all integrating the identified desaturase domain with the sequences HDSGH, HNAHH, and QLEHH. These regions were shown to be conserved between both Arabidopsis and Eutrema, as they are to the first report of the Δ^8-desaturase in sunflower, where only the first region differs from HD**A**GH in sunflower to HD**S**GH, where the alanine (A) was replaced by a serine (S) residue.

5.2.2 *Production of Transgenic Lines*

The functionality of the Eutrema *SLD* gene was tested by overexpressing the identified genes, *ThSLD1* and *ThSLD2,* in two Arabidopsis backgrounds i.e. Col-0 and *sld1sld2*. The wild-type ecotype Col-0 was used to change the LCB desaturation phenotype. Expressing each of the *ThSLD* genes in the Arabidopsis *sdl1sld2* double would determine the functionality of the *ThSLD* genes, the level of complementation between *ThSLD1* and *ThSLD2* respectively, and the role of each gene in LCB desaturation. The Arabidopsis *sld1sld2* double mutant was obtained from two SALK collection single mutants *sld1-1* and *sld2* as previously described (Chen *et al.* 2012). The *sld1-1* line (SALK_010384) had a T-DNA insertion approximately 1050 bp downstream of the *AtSLD1* start codon, whilst the T-DNA insertion site for *sld2* (SALK_013243) was approximately 370 bp downstream of the *AtSLD2* start codon (Figure 5.3). According to the identified domains (Figure 5.2), the T-DNA insertion in *AtSLD1* would disrupt the end of the desaturase domain, while *sld2* showed the T-DNA insertion sooner, nearer the start codon, which disrupted the transmembrane domain.

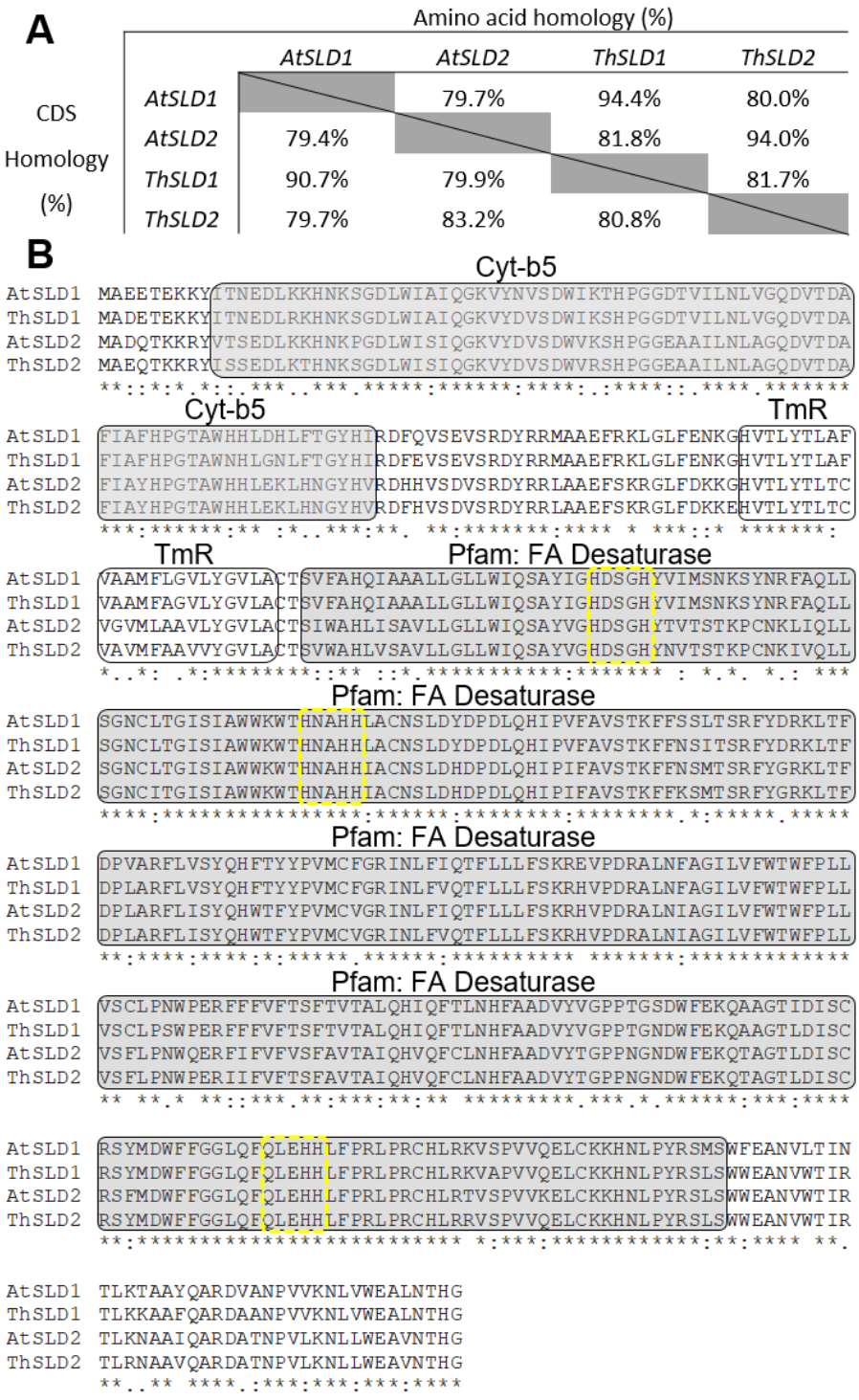

Figure 5.2 Arabidopsis and Eutrema SLD Sequence Homology

(A) Amino acid and coding sequence (CDS) homology between *SLD1* and *SLD2*, sequences analysed in Geneious® 10.2.3. (B) Amino acid alignment by CLUSTAL multiple sequence alignment (MUSCLE 3.8, (Madeira *et al.* 2019)). ***** (asterisk) single, fully conserved residue; weak "**.**" (period) or strong "**:**" (colon) conservation between groups (score ≤0.5 and >0.5, respectively, Gonnet PAM 250 matrix). Histidine conserved regions marked in yellow (■). At, *Arabidopsis thaliana*; Th, *Eutrema salsugineum*. Domain prediction by SMART online software (Letunic and Bork 2018). Cyt-b5, cytochrome b5-like domain; TmR, Transmembrane Region; Pfam: FA Desaturase, Protein family Fatty Acid Desaturase domain.

The CaMV 35S promoter was used to achieve ubiquitous high expression levels of the *ThSLD* cDNAs (Gronenborn *et al.* 1981, Benfey and Chua 1990). Kanamycin was used as a selective marker for the transformation of the Arabidopsis wild-type Col-0. Kanamycin is an aminoglycoside antibiotic that binds the ribosomal 30S subunit which causes mistranslation and growth impairment (Errampalli *et al.* 1991, de Vries and Wackernagel 1998, Harrison *et al.* 2006). The transformation of Arabidopsis double mutant *sld1sld2* used DsRED fluorescence as selective marker (Jach *et al.* 2001), as kanamycin resistance was previously used to generate the *sld1sld2* mutant (Chen *et al.* 2012). DsRED is a red fluorescent protein isolated from the red coral *Discosoma sp*. with an excitation peak of 553 nm (Matz *et al.* 1999), and it was shown as a reporter *in planta* by Jach *et al.* (Jach *et al.* 2001). It can emit red fluorescence through the seed coat, visible under a DsRED filter, allowing identification and selection of transformed seeds. The *ThSLD* constructs were introduced to Arabidopsis backgrounds Col-0 and *sld1sld2* via *Agrobacterium*-mediated transformation [(Clough and Bent 1998), Section 2.3]. Each of the transformation events were treated as independent lines, and to ensure reproducibility of the *ThSLD* gene characterisation in the genotypes produced, three lines per genotype were selected, each from an independent transformation event.

The transformed lines genotype was confirmed (Figure 5.3). The Arabidopsis endogenous genes were tested in all lines with an expected fragment size of 1129 bp for *AtSLD1* and 1036 bp for *AtSLD2* for Col-0, and the overexpressing lines Col-0:*ThSLD1* and Col-0:*ThSLD2* (Figure 5.3 A-B). A BLAST using the NCBI database confirmed the uniqueness of each primer. Both right (RP) and left (LP) primers for *AtSLD2* matched *AtSLD2* mRNA (accession number NM_130183.4) and the mRNA for the *U11/U12 SMALL NUCLEAR RIBONUCLEOPROTEIN* (accession number NM_001337179.1) with 21 out of 21 matching nucleotides (100% percentage of identity). This did not seem to have affected the results, no gDNA fragment was produced when using this primer pair in the mutant line *sld1sld2* or in either line *sld1sld2*:*ThSLD1* and *sld1sld2*:*ThSLD2*,

confirming the absence of *AtSLD2* wild-type sequence from these lines (Figure 5.3 E). The Eutrema *ThSLD* cDNAs were expected to produce fragment sizes of 300 and 299 bp for *ThSLD1* and *ThSLD2*, respectively (Figure 5.3 C-D). The *ACTIN2* (*AtACT2*) gene was used as a reference gene, serving also as a positive control for the PCR and the gDNA extraction. The *AtACT2* 156 bp fragment was present in all lines confirming both PCR analysis and gDNA extraction protocols worked. Col-0, and the overexpressing lines with a Col-0 background, showed the presence of the *AtSLD* genes and no T-DNA insertion. The *sld1sld2* background lines showed the disruption of the *AtSLD* genes along with the presence of the T-DNA. The presence of the transgenes *ThSLD1* and *ThSLD2* was also confirmed in the respective transformed lines (Figure 5.3 E).

5.2.3 *Quantitative Analysis of ThSLD transgenes Overexpression*

Targeted analysis of mRNA through RT-qPCR was used to quantify the expression of *ThSLD1* and *ThSLD2* transgenes [(Le *et al.* 2015), Section 2.4]. The *ThSLD* genes are composed of only one exon (Figure 5.3 C-D), thus no intron spanning primers were necessary. Primer pairs were designed for the amplification of 67 and 68 bp mRNA fragments for *ThSLD1* (Figure 5.3 C) and *ThSLD2* (Figure 5.3 D), respectively, targeting the coding sequence corresponding to the desaturase domain. The primers used for the analysis of the *ThSLD* transgenes were confirmed to be unique to the respective sequences, and would not anneal to Arabidopsis, as predicted by a BLAST search conducted on NCBI database. Only the reverse primer for *ThSLD2* (Section 2.4.2) showed 21 out of 23 identical nucleotides to the *AtSLD2* gene (91% identity), with two mismatched nucleotides in the middle of the sequence. The expression analysis was performed in rosette leaves of adult plants at 19 DAS.

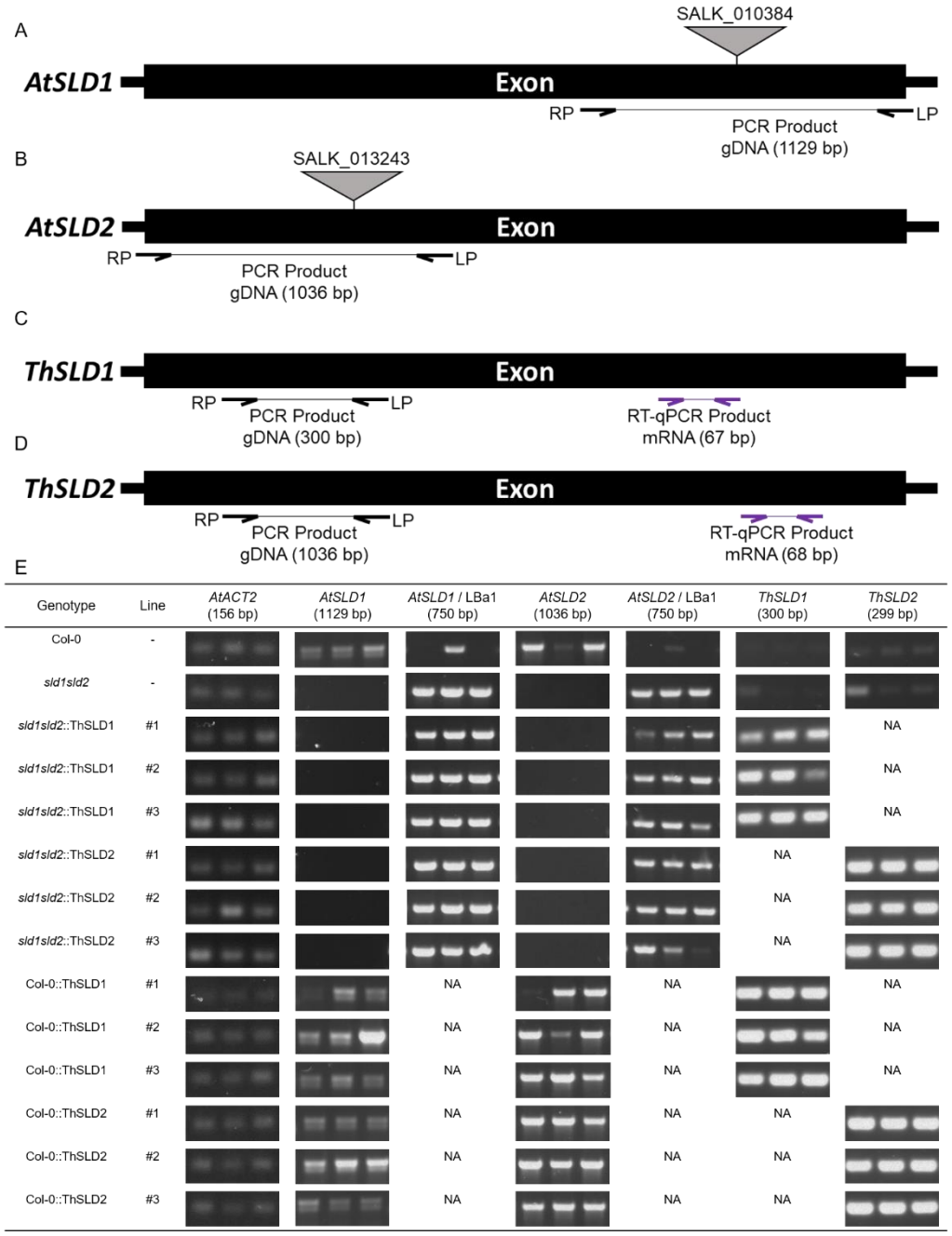

Figure 5.3 SLD Genes and Overexpressing Lines Genotype

Gene structure with T-DNA insertions (▼) for (A) *AtSLD1* SALK_010384 at 1050 bp and (B) *AtSLD2* SALK_013243 at 370 bp, both from start codon, (C) *ThSLD1* and (D) *ThSLD2* gene structure. All genes have one exon, primer binding sites are marked by half arrows; RP, Right Primer; LP, Left Primer. Presence of T-DNA was analysed by the RP for each gene and the left border primer for the T-DNA (LBa1). (E) PCR results for the presence and/or absence of *AtSLD* and *ThSLD* genes, and presence of the T-DNA insertion in the double mutant lines. *ACTIN2* (*AtACT2*) was used as a reference gene, size of the fragment in base pairs (bp). Electrophoresis gel details in Section 2.4.4.

The genotypes *sld1sld2*:*ThSLD1* and Col-0:*ThSLD1* were tested for the quantification of the *ThSLD1* transgene expression, whilst the genotypes

sld1sld2:*ThSLD2* and Col-0:*ThSLD2* for the expression of transgene *ThSLD2* (Figure 5.4), all in relation to the reference gene *AtUBC21* expression. Three independent lines per genotype were selected and used for the characterisation the SLD function. The statistical analysis was performed using a square root (√) transformation of the relative expression to *AtUBC21*, which allowed for a balanced ANOVA analysis. The expression levels were statistically analysed to determine overexpression in each line by comparing to the 95% CI limits (Figure 5.4 A). *AtUBC21* is reported as a stable reference gene for Arabidopsis, suitable for use in RT-qPCR analysis of multiple tissues at different developmental stages (He *et al.* 2016). The expression analysis of the transgenes was also confirmed with a second reference gene, *AtACT2* which showed the same trend as found with *AtUBC21* (Joseph *et al.* 2018). In all selected lines this was observed not only in the mean squared values, but also the lower limit of the 95% CI (CI_{LL}). Line #6 of *sld1sld1*:*ThSLD2* showed the lowest CI_{LL} of 1.82 (mean 14.36), with only two other lines showing a CI_{LL} lower than ten, i.e. lines #9 and #11 of genotypes Col-0:*ThSLD1* and Col-0:*ThSLD2*, respectively (Figure 5.4). The CI at 95% level can be interpreted as range of values with a 95% probability of containing the true mean of the population. The transgene expression showed a wide range of values in the 95% CI for all lines tested, which could be explained by the use of three biological replicates, i.e. three leaves from different plants per line were used for the RNA extraction and cDNA synthesis. The analysis of variance (ANOVA) showed significant differences between genotypes ($p<0.001$) and between lines within each of the genotypes ($p<0.001$) (Figure 5.4 B). These differences seemed to result from the high levels of *ThSLD1* and *ThSLD2* overexpression in lines #7 (mean 618.02) and #10 (mean 671.33) in the Col-0 background. Line #12 also showed an overexpression with a mean of 315.06, hence contributing to the differences between genotypes. In contrast all three lines for each *sld1sld2*:*ThSLD1* (#1 - #3) and *sld1sld2*:*ThSLD2* (#4 - #6) genotypes showed a more evenly balanced spread of over-expression, with only line #6 of note due to the lowest transgene expression (mean 14.36). The

similarity in the transgene expression between these lines aided the subsequent biochemical profiling of the genotypes. Col-0:*ThSLD1* (#7 - #9) and Col-0:*ThSLD2* (#10 - #12) were also tested and the relationship between overexpression levels and phenotype will be discussed in the following sections.

5.2.4 *ThSLD2 Alters the Cis/Trans Ratio in the t18:1 LCB*

To ascertain the impact of each *SLD* gene in the different genotypes produced, the LCB profile was analysed in plants grown under control conditions (Section 2.5.5). For this analysis, an extraction method was used that allowed the assessment of the total LCB profile changes by analysing the pool of LCBs extracted from more complex lipids. The LCBs were extracted from 18 DAS fresh leaf tissue, using a strong alkaline hydrolysis for the release of the LCBs from the complex sphingolipids structure, and then converted to dinitrophenyl derivatives (Sperling *et al.* 1998). This approach allowed for the assessment of the *cis*/*trans* t18:1 isomers ratio (t18:1$^{\Delta 8Z}$/t18:1$^{\Delta 8E}$ ratio). As the *SLD* genes encode for the sphingolipid LCB Δ^8-desaturase, assessing the contribution of each *ThSLD1* and *ThSLD2* to the partition of the Δ^8-4-hydroxysphingenine (t18:1) isomers t18:1$^{\Delta 8Z}$ (*cis*) to t18:1$^{\Delta 8E}$ (*trans*) was one of the main aims of this work. The LCB profile for the transgenic lines and the double mutant *sld1sld2* was shown to be affected when compared to the wild-type Col-0 (Figure 5.5). Col-0 was dominated by the trihydroxy LCB species, with an emphasis on the unsaturated t18:1, which constituted 77% of the total LCB pool, as would be expected as these are reported to be the main LCB present in plants (Michaelson *et al.* 2016). On the contrary, the double mutant *sld1sld2* showed an almost negligible content in the desaturated LCBs d18:1 and t18:1, as previously reported (Chen *et al.* 2012). Furthermore, this effect was observed in both isomers of t18:1, t18:1$^{\Delta 8Z}$ and t18:1$^{\Delta 8E}$, demonstrating how the Δ^8-desaturase can place the double bond in both positions.

A

Genotype	Line	Mean (√)	Mean	CI_{LL} (√)	CI_{LL}	CI_{UL} (√)	CI_{UL}
sld1sld2::ThSLD1	#1	8.08	65.29	5.64	31.81	10.52	110.67
	#2	5.85	34.22	3.42	11.66	8.29	68.72
	#3	5.86	34.34	3.42	11.70	8.30	68.89
sld1sld2::ThSLD2	#4	6.19	38.32	3.75	14.06	8.63	74.48
	#5	7.46	55.65	5.02	25.23	9.90	98.01
	#6	3.79	14.36	1.35	1.82	6.22	38.69
Col-0::ThSLD1	#7	24.86	618.02	22.42	502.84	27.30	745.29
	#8	5.62	31.58	3.18	10.11	8.06	64.96
	#9	4.80	23.04	2.37	5.59	7.24	52.42
Col-0::ThSLD2	#10	25.91	671.33	23.47	551.03	28.35	803.72
	#11	5.02	25.20	2.59	6.68	7.46	55.65
	#12	17.75	315.06	15.31	234.40	20.19	407.64

B

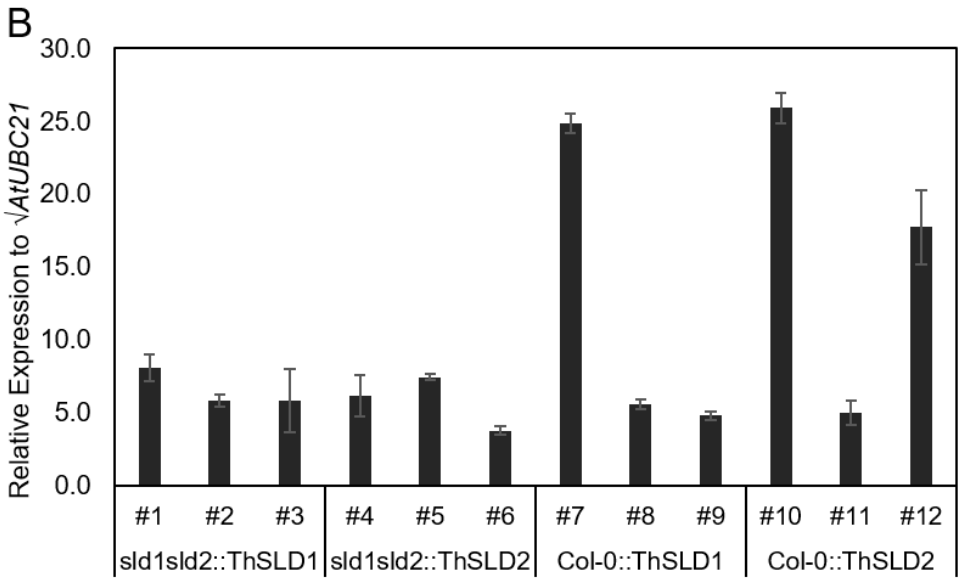

Figure 5.4 Expression Analysis of the SLD genes

The expression of the transgenes *ThSLD1* and *ThSLD2* for three independent lines for each *sld1sld2*:*ThSLD1*, *sld1sld2*:*ThSLD2*, Col-0:*ThSLD1*, and Col-0:*ThSLD2* was quantified by RT-qPCR in relation to the reference gene *AtUBC21*. RNA was extracted from three weeks old leaves from three different plants, and the RT-qPCR was performed with two technical replicates. (A) Table details mean, lower (CI_{LL}) and upper (CI_{UL}) limits for the 95% confidence interval for each line and genotype. (√) represent squared root values. (B) Square root mean ± Standard Error (SE) for the expression values used for the ANOVA, showing significant differences between genotypes ($p<0.001$), and lines within genotypes ($p<0.001$).

Concomitantly, the double mutant showed an accumulation of the unsaturated forms d18:0 and t18:0 which contributed to 99.4% of the total pool of LCBs in *sld1sld2*, where d18:0 represented 11.6% and t18:0 87.7% of the total (Figure 5.5 A). This showed that despite the absence

of the Δ^8-desaturase, the ratio of trihydroxy to dihydroxy LCB species was maintained. The trend was also confirmed by the total content of LCB in *sld1sld2* (Figure 5.5 C), which did not show any difference to the wild-type. Additionally, despite the LCB profile changes that were a consequence of the different genotypes produced, no differences were found amongst genotypes (p=0.712), or between lines within each genotype (p=0.173, Figure 5.5 C).

The *ThSLD1* transgene overexpression in *sld1sld2*:*ThSLD1* resulted in a general recovery of the double mutant profile to wild-type values, with a consistent behaviour in all three lines (Figure 5.5 A). Including the recovery of t18:1$^{\Delta 8Z}$ and t18:1$^{\Delta 8E}$ isoforms to 76.5% and 85% of the wild-type values. *ThSLD1* introduced in the wild-type background did not show the expected LCB profile potentially caused by the additive overexpression of the *ThSLD* and endogenous *AtSLD*. The LCB profile was unchanged between Col-0 and *sld1sld2*:*ThSLD1*. Of note, line #7 that previously reported a high expression of the *ThSLD1* transgene (mean 618.02, Figure 5.4), showed an increased content of the total LCB content, which reflected the 1.6- and 2.0-fold increase in t18:1$^{\Delta 8E}$ and d18:2. Despite this, its standard error suggested an outlier behaviour, which was confirmed by the ANOVA not to be significantly different from the remaining lines of the same genotype. The genotypes expressing *ThSLD2*, *sld1sld2*:*ThSLD2* and Col-0:*ThSLD2* showed a distinct LCB phenotype to the *ThSLD1* lines. This was the result of the different partitioning of the t18:1 *cis* (t18:1$^{\Delta 8Z}$) and *trans* (t18:1$^{\Delta 8E}$) isomers. In *sld1sld2*:*ThSLD2,* a clear *ThSLD2* driven recovery of t18:1$^{\Delta 8E}$ reached an average across the three lines of 0.37 nmol/mg fresh weight representing 92.5% of Col-0 t18:1$^{\Delta 8E}$ (Figure 5.5 A). However, the same was not observed for the *cis* isomer t18:1$^{\Delta 8Z}$, which showed an average of 0.04 nmol/mg fresh weight, representing 10% of the wild-type t18:1Δ^{8Z} content. The same trend was observed for Col-0:*ThSLD2*, with an average t18:1$^{\Delta 8Z}$ of 0.09 nmol/mg fresh weight, which was less than 25% of the wild-type content. The partition of the t18:1$^{\Delta 8Z}$ to t18:1$^{\Delta 8E}$ isomers is shown in Figure 5.5 B, where the *cis/trans* ratio was analysed for all

the genotypes. Confirming the results obtained from the LCB profile (Figure 5.5 A), the *cis*/*trans* ratio of the genotypes overexpressing *ThSLD1* showed no difference to the wild-type Col-0, however these were significantly different from the reduced ratio observed in Col-0:*ThSLD2*. Whilst the double mutant *sld1sld2* and *sld1sld2*:*ThSLD2* were shown to be significantly different from all other genotypes, but not amongst each other. No differences were found between lines within each genotype, showing consistency in the genotype results. Three levels of *cis*/*trans* ratio were found amongst the genotypes studied, as described previously in Section 5.1.2, this ratio varies with species and is thought to be a factor contributing to the plants resilience to chilling. *ThSLD2* did not seem to be able to recover the double mutant phenotype when expressed in the *sld1sld2* background. However, when expressed in the wild-type Col-0 the genotype showed an intermediate profile, showing higher *cis*/*trans* relative to *sld1sld2* and *sld1sld2*:*ThSLD2,* as a probable consequence of the endogenous expression of the *AtSLD* genes. Nevertheless, the effect of *ThSLD2* was still visible in the reduced production of the t18:1$^{\Delta 8Z}$ (*cis*) isomer.

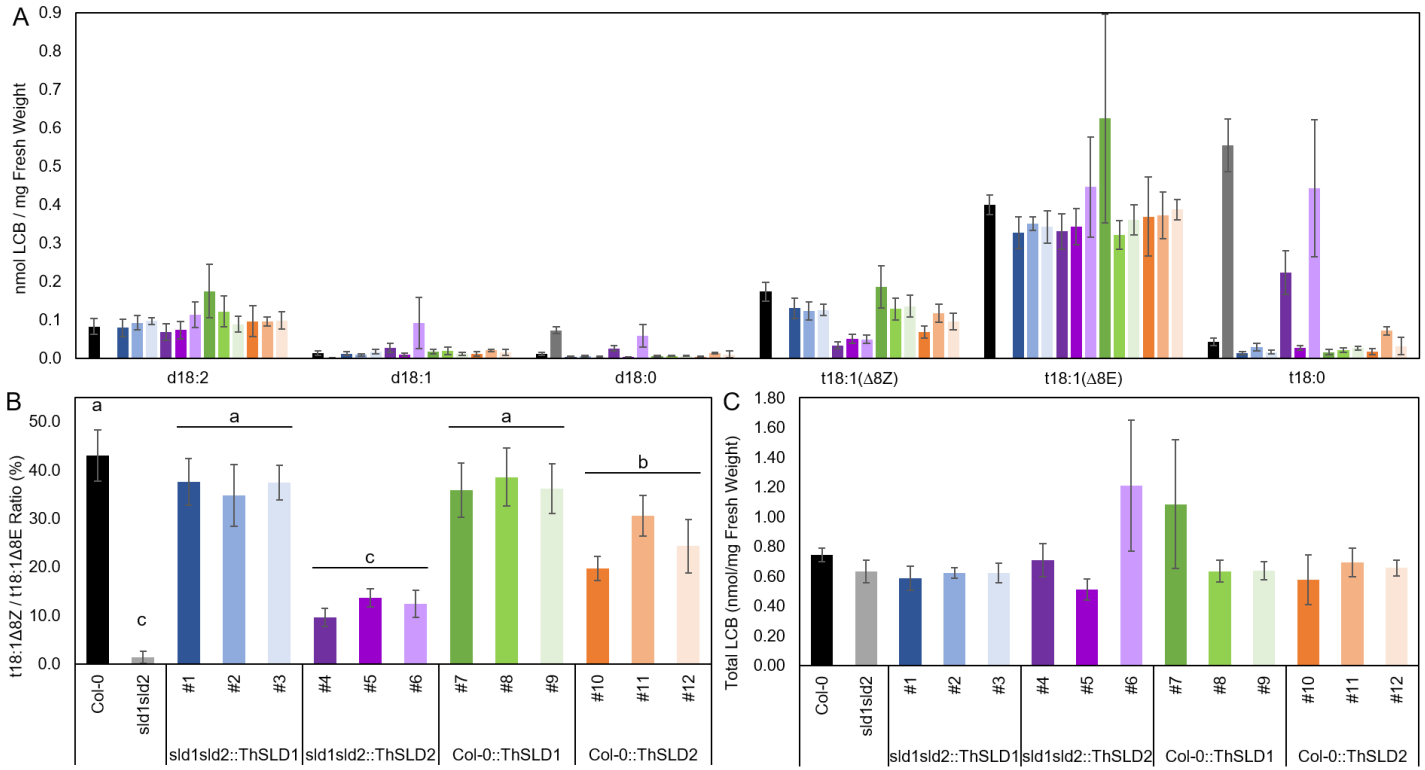

Figure 5.5 LCB Profile for the SLD Lines

(A) LCB profile; (B) t18:1$^{\Delta 8E}$ (*cis*) to t18:1$^{\Delta 8Z}$ (*trans*) ratio; (C) total content of LCB for Col-0 (■), *sld1sld2* (■), *sld1sld2*:*ThSLD1* lines #1 (■), #2 (■), #3 (■); *sld1sld2*:*ThSLD2* lines #4 (■), #5 (■), #6 (■); Col-0:*ThSLD1* lines #7 (■), #8 (■), #9 (■); and of Col-0:*ThSLD2* lines #10 (■), #11 (■), #12 (■). Bars represent mean ± standard error, N=6. ANOVA for differences amongst genotypes (B, p<0.001; C, p=0.712), and lines within genotypes (B, p=0.863; C, p=0.173). Bonferroni test used in B, results shown in lowercase letters sorted in descending order.

5.2.5 *The Sphingolipid Profile Changed with the Genotype*

Sphingolipids can be grouped in different pools that include ceramides, hydroxyceramides and the complex forms glucosylceramides and GIPCs (Michaelson *et al.* 2016). As building blocks of complex sphingolipids, changes in LCB metabolism are expected to have an impact on wider sphingolipid biosynthesis, and especially in glucosylceramides and GIPCs (Chen *et al.* 2012). The sphingolipid profile was firstly analysed in the genotypes *sld1sld2*:*ThSLD1* (#1 - #3), and *sld1sld2*:*ThSLD2* (#4 - #6), together with the wild-type Col-0 and the double mutant *sld1sld2* under 23°C control temperature. The aim was to ascertain the impact of the transgenes *ThSLD1* and *ThSLD2* in the sphingolipid profile, when overexpressed in the absence of Δ^8-desaturation in the double mutant *sld1sld2.* As shown above, the ratio of the *cis/trans* isomers of t18:1 driven by *ThSLD2,* with a detrimental effect on the production of the *cis* form. Furthermore, Δ^8-desaturation was previously reported to be involved in the synthesis of complex sphingolipids glucosylceramides and GIPCs in Arabidopsis (Chen *et al.* 2012). Profiling was completed using sphingolipids extracted from freeze-dried whole plant tissue collected after 18 DAS grown under control conditions. The heterogeneity within the sphingolipid classes and their relatively low abundance in plant tissues are a limitation on the quantification methods available (Markham and Jaworski 2007). Markham *et al.* (Markham 2013) optimised a method that relies first on the elution of the sphingolipid extract using HPLC, followed by ESI-MS/MS in MRM mode to identify specific sphingolipid species. The ESI-MS/MS system offers high specificity (because the daughter ions originate only from the selected parent ion) and sensitivity, whilst the MRM mode allows for the simultaneous analysis of a large number of compounds (Gergov *et al.* 2003, Markham and Jaworski 2007). The resulting analysis yielded paired fatty acid and LCB profiles for each of the sphingolipid classes ceramides, hydroxyceramides, glucosylceramides and GIPCs.

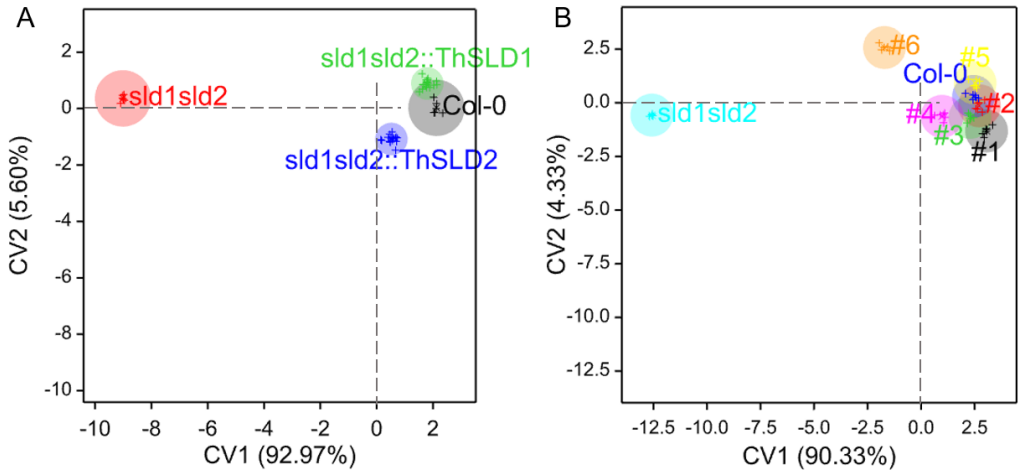

Figure 5.6 Sphingolipid Multivariate Canonical Analysis

Complete sphingolipid dataset analysed by canonical variate (CV) analysis with genotype (A) or lines (B) as a grouping factor. Two dimensions (CV1, CV2) were found to explain the variability of the data. Graph A: *sld1sld2* (■); Col-0 (■); *sld1sld2*:*ThSLD1* (■); *sld1sld2*:*ThSLD2* (■). Graph B: *sld1sld2* (■); Col-0 (■); *sld1sld2*:*ThSLD1* lines #1 (■), #2 (■), #3 (■); *sld1sld2*:*ThSLD2* lines #4 (■), #5 (■), #6 (■). Circles around means (×) represent 95% confidence intervals, individual points are represented by "+". Dashed lines represent zero in both axis. CV loadings in Appendix 16.

The complete sphingolipid dataset was analysed using canonical variate analysis (CVA) that included each fatty acid (16:0, 18:0, 20:0, 20:1, 22:0, 22:1, 24:0, 24:1, 26:0, 26:1) for each LCB class (d18:0, d18:1, t18:0, t18:1) of each pool of ceramides, glucosylceramides, GIPCs and hydroxyceramides. This multivariate approach was used to assess the global changes in the sphingolipid profile of the four genotypes *per se* (Figure 5.6 A), and of each of the lines (Figure 5.6 B). Using either genotype or line as grouping factor showed that two dimensions were sufficient to account for at least 94.7% of the variation, with the first canonical variate (CV1) as the main component with a score of 90.33% using lines as grouping factor (Figure 5.6 B), or 92.97% with genotype (Figure 5.6 A). Furthermore, the components (vector loadings) that contributed to the CV in the genotype analysis were analysed revealing d18:1 and hydroxyceramides as the major contributors for CV1 as oposed to GIPCs and t18:0 that were the main contributors to the negative loadings (31.25% and 29.69%, respectively). The second CV (CV2) showed a similar trend for the positive vectors with d18:1 (28.24%) and hydroxyceramides (28.24%) together with glucosylceramides

(28.24%) as main contributors. Whilst the negative pool of the CV2 vectors found d18:0 to be the main LCB contributor (29.73%), contrary to what was found in the CV1. No differences were found in the saturated to unsaturated fatty acids, nor the carbon chain length contribution to both dimensions. The double mutant *sld1sld2* showed the most distinctive response of all the genotypes analysed, as it would be expected when no Δ8 desaturation was present, illustrating the significant impact of this enzyme on the sphingolipid profile of Arabidopsis. Both genotypes *sld1sld2*:*ThSLD1* and *sld1sld2*:*ThSLD2* showed a sphingolipid profile closer to the observed for the wild-type Col-0 (Figure 5.6 A), which suggested that the sphingolipid biochemical phenotype was recovered by the Eutrema transgenes. The *sld1sld2*:*ThSLD1* profile showed closer resemblance to Col-0, with a partial overlap of the 95% confidence intervals, whilst *sld1sld2*:*ThSLD2* showed a lower CV1 value. This trend could be explained by the lower CV1 values observed in lines #4 and #6 from *sld1sld2*:*ThSLD2*, more similar to the double mutant (Figure 5.6 B). This effect suggested the predominance of the *ThSLD1* gene, as it recovered the double mutant phenotype to wild-type values in all three lines (#1 - #3) as reported in Arabidopsis by Chen *et al.* (2012) (Chen *et al.* 2012). Additionally, lines #5 and #6 showed higher CV2 values which, despite only accounting for 4.33% of the variability of the data, might suggest a contribution of the glucosylceramides and hydroxyceramides, to the detriment of GIPCs, for the observed shift in the profile (Figure 5.6 B).

In a parallel experiment, under the same growth conditions, the sphingolipid profile of the overexpressing lines #7 of Col-0:*ThSLD1* and #10 for Col-0:*ThSLD2* was assessed, together with *sld1sld2* and Col-0 as control (Figure 5.7). One representative line per genotype was analysed for its sphingolipid content, due to the high expression values obtained for each of the transgenes *ThSLD1* and *ThSLD2*, lines #1 and #4 were respectively chosen. The profiles were also analysed with the mutltivariate CVA, which showed the same trend as for the *sld1sld2*:*ThSLD* gentoypes (Figure 5.7). Two dimensions were

necessary to account for 97.6% of the variation. CV1 accounted for 84.1% of the variation and showed a predominance of ceramides in the positive loading vectors against the predominance of glucosylceramides in the negative pool of vector loadings. CV1 showed a clear distinction and distance of *sld1sld2* from the remaining three gentoypes. This could suggest a predominance of ceramides in the profile of the double mutant *sld1sld2*, as suggested by Chen *et al.* (Chen *et al.* 2012). As observed in the LCB profile, the genotypes Col-0:*ThSLD1* and Col-0:*ThSLD2* did not show a changed sphingolipid content compared to the wild-type Col-0. On the contrary, both genotypes showed a CV1 profile similar to the wild-type Col-0, however these were distinguished by CV2, where Col-0:*ThSLD1* and Col-0:*ThSLD2* grouped together and distanced themselves from Col-0 (Figure 5.7). CV2 had a predominance of GIPCs in its positive loadings, where hydroxyceramides contributed the least. The composition of the CV2 dimension may suggest a shift towards increased GIPC content, especially in the genotype overexpressing *ThSLD2*. However, further analysis of the individual profiles for each class is necessary to assess structural differences that might have arisen from each of the overexpressed transgenes.

5.2.6 *ThSLD1 and ThSLD2 Recovered the Glucosylceramide Content in the sld1sld2 Background*

The CVA on the complete dataset presented and discussed above served as a first approach to the analysis of the sphingolipid content of the genotypes studied. Each class of sphingolipid was then analysed separately to assess specific changes in each profile that might elucidate the role of each *SLD* gene in the sphingolipid metabolism. Glucosylceramides and GIPCs are complex sphingolipids with a polar head group usually a glycosyl residue or an inositol-glucuronic acid, respectively, linked to the ceramide backbone. GIPCs are the predominant class in plants (Markham *et al.* 2006), and glucosylceramides comprise approximately 30% of the sphingolipids in Arabidopsis leaves (Markham *et al.* 2006, Markham and Jaworski 2007).

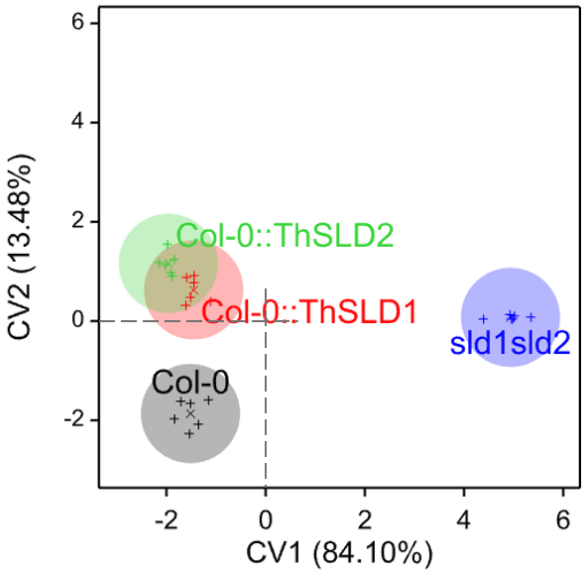

Figure 5.7 Sphingolipid Multivariate Analysis for Col-0:ThSLD

Sphingolipid profile analysed by canonical variate (CV) analysis, genotype as grouping factor for Col-0 (■), *sld1sld2* (■), line #1 of Col-0:*ThSLD1* (■), and line #4 of Col-0:*ThSLD2* (■). Two dimensions (CV1, CV2) were found to explain the variability of the data. Circles around means (×) represent 95% confidence intervals, individual points are represented by "+". Dashed lines represent zero in both CV1 and CV2. CV loadings in Appendix 17.

The glucosylceramide and GIPC profiles for the tested genotypes are shown in Figure 5.8, where each panel shows the fatty acid profile (carbon chain length: double bonds) for each of the main LCBs classes (panels A – D for glucosylceramides, and E – H for GIPCs). The four main LCBs classes analysed consisted in the di- and tri-hydroxylated (d18 and t18) forms, in either saturated d18:0 and t18:0, or unsaturated d18:1 and t18:1 forms. A clear difference in the double mutant *sld1sld2* profile was observed in both sphingolipid classes, with an almost complete ablation of lipid content in the unsaturated LCBs d18:1 and t18:1, whilst increasing d18:0 and t18:0 content. This trend was observed in both classes, however a higher impact in the glucosylceramide profile was observed. For example an average fold change increase of 59 in the content of the fatty acid 16:0 in d18:0 (Figure 5.8 A), or 134-fold change in the same fatty acid content in t18:0 (Figure 5.8 B) were observed. Longer carbon chain fatty acids also showed this trend, with an increase of 24:1 and 26:1 in t18:0 of on average 45.1- and 37.3-fold, respectively. A principal

component analysis (PCA) on the glucosylceramide pool confirmed this trend, where two (PC-1 and PC-2) out of the three dimensions necessary to explain the variability in the data showed a clear distinction between the double mutant and the remaining genotypes analysed (Appendix 20). The PCA showed the double mutant with a low negative PC-1, which was predominantly influenced by unsaturated LCBs t18:1 and d18:1 in its positive loadings (85.7% of LCBs, no t18:0 was found in the positive loadings), whereas its negative loadings were characterized by 89.5% of saturated LCBs (no t18:1 was found). PC-2, in which positive loadings included 54.3% of desaturated LCBs (t18:0 and d18:0), placed *sld1sld2* pool on the positive region. These results agreed with the observed glucosylceramide profile previously published (Chen *et al.* 2012), illustrating the role of Δ^8-desaturation in the biosynthesis pathway of the glucosylceramide pool. A similar trend was found in the double mutant GIPC pool, where a PCA also identified three dimensions that accounted for 87.1% of the variation (Appendix 21). Despite the distinct profile of the double mutant *sld1sld2*, this was not as marked an effect as observed for the glucosylceramide profile. This was reflected in both PCAs and in the long chain fatty acids of d18:0 and t18:0 LCB profile (Figure 5.8 E, F) where the lipid concentration did not surpass Col-0, as it would be expected after being reported (Chen *et al.* 2012). The PCA results show a separation of *sld1sld2* from the remaining genotypes, which again could be explained by a low PC-1 and high PC-2. This analysis also revealed the presence of a replicate with a consistent outlier profile, which, even after three dimensions (PC-2 vs PC-3), stood out from the remainder of the *sld1sld2* population.

The genotypes overexpressing the transgenes *sld1sld2*:*ThSLD1* and *sld1sld2*:*ThSLD2* showed a general recovery in the glucosylceramide profile to Col-0 values. Yet, some differences between lines within each genotype were found. Line #6 showed only a partial recovery in its glucosylceramide profile compared to the other two lines (#4 and #5) of *sld1sld2*:*ThSLD2*, with a profile that showed similar trends to the double mutant *sld1sld2*. The 21-fold increase in content of 16:0 in d18:0

compared to Col-0 (Figure 5.8 A), or 17-fold change in 24:1 fatty acid of t18:0 (Figure 5.8 B) show more similarity to the *sld1sld2* profile than to wild-type. This trend was also verified in the PCA (Appendix 20), where the data representing line #6 tended towards negative values in PC-1 combined with positive PC-2, which resulted in a separation from the remaining lines towards the *sld1sld2* pool. Concomitantly, this same line was previously shown (Figure 5.4, Section 5.2.3) to have the lowest transgene expression rate of the selected lines, which might be a contributing factor to the observed results. Moreover, the lines that showed higher expression levels, #1 for *sld1sld2*:*ThSLD1* and line #5 of *sld1sld2*:*ThSLD2* correspondingly showed an increased content of glucosylceramides, compared to the wild-type. This could be observed in the unsaturated LCBs, where lines #1 and #5 showed a respectively a 5.0% and 15.1% increase in the 16:0 fatty acid of d18:1 (Figure 5.8 C), or in the t18:1, an increase of 26.4% for line #5 and 9.8% for line #1 in 24:1 (Figure 5.8 D). The PCA (Appendix 20) showed one of the line #1 replicates to stand out from the remaining pool, suggesting it to be an outlier, which could be skewing the mean represented in Figure 5.8. The PCA also did not show any separation of the lines from the wild-type Col-0 pool, indicating that these differences were not significant and an overall similar behaviour to the wild-type. The GIPC profile revealed a different behaviour of the overexpressing lines *sld1sld2*:*ThSLD1* and *sld1sld2*:*ThSLD2*, where the first showed a recovered or augmented profile to wild-type values, whilst the latter showed an intermediate profile (Figure 5.8 E-H). Discrete increases in the GIPC content were observed for some lines of *sld1sld2*:*ThSLD1*. Some examples are shown in the d18:0 profile (Figure 5.8 E) with an average 60% increase in fatty acid 22:1 in lines #1 and #3, or in the d18:1 LCB (Figure 5.8 G) where line #1 showed an increased content in the fatty acids 16:0 (41.9%), 22:0 (64.2%), 24:0 (34.8%), and in 24:1 (51.7%). The *ThSLD2* transgene, however, only showed a partial recovery of the GIPC profile. This effect was present throughout, and especially evident in the profile of LCB d18:1 (Figure 5.8 G), with an average difference of *sld1sld2*:*ThSLD2* to Col-0 of 47.7% in 16:0 or 53.8% in 26:0. Or in the t18:1 profile that

reached values of 38.8% for 26:0 or 48.4% in 22:1 (Figure 5.8 H). Again, lines #5 and #6 showed the biggest differences in their profiles. The differences observed amongst the lines of each genotype were consistent with the glucosylceramide profile, as lines #1, #5 and #6 stood out (Figure 5.8 E-H), but not in the PCA performed (Appendix 21). This analysis also did not distinguish any of the genotypes, except the double mutant as discussed before, possibly indicating that the observed changes in some molecular species may be compensated throughout each profile. The total content of glucosylceramides and GIPCs was also analysed to assess if the changes revealed in the profile were reflected in the overall amount of these sphingolipids as it is discussed below.

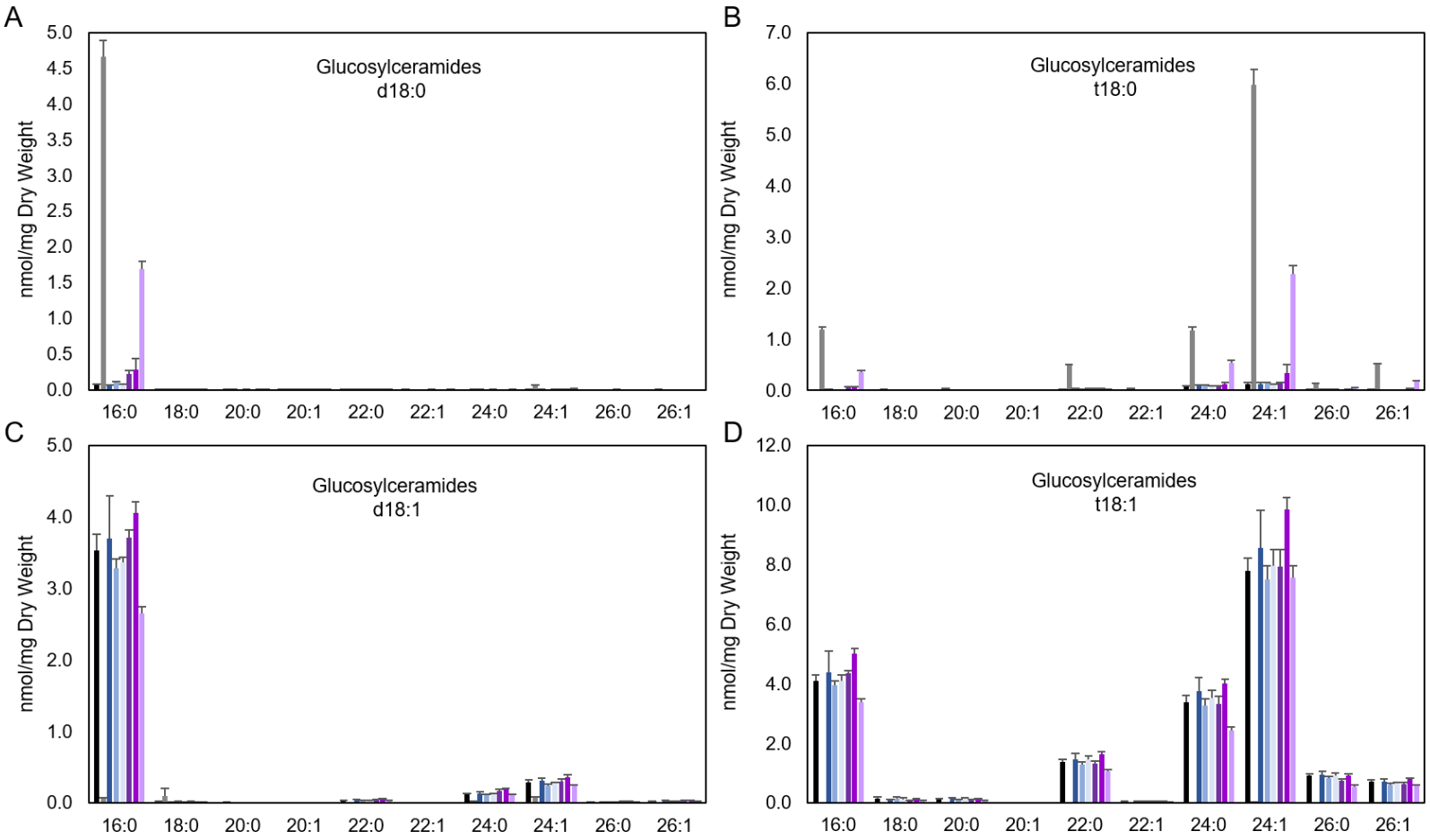

(Continued on the next page)

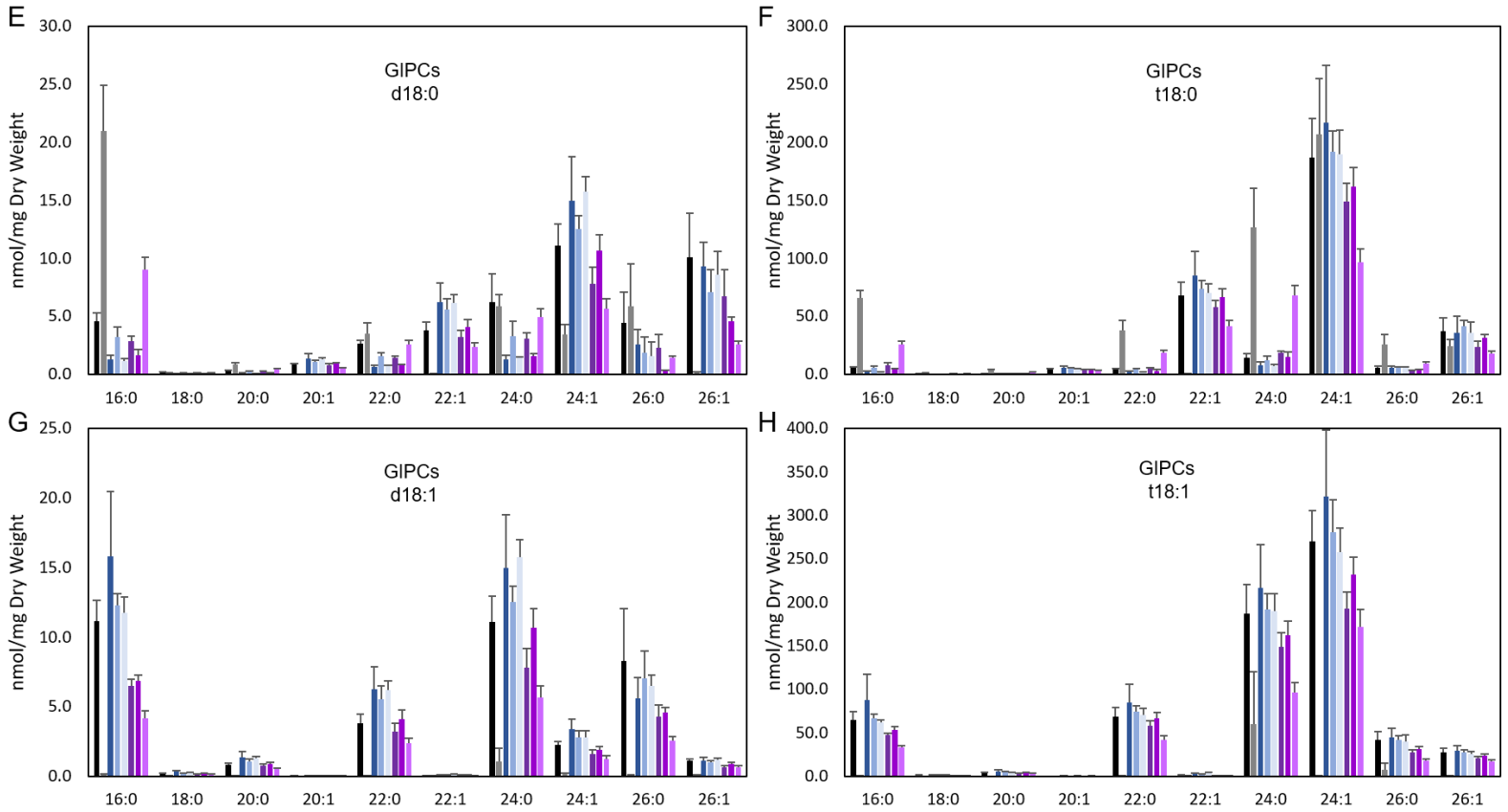

Figure 5.8 Glucosylceramide and GIPC Content of the SLD Lines

Glucosylceramide (A-D) and GIPC (E-H) fatty acid profile for the LCBs d18:0 (A, E), t18:0 (B, F), d18:1 (C, G), and t18:1 (D, H) for Col-0 (■), *sld1sld2* (■), the three lines #1 (■), #2 (■) and #3 (■) of *sld1sld2*:*ThSLD1* and lines #4 (■), #5 (■) and #6 (■) for *sld1sld2*:*ThSLD2*. Bars represent mean + standard error, N=6.

Despite the observed differences in each line of *sld1sld2*:*ThSLD1* and *sld1sld2*:*ThSLD2*, this did not translate in to significant differences between lines of the same genotype in the total content of glucosylceramides or GIPCs (Figure 5.9). The total content of each sphingolipid class was tested with an ANOVA to assess differences between genotypes and between lines within genotypes. Differences amongst genotypes were found in both classes, with $p<0.001$ for glucosylceramides and $p_{log10}<0.001$ for GIPCs, for which a Bonferroni test was used for comparisons between genotypes. The total glucosylceramide content was significantly reduced in the double mutant *sld1sld2*, which accumulated 14.7 nmol/mg of (whole plant) dry weight showing a 36.4% reduction compared to Col-0. Whilst the genotypes *sld1sld2*:*ThSLD1* and *sld1sld2*:*ThSLD2* showed a mean total content of 23.3 and 25.3 nmol/mg dry weight, respectively, showing no differences to the wild-type Col-0 with 23.1 nmol/mg dry weight (Figure 5.9 A). The GIPC total content used a $\log_{10}$ transformation for the ANOVA (Figure 5.9 B), which showed a more balanced distribution of the residuals, resulting in a stronger analysis. GIPC analysis showed the same trend for *sld1sld2* with a significantly reduced content of 602.1 nmol/mg dry weight compared to wild-type Col-0 (1073.8 nmol/mg dry weight) and *sld1sld2*:ThSLD1 (1132.8 nmol/mg dry weight). The resulting GIPC total content was thus not in agreement with the published data by Chen *et al.* (Chen *et al.* 2012), which showed an accumulation of GIPCs in both single *sld1* and double *sld1sld2* mutants. This could be traced to the class's LCB profile, where in the published data showed an increased t18:0 profile in the double mutant *sld1sld2* ranging approximately from 9- to 50-fold, whilst in the data presented here this range reached a maximum average of 11.5-fold increase. The *sld1sld2*:*ThSLD2* genotype, however, showed an intermediate content of 815.2 nmol GIPC/mg dry weight that was not distinguished from any of the remaining genotypes *sld1sld2*, Col-0 or *sld1sld2*:ThSLD1, but showed only a partial recovery of the sphingolipid profile by the overexpression of the transgene *ThSLD2*.

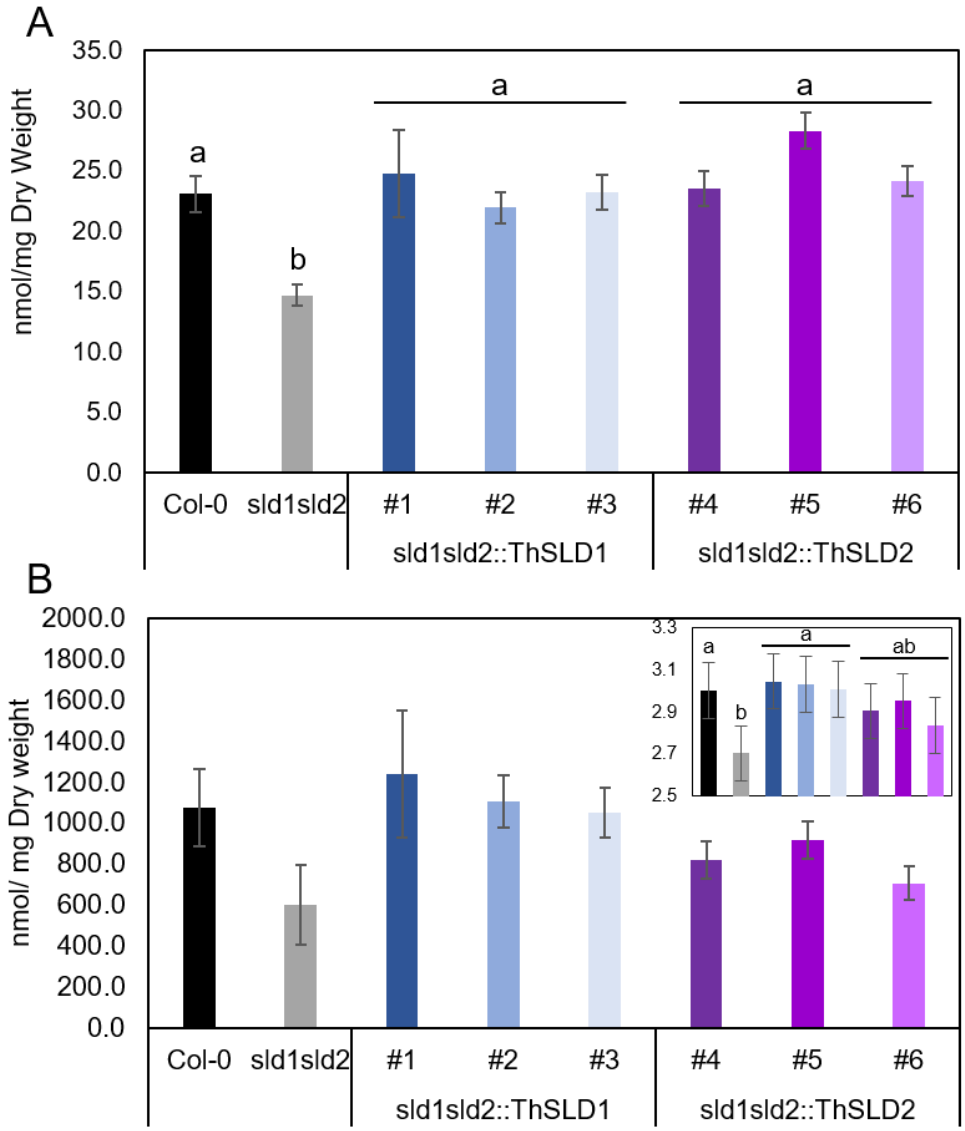

Figure 5.9 Total Glucosylceramide and GIPC Content

(A) Glucosylceramide and (B) GIPC total content for Col-0 (■), *sld1sld2* (■), the three lines #1 (■), #2 (■) and #3 (■) of *sld1sld2*:*ThSLD1* and lines #4 (■), #5 (■) and #6 (■) of *sld1sld2*:*ThSLD2*. Insert in B represents GIPC data transformed with $\log_{10}$ to allow a balanced distribution of residuals. Bars represent mean ± standard error, N=6. ANOVA showed differences amongst genotypes (A, $p<0.001$; B, $p_{\log_{10}}<0.001$), but not between lines within genotypes (A, $p=0.172$; B, $p_{\log_{10}}=0.769$). Bonferroni test used to compare genotypes are shown in lowercase letters sorted in descending order.

5.2.7 *sld1sld2 Showed an Accumulation of Ceramides*

The free ceramide profile was analysed, to assess the impact of the *SLD* genes in its specific biosynthesis pathway. Previously, ceramides were

demonstrated to follow the same trend as the glucosylceramides or the GIPCs in the double mutant's profile (Chen *et al.* 2012). Figure 5.10 shows the ceramide profile for the studied lines, where the main contributors for the ceramide pool were shown to be the LCBs 4-hydroxysphinganine t18:0 and the 4-hydroxy-8-sphingenine t18:1 (t18:1^8), as expected from the predominant LCBs found in plant species (Michaelson *et al.* 2016). Both saturated and unsaturated LCBs d18:0 and d18:1 (Figure 5.10 A, C), respectively, accumulated at low levels and did not reach 1.0 nmol/mg dry weight. Both t18:0 and t18:1 showed contrasting responses from the studied lines as expected. No t18:1 content was found in *sld1sld2* showing instead an exacerbated t18:0 profile (Figure 5.10 B, D), whereas the *sld1sld2* genotypes carrying the *ThSLD* transgenes showed a general recovery of the profile compared with wild-type. The analysis of the ceramides revealed higher variability within the lines of each *sld1sld2*:*ThSLD1* and *sld1sld2*:*ThSLD2* genotypes.

Initial PCA analysis (results not shown), revealed the need for at least four dimensions to explain up to 84.33% of the variability of the data, where the first two, PC-1 and PC-2 showed similar values of 34.94% and 32.83%, respectively (PC-3, 9.50%; PC-4, 7.06%). Instead, a CVA was used to account for the genotype effect (Figure 5.11). This revealed a clear separation of the genotypes, with CV1 distinguishing *sld1sld2* in its positive limit, and in the lower negative region *sld1sld2*:*ThSLD1* together with Col-0, followed by *sld1sld2*:*ThSLD2* closer to zero (Figure 5.11 B). CV2 showed an interesting result by pulling apart Col-0 and *sld1sld2*:*ThSLD1* genotypes, while showing the proximity of *sld1sld2*:*ThSLD2* and *sld1sld2* (Figure 5.11 A). Yet, the third dimension was also informative, despite only accounting for 7.14% of the variability, where *sld1sld2*:*ThSLD2* stood out from the remaining three genotypes (Figure 5.11 C). The analysis of the vector loadings revealed CV1 and CV3 with a similar positive influence of long carbon acyl fatty acid chains in d18:0. CV2 showed a more varied LCB profile on its top five positive loadings, with predominant intermediate carbon length fatty acid

molecular species between 20 and 22 carbons, whereas it was negatively influenced by d18:1:22:1, and t18:0's fatty acids 18:0 and 20:1. These suggested a pattern, where the wild-type Col-0 and *sld1sld2*:*ThSLD1* showed a rich profile in intermediate chain length fatty acids in their ceramides, whilst the absence of the *AtSLD* genes, which did not seem to be fully recovered by *ThSLD2,* showed a predominance of long chain fatty acids in their ceramide profile. Despite the absence of Δ^8-desaturation in *sld1sld2*, residual amounts of d18:1 were present in the double mutant's profile (Figure 5.10 C). An effect that could be explained by the presence of the Δ^4-desaturase, which produced 4-sphingenine d18:1^4, and remained active in the double mutant *sld1sld2* (Michaelson *et al.* 2009). The total content of ceramides (Figure 5.12) was also analysed and ANOVA analysis showed no differences between the lines within each genotype ($p=0.368$). However, significant differences between genotypes ($p<0.01$) were identified, showing a significantly higher accumulation of ceramides in the double mutant *sld1sld2* than in any other genotype. Such a trend could be explained by the increased content of t18:0, which showed the highest concentration of the four LCB classes of ceramides, as presented in Figure 5.10.

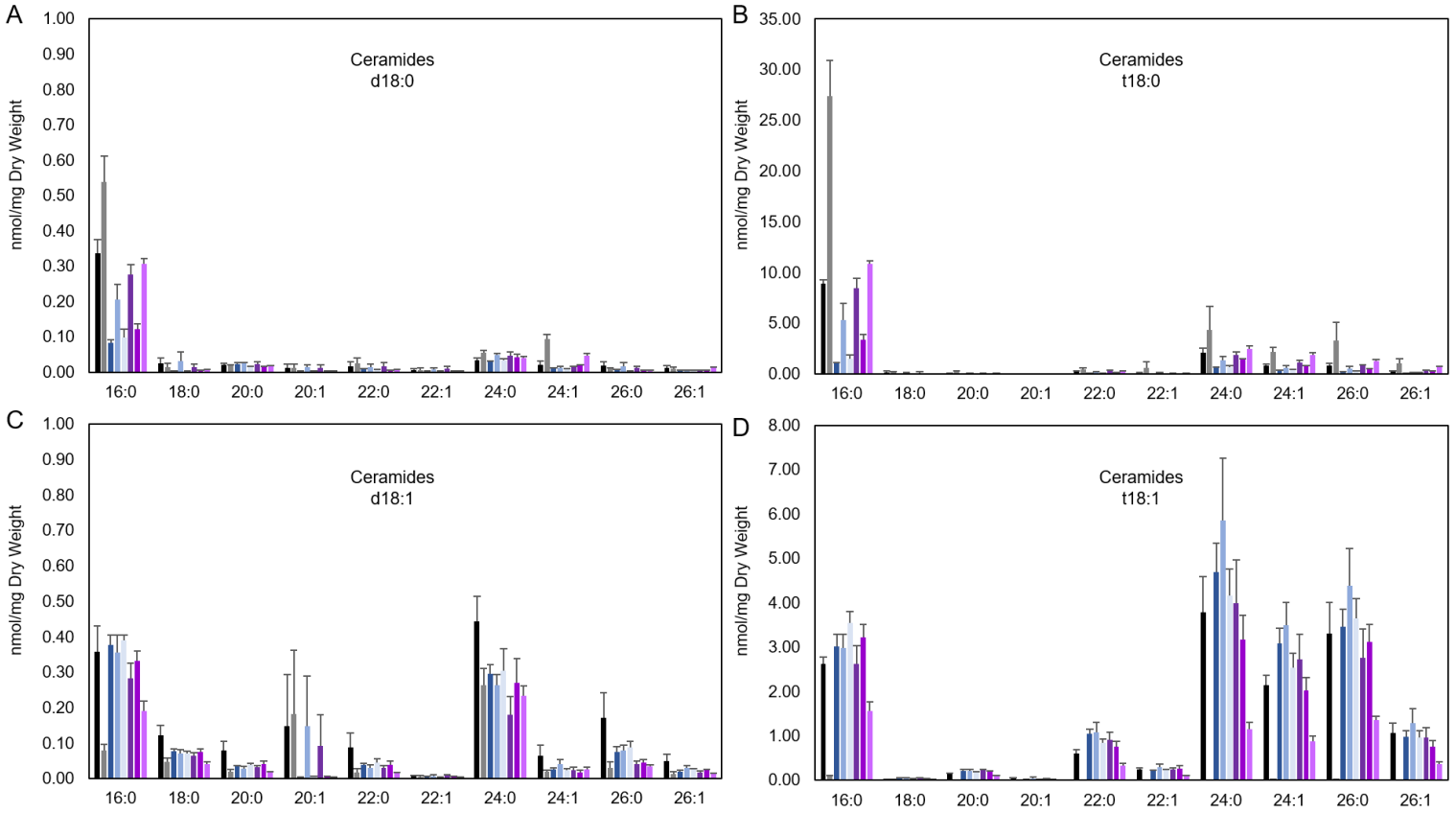

Figure 5.10 Ceramide Profile of the SLD lines

Ceramide fatty acid profile for the LCBs d18:0 (A), t18:0 (B), d18:1 (C), and t18:1 (D) for Col-0 (■), *sld1sld2* (■), the three lines #1 (■), #2 (■) and #3 (■) of *sld1sld2*:*ThSLD1* and lines #4 (■), #5 (■) and #6 (■) for *sld1sld2*:*ThSLD2*. Bars represent mean + standard error, N=6.

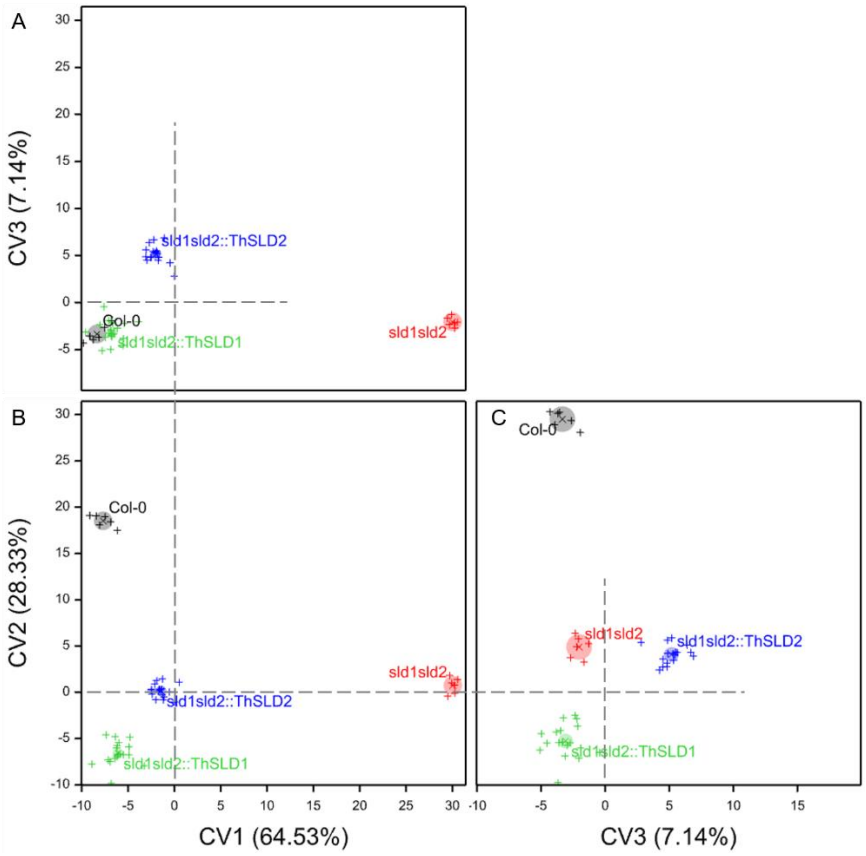

Figure 5.11 Canonical Variates Analysis of Ceramide Profile of SLD Lines

Canonical variate (CV) analysis of ceramide profule with genotype as a grouping factor. The three dimensions (CV1, CV2, CV3) were used to explain the variability of the data (A-C). Col-0 (■); *sld1sld2* (■); *sld1sld2*:*ThSLD1* (■); *sld1sld2*:*ThSLD2* (■). Circles around means (×) represent 95% confidence intervals, individual points are represented by "+". Dashed lines represent zero. CV loadings in Appendix 18.

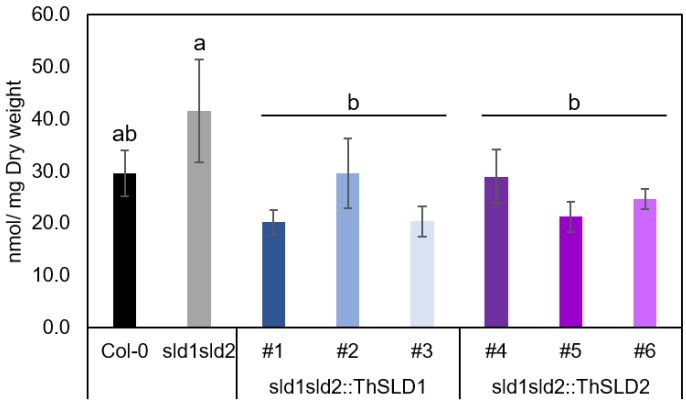

Figure 5.12 Total Ceramide Content in the SLD Lines

Ceramide total content for Col-0 (■), *sld1sld2* (■), the three lines #1 (■), #2 (■) and #3 (■) of *sld1sld2*:*ThSLD1* and lines #4 (■), #5 (■) and #6 (■) of *sld1sld2*:*ThSLD2*. Bars represent mean ± standard error, N=6. ANOVA showed differences amongst genotypes ($p<0.01$), but not between lines within genotypes ($p=0.368$). Bonferroni test used to compare genotypes shown in lowercase letters sorted in descending order.

5.2.8 *The Hydroxyceramide Profile Changed in sld1sld2*

The total content of hydroxyceramides showed a reduced overall content in *sld1sld2* to a mean of 115.7 nmol/mg dry weight. Both overexpressing genotypes, *sld1sld2*:*ThSLD1* and *sld1sld2*:*ThSLD2* showed a total concentration of 150.9 and 154.0 nmol/mg dry weight, respectively, displaying an higher concentration compared to wild-type Col-0 (139.9 nmol/mg dry weight; Figure 5.13). The statistical analysis performed with ANOVA used a logarithmic transformation (log_{10}), which allowed a more balanced distribution of the residuals, and hence more power to the analysis (insert in Figure 5.13). The observed differences amongst lines within each genotype were not significant (p=0.431), however the genotype factor showed a significant *p* value (<0.05). The Bonferroni comparison test showed the contrasting behaviour of *sld1sld2* against *sld1sld2*:*ThSLD1* and *sld1sld2*:*ThSLD2*, however neither of these genotypes were found to be significantly different from Col-0. Such result could suggest that either absence or overexpression of the *SLD* genes did not show a significant impact on the hydroxyceramide content.

Further analysis of the hydroxyceramide profile was performed to assess specific differences in each of the LCBs profile (Figure 5.14). The LCB class t18:1 showed the highest contribution to the total pool of hydroxyceramides reaching 85% in the wild-type Col-0. As before, the hydroxyceramide profile was found to follow the same trend as other sphingolipid classes, reflecting also the results observed for its total content. The distinction in the profile of the double mutant *sld1sld2* was shown by the 27- and 28-fold increased content of the LCBs profile d18:0 and t18:0, respectively (Figure 5.14 A, B), and a correspondent drop of 62.4% in d18:1 and 99.7% in t18:1 (Figure 5.14 C, D). The transgenes *ThSLD1* and *ThSLD2* contributed to the recovery of the double mutant's phenotype to Col-0 values. Consistently, the same variances previously found in the different lines for each genotype were also represented in the hydroxyceramide profile. The *sld1sld2*:*ThSLD2* line #6 showed similarities to the double mutant. This was especially observed in the increased concentrations of fatty acid 16:0 in d18:0 by 10-fold (Figure

5.14 A), or in LCB t18:0 where fatty acids 16:0, 24:0 and 24:1 showed a 15-, 4-, and 13-fold increase compared to the wild-type, respectively (Figure 5.14 B). Lines #1 and #5 showed a slight increased content of hydroxyceramides, as before. Line #1, which overexpressed *ThSLD1* transgene, showed a 20% increase in the total concentration of unsaturated LCBs d18:1 and t18:1, whilst in line #5 overexpressing *ThSLD2* this response was more variable with a total increase of d18:1 by 25% and t18:1 in a lesser extent with 18% increase.

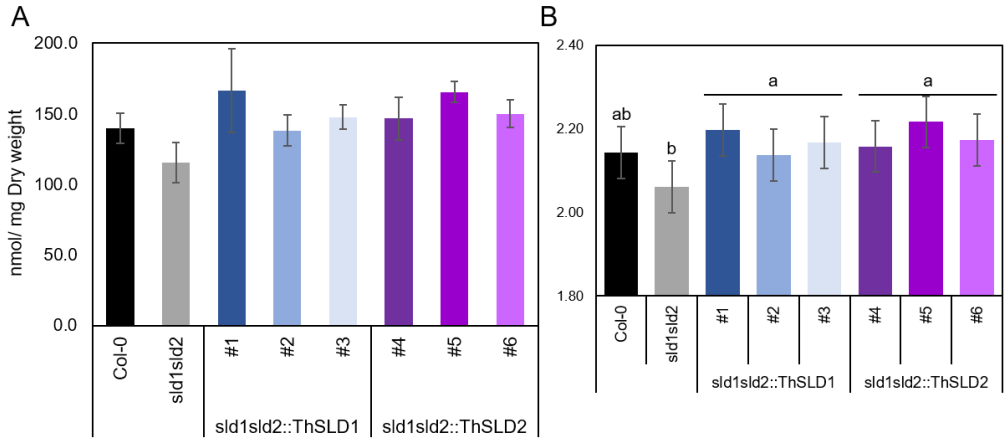

Figure 5.13 Total Hydroxyceramide Content for the SLD Lines

Hydroxyceramide total content for Col-0 (■), *sld1sld2* (■), lines #1 (■), #2 (■) and #3 (■) of *sld1sld2*:*ThSLD1* and lines #4 (■), #5 (■) and #6 (■) of *sld1sld2*:*ThSLD2*. Bars represent mean ± standard error, N=6. (A) Original data, (B) $\log_{10}$ transformed data to allow a balanced distribution of residuals in the ANOVA, which showed differences amongst genotypes ($p<0.05$), but not between lines within genotypes ($p=0.431$). Bonferroni test used to compare genotypes are shown in lowercase letters sorted in descending order.

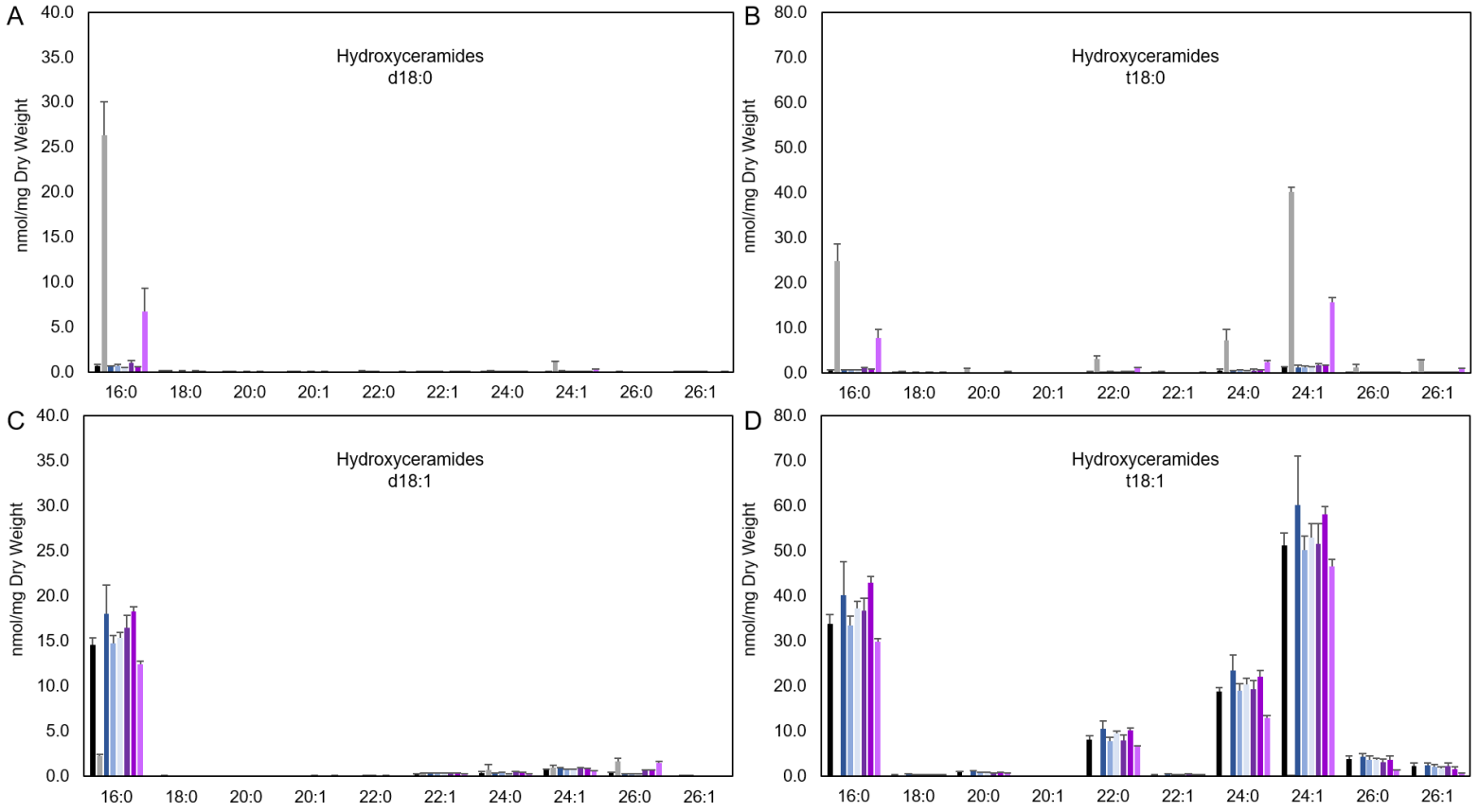

Figure 5.14 Hydroxyceramide Profile for the SLD lines

Hydroxyceramide fatty acid profile for the LCBs d18:0 (A), t18:0 (B), d18:1 (C), and t18:1 (D) for Col-0 (■), *sld1sld2* (■), the three lines #1 (■), #2 (■) and #3 (■) of *sld1sld2*:*ThSLD1* and lines #4 (■), #5 (■) and #6 (■) for *sld1sld2*:*ThSLD2*. Bars represent mean + standard error, N=6.

5.2.9 *Col-0:ThSLD1 and Col-0:ThSLD2 Total Sphingolipid Class Content*

The sphingolipid classes were also analysed for the genotypes Col-0:*ThSLD1* and Col-0:*ThSLD2* in comparison with the wild-type Col-0. The previously discussed CVA for this dataset (Figure 5.7) showed the clear distinction of *sld1sld2* by CV1 (84.10%). This relationship has been extensively analysed in the above sections, where *sld1sld2* genotype was compared to the wild-type Col-0, and the recovery genotypes *sld1sld2*:*ThSLD1* and *sld1sld2*:*ThSLD1*. Thus, this section focuses on the comparison of both Col-0:*ThSLD1* and Col-0:*ThSLD2* with the wild-type Col-0. The relationship amongst these three genotypes was shown, by the CVA on the total sphingolipid dataset, to be differentiated by CV2 which was positively influenced by GIPCs, distinguished both Col-0:*ThSLD1* and Col-0:*ThSLD2* from Col-0 (details in Section 5.2.5). However, this trend did not translate into the total content of each of the different classes (Figure 5.15). Quite a specific pattern was observed when *ThSLD1* and *ThSLD2* were overexpressed in the wild-type background. No impact was observed in the total content of GIPCs nor glucosylceramides where the ANOVA showed p=0.390, and p=0.2674, respectively (Figure 5.15 E). On the contrary, the total content of ceramides and hydroxyceramides significantly increased in both overexpressors with a significant difference amongst each other and to Col-0 (Figure 5.15 E). The hydroxyceramides showed to accumulate in the overexpressors almost to the extent of the predominant class GIPC which resulted from an increased content of the unsaturated LCBs, with a greater effect observed on t18:1. Col-0:*ThSLD2* showed the highest accumulation of both classes, followed by Col-0:*ThSLD1*. The ceramide content registered the highest increase in Col-0:*ThSLD2* profile of 3.5-fold compared to Col-0, and 1.4-fold compared to Col-0:*ThSLD1* (Figure 5.15 B). Col-0:*ThSLD1* showed a balanced response in both ceramide and hydroxyceramide content with a 2.6- and 2.25-fold increase when compared to Col-0 (Figure 5.15 B, D).

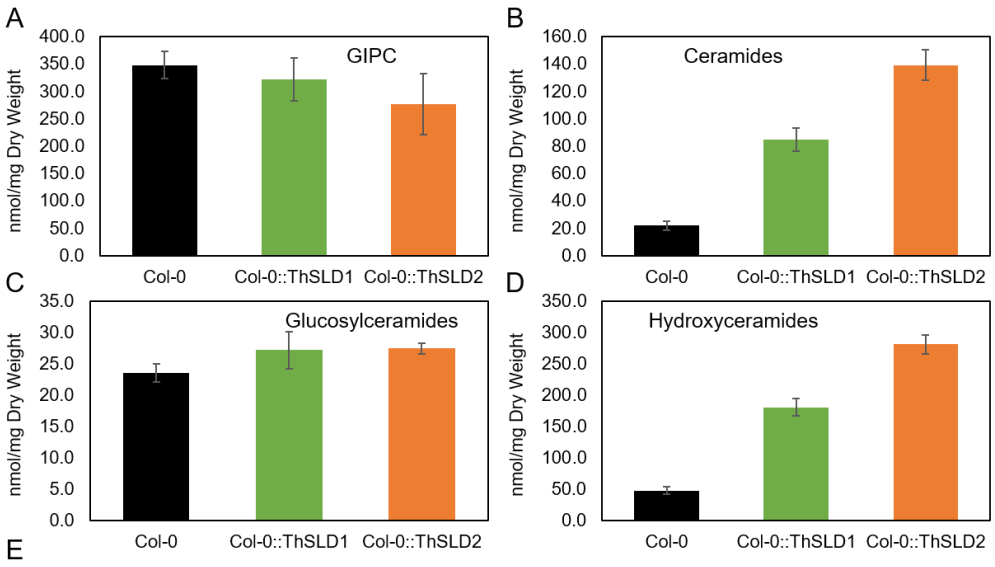

E

	GIPC	Ceramides	Glucosylceramides	Hydroxyceramides
Genotype	p=0.390	*** (p<0.001)	p=0.264	*** (p<0.001)
Col-0	2.54 ± 0.15	1.32 ± 0.07 (c)	1.37 ± 0.04	1.66 ± 0.06 (c)
Col-0::*ThSLD1*	2.49 ± 0.15	1.92 ± 0.07 (b)	1.42 ± 0.04	2.25 ± 0.06 (b)
Col-0::*ThSLD2*	2.33 ± 0.15	2.14 ± 0.07 (a)	1.44 ± 0.04	2.45 ± 0.06 (a)

Figure 5.15 Total Content of Sphingolipids in Col-0:ThSLD Genotypes

(A) GIPC, (B) Ceramide, (C) Glucosylceramide, and (D) Hydroxyceramide total content (original data) for Col-0 (■), Col-0:*ThSLD1* line #7 (■), and Col-0:*ThSLD2* line #10 (■). Bars represent mean + standard error, N=6. (E) ANOVA results table for genotype differences, mean ± standard error of difference on $\log_{10}$ scale. Bonferroni test to compare genotypes is in parentheses as lowercase letters sorted in descending order.

5.2.10 *SLD Overexpression Showed no Impact on Arabidopsis Growth*

The biochemical profile of the different genotypes showed significant differences in the impact of each *ThSLD* gene. Previously, it was demonstrated that the *SLD* mutants in Arabidopsis did not have a significant impact in the growth phenotype, even when *sld1sld2* was complemented with *AtSLD1* (Chen *et al.* 2012). When the lines were exposed to freezing stress at 0°C, however, the complemented genotype maintained green pigmentation even after eight weeks of stress conditions (Chen *et al.* 2012). This led to the suggestion of *AtSLD1* as candidate gene for cold stress endurance. To test this hypothesis, the

genotypes overexpressing *ThSLD1* and *ThSLD2* were analysed for distinct growth patterns under control conditions and, in a first experiment, under cold stress at 4°C for eight days. A period of eight days was used as tested in Chapter 3. Furthermore, it has been demonstrated that seven days of cold acclimation to be enough for the plant to reach maximal freezing tolerance (Livingston *et al.* 2007). Each of the three lines for *sld1sld2*:*ThSLD1* (#1 - #3), *sld1sld2*:*ThSLD2* (#4 - #6), Col-0:*ThSLD1* (#7 - #9) and Col-0:*ThSLD2* (#10 - #12) were grown together with the wild-type Col-0 and the double mutant *sld1sld2*. Six plants for each line were grown under control conditions of 23°C temperature (Section 2.2.3) for 26 DAS. A second set of plants was grown under the same control conditions for 18 DAS, after which they were moved to cold 4°C conditions for eight days (Section 2.2.4). Exposing the different genotypes to control and cold temperatures allowed the assessment of the growth phenotype, first, and then the ability of each genotype to withstand cold stress (Figure 5.16). Under control conditions no visual differences between the lines, nor between genotypes, were found that would distinguish any of the overexpressing *ThSLD1* or *ThSLD2* lines from each other or from the wild-type (Figure 5.16 A-F). The effect of the cold stress was visible after the eight days of exposure, as plants showed an arrested development, displayed a yellow hue on the developed leaves with anthocyanins forming in the centre of the rosette (Figure 5.16 G-L). Despite the visible impact of the cold temperatures in the development of the plants there was no significant alteration in this pattern between lines. Surprisingly, even the double mutant *sld1sld2* did not differentiate from wild-type. These observations differ from those described by Chen *et al.* (Chen *et al.* 2012). Several factors could contribute to this, e.g. the specific cold stress temperature or the exposure time may not have been enough to trigger a response.

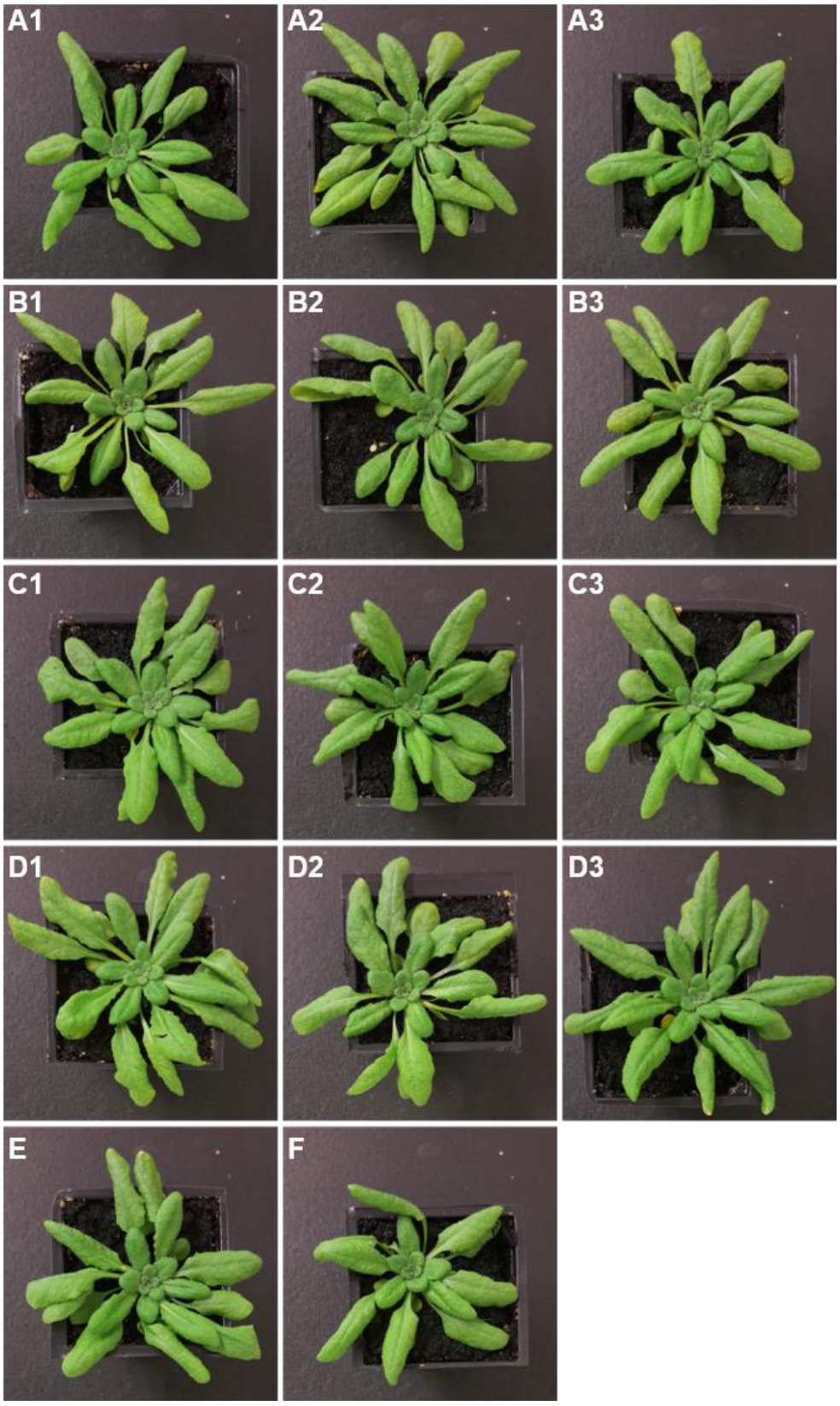

(Continued on the next page)



Figure 5.16 Growth Phenotype of the SLD Lines

Phenotype of SLD lines after 26 DAS of control 23/18°C day/night (A-F) and after eight days of cold 4°C (G-L). One representative plant is shown for each genotype and temperature, each of the overexpressing genotypes have three independent lines 1 to 3. (A1-A3, G1-G3) *sld1sld2*:*ThSLD1*; (B1-B3, H1-H3) *sld1sld2*:*ThSLD2*; (C1-C3, I1-I3) Col-0:*ThSLD1*; (D1-D3, J1-J3) Col-0:*ThSLD2*; (E, K) *sld1sld2*; (F, L) wild-type Col-0.

5.2.11 *SLD Showed No Effect in Membrane Damage Under Cold*

The plants from the control and cold stress growth phenotype experiment were analysed for their levels of electrolyte leakage. As described in Chapter 3 (Section 3.2.7), electrolyte leakage is a measure of the level of membrane damage. Thus, an increase in the relative conductivity can be related to the extent of the cellular damage under stress, which is used as a method of assessing stress response (Jaglo-Ottosen *et al.* 1998). In this experiment, five leaf discs per plant from five plants per line were used to measure the water conductivity after 24h of collection, and total conductivity was quantified after exposing the sample of 90 min at 90°C. The relative conductivity was determined and used to calculate the injury index (I_d, %) associated with membrane damage caused by the eight days of exposure to cold stress (Whitlow *et al.* 1992). The relative conductivity (Figure 5.17 A) showed a response to the temperature change ($p<0.001$) in all lines, however no differences were found amongst the genotypes ($p=0.619$) nor between lines within genotype ($p=0.104$). The injury index (Figure 5.17 B) reflected the percentage increase in the membrane damage of each line. Line #6 of *sld1sld2*:*ThSLD2* showed a 5.45% decrease in the averaged membrane damage, however the variability associated with the measurement did not allow for a statistical significance. This was evident in the ANOVA test which, as before, did not show any differences amongst lines within genotypes ($p=0.058$), nor between genotypes ($p=0.229$). These results reflected the observed lack of differentiation in the genotypes' growth phenotype.

5.2.12 *Acyl-CoA Accumulated under Cold Stress*

The acyl-CoA pool is directly involved in the biosynthetic pathway of sphingolipids (Markham *et al.* 2013). The acyl Co-A profile was analysed in the *sld1sld2*:*ThSLD1* and *sld1sld2*:*ThSLD2* genotypes, together with Col-0 and *sld1sld2*. The analysis was performed on the same two sets of control and cold plants as described above (see Section 5.2.10).

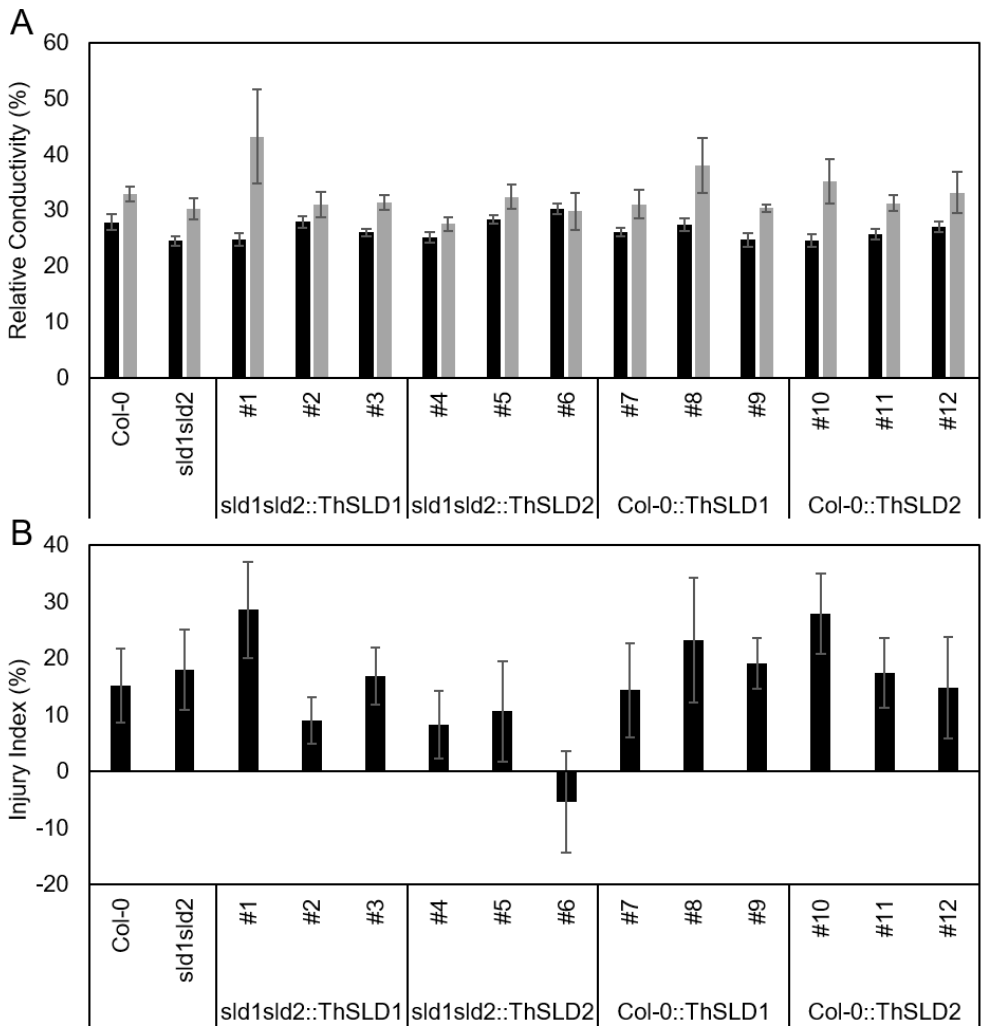

Figure 5.17 Membrane Damage in the SLD Lines Under Cold Stress

(A) Relative conductivity under control (■) and after eight days of cold stress (■); (B) Injury index calculated using the relative conductivity of control and stress for each line. Bars represent mean + standard error, N=6. ANOVA performed for differences between genotype (A, p=0.619; B, p=0.058), line within genotype (A, p=0.104; B, p=0.229), and temperature (A, p<0.001).

This experimental design allowed the assessment of the acyl-CoA profile, not only in response to the *SLD* genes, but also the influence of the cold response in the plants' metabolic adaptation. Under both control (Figure 5.18 A) and cold (Figure 5.18 B) temperatures no significant alterations in the profiles of each genotype was observed. *sld1sld2* showed a subtle increase in the very-long chain acyl-CoA species under control conditions, observed in species 24:0 through 28:0, showing the highest

average increase of 35.9% in 24:1 and 58.8% in 26:1 compared to Col-0 (Figure 5.18 A). This trend was not observed in cold conditions, where instead a general reduction in the very-long chain acyl-CoA was observed. Concomitantly, cold stress caused a shift in the acyl-CoA profile by increasing the content of long-chain 16:0 and 18:3. Under the imposed cold conditions, *sld1sld2*:*ThSLD2* showed the highest 16:0 accumulation with an average across its three lines of 45.77% of the total content, whereas Col-0 showed an average of 40.42% (Figure 5.18 B). Due to the low concentration and challenges of measuring the acyl-CoA pool in vegetative tissues, measurement errors were incurred. This is observed in the CVA performed for the control and cold conditions datasets. This analysis was performed for both growth conditions, using either genotype ((Figure 5.18 C, D) or line (Figure 5.18 E, F) as grouping factors. Figure 5.18 (C-F) shows the results for this analysis where, for simplicity, only two CV are shown for each analysis, however in any of the analysis both CVs accounted for less than 90% of the variability of the dataset, further illustrating the dispersion in the data. Still, differences amongst the genotypes were observed, allowing some extrapolation to their specific response to the different temperatures. Under control temperature, *sld1sld2* showed a distinct behaviour to the other genotypes with positive CV1 values. The relationship of Col-0, *sld1sld2*:*ThSLD1* and *sld1sld2*:*ThSLD2* showed a similar trend with that observed for the sphingolipid profile described above, where *sld1sld2*:*ThSLD1* complemented the *sld1sld2* phenotype to Col-0 values. The shift in the genotypes' response to cold stress was also shown in the CVA (Figure 5.18 F), with a surprising similarity of *sld1sld2* and Col-0 profiles. The complemented genotypes, however, showed contrasting responses, *sld1sld2*:*ThSLD2* showed a higher CV2, whilst *sld1sld2*:*ThSLD1* a higher CV1, when comparing both to Col-0.

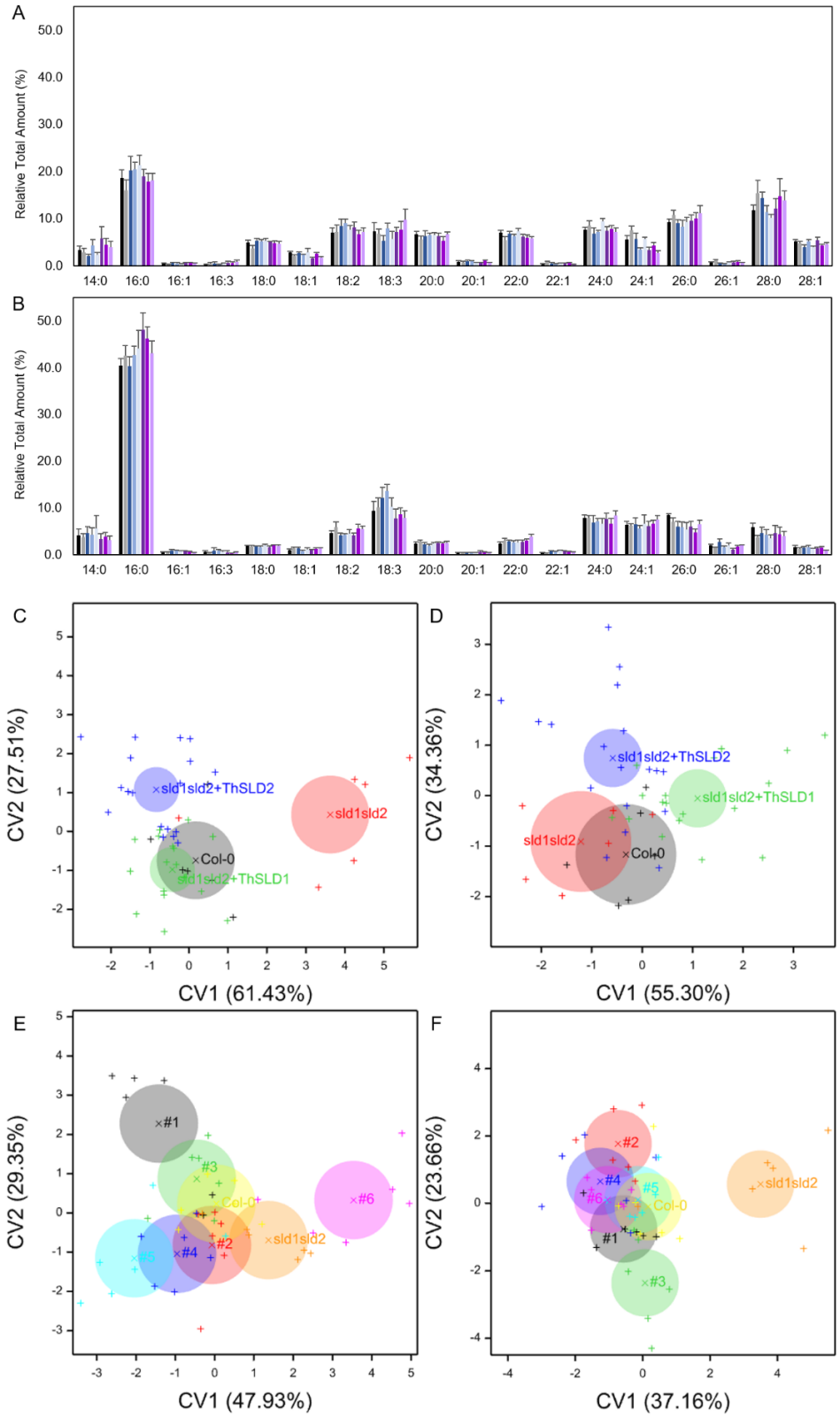

Figure 5.18 Acyl-CoA Profile under Control and Cold Temperatures

Acyl-CoA profile at control (A) and eight days of cold (B) for Col-0 (■), *sld1sld2* (■), lines #1 (■), #2 (■) and #3 (■) of *sld1sld2*:*ThSLD1* and lines #4 (■), #5 (■) and #6 (■) for *sld1sld2*:*ThSLD2*. Bars represent mean + standard error, N=6. CVA for control (C, E) and cold (D, F) temperatures using genotype (C, D) or lines (E, F) as grouping factors. CV loadings in Appendix 19.

5.2.13 *Higher Recovery Rate in the ThSLD2 Complemented Lines*

No visible growth phenotype was observed for the SLD lines under control nor after eight days of cold stress at 4°C. The same result was registered when the membrane electrolyte leakage was assessed showing no significant differences amongst genotypes. The previously described phenotype for the *sld* mutants and the double mutant complemented with *AtSLD1*, showed the resilience of the latter *sld1sld2*:*AtSLD1* to eight weeks of 0°C by retaining leaf colouration and delaying senescence (Chen *et al.* 2012). Taken together with the results obtained in this project, where no distinguishable features were found under cold stress at 4°C, the recovery capacity of the overexpressing lines was questioned. To assess this, the plants were subjected to further testing by analysing the recovery rate after a short freezing period. Five plants for each Col-0, *sld1sld2*, the three lines #1 - #3 of *sld1sld2*:*ThSLD1*, #4 - #6 of *sld1sld2*:*ThSLD2*, #7 - #9 of Col-0:*ThSLD1*, and the final three lines #10 - #12 of Col-0:*ThSLD2* were studied.

The experimental design (Figure 5.19 A) began with plants grown in control conditions of 23°C for 19 DAS, followed by a cold acclimation period of eight days at 4°C (Sections 2.2.3-2.2.4). The primed plants were then exposed to -5°C for 24h (temperature decreased at a rate of 0.10°C/min), recovered first to 4°C for four days, and then to control temperature of 23°C for up to eleven days. As with the previous experiment, no differences were found between the genotypes during cold or freezing stresses. However, the recovery rate showed different responses amongst genotypes. This was assessed by measuring the rosette diameter (Figure 5.19 B) and shoot height (Figure 5.19 C), when present, in the plants after four and eleven days of recovery to 23°C. After four days of recovery, no differences in the rosette size were found amongst genotypes ($p=0.268$) nor between lines within of each genotype ($p=0.129$). However, after 11 days at 23°C there was sufficient differentiation in the rosette diameter between lines ($p=0.018$), which was reflected in the respective genotype differences ($p<0.001$).

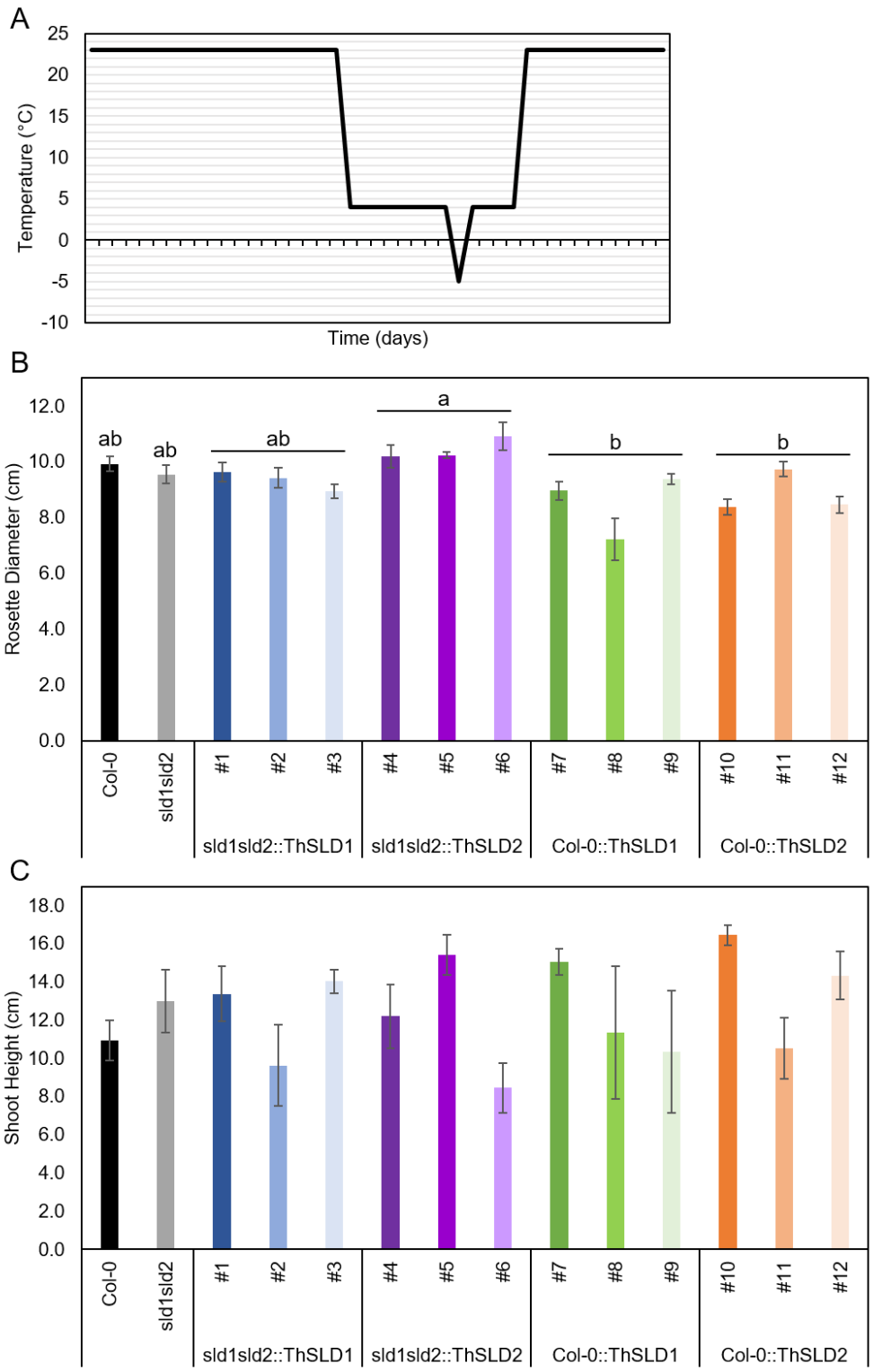

Figure 5.19 Recovery Rate of the SLD Lines after Freezing Stress

(A) Experimental design of 23°C growth for 19 DAS, cold acclimation of eight days at 4°C, drop to -5°C for 24h, and recover to 4°C for four days followed by 23°C for eleven days. (B) Rosette diameter (cm), and (C) shoot height (cm) at 11 days of recovery. Bars represent mean + standard error, N=5. ANOVA used for differences amongst genotypes (B, $p<0.001$; C, $p=0.638$), and lines within genotypes (B, $p=0.018$; C, $p=0.004$). Bonferroni test used in B for genotype differences, results shown in lowercase letters sorted in descending order.

sld1sld2:*ThSLD2* showed the largest rosettes with an average across its lines of 10.5 cm diameter, compared to 9.9 cm of Col-0 or 9.3 cm on average for *sld1sld2*:*ThSLD1* plants (Figure 5.19 B). Col-0:*ThSLD1* and Col-0:*ThSLD2* showed the slowest recovery rate, with an average rosette sizes of 8.5 and 8.9 cm after 11 days of recovery, however these changes were not significantly different to the wild-type. The shoot height was also measured after the eleven days of recovery under 23°C where at least 80% of the plants throughout all lines showed a developing shoot. No differences were found between genotypes ($p=0.638$), however differences between lines ($p<0.05$) distinguished line #10 of Col-0:*ThSLD2* 16.5 cm from line #6 of *sld1sld2*:*ThSLD2* that showed the lowest shoot height of 8.5 cm (Figure 5.19 C). All other lines showed an intermediate height profile that was not distinguishable from either of these two lines. With the high variability in this dataset, shoot height was not the right indicator for recovery. Overall these results did not show the same trend as previously published, which reported *SLD1* as the predominant gene with an impact in the plant's cold stress resilience. Instead, the results obtained here suggest that *SLD2* might have a role in the plant's ability to recover from stress.

5.3 DISCUSSION

The aims of this chapter were to characterise the extremophile Eutrema *ThSLD* genes in the sphingolipid biosynthetic pathway. To achieve this, two genes, *ThSLD1* and *ThSLD2* sharing 94% and 94.4% of sequence identity with the respective amino acid sequences of the Arabidopsis homologs, were identified. The conserved histidine regions in the fatty acid desaturase domain, preceded by the cytochrome b_5 and transmembrane domains that are characteristic of the membrane-bound desaturase family (Sperling *et al.* 1995, Shanklin and Cahoon 1998, Sperling *et al.* 1998), were also identified. All these factors suggested the correct identification of the Eutrema genes responsible for the addition of a C8 double bond in the LCB chain. The coding sequences were cloned and overexpressed in two Arabidopsis backgrounds for the

characterisation of their function *in vivo*. The ubiquitous expression of either *ThSLD1* or *ThSLD2* in the double mutant for the Arabidopsis endogenous *AtSLD* genes, *sld1sld2*, allowed the investigation of the impact of each gene on the partition of the *cis* to *trans* isomer ratio of the phytosphingenine t18:1, and the consequential impact on the sphingolipid classes production.

The Eutrema genes were also overexpressed in the Arabidopsis wild-type Col-0 background, and the regulation between the endogenous and the transgenes in the sphingolipid profile of these lines was analysed. Three lines from independent transformation events were obtained, to ascertain the reproducibility of the methods and confirmation of the profile for each genotype. Throughout the obtained results, statistical analysis confirmed there were no differences amongst the lines within each genotype, rather establishing significant differences, when present, between the genotypes. The genotypes produced in this project were *sld1sld2*:*ThSLD1*, *sld1sld2*:*ThSLD2*, Col-0:*ThSLD1* and Col-0:*ThSLD2*, which were biochemically analysed together with Col-0 and the double mutants as controls. The transgene expression was also analysed for each of the lines, which confirmed the overexpression in each respective line driven by the CaMV 35S promoter. The expression of the endogenous *AtSLD* genes was not assessed in the wild-type Col-0 nor in the *sld1sld2* background lines. As the T-DNA insertion does not guarantee the disruption of the entire coding sequence, which could have still been translated and hence shown as being expressed. However, the T-DNA can disrupt essential domains for the function of the protein, in which case despite translation it would not be functional. *AtSLD1* had the fatty acid desaturase domain disrupted, whilst in the *AtSLD2* the transmembrane domain was affected. In either case the disrupted domains would affect the functional proteins. The PCR confirmed the presence of the T-DNA in the *sld1sld2* lines, and the biochemical profile determined the efficacy of the T-DNA insertion.

5.3.1 *Conserved SLD1 and SLD2 between Arabidopsis and Eutrema*

The Arabidopsis and Eutrema *SLD* genes shared a sequence identity in their coding sequences of 90.7% for *SLD1* and 83.2% for *SLD2*, which corresponded to the 94.4% and 94.0% of amino acid sequence identity. These results showed a higher sequence similarity between the *SLD1* sequences than for the *SLD2*. *AtSLD1* was previously described as being ubiquitously expressed in the whole plant (Chen *et al.* 2012). Furthermore, in the RNA-Seq analysis performed in Arabidopsis and Eutrema after three days of exposure to cold temperatures of 4°C, *SLD1* was found to be upregulated in both species, with a $\log_2$ fold change of 0.61 ($p<0.001$) and 0.75 ($p<0.01$), respectively (Appendix 3). *SLD2* was not found in the differentially expressed gene (DEG) pool, this was expected as this gene was only found to be expressed in the flowers and siliques of Arabidopsis (Chen *et al.* 2012). Taken together, these results agree with the proposed hypothesis that *SLD1* is the gene responsible for the majority of the LCB Δ^8-desaturase activity. However, the role of the *SLD2* is still not completely understood, as no complementation studies using only this gene have been found.

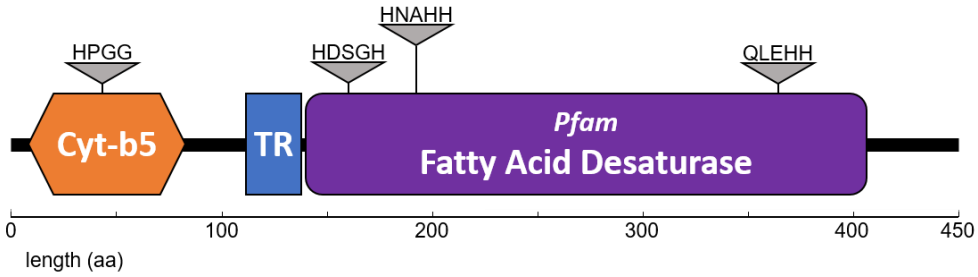

Figure 5.20 SLD Amino Acid Predicted Domains

Amino acid domains for the SLD protein predicted by SMART online software (Letunic and Bork 2018). (■) Cyt-*b*5, cytochrome b_5-like domain; (■) TmR, Transmembrane Region; (■) Pfam: FA Desaturase, Protein family Fatty Acid Desaturase domain. Histidine motifs in domains marked with a triangle (▼). Sequence length of 449 amino acids, scale is shown in the bottom of the picture as amino acid (aa) length.

The Arabidopsis and Eutrema amino acid sequences were shown to be highly conserved and included the distinctive histidine (**H**) motif of the membrane-bound family of desaturases (Sperling *et al.* 1995, Shanklin and Cahoon 1998). In this particular case the motif could be described as **H** $X_{(3)}$ **H** $X_{(32)}$ **H** $X_{(2)}$ **HH** $X_{(172)}$ **Q** $X_{(2)}$ **HH** (Figure 5.20), which included the switch from a histidine to a glutamine (**Q**) residue in the beginning of the third motif (Sperling *et al.* 1995). The histidine motifs were included in the region where the *Pfam* domain fatty acid desaturase was identified by the SMART online software (Figure 5.20) (Letunic and Bork 2018). These motifs were intercalated with the six transmembrane domains in Arabidopsis, and the five in Eutrema sequences. This conforms to the described range of four to six membrane spanning helices in the membrane bound family of desaturases (Shanklin and Cahoon 1998, Sperling *et al.* 2003). The transmembrane domains span the ER membrane and the N-terminal cytochrome b_5-like domain and the three histidine motifs face the lumen of the organelle (Sperling *et al.* 2003). The cytochrome b_5-like domain included in the membrane-bound desaturase active centre bares a functional advantage, as it is the immediate electron donor required for the insertion of the double bond by the desaturase into the fatty acid residues (Sperling *et al.* 1998, Gostincar *et al.* 2010). The cytochrome b_5-like domain is characterised by the **HPGG** motif in which the histidine residue is essential to the electron supply (Sayanova *et al.* 1999, Gostincar *et al.* 2010). In the identified amino acids sequences for SLD1 and SLD2 in both Arabidopsis and Eutrema, this motif was conserved and present in the residues 42 to 45 (Figure 5.20), as identified in the first Δ^8-desaturase report in sunflower (Sperling *et al.* 1995) and later in Arabidopsis and *B. napus* (Sperling *et al.* 1998).

5.3.2 *Is There a Stereospecificity Correlated with Each SLD Gene?*

The singularity of the LCB Δ^8-desaturase as a stereounselective enzyme has been characterised by the analysis of the *cis* to *trans* ratios in different plant species (Imai *et al.* 1997, Sperling *et al.* 1998, Imai *et al.*

2000, Markham *et al.* 2006). However, its underlying molecular mechanism is not yet fully understood. This desaturase can use either t18:0 or d18:0 as substrates, but the phytosphingenine t18:1 has been shown to be the most abundant LCB in plant tissues (Markham *et al.* 2006). The same result was demonstrated here for all the genotypes, except for the double mutant *sld1sld2*. This mutant showed an almost complete ablation of the unsaturated LCB species, concomitantly with an increased d18:0 and t18:0 that did not impact the total content of LCBs, which showed no differences between genotypes. These results confirm the identity of the *SLD* genes as the coding sequences for the LCB Δ^8-desaturase (Chen *et al.* 2012). *ThSLD1* was biochemically confirmed to code for the stereounselective, LCB Δ^8-desaturase as both isomers t18:1$^{\Delta 8Z}$ (*cis*) and t18:1$^{\Delta 8E}$ (*trans*) content were recovered to wild-type range of values in *sld1sld2*:*ThSLD1*. In contrast, *ThSLD2* showed an interesting response when overexpressed in the double mutant, by recovering the *trans* t18:1$^{\Delta 8E}$ isomer to wild-type values, but not the *cis* t18:1$^{\Delta 8Z}$ causing a decrease in the *cis*/*trans* ratio of the genotype *sld1sld2*:*ThSLD2*. In Arabidopsis, *AtSLD2* has been found to have a tissue specific expression, e.g. flower and silique, which would suggest a physiological role of this enzyme. However, the absence of both *AtSLD1* and *AtSLD2* enzymes is not lethal, as the respective single and double mutant *sld1sld2* were able to produce viable flowers and seeds under control conditions without any visible impairment (Chen *et al.* 2012).

Besides the physiological significance of *SLD2*, the results also suggested a relationship between each gene and the stereoselectivity of the resulting desaturase. This was further emphasized by the overexpression of *ThSLD2* in the wild-type Col-0 background. The resulting LCB profile showed an interesting response, with an intermediate profile incorporating a significantly reduced t18:1 *cis*/*trans* ratio when compared to Col-0 and genotypes overexpressing *ThSLD1*, due to a lower *cis* t18:1$^{\Delta 8Z}$ content. However, this ratio was also higher than that observed for *sld1sld2*:*ThSLD2*, indicating a regulation between the products of both *ThSLD1* and *ThSLD2* driven enzymes. The potential

mode of action to produce both isomers proposed by Sperling *et al.* (Sperling *et al.* 2003) suggested a conformational reason, in terms of the geometry and the size of the hydrophobic cavity in the immediate neighbourhood of the di-iron reactive centre. Later, the isomer analysis showed the substrate conformation could be a determinant factor in the resulting stereochemistry of the products, where it was also suggested a likely combination with the shape of the di-iron centre to produce either *cis* or *trans* products (Habel *et al.* 2010). The results presented here suggest also the role of the enzyme in the production of each isomer, with *ThSLD2* showing a preference for the *trans* isomer. As discussed above, both *ThSLD1* and *ThSLD2* showed a conserved cytochrome b_5-like and histidine – motif – containing fatty acid desaturase domains to the previously described Δ^8-desaturases (Sperling *et al.* 1995, Sperling *et al.* 1998, Michaelson *et al.* 2002).

5.3.3 *Expected and Unexpected Changes in Sphingolipid Profile*

As a consequence of the changes in the LCB profile, and according to the literature, specific changes in the sphingolipid profile were expected, as previously demonstrated that the absence of the *SLD* genes leads to a reduction of the glucosylceramide content, resulting in the accumulation of GIPCs (Chen *et al.* 2012). Together with previous characterisation of the specific LCB content in both sphingolipid classes (Sperling *et al.* 2005, Markham *et al.* 2006), it was suggested that the Arabidopsis Δ^8-desaturase *per se* did not directly influence the sphingolipid class content. But, its unsaturated products would be essential for the differential transport of the isomers between the ER and the Golgi compartment, where the IPCS enzymes synthesise the complex forms of GIPC (Chen *et al.* 2012). The results also showed the decreased accumulation of glucosylceramides in the double mutant *sld1sld2*. However, this was reflected in the accumulation of ceramides only instead of GIPCs. The latter also showed a reduction in its total content, together with the hydroxyceramide content. These results

suggest a significant impact of the *SLD* genes in the plant's ability to produce complex sphingolipid classes with the concomitant accumulation of the ceramide pool. The overexpression of *ThSLD1* and *ThSLD2* in the *sld1sld2* background recovered the sphingolipid profile to wild-type values, indicating that the resulting Δ^8-desaturase activity is sufficient to restore complex sphingolipid biosynthesis. The only exception was observed for *sld1sld2*:*ThSLD2* which was not able to fully recover its GIPC content, possibly indicating the need for a balanced *cis* to *trans* ratio homeostasis in the ER for the correct partitioning, and perhaps transport of the isomers to the Golgi for GIPC biosynthesis.

When overexpressed in the Col-0 background, both genes showed a higher accumulation of ceramides and hydroxyceramides with no differences found in the GIPCs or glucosylceramides, and the highest accumulation registered by *ThSLD2*. These results could suggest an increased desaturation of the LCB d18:0 and t18:0 substrates that would impact the assimilation rate into the complex glucosylceramides, or even the respective transport to the Golgi compartment? Potential measurement errors could also have been a possibility, as the complex glycosylated structure of the GIPCs makes their extraction difficult when using common organic solvents such as chloroform/methanol (Sperling and Heinz 2003, Markham *et al.* 2006). However, the extraction and analysis protocols used here followed methods previously developed that allowed an efficient extraction (Markham 2013). Li *et al.* showed a relationship between the accumulation of hydroxyceramides to the increased susceptibility to oxidative stress (Li *et al.* 2015). A possibility that could be tested using the genotypes Col-0:*ThSLD1* and Col-0:*ThSLD2*, since they accumulated a significant amount of hydroxyceramides compared to the wild-type, and perhaps a new physiological role for the *SLD* genes.

5.3.4 *The SLD impact in the Cold Stress and Recovery*

The hypothesis that the LCB Δ^8-desaturation has an impact on the plant's response to cold stress was tested (Figure 5.21), as previous

characterisation of the Arabidopsis *AtSLD1* and *AtSLD2* genes showed the ablation of both genes would comprise the plant's survival to long-term exposure to freezing (0°C) temperatures (Chen *et al.* 2012). Furthermore, in Arabidopsis seedlings, 1h exposure to 4°C sufficed to reduce the total content of the LCB pool, mainly influenced by the reduction of t18:1 content up to 53% (Guillas *et al.* 2013). Here, the SLD genotypes were firstly exposed to eight days at 4°C, after which no visible changes in the morphology were detected in any of the genotypes. These conditions had however been previously tested in Chapter 3 which detrimental effects in the plant's health allowed the identification of two genes with a proposed role in the plant's cold acclimation. Furthermore, an impact of the cold stress was observed in the acyl-CoA pool of the SLD genotypes. A general decrease in the VLCFA molecular species was concomitant with the accumulation of 16:0, the highest being found in *sld1sld2*:*ThSLD2* (Figure 5.18, Section 5.2.12). The acyl-CoA pool is a key element in the biosynthetic pathway of the sphingolipids as a source of acyl substrates [(Zheng *et al.* 2005); further reviewed in Chapter 1]. Thus, the profile observed in the sphingolipid profile of the transgenic lines might have affected the regulation of the acyl-CoA pool, which was also shown to be perturbed by cold stress.

Sphingolipids are a major component of the plasma membrane (Mamode Cassim *et al.* 2019), which is one of the first lines of defence against freezing stress (Steponkus 1984). Freezing damage to the membranes can lead to leakiness caused by the formation of extracellular ice (Uemura *et al.* 1995). The correlation between sphingolipids and the plants' adaptive strategies to cold stress has been previously demonstrated and are thought to be related of the desaturation level of the LCB moiety of complex sphingolipids (Lynch and Steponkus 1987, Yoshida *et al.* 1988). Imai *et al.* showed a variety of chilling-resistant plants to have an increased t18:1 *cis* isomer, relative to what was found in the chilling-sensitive plants (Imai *et al.* 1997), further confirmed in different freezing-resistant grapevine varieties (Kawaguchi *et al.* 2000). The freezing sensitivity of the SLD genotypes was tested here, revealing

sld1sld2:*ThSLD2* with a higher post-stress recovery rate. As discussed, the genotypes produced showed different levels of LCB desaturation. *ThSLD2* in particular, showed a reduced t18:1 *cis/trans* ratio, with a preference to produce t18:1$^{\Delta 8}$ *trans* isomer, with an impact in the accumulation of GIPCs. Despite the published evidence that relates the different ratios of the t18:1$^{\Delta 8}$ isomers with the plants ability to withstand freezing stress, the detailed mechanism in which this ratio intervenes is still unknown. The ablation of both *SLD* genes in Arabidopsis does not produce a lethal phenotype, even when exposed to freezing stress. Conceivably allowing the extrapolation that the t18:1$^{\Delta 8}$ *cis*/*trans* ratio per se might not directly influence the plant's chances of survival but rather as a result of the partitioning of the LCB moiety to the different sphingolipid classes. Further study into this relationship is necessary, for which the extremophile Eutrema could be of further assistance, e.g. disruption of the *ThSLD1* and *ThSLD2* sequences using techniques such as CRISPR/Cas9 that would allow precise changes in the enzymes structure and regulation.

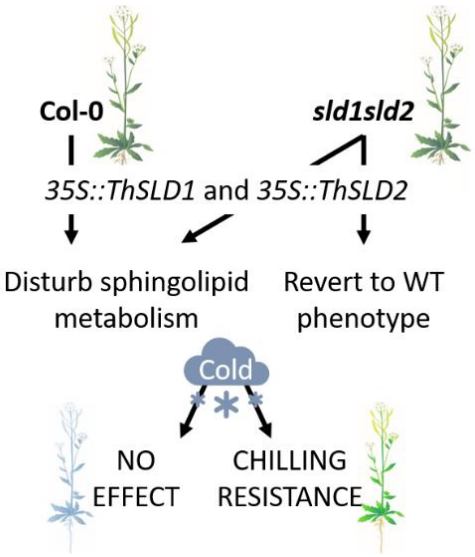

Figure 5.21 Expected Results for the SLD Overexpressing Lines

Schematic representation of the expected results from overexpressing *ThSLD1* and *ThSLD2* in two Arabidopsis backgrounds, Col-0 and *sld1sld2*. *35S:ThSLD1* and *35S:ThSLD2* represent the vector using the Cauliflower Mosaic Virus 35S promoter (35S) to drive the expression of the *SLD* genes.

5.4 CONCLUSION

The Eutrema stereounselective sphingoid LCB Δ^8-desaturase genes, *ThSLD1* and *ThSLD2* were here identified and characterised. Both Eutrema genes showed the characteristic cytochrome b_5-like domain in the N-terminal region of the sequence, and the three highly conserved histidine motifs characteristic of the membrane-bound desaturase family, intercalated with five hydrophobic regions interpreted as the transmembrane domains. The biochemical profile of each gene, when expressed in two Arabidopsis backgrounds, was also characterised. By overexpressing each coding sequence in the double mutant *sld1sld2*, it was demonstrated that *ThSLD2* has capacity to produce *trans* t18:1$^{\Delta 8E}$ isomer, but not the *cis* form. Such observation reinstated the discussion around the role of the conformation of the catalytic cavity of the Δ^8-desaturase in the production of the isomers. Whereas *ThSLD1*, as with *AtSLD1*, revealed to fully recover the LCB *cis*/*trans* ratio. Such differences in the LCB profile translated in the incomplete recovery of the GIPC sphingolipid profile in *sld1sld2*:*ThSLD2*. When each of these genes were overexpressed in the wild-type Col-0 background, the same shift in the t18:1 *cis*/*trans* ratio was observed, which corresponded to a significant accumulation of ceramides and hydroxyceramides with a higher content associated with *ThSLD2*. Finally, the genotypes were tested under cold and freezing stress conditions to assess the role of each gene and of the LCB Δ^8-desaturation in the plant's ability to cope with stress. The short-term stresses applied did not allow for any differences to emerge. However, when the post-freezing recovery rate was analysed, the double mutant complemented with *ThSLD2* showed a potential role in the recovery capacity of the plants.

Chapter 6.
Contribution of the Chloroplastidial Fatty Acid Desaturases to *Eutrema salsugineum* Cold Adaptation

6.1 INTRODUCTION

Extremophile plants are excellent models for unravelling the strategies that plants use to endure stress conditions. As introduced in Chapter 1 (Section 1.1), Eutrema is known for its resilience to low temperatures, capable of surviving temperatures of -26°C in the most extreme habitat conditions of the Yakutsk accession (Lee *et al.* 2012), high salinity where 250 mM sodium chloride (NaCl) is considered a moderate stress (Gong *et al.* 2005), or repeated drought treatments (MacLeod *et al.* 2015). The similarity level between genomes of Eutrema and Arabidopsis allow a direct comparison between genes and their function (Bressan *et al.* 2001, Wang *et al.* 2004, Wong *et al.* 2005). Plant survival strategies in adverse environments are complex, involving a multitude of molecular, metabolic and physiological adaptations, as studied in Eutrema [(Wong *et al.* 2006, Gao *et al.* 2009, Benina *et al.* 2013, Khanal *et al.* 2015, Khanal *et al.* 2017, Tang *et al.* 2018), further reviewed in Chapter 1]. In a proteomic study of cold stress tolerance in the Shandong ecotype, Gao *et al*. (2009) showed that the largest changes with cold adaptation were related to photosynthesis, defence and stress-related proteins (Gao *et al.* 2009). Interestingly, these were all predicted to be localised in the chloroplast suggesting a major role for this organelle in Eutrema's adaptation to low temperatures. Other reports also suggest Eutrema has the capacity to mitigate the effects of photoinhibition with a photosystem that rapidly and efficiently responds to abiotic stress, by downregulating photosynthesis-related genes that represent 15% of the total down-regulated transcripts (Wong *et al.* 2006, Wang *et al.* 2017). Moreover, a categorisation of Eutrema's genes using gene ontology identified 17.6% of the products to be associated with the chloroplast (Wong *et al.* 2005). The same study showed that from the identified genes, 37.5% were cold-related, while only 22.5% and 24.4% related to salinity or drought stresses (Wong *et al.* 2005), indicating an unexplored pool of information on how the plant copes with cold stress.

6.1.1 *Chloroplast Fatty Acid Desaturases*

Cold acclimation involves an increased content of membrane polyunsaturated fatty acids, such as trienoic acids in the membranes (Sakamoto and Murata 2002). Several examples described in the literature show the relationship between cold acclimation and the degree of fatty acid unsaturation (Kodama *et al.* 1994, Roman *et al.* 2012, Roman *et al.* 2015). In Arabidopsis, the reported rise in basal fluorescence with temperature is strongly correlated with the fluidity of thylakoid membranes [(Tovuu *et al.* 2013), and discussed in Chapter 3]. In plants, the FAD family, responsible for the unsaturation of fatty acids by conversion of single to double bonds, is extensive (Shanklin and Cahoon 1998). As the active site of photosynthesis, plastid membranes have an active role in the plant's adaptation to cold stress (Fernie 2019, Holzl and Dormann 2019, Koochak *et al.* 2019). In this organelle two FADs are responsible for the production of trienoic fatty acids with a described impact on cold stress. Both FAD7 and FAD8 are ω-3 fatty acid desaturases, with a third FAD3 localised in the ER (Browse *et al.* 1985, Browse *et al.* 1986, Miquel *et al.* 1993, Mcconn *et al.* 1994, McConn and Browse 1996, Shah *et al.* 1997). In Arabidopsis, *AtFAD7* and *AtFAD8* genes have been identified and the mutants characterized as temperature sensitive ω-3 desaturases located in the chloroplastidial membrane (Browse *et al.* 1985, Browse *et al.* 1986, Gibson *et al.* 1994, Mcconn *et al.* 1994). *AtFAD7* (At3g11170) was first identified by screening leaf fatty acid content in a ethyl methanesulfonate (EMS) mutagenized population using direct gas chromatography (GC) (Browse *et al.* 1985). The decreased values of 16:3 and 18:3 fatty acid levels, compensated by the increase in the 16:2 and 18:2 precursors in the mutant, led to the identification of this enzyme (Browse *et al.* 1986). *AtFAD8* (At5g05580) was identified a few years later by EMS mutation on the *fad7-1* background, which accentuated the decrease in the trienoic FAs compared to the single mutant *fad7-1* and a corresponding increase in the 16:2 and 18:2 FAs (Gibson *et al.* 1994, Mcconn *et al.* 1994). There is a third, ER localized, ω-3 desaturase *FAD3* in Arabidopsis (Browse *et*

al. 1993, Shah *et al.* 1997). However, the triple mutant *fad3fad7fad8* in Arabidopsis was shown to be male sterile, a phenotype that can be reversed by the application of jasmonic acid (McConn and Browse 1996). The relationship between trienoic fatty acid content and cold acclimation has been further investigated in Arabidopsis (Routaboul *et al.* 2000, Shi *et al.* 2011, Routaboul *et al.* 2012), and other species e.g. tomato (Dominguez *et al.* 2010) and rice (Tovuu *et al.* 2016). Reports of a transgenic tobacco overexpressing *FAD7* significantly increased its trienoic acid content e.g., 16:3 and 18:3, which translated into higher leaf area and no symptoms of leaf chlorosis under cold conditions (Kodama *et al.* 1994). The absence of *FAD8* in the rice mutant *osfad8* caused growth impairment and decreased fluidity in the thylakoid membranes, resulting in higher susceptibility to photoinhibition during cold acclimation (Tovuu *et al.* 2016). Despite its status as an abiotic stress model plant, no studies were yet published relating Eutrema's response to cold acclimation with a modification of trienoic fatty acid profile. This relationship would be of interest, not only for the study of the functional characteristics of these enzymes in an extremophile context, but to further explore the apparent relationship between Eutrema chloroplast regulation and its improved performance under low temperature stress.

6.1.2 *The Advantage of Genome Editing Technologies*

Genome editing technologies allow for precise editing creating specific targeted mutations which lead to key functional changes. Zinc finger nucleases (ZFN) and Transcriptor Activator-Like Effector Nucleases (TALENs) are powerful tools for targeted gene editing, together with the recently developed Clustered Regulatory Interspaced Short Palindromic Repeats technique with the associated protein 9 (CRISPR/Cas9; Figure 6.1). ZFN are chimeric proteins composed of DNA-binding motifs fused to an endonuclease domain, the restriction enzyme *FokI* (Kim *et al.* 1996). This complex guides the cleavage of specific DNA sequences creating double-strand breaks (DSB), which are then subjected to the cell's repair systems leading to localised mutagenesis events (Kim *et al.*

2005, Kim and Kang 2006, Qi *et al.* 2013). Like ZFN, TALENs comprise a target sequence-specific DNA-binding domains derived from TALE proteins fused to *FokI*, originating targeted DSBs (Gaj *et al.* 2013). CRISPR *loci* are variable short spacers separated by short repeats, which are transcribed and processed into short non-coding RNAs (Belhaj *et al.* 2015). These short RNAs can form a functional complex with Cas proteins and guide the complex to cleave complementary DNA producing DSB (Hsu *et al.* 2013, Belhaj *et al.* 2015, Liu *et al.* 2015). This system was originally found in bacteria and archaea as an integrated part of their immune system (Bhaya *et al.* 2011), and type II CRISPR/Cas system derived from *Streptococcus pyogenes* (SpCas9) is the most widely used for gene editing (Jinek *et al.* 2012, Cong *et al.* 2013, Gaj *et al.* 2013). The Cas proteins require a protospacer adjacent motif (PAM) for DNA target recognition, with the SpCas9 recognizing a 5'-*NGG* PAM of two guanine bp (N represents any of the four bp) (Jinek *et al.* 2012, Belhaj *et al.* 2015). The development of a single guide RNA (gRNA), that incorporates the 20-nucleotide target sequence with the PAM sequence increased the simplicity of this technique (Jinek *et al.* 2012). After cleavage, DSBs are repaired through the cell's own DNA repair systems, commonly by non-homologous end-joining (NHEJ) or homologous recombination (HR). The most common repair system in plants is the NHEJ which can produce small insertional or deletion mutations (indels) often inducing frameshift mutations (Kim and Kim 2014). This error-prone characteristic is advantageous, and its application is suitable for the production of loss-of-function targeted mutations.

Genome editing provides a series of advantages when compared to other methods of traditional breeding. EMS mutant lines can have undetermined background mutations (Sega 1984, Kim *et al.* 2006), or T-DNA insertions that can occur at random sites, completely disrupting gene expression (Thorneycroft *et al.* 2001). Post-transcriptional gene silencing is limited as variable gene silencing can occur without a possible control, or the unstable expression depending on the promoter used and tissue (Bourque 1995, Thorneycroft *et al.* 2001). An alternative

is the use of RNAi, where RNA molecules inhibit or knockdown gene expression (McManus and Sharp 2002), this can have unpredictable non-targeted effects and low reproducibility (Gaj *et al.* 2013). Comparatively, ZFN and TALEN require the design and generation of a new nuclease pair for every genomic target, whilst in CRISPR/Cas9 the only variable component is the short 20-nucleotide target-specific portion of the gRNA, that can be easily adapted (Gaj *et al.* 2013). Thus, allowing a multiplex approach, which can be achieved by producing up to 20 gRNAs that can be expressed by a single scaffold (Ma *et al.* 2015, Xie *et al.* 2015). Thus, this technique is one of the most scalable genome editing technologies available, which is demonstrated by the quantity of published work in such widespread research areas from human (Chen *et al.* 2013), to the model plant Arabidopsis (Li *et al.* 2013, Li *et al.* 2014, Yan *et al.* 2015), and crops such as tomato (Cermak *et al.* 2015) or wheat (Shan *et al.* 2014, Zhang *et al.* 2019). Other advantages include precision due to the low rate of off-target mutations, speed by avoiding lengthy crosses, or the possibility of multiplexing by targeting few selected genes simultaneously. Furthermore, once the homozygous mutated generation is obtained, progressive segregation analysis can be used to remove the Cas9 containing vector, facilitating the production of “transgenic free” lines without the integration of exogenous DNA (Hahn *et al.* 2017, Danilo *et al.* 2019).

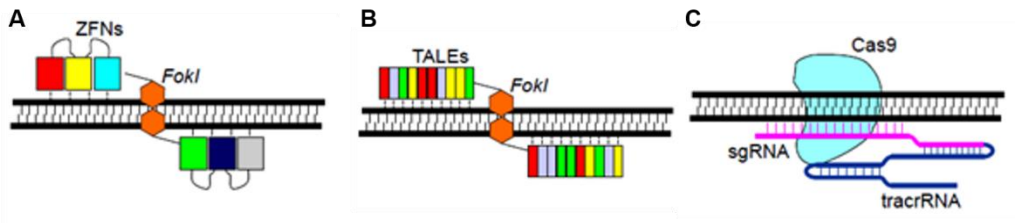

Figure 6.1 Comparison between ZFN, TALEN and CRISPR Systems

(A) Zinc finger nucleases (ZFN), (B) Transcriptor Activator-Like Effector Nucleases (TALENs), and (C) Clustered Regulatory Interspaced Short Palindromic Repeats technique with the associated protein 9 (CRISPR/Cas9) systems for gene editing. Adapted from ProteinTech® Group (https://tinyurl.com/y54q4kfr).

6.1.3 *Chapter Aims*

This experiment aimed to characterise chloroplastidial fatty acid desaturases, FAD7 and FAD8, in the extremophile background of Eutrema ecotype Shandong. These enzymes have an established role in the cold stress response of Arabidopsis and other economically interesting crops, e.g. tomato and rice. Furthermore, chloroplasts have a crucial role in the cold acclimation process of Eutrema. To investigate the role of FAD7 and FAD8 in Eutrema, mutant lines were created using the genome editing technique CRISPR/Cas9, and thereby determinate the importance of trienoic fatty acid desaturation in the extremophile adaptation to cold. The workflow designed to achieve the proposed aims for this chapter is shown in Figure 6.2. Therefore, efficient germination and transformation protocols were firstly developed. This was important as an efficient transformation technique is required for the CRISPR/Cas9 system. The genomic sequences for *ThFAD7* and *ThFAD8* were identified in Eutrema, based on the respective Arabidopsis amino acid sequences, and a multiplex approach was designed using four specific gRNAs to target the two genes. The design of the gRNA sequences included consideration of off-target events, mismatch possibilities, the out-of-frame score and sequence identity to other genes in Eutrema. The vector was obtained, cloned using the Gateway protocol, delivered by *Agrobacterium*-mediated floral dip (Clough and Bent 1998), and six candidates for edited lines identified in the T1 population.

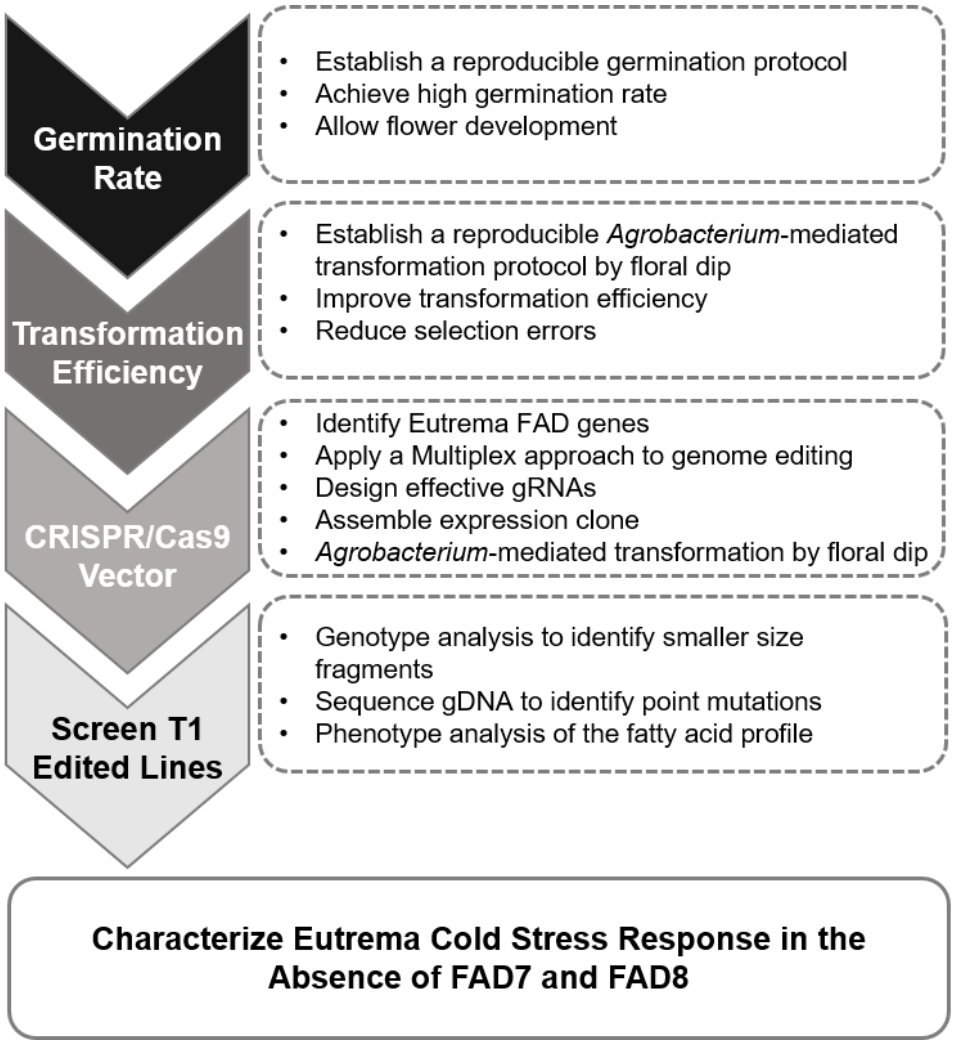

Figure 6.2 Workflow for Editing the Genome of Eutrema

The figure shows the workflow planned to achieve the aims proposed for this chapter.

6.2 RESULTS

6.2.1 *Efficient Germination Achieved by Direct Sow*

Germination and transformation protocols are publicly available for Eutrema [http://thellungiella.org/protocols.htm, (Clough and Bent 1998, Li *et al.* 2007)], nonetheless it was important to demonstrate the efficiency, adapt such protocols to the lab conditions available and establish replicable protocols. Anecdotal evidence (pers. comm. Prof. Christoph Benning, MSU-DOE Plant Research Laboratory) from groups working with Eutrema identified antibiotic selection as a challenge in the

generation of transgenic lines. To this end, three germination protocols were tested with stratification periods that varied from one to three weeks at 4ºC and darkness. A seed sterilisation method adapted from Arabidopsis was used (detailed in Section 2.2.1.2), where seeds were firstly sterilised with ethanol, and placed in sterilised growth medium. For the two other methods the seeds were sown directly in soil, with or without a previous sandpaper treatment as a mechanical scarification step. The wild-type Arabidopsis Columbia (Col-0) ecotype seeds were used as a germination control, and the number of seeds with radicle protrusion or leaf development was used as a scoring method to analyse germination rate. The seed sterilization protocol was proven to be more efficient for Arabidopsis with a germination rate higher than 90% with either stratification period, while only 10% of the sterilised Eutrema seeds germinated after three weeks of stratification (Figure 6.3). One week of stratification was tested for all three protocols, however no Eutrema seed germinated under this period with any protocol. Figure 6.3 panel A shows the result of one week of stratification for sterilised Eutrema seeds when compared to Arabidopsis, the results for the other methods after only one week of stratification are not shown. The direct sow method proved to be more effective for the germination of Eutrema after three weeks of stratification (Figure 6.3 C-E). Mechanical scarification using sandpaper was shown to be more efficient reaching 85%, as it would be expected to break the outer seed coat triggering germination (Li *et al.* 2015). The Arabidopsis seeds, however, responded better without the scarification pre-treatment, but still achieved higher germination rates than Eutrema under the same conditions (Figure 6.3 D-E). As the results suggest, direct sowing of Eutrema seeds was the most efficient protocol, and whenever possible with the application of a scarification pre-treatment to enhance this effect.

The existing transformation protocols for Eutrema use *Agrobacterium tumefaciens*-mediated transformation, the floral dip method (Clough and Bent 1998), or leaf explants (Li *et al.* 2007) as delivery methods. However, as the genome editing CRISPR/ Cas9 method required a

transformable species (Bortesi and Fischer 2015), the importance of developing a reproducible protocol arose. To test the *Agrobacterium tumefaciens*-mediated transformation method and assess its efficiency, the transformation protocol developed in Chapter 5 for Arabidopsis was firstly used and applied to Eutrema flowering plants (Section 2.3). The expression clones containing the Eutrema *SLD* genes (*ThSLD1* and *ThSLD2*) under the transcription regulation of the constitutive CaMV 35S promoter (35S), and the DsRED fluorescence gene as a selection marker (Matz *et al.* 1999, Jach *et al.* 2001). Eutrema flowers for a long period (eight–ten weeks), continuing to develop fresh floral structures, therefore a protocol was designed with three repetitive flower dip events, with the first flower dip applied when the flower buds started to develop in at least 50% of the plants in each pot (Figure 6.4 A). The flowering times varied between ten to thirty days after the seedlings were sown. The three repetitive flower dip events were included to account for the long flowering periods shown by Eutrema and were applied twelve to sixteen days apart depending on the plant's health state. This was monitored by visible signs of stress, such as yellow or withered leaves and flower or silique abortion. However, no such symptoms were found and even after the three floral dips plants were still flowering and setting seed (Figure 6.4 C). The number of independent transformation events corresponded to the number of pots, each of these containing nine plants, so for the *ThSLD1* expression clone, nine transformations events (nine pots) were used, while for the *ThSLD2* clone there were eight.

Due to the long flowering periods of Eutrema, there was a gradient of seed maturation of the transformed plants, which started to be collected one month after the last floral dip and continued for a further three weeks. Once collected and examined with a light microscope, T1 seeds were identified as DsRED positive marking for the presence of the transgene, thus showing that the *Agrobacterium*-mediated transformation by flower dip was successful. Its efficiency however, was low with only five transformation events showing DsRED positive seeds for the *ThSLD1* clone, and six (out of eight) transformation events for *ThSLD2*. The

number of transformed DsRED positive seeds was also low, ranging between one and four seeds per transformation event. This experiment was repeated, with no improvement in the amount of seeds transformed. Despite the low efficiency obtained, Eutrema was successfully transformed, and the use of DsRED as a selection marker was proven. This is of significance as the stress resilience and waxy leaves (Teusink *et al.* 2002, Tang *et al.* 2018) characteristic of this species could interfere with the application of herbicides as a selective marker, potentially allowing for false positives.

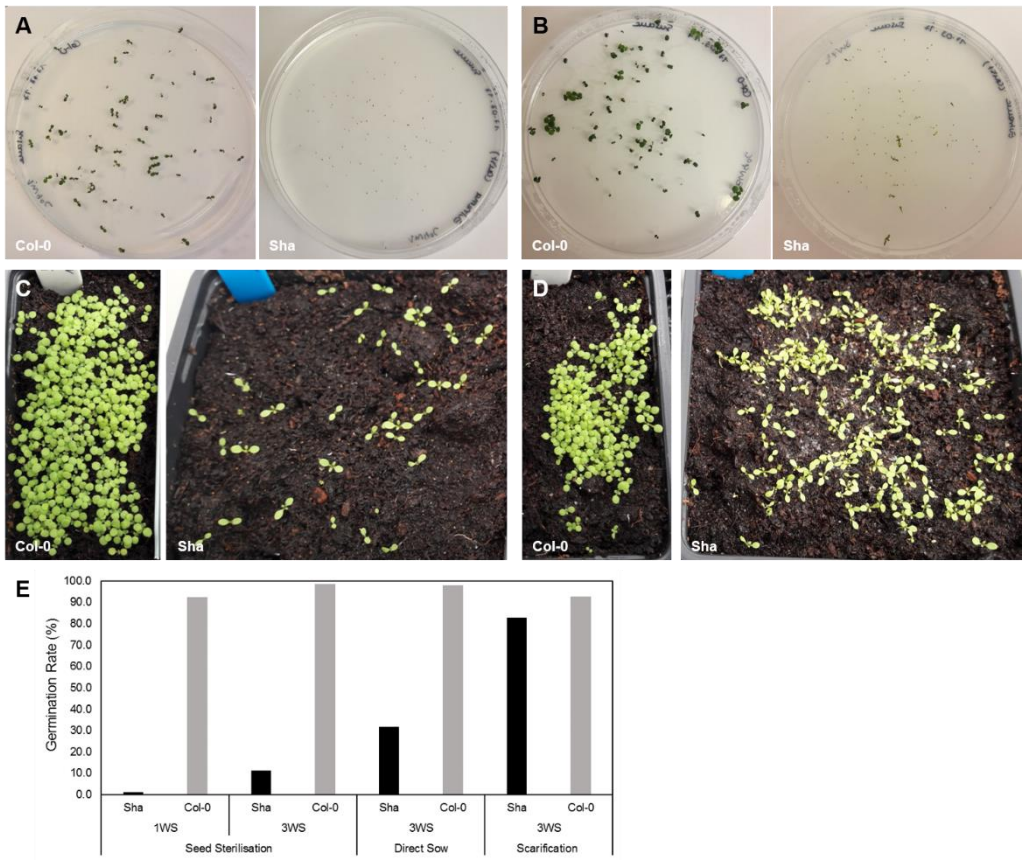

Figure 6.3 Germination Efficiency of Eutrema salsugineum

Germination efficiency for the different protocols, seed sterilisation with one (A) and three (B) weeks of stratification; direct sow without (C) and with mechanical scarification (D), both after three weeks of stratification. (E) Graphical representation of the germination rate for each protocol, stratification period and ecotype. Col-0, *Arabidopsis thaliana* ecotype Columbia; Sha, *Eutrema salsugineum* ecotype Shandong; 1WS, one week of stratification; 3WS, three weeks of stratification.

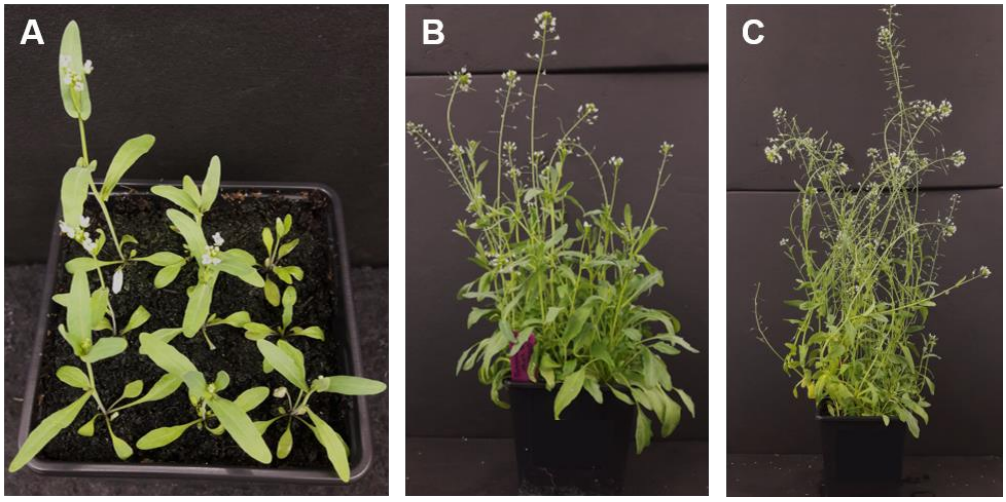

Figure 6.4 Eutrema Plants during Transformation

The Eutrema plants used to test the *Agrobacterium*-mediated floral dip transformation protocol showing the plant's developmental stage when the first (A), second (B) and third (C) floral dip events were applied. One pot per independent transformation event was used, each pot (9x9 cm) contained nine plants sown at the same time.

6.2.2 *Identification of Eutrema FATTY ACID DESATURASE*

The Eutrema FAD7 and FAD8 sequences were identified based on the amino acid sequence of the respective Arabidopsis homologs *AtFAD7* (At3g11170) and *AtFAD8* (At5g05580) in the online database *Phytozome 12*. The respective entries were identified as Thhalv10020755m.g and Thhalv10013625m.g by sharing a protein sequence similarity of 92.4% and 93.0% with the AtFAD7 and AtFAD8, respectively, and henceforth referred to as *ThFAD7* and *ThFAD8*. The detailed alignment of the amino acid SLD sequences between the two species was performed with MUSCLE 3.8 [(Madeira *et al.* 2019), Figure 6.5]. Domain search (Letunic and Bork 2018) identified the fatty acid desaturase domains for each sequence (Figure 6.5). *ThFAD7* was identified as an ω-3 fatty acid desaturase, a chloroplast desaturase, in the NCBI database (LOC18023475, EUTSA_v10020755mg), and *ThFAD8* was identified as a temperature-sensitive sn-2 acyl-lipid ω-3 chloroplast desaturase (LOC18018373, EUTSA_v10013625mg). The three fatty acid desaturase characteristic histidine regions [reviewed in Chapter 5 (Sperling *et al.* 1995, Shanklin and Cahoon 1998)] were also identified (Figure 6.5).

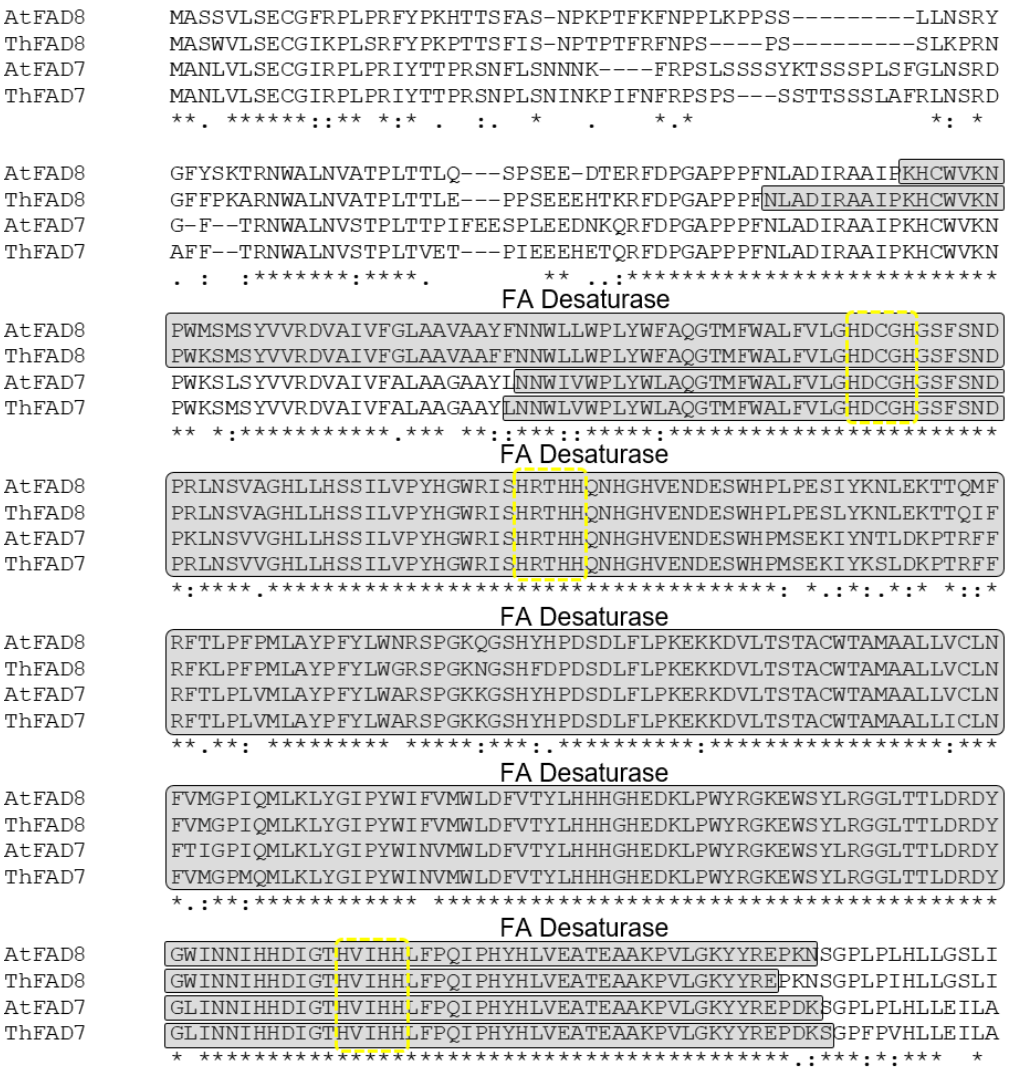

Figure 6.5 Multiple Sequence Alignment for the FAD genes

FAD8 and FAD7 amino acid sequence alignment for Arabidopsis (At) and Eutrema (Th) by CLUSTAL multiple sequence alignment (MUSCLE 3.8, (Madeira *et al.* 2019)). ***** (asterisk) single, fully conserved residue; weak "**.**" (period) or strong "**:**" (colon) conservation between groups (score ≤0.5 and >0.5, respectively, Gonnet PAM 250 matrix). Histidine conserved regions marked in yellow (■). Domain prediction by SMART software (Letunic and Bork 2018). FA Desaturase, Fatty Acid Desaturase domain.

These were localised within the desaturase domain with the sequences HDCGH, HRTHH, and HVIHH. These regions were shown to be conserved between both Arabidopsis and Eutrema FAD7 and FAD8 sequences (Figure 6.5). Furthermore, the UniProt database identified *ThFAD7* as V4NQN1_EUTSA, while *ThFAD8* was identified as

V4KR96_EUTSA with both entries described as *unreviewed*. No published evidence was found on the function of the two Eutrema genes, as described for the ω-3 desaturases FAD7 and FAD8 in Arabidopsis (Browse *et al.* 1985, Browse *et al.* 1986, Browse *et al.* 1993, Miquel *et al.* 1993, Yadav *et al.* 1993).

Both *ThFAD7* and *ThFAD8* were characterised by eight exons and seven intron regions (Figure 6.7), encoding peptide sequences of 438 and 428 amino acids, respectively. However, the two genes share only 65.5% of similarity in the genomic DNA (gDNA) sequences (Figure 6.5). According to the UniProt database, the first 132 amino acid residues for *ThFAD7* and the first 123 residues of *ThFAD8* were identified as domains of unknown function, followed by the respective FAD domain in the residues 140 to 394 for *ThFAD7* and 131 to 385 of *ThFAD8*. The first domain amino acid sequences were used to identify a potential subcellular location domain with the aid of the online tool TargetP 1.1 Server (Emanuelsson *et al.* 2007). In both cases, the domains were predicted as a chloroplast transit peptide with a reliability class (RC) calculated of two for *ThFAD7* and one for *ThFAD8*, where one is the highest in a scale from one to five (Table 6.1). The RC is a measure of the size of the difference between the highest and the second highest output scores, where one corresponds to a difference higher than 0.800 and two a difference between 0.800 and 0.600 (Emanuelsson *et al.* 2000, Emanuelsson *et al.* 2007).

Table 6.1 Prediction for Targeting Peptide

The results from the TargetP 1.1 Server for the prediction of the first domain sequence for *ThFAD7* (V4NQN1) amino acid residues 1 – 132, and *ThFAD8* (V4KR96) residues 1-123. cTP, chloroplast Transit Peptide; mTP, mitochondrial Targeting Peptide; SP, Signal Peptide; RC, Reliability Class.

Gene	Name	Sequence Length	cTP	mTP	SP	other	Localisation	RC
ThFAD7	Tr_V4NQN1_1-132	132	0.891	0.126	0.002	0.031	Chloroplast	2
ThFAD8	Tr_V4KR96_1-123	123	0.939	0.032	0.011	0.081	Chloroplast	1

6.2.3 *Eutrema Showed a Higher Fatty Acid Ratio of 16:1/16:2 Than Arabidopsis*

Shandong (Sha) fatty acid profile was analysed against Arabidopsis wild-type Col-0 to assess the wild-type phenotype of the extremophile. Furthermore, the Arabidopsis double mutant for *AtFAD7* and *AtFAD8, fad7-1fad8* was obtained and, after confirmed to be homozygous (Appendix 22), the fatty acid profile analysed as a reference for the eventually produced Eutrema CRISPR mutant lines. The total Sha fatty acid content did not show any differences from the Arabidopsis wild-type (Figure 6.6 A), however it showed a higher ratio of 16:2/16:3 showing an opposite trend to Col-0 by producing 16:2 in detriment of 16:3 (Figure 6.6 B).The ratio of 18:2/18:3 in Sha was lower than Col-0 (Figure 6.6 C).

The Arabidopsis double mutant *fad7fad8* was previously originated from the cross of the two EMS single mutants *fad7* and *fad8*, and obtained from the European Arabidopsis Stock Centre (NASC) The double mutant *fad7fad8* was confirmed to be homozygous by gDNA sequencing, which confirmed the point mutation of a guanine (G) to an adenine (A) on the amino acid 141 of the FAD7 protein, and on the amino acid residue 149 of FAD8 (Appendix 22). This substitution mutation replaced a tryptophan (W) residue for a STOP codon, which terminates the protein before the first histidine box essential for the desaturase function (Shanklin *et al.* 1994, Shanklin and Cahoon 1998). The fatty acid profile for the double mutant showed no production of the trienoic 16-carbon fatty acid (Figure 6.6 A-B). Whilst, the increased production of 18:2 combined with a 78% reduction in the 18:3, when compared to both Sha and Col-0, reflected a nine-fold increase of the 18:2/18:3 ratio (Figure 6.6 C). These results are in accordance with the published data for the same SALK lines published by Roman *et al.* (Roman *et al.* 2015). Additionally, as the profiles for Eutrema and Arabidopsis *fad7fad8* were established, the profiling of the fatty acid content of the T1 CRISPR lines could be applied as an effective and rapid screen for the identification of edited lines.

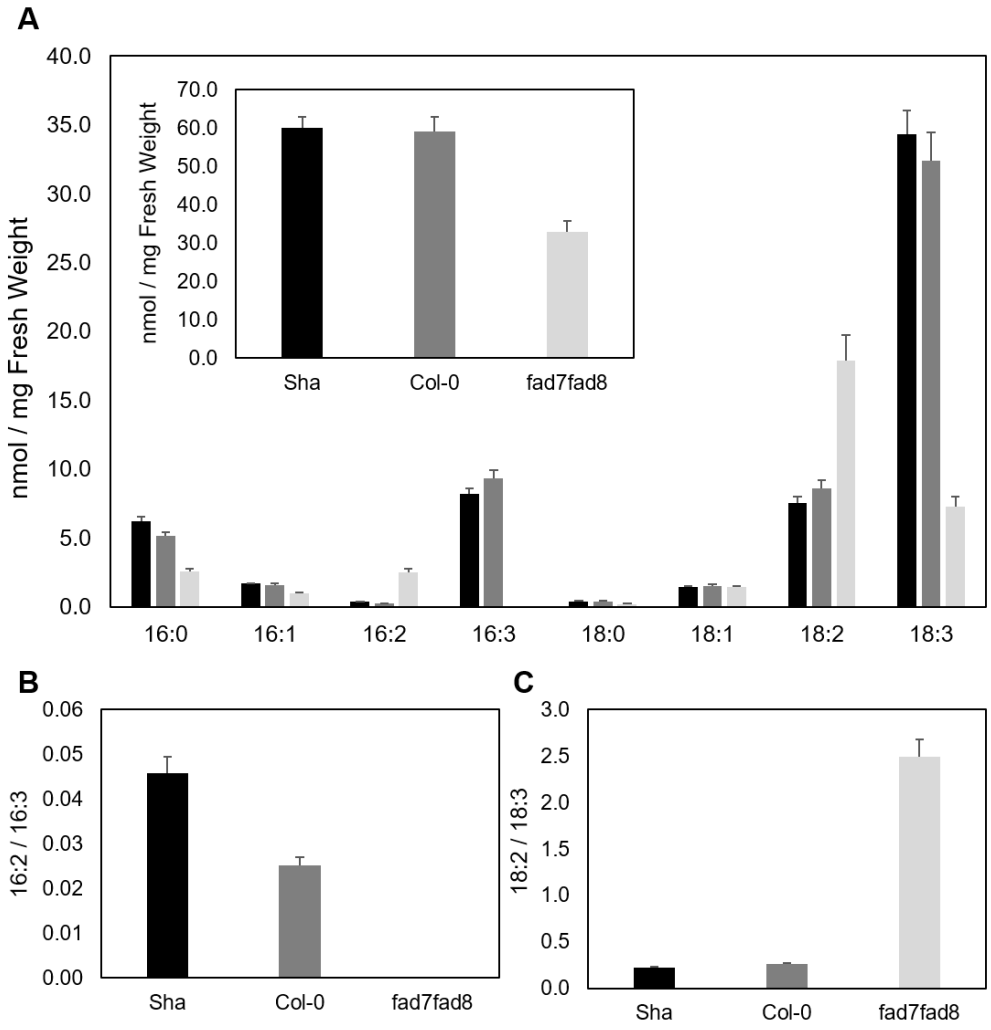

Figure 6.6 Fatty Acid Profile for Eutrema and Arabidopsis

Fatty acid profile measured for Eutrema wild-type Sha (■), Arabidopsis wild-type Col-0 (■) and double mutant for *AtFAD7* and *At FAD8* genes *fad7fad8* (■). (A) Quantification of fatty acid methyl esters (FAMEs) of each molecular species represented as number of carbons:double bonds, the insert shows the total content. Ratios of 16:2 to 16:3 (B), and 18:2 to 18:3 (C) content in the three genotypes. Average + standard error is shown, N_{Sha}=9, N_{Col-0}=5, $N_{fad7fad8}$=5. FAMEs were analysed in two-weeks old rosette leaves grown under control 23°C (further details in Sections 2.2.3 - 2.2.4).

6.2.4 *A Multiplex Approach was Used for the Genome Editing*

The design of the gRNA followed a multiplex genome editing approach (Ma *et al.* 2015), where four gRNAs were designed to target the two genes *ThFAD7* and *ThFAD8* aiming to increase the probability and the size of deletion. Two conserved gRNAs were designed to target the conserved regions of *ThFAD7* and *ThFAD8* in exon 1 (gRNA1) and exon

7 (gRNA2), while two unique gRNAs were designed to target exon 1 of *ThFAD7* (gRNA3) and exon 1 of *ThFAD8* (gRNA4) (Figure 6.7). Geneious® software was used to find all potential gRNA sequences for both genes, which were firstly analysed according to their position where a target region within an exon, especially the first exon, was prioritised. For the conserved regions, five possibilities for the first exon and one for exon seven of both *ThFAD7* and *ThFAD8* were considered. This reduced number of possible gRNAs was due to the low (65.5 %) sequence identity between the nucleotide sequences, gRNAs were only selected if they showed a complete match in the respective 20 nucleotide sequence in both target genes. The search for the unique gRNA yielded 217 gRNA possibilities for *ThFAD7* and 239 for *ThFAD8*, which were then reduced by focusing in gRNAs which targeted the first exon and were localised at least 160 bp upstream from the gRNA1 and 2.

The gRNAs were further filtered according to the predictive scores of the online tool CRISPOR for the specificity score, off-target counts, mismatches, out-of-frame score, and frameshift mutation analysis (Haeussler *et al.* 2016, Concordet and Haeussler 2018). The results for the four gRNAs chosen are shown in Table 6.2, along with the respective targeted gene, exon and guide sequences. The specificity score for the two conserved (gRNA1 and gRNA2) guides was under the limit recommended by CRISPOR of >50, on a scale of 0 – 100, which also showed a high number of off-targets with 17 for gRNA1 and nine for gRNA2. The unique independent gRNAs 3 and 4 showed high specificity with scores of 99 and 100, respectively, which corresponded to only three off-target counts for gRNA3 and one for gRNA4. Despite the high number of off-target counts in the two conserved gRNAs, the analysis of the 0-1-2-3-4 mismatches (Table 6.2) showed that most of the off-target sequences have three to four mismatches reducing the probability of these being affected by the CRISPR system. The off-target sequences and respective mismatch positions, counts, and location in the chromosome (or in the case of Eutrema, scaffold) are shown in Table 6.3 for the selected gRNAs which were analysed within each of the genes

ThFAD7 and *ThFAD8*. Hence the table shows that for the two conserved gRNAs, the only identified off-target with zero mismatches, and the most likely to be affected, were the target regions of the other gene. For example, when analysing gRNA1 in *ThFAD7* the off-target sequence with zero mismatches was localised in the scaffold 2, which corresponds to the location of *ThFAD8*, the opposite was then observed when analysing the same gRNA, but in the *ThFAD8* gene. This is also shown when analysing gRNA2, but not in the analysis of gRNAs 3 and 4, confirming both the conserved and unique characteristic of gRNAs 1-2, and 3-4, respectively. Further analysis on the location of the off-target location, gRNA1 showed three off-targets in the scaffold 2, where *ThFAD8* is also localised, but the mismatches are located within 5 bp of the PAM sequences reducing the chances of being affected (Table 6.3). Despite only showing one off-target for gRNA2 in scaffold 13, where *ThFAD7* is located, there is no mismatch in the 11 bp adjacent to the PAM sequence, suggesting a potentially real off-target site (Table 6.3). The gRNAs 3 and 4 also showed off-targets located in the scaffolds 2 and 13, respectively, but again the mismatch positions are near the PAM sequence (Table 6.3). The efficiency of the guide can be also reduced by in-frame mutations caused due to microhomology regions observed in the sequence adjacent to the target (Morton *et al.* 2006, Qi *et al.* 2013). Bae *et al* (Bae *et al.* 2014) developed a method that allows the prediction of these events, considering factors such as the frequency of the microhomology related deletions, caused by the size of the microhomology and by the length of the deletion, in the out-of-frame score. It ranges from 0 to 100, and it is a prediction of how likely out-of-frame deletions will be using a determined guide. Appendix 25 shows the microhomology predicted deletions associated with each of the four gRNAs used in this study, it also includes the respective effect in number of bp deleted and if it is predicted to cause a frameshift or no-frameshift deletion event.

The two conserved gRNAs 1 and 2 were 1299 bp apart in the full genomic sequence for *ThFAD8* and 1417 bp apart in *ThFAD7* (distance between

PAM sequences), whilst the specific gRNAs were localised in the first exon, but at a distance from gRNA1 of 191 bp for *ThFAD7* gRNA3, and 190 bp for *ThFAD8* gRNA4 (distance between PAM sequences, Figure 6.7 A). In the *ThFAD7* gRNA3 mutation site, three bp after the PAM sequence, the target was the amino acid glycine (Gly, residue 90), while gRNA1 targeted a phenylalanine (Phe) on residue 152. Whilst in *ThFAD8*, gRNA4 targeted residue 82, an alanine (Ala), and gRNA1 a Phe (residue 145) as in *ThFAD7*. gRNA2 was localised in the seventh exon in both genes and targeted a tyrosine (Tyr) in residue 377 of *ThFAD7*, and residue 368 of *ThFAD8*. Each of the gRNAs were designed to be transcribed from a different RNA polymerase III (Pol III) promoter (Figure 6.7 B), and four Arabidopsis small RNA promoters were selected from the literature that were previously used in genome editing experiments (Ma *et al.* 2015, Morineau *et al.* 2016). gRNA1 was expressed under a U3 promoter, while gRNA2, 3, and 4 used different U6 promoters. These U-snRNA promoters are transcribed by Pol III and encode for small nuclear RNAs (snRNA) involved in the RNA processing (Filipowicz *et al.* 1990, Waibel and Filipowicz 1990, 1990). The requirement for a specific nucleotide adenine(A) for pU3 and of a guanine (G) for pU6 were met for gRNA1 and gRNA2, whereas there was the need of adding a “G” to the 5’ end of the guide sequences of gRNA3 and gRNA4 (Belhaj *et al.* 2015).

Table 6.2 Summary of the gRNA Properties

Summary table of the four gRNAs properties designed for this experiment. The PAM sequence is marked in bold at the 3' end of the gRNA sequence, the specificity score, off-target counts, mismatches, out-of-frame score, and frameshift mutation analysis were performed with CRISPOR online tool [101, 102]. The score for Off-Targets for 0-1-2-3-4 Mismatches reads as: for each number of mismatches, the number of off-targets is indicated (example: 1-3-20-50-60 means 1 off-target with 0 mismatches, 3 off-targets with 1 mismatch, 20 off-targets with 2 mismatches, etc). For the frameshift mutation, uppercase letters refer to the nucleotides adenine (A), thymine (T), guanine (G) and cytosine (C); and the three letter codes refer to the respective amino acids phenylalanine (She), serine (Ser), isoleucine (Ile), leucine (Leu), tyrosine (Tyr), glycine (Gly), alanine (Ala), and arginine (Arg).

gRNA	Gene Target	Exon	Sequence 5' … 3'	Specificity Score	Off-Target Counts	Off-Target for 0-1-2-3-4 Mismatches	Out-of-Frame Score	Frameshift Mutation
gRNA1	*ThFAD7*, *ThFAD8*	1st	AACAAAGAGAGCCCAGAACA**TGG**	49	17	1-0-0-5-11	68	T**T**C (Phe) > TCT (Ser)
gRNA2	*ThFAD7*, *ThFAD8*	7th	GCTTCTACTAGATGATAATG**TGG**	49	9	1-0-0-2-6	54	*ThFAD7*: AT**T** (Ile) > ATA (Ile) *ThFAD8*: T**T**A (Leu) > TAT (Tyr)
gRNA3	*ThFAD7*	1st	GTGAACGGAGGAGGCGCGCCT**GGG**	99	3	0-0-0-1-2	64	GG**C** (Gly) > GGG (Gly)
gRNA4	*ThFAD8*	1st	GTTGAAGGGAGGGGGCGCACC**TGG**	100	1	0-0-0-1-0	62	**G**CG (Ala) > CGC (Arg)

Table 6.3 Off-targets for the Designed gRNAs

Off-target scores and sequences, mismatch counts and sequences, and respective genomic positions for the four gRNAs selected to target *ThFAD7* and *ThFAD8*. Ex, Exon; MC, Mismatch Counts; st, strand

gRNA	Gene	Ex	Off-Target Sequence	Mismatch Position	MC	(mit) Off-Target Score	(cfd) Off-Target Score	Location	st
gRNA1 [Conserved]	*ThFAD7*	1st	AACAAAGAGAGCCCAGAACATGG	.....	0	100	1	scaffold_2	-
	ThFAD8	1st	AACAAAGAGAGCCCAGAACATGG	.....	0	100	1	scaffold_13	+
	ThFAD7 and *ThFAD8*	1st	AATTAAGAGAACCCAGAACAAGG	..**.....*.....	3	1.462	0.437	scaffold_1	-
			GATAAAGAGAGCTCAGAACAGAG	*.*.....*.....	3	0.227	0.125	scaffold_15	+
			ACCAAACAAAGCCCAGAACACAG	.*....*.*.....	3	0.212	0.090	scaffold_1	-
			TCCAAAGAGAGCCCAGAAAACAG	**.....*.	3	0.225	0.087	scaffold_2	-
			AATACAGAGAGACCAGAACAGAG	..*.*.....*.....	3	0.259	0.064	scaffold_10	-
			CAAAAAGAGAGCCCAAAACTTGG	*.*.....*...*	4	0.118	0.446	scaffold_9	+
			AACAAAGAGTGATCAGAATAAGG	.....*.**.....*.	4	0.079	0.204	scaffold_3	-
			ATCAAAGAATGCCCAGAATAAGG	.*.....**.....*.	4	0.281	0.190	scaffold_7	+
			ATCAAAGAGAGACCAGATCTTGG	.*.....*.....*.*	4	0.067	0.156	scaffold_24	+
			AACAAAGCGAACCTAGAAAAAGG	.....*..*..*....*.	4	0.037	0.135	scaffold_7	+
			TATAAAGAGAGCCCAACACATGG	*.*.....**...	4	0.103	0.121	scaffold_2	+
			CTCAAAGGGAGCCCAGGACAAGG	**.....*.....*...	4	0.610	0.081	scaffold_40	-
			AACCAAGTGAGCTCAGAATAAGG	...*...*....*.....*.	4	0.193	0.049	scaffold_19	+
			AACAAAGAGGGCTCAAAAGATGG	.....*..*..*..*.	4	0.028	0.049	scaffold_1	+
			AACTTAGAGATCCCAGAAAAGGG	...**.....*.....*.	4	0.277	0.038	scaffold_1	-
			GACAAAGAGAGCTAAGAAGACGG	*.....**....*.	4	0.030	0.031	scaffold_2	+

(Continued on the next page)

gRNA	Gene	Ex	Off-Target Sequence	Mismatch Position	MC	(mit) Off-Target Score	(cfd) Off-Target Score	Location	st
gRNA2 [Conserved]	*ThFAD7*	7th	GCTTCTACTAGATGATAATG**TGG**	.....	0	100	1	scaffold_2	-
	ThFAD8	7th	GCTTCTACTAGATGATAATG**TGG**	.....	0	100	1	scaffold_13	+
	ThFAD7 and *ThFAD8*	7th	TCTTCTAAGAGATGATAATGCAG	*.....**.....	3	0.326554149	0.104320988	scaffold_13	+
			CCTACTACTCGATGATAATGAGA	*..*.....*.....	3	0.492236287	0.00787352	scaffold_1	-
			GCTGCGAATTGATGATAATGGGG	...*.*.*.*.....	4	0.760552802	0.204831933	scaffold_20	+
			GCTACTGCTCGATGATAATAAGG	...*..*..*.....*	4	0.415325641	0.105042017	scaffold_8	+
			TCTTATACTAGATGATAAGTCGG	*...*.....**	4	0.219695863	0.1	scaffold_7	+
			GCTTGTACTCTATGATAATCAGG	....*....**.....*	4	0.337490089	0.032967033	scaffold_11	+
			GCTTCATCTAGTTGATGATGAGG	.....**....*....*...	4	0.111984377	0.022303922	scaffold_6	+
			ACTTCTTCTAGATGATGACGAGG	*.....*.....*.*.	4	0.138537471	0.019168357	scaffold_23	+
gRNA3 [Unique]	*ThFAD7*	1st	TGAAGGGAGGGGGCGCACCTGGG	....*.....*.....*...	3	0.635	0.364	scaffold_2	-
			AGAACGAAGGAGACGCGCCAAGG	*.....*.....*.....*	4	0.184	0.519	scaffold_15	+
			TGAACAGAGGCAACGCGCCTTGG	.....*....***.....	4	0.087	0.345	scaffold_2	-
gRNA4 [Unique]	*ThFAD8*	1st	TTGAACGGAGGAGGCGCGCCTGG	.....*.....*.....*..	3	0.173471962	0.254545455	scaffold_13	+

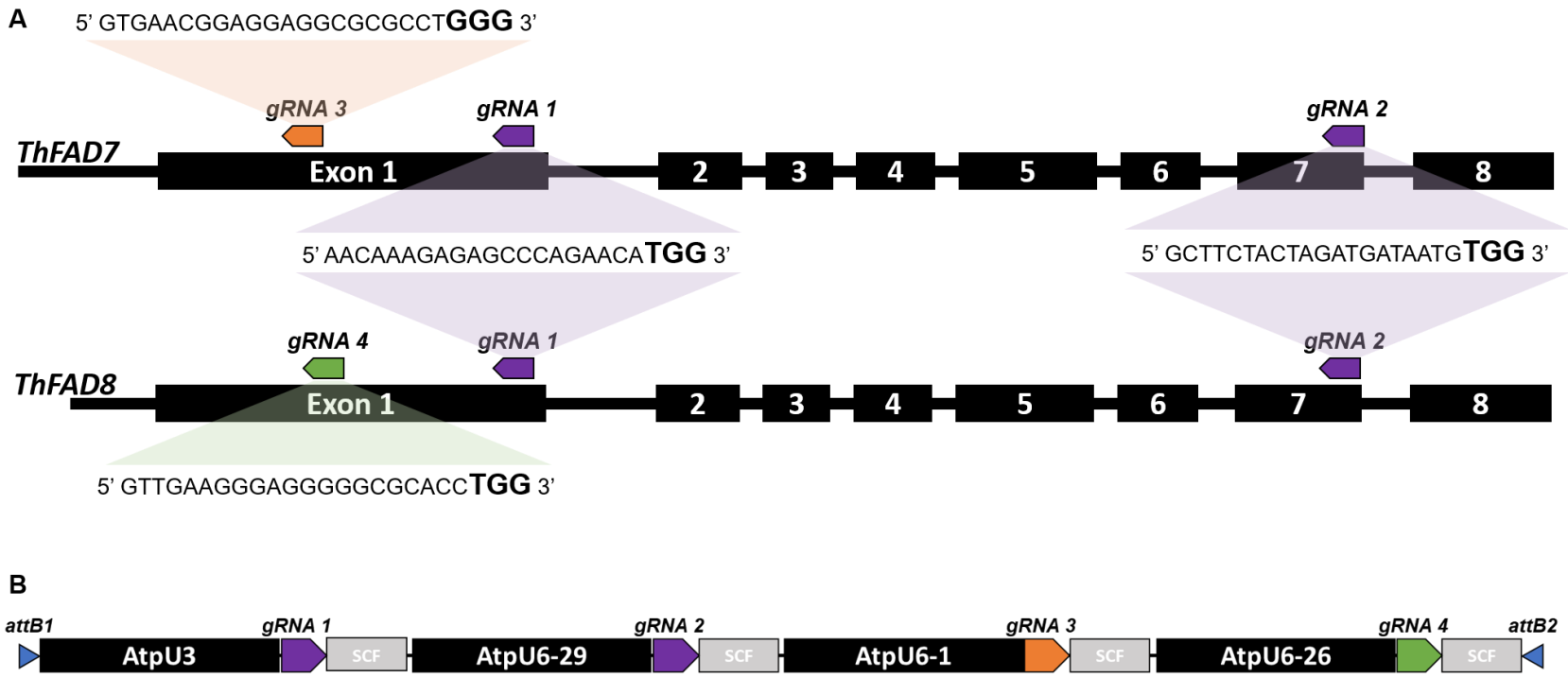

Figure 6.7 Gene Structures and gRNAs of ThFAD7 and ThFAD8

(A) *ThFAD7* and *ThFAD8* gene structure composed of eight exons (■). Localisation and sequence of gRNA targets is shown for the two conserved gRNA1 (■) and gRNA2 (■) in exons 1 and 7, the unique gRNAs for *ThFAD7* gRNA3 (■) and *ThFAD8* gRNA4 (■), both in exon 1. The protospacer adjacent motif (PAM) is represented in **bold** by the three last nucleotides on the 3' side of each gRNA sequence. (B) Scheme of the cloned fragment containing the four gRNAs, each preceded by the respective promoter (AtpU3, AtpU6-29, AtpU6-1, and AtpU6-26), and followed by the gRNA scaffold sequence (SCF, ■). Flanking each side of the clone are the *attB* Gateway® recombination sites (■).

6.2.5 *gRNA:Cas9:DsRED Expression Clone Production*

The Gateway™ cloning protocol was used to assemble the gRNA *cassette* with the Cas9-DsRED containing vector, pDE-Cas9-proDsREDter (15,821 bp) [(Morineau *et al.* 2016), protocol detailed in Section 2.7.6]. The gRNA *cassette* was isolated from the pUC19 vector using a high-fidelity polymerase, to guarantee the correct replication of the gRNA template by reducing potential errors. The PCR product was then used in the *BP* reaction for the assembly of the entry clones. The number of colonies formed after transformation of competent *E. coli* was assessed, the *BP* reactions 1, 2, and 3 showed 8, 4, and 29 colonies, respectively, while no colonies were found in the negative control. No presence of colonies in the negative control showed the efficiency of the reaction and limited the possibility of false positives in the *BP* reaction colonies, which were analysed by restriction analysis and DNA Sanger sequencing (Figure 6.8). The restriction analysis was performed with *Hind*III, due to the location of its two recognition sites in the entry clone, namely, before gRNA2 and after the hairpin sequence for gRNA3. These were expected to yield two fragments with different sizes of 5,256 bp and 1048 bp, which allowed the breakdown of the entry clone targeting the gRNA *cassette*. Three colonies per reaction were analysed, and two out of three reactions showed the correct restriction pattern (Figure 6.8 A). DNA sequencing confirmed these results for reactions 1 and 2, which was performed with the standard *M13* primer pair to confirm the correct insertion of the gRNA cassette into the donor vector. All three replicates per reaction showed a high consensus identity in both ends of the gRNA *cassette*, which suggests the correct insertion into the destination vector pDONR221™ (Figure 6.8 B). DNA sequencing also confirmed the error in the assembly of reaction three which was discarded after the analysis (results not shown).

As the entry clones were confirmed, six *LR* reactions were performed to assemble the entry clones with the destination vector pDE-Cas9-proDsREDter to produce the final expression clone containing the gRNA

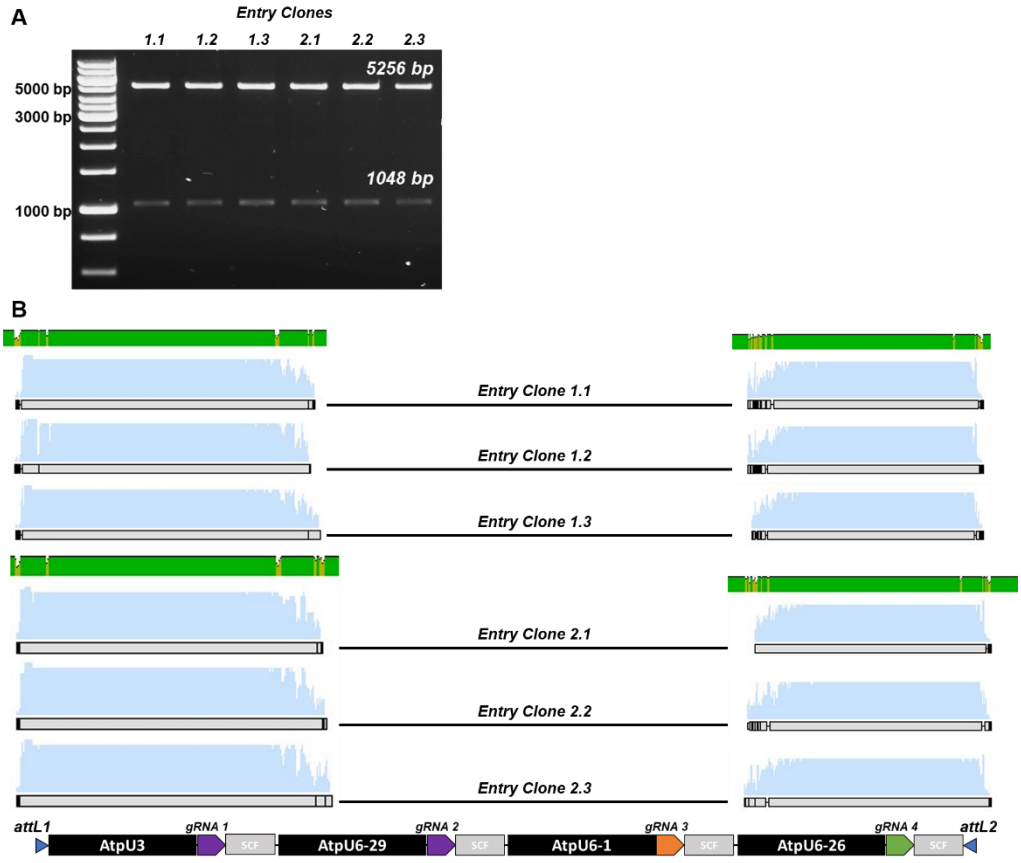

Figure 6.8 Entry Clones Analysis

(A) Restriction analysis of the two entry clones, each analysed in triplicate (1.1 – 1.3 and 2.1 – 2.3), performed with *HindIII* enzyme in a 1% agarose gel, with Thermo Scientific™ GeneRuler 1 kb DNA ladder for DNA fragments size reference. The two fragment sizes from the restriction analysis were expected to be 5,256 bp and 1048 bp. (B) DNA sequencing results for the two entry clones, each entry clone was analysed in triplicate (1.1 – 1.3 and 2.1 – 2.3). Sequencing was performed with the standard primer pair M13uni-21 / M13rev-29, and sequence alignment was performed with Geneious® against the designed clone (bottom of the panel) showing the entry clone *attL* Gateway® recombination sites (■). Green bars (■) represent the sequence identity between the three replicates per entry clone.

cassette, the Cas9, and the selection marker DsRED in a final 17,927 bp vector. Again, the efficiency of the reaction was assessed by the number of colonies and confirmed using restriction analysis with the enzymes *Not*I and *Nhe*I, and finally by DNA sequencing (Figure 6.9). Each of the six *LR* transformed *E. coli* yielded a significant number of colonies, whilst the negative control with no added entry clone showed no colonies and the positive control, that replaced the entry clone for the pENTR™ vector, showed a significant number of colonies, which confirmed the efficiency of the reaction. The restriction analysis was performed with the enzymes

*Not*I and *Nhe*I, with three recognition sites each targeting the expression clone breaking it down in six fragments for an accurate analysis. The six expected fragments varied in size from 6529 bp, 5467 bp, 3109 bp, 1532 bp, 698 bp to 592 bp. The restriction analysis showed that all six replicates have the right number and size fragments as predicted (Figure 6.9 A), confirming high efficiency of the reaction. DNA sequencing analysis was done to confirm that the gRNA *cassette* was correctly cloned and replicated into the pDE-Cas9 vector. For this, four primer pairs were specifically designed (Section 2.7.6) to cover the 3.7 kb gRNA *cassette* (Figure 6.7), from the AtpU3 promoter to the terminator sequence of gRNA4, due to the limitation of the sequencing reads (maximum length approximately 1000 bp). All six expression clones were analysed to assess the ones with the highest sequence identity to the gRNA *cassette* designed. The expression clones 2.2 and 2.3 (Figure 6.9 B – C) showed the most complete sequence results for the integral part of the gRNA *cassette*, with only minor disruptions, these were used for the transformation of *Agrobacterium*. Competent *Agrobacterium tumefaciens* cells strain AGL-1 (Lazo *et al.* 1991) were then transformed by electroporation as described in Section 2.3.4, and after two days of incubation, four independent colonies were selected and transferred to SOC medium to proceed with the floral dip protocol.

6.2.6 *Eutrema Showed High Transformation Efficiency with One Flower Dip*

The transformation of the Eutrema plants was performed according to the *Agrobacterium*-mediated flower dip method previously tested (detailed in section 6.2.1) and done in two batches. Batch A was subjected to three flower dip sessions to account for the longer flower period and the high stress resilience characteristic of this species as discussed in Section 6.2.1, while Lot B had only one flower dip. In both cases, transformation started at the onset of the flower buds as shown in Figure 6.10 A. The repeated flower dip events in batch A were spaced by fifteen-day intervals, which was previously demonstrated to allow enough time for

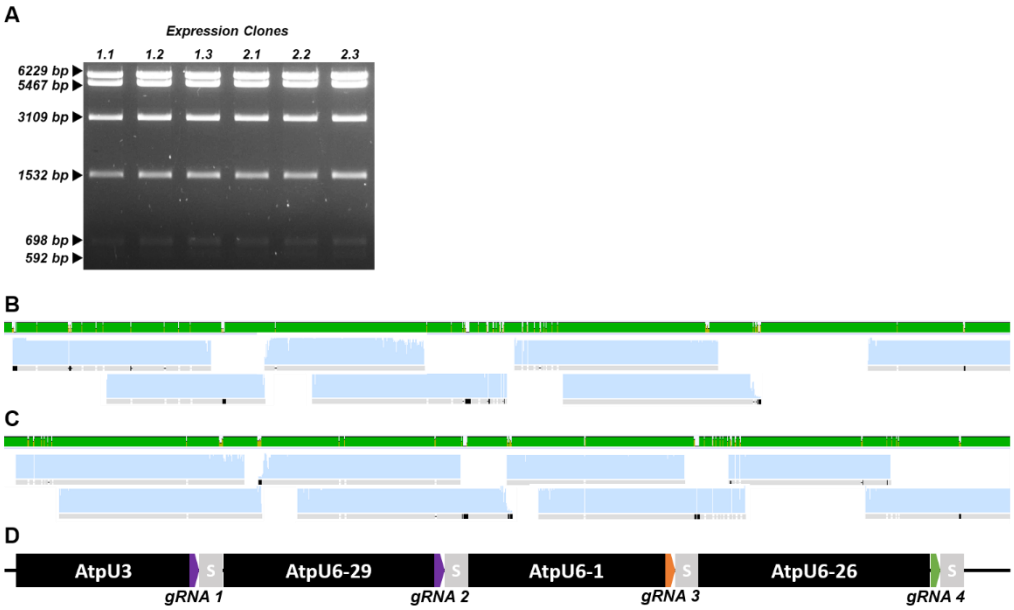

Figure 6.9 Expression Clones Analysis

(A) Analysis of the restriction pattern for the six expression clones performed with the enzymes *NotI* and *NheI* in a 1% agarose gel, with the Thermo Scientific™ GeneRuler 1 kb DNA ladder for DNA fragments size reference. Six fragments were expected to result from the restriction reaction with the sizes of 6529 bp, 5467 bp, 3109 bp, 1532 bp, 698 bp and 592 bp (►). DNA sequencing for the expression clones 2.2 (B) and 2.3 (C). Sequencing was performed with the primers for the promoters AtpU3, AtpU6-29, AtpU6-1, and AtpU6-26 (■) (Section 2.7.6). Within each panel the consensus identity (■) shows the result of the sequencing. The alignment of the sequences was performed with Geneious® against the designed gRNA *cassette* (D). S, gRNA scaffold.

the plants to recover (Section 6.2.1).The transformed T1 seeds were identified using the DsRED filter in a light microscope to facilitate the identification of the fluorescence in the seed coat (Figure 6.10 B-C). Batch A had a total of 31 transformed seeds identified, with five of the 11 transformation events with no transformed seeds, while batch B had 92 DsRED positive seeds and only two transformation events of 10 with no results, a total of 123 DsRED positive seeds.

On the T1 generation, 66 plants germinated representing a germination rate of 53.7%. Of these, 31.8% of the population (21 plants out of 66) did not develop any flower buds after seven weeks of control conditions, despite the three weeks of stratification applied, tested previously as enough time to allow for the onset of flowering later in the cycle. The remaining 45 flowering plants were then analysed for gene editing.

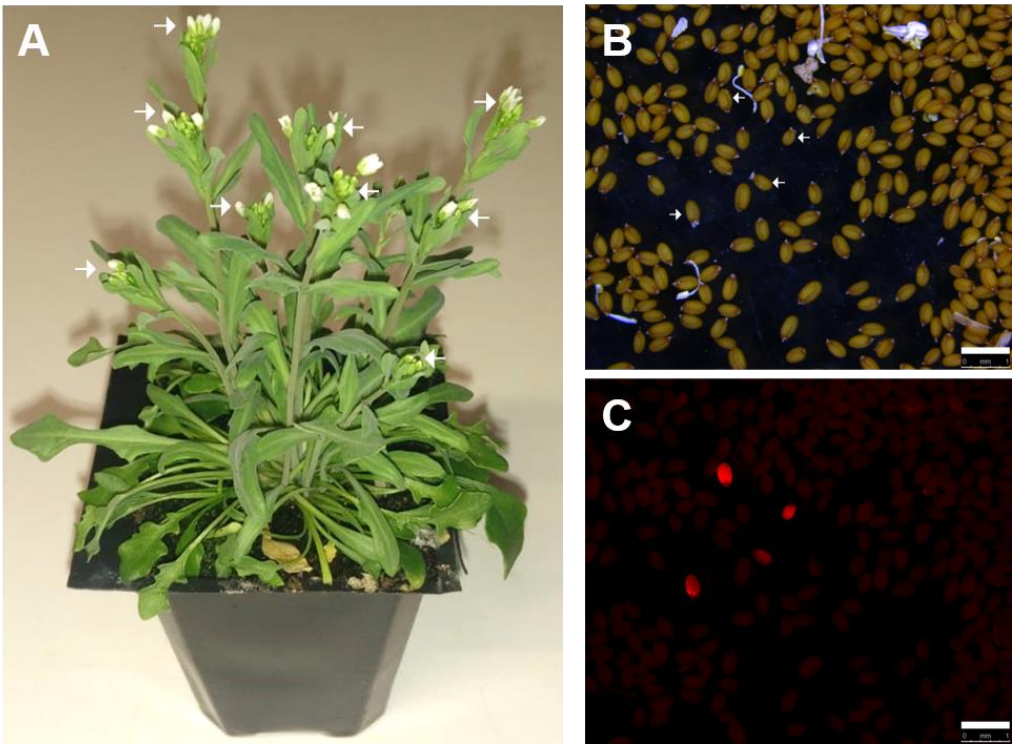

Figure 6.10 Eutrema Transformation with the CRISPR Vector

(A) Representative plant of the T0 wild-type Eutrema used for floral dip transformation with the CRISPR vector showing the first flower buds (white arrows) stage at which the first floral dip event took place. (B) Bright field image of the transformed T1 seeds, the white arrows show the DsRED positive seeds identified in (C) using the DsRED filter. The white bar represents 1.0 mm size scale.

Table 6.4 Eutrema Transformation Summary

Number of events for each stage of the *Agrobacterium*-mediated transformation protocol, and to produce the T1 CRISPR lines.

	Batch A	Batch B	Total
Transformation events	11	10	21
Transformation events with DsRED seeds	6	8	14
Number DsRED seeds	31	92	123
Germinated Seeds	16	50	66
T1 Flowered plants	11	34	45

6.2.7 *Six Edited Candidates were Identified Based on Fragment Size*

T1 plants were screened for edition of genes *ThFAD7* and *ThFAD8* by PCR analysis of gDNA to identify any size shift in the target fragments in comparison to wild-type, and gDNA sequencing was used to detect smaller indels of a few nucleotides. As the targeted genes have an impact reducing the production of trienoic fatty acids (Browse *et al.* 1985, Browse *et al.* 1986, Mcconn *et al.* 1994) the analysis of the fatty acid profile of each of the plants was also assessed (GC-FID analysis of methylated fatty acids detailed in Section 2.5.4).

The genotype of the T1 CRISPR lines was analysed by amplifying two regions of each gene that included the gRNA target sequences (Figure 6.11), to identify lines with a shift in the respective fragment size which might indicate editing. The 45 flowering plants were genotyped, from which six (8, 9, 10, 15, 16, and 18) appeared to show a second fragment of smaller size for *ThFAD8* exon 1 (*ThFAD8.1*), reduced from 351 bp to approximately 100 bp (Figure 6.11 B). The same effect was also observed only for line 10 in exon 1 of *ThFAD7* (*ThFAD7.1*) with a second fragment of approximately 100 bp (Figure 6.11). No other lines showed any changes in fragment size which corresponded to the size of the wild-type Shandong (Sha) tested. The six lines 8, 9, 10, 15, 16, and 18 were therefore treated as potential edited lines, and the gDNA sequencing and fatty acid profile for these lines is presented below, which also included a line as a negative control (e.g. not showing a smaller size fragment).

As the genotype results were promising, gDNA Sanger sequencing was performed after the PCR was repeated with a high-fidelity polymerase to decrease the chance of errors. These reactions were analysed in a 1% agarose gel prior to sequencing. Unfortunately, the results observed for the lines 8, 9, 10, 15, 16 and 18 were not replicated and no second smaller fragment was found (results not shown). Still, the reactions were sequenced to search for small indels that might not have been detected in the first analysis. No changes in any of the target sequences for any of

the designed gRNAs were found (Figure 6.12). The sequencing efficiency showed in Figure 6.12 F for the gRNA4 target in exon 1 of *ThFAD8* was quite low, despite this there was no evidence of any change and the test was not repeated. As no deletion of big fragments were found, the sequencing results were analysed for the specific target sequence of each of the gRNA, as its induced mutation(s) occur three bp after the PAM sequence. Line 17 showed an overlap in the sequencing of an adenine (A) over five bp (CTGGG) spanning the 8th to the 12th bp in the gRNA1 sequence target, but due to the low sequencing efficiency this result was again inconclusive (Figure 6.12 A). No other mutation was found for any of the T1 lines, hence change in the target sequences of the gRNAs (detailed results in Appendix 22). The analysis for edited lines was performed in the T1 generation where, if any mutation occurred, only one copy of the edited gene would be present as the lines were still heterozygous. This explains the presence of the wild-type fragment together with the reduced size fragment observed for the six lines 8, 9, 10, 15, 16, and 18 (Figure 6.11). As such, a double trace for the mutation site in the DNA sequencing results, without affecting the sequencing performance, could have also indicated an edited line.

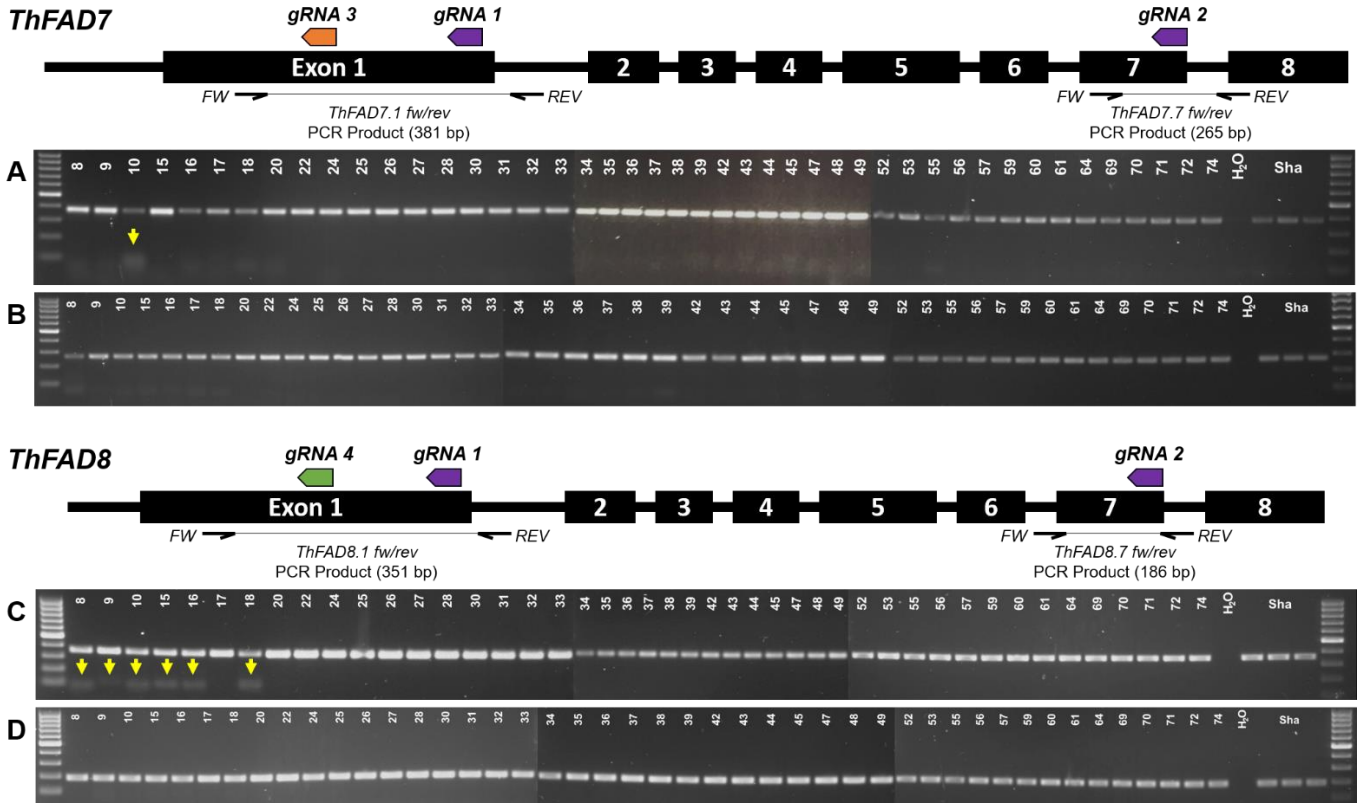

Figure 6.11 T1 CRISPR Lines Genotype Analysis

T1 CRISPR lines were genotyped by amplifying two regions of each gene targeted by the four gRNAs. The analysis of *ThFAD7* is shown in (A) exon 1 (*ThFAD7.1*) 381 bp, and (B) exon 7 (*ThFAD7.7*) 265 bp regions. The analysis of *ThFAD8* is shown in (C) exon 1 (*ThFAD8.1*) 351 bp, and (D) exon 7 (*ThFAD8.7*) 186 bp regions. Numbers on top of each fragment represent the 45 plants tested for shifts in band size (yellow arrows, ▼), water (H_2O) and Eutrema (Sha) were used as negative and positive controls, respectively. Thermo Scientific™ GeneRuler 100 bp DNA ladder was used for DNA fragments size reference.

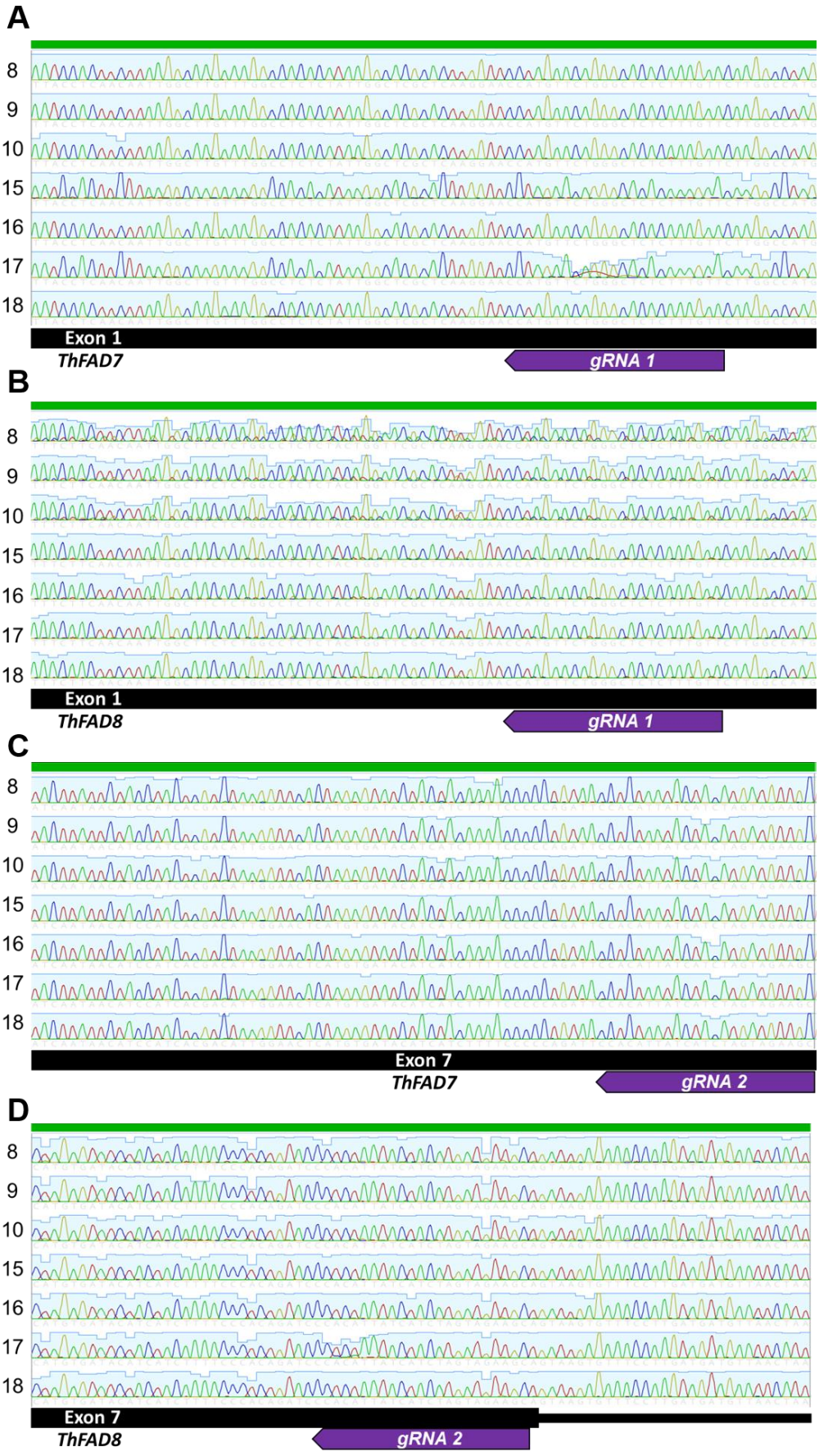

(Continued on the next page)

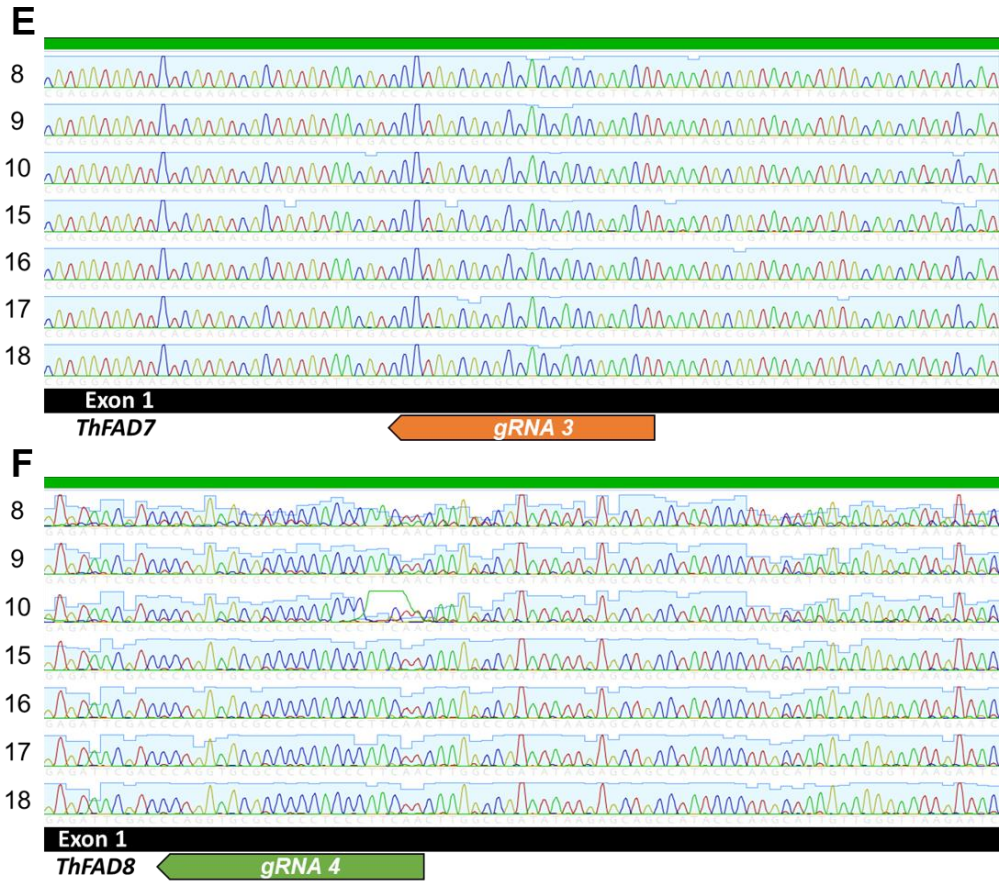

Figure 6.12 T1 CRISPR Lines Sequencing Results

Sequencing results for the six T1 lines 8, 9, 10, 15, 16, 17, and 18 showing the gRNA gene target sequences. gRNA1 (■) target sequence in *ThFAD7* (A) and in *ThFAD8* (B); gRNA2 (■) for *ThFAD7* (C) and *ThFAD8* (D); gRNA3 (■) target in *ThFAD7* (E); and gRNA4 (■) in *ThFAD8* (F). Sequence alignment was performed with Geneious® against the database FASTA sequences and the designed gRNAs (bottom of each panel). gRNA PAM sequence represented in the arrow tip of each of the gRNAs. Green bar (■) on top of each panel represents sequence identity, and the traces show bases adenine (A, —), thymine (T, —), guanine (G, —), and cytosine (C, —).

Finally, the fatty acid profile of the T1 lines was measured through the analysis of the fatty acid methyl esters (FAMEs, Section 2.5.4) to account for any change in the content of trienoic acids that could indicate an edited line. As previously described (section 6.2.3), the double mutant profile was characterised by a reduction in the production of trienoic acids, with a higher impact in the 16:2/16:3 ratio. Figure 6.13 shows the fatty acid ratio of 16:2/16:3 and 18:2/18:3 for the T1 edited candidates compared to the wild-type Sha. No dramatic decrease in the 16:2/16:3 ratio was found in any of the T1 lines shown that could immediately

suggest an edited line. However, line 9 showed a 21% decreased content of 16:2/16:3 and of 19% in 18:2/18:3. And, despite the 34% reduction observed in the ratio 18:2/18:3 in line 10, its 16:2/16:3 content increased by 17% showing an opposite trend to the previously described. As these were T1 lines no replication was possible as each plant was considered an independent line which could present a biased analysis of the profile. Furthermore, as they were heterozygous the effects of any potentially edited lines might be limited due to the presence of only one edited copy in simultaneous with the wild-type copy. Six potentially edited T1 lines were identified by the presence of a second fragment in the gDNA PCR analysis of exon 1 of *ThFAD8*. However, no confirmation of these results was possible using gDNA sequencing or the fatty acid profile. Nonetheless, these six lines were carried through to T2 in order to analyse segregation pattern and confirm the presence of edited genes, whilst also allowing further edition events to occur. Time prevented the conclusion of this work and establishment of *ThFAD7* and *ThFAD8* mutated lines in Eutrema, however subsequent stages are discussed below.

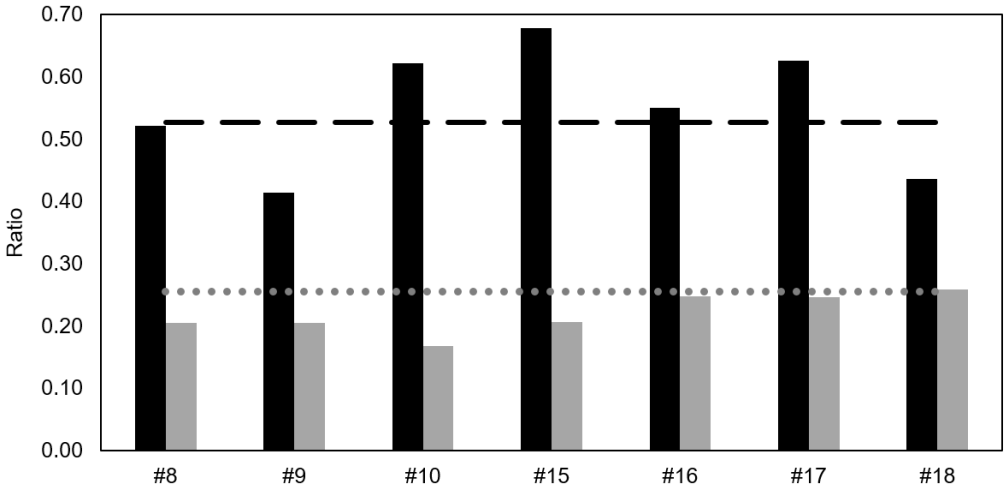

Figure 6.13 Fatty Acid Profile of the T1 CRISPR Lines

The ratio of the fatty acids 16:2/16:3 (■) and 18:2/18:3 (■) was measured in each of the T1 CRISPR lines 8, 9, 10, 15, 16, 17, and 18, and compared against the wild-type Eutrema Shandong represented by ▬ ▬ for 16:2/16:3 ratio, and as ●●● for 18:2/18:3 ratio. Each plant was considered an independent line, so no replication was possible. Fatty acids are represented as number of carbons: double bonds.

6.3 DISCUSSION

The work developed in this chapter aimed to propose Eutrema as a plant model for abiotic stress, by producing mutated Eutrema genotypes using the CRISPR/Cas9 system as means to target the chloroplast fatty acid desaturases *ThFAD7* and *ThFAD8*. Firstly, efficient and reproducible germination and transformation protocols for Eutrema were established, allowing the development of a CRISPR/Cas9 driven mutagenesis protocol. Secondly, the ThFAD7 and ThFAD8 sequences were identified through the homologue amino acid sequences of AtFAD7 and AtFAD8 in Arabidopsis. The respective fatty acid desaturase domains including the characteristic conserved histidine boxes were found through bioinformatics. Thirdly, a multiplex approach was designed allowing for three sequences within each *ThFAD7* and *ThFAD8* to be targeted by four gRNAs delivered by the same scaffold system (Ma *et al.* 2015, Xie *et al.* 2015). Finally, the transformation protocol produced a total of 123 transformed seeds, which upon germination were analysed for mutations. From these six potentially mutated lines were identified. The results obtained are discussed below, with focus on the advances made here for the establishment of Eutrema as a plant model for abiotic stress studies.

6.3.1 *Establishing Reliable Protocols for Eutrema*

Understanding the germination strategy of a candidate plant model is essential for its successful establishment. Halophytes such as Eutrema, hold several different ecological strategies for seed germination (Song *et al.* 2005), so the present chapter started by exploring the ecotype Shandong (Sha) germination efficiency by testing three protocols. As Eutrema seems to control its dormancy for longer periods (Li *et al.* 2015), one and three weeks of stratification were tested. Three weeks was shown to be essential for the ability of the plant to germinate and flower as it has an obligatory vernalization requirement (Bressan *et al.* 2001). The established protocol was then to sow the seeds directly to soil, with a sandpaper pre-treatment whenever possible. This was recommended

to be followed by a stratification period of three weeks at 4°C and dark conditions to achieve higher germination rates and guarantee the onset of flowering. This stratification period was enough for the plants to flower as shown in Figure 6.14, without the requirement of a vernalisation period during growth (Amtmann 2009). Seed storage was also an important factor to consider for maintenance of seed stocks, and Eutrema seemed to be particularly sensitive to this. A treatment of seven days at -80 °C after seed collection was used to improve germination efficiency after medium to long periods of storage. Despite the tested protocol, germination rate varied reaching up to 85% only when a mechanical scarification was applied (Figure 6.3 E). The 53% germination rate observed with direct sowing for the T1 CRISPR DsRED positive seeds was the highest obtained without the application of mechanical scarification. This meant that the chances of identifying edited lines in the T1 screen were reduced by half. Furthermore, 30% of the germinated T1 plants did not flower despite three-week stratification period, an effect which was not observed before. After 35 days of control conditions, these plants did not present any shoot nor bud development, thus were not considered for the screening as no seeds would be produced to continue with the segregation analysis.

The successful transformation of Eutrema using the traditional *Agrobacterium*-mediated floral dip method (Clough and Bent 1998) was fundamental for the delivery of the CRISPR/Cas9 vector. However, and despite the recommended eight to ten *Agrobacterium* treatments in the literature (http://thellungiella.org/) and the three tested, one floral dip revealed higher efficiency in the production of DsRED positive seeds than multiple floral dips. This leads to a debate around the correct flower developmental stage as a determinant factor in the efficiency transformation with *Agrobacterium.* Despite no visible signs of stress, multiple floral dips might have caused silique abortion and hence reduced the number of transformed seeds identified. The use of DsRED fluorescence as a selection marker improved the efficiency with which transformed seeds were selected. DsRED is a red fluorescent protein

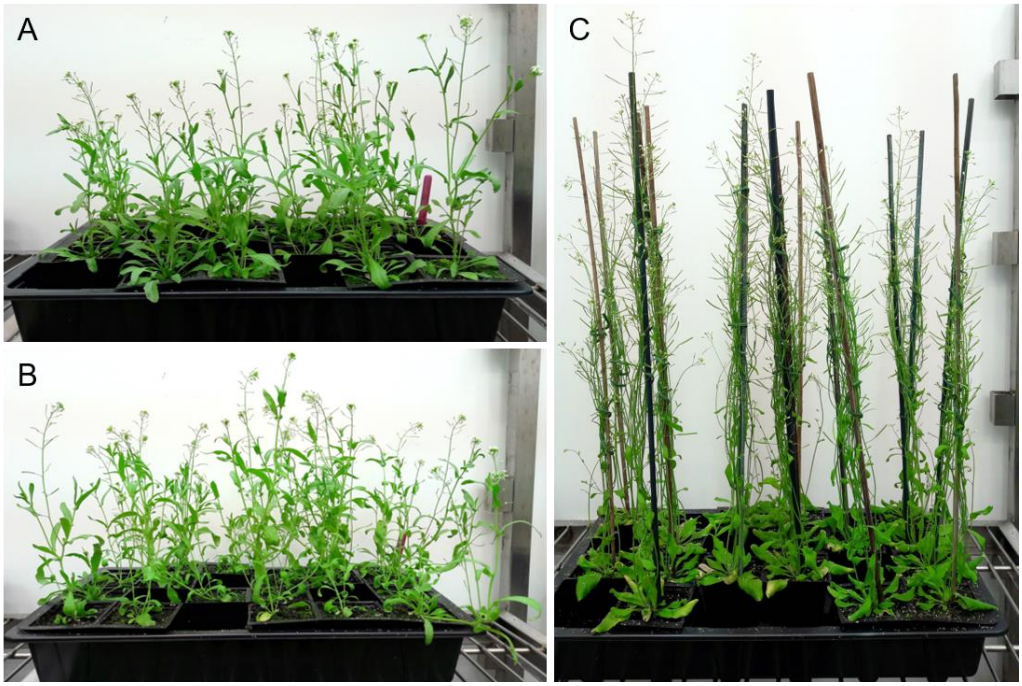

Figure 6.14 Eutrema (Sha) and Arabidopsis (Col-0) Flowering Plants

Eutrema Shandong ecotype (Sha) plants (A, B) and Arabidopsis ecotype Columbia (Col-0) plants (C) at 41 DAS (days after sowing) originated from the germination efficiency test. (A) Sha direct sow, (B) Sha direct sow with mechanical scarification, (C) Col-0 mix of direct sow.

isolated from red coral *Discosoma* sp. with an excitation peak of 553 nm (Matz *et al.* 1999), and it was first shown as a reporter *in planta* by Jach *et al.* (Jach *et al.* 2001) with the advantage of being easier to visualise when compared to GFP that can be difficult to distinguish from the autofluorescence background caused by green tissues. DsRED was expressed through the seed coat emitting red fluorescence glow under the appropriate filter (Matz *et al.* 1999, Jach *et al.* 2001), which allowed for a rapid identification of the transformed seeds (Figure 6.10). Eutrema has been demonstrated to have 13 times higher wax content than Arabidopsis (Teusink *et al.* 2002), and its stem leaves show low cuticle permeability (Tang *et al.* 2018) thought to be a physical protection mechanism against the extreme conditions. Thus, the use of DsRED as a selection marker opened the possibility of a more suitable choice for Eutrema transformation than the traditional use of antibiotics or herbicides, which need to be absorbed by the leaves to act. CRISPR/Cas9 induced mutations are known to be carried over through

the generations independently of the presence or absence of Cas9 following a Mendelian proportion (Feng *et al.* 2014, Jiang *et al.* 2014, Hahn *et al.* 2017). As the mutations are stably inherited, once the edited lines are identified it is recommended that the gRNA/Cas9 *cassette* should be lost by segregation to avoid the possibility of newer or increased off-target mutations by the active CRISPR system (Hahn *et al.* 2017, Danilo *et al.* 2019). In protocols that use of antibiotics or herbicides, this segregation selection needs to be carried over at least to T4 or T5 grown in non-selective medium (Hahn *et al.* 2017), and thus losing the selective benefit. On the contrary, DsRED carries the advantage to allow selection of “Cas9 free” progeny in the T2 generation seed pool avoiding the lengthy process of segregation analysis. Even more of an advantage if the length of Eutrema average life cycle of three weeks of vernalisation, two weeks of germination, and ten to 12 weeks to set seed is to be considered.

6.3.2 *Off-Target Analysis of the gRNAs Designed*

For the CRISPR/Cas9 method, a multiplex strategy (Cong *et al.* 2013, Li *et al.* 2013, Xing *et al.* 2014, Ma *et al.* 2015) was applied by designing four gRNAs to target exon 1 and 7 in both *ThFAD* genes, increasing the chances of deletion and ensure gene knockout (Li *et al.* 2013), especially in the first exon targeted by two gRNAs. gRN3 for *ThFAD7* and gRNA4 for *ThFAD8* were designed to target the predicted chloroplast targeting signal, while the fatty acid desaturase domain was targeted in both genes by gRNA1 and gRNA2. This design rendered a multitude of possible mutations, increasing the probability of frameshift mutations causing an alteration in the gene’s reading frame (Jiang *et al.* 2017). Thus, if translation is not interrupted, then it could affect the ability of the proteins to be targeted to the chloroplast and/or their desaturase domain activity. As key domains for the correct function of the desaturases (Shanklin and Cahoon 1998), any mutation occurring in any of these regions would render the protein inactive. Nonetheless, in-frame mutations that do not alter the protein activity were also considered. The Bae score (Bae *et al.*

2014), used to determine the out-of-frame probability which determines the percentage of clones that will have out-of-frame deletions, based on the micro-homology regions flanking the target sequence. Despite the predicted high count of out-of-frame score, these are of more importance in the case of experiments using only one gRNA, where predicting the potential deletions is a key aspect for the efficiency of the gene editing (Bae *et al.* 2014). The endonuclease activity of the Cas9, guided by the engineered gRNAs, most frequently creates a blunt-ended double-strand break (DSB) three nucleotides upstream of the PAM sequence (Jinek *et al.* 2012). Depending on the micro-homology of the adjacent area to the target site, the DSB can cause a frameshift mutation. However, no frameshift events can also occur which can lead to a less affected protein. The micro-homology predicted deletions calculated by CRISPOR (Appendix 25) showed that gRNA 1 – 3 71 to 78 bp deletions could occur which would not cause a frameshift, whilst for gRNA4 a total of 54 bp deletions can occur to achieve the same effect. gRNA1 showed the lowest chance of no frameshift mutations, with 30.7% from an analysed pool of 88. On the other hand, gRNA2 showed the highest probability, with 38.6% no frameshift possibilities out of 70 mutations with two to 75 bp deleted. An average of 70% of the possible deletions as a frameshift mutation resulting from each of the gRNAs was still considered high, increasing the possibility of a non-functional protein.

The specificity score measured the uniqueness of the guide sequence in the respective genome with a recommended value of ≥ 50 (out of 100), since a high specificity score value will reduce the probability of off-target effects (Hsu *et al.* 2013). Correspondingly, the relatively low specificity score of the gRNAs 1 and 2 (both under 50) was associated with a high number of predicted off-targets, whilst gRNA4 showed the maximum specificity score of 100 and only one predicted off-target. The off-target count identified a possible 20 nucleotide sequences matching any of the designed gRNAs, which are followed by a PAM sequence, hence being a possible Cas9 nuclease target (Lin *et al.* 2014). The count for the conserved gRNAs 1 and 2 was quite high (Table 6.2), especially for

gRNA1 with 17 possible off-target sequences. Despite the considerable number of predicted off-targets for the chosen gRNA, some of them might be considered as false-positive and not real targets, while only a few will have higher probability of being cleaved (Haeussler *et al.* 2016). The number and position in the sequence of the mismatches are an important factor to consider, as the closer they are to the PAM sequence, the lower the probability of occurring due to reduced DNA binding (Swarts and Jinek 2018). The analysis of the mismatch counts for gRNA1 showed that 11 (65%) of these off-targets would have four mismatches in their sequence, and five (29%) with three mismatches. Leaving only one off-target to account for with zero mismatches that corresponds to the right *ThFAD* exon 1 target. The off-target scores and mismatch positions in Table 6.3 confirm these results, showing only one off-target with a high score due to the presence of a mismatch nine bp away from the PAM sequence. However, according to NCBI BLAST, the off-target sequence did not show any significant alignment for the whole 20 nucleotide sequence. The most significant results with 100% of identity were for the last 12 bp of the off-target sequence for a predicted hydroxyproline O-galactosyltransferase GALT5 (LOC18009077), and for the 12 first bp from the PAM sequence for an uncharacterised mRNA LOC18993225. In Arabidopsis, GALT5 is involved in the arabinogalactan protein glycosylation essential to the growth and development of the plant (Basu *et al.* 2015). LOC18993225 has an enhancer of polycomb-like (EPL1) conserved domain, which is involved in histone acetylation in transcription regulation in yeast (Boudreault *et al.* 2003). The analysis of the designed gRNAs properties displayed the uniqueness and the potential effectiveness in editing the two targeted *FAD* genes. As to the potential non-targeted mutations, these can be identified based on CRISPOR predictions, which include a simpler way to design specific primers, for which PCR and sequencing analysis can be performed. By identifying edited lines without non-targeted mutations these effects can be mitigated.

6.3.3 *Investigating Screen Methods*

Despite all efforts, it was not possible to perform genotype analysis on the T2 generation. The analyses performed in the T1 were not conclusive as to the presence of edited lines, nor the nature of the edition, with only six lines showing a second smaller size fragment for exon 1 of *ThFAD8*, and only one of these six lines showing the same result for exon 1 of *ThFAD7* (Figure 6.11). From these results, it could be extrapolated that there was a deletion of approximately 200 bp in these six lines, which would mean that the area between the targeted sequences in exon 1 for the two gRNAs was deleted. The distance between the gRNA1 and gRNA3 PAM sites in *ThFAD7* was 191 bp, while in *ThFAD8* the distance from gRNA1 to gRNA4 was 190 bp (Figure 6.7). This design was planned to avoid competition from the Cas9, whilst targeting two areas in the first exon to increase the chances of deletion. The distances between gRNAs could therefore correspond to the reduction in size of the second fragment observed in Figure 6.11. However, no evidence for this was found with Sanger sequencing, which was performed in gDNA amplified with a high-fidelity polymerase. As the second small size fragments were identified in a 1% agarose gel perhaps the isolation of this fragment and cloning prior to Sanger DNA sequencing might have revealed the nature of the second fragments, and positively identified edited lines. However, small insertions or deletions of a few base pairs, or frameshift mutations could also occur according to the predictions shown in Appendix Appendix 25. Such mutational events might not have been detected by the gDNA PCR analyses performed. Other sequencing methods, such as Next Generation Sequencing (NGS) could be an alternative method to characterise these mutational events (Shendure and Ji 2008). Restriction analysis on the fragments amplified by PCR was also considered (Jiang *et al.* 2017). However, only the gRNA3 target sequence had a restriction site on the third bp from the PAM sequence, the prime site for any mutation that might occur. This enzyme was *PteI* (with isoschizomers *BsePI*, *BssHII*, and *PauI*) with the recognition site G|CGCGC (“|” represents the cutting site), producing two fragments of 307 and 78 bp

respectively, from the *ThFAD7* exon 1 amplified fragment of 381 bp (Figure 6.11). All other gRNA targets had cutting sites before or after this prime mutation site, rendering a false negative in the case of indel(s) of one to four bp. As the screen for edited lines was not conclusive, other analysis could have been performed to confirm the presence of the expression clone in the T1 CRISPR lines. PCR analysis to amplify the Cas9 genomic sequence, or the promoter-gRNA *cassette* could have indicated the presence of any of these elements essential for the CRISPR system. Regarding the apparent difference in gRNA-induced mutations efficiency, such cases have been previously reported. Mourineau *et al*. (Morineau *et al.* 2016) reported the use of two gRNAs targeting three homologous *CsFAD2* genes in *Camelina sativa* (Camelina) where the T1 generation showed a mutation in 26% of the lines transformed with gRNA2, whilst gRNA1 caused no mutations in T1. It was clear that our understanding the impact of each of the CRISPR/Cas9 in the production of specific mutations is still not fully understood (Gisler *et al.* 2019).

6.3.4 *The Contribution of FAD Genes to Cold Stress*

No published work linked the function of the *ThFAD7* and *ThFAD8* genes with the cold stress response in Eutrema, however, these genes were found to be upregulated in the RNA-Seq analysis (Appendix 3). The Eutrema transcriptome data showed both transcripts to be upregulated after exposure to three days of cold stress (4°C). *ThFAD7* had a Log_2 ratio of 0.759, and *ThFAD8* of 0.709. Despite low fold change values, these suggest a possible role in the cold stress response of Eutrema. Evidence suggests that a highly stress-specific translational and transcriptional reprogramming occurs in Eutrema under abiotic stresses, which ultimately leads to metabolic and signalling changes (Mucha *et al.* 2015). According to Taji *et al.* (Taji *et al.* 2004), only six Eutrema genes were salt stress-inducible whose log_2 ratios of salt versus control were ≥1.5, whereas the same experiment in Arabidopsis showed 40 such salt stress-inducible genes. In Camelina, the disruption of *CsFAD2* using a similar CRISPR/Cas9 approach to the one presented here resulted

mostly in frameshift mutations or indels of large portions of the gene. This led to a perturbed fatty acid desaturation ratio, due to the almost complete reduction of dienoic acids, and in particular 18:2, with the concomitant decrease in trienoic acids and accumulation of monounsaturated species such as 18:1 and 20:1 (Morineau *et al.* 2016, Jiang *et al.* 2017). Extrapolation of these results into the context of the work developed in this chapter could allow a predictive scenario. Considering the six mutated candidates identified in T1 for *ThFAD8* and the one candidate for *ThFAD7,* an approximately 200 bp deletion was observed in the 5' portion of the genes. Disruption of the reading frame was thus likely to occur, leading to a non-functional protein. In such case, reduction of the trienoic acid content in the mutated lines could be predicted, allowing investigations of the importance of such stress responses in the context of an extremophile metabolism. The extent of damage caused by cold and freezing stress to the Eutrema mutated plants lacking polyunsaturated fatty acids could then be asserted using the high-throughput cold screen test developed in Chapter 3. Moreover, as the test uses chlorophyll *a* fluorescence to measure the plant's cold adaptation, the role of polyunsaturated fatty acid content as a protective mechanism and its relationship with the photosynthetic response in Eutrema could be studied.

6.4 CONCLUSION

In the present chapter, a series of tasks were proposed with the objective of establishing the extremophile plant Eutrema as a plant model for abiotic stress. Firstly, reliable and reproducible germination and transformation protocols were developed. It was established that three weeks of stratification were the minimum requirement period for an effective germination rate and onset of flowering. Once the plants start to develop the first flower buds, the *Agrobacterium*-mediated floral dip should be applied, where one application would suffice for the successful transformation of Eutrema. The recently developed CRISPR/Cas9 gene editing technique was then applied, to produce Eutrema lines with

mutated versions of the fatty acid desaturases FAD7 and FAD8. This would allow to model Eutrema's response to cold stress in the absence of these two lipid metabolism genes, essential to the cold stress response as demonstrated in Arabidopsis. The Eutrema *ThFAD7* and *ThFAD8* were identified *in silico*, based in the respective Arabidopsis sequences. Four gRNAs were designed and chosen based on specificity, off-targets and frameshift mutations to allow mutagenesis of the target sequences. Eutrema wild-type Sha were transformed using *Agrobacterium*-mediated floral dip, which revealed the flower development stage to be key for the successful transformation. Six CRISPR transformed T1 lines were identified as potentially edited lines. Despite efforts, the work did not progress with the plant characterisation, however it was shown that a multiplex strategy to genome editing by CRISPR/Cas9 is achievable in Eutrema. A key element to this was the choice of DsRED fluorescence marker for the selection of transformed seeds, which can then be used to simplify the segregation analysis. Improvements to the protocol used were also discussed, in particular increasing the number of transformed plants in an effort to bypass the low germination rates observed. The use of tRNA expression systems to drive simultaneous expression of multiple gRNAs could also be considered (Xie *et al.* 2015). Further improvements and screening are yet required to demonstrate the efficacy of the CRISPR approach. However, the work developed here demonstrates the potential of Eutrema as plant model for abiotic stresses, and of CRISPR approaches as a tool to decrypt stress resilience mechanisms.

Chapter 7.
General Discussion

The work developed during this project addressed the hypothesis that lipid remodelling plays a key role in plant cold acclimation strategies. Plants growing in extreme environmental conditions evolve their tolerance to cold temperatures. However, a complex trait like cold adaption remains a major challenge. To decrypt the role of lipids in low temperature tolerance two model species with contrasting capacities for cold adaption, the extremophile *Eutrema salsugineum* (Eutrema) and *Arabidopsis thaliana* (Arabidopsis), were used to reveal the cold-induced mechanisms that plants use. A summary of the main results obtained in each chapter is shown in Figure 7.1 (colour-coded in relation to each chapter in the top panel). The project comprised the analysis of the cold-induced transcriptomic changes in Arabidopsis, after a three-day period under cold stress conditions at 4°C, from which potential candidate genes were selected. To assess the impact of the candidate genes on the plant health under cold stress their respective T-DNA insertion lines were screened using photochemical performance. The cold screen proposed *AtPES1* and *AtPGR5L1A* to be involved in Arabidopsis cold response, which have also been reported in previous abiotic stress studies (DalCorso *et al.* 2008, Lippold *et al.* 2012). To further analyse the influence of these genes the T-DNA insertion lines *pes1* and *pgr5l1a*, together with *ipcs3*, were subject to a preliminary characterisation of their lipid profiles under control (23°C) and cold stress (4°C) conditions. Analysis involved phenological assessment and targeted lipidome profiling, to ascertain the specific contributions of each gene in the plant's lipid metabolism. PGR5L1A is involved in the cyclic electron flow around PSI, which absence under cold stress caused compositional changes in FFA and TAG. Cold stress also affected TAG, DAG and galactolipid composition in the *PES1* mutant. Finally, IPCS3 as an inositol phosphoryl ceramide synthase, showed a perturbed sphingolipid profile, with a shift in the composition of its ceramide and GIPC profiles.

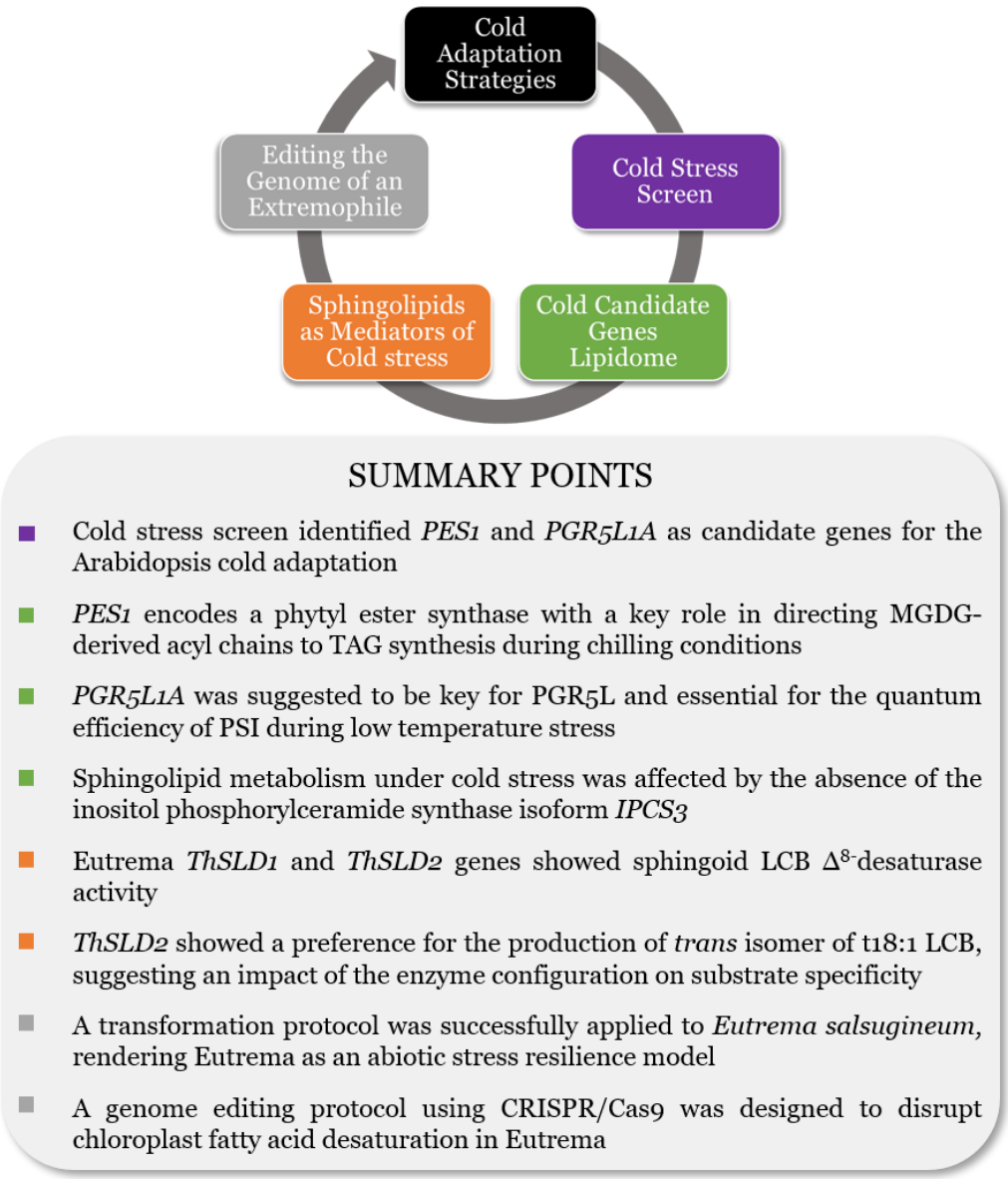

Figure 7.1 Summary of the Results Obtained in this Project

Connection between the chapters developed and the central theme explored (top panel). Main results obtained in each chapter of this project (bottom panel).

Continuing the investigation of the sphingolipid metabolism, the project then focused on the sphingoid LCB Δ^8-desaturase genes, *SLD1* and *SLD2*, previously proposed to be involved in cold acclimation (Chen *et al.* 2012). The identification and characterisation of the Eutrema genes was performed, which revealed a preference of *ThSLD2* to produce t18:1 *trans* isomers resulting in an altered t18:1 *cis*/*trans* ratio with an impact on the GIPC content. Lastly, Eutrema cold adaptation strategy was challenged by editing the chloroplastidial *ThFAD7* and *ThFAD8,* as a

proposed plant model for abiotic studies. To this aim, the germination and transformation protocols were improved, followed by the development of the first reported gene editing protocol using CRISPR/Cas9 in Eutrema. The results obtained were thoroughly discussed within in each section, being presented here as a general discussion into their role in the context of the plant's strategy under abiotic stress conditions.

Throughout this project a parallel strategy has been used to contrast the cold acclimation responses in Arabidopsis with those of Eutrema. Extremophile species provide a unique resource to understand the metabolic mechanisms that enable the transition from temperate to extreme climates (Griffith *et al.* 2007). Adaption to cold climates is crucial and Eutrema sheds light on how complex adaptive traits have evolved in Brassicaceae. Moreover, a greater understanding of these mechanisms provides the foundations for the development of climate-smart staple crops for agriculture (Acuna-Rodriguez *et al.* 2019). Research into the role of lipids in adaption to cold temperatures has largely focused on increasing membrane lipid unsaturation, chain shortening and alterations in the lipid class composition. However, the availability of improved analytical capacity, molecular tools and diverse genetic resources, has enabled researchers to move beyond structural responses and examine more diverse metabolic responses. Despite reports on the ability of Eutrema to withstand cold and freezing temperatures, its underlying mechanisms are still unclear. Eutrema can be viewed as a powerful tool and a bridge between Arabidopsis with reduced range of resistance to stressful environment conditions, and extreme cases such as resurrection plants, e.g. *Haberlea rhodopensis* (Benina *et al.* 2013). Despite being sequenced (Wang *et al.* 2004) and its close relationship with Arabidopsis (Beilstein *et al.* 2008), its morphology, life cycle and resilience to stress limited its use for research. With the development of the CRISPR/Cas9 protocol in Eutrema reported here (Chapter 6) the possibilities for research into specific lipid pathways becomes attainable. As reported in this work, multiplex CRISPR was used in three targets of the coding sequence of *ThFAD7* and *ThFAD8*, disrupting the production

of trienoic acids essential for the plants adaptation to temperature fluctuation (Roman *et al.* 2012, Roman *et al.* 2015, Tovuu *et al.* 2016, Wang *et al.* 2017). The relationship between the unsaturated fatty acids and photosynthetic ability under cold stress has been previously discussed in the rice mutant for the *OsFAD8* gene (Tovuu *et al.* 2016). As the homozygous single and double mutated lines for *ThFAD7* and *ThFAD8* in Eutrema would be established, it would be of interest to apply the fluorescence screen used in Chapter 3 to elucidate the impact of impaired trienoic fatty acid production in the photochemical performance of Eutrema, and establish its importance on the extremophile cold acclimation strategies (Mishra *et al.* 2011). Increasing evidence demonstrates the importance of lipid species in the orientation and activity of light harvesting complexes in the thylakoid membrane. Indeed, the specific spatial distribution of MGDG, DGDG and PG in the different regions of the thylakoid must require complex editing and maintenance; undoubtedly these mechanisms have a role in plant adaptation. One of the proposed hypothesis for Eutrema's cold tolerance ability is its highly efficient photosystem (Wong *et al.* 2006, Gao *et al.* 2009). Higher plasticity was found in the ecotype Shandong (used here) in contrast to Yukon (Wong *et al.* 2006, Gao *et al.* 2009, Khanal *et al.* 2017). Alternatively, *Eutrema parvulum* that did not show any damage to F_v/F_m under high salinity by producing reactive oxygen species (ROS), antioxidants, and regulation of the electron transport in the chloroplast (Uzilday *et al.* 2015). *PGR5L1A* is a contributor to the CEF in PSI acting as a photoprotection mechanism, with evidence suggesting a role of the PGR5-PGR5L1 complex in the chilling response of tomato (Wang *et al.* 2017), making *PGR5L1A* a potential candidate to be studied in Eutrema. The analysis of DEGs in Eutrema and Arabidopsis following three days of cold stress showed *PGR5L1A* to be downregulated. This relationship has been seen before in Eutrema (Yukon), where a large percentage of the photosynthetic related transcripts were found to be downregulated under low temperature, whilst the plants still demonstrated a high-tolerance to photoinhibition (Wong *et al.* 2006).

As with *PGR5L1A*, other gene candidates were also found to be differentially expressed in the Eutrema RNA-Seq (Appendix 3), *PES1* (log_2 fold change 2.26), *PGR5L1B* (log_2 fold change -2.08), or *SLD1* (log_2 fold change 0.75) suggesting a commonality with Arabidopsis in its response to cold acclimation. As the Eutrema *SLD* gene sequences were identified and overexpressed in Arabidopsis (Chapter 5) these are also a potential target. The production of a library of mutants targeting the different histidine box motifs found in both *ThSLD1* and *ThSLD2* would aid in the elucidation of the correlation between the enzyme conformation and the production of either *cis* or *trans* isomers. Taking advantage of the extremophile context of Eutrema, the relationship between the perturbed sphingolipid profile and its cold adaptation strategies could be investigated, as so far, no work was found to establish this relationship. Moreover, the demonstrated changes in the sphingolipid profile induced by *ThSLD2* were shown to influence the ability of Arabidopsis to recover from the cold acclimation followed by freezing period faster than its *SLD1* counterpart. This might suggest an involvement in deacclimation, a regulated process that guarantees the recovery and adaption of the plant metabolism to spring, when it resumes flowering (Vyse *et al.* 2019). The rate and control of deacclimation are a key component of this strategy, as a slow or late timing can reduce recovery and jeopardise seed production.

The work presented here considered the role of specific organelles within the cell. PES1, PGR5L1A and the desaturases FAD7 and FAD8 have an active role in the chloroplast metabolism. Whereas investigations into sphingolipid metabolism explored the ER, where cold-induced IPCS3 or the contributions of the LCB Δ^8-desaturase (*SLD1* and *SLD2*) were investigated. The complex glucosylceramides or hydroxyceramides are produced in the ER, whilst GIPCs are produced in the Golgi by the IPCS. The production of GIPC is thought to preferably use trihydroxy desaturated LCB t18:1-containing ceramides, to which the relationship of *cis* and *trans* isomers is thought to play a key role. Typically, the response of specific sub-cellular compartments is not considered, however,

metabolic responses are often defined by compartment specific pathways, therefore a clear understanding of metabolic cold adaption would require sub-cellular resolution.

When taken apart and individually studied, the functional characterisation of genes can lead to the successful identification of key players in the plant's metabolism. In such a way that, through the genetic manipulation of their expression, allows the improvement of crops (Napier *et al.* 2014, Usher *et al.* 2017, Tocher *et al.* 2019). However, such approaches lack the context in which is expressed by the cell and plant, which can in turn result in a biased view of a pathway or acclimation response. The idea of physical interactions amongst enzymes and pathways, also referred as interactome, is one such example. In mammals, the physical interaction between lipid biosynthesis enzymes have been reported (Coleman 2019). In plants, the identification of physical interactions between acyl editing enzymes were found in the oilseed flax (*Linun usitatissimum*). Diacylglycerol acyltransferases were found to interact with PDCT (phosphatidylcholine diacylglycerol choline phosphotransferase) and LPCAT (lysophosphatidylcoline acyltransferase), resulting in the accumulation of polyunsaturated fatty acids from PC to TAG (Xu *et al.* 2019). The interactome view can also be expanded to the network analysis, for which a database in Arabidopsis has been developed (Braun *et al.* 2011). In the context of cold acclimation, this could be a very useful tool, as the environmental cues perceived by the plant activate cold-responsive TF that lead to the up- or down-regulation of expression of genes that contribute to the metabolic changes necessary to survival. Moreover, the straight-forward overexpression of a single activity is unlikely to provide cold-adaption. Rather it is the modulation of a precisely regulated network of activities that enable the complex metabolic adjustment that defines stress adaption. Over recent decades considerable progress has been made in understanding the responses of plants to abiotic stresses and their signal networks in Arabidopsis (Hou *et al.* 2016, Hilker and Schmulling 2019). However, naturally stress resistant plants, such as Eutrema, have the potential to provide new

solutions. Compared to Arabidopsis, Eutrema has undergone extensive genome expansion, increasing the copy number of specific gene families associated with the stress response network. The role of lipids within the metabolic response to abiotic stress is significant and remains to be fully determined. Although understanding the mechanisms and evolution of stress adaptation traits could provide new perspectives on how to engineer other plants to be stress resistant crops, it is still a significant challenge to incorporate these approaches into traditional agricultural crops. Finally, a series of open questions raised from the results obtained in this work were formulated and are presented in Figure 7.2. Whilst the answers might still be unclear, they may also serve as a cue for further work to be developed.

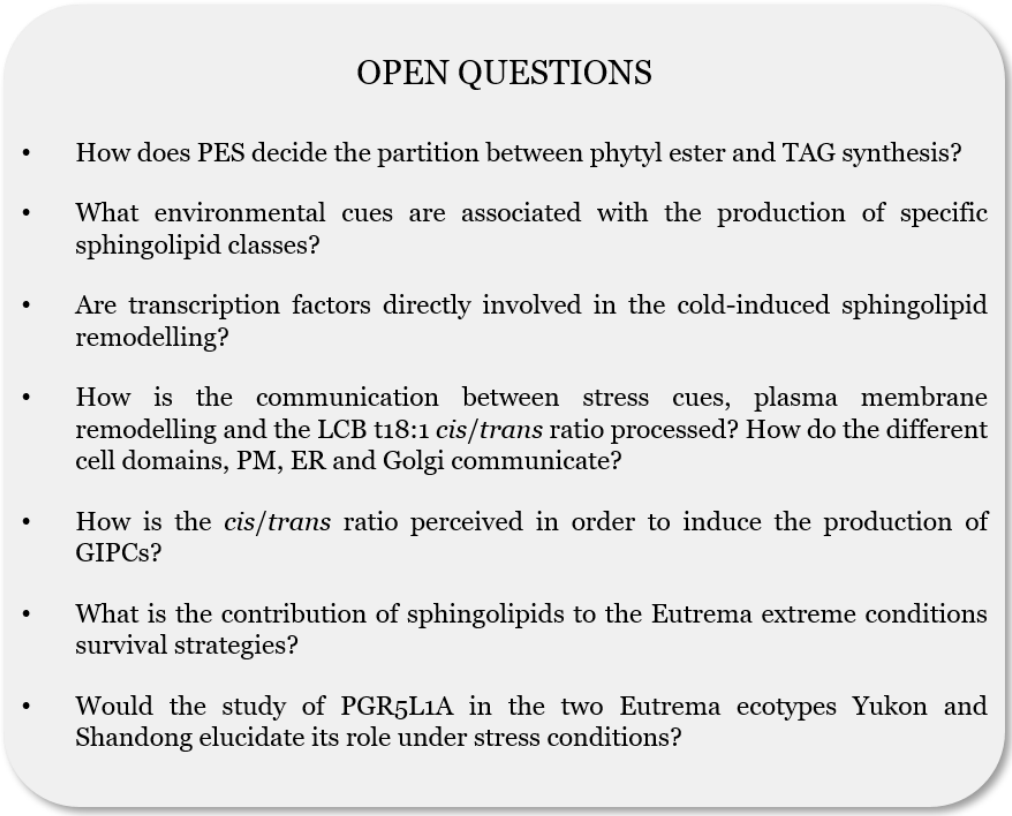

Figure 7.2 Open Questions Following the Work Developed in this Project

References

Acuna-Rodriguez, I. S., H. Hansen, J. Gallardo-Cerda, C. Atala and M. A. Molina-Montenegro (2019). "Antarctic Extremophiles: Biotechnological Alternative to Crop Productivity in Saline Soils." *Frontiers in Bioengineering and Biotechnology* **7**.

Agarwal, M., Y. J. Hao, A. Kapoor, C. H. Dong, H. Fujii, X. W. Zheng and J. K. Zhu (2006). "A R2R3 type MYB transcription factor is involved in the cold regulation of CBF genes and in acquired freezing tolerance." *Journal of Biological Chemistry* **281**(49): 37636-37645.

Akhtar, P., F. Gorfol, G. Garab and P. H. Lambrev (2019). "Dependence of chlorophyll fluorescence quenching on the lipid-to-protein ratio in reconstituted light-harvesting complex II membranes containing lipid labels." *Chemical Physics* **522**: 242-248.

Alcazar, R., J. C. Cuevas, J. Planas, X. Zarza, C. Bortolotti, P. Carrasco, J. Salinas, A. F. Tiburcio and T. Altabella (2011). "Integration of polyamines in the cold acclimation response." *Plant Sci* **180**(1): 31-38.

Ali, U., H. H. Li, X. M. Wang and L. Guo (2018). "Emerging Roles of Sphingolipid Signaling in Plant Response to Biotic and Abiotic Stresses." *Molecular Plant* **11**(11): 1328-1343.

Allen, G. J., J. M. Kwak, S. P. Chu, J. Llopis, R. Y. Tsien, J. F. Harper and J. I. Schroeder (1999). "Cameleon calcium indicator reports cytoplasmic calcium dynamics in Arabidopsis guard cells." *Plant Journal* **19**(6): 735-747.

Alonso, J. M. (2003). "Genome-wide insertional mutagenesis of Arabidopsis thaliana (vol 301, pg 653, 2003)." *Science* **301**(5641): 1849-1849.

Amid, A., A. Lytovchenko, A. R. Fernie, G. Warren and G. J. Thorlby (2012). "The sensitive to freezing3 mutation of Arabidopsis thaliana is a cold-sensitive allele of homomeric acetyl-CoA carboxylase that results in cold-induced cuticle deficiencies." *J Exp Bot* **63**(14): 5289-5299.

Amtmann, A. (2009). "Learning from Evolution: Thellungiella Generates New Knowledge on Essential and Critical Components of Abiotic Stress Tolerance in Plants." *Molecular Plant* **2**(1): 3-12.

Amtmann, A., H. J. Bohnert and R. A. Bressan (2005). "Abiotic stress and plant genome evolution. Search for new models." *Plant Physiology* **138**(1): 127-130.

Andersson, M. X. and P. Dormann (2009). Chloroplast membrane lipid biosynthesis and transport. Berlin, *Heidelberg: Springer*.

Arnon, D. I., M. B. Allen and F. R. Whatley (1954). "Photosynthesis by Isolated Chloroplasts." *Nature* **174**(4426): 394-396.

Artus, N. N., M. Uemura, P. L. Steponkus, S. J. Gilmour, C. T. Lin and M. F. Thomashow (1996). "Constitutive expression of the cold-regulated Arabidopsis thaliana COR15a gene affects both chloroplast and protoplast freezing tolerance." *Proceedings of the National Academy of Sciences of the United States of America* **93**(23): 13404-13409.

Aslan, S., C. X. Sun, S. Leonova, P. Dutta, P. Dormann, F. Domergue, S. Stymne and P. Hofvander (2014). "Wax esters of different compositions produced via engineering of leaf chloroplast metabolism in Nicotiana benthamiana." *Metabolic Engineering* **25**: 103-112.

Aubourg, S., M. Kreis and A. Lecharny (1999). "The DEAD box RNA helicase family in Arabidopsis thaliana." *Nucleic Acids Research* **27**(2): 628-636.

Awai, K., E. Marechal, M. A. Block, D. Brun, T. Masuda, H. Shimada, K. Takamiya, H. Ohta and J. Joyard (2001). "Two types of MGDG synthase genes, found widely in both 16 : 3 and 18 : 3 plants, differentially mediate galactolipid syntheses in photosynthetic and nonphotosynthetic tissues in Arabidopsis thaliana." *Proceedings of the National Academy of Sciences of the United States of America* **98**(19): 10960-10965.

Bae, S., J. Kweon, H. S. Kim and J. S. Kim (2014). "Microhomology-based choice of Cas9 nuclease target sites." *Nature Methods* **11**(7): 705-706.

Baird, G. S., D. A. Zacharias and R. Y. Tsien (2000). "Biochemistry, mutagenesis, and oligomerization of DsRed, a red fluorescent protein from coral." *Proc Natl Acad Sci U S A* **97**(22): 11984-11989.

Bajji, M., J. M. Kinet and S. Lutts (2002). "The use of the electrolyte leakage method for assessing cell membrane stability as a water stress tolerance test in durum wheat." *Plant Growth Regulation* **36**(1): 61-70.

Baker, N. R. and E. Rosenqvist (2004). "Applications of chlorophyll fluorescence can improve crop production strategies: an examination of future possibilities." *Journal of Experimental Botany* **55**(403): 1607-1621.

Baker, S. S., K. S. Wilhelm and M. F. Thomashow (1994). "The 5'-Region of Arabidopsis-Thaliana Cor15a Has Cis-Acting Elements That Confer Cold-Regulated, Drought-Regulated and Aba-Regulated Gene-Expression." *Plant Molecular Biology* **24**(5): 701-713.

Balakrishnan, C. N., Y. C. Lin, S. E. London and D. F. Clayton (2012). "RNA-seq transcriptome analysis of male and female zebra finch cell lines." *Genomics* **100**(6): 363-369.

Barbagallo, R. P., K. Oxborough, K. E. Pallett and N. R. Baker (2003). "Rapid, noninvasive screening for perturbations of metabolism and plant growth using chlorophyll fluorescence imaging." *Plant Physiology* **132**(2): 485-493.

Barbaglia, A. M. and S. Hoffmann-Benning (2016). "Long-Distance Lipid Signaling and its Role in Plant Development and Stress Response." *Subcell Biochem* **86**: 339-361.

Bargmann, B. O. and T. Munnik (2006). "The role of phospholipase D in plant stress responses." *Current Opinion in Plant Biology* **9**(5): 515-522.

Bargmann, B. O. R., A. M. Laxalt, B. ter Riet, B. van Schooten, E. Merquiol, C. Testerink, M. A. Haring, D. Bartels and T. Munnik (2009). "Multiple PLDs Required for High Salinity and Water Deficit Tolerance in Plants." *Plant and Cell Physiology* **50**(1): 78-89.

Barnes, A. C., C. Benning and R. L. Roston (2016). "Chloroplast Membrane Remodeling during Freezing Stress Is Accompanied by Cytoplasmic Acidification Activating SENSITIVE TO FREEZING2." *Plant Physiology* **171**(3): 2140-2149.

Barrero-Sicilia, C., S. Silvestre, R. P. Haslam and L. V. Michaelson (2017). "Lipid remodelling: Unravelling the response to cold stress in Arabidopsis and its extremophile relative Eutrema salsugineum." *Plant Science* **263**: 194-200.

Barthole, G., L. Lepiniec, P. M. Rogowsky and S. Baud (2012). "Controlling lipid accumulation in cereal grains." *Plant Science* **185**: 33-39.

Basu, D., W. D. Wang, S. Y. Ma, T. DeBrosse, E. Poirier, K. Emch, E. Soukup, L. Tian and A. M. Showalter (2015). "Two Hydroxyproline Galactosyltransferases, GALT5 and GALT2, Function in Arabinogalactan-Protein Glycosylation, Growth and Development in Arabidopsis." *Plos One* **10**(5).

Bate, N. J., S. Sivasankar, C. Moxon, J. M. C. Riley, J. E. Thompson and S. J. Rothstein (1998). "Molecular characterization of an Arabidopsis gene

encoding hydroperoxide lyase, a cytochrome P-450 that is wound inducible." *Plant Physiology* **117**(4): 1393-1400.

Baud, S., V. Guyon, J. Kronenberger, S. Wuilleme, M. Miquel, M. Caboche, L. Lepiniec and C. Rochat (2003). "Multifunctional acetyl-CoA carboxylase 1 is essential for very long chain fatty acid elongation and embryo development in Arabidopsis." *Plant Journal* **33**(1): 75-86.

Beilstein, M. A., I. A. Al-Shehbaz, S. Mathews and E. A. Kellogg (2008). "Brassicaceae Phylogeny Inferred from Phytochrome a and Ndhf Sequence Data: Tribes and Trichomes Revisited." *American Journal of Botany* **95**(10): 1307-1327.

Belhaj, K., A. Chaparro-Garcia, S. Kamoun, N. J. Patron and V. Nekrasov (2015). "Editing plant genomes with CRISPR/Cas9." *Curr Opin Biotechnol* **32**: 76-84.

Ben-Yaakov, E., S. Harpaz-Saadi, D. Galili, Y. Eyal and E. Goldschmidt (2006). "The relationship between chlorophyllase activity and chlorophyll degradation during the course of leaf senescence in various plant species." *Israel Journal of Plant Sciences* **54**(2): 129-135.

Benfey, P. N. and N. H. Chua (1990). "The Cauliflower Mosaic Virus-35s Promoter - Combinatorial Regulation of Transcription in Plants." *Science* **250**(4983): 959-966.

Benina, M., T. Obata, N. Mehterov, I. Ivanov, V. Petrov, V. Toneva, A. R. Fernie and T. S. Gechev (2013). "Comparative metabolic profiling of Haberlea rhodopensis, Thellungiella halophyla, and Arabidopsis thaliana exposed to low temperature." *Frontiers in Plant Science* **4**.

Benning, C. (2008). "A role for lipid trafficking in chloroplast biogenesis." *Progress in Lipid Research* **47**(5): 381-389.

Benning, C. (2009). "Mechanisms of Lipid Transport Involved in Organelle Biogenesis in Plant Cells." *Annual Review of Cell and Developmental Biology* **25**: 71-91.

Benning, C. and H. Ohta (2005). "Three enzyme systems for galactoglycerolipid biosynthesis are coordinately regulated in plants." *Journal of Biological Chemistry* **280**(4): 2397-2400.

Bhaya, D., M. Davison and R. Barrangou (2011). "CRISPR-Cas Systems in Bacteria and Archaea: Versatile Small RNAs for Adaptive Defense and Regulation." *Annual Review of Genetics, Vol 45* **45**: 273-297.

Bilger, W. and O. Bjorkman (1990). "Role of the xanthophyll cycle in photoprotection elucidated by measurements of light-induced absorbance changes, fluorescence and photosynthesis in leaves of Hedera canariensis." *Photosynth Res* **25**(3): 173-185.

Bjorkman, O. and B. Demmig (1987). "Photon Yield of O-2 Evolution and Chlorophyll Fluorescence Characteristics at 77-K among Vascular Plants of Diverse Origins." *Planta* **170**(4): 489-504.

Bligh, E. G. and W. J. Dyer (1959). "A Rapid Method of Total Lipid Extraction and Purification." *Canadian Journal of Biochemistry and Physiology* **37**(8): 911-917.

Block, M. A., A. J. Dorne, J. Joyard and R. Douce (1983). "Preparation and Characterization of Membrane-Fractions Enriched in Outer and Inner Envelope Membranes from Spinach-Chloroplasts .2. Biochemical-Characterization." *Journal of Biological Chemistry* **258**(21): 3281-3286.

Bolle, C., G. Huep, N. Kleinbolting, G. Haberer, K. Mayer, D. Leister and B. Weisshaar (2013). "GABI-DUPLO: a collection of double mutants to overcome genetic redundancy in Arabidopsis thaliana." *Plant Journal* **75**(1): 157-171.

Borner, G. H. H., D. J. Sherrier, T. Weimar, L. V. Michaelson, N. D. Hawkins, A. MacAskill, J. A. Napier, M. H. Beale, K. S. Lilley and P. Dupree (2005).

"Analysis of detergent-resistant membranes in Arabidopsis. Evidence for plasma membrane lipid rafts." *Plant Physiology* **137**(1): 104-116.

Bortesi, L. and R. Fischer (2015). "The CRISPR/Cas9 system for plant genome editing and beyond." *Biotechnol Adv* **33**(1): 41-52.

Botella, C., J. Jouhet and M. A. Block (2017). "Importance of phosphatidylcholine on the chloroplast surface." *Progress in Lipid Research* **65**: 12-23.

Boudreault, A. A., D. Cronier, W. Selleck, N. Lacoste, R. T. Utley, S. Allard, J. Savard, W. S. Lane, S. Tan and J. Cote (2003). "Yeast enhancer of polycomb defines global Esa1-dependent acetylation of chromatin." *Genes Dev* **17**(11): 1415-1428.

Bourque, J. E. (1995). "Antisense Strategies for Genetic Manipulations in Plants." *Plant Science* **105**(2): 125-149.

Braun, P., A. R. Carvunis, B. Charloteaux, M. Dreze, J. R. Ecker, D. E. Hill, F. P. Roth, M. Vidal, M. Galli, P. Balumuri, V. Bautista, J. D. Chesnut, R. C. Kim, C. de los Reyes, P. Gilles, C. J. Kim, U. Matrubutham, J. Mirchandani, E. Olivares, S. Patnaik, R. Quan, G. Ramaswamy, P. Shinn, G. M. Swamilingiah, S. Wu, J. R. Ecker, M. Dreze, D. Byrdsong, A. Dricot, M. Duarte, F. Gebreab, B. J. Gutierrez, A. MacWilliams, D. Monachello, M. S. Mukhtar, M. M. Poulin, P. Reichert, V. Romero, S. Tam, S. Waaijers, E. M. Weiner, M. Vidal, D. E. Hill, P. Braun, M. Galli, A. R. Carvunis, M. E. Cusick, M. Dreze, V. Romero, F. P. Roth, M. Tasan, J. Yazaki, P. Braun, J. R. Ecker, A. R. Carvunis, Y. Y. Ahn, A. L. Barabasi, B. Charloteaux, H. M. Chen, M. E. Cusick, J. L. Dangl, M. Dreze, J. R. Ecker, C. Y. Fan, L. T. Gai, M. Galli, G. Ghoshal, T. Hao, D. E. Hill, C. Lurin, T. Milenkovic, J. Moore, M. S. Mukhtar, S. J. Pevzner, N. Przulj, S. Rabello, E. A. Rietman, T. Rolland, F. P. Roth, B. Santhanam, R. J. Schmitz, W. Spooner, J. Stein, M. Tasan, J. Vandenhaute, D. Ware, P. Braun, M. Vidal, P. Braun, A. R. Carvunis, B. Charloteaux, M. Dreze, M. Galli, M. Vidal and A. I. M. Co (2011). "Evidence for Network Evolution in an Arabidopsis Interactome Map." *Science* **333**(6042): 601-607.

Bressan, R. A., C. Q. Zhang, H. Zhang, P. M. Hasegawa, H. J. Bohnert and J. K. Zhu (2001). "Learning from the Arabidopsis experience. The next gene search paradigm." *Plant Physiology* **127**(4): 1354-1360.

Bromley, P. E., Y. O. Li, S. M. Murphy, C. M. Sumner and D. V. Lynch (2003). "Complex sphingolipid synthesis in plants: characterization of inositolphosphorylceramide synthase activity in bean microsomes." *Arch Biochem Biophys* **417**(2): 219-226.

Browse, J., M. Mcconn, D. James and M. Miquel (1993). "Mutants of Arabidopsis Deficient in the Synthesis of Alpha-Linolenate - Biochemical and Genetic-Characterization of the Endoplasmic-Reticulum Linoleoyl Desaturase." *Journal of Biological Chemistry* **268**(22): 16345-16351.

Browse, J., P. Mccourt and C. Somerville (1986). "A Mutant of Arabidopsis Deficient in C18-3 and C16-3 Leaf Lipids." *Plant Physiology* **81**(3): 859-864.

Browse, J., P. Mccourt and C. R. Somerville (1985). "A Mutant of Arabidopsis Lacking a Chloroplast-Specific Lipid." *Science* **227**(4688): 763-765.

Browse, J. and C. Somerville (1991). "Glycerolipid Synthesis - Biochemistry and Regulation." *Annual Review of Plant Physiology and Plant Molecular Biology* **42**: 467-506.

Bruce, T. J. A., M. C. Matthes, J. A. Napier and J. A. Pickett (2007). "Stressful "memories" of plants: Evidence and possible mechanisms." *Plant Science* **173**(6): 603-608.

Bure, C., J. L. Cacas, S. Mongrand and J. M. Schmitter (2014). "Characterization of glycosyl inositol phosphoryl ceramides from plants and fungi by mass spectrometry." *Analytical and Bioanalytical Chemistry* **406**(4): 995-1010.

Bustin, S. and J. Huggett (2017). "qPCR primer design revisited." *Biomolecular Detection and Quantification* **14**: 19-28.

Cacas, J. L., C. Bure, K. Grosjean, P. Gerbeau-Pissot, J. Lherminier, Y. Rombouts, E. Maes, C. Bossard, J. Gronnier, F. Furt, L. Fouillen, V. Germain, E. Bayer, S. Cluzet, F. Robert, J. M. Schmitter, M. Deleu, L. Lins, F. Simon-Plas and S. Mongrand (2016). "Revisiting Plant Plasma Membrane Lipids in Tobacco: A Focus on Sphingolipids." *Plant Physiology* **170**(1): 367-384.

Cacas, J. L., F. Furt, M. Le Guedard, J. M. Schmitter, C. Bure, P. Gerbeau-Pissot, P. Moreau, J. J. Bessoule, F. Simon-Plas and S. Mongrand (2012). "Lipids of plant membrane rafts." *Progress in Lipid Research* **51**(3): 272-299.

Cahoon, E. B. and D. V. Lynch (1991). "Analysis of Glucocerebrosides of Rye (Secale-Cereale L Cv Puma) Leaf and Plasma-Membrane." *Plant Physiology* **95**(1): 58-68.

Calixto, C. P. G., W. B. Guo, A. B. James, N. A. Tzioutziou, J. C. Entizne, P. E. Panter, H. Knight, H. G. Nimmo, R. X. Zhang and J. W. S. Brown (2018). "Rapid and Dynamic Alternative Splicing Impacts the Arabidopsis Cold Response Transcriptome." *Plant Cell* **30**(7): 1424-1444.

Campos, P. S., V. Quartin, J. C. Ramalho and M. A. Nunes (2003). "Electrolyte leakage and lipid degradation account for cold sensitivity in leaves of Coffea sp plants." *Journal of Plant Physiology* **160**(3): 283-292.

Casazza, A. P., S. Rossini, M. G. Rosso and C. Soave (2005). "Mutational and expression analysis of ELIP1 and ELIP2 in Arabidopsis thaliana." *Plant Molecular Biology* **58**(1): 41-51.

Cassagne, C. and R. Lessire (1978). "Biosynthesis of Saturated Very Long-Chain Fatty-Acids by Purified Membrane-Fractions from Leek Epidermal-Cells." *Archives of Biochemistry and Biophysics* **191**(1): 146-152.

Cassagne, C., R. Lessire, J. J. Bessoule, P. Moreau, A. Creach, F. Schneider and B. Sturbois (1994). "Biosynthesis of Very Long-Chain Fatty-Acids in Higher-Plants." *Progress in Lipid Research* **33**(1-2): 55-69.

Cecchini, N. M., K. Steffes, M. R. Schlappi, A. N. Gifford and J. T. Greenberg (2015). "Arabidopsis AZI1 family proteins mediate signal mobilization for systemic defence priming." *Nature Communications* **6**.

Cermak, T., N. J. Baltes, R. Cegan, Y. Zhang and D. F. Voytas (2015). "High-frequency, precise modification of the tomato genome." *Genome Biology* **16**.

Chae, K., C. A. Kieslich, D. Morikis, S. C. Kim and E. M. Lord (2009). "A gain-of-function mutation of Arabidopsis lipid transfer protein 5 disturbs pollen tube tip growth and fertilization." *Plant Cell* **21**(12): 3902-3914.

Chen, B. H., L. A. Gilbert, B. A. Cimini, J. Schnitzbauer, W. Zhang, G. W. Li, J. Park, E. H. Blackburn, J. S. Weissman, L. S. Qi and B. Huang (2013). "Dynamic Imaging of Genomic Loci in Living Human Cells by an Optimized CRISPR/Cas System." *Cell* **155**(7): 1479-1491.

Chen, J. H., H. W. Jiang, E. J. Hsieh, H. Y. Chen, C. T. Chien, H. L. Hsieh and T. P. Lin (2012). "Drought and Salt Stress Tolerance of an Arabidopsis Glutathione S-Transferase U17 Knockout Mutant Are Attributed to the Combined Effect of Glutathione and Abscisic Acid." *Plant Physiology* **158**(1): 340-351.

Chen, M., G. S. Han, C. R. Dietrich, T. M. Dunn and E. B. Cahoon (2006). "The essential nature of sphingolipids in plants as revealed by the functional identification and characterization of the Arabidopsis LCB1 subunit of serine palmitoyltransferase." *Plant Cell* **18**(12): 3576-3593.

Chen, M., J. E. Markham and E. B. Cahoon (2012). "Sphingolipid delta 8 unsaturation is important for glucosylceramide biosynthesis and low-temperature performance in Arabidopsis." *Plant Journal* **69**(5): 769-781.

Chen, M., J. E. Markham, C. R. Dietrich, J. G. Jaworski and E. B. Cahoon (2008). "Sphingolipid long-chain base hydroxylation is important for growth and regulation of sphingolipid content and composition in Arabidopsis." *Plant Cell* **20**(7): 1862-1878.

Chen, M. and J. J. Thelen (2016). "Acyl-lipid desaturase 1 primes cold acclimation response in Arabidopsis." *Physiol Plant* **158**(1): 11-22.

Chen, M. J. and J. J. Thelen (2013). "ACYL-LIPID DESATURASE2 Is Required for Chilling and Freezing Tolerance in Arabidopsis." *Plant Cell* **25**(4): 1430-1444.

Chen, M. X., Z. Wang, Y. N. Zhu, Z. L. Li, N. Hussain, L. J. Xuan, W. L. Guo, G. P. Zhang and L. X. Jiang (2012). "The Effect of TRANSPARENT TESTA2 on Seed Fatty Acid Biosynthesis and Tolerance to Environmental Stresses during Young Seedling Establishment in Arabidopsis." *Plant Physiology* **160**(2): 1023-1036.

Chen, M. X., L. J. Xuan, Z. Wang, L. H. Zhou, Z. L. Li, X. Du, E. Ali, G. P. Zhang and L. X. Jiang (2014). "TRANSPARENT TESTA8 Inhibits Seed Fatty Acid Accumulation by Targeting Several Seed Development Regulators in Arabidopsis." *Plant Physiology* **165**(2): 905-916.

Chen, N. M., B. Song, S. Tang, J. Q. He, Y. J. Zhou, J. C. Feng, S. Shi and X. J. Xu (2018). "Overexpression of the ABC transporter gene TsABCG11 increases cuticle lipids and abiotic stress tolerance in Arabidopsis." *Plant Biotechnology Reports* **12**(5): 303-313.

Chen, Q. F., S. Xiao and M. L. Chye (2008). "Overexpression of the Arabidopsis 10-kilodalton acyl-coenzyme A-binding protein ACBP6 enhances freezing tolerance." *Plant Physiology* **148**(1): 304-315.

Cheng, C. Y., V. Krishnakumar, A. P. Chan, F. Thibaud-Nissen, S. Schobel and C. D. Town (2017). "Araport11: a complete reannotation of the Arabidopsis thaliana reference genome." *Plant J* **89**(4): 789-804.

Cheng, F., J. Wu, L. Fang and X. W. Wang (2012). "Syntenic gene analysis between Brassica rapa and other Brassicaceae species." *Frontiers in Plant Science* **3**.

Chinnusamy, V., M. Ohta, S. Kanrar, B. H. Lee, X. H. Hong, M. Agarwal and J. K. Zhu (2003). "ICE1: a regulator of cold-induced transcriptome and freezing tolerance in Arabidopsis." *Genes & Development* **17**(8): 1043-1054.

Chinnusamy, V., J. K. Zhu and R. Sunkar (2010). "Gene regulation during cold stress acclimation in plants." *Methods Mol Biol* **639**: 39-55.

Clarke, J. E. and G. N. Johnson (2001). "In vivo temperature dependence of cyclic and pseudocyclic electron transport in barley." *Planta* **212**(5-6): 808-816.

Clough, S. J. and A. F. Bent (1998). "Floral dip: a simplified method for Agrobacterium-mediated transformation of Arabidopsis thaliana." *Plant Journal* **16**(6): 735-743.

Coleman, R. A. (2019). "It takes a village: channeling fatty acid metabolism and triacylglycerol formation via protein interactomes." *Journal of Lipid Research* **60**(3): 490-497.

Collakova, E. and D. DellaPenna (2003). "The role of homogentisate phytyltransferase and other tocopherol pathway enzymes in the

regulation of tocopherol synthesis during abiotic stress." *Plant Physiology* **133**(2): 930-940.

Concordet, J. P. and M. Haeussler (2018). "CRISPOR: intuitive guide selection for CRISPR/Cas9 genome editing experiments and screens." *Nucleic Acids Research* **46**(W1): W242-W245.

Cong, L., F. A. Ran, D. Cox, S. L. Lin, R. Barretto, N. Habib, P. D. Hsu, X. B. Wu, W. Y. Jiang, L. A. Marraffini and F. Zhang (2013). "Multiplex Genome Engineering Using CRISPR/Cas Systems." *Science* **339**(6121): 819-823.

Contreras-Lopez, O., T. C. Moyano, D. C. Soto and R. A. Gutierrez (2018). "Step-by-Step Construction of Gene Co-expression Networks from High-Throughput Arabidopsis RNA Sequencing Data." *Methods Mol Biol* **1761**: 275-301.

Coursol, S., L. M. Fan, H. Le Stunff, S. Spiegel, S. Gilroy and S. M. Assmann (2003). "Sphingolipid signalling in Arabidopsis guard cells involves heterotrimeric G proteins." *Nature* **423**(6940): 651-654.

Coursol, S., H. Le Stunff, D. V. Lynch, S. Gilroy, S. M. Assmann and S. Spiegel (2005). "Arabidopsis sphingosine kinase and the effects of phytosphingosine-1-phosphate on stomatal aperture." *Plant Physiol* **137**(2): 724-737.

DalCorso, G., P. Pesaresi, S. Masiero, E. Aseeva, D. S. Nemann, G. Finazzi, P. Joliot, R. Barbato and D. Leister (2008). "A complex containing PGRL1 and PGR5 is involved in the switch between linear and cyclic electron flow in Arabidopsis." *Cell* **132**(2): 273-285.

Danilo, B., L. Perrot, K. Mara, E. Botton, F. Nogue and M. Mazier (2019). "Efficient and transgene-free gene targeting using Agrobacterium-mediated delivery of the CRISPR/Cas9 system in tomato." *Plant Cell Reports* **38**(4): 459-462.

Dassanayake, M., D. H. Oh, J. S. Haas, A. Hernandez, H. Hong, S. Ali, D. J. Yun, R. A. Bressan, J. K. Zhu, H. J. Bohnert and J. M. Cheeseman (2011). "The genome of the extremophile crucifer Thellungiella parvula." *Nature Genetics* **43**(9): 913-U137.

de Freitas, G. P. M., S. Basu, V. Ramegowda, J. Thomas, L. C. Benitez, E. B. Braga and A. Pereira (2019). "Physiological and transcriptional responses to low-temperature stress in rice genotypes at the reproductive stage." *Plant Signaling & Behavior* **14**(4).

De Palma, M., S. Grillo, I. Massarelli, A. Costa, G. Balogh, L. Vigh and A. Leone (2008). "Regulation of desaturase gene expression, changes in membrane lipid composition and freezing tolerance in potato plants." *Molecular Breeding* **21**(1): 15-26.

de Vries, J. and W. Wackernagel (1998). "Detection of nptII (kanamycin resistance) genes in genomes of transgenic plants by marker-rescue transformation." *Mol Gen Genet* **257**(6): 606-613.

Demmig-Adams, B. (1990). "Carotenoids and Photoprotection in Plants - a Role for the Xanthophyll Zeaxanthin." *Biochimica Et Biophysica Acta* **1020**(1): 1-24.

Denic, V. and J. S. Weissman (2007). "A molecular caliper mechanism for determining very long-chain fatty acid length." *Cell* **130**(4): 663-677.

Depicker, A., S. Stachel, P. Dhaese, P. Zambryski and H. M. Goodman (1982). "Nopaline synthase: transcript mapping and DNA sequence." *J Mol Appl Genet* **1**(6): 561-573.

Devaiah, S. P., M. R. Roth, E. Baughman, M. Y. Li, P. Tamura, R. Jeannotte, R. Welti and X. M. Wang (2006). "Quantitative profiling of polar glycerolipid species from organs of wild-type Arabidopsis and a

PHOSPHOLIPASE D alpha 1 knockout mutant." *Phytochemistry* **67**(17): 1907-1924.

DeWald, D. B., J. Torabinejad, C. A. Jones, J. C. Shope, A. R. Cangelosi, J. E. Thompson, G. D. Prestwich and H. Hama (2001). "Rapid accumulation of phosphatidylinositol 4,5-bisphosphate and inositol 1,4,5-trisphosphate correlates with calcium mobilization in salt-stressed Arabidopsis." *Plant Physiology* **126**(2): 759-769.

Dhankher, O. P. and C. H. Foyer (2018). "Climate resilient crops for improving global food security and safety." *Plant Cell and Environment* **41**(5): 877-884.

Di Paolo, G. and P. De Camilli (2006). "Phosphoinositides in cell regulation and membrane dynamics." *Nature* **443**(7112): 651-657.

Djanaguiraman, M., D. L. Boyle, R. Welti, S. V. K. Jagadish and P. V. V. Prasad (2018). "Decreased photosynthetic rate under high temperature in wheat is due to lipid desaturation, oxidation, acylation, and damage of organelles." *Bmc Plant Biology* **18**.

Djanaguiraman, M., P. V. V. Prasad and M. Seppanen (2010). "Selenium protects sorghum leaves from oxidative damage under high temperature stress by enhancing antioxidant defense system." *Plant Physiology and Biochemistry* **48**(12): 999-1007.

Doherty, C. J., H. A. Van Buskirk, S. J. Myers and M. F. Thomashow (2009). "Roles for Arabidopsis CAMTA Transcription Factors in Cold-Regulated Gene Expression and Freezing Tolerance." *Plant Cell* **21**(3): 972-984.

Dominguez, T., M. L. Hernandez, J. C. Pennycooke, P. Jimenez, J. M. Martinez-Rivas, C. Sanz, E. J. Stockinger, J. J. Sanchez-Serrano and M. Sanmartin (2010). "Increasing omega-3 Desaturase Expression in Tomato Results in Altered Aroma Profile and Enhanced Resistance to Cold Stress." *Plant Physiology* **153**(2): 655-665.

Donahue, J. L., S. R. Alford, J. Torabinejad, R. E. Kerwin, A. Nourbakhsh, W. K. Ray, M. Hernick, X. Y. Huang, B. M. Lyons, P. P. Hein and G. E. Gillaspy (2010). "The Arabidopsis thaliana Myo-Inositol 1-Phosphate Synthase1 Gene Is Required for Myo-inositol Synthesis and Suppression of Cell Death." *Plant Cell* **22**(3): 888-903.

Dormann, P. and C. Benning (2002). "Galactolipids rule in seed plants." *Trends in Plant Science* **7**(3): 112-118.

Dorne, A. J., J. Joyard and R. Douce (1990). "Do Thylakoids Really Contain Phosphatidylcholine." *Proceedings of the National Academy of Sciences of the United States of America* **87**(1): 71-74.

Du, Z. Y., B. F. Lucker, K. Zienkiewicz, T. E. Miller, A. Zienkiewicz, B. B. Sears, D. M. Kramer and C. Benning (2018). "Galactoglycerolipid Lipase PGD1 Is Involved in Thylakoid Membrane Remodeling in Response to Adverse Environmental Conditions in Chlamydomonas." *Plant Cell* **30**(2): 447-465.

Du, Z. Y., S. Xiao, Q. F. Chen and M. L. Chye (2010). "Depletion of the membrane-associated acyl-coenzyme A-binding protein ACBP1 enhances the ability of cold acclimation in Arabidopsis." *Plant Physiol* **152**(3): 1585-1597.

Dubos, C., R. Stracke, E. Grotewold, B. Weisshaar, C. Martin and L. Lepiniec (2010). "MYB transcription factors in Arabidopsis." *Trends in Plant Science* **15**(10): 573-581.

Dutilleul, C., G. Benhassaine-Kesri, C. Demandre, N. Reze, A. Launay, S. Pelletier, J. P. Renou, A. Zachowski, E. Baudouin and I. Guillas (2012). "Phytosphingosine-phosphate is a signal for AtMPK6 activation and Arabidopsis response to chilling." *New Phytologist* **194**(1): 181-191.

Dutilleul, C., H. Chavarria, N. Reze, B. Sotta, E. Baudouin and I. Guillas (2015). "Evidence for ACD5 ceramide kinase activity involvement in Arabidopsis response to cold stress." *Plant Cell Environ* **38**(12): 2688-2697.

Eberhard, S., G. Finazzi and F. A. Wollman (2008). "The Dynamics of Photosynthesis." *Annual Review of Genetics* **42**: 463-515.

Ejsing, C. S., E. Duchoslav, J. Sampaio, K. Simons, R. Bonner, C. Thiele, K. Ekroos and A. Shevchenko (2006). "Automated identification and quantification of glycerophospholipid molecular species by multiple precursor ion scanning." *Anal Chem* **78**(17): 6202-6214.

El-Gebali, S., J. Mistry, A. Bateman, S. R. Eddy, A. Luciani, S. C. Potter, M. Qureshi, L. J. Richardson, G. A. Salazar, A. Smart, E. L. L. Sonnhammer, L. Hirsh, L. Paladin, D. Piovesan, S. C. E. Tosatto and R. D. Finn (2019). "The Pfam protein families database in 2019." *Nucleic Acids Research* **47**(D1): D427-D432.

Emanuelsson, O., S. Brunak, G. von Heijne and H. Nielsen (2007). "Locating proteins in the cell using TargetP, SignalP and related tools." *Nature Protocols* **2**(4): 953-971.

Emanuelsson, O., H. Nielsen, S. Brunak and G. von Heijne (2000). "Predicting subcellular localization of proteins based on their N-terminal amino acid sequence." *Journal of Molecular Biology* **300**(4): 1005-1016.

Errampalli, D., D. Patton, L. Castle, L. Mickelson, K. Hansen, J. Schnall, K. Feldmann and D. Meinke (1991). "Embryonic Lethals and T-DNA Insertional Mutagenesis in Arabidopsis." *Plant Cell* **3**(2): 149-157.

Essigmann, B., S. Guler, R. A. Narang, D. Linke and C. Benning (1998). "Phosphate availability affects the thylakoid lipid composition and the expression of SQD1, a gene required for sulfolipid biosynthesis in Arabidopsis thaliana." *Proceedings of the National Academy of Sciences of the United States of America* **95**(4): 1950-1955.

Faergeman, N. J. and J. Knudsen (1997). "Role of long-chain fatty acyl-CoA esters in the regulation of metabolism and in cell signalling." *Biochemical Journal* **323**: 1-12.

Fauser, F., S. Schiml and H. Puchta (2014). "Both CRISPR/Cas-based nucleases and nickases can be used efficiently for genome engineering in Arabidopsis thaliana." *Plant Journal* **79**(2): 348-359.

Fedoroff, N. (2000). "Transposons and genome evolution in plants." *Proceedings of the National Academy of Sciences of the United States of America* **97**(13): 7002-7007.

Feng, Z. Y., Y. F. Mao, N. F. Xu, B. T. Zhang, P. L. Wei, D. L. Yang, Z. Wang, Z. J. Zhang, R. Zheng, L. Yang, L. Zeng, X. D. Liu and J. K. Zhu (2014). "Multigeneration analysis reveals the inheritance, specificity, and patterns of CRISPR/Cas-induced gene modifications in Arabidopsis." *Proceedings of the National Academy of Sciences of the United States of America* **111**(12): 4632-4637.

Fernie, A. R. (2019). "Seeing is believing: the three-way division of labor in the photosynthetic thylakoid membrane." *Plant Journal* **97**(3): 410-411.

Filipowicz, W., T. Kiss, C. Marshallsay and F. Waibel (1990). "U-Snrna Genes, U-Snrnas and U-Snrnps of Higher-Plants." *Molecular Biology Reports* **14**(2-3): 125-129.

Fleming, I. (1967). "Absolute Configuration and Structure of Chlorophyll." *Nature* **216**(5111): 151-&.

Fourrier, N., J. Bedard, E. Lopez-Juez, A. Barbrook, J. Bowyer, P. Jarvis, G. Warren and G. Thorlby (2008). "A role for SENSITIVE TO FREEZING2 in protecting chloroplasts against freeze-induced damage in Arabidopsis." *Plant Journal* **55**(5): 734-745.

Fowler, S. and M. F. Thomashow (2002). "Arabidopsis transcriptome profiling indicates that multiple regulatory pathways are activated during cold acclimation in addition to the CBF cold response pathway." *Plant Cell* **14**(8): 1675-1690.

Fujii, S., K. Kobayashi, N. Nagata, T. Masuda and H. Wada (2018). "Digalactosyldiacylglycerol Is Essential for Organization of the Membrane Structure in Etioplasts." *Plant Physiology* **177**(4): 1487-1497.

Fursova, O. V., G. V. Pogorelko and V. A. Tarasov (2009). "Identification of ICE2, a gene involved in cold acclimation which determines freezing tolerance in Arabidopsis thaliana." *Gene* **429**(1-2): 98-103.

Gaj, T., C. A. Gersbach and C. F. Barbas (2013). "ZFN, TALEN, and CRISPR/Cas-based methods for genome engineering." *Trends in Biotechnology* **31**(7): 397-405.

Gao, F., P. J. Ma, Y. X. Wu, Y. J. Zhou and G. F. Zhang (2019). "Quantitative Proteomic Analysis of the Response to Cold Stress in Jojoba, a Tropical Woody Crop." *International Journal of Molecular Sciences* **20**(2).

Gao, F., Y. Zhou, W. Zhu, X. Li, L. Fan and G. Zhang (2009). "Proteomic analysis of cold stress-responsive proteins in Thellungiella rosette leaves." *Planta* **230**(5): 1033-1046.

Gao, F., Y. J. Zhou, W. P. Zhu, X. F. Li, L. M. Fan and G. F. Zhang (2009). "Proteomic analysis of cold stress-responsive proteins in Thellungiella rosette leaves." *Planta* **230**(5): 1033-1046.

Gao, S., W. Y. Guo, W. Feng, L. Liu, X. R. Song, J. Chen, W. Hou, H. X. Zhu, S. J. Tang and J. Hu (2016). "LTP3 contributes to disease susceptibility in Arabidopsis by enhancing abscisic acid (ABA) biosynthesis." *Molecular Plant Pathology* **17**(3): 412-426.

Gardiner, J. C., J. D. I. Harper, N. D. Weerakoon, D. A. Collings, S. Ritchie, S. Gilroy, R. J. Cyr and J. Marc (2001). "A 90-kD phospholipase D from tobacco binds to microtubules and the plasma membrane." *Plant Cell* **13**(9): 2143-2158.

Gaude, N., C. Brehelin, G. Tischendorf, F. Kessler and P. Dormann (2007). "Nitrogen deficiency in Arabidopsis affects galactolipid composition and gene expression and results in accumulation of fatty acid phytyl esters." *Plant Journal* **49**(4): 729-739.

Gaudet, P., M. S. Livstone, S. E. Lewis and P. D. Thomas (2011). "Phylogenetic-based propagation of functional annotations within the Gene Ontology consortium." *Briefings in Bioinformatics* **12**(5): 449-462.

Gauvrit, C. and P. Gaillardon (1991). "Effect of Low-Temperatures on 2,4-D Behavior in Maize Plants." *Weed Research* **31**(3): 135-142.

Genty, B., J. M. Briantais and N. R. Baker (1989). "The Relationship between the Quantum Yield of Photosynthetic Electron-Transport and Quenching of Chlorophyll Fluorescence." *Biochimica Et Biophysica Acta* **990**(1): 87-92.

Gergov, M., I. Ojanpera and E. Vuori (2003). "Simultaneous screening for 238 drugs in blood by liquid chromatography-ionspray tandem mass spectrometry with multiple-reaction monitoring." *Journal of Chromatography B-Analytical Technologies in the Biomedical and Life Sciences* **795**(1): 41-53.

German, D. A. and M. A. Koch (2017). "Eutrema salsugineum (Cruciferae) new to Mexico: a surprising generic record for the flora of Middle America." *Phytokeys*(76): 13-21.

Gibson, S., V. Arondel, K. Iba and C. Somerville (1994). "Cloning of a Temperature-Regulated Gene Encoding a Chloroplast Omega-3 Desaturase from Arabidopsis-Thaliana." *Plant Physiology* **106**(4): 1615-1621.

Gilmour, S. J., R. K. Hajela and M. F. Thomashow (1988). "Cold Acclimation in Arabidopsis thaliana." *Plant Physiol* **87**(3): 745-750.

Giorgi, F. M., C. Del Fabbro and F. Licausi (2013). "Comparative study of RNA-seq- and Microarray-derived coexpression networks in Arabidopsis thaliana." *Bioinformatics* **29**(6): 717-724.

Gipson, A. B., K. J. Morton, R. J. Rhee, S. Simo, J. A. Clayton, M. E. Perrett, C. G. Binkley, E. L. Jensen, D. L. Oakes, M. F. Rouhier and K. A. Rouhier (2017). "Disruptions in valine degradation affect seed development and germination in Arabidopsis." *Plant Journal* **90**(6): 1029-1039.

Gisler, S., J. P. Goncalves, W. Akhtar, J. de Jong, A. V. Pindyurin, L. F. A. Wessels and M. van Lohuizen (2019). "Multiplexed Cas9 targeting reveals genomic location effects and gRNA-based staggered breaks influencing mutation efficiency." *Nat Commun* **10**(1): 1598.

Gombos, Z., H. Wada and N. Murata (1994). "The Recovery of Photosynthesis from Low-Temperature Photoinhibition Is Accelerated by the Unsaturation of Membrane-Lipids - a Mechanism of Chilling Tolerance." *Proceedings of the National Academy of Sciences of the United States of America* **91**(19): 8787-8791.

Gong, Q., P. Li, S. Ma, S. Indu Rupassara and H. J. Bohnert (2005). "Salinity stress adaptation competence in the extremophile Thellungiella halophila in comparison with its relative Arabidopsis thaliana." *Plant J* **44**(5): 826-839.

Gong, Z. Z., C. H. Dong, H. Lee, J. H. Zhu, L. M. Xiong, D. M. Gong, B. Stevenson and J. K. Zhu (2005). "A DEAD box RNA helicase is essential for mRNA export and important for development and stress responses in Arabidopsis." *Plant Cell* **17**(1): 256-267.

Gong, Z. Z., H. Lee, L. M. Xiong, A. Jagendorf, B. Stevenson and J. K. Zhu (2002). "RNA helicase-like protein as an early regulator of transcription factors for plant chilling and freezing tolerance." *Proceedings of the National Academy of Sciences of the United States of America* **99**(17): 11507-11512.

Gostincar, C., M. Turk and N. Gunde-Cimerman (2010). "The Evolution of Fatty Acid Desaturases and Cytochrome b5 in Eukaryotes." *Journal of Membrane Biology* **233**(1-3): 63-72.

Goubet, F., C. J. Barton, J. C. Mortimer, X. L. Yu, Z. N. Zhang, G. P. Miles, J. Richens, A. H. Liepman, K. Seffen and P. Dupree (2009). "Cell wall glucomannan in Arabidopsis is synthesised by CSLA glycosyltransferases, and influences the progression of embryogenesis." *Plant Journal* **60**(3): 527-538.

Goulas, E., M. Schubert, T. Kieselbach, L. A. Kleczkowski, P. Gardestrom, W. Schroder and V. Hurry (2006). "The chloroplast lumen and stromal proteomes of Arabidopsis thaliana show differential sensitivity to short- and long-term exposure to low temperature." *Plant Journal* **47**(5): 720-734.

Griffith, M., M. Timonin, A. C. Wong, G. R. Gray, S. R. Akhter, M. Saldanha, M. A. Rogers, E. A. Weretilnyk and B. Moffatt (2007). "Thellungiella: an Arabidopsis-related model plant adapted to cold temperatures." *Plant Cell Environ* **30**(5): 529-538.

Gronenborn, B., R. C. Gardner, S. Schaefer and R. J. Shepherd (1981). "Propagation of Foreign DNA in Plants Using Cauliflower Mosaic-Virus as Vector." *Nature* **294**(5843): 773-776.

Gronnier, J., V. Germain, P. Gouguet, J. L. Cacas and S. Mongrand (2016). "GIPC: Glycosyl Inositol Phospho Ceramides, the major sphingolipids on earth." *Plant Signal Behav* **11**(4): e1152438.

Gu, Y., L. He, C. Zhao, F. Wang, B. Yan, Y. Gao, Z. Li, K. Yang and J. Xu (2017). "Biochemical and Transcriptional Regulation of Membrane Lipid Metabolism in Maize Leaves under Low Temperature." *Front Plant Sci* **8**: 2053.

Guillas, I., A. Guellim, N. Reze and E. Baudouin (2013). "Long chain base changes triggered by a short exposure of Arabidopsis to low temperature are altered by AHb1 non-symbiotic haemoglobin overexpression." *Plant Physiology and Biochemistry* **63**: 191-195.

Guo, L., G. Mishra, K. Taylor and X. Wang (2011). "Phosphatidic acid binds and stimulates Arabidopsis sphingosine kinases." *J Biol Chem* **286**(15): 13336-13345.

Guo, L., H. B. Yang, X. Y. Zhang and S. H. Yang (2013). "Lipid transfer protein 3 as a target of MYB96 mediates freezing and drought stress in Arabidopsis." *Journal of Experimental Botany* **64**(6): 1755-1767.

Guo, Y., L. Xiong, M. Ishitani and J. K. Zhu (2002). "An Arabidopsis mutation in translation elongation factor 2 causes superinduction of CBF/DREB1 transcription factor genes but blocks the induction of their downstream targets under low temperatures." *Proceedings of the National Academy of Sciences of the United States of America* **99**(11): 7786-7791.

Gutbrod, K., J. Romer and P. Dormann (2019). "Phytol metabolism in plants." *Progress in Lipid Research* **74**: 1-17.

Guy, C., F. Kaplan, J. Kopka, J. Selbig and D. K. Hincha (2008). "Metabolomics of temperature stress." *Physiologia Plantarum* **132**(2): 220-235.

Habel, A., P. Sperling, S. Bartram, E. Heinz and W. Boland (2010). "Conformational Studies on the Delta(8)(E,Z)-Sphingolipid Desaturase from Helianthus annuus with Chiral Fluoropalmitic Acids As Mechanistic Probes." *Journal of Organic Chemistry* **75**(15): 4975-4982.

Haeussler, M., K. Schonig, H. Eckert, A. Eschstruth, J. Mianne, J. B. Renaud, S. Schneider-Maunoury, A. Shkumatava, L. Teboul, J. Kent, J. S. Joly and J. P. Concordet (2016). "Evaluation of off-target and on-target scoring algorithms and integration into the guide RNA selection tool CRISPOR." *Genome Biology* **17**.

Hahn, F., O. Mantegazza, A. Greiner, P. Hegemann, M. Eisenhut and A. P. M. Weber (2017). "An Efficient Visual Screen for CRISPR/Cas9 Activity in Arabidopsis thaliana." *Frontiers in Plant Science* **8**.

Hanada, K. and M. Nishijima (2003). "Purification of mammalian serine palmitoyltransferase, a hetero-subunit enzyme for sphingolipid biosynthesis, by affinity-peptide chromatography." *Methods Mol Biol* **228**: 163-174.

Harris, M. A., J. Clark, A. Ireland, J. Lomax, M. Ashburner, R. Foulger, K. Eilbeck, S. Lewis, B. Marshall, C. Mungall, J. Richter, G. M. Rubin, J. A. Blake, C. Bult, M. Dolan, H. Drabkin, J. T. Eppig, D. P. Hill, L. Ni, M. Ringwald, R. Balakrishnan, J. M. Cherry, K. R. Christie, M. C. Costanzo, S. S. Dwight, S. Engel, D. G. Fisk, J. E. Hirschman, E. L. Hong, R. S. Nash, A. Sethuraman, C. L. Theesfeld, D. Botstein, K. Dolinski, B. Feierbach, T. Berardini, S. Mundodi, S. Y. Rhee, R. Apweiler, D. Barrell, E. Camon, E. Dimmer, V. Lee, R. Chisholm, P. Gaudet, W. Kibbe, R. Kishore, E. M. Schwarz, P. Sternberg, M. Gwinn, L. Hannick, J. Wortman, M. Berriman, V. Wood, N. de la Cruz, P. Tonellato, P. Jaiswal, T. Seigfried, R. White and G. O. Consortium (2004). "The Gene Ontology (GO) database and informatics resource." *Nucleic Acids Research* **32**: D258-D261.

Harris, M. A., J. I. Clark, A. Ireland, J. Lomax, M. Ashburner, R. Collins, K. Eilbeck, S. Lewis, C. Mungall, J. Richter, G. M. Rubin, S. Q. Shu, J. A. Blake, C. J. Bult, A. D. Diehl, M. E. Dolan, H. J. Drabkin, J. T. Eppig, D.

P. Hill, L. Ni, M. Ringwald, R. Balakrishnan, G. Binkley, J. M. Cherry, K. R. Christie, M. C. Costanzo, Q. Dong, S. R. Engel, D. G. Fisk, J. E. Hirschman, B. C. Hitz, E. L. Hong, C. Lane, S. Miyasato, R. Nash, A. Sethuraman, M. Skrzypek, C. L. Theesfeld, S. A. Weng, D. Botstein, K. Dolinski, R. Oughtred, T. Berardini, S. Mundodi, S. Y. Rhee, R. Apweiler, D. Barrell, E. Camon, E. Dimmer, N. Mulder, R. Chisholm, P. Fey, P. Gaudet, W. Kibbe, K. Pilcher, C. A. Bastiani, R. Kishore, E. M. Schwarz, P. Sternberg, K. Van Auken, M. Gwinn, L. Hannick, J. Wortman, M. Aslett, M. Berriman, V. Wood, S. Bromberg, C. Foote, H. Jacob, D. Pasko, V. Petri, D. Reilly, K. Seiler, M. Shimoyama, J. Smith, S. Twigger, P. Jaiswal, T. Seigfried, C. Collmer, D. Howe and M. Westerfield (2006). "The Gene Ontology (GO) project in 2006." *Nucleic Acids Research* **34**: D322-D326.

Harrison, S. J., E. K. Mott, K. Parsley, S. Aspinall, J. C. Gray and A. Cottage (2006). "A rapid and robust method of identifying transformed Arabidopsis thaliana seedlings following floral dip transformation." *Plant Methods* **2**.

Harwood, J. L. (1996). "Recent advances in the biosynthesis of plant fatty acids." *Biochimica Et Biophysica Acta-Lipids and Lipid Metabolism* **1301**(1-2): 7-56.

Hashimoto, K., A. C. Yoshizawa, S. Okuda, K. Kuma, S. Goto and M. Kanehisa (2008). "The repertoire of desaturases and elongases reveals fatty acid variations in 56 eukaryotic genomes." *Journal of Lipid Research* **49**(1): 183-191.

Haslam, T. M. and L. Kunst (2013). "Extending the story of very-long-chain fatty acid elongation." *Plant Science* **210**: 93-107.

He, Y. H., H. L. Yan, W. P. Hua, Y. Y. Huang and Z. Z. Wang (2016). "Selection and Validation of Reference Genes for Quantitative Real-time PCR in Gentiana macrophylla." *Frontiers in Plant Science* **7**.

Hendry, G. A. F., J. D. Houghton and S. B. Brown (1987). "Tansley Review No-11 - the Degradation of Chlorophyll - a Biological Enigma." *New Phytologist* **107**(2): 255-302.

Hertle, A. P., T. Blunder, T. Wunder, P. Pesaresi, M. Pribil, U. Armbruster and D. Leister (2013). "PGRL1 Is the Elusive Ferredoxin-Plastoquinone Reductase in Photosynthetic Cyclic Electron Flow." *Molecular Cell* **49**(3): 511-523.

Hietala, T., N. Mozes, M. J. Genet, H. Rosenqvist and S. Laakso (1997). "Surface lipids and their distribution on willow (Salix) leaves: A combined chemical, morphological and physicochemical study." *Colloids and Surfaces B-Biointerfaces* **8**(4-5): 205-215.

Higashi, Y. and K. Saito (2019). "Lipidomic studies of membrane glycerolipids in plant leaves under heat stress." *Progress in Lipid Research* **75**.

Hilker, M. and T. Schmulling (2019). "Stress priming, memory, and signalling in plants." *Plant Cell and Environment* **42**(3): 753-761.

Hincha, D. K. and E. Zuther (2014). "Plant cold acclimation and freezing tolerance." *Methods Mol Biol* **1166**: 1-6.

Hittinger, C. T. and S. B. Carroll (2007). "Gene duplication and the adaptive evolution of a classic genetic switch." *Nature* **449**(7163): 677-U671.

Hnilickova, H., F. Hnilicka, M. Orsak and V. Hejnak (2019). "Effect of salt stress on growth, electrolyte leakage, Na+ and K+ content in selected plant species." *Plant Soil and Environment* **65**(2): 90-96.

Holzl, G. and P. Dormann (2019). "Chloroplast Lipids and Their Biosynthesis." *Annual Review of Plant Biology, Vol 70* **70**: 51-81.

Hortensteiner, S. (2006). "Chlorophyll degradation during senescence." *Annual Review of Plant Biology* **57**: 55-77.

Horton, P., A. V. Ruban and R. G. Walters (1994). "Regulation of Light-Harvesting in Green Plants - Indication by Nonphotochemical Quenching of Chlorophyll Fluorescence." *Plant Physiology* **106**(2): 415-420.

Horton, P., A. V. Ruban and R. G. Walters (1996). "Regulation of light harvesting in green plants." *Annual Review of Plant Physiology and Plant Molecular Biology* **47**: 655-684.

Hou, Q., G. Ufer and D. Bartels (2016). "Lipid signalling in plant responses to abiotic stress." *Plant Cell Environ* **39**(5): 1029-1048.

Hsu, P. D., D. A. Scott, J. A. Weinstein, F. A. Ran, S. Konermann, V. Agarwala, Y. Q. Li, E. J. Fine, X. B. Wu, O. Shalem, T. J. Cradick, L. A. Marraffini, G. Bao and F. Zhang (2013). "DNA targeting specificity of RNA-guided Cas9 nucleases." *Nature Biotechnology* **31**(9): 827-+.

Huby, E., J. A. Napier, F. Baillieul, L. V. Michaelson and S. Dhondt-Cordelier (2019). "Sphingolipids: towards an integrated view of metabolism during the plant stress response." *New Phytologist*.

Hunkapiller, T., R. J. Kaiser, B. F. Koop and L. Hood (1991). "Large-scale and automated DNA sequence determination." *Science* **254**(5028): 59-67.

Hurlock, A. K., R. L. Roston, K. Wang and C. Benning (2014). "Lipid Trafficking in Plant Cells." *Traffic* **15**(9): 915-932.

Imai, H., Y. Morimoto and K. Tamura (2000). "Sphingoid base composition of monoglucosylceramide in Brassicaceae." *Journal of Plant Physiology* **157**(4): 453-456.

Imai, H., M. Ohnishi, K. Hotsubo, M. Kojima and S. Ito (1997). "Sphingoid base composition of cerebrosides from plant leaves." *Bioscience Biotechnology and Biochemistry* **61**(2): 351-353.

Imai, H., M. Ohnishi, M. Kinoshita, M. Kojima and S. Ito (1995). "Structure and Distribution of Cerebroside Containing Unsaturated Hydroxy Fatty-Acids in Plant-Leaves." *Bioscience Biotechnology and Biochemistry* **59**(7): 1309-1313.

Imai, H., K. Yamamoto, A. Shibahara, S. Miyatani and T. Nakayama (2000). "Determining double-bond positions in monoenoic 2-hydroxy fatty acids of glucosylceramides by gas chromatography-mass spectrometry." *Lipids* **35**(2): 233-236.

Inan, G., Q. Zhang, P. H. Li, Z. L. Wang, Z. Y. Cao, H. Zhang, C. Q. Zhang, T. M. Quist, S. M. Goodwin, J. H. Zhu, H. H. Shi, B. Damsz, T. Charbaji, Q. Q. Gong, S. S. Ma, M. Fredricksen, D. W. Galbraith, M. A. Jenks, D. Rhodes, P. M. Hasegawa, H. J. Bohnert, R. J. Joly, R. A. Bressan and J. K. Zhu (2004). "Salt cress. A halophyte and cryophyte Arabidopsis relative model system and its applicability to molecular genetic analyses of growth and development of extremophiles." *Plant Physiology* **135**(3): 1718-1737.

Ischebeck, T., A. M. Zbierzak, M. Kanwischer and P. Dormann (2006). "A salvage pathway for phytol metabolism in Arabidopsis." *Journal of Biological Chemistry* **281**(5): 2470-2477.

Ishitani, M., L. Xiong, H. Lee, B. Stevenson and J. K. Zhu (1998). "HOS1, a genetic locus involved in cold-responsive gene expression in arabidopsis." *Plant Cell* **10**(7): 1151-1161.

Jach, G., E. Binot, S. Frings, K. Luxa and J. Schell (2001). "Use of red fluorescent protein from Discosoma sp (dsRED) as a reporter for plant gene expression." *Plant Journal* **28**(4): 483-491.

Jaglo-Ottosen, K. R., S. J. Gilmour, D. G. Zarka, O. Schabenberger and M. F. Thomashow (1998). "Arabidopsis CBF1 overexpression induces COR genes and enhances freezing tolerance." *Science* **280**(5360): 104-106.

Janska, A., P. Marsik, S. Zelenkova and J. Ovesna (2010). "Cold stress and acclimation - what is important for metabolic adjustment?" *Plant Biol (Stuttg)* **12**(3): 395-405.

Jarvis, P., P. Dormann, C. A. Peto, J. Lutes, C. Benning and J. Chory (2000). "Galactolipid deficiency and abnormal chloroplast development in the Arabidopsis MGD synthase 1 mutant." *Proceedings of the National Academy of Sciences of the United States of America* **97**(14): 8175-8179.

Jaworski, J. G., R. C. Clough, S. R. Barnum, D. Postbeittenmiller and J. B. Ohlrogge (1990). "Initial Reactions of Fatty-Acid Synthesis and Their Regulation." *Plant Lipid Biochemistry, Structure and Utilization*: 97-104.

Jiang, W. Z., I. M. Henry, P. G. Lynagh, L. Comai, E. B. Cahoon and D. P. Weeks (2017). "Significant enhancement of fatty acid composition in seeds of the allohexaploid, Camelina sativa, using CRISPR/Cas9 gene editing." *Plant Biotechnology Journal* **15**(5): 648-657.

Jiang, W. Z., B. Yang and D. P. Weeks (2014). "Efficient CRISPR/Cas9-Mediated Gene Editing in Arabidopsis thaliana and Inheritance of Modified Genes in the T2 and T3 Generations." *Plos One* **9**(6).

Jinek, M., K. Chylinski, I. Fonfara, M. Hauer, J. A. Doudna and E. Charpentier (2012). "A Programmable Dual-RNA-Guided DNA Endonuclease in Adaptive Bacterial Immunity." *Science* **337**(6096): 816-821.

Joet, T., L. Cournac, G. Peltier and M. Havaux (2002). "Cyclic electron flow around photosystem I in C(3) plants. In vivo control by the redox state of chloroplasts and involvement of the NADH-dehydrogenase complex." *Plant Physiol* **128**(2): 760-769.

Johnova, P., J. Skalak, I. Saiz-Fernandez and B. Brzobohaty (2016). "Plant responses to ambient temperature fluctuations and water-limiting conditions: A proteome-wide perspective." *Biochimica Et Biophysica Acta-Proteins and Proteomics* **1864**(8): 916-931.

Johnson, G. N. (2011). "Physiology of PSI cyclic electron transport in higher plants." *Biochimica Et Biophysica Acta-Bioenergetics* **1807**(3): 384-389.

Joseph, J. T., N. J. Poolakkalody and J. M. Shah (2018). "Plant reference genes for development and stress response studies." *Journal of Biosciences* **43**(1): 173-187.

Jung, H. W., T. J. Tschaplinski, L. Wang, J. Glazebrook and J. T. Greenberg (2009). "Priming in Systemic Plant Immunity." *Science* **324**(5923): 89-91.

Kasuga, M., Q. Liu, S. Miura, K. Yamaguchi-Shinozaki and K. Shinozaki (1999). "Improving plant drought, salt, and freezing tolerance by gene transfer of a single stress-inducible transcription factor." *Nature Biotechnology* **17**(3): 287-291.

Kaur, H., L. Wang, N. Stawniak, R. Sloan, H. van Erp, P. Eastmond and I. Bancroft (2019). "The impact of reducing fatty acid desaturation on the composition and thermal stability of rapeseed oil." *Plant Biotechnol J*.

Kawaguchi, M., H. Imai, M. Naoe, Y. Yasui and M. Ohnishi (2000). "Cerebrosides in grapevine leaves: Distinct composition of sphingoid bases among the grapevine species having different tolerances to freezing temperature." *Bioscience Biotechnology and Biochemistry* **64**(6): 1271-1273.

Kelly, A. A., J. E. Froehlich and P. Dormann (2003). "Disruption of the two digalactosyldiacylglycerol synthase genes DGD1 and DGD2 in Arabidopsis reveals the existence of an additional enzyme of galactolipid synthesis." *Plant Cell* **15**(11): 2694-2706.

Kelly, A. A., B. Kalisch, G. Holzl, S. Schulze, J. Thiele, M. Melzer, R. L. Roston, C. Benning and P. Dormann (2016). "Synthesis and transfer of

galactolipids in the chloroplast envelope membranes of Arabidopsis thaliana." *Proceedings of the National Academy of Sciences of the United States of America* **113**(38): 10714-10719.

Khanal, N., G. E. Bray, A. Grisnich, B. A. Moffatt and G. R. Gray (2017). "Differential Mechanisms of Photosynthetic Acclimation to Light and Low Temperature in Arabidopsis and the Extremophile Eutrema salsugineum." *Plants (Basel)* **6**(3).

Khanal, N., B. A. Moffatt and G. R. Gray (2015). "Acquisition of freezing tolerance in Arabidopsis and two contrasting ecotypes of the extremophile Eutrema salsugineum (Thellungiella salsuginea)." *J Plant Physiol* **180**: 35-44.

Khodakovskaya, M., R. McAvoy, J. Peters, H. Wu and Y. Li (2006). "Enhanced cold tolerance in transgenic tobacco expressing a chloroplast omega-3 fatty acid desaturase gene under the control of a cold-inducible promoter." *Planta* **223**(5): 1090-1100.

Kim, H. and J. S. Kim (2014). "A guide to genome engineering with programmable nucleases." *Nature Reviews Genetics* **15**(5): 321-334.

Kim, Y., K. S. Schumaker and J. K. Zhu (2006). "EMS mutagenesis of Arabidopsis." *Methods Mol Biol* **323**: 101-103.

Kim, Y. G., J. Cha and S. Chandrasegaran (1996). "Hybrid restriction enzymes: zinc finger fusions to Fok I cleavage domain." *Proc Natl Acad Sci U S A* **93**(3): 1156-1160.

Kim, Y. O. and H. Kang (2006). "The role of a zinc finger-containing glycine-rich RNA-binding protein during the cold adaptation process in Arabidopsis thaliana." *Plant Cell Physiol* **47**(6): 793-798.

Kim, Y. O., J. S. Kim and H. Kang (2005). "Cold-inducible zinc finger-containing glycine-rich RNA-binding protein contributes to the enhancement of freezing tolerance in Arabidopsis thaliana." *Plant J* **42**(6): 890-900.

Kleinboelting, N., G. Huep, A. Kloetgen, P. Viehoever and B. Weisshaar (2012). "GABI-Kat SimpleSearch: new features of the Arabidopsis thaliana T-DNA mutant database." *Nucleic Acids Research* **40**(D1): D1211-D1215.

Klimyuk, V. I., B. J. Carroll, C. M. Thomas and J. D. G. Jones (1993). "Alkali Treatment for Rapid Preparation of Plant-Material for Reliable Pcr Analysis." *Plant Journal* **3**(3): 493-494.

Knight, H., S. G. Mugford, B. Ulker, D. H. Gao, G. Thorlby and M. R. Knight (2009). "Identification of SFR6, a key component in cold acclimation acting post-translationally on CBF function." *Plant Journal* **58**(1): 97-108.

Kobayashi, K. (2016). "Role of membrane glycerolipids in photosynthesis, thylakoid biogenesis and chloroplast development." *Journal of Plant Research* **129**(4): 565-580.

Koch, M. A. and D. A. German (2013). "Taxonomy and systematics are key to biological information: Arabidopsis, Eutrema (Thellungiella), Noccaea and Schrenkiella (Brassicaceae) as examples." *Front Plant Sci* **4**: 267.

Kodama, H., T. Hamada, G. Horiguchi, M. Nishimura and K. Iba (1994). "Genetic Enhancement of Cold Tolerance by Expression of a Gene for Chloroplast Omega-3-Fatty-Acid Desaturase in Transgenic Tobacco." *Plant Physiology* **105**(2): 601-605.

Konig, S., K. Feussner, M. Schwarz, A. Kaever, T. Iven, M. Landesfeind, P. Ternes, P. Karlovsky, V. Lipka and I. Feussner (2012). "Arabidopsis mutants of sphingolipid fatty acid alpha-hydroxylases accumulate ceramides and salicylates." *New Phytologist* **196**(4): 1086-1097.

Koochak, H., S. Puthiyaveetil, D. L. Mullendore, M. Li and H. Kirchhoff (2019). "The structural and functional domains of plant thylakoid membranes." *Plant Journal* **97**(3): 412-429.

Krank, J., R. C. Murphy, R. M. Barkley, E. Duchoslav and A. McAnoy (2007). "Qualitative analysis and quantitative assessment of changes in neutral glycerol lipid molecular species within cells." *Lipidomics and Bioactive Lipids: Mass-Spectrometry-Based Lipid Analysis* **432**: 1-20.

Kreps, J. A., Y. Wu, H. S. Chang, T. Zhu, X. Wang and J. F. Harper (2002). "Transcriptome changes for Arabidopsis in response to salt, osmotic, and cold stress." *Plant Physiol* **130**(4): 2129-2141.

Kreyling, J., S. Schmid and G. Aas (2015). "Cold tolerance of tree species is related to the climate of their native ranges." *Journal of Biogeography* **42**(1): 156-166.

Kunst, L., J. Browse and C. Somerville (1989). "A Mutant of Arabidopsis Deficient in Desaturation of Palmitic Acid in Leaf Lipids." *Plant Physiology* **90**(3): 943-947.

Lamesch, P., T. Z. Berardini, D. H. Li, D. Swarbreck, C. Wilks, R. Sasidharan, R. Muller, K. Dreher, D. L. Alexander, M. Garcia-Hernandez, A. S. Karthikeyan, C. H. Lee, W. D. Nelson, L. Ploetz, S. Singh, A. Wensel and E. Huala (2012). "The Arabidopsis Information Resource (TAIR): improved gene annotation and new tools." *Nucleic Acids Research* **40**(D1): D1202-D1210.

Lang, V., E. Mantyla, B. Welin, B. Sundberg and E. T. Palva (1994). "Alterations in Water Status, Endogenous Abscisic-Acid Content, and Expression of Rab18 Gene during the Development of Freezing Tolerance in Arabidopsis-Thaliana." *Plant Physiology* **104**(4): 1341-1349.

Larson, T. R. and I. A. Graham (2001). "Technical Advance: a novel technique for the sensitive quantification of acyl CoA esters from plant tissues." *Plant J* **25**(1): 115-125.

Lazo, G. R., P. A. Stein and R. A. Ludwig (1991). "A DNA Transformation-Competent Arabidopsis Genomic Library in Agrobacterium." *Bio-Technology* **9**(10): 963-967.

Le, M. Q., M. Pagter and D. K. Hincha (2015). "Global changes in gene expression, assayed by microarray hybridization and quantitative RT-PCR, during acclimation of three Arabidopsis thaliana accessions to sub-zero temperatures after cold acclimation." *Plant Mol Biol* **87**(1-2): 1-15.

Lee, B. H., D. A. Henderson and J. K. Zhu (2005). "The Arabidopsis cold-responsive transcriptome and its regulation by ICE1." *Plant Cell* **17**(11): 3155-3175.

Lee, H., Y. Guo, M. Ohta, L. Xiong, B. Stevenson and J. K. Zhu (2002). "LOS2, a genetic locus required for cold-responsive gene transcription encodes a bi-functional enolase." *EMBO J* **21**(11): 2692-2702.

Lee, H. J., L. M. Xiong, Z. Z. Gong, M. Ishitani, B. Stevenson and J. K. Zhu (2001). "The Arabidopsis HOS1 gene negatively regulates cold signal transduction and encodes a RING finger protein that displays cold-regulated nucleo-cytoplasmic partitioning." *Genes & Development* **15**(7): 912-924.

Lee, J., R. Welti, W. T. Schapaugh and H. N. Trick (2011). "Phospholipid and triacylglycerol profiles modified by PLD suppression in soybean seed." *Plant Biotechnology Journal* **9**(3): 359-372.

Lee, Y. P., A. Babakov, B. de Boer, E. Zuther and D. K. Hincha (2012). "Comparison of freezing tolerance, compatible solutes and polyamines in geographically diverse collections of Thellungiella sp. and Arabidopsis thaliana accessions." *Bmc Plant Biology* **12**.

Lee, Y. P., C. Funk, A. Erban, J. Kopka, K. I. Kohl, E. Zuther and D. K. Hincha (2016). "Salt stress responses in a geographically diverse collection of

Eutrema/Thellungiella spp. accessions." *Functional Plant Biology* **43**(7): 590-606.

Lee, Y. P., F. M. Giorgi, M. Lohse, K. Kvederaviciute, S. Klages, B. Usadel, I. Meskiene, R. Reinhardt and D. K. Hincha (2013). "Transcriptome sequencing and microarray design for functional genomics in the extremophile Arabidopsis relative Thellungiella salsuginea (Eutrema salsugineum)." *Bmc Genomics* **14**.

Lee, Y. S., Y. B. Choi, S. Suh, J. Lee, S. M. Assmann, C. O. Joe, J. F. Kelleher and R. C. Crain (1996). "Abscisic acid-induced phosphoinositide turnover in guard cell protoplasts of Vicia faba." *Plant Physiology* **110**(3): 987-996.

Lessire, R., H. Juguelin, P. Moreau and C. Cassagne (1985). "Nature of the Reaction-Product of [1-C-14] Stearoyl-Coa Elongation by Etiolated Leek Seedling Microsomes." *Archives of Biochemistry and Biophysics* **239**(1): 260-269.

Letunic, I. and P. Bork (2018). "20 years of the SMART protein domain annotation resource." *Nucleic Acids Research* **46**(D1): D493-D496.

Li-Beisson, Y., B. Shorrosh, F. Beisson, M. X. Andersson, V. Arondel, P. D. Bates, S. Baud, D. Bird, A. Debono, T. P. Durrett, R. B. Franke, I. A. Graham, K. Katayama, A. A. Kelly, T. Larson, J. E. Markham, M. Miquel, I. Molina, I. Nishida, O. Rowland, L. Samuels, K. M. Schmid, H. Wada, R. Welti, C. Xu, R. Zallot and J. Ohlrogge (2013). "Acyl-lipid metabolism." *Arabidopsis Book* **11**: e0161.

Li, H. M. and C. W. Yu (2018). "Chloroplast Galactolipids: The Link Between Photosynthesis, Chloroplast Shape, Jasmonates, Phosphate Starvation and Freezing Tolerance." *Plant and Cell Physiology* **59**(6): 1128-1134.

Li, H. Q., J. Xu, L. Chen and M. R. Li (2007). "Establishment of an efficient Agrobacterium tumefaciens-mediated leaf disc transformation of Thellungiella halophila." *Plant Cell Rep* **26**(10): 1785-1789.

Li, J., F. C. Bi, J. Yin, J. X. Wu, C. Rong, J. L. Wu and N. Yao (2015). "An Arabidopsis neutral ceramidase mutant ncer1 accumulates hydroxyceramides and is sensitive to oxidative stress." *Frontiers in Plant Science* **6**.

Li, J. F., J. E. Norville, J. Aach, M. McCormack, D. D. Zhang, J. Bush, G. M. Church and J. Sheen (2013). "Multiplex and homologous recombination-mediated genome editing in Arabidopsis and Nicotiana benthamiana using guide RNA and Cas9." *Nature Biotechnology* **31**(8): 688-691.

Li, J. F., D. D. Zhang and J. Sheen (2014). "Cas9-Based Genome Editing in Arabidopsis and Tobacco." *Use of Crispr/Cas9, Zfns, and Talens in Generating Site-Specific Genome Alterations* **546**: 459-472.

Li, M., N. Sui, L. Lin, Z. Yang and Y. Zhang (2019). "Transcriptomic profiling revealed genes involved in response to cold stress in maize." *Funct Plant Biol*.

Li, Q., Q. Zheng, W. Shen, D. Cram, D. B. Fowler, Y. Wei and J. Zou (2015). "Understanding the biochemical basis of temperature-induced lipid pathway adjustments in plants." *Plant Cell* **27**(1): 86-103.

Li, W., R. Wang, M. Li, L. Li, C. Wang, R. Welti and X. Wang (2008). "Differential degradation of extraplastidic and plastidic lipids during freezing and post-freezing recovery in Arabidopsis thaliana." *Journal of Biological Chemistry* **283**(1): 461-468.

Li, W. Q., M. A. Khan, S. Yamaguchi and X. J. Liu (2015). "Hormonal and environmental regulation of seed germination in salt cress (Thellungiella halophila)." *Plant Growth Regulation* **76**(1): 41-49.

Li, W. Q., M. Y. Li, W. H. Zhang, R. Welti and X. M. Wang (2004). "The plasma membrane-bound phospholipase D delta enhances freezing tolerance in Arabidopsis thaliana." *Nature Biotechnology* **22**(4): 427-433.

Li, X. G., W. Duan, Q. W. Meng, Q. Zou and S. J. Zhao (2004). "The function of chloroplastic NAD(P)H dehydrogenase in tobacco during chilling stress under low irradiance." *Plant and Cell Physiology* **45**(1): 103-108.

Li, X. P., O. Bjorkman, C. Shih, A. R. Grossman, M. Rosenquist, S. Jansson and K. K. Niyogi (2000). "A pigment-binding protein essential for regulation of photosynthetic light harvesting." *Nature* **403**(6768): 391-395.

Li, Y., W. Sun, F. L. Liu, J. Cheng, X. J. Zhang, H. Zhang and Y. X. Zhao (2019). "Methods for grafting Arabidopsis thaliana and Eutrema salsugineum." *Plant Methods* **15**(1).

Liang, H., N. Yao, L. T. Song, S. Luo, H. Lu and L. T. Greenberg (2003). "Ceramides modulate programmed cell death in plants." *Genes & Development* **17**(21): 2636-2641.

Liepman, A. H., C. G. Wilkerson and K. Keegstra (2005). "Expression of cellulose synthase-like (Csl) genes in insect cells reveals that CslA family members encode mannan synthases." *Proceedings of the National Academy of Sciences of the United States of America* **102**(6): 2221-2226.

Lin, Y., T. J. Cradick, M. T. Brown, H. Deshmukh, P. Ranjan, N. Sarode, B. M. Wile, P. M. Vertino, F. J. Stewart and G. Bao (2014). "CRISPR/Cas9 systems have off-target activity with insertions or deletions between target DNA and guide RNA sequences." *Nucleic Acids Res* **42**(11): 7473-7485.

Lindquist, E. and H. Aronsson (2018). "Chloroplast vesicle transport." *Photosynthesis Research* **138**(3): 361-371.

Lippold, F., K. vom Dorp, M. Abraham, G. Holzl, V. Wewer, J. L. Yilmaz, I. Lager, C. Montandon, C. Besagni, F. Kessler, S. Stymne and P. Dormann (2012). "Fatty Acid Phytyl Ester Synthesis in Chloroplasts of Arabidopsis." *Plant Cell* **24**(5): 2001-2014.

Liu, D., L. Hou, W. C. Li, J. F. Cheng and Y. Q. Fu (2014). "COR15B expression is affected by chloroplast functionality and its role in response to salt stress in Arabidopsis thaliana." *Biologia Plantarum* **58**(4): 667-675.

Liu, J., D. Moyankova, D. Djilianov and X. Deng (2019). "Common and Specific Mechanisms of Desiccation Tolerance in Two Gesneriaceae Resurrection Plants. Multiomics Evidences." *Frontiers in Plant Science* **10**(1067).

Liu, Q., M. Kasuga, Y. Sakuma, H. Abe, S. Miura, K. Yamaguchi-Shinozaki and K. Shinozaki (1998). "Two transcription factors, DREB1 and DREB2, with an EREBP/AP2 DNA binding domain separate two cellular signal transduction pathways in drought- and low-temperature-responsive gene expression, respectively, in Arabidopsis." *Plant Cell* **10**(8): 1391-1406.

Liu, Y., W. Tao, S. Wen, Z. Li, A. Yang, Z. Deng and Y. Sun (2015). "In Vitro CRISPR/Cas9 System for Efficient Targeted DNA Editing." *MBio* **6**(6): e01714-01715.

Livak, K. J. and T. D. Schmittgen (2001). "Analysis of relative gene expression data using real-time quantitative PCR and the 2(T)(-Delta Delta C) method." *Methods* **25**(4): 402-408.

Livingston, D. P., K. Van, R. Premakumar, S. P. Tallury and E. M. Herman (2007). "Using Arabidopsis thaliana as a model to study subzero acclimation in small grains." *Cryobiology* **54**(2): 154-163.

Long, T. A., Y. Okegawa, T. Shikanai, G. W. Schmidt and S. F. Covert (2008). "Conserved role of PROTON GRADIENT REGULATION 5 in the regulation of PSI cyclic electron transport." *Planta* **228**(6): 907-918.

Love, M. I., W. Huber and S. Anders (2014). "Moderated estimation of fold change and dispersion for RNA-seq data with DESeq2." *Genome Biology* **15**(12).

Lynch, D. V. and T. M. Dunn (2004). "An introduction to plant sphingolipids and a review of recent advances in understanding their metabolism and function." *New Phytologist* **161**(3): 677-702.

Lynch, D. V. and P. L. Steponkus (1987). "Plasma-Membrane Lipid Alterations Associated with Cold-Acclimation of Winter Rye Seedlings (Secale-Cereale L-Cv Puma)." *Plant Physiology* **83**(4): 761-767.

Ma, X. L., Q. Y. Zhang, Q. L. Zhu, W. Liu, Y. Chen, R. Qiu, B. Wang, Z. F. Yang, H. Y. Li, Y. R. Lin, Y. Y. Xie, R. X. Shen, S. F. Chen, Z. Wang, Y. L. Chen, J. X. Guo, L. T. Chen, X. C. Zhao, Z. C. Dong and Y. G. Liu (2015). "A Robust CRISPR/Cas9 System for Convenient, High-Efficiency Multiplex Genome Editing in Monocot and Dicot Plants." *Molecular Plant* **8**(8): 1274-1284.

MacLeod, M. J., J. Dedrick, C. Ashton, W. W. Sung, M. J. Champigny and E. A. Weretilnyk (2015). "Exposure of two Eutrema salsugineum (Thellungiella salsuginea) accessions to water deficits reveals different coping strategies in response to drought." *Physiol Plant* **155**(3): 267-280.

Madeira, F., Y. M. Park, J. Lee, N. Buso, T. Gur, N. Madhusoodanan, P. Basutkar, A. R. N. Tivey, S. C. Potter, R. D. Finn and R. Lopez (2019). "The EMBL-EBI search and sequence analysis tools APIs in 2019." *Nucleic Acids Research* **47**(W1): W636-W641.

Magnin-Robert, M., D. Le Bourse, J. Markham, S. Dorey, C. Clement, F. Baillieul and S. Dhondt-Cordelier (2015). "Modifications of Sphingolipid Content Affect Tolerance to Hemibiotrophic and Necrotrophic Pathogens by Modulating Plant Defense Responses in Arabidopsis." *Plant Physiol* **169**(3): 2255-2274.

Mamode Cassim, A., P. Gouguet, J. Gronnier, N. Laurent, V. Germain, M. Grison, Y. Boutte, P. Gerbeau-Pissot, F. Simon-Plas and S. Mongrand (2019). "Plant lipids: Key players of plasma membrane organization and function." *Prog Lipid Res* **73**: 1-27.

Markham, J. E. (2013). "Detection and quantification of plant sphingolipids by LC-MS." *Methods Mol Biol* **1009**: 93-101.

Markham, J. E. and J. G. Jaworski (2007). "Rapid measurement of sphingolipids from Arabidopsis thaliana by reversed-phase high-performance liquid chromatography coupled to electrospray ionization tandem mass spectrometry." *Rapid Communications in Mass Spectrometry* **21**(7): 1304-1314.

Markham, J. E., J. Li, E. B. Cahoon and J. G. Jaworski (2006). "Separation and identification of major plant sphingolipid classes from leaves." *Journal of Biological Chemistry* **281**(32): 22684-22694.

Markham, J. E., D. V. Lynch, J. A. Napier, T. M. Dunn and E. B. Cahoon (2013). "Plant sphingolipids: function follows form." *Current Opinion in Plant Biology* **16**(3): 350-357.

Marla, S. R., S. Shiva, R. Welti, S. Liu, J. J. Burke and G. P. Morris (2017). "Comparative Transcriptome and Lipidome Analyses Reveal Molecular Chilling Responses in Chilling-Tolerant Sorghums." *Plant Genome* **10**(3).

Martiniere, A., M. Shvedunova, A. J. W. Thomson, N. H. Evans, S. Penfield, J. Runions and H. G. McWatters (2011). "Homeostasis of plasma

membrane viscosity in fluctuating temperatures." *New Phytologist* **192**(2): 328-337.

Matos, A. R., C. Hourton-Cabassa, D. Cicek, N. Reze, J. D. Arrabaca, A. Zachowski and F. Moreau (2007). "Alternative oxidase involvement in cold stress response of Arabidopsis thaliana fad2 and FAD3+ cell suspensions altered in membrane lipid composition." *Plant Cell Physiol* **48**(6): 856-865.

Matz, M. V., A. F. Fradkov, Y. A. Labas, A. P. Savitsky, A. G. Zaraisky, M. L. Markelov and S. A. Lukyanov (1999). "Fluorescent proteins from nonbioluminescent Anthozoa species." *Nature Biotechnology* **17**(10): 969-973.

Maxwell, K. and G. N. Johnson (2000). "Chlorophyll fluorescence - a practical guide." *Journal of Experimental Botany* **51**(345): 659-668.

McAusland, L., J. A. Atkinson, T. Lawson and E. H. Murchie (2019). "High throughput procedure utilising chlorophyll fluorescence imaging to phenotype dynamic photosynthesis and photoprotection in leaves under controlled gaseous conditions." *Plant Methods* **15**: 109.

McConn, M. and J. Browse (1996). "The critical requirement for linolenic acid is pollen development, not photosynthesis, in an arabidopsis mutant." *Plant Cell* **8**(3): 403-416.

Mcconn, M., S. Hugly, J. Browse and C. Somerville (1994). "A Mutation at the Fad8 Locus of Arabidopsis Identifies a 2nd Chloroplast Omega-3 Desaturase." *Plant Physiology* **106**(4): 1609-1614.

McGlew, K., V. Shaw, M. Zhang, R. J. Kim, W. L. Yang, B. Shorrosh, M. C. Suh and J. Ohlrogge (2015). "An annotated database of Arabidopsis mutants of acyl lipid metabolism." *Plant Cell Reports* **34**(4): 519-532.

McManus, M. T. and P. A. Sharp (2002). "Gene silencing in mammals by small interfering RNAs." *Nature Reviews Genetics* **3**(10): 737-747.

Meshi, T. and M. Iwabuchi (1995). "Plant transcription factors." *Plant and Cell Physiology* **36**(8): 1405-1420.

Michaelson, L. V., A. J. Longman, O. Sayanova, A. K. Stobart and J. A. Napier (2002). "Isolation and characterization of a cDNA encoding a Delta8 sphingolipid desaturase from Aquilegia vulgaris." *Biochem Soc Trans* **30**(Pt 6): 1073-1075.

Michaelson, L. V., J. A. Napier, D. Molino and J. D. Faure (2016). "Plant sphingolipids: Their importance in cellular organization and adaption." *Biochim Biophys Acta* **1861**(9 Pt B): 1329-1335.

Michaelson, L. V., S. Zauner, J. E. Markham, R. P. Haslam, R. Desikan, S. Mugford, S. Albrecht, D. Warnecke, P. Sperling, E. Heinz and J. A. Napier (2009). "Functional Characterization of a Higher Plant Sphingolipid Delta 4-Desaturase: Defining the Role of Sphingosine and Sphingosine-1-Phosphate in Arabidopsis." *Plant Physiology* **149**(1): 487-498.

Michaud, M. and J. Jouhet (2019). "Lipid Trafficking at Membrane Contact Sites During Plant Development and Stress Response." *Frontiers in Plant Science* **10**.

Mina, J. G., Y. Okada, N. K. Wansadhipathi-Kannangara, S. Pratt, H. Shams-Eldin, R. T. Schwarz, P. G. Steel, T. Fawcett and P. W. Denny (2010). "Functional analyses of differentially expressed isoforms of the Arabidopsis inositol phosphorylceramide synthase." *Plant Molecular Biology* **73**(4-5): 399-407.

Minami, A., M. Fujiwara, A. Furuto, Y. Fukao, T. Yamashita, M. Kamo, Y. Kawamura and M. Uemura (2009). "Alterations in detergent-resistant plasma membrane microdomains in Arabidopsis thaliana during cold acclimation." *Plant Cell Physiol* **50**(2): 341-359.

Minami, A., A. Furuto and M. Uemura (2010). "Dynamic compositional changes of detergent-resistant plasma membrane microdomains during plant cold acclimation." *Plant Signal Behav* **5**(9): 1115-1118.

Miquel, M., D. James, H. Dooner and J. Browse (1993). "Arabidopsis Requires Polyunsaturated Lipids for Low-Temperature Survival." *Proceedings of the National Academy of Sciences of the United States of America* **90**(13): 6208-6212.

Mironov, K. S., R. A. Sidorov, M. S. Trofimova, V. S. Bedbenov, V. D. Tsydendambaev, S. I. Allakhverdiev and D. A. Los (2012). "Light-dependent cold-induced fatty acid unsaturation, changes in membrane fluidity, and alterations in gene expression in Synechocystis." *Biochimica Et Biophysica Acta-Bioenergetics* **1817**(8): 1352-1359.

Mishra, A., K. B. Mishra, Hoermiller, II, A. G. Heyer and L. Nedbal (2011). "Chlorophyll fluorescence emission as a reporter on cold tolerance in Arabidopsis thaliana accessions." *Plant Signal Behav* **6**(2): 301-310.

Missihoun, T. D., H. H. Kirch and D. Bartels (2012). "T-DNA insertion mutants reveal complex expression patterns of the aldehyde dehydrogenase 3H1 locus in Arabidopsis thaliana." *Journal of Experimental Botany* **63**(10): 3885-3898.

Mizusawa, N. and H. Wada (2012). "The role of lipids in photosystem II." *Biochimica Et Biophysica Acta-Bioenergetics* **1817**(1): 194-208.

Moellering, E. R., B. Muthan and C. Benning (2010). "Freezing Tolerance in Plants Requires Lipid Remodeling at the Outer Chloroplast Membrane." *Science* **330**(6001): 226-228.

Molina, A. and F. Garcia-Olmedo (1993). "Developmental and pathogen-induced expression of three barley genes encoding lipid transfer proteins." *Plant J* **4**(6): 983-991.

Molina, A. and F. GarciaOlmedo (1997). "Enhanced tolerance to bacterial pathogens caused by the transgenic expression of barley lipid transfer protein LTP2." *Plant Journal* **12**(3): 669-675.

Mongrand, S., J. Morel, J. Laroche, S. Claverol, J. P. Carde, M. A. Hartmann, M. Bonneu, F. Simon-Plas, R. Lessire and J. J. Bessoule (2004). "Lipid rafts in higher plant cells - Purification and characterization of triton X-100-insoluble microdomains from tobacco plasma membrane." *Journal of Biological Chemistry* **279**(35): 36277-36286.

Morineau, C., Y. Bellec, F. Tellier, L. Gissot, Z. Kelemen, F. Nogue and J. D. Faure (2016). "Selective gene dosage by CRISPR-Cas9 genome editing in hexaploid Camelina sativa." *Plant Biotechnol J*.

Morineau, C., L. Gissot, Y. Bellec, K. Hematy, F. Tellier, C. Renne, R. Haslam, F. Beaudoin, J. Napier and J. D. Faure (2016). "Dual Fatty Acid Elongase Complex Interactions in Arabidopsis." *PLoS One* **11**(9): e0160631.

Morton, J., M. W. Davis, E. M. Jorgensen and D. Carroll (2006). "Induction and repair of zinc-finger nuclease-targeted double-strand breaks in Caenorhabditis elegans somatic cells." *Proceedings of the National Academy of Sciences of the United States of America* **103**(44): 16370-16375.

Msanne, J., M. Chen, K. D. Luttgeharm, A. M. Bradley, E. S. Mays, J. M. Paper, D. L. Boyle, R. E. Cahoon, K. Schrick and E. B. Cahoon (2015). "Glucosylceramides are critical for cell-type differentiation and organogenesis, but not for cell viability in Arabidopsis." *Plant Journal* **84**(1): 188-201.

Mucha, S., D. Walther, T. M. Muller, D. K. Hincha and E. Glawischnig (2015). "Substantial reprogramming of the Eutrema salsugineum (Thellungiella

salsuginea) transcriptome in response to UV and silver nitrate challenge." *BMC Plant Biol* **15**: 137.

Munekaga, Y., M. Hashimoto, C. Miyaka, K. I. Tomizawa, T. Endo, M. Tasaka and T. Shikanai (2004). "Cyclic electron flow around photosystem I is essential for photosynthesis." *Nature* **429**(6991): 579-582.

Munekage, Y., M. Hojo, J. Meurer, T. Endo, M. Tasaka and T. Shikanai (2002). "PGR5 is involved in cyclic electron flow around photosystem I and is essential for photoprotection in Arabidopsis." *Cell* **110**(3): 361-371.

Munnik, T. (2001). "Phosphatidic acid: an emerging plant lipid second messenger." *Trends in Plant Science* **6**(5): 227-233.

Murata, N., S. Takahashi, Y. Nishiyama and S. I. Allakhverdiev (2007). "Photoinhibition of photosystem II under environmental stress." *Biochimica Et Biophysica Acta-Bioenergetics* **1767**(6): 414-421.

Murchie, E. H. and T. Lawson (2013). "Chlorophyll fluorescence analysis: a guide to good practice and understanding some new applications." *Journal of Experimental Botany* **64**(13): 3983-3998.

Murray, M. B., J. N. Cape and D. Fowler (1989). "Quantification of Frost Damage in Plant-Tissues by Rates of Electrolyte Leakage." *New Phytologist* **113**(3): 307-311.

Nagele, T., S. Stutz, Hormiller, II and A. G. Heyer (2012). "Identification of a metabolic bottleneck for cold acclimation in Arabidopsis thaliana." *Plant J* **72**(1): 102-114.

Nagler, M., E. Nukarinen, W. Weckwerth and T. Nagele (2015). "Integrative molecular profiling indicates a central role of transitory starch breakdown in establishing a stable C/N homeostasis during cold acclimation in two natural accessions of Arabidopsis thaliana." *BMC Plant Biol* **15**: 284.

Nakamura, Y. (2017). "Plant Phospholipid Diversity: Emerging Functions in Metabolism and Protein-Lipid Interactions." *Trends Plant Sci* **22**(12): 1027-1040.

Napier, J. A., R. P. Haslam, F. Beaudoin and E. B. Cahoon (2014). "Understanding and manipulating plant lipid composition: Metabolic engineering leads the way." *Current Opinion in Plant Biology* **19**: 68-75.

Natali, A., J. M. Gruber, L. Dietzel, M. C. A. Stuart, R. van Grondelle and R. Croce (2016). "Light-harvesting Complexes (LHCs) Cluster Spontaneously in Membrane Environment Leading to Shortening of Their Excited State Lifetimes." *Journal of Biological Chemistry* **291**(32): 16730-16739.

Navarro-Retamal, C., A. Bremer, H. I. Ingolfsson, J. Alzate-Morales, J. Caballero, A. Thalhammer, W. Gonzalez and D. K. Hincha (2018). "Folding and Lipid Composition Determine Membrane Interaction of the Disordered Protein COR15A." *Biophysical Journal* **115**(6): 968-980.

Nawrocki, W. J., B. Bailleul, D. Picot, P. Cardol, F. Rappaport, F. A. Wollman and P. Joliot (2019). "The mechanism of cyclic electron flow." *Biochimica Et Biophysica Acta-Bioenergetics* **1860**(5): 433-438.

Negi, J., S. Munemasa, B. Song, R. Tadakuma, M. Fujita, T. Azoulay-Shemer, C. B. Engineer, K. Kusumi, I. Nishida, J. I. Schroeder and K. Iba (2018). "Eukaryotic lipid metabolic pathway is essential for functional chloroplasts and CO2 and light responses in Arabidopsis guard cells." *Proceedings of the National Academy of Sciences of the United States of America* **115**(36): 9038-9043.

Ng, C. K. Y., K. Carr, M. R. McAinsh, B. Powell and A. M. Hetherington (2001). "Drought-induced guard cell signal transduction involves sphingosine-1-phosphate." *Nature* **410**(6828): 596-599.

Nikolau, B. J., J. B. Ohlrogge and E. S. Wurtele (2003). "Plant biotin-containing carboxylases." *Archives of Biochemistry and Biophysics* **414**(2): 211-222.

Nilsson, A. K., P. Fahlberg, O. N. Johansson, M. Hamberg, M. X. Andersson and M. Ellerstrom (2016). "The activity of HYDROPEROXIDE LYASE 1 regulates accumulation of galactolipids containing 12-oxo-phytodienoic acid in Arabidopsis." *Journal of Experimental Botany* **67**(17): 5133-5144.

Novillo, F., J. M. Alonso, J. R. Ecker and J. Salinas (2004). "CBF2/DREB1C is a negative regulator of CBF1/DREB1B and CBF3/DREB1A expression and plays a central role in, stress tolerance in Arabidopsis." *Proceedings of the National Academy of Sciences of the United States of America* **101**(11): 3985-3990.

O'Malley, R. C. and J. R. Ecker (2010). "Linking genotype to phenotype using the Arabidopsis unimutant collection." *Plant Journal* **61**(6): 928-940.

Oh, D. H., M. Dassanayake, H. J. Bohnert and J. M. Cheeseman (2012). "Life at the extreme: lessons from the genome." *Genome Biology* **13**(3).

Ohlrogge, J. and J. Browse (1995). "Lipid biosynthesis." *Plant Cell* **7**(7): 957-970.

Ohlrogge, J. B. and J. G. Jaworski (1997). "Regulation of fatty acid synthesis." *Annual Review of Plant Physiology and Plant Molecular Biology* **48**: 109-136.

Ohta, M., K. Matsui, K. Hiratsu, H. Shinshi and M. Ohme-Takagi (2001). "Repression domains of class II ERF transcriptional repressors share an essential motif for active repression." *Plant Cell* **13**(8): 1959-1968.

Onate-Sanchez, L. and J. Vicente-Carbajosa (2008). "DNA-free RNA isolation protocols for Arabidopsis thaliana, including seeds and siliques." *BMC Res Notes* **1**: 93.

Orsini, F., M. P. D'Urzo, G. Inan, S. Serra, D. H. Oh, M. V. Mickelbart, F. Consiglio, X. Li, J. C. Jeong, D. J. Yun, H. J. Bohnert, R. A. Bressan and A. Maggio (2010). "A comparative study of salt tolerance parameters in 11 wild relatives of Arabidopsis thaliana." *Journal of Experimental Botany* **61**(13): 3787-3798.

Oxborough, K. (2004). "Imaging of chlorophyll a fluorescence: theoretical and practical aspects of an emerging technique for the monitoring of photosynthetic performance." *Journal of Experimental Botany* **55**(400): 1195-1205.

Ozols, J. (1989). "Structure of Cytochrome-B5 and Its Topology in the Microsomal Membrane." *Biochimica Et Biophysica Acta* **997**(1-2): 121-130.

Pagnussat, L. A., N. Oyarburo, C. Cimmino, M. L. Pinedo and L. de la Canal (2015). "On the role of a Lipid-Transfer Protein. Arabidopsis ltp3 mutant is compromised in germination and seedling growth." *Plant Signaling & Behavior* **10**(12).

Park, J. A., T. W. Kim, S. K. Kim, W. T. Kim and H. S. Pai (2005). "Silencing of NbECR encoding a putative enoyl-CoA reductase results in disorganized membrane structures and epidermal cell ablation in Nicotiana benthamiana." *Febs Letters* **579**(20): 4459-4464.

Pata, M. O., Y. A. Hannun and C. K. Ng (2010). "Plant sphingolipids: decoding the enigma of the Sphinx." *New Phytol* **185**(3): 611-630.

Pinneh, E. C., J. G. Mina, M. J. R. Stark, S. D. Lindell, P. Luemmen, M. R. Knight, P. G. Steel and P. W. Denny (2019). "The identification of small molecule inhibitors of the plant inositol phosphorylceramide synthase which demonstrate herbicidal activity." *Scientific Reports* **9**.

Pinneh, E. C., R. Stoppel, H. Knight, M. R. Knight, P. G. Steel and P. W. Denny (2019). "Expression levels of inositol phosphorylceramide synthase

modulate plant responses to biotic and abiotic stress in Arabidopsis thaliana." *Plos One* **14**(5).

Pinnola, A. and R. Bassi (2018). "Molecular mechanisms involved in plant photoprotection." *Biochemical Society Transactions* **46**: 467-482.

Porra, R. J., W. A. Thompson and P. E. Kriedemann (1989). "Determination of Accurate Extinction Coefficients and Simultaneous-Equations for Assaying Chlorophyll-a and Chlorophyll-B Extracted with 4 Different Solvents - Verification of the Concentration of Chlorophyll Standards by Atomic-Absorption Spectroscopy." *Biochimica Et Biophysica Acta* **975**(3): 384-394.

Preite, V., C. Sailer, L. Syllwasschy, S. Bray, H. Ahmadi, U. Kramer and L. Yant (2019). "Convergent evolution in Arabidopsis halleri and Arabidopsis arenosa on calamine metalliferous soils." *Philosophical Transactions of the Royal Society B-Biological Sciences* **374**(1777).

Qi, Y. P., Y. Zhang, F. Zhang, J. A. Baller, S. C. Cleland, Y. G. Ryu, C. G. Starker and D. F. Voytas (2013). "Increasing frequencies of site-specific mutagenesis and gene targeting in Arabidopsis by manipulating DNA repair pathways." *Genome Research* **23**(3): 547-554.

Rahman, L. N., L. Chen, S. Nazim, V. V. Bamm, M. W. Yaish, B. A. Moffatt, J. R. Dutcher and G. Harauz (2010). "Interactions of intrinsically disordered Thellungiella salsuginea dehydrins TsDHN-1 and TsDHN-2 with membranes - synergistic effects of lipid composition and temperature on secondary structure." *Biochemistry and Cell Biology-Biochimie Et Biologie Cellulaire* **88**(5): 791-807.

Raju, S. K. K., A. C. Barnes, J. C. Schnable and R. L. Roston (2018). "Low-temperature tolerance in land plants: Are transcript and membrane responses conserved?" *Plant Science* **276**: 73-86.

Reddy, A. S., M. L. Nuccio, L. M. Gross and T. L. Thomas (1993). "Isolation of a Delta-6-Desaturase Gene from the Cyanobacterium Synechocystis Sp Strain Pcc-6803 by Gain-of-Function Expression in Anabaena Sp Strain Pcc-7120." *Plant Molecular Biology* **22**(2): 293-300.

Reyes-Diaz, M., N. Ulloa, A. Zuniga-Feest, A. Gutierrez, M. Gidekel, M. Alberdi, L. J. Corcuera and L. A. Bravo (2006). "Arabidopsis thaliana avoids freezing by supercooling." *J Exp Bot* **57**(14): 3687-3696.

Rhee, S. Y. and M. Mutwil (2014). "Towards revealing the functions of all genes in plants." *Trends in Plant Science* **19**(4): 212-221.

Richmond, T. A. and C. R. Somerville (2000). "The cellulose synthase superfamily." *Plant Physiology* **124**(2): 495-498.

Rizza, A., A. Boccaccini, I. Lopez-Vidriero, P. Costantino and P. Vittorioso (2011). "Inactivation of the ELIP1 and ELIP2 genes affects Arabidopsis seed germination." *New Phytologist* **190**(4): 896-905.

Roesler, K. R., B. S. Shorrosh and J. B. Ohlrogge (1994). "Structure and Expression of an Arabidopsis Acetyl-Coenzyme-a Carboxylase Gene." *Plant Physiology* **105**(2): 611-617.

Roman, A., V. Andreu, M. L. Hernandez, B. Lagunas, R. Picorel, J. M. Martinez-Rivas and M. Alfonso (2012). "Contribution of the different omega-3 fatty acid desaturase genes to the cold response in soybean." *Journal of Experimental Botany* **63**(13): 4973-4982.

Roman, A., M. L. Hernandez, A. Soria-Garcia, S. Lopez-Gomollon, B. Lagunas, R. Picorel, J. M. Martinez-Rivas and M. Alfonso (2015). "Non-redundant Contribution of the Plastidial FAD8 omega-3 Desaturase to Glycerolipid Unsaturation at Different Temperatures in Arabidopsis." *Molecular Plant* **8**(11): 1599-1611.

Routaboul, J. M., S. F. Fischer and J. Browse (2000). "Trienoic fatty acids are required to maintain chloroplast function at low temperatures." *Plant Physiology* **124**(4): 1697-1705.

Routaboul, J. M., C. Skidmore, J. G. Wallis and J. Browse (2012). "Arabidopsis mutants reveal that short- and long-term thermotolerance have different requirements for trienoic fatty acids." *Journal of Experimental Botany* **63**(3): 1435-1443.

Ruban, A. V., M. P. Johnson and C. D. Duffy (2012). "The photoprotective molecular switch in the photosystem II antenna." *Biochim Biophys Acta* **1817**(1): 167-181.

Ruelland, E., C. Cantrel, M. Gawer, J. C. Kader and A. Zachowski (2002). "Activation of phospholipases C and D is an early response to a cold exposure in Arabidopsis suspension cells." *Plant Physiology* **130**(2): 999-1007.

Ruhle, T., B. Reiter and D. Leister (2018). "Chlorophyll Fluorescence Video Imaging: A Versatile Tool for Identifying Factors Related to Photosynthesis." *Frontiers in Plant Science* **9**.

Ruiz-Lopez, N., R. P. Haslam, J. A. Napier and O. Sayanova (2014). "Successful high-level accumulation of fish oil omega-3 long-chain polyunsaturated fatty acids in a transgenic oilseed crop." *Plant Journal* **77**(2): 198-208.

Ryan, P. R., Q. Liu, P. Sperling, B. Dong, S. Franke and E. Delhaize (2007). "A higher plant Delta 8 sphingolipid desaturase with a preference for (Z)-isomer formation confers aluminum tolerance to yeast and plants." *Plant Physiology* **144**(4): 1968-1977.

Sakamoto, T. and N. Murata (2002). "Regulation of the desaturation of fatty acids and its role in tolerance to cold and salt stress." *Current Opinion in Microbiology* **5**(2): 206-210.

Sanchez-Rangel, D., M. R. S. Vicente, M. E. de la Torre-Hernandez, M. Najera-Martinez and J. Plasencia (2015). "Deciphering the link between salicylic acid signaling and sphingolipid metabolism." *Frontiers in Plant Science* **6**.

Sanchez, J. P. and N. H. Chua (2001). "Arabidopsis PLC1 is required for secondary responses to abscisic acid signals." *Plant Cell* **13**(5): 1143-1154.

Sanger, F., G. M. Air, B. G. Barrell, N. L. Brown, A. R. Coulson, C. A. Fiddes, C. A. Hutchison, P. M. Slocombe and M. Smith (1977). "Nucleotide sequence of bacteriophage phi X174 DNA." *Nature* **265**(5596): 687-695.

Sato, N. (2004). "Roles of the acidic lipids sulfoquinovosyl diacylglycerol and phosphatidylglycerol in photosynthesis: their specificity and evolution." *Journal of Plant Research* **117**(6): 495-505.

Sayanova, O., P. R. Shewry and J. A. Napier (1999). "Histidine-41 of the cytochrome b(5) domain of the borage Delta(6) fatty acid desaturase is essential for enzyme activity." *Plant Physiology* **121**(2): 641-646.

Sayanova, O., M. A. Smith, P. Lapinskas, A. K. Stobart, G. Dobson, W. W. Christie, P. R. Shewry and J. A. Napier (1997). "Expression of a borage desaturase cDNA containing an N-terminal cytochrome b5 domain results in the accumulation of high levels of delta6-desaturated fatty acids in transgenic tobacco." *Proc Natl Acad Sci U S A* **94**(8): 4211-4216.

Schaller, S., D. Latowski, M. Jemiola-Rzeminska, A. Dawood, C. Wilhelm, K. Strzalka and R. Goss (2011). "Regulation of LHCII aggregation by different thylakoid membrane lipids." *Biochimica Et Biophysica Acta-Bioenergetics* **1807**(3): 326-335.

Schreiber, U., U. Schliwa and W. Bilger (1986). "Continuous recording of photochemical and non-photochemical chlorophyll fluorescence quenching with a new type of modulation fluorometer." *Photosynth Res* **10**(1-2): 51-62.

Sega, G. A. (1984). "A Review of the Genetic-Effects of Ethyl Methanesulfonate." *Mutation Research* **134**(2-3): 113-142.

Seo, P. J., S. B. Lee, M. C. Suh, M. J. Park, Y. S. Go and C. M. Park (2011). "The MYB96 Transcription Factor Regulates Cuticular Wax Biosynthesis under Drought Conditions in Arabidopsis." *Plant Cell* **23**(3): 1138-1152.

Shah, S., Z. G. Xin and J. Browse (1997). "Overexpression of the FAD3 desaturase gene in a mutant of Arabidopsis." *Plant Physiology* **114**(4): 1533-1539.

Shan, Q. W., Y. P. Wang, J. Li and C. X. Gao (2014). "Genome editing in rice and wheat using the CRISPR/Cas system." *Nature Protocols* **9**(10): 2395-2410.

Shanklin, J. and E. B. Cahoon (1998). "Desaturation and related modifications of fatty acids." *Annual Review of Plant Physiology and Plant Molecular Biology* **49**: 611-641.

Shanklin, J., E. Whittle and B. G. Fox (1994). "Eight histidine residues are catalytically essential in a membrane-associated iron enzyme, stearoyl-CoA desaturase, and are conserved in alkane hydroxylase and xylene monooxygenase." *Biochemistry* **33**(43): 12787-12794.

Sharma, D. K., S. B. Andersen, C. O. Ottosen and E. Rosenqvist (2015). "Wheat cultivars selected for high F-v/F-m under heat stress maintain high photosynthesis, total chlorophyll, stomatal conductance, transpiration and dry matter." *Physiologia Plantarum* **153**(2): 284-298.

Shaw, C. H. (1996). Plant Gene Transfer and Expression Protocols, *Humana Press*.

Shendure, J. and H. Ji (2008). "Next-generation DNA sequencing." *Nat Biotechnol* **26**(10): 1135-1145.

Shepherd, T. and D. W. Griffiths (2006). "The effects of stress on plant cuticular waxes." *New Phytologist* **171**(3): 469-499.

Shi, Y. L., L. Z. An, X. R. Li, C. H. Huang and G. X. Chen (2011). "The octadecanoid signaling pathway participates in the chilling-induced transcription of omega-3 fatty acid desaturases in Arabidopsis." *Plant Physiology and Biochemistry* **49**(2): 208-215.

Shikanai, T. (2007). "Cyclic electron transport around photosystem I: Genetic approaches." *Annual Review of Plant Biology* **58**: 199-217.

Shimojima, M. (2011). "Biosynthesis and functions of the plant sulfolipid." *Progress in Lipid Research* **50**(3): 234-239.

Shinozaki, K. and K. Yamaguchi-Shinozaki (2000). "Molecular responses to dehydration and low temperature: differences and cross-talk between two stress signaling pathways." *Current Opinion in Plant Biology* **3**(3): 217-223.

Shinozaki, K., K. Yamaguchi-Shinozaki and M. Seki (2003). "Regulatory network of gene expression in the drought and cold stress responses." *Curr Opin Plant Biol* **6**(5): 410-417.

Shinwari, Z. K., K. Nakashima, S. Miura, M. Kasuga, M. Seki, K. Yamaguchi-Shinozaki and K. Shinozaki (1998). "An Arabidopsis gene family encoding DRE/CRT binding proteins involved in low-temperature-responsive gene expression." *Biochemical and Biophysical Research Communications* **250**(1): 161-170.

Siegenthaler, P. A. and N. Murata (1998). Lipids in Photosynthesis: Structure, Function and Genetics. Dordrecht, The Netherlands, *Kluwer Academic Press*.

Silvestre, S., S. Araujo Sde, M. C. Vaz Patto and J. Marques da Silva (2014). "Performance index: An expeditious tool to screen for improved drought resistance in the Lathyrus genus." *J Integr Plant Biol* **56**(7): 610-621.

Smith, M. A., M. Dauk, H. Ramadan, H. Yang, L. E. Seamons, R. P. Haslam, F. Beaudoin, I. Ramirez-Erosa and L. Forseille (2013). "Involvement of Arabidopsis ACYL-COENZYME A DESATURASE-LIKE2 (At2g31360) in the Biosynthesis of the Very-Long-Chain Monounsaturated Fatty Acid Components of Membrane Lipids." *Plant Physiology* **161**(1): 81-96.

Song, J., G. Feng, C. Tian and F. Zhang (2005). "Strategies for adaptation of Suaeda physophora, Haloxylon ammodendron and Haloxylon persicum to a saline environment during seed-germination stage." *Ann Bot* **96**(3): 399-405.

Sperling, P., S. Franke, S. Luthje and E. Heinz (2005). "Are glucocerebrosides the predominant sphingolipids in plant plasma membranes?" *Plant Physiol Biochem* **43**(12): 1031-1038.

Sperling, P. and E. Heinz (2003). "Plant sphingolipids: structural diversity, biosynthesis, first genes and functions." *Biochimica Et Biophysica Acta-Molecular and Cell Biology of Lipids* **1632**(1-2): 1-15.

Sperling, P., B. Libisch, U. Zahringer, J. A. Napier and E. Heinz (2001). "Functional identification of a Delta(8)-sphingolipid desaturase from Borago officinalis." *Archives of Biochemistry and Biophysics* **388**(2): 293-298.

Sperling, P., H. Schmidt and E. Heinz (1995). "A cytochrome-b5-containing fusion protein similar to plant acyl lipid desaturases." *Eur J Biochem* **232**(3): 798-805.

Sperling, P., P. Ternes, H. Moll, S. Franke, U. Zahringer and E. Heinz (2001). "Functional characterization of sphingolipid C4-hydroxylase genes from Arabidopsis thaliana." *Febs Letters* **494**(1-2): 90-94.

Sperling, P., P. Ternes, T. K. Zank and E. Heinz (2003). "The evolution of desaturases." *Prostaglandins Leukotrienes and Essential Fatty Acids* **68**(2): 73-95.

Sperling, P., U. Zahringer and E. Heinz (1998). "A sphingolipid desaturase from higher plants. Identification of a new cytochrome b5 fusion protein." *J Biol Chem* **273**(44): 28590-28596.

Steponkus, P. L. (1984). "ROLE OF THE PLASMA-MEMBRANE IN FREEZING-INJURY AND COLD-ACCLIMATION." *Annual Review of Plant Physiology and Plant Molecular Biology* **35**: 543-584.

Steponkus, P. L. (1999). "Freeze-induced dehydration and the cryostability of biological membranes." *Water Management in the Design and Distribution of Quality Foods*: 53-85.

Steponkus, P. L., M. Uemura, R. A. Joseph, S. J. Gilmour and M. F. Thomashow (1998). "Mode of action of the COR15a gene on the freezing tolerance of Arabidopsis thaliana." *Proceedings of the National Academy of Sciences of the United States of America* **95**(24): 14570-14575.

Stockinger, E. J., S. J. Gilmour and M. F. Thomashow (1997). "Arabidopsis thaliana CBF1 encodes an AP2 domain-containing transcriptional activator that binds to the C-repeat/DRE, a cis-acting DNA regulatory element that stimulates transcription in response to low temperature and water deficit." *Proceedings of the National Academy of Sciences of the United States of America* **94**(3): 1035-1040.

Swarts, D. C. and M. Jinek (2018). "Cas9 versus Cas12a/Cpf1: Structure-function comparisons and implications for genome editing." *Wiley Interdisciplinary Reviews-Rna* **9**(5).

Swerdlow, H., S. L. Wu, H. Harke and N. J. Dovichi (1990). "Capillary gel electrophoresis for DNA sequencing. Laser-induced fluorescence detection with the sheath flow cuvette." *J Chromatogr* **516**(1): 61-67.

Taji, T., M. Seki, M. Satou, T. Sakurai, M. Kobayashi, K. Ishiyama, Y. Narusaka, M. Narusaka, J. K. Zhu and K. Shinozaki (2004). "Comparative genomics in salt tolerance between Arabidopsis and Arabidopsis-related halophyte salt cress using Arabidopsis microarray." *Plant Physiology* **135**(3): 1697-1709.

Takahashi, S. and N. Murata (2005). "Interruption of the Calvin cycle inhibits the repair of Photosystem II from photodamage." *Biochimica Et Biophysica Acta-Bioenergetics* **1708**(3): 352-361.

Tang, S., N. Chen, B. Song, J. He, Y. Zhou, M. A. Jenks and X. Xu (2018). "Compositional and transcriptomic analysis associated with cuticle lipid production on rosette and inflorescence stem leaves in the extremophyte Thellungiella salsuginea." *Physiol Plant*.

Tarca, A. L., R. Romero and S. Draghici (2006). "Analysis of microarray experiments of gene expression profiling." *American Journal of Obstetrics and Gynecology* **195**(2): 373-388.

Ternes, P., S. Franke, U. Zahringer, P. Sperling and E. Heinz (2002). "Identification and characterization of a sphingolipid Delta 4-desaturase family." *Journal of Biological Chemistry* **277**(28): 25512-25518.

Testerink, C. and T. Munnik (2005). "Phosphatidic acid: a multifunctional stress signaling lipid in plants." *Trends in Plant Science* **10**(8): 368-375.

Teusink, R. S., M. Rahman, R. A. Bressan and M. A. Jenks (2002). "Cuticular waxes on Arabidopsis thaliana close relatives Thellungiella halophila and Thellungiella parvula." *International Journal of Plant Sciences* **163**(2): 309-315.

Thalhammer, A., G. Bryant, R. Sulpice and D. K. Hincha (2014). "Disordered cold regulated15 proteins protect chloroplast membranes during freezing through binding and folding, but do not stabilize chloroplast enzymes in vivo." *Plant Physiol* **166**(1): 190-201.

Thalhammer, A., M. Hundertmark, A. V. Popova, R. Seckler and D. K. Hincha (2010). "Interaction of two intrinsically disordered plant stress proteins (COR15A and COR15B) with lipid membranes in the dry state." *Biochimica Et Biophysica Acta-Biomembranes* **1798**(9): 1812-1820.

Thomashow, M. and M. Thomashow (2010). "Plant Cold Acclimation Identifying Gene Regulons Involved in Freezing Tolerance." *In Vitro Cellular & Developmental Biology-Animal* **46**: S78-S79.

Thomashow, M. E. (2005). "Gene regulons and regulatory networks involved in plant cold acclimation." *In Vitro Cellular & Developmental Biology-Animal* **41**: 14a-14a.

Thomashow, M. F. (1994). *Arabidopsis thaliana* as a Model for Studying Mechanisms of Plant Cold Tolerance. USA, *Cold Spring Harbor Laboratory Press*.

Thomashow, M. F. (1998). "Role of cold-responsive genes in plant freezing tolerance." *Plant Physiol* **118**(1): 1-8.

Thomashow, M. F. (1999). "Plant cold acclimation: Freezing tolerance genes and regulatory mechanisms." *Annual Review of Plant Physiology and Plant Molecular Biology* **50**: 571-599.

Thomashow, M. F., N. Artus, S. Gilmour, E. Stockinger, K. Wilhelm, D. Zarka, R. A. Joseph, M. Uemura and P. L. Steponkus (1996). "Function and regulation of Arabidopsis thaliana COR (cold-regulated) genes." *Plant Physiology* **111**(2): 81003-81003.

Thomashow, M. F., S. J. Gilmour, R. Hajela, D. Horvath, C. Lin and W. Guo (1990). "Studies on Cold-Acclimation in Arabidopsis-Thaliana." *Horticultural Biotechnology* **11**: 305-314.

Thorlby, G., N. Fourrier and G. Warren (2004). "The SENSITIVE TO FREEZING2 gene, required for freezing tolerance in Arabidopsis thaliana, encodes a beta-glucosidase." *Plant Cell* **16**(8): 2192-2203.

Thorneycroft, D., S. M. Sherson and S. M. Smith (2001). "Using gene knockouts to investigate plant metabolism." *Journal of Experimental Botany* **52**(361): 1593-1601.

Tietje, C. and E. Heinz (1998). "Uridine-diphospho-sulfoquinovose: diacylglycerol sulfoquinovosyltransferase activity is concentrated in the inner membrane of chloroplast envelopes." *Planta* **206**(1): 72-78.

Tocher, D. R., M. B. Betancor, M. Sprague, R. E. Olsen and J. A. Napier (2019). "Omega-3 Long-Chain Polyunsaturated Fatty Acids, EPA and DHA: Bridging the Gap between Supply and Demand." *Nutrients* **11**(1).

Tovuu, A., I. S. Zulfugarov and C. H. Lee (2013). "Correlations between the temperature dependence of chlorophyll fluorescence and the fluidity of thylakoid membranes." *Physiologia Plantarum* **147**(4): 409-416.

Tovuu, A., I. S. Zulfugarov, G. X. Wu, I. S. Kang, C. Kim, B. Y. Moon, G. An and C. H. Lee (2016). "Rice mutants deficient in omega-3 fatty acid desaturase (FAD8) fail to acclimate to cold temperatures." *Plant Physiology and Biochemistry* **109**: 525-535.

Uemura, M., S. J. Gilmour, M. F. Thomashow and P. L. Steponkus (1996). "Effects of COR6.6 and COR15am polypeptides encoded by COR (cold-regulated) genes of Arabidopsis thaliana on the freeze-induced fusion and leakage of liposomes." *Plant Physiology* **111**(1): 313-327.

Uemura, M., R. A. Joseph and P. L. Steponkus (1995). "Cold-Acclimation of Arabidopsis-Thaliana - Effect on Plasma-Membrane Lipid-Composition and Freeze-Induced Lesions." *Plant Physiology* **109**(1): 15-30.

Uemura, M. and P. L. Steponkus (1997). "Effect of cold acclimation on the lipid composition of the inner and outer membrane of the chloroplast envelope isolated from rye leaves." *Plant Physiology* **114**(4): 1493-1500.

Uno, Y., T. Furihata, H. Abe, R. Yoshida, K. Shinozaki and K. Yamaguchi-Shinozaki (2000). "Arabidopsis basic leucine zipper transcription factors involved in an abscisic acid-dependent signal transduction pathway under drought and high-salinity conditions." *Proceedings of the National Academy of Sciences of the United States of America* **97**(21): 11632-11637.

Upchurch, R. G. (2008). "Fatty acid unsaturation, mobilization, and regulation in the response of plants to stress." *Biotechnology Letters* **30**(6): 967-977.

Usher, S., L. H. Han, R. P. Haslam, L. V. Michaelson, D. Sturtevant, M. Aziz, K. D. Chapman, O. Sayanova and J. A. Napier (2017). "Tailoring seed oil composition in the real world: optimising omega-3 long chain polyunsaturated fatty acid accumulation in transgenic Camelina sativa." *Scientific Reports* **7**.

Uzilday, B., R. Ozgur, A. H. Sekmen, E. Yildiztugay and I. Turkan (2015). "Changes in the alternative electron sinks and antioxidant defence in chloroplasts of the extreme halophyte Eutrema parvulum (Thellungiella parvula) under salinity." *Ann Bot* **115**(3): 449-463.

Valentin, H. E., K. Lincoln, F. Moshiri, P. K. Jensen, Q. G. Qi, T. V. Venkatesh, B. Karunanandaa, S. R. Baszis, S. R. Norris, B. Savidge, K. J. Gruys and R. L. Last (2006). "The Arabidopsis vitamin E pathway gene5-1 mutant reveals a critical role for phytol kinase in seed tocopherol biosynthesis." *Plant Cell* **18**(1): 212-224.

van Etten, J., K. de Sousa, A. Aguilar, M. Barrios, A. Coto, M. Dell'Acqua, C. Fadda, Y. Gebrehawaryat, J. van de Gevel, A. Gupta, A. Y. Kiros, B. Madriz, P. Mathur, D. K. Mengistu, L. Mercado, J. N. Mohammed, A. Paliwal, M. E. Pe, C. F. Quiros, J. C. Rosas, N. Sharma, S. S. Singh, I. S. Solanki and J. Steinke (2019). "Crop variety management for climate adaptation supported by citizen science." *Proceedings of the National Academy of Sciences of the United States of America* **116**(10): 4194-4199.

van Leeuwen, W., J. E. Vermeer, T. W. Gadella, Jr. and T. Munnik (2007). "Visualization of phosphatidylinositol 4,5-bisphosphate in the plasma membrane of suspension-cultured tobacco BY-2 cells and whole Arabidopsis seedlings." *Plant J* **52**(6): 1014-1026.

Vergnolle, C., M. N. Vaultier, L. Taconnat, J. P. Renou, J. C. Kader, A. Zachowski and E. Ruelland (2005). "The cold-induced early activation of phospholipase C and D pathways determines the response of two distinct clusters of genes in Arabidopsis cell suspensions." *Plant Physiology* **139**(3): 1217-1233.

Vijayan, P. and J. Browse (2002). "Photoinhibition in mutants of Arabidopsis deficient in thylakoid unsaturation." *Plant Physiology* **129**(2): 876-885.

Vogel, J. T., D. G. Zarka, H. A. Van Buskirk, S. G. Fowler and M. F. Thomashow (2005). "Roles of the CBF2 and ZAT12 transcription factors in configuring the low temperature transcriptome of Arabidopsis." *Plant Journal* **41**(2): 195-211.

vom Dorp, K., G. Holzl, C. Plohmann, M. Eisenhut, M. Abraham, A. P. M. Weber, A. D. Hanson and P. Dormann (2015). "Remobilization of Phytol from Chlorophyll Degradation Is Essential for Tocopherol Synthesis and Growth of Arabidopsis." *Plant Cell* **27**(10): 2846-2859.

Vu, H. S., M. R. Roth, P. Tamura, T. Samarakoon, S. Shiva, S. Honey, K. Lowe, E. A. Schmelz, T. D. Williams and R. Welti (2014). "Head-group acylation of monogalactosyldiacylglycerol is a common stress response, and the acyl-galactose acyl composition varies with the plant species and applied stress." *Physiologia Plantarum* **150**(4): 517-528.

Vu, H. S., S. Shiva, A. S. Hall and R. Welti (2014). "A lipidomic approach to identify cold-induced changes in Arabidopsis membrane lipid composition." *Methods Mol Biol* **1166**: 199-215.

Vu, H. S., P. Tamura, N. A. Galeva, R. Chaturvedi, M. R. Roth, T. D. Williams, X. M. Wang, J. Shah and R. Welti (2012). "Direct Infusion Mass Spectrometry of Oxylipin-Containing Arabidopsis Membrane Lipids Reveals Varied Patterns in Different Stress Responses." *Plant Physiology* **158**(1): 324-339.

Vyse, K., M. Pagter, E. Zuther and D. K. Hincha (2019). "Deacclimation after cold acclimation - a crucial, but widely neglected part of plant winter survival." *J Exp Bot*.

Wada, H. and N. Murata (2007). "The essential role of phosphatidylglycerol in photosynthesis." *Photosynthesis Research* **92**(2): 205-215.

Waibel, F. and W. Filipowicz (1990). "Rna-Polymerase Specificity of Transcription of Arabidopsis U-Snrna Genes Determined by Promoter Element Spacing." *Nature* **346**(6280): 199-202.

Waibel, F. and W. Filipowicz (1990). "U6 Snrna Genes of Arabidopsis Are Transcribed by Rna Polymerase-Iii but Contain the Same 2 Upstream Promoter Elements as Rna Polymerase-Ii-Transcribed U-Snrna Genes." *Nucleic Acids Research* **18**(12): 3451-3458.

Wallis, J. G. and J. Browse (2002). "Mutants of Arabidopsis reveal many roles for membrane lipids." *Progress in Lipid Research* **41**(3): 254-278.

Walton, D. C. (1980). "BIOCHEMISTRY AND PHYSIOLOGY OF ABSCISIC-ACID." *Annual Review of Plant Physiology and Plant Molecular Biology* **31**: 453-489.

Wang, F., N. Wu, L. Zhang, G. J. Ahammed, X. Chen, X. Xiang, J. Zhou, X. Xia, K. Shi, J. Yu, C. H. Foyer and Y. Zhou (2017). "Light Signaling-dependent Regulation of Photoinhibition and Photoprotection in Tomato." *Plant Physiol*.

Wang, J. S., Q. Zhang, F. Cui, L. Hou, S. Z. Zhao, H. Xia, J. J. Qiu, T. T. Li, Y. Zhang, X. J. Wang and C. Z. Zhao (2017). "Genome-Wide Analysis of Gene Expression Provides New Insights into Cold Responses in Thellungiella salsuginea." *Frontiers in Plant Science* **8**.

Wang, W. M., X. H. Yang, S. Tangchaiburana, R. Ndeh, J. E. Markham, Y. Tsegaye, T. M. Dunn, G. L. Wang, M. Bellizzi, J. F. Parsons, D. Morrissey, J. E. Bravo, D. V. Lynch and S. Y. Xiao (2008). "An Inositolphosphorylceramide Synthase Is Involved in Regulation of Plant Programmed Cell Death Associated with Defense in Arabidopsis." *Plant Cell* **20**(11): 3163-3179.

Wang, X. J., D. C. Shi, X. Y. Wang, J. Wang, Y. S. Sun and J. Q. Liu (2015). "Evolutionary Migration of the Disjunct Salt Cress Eutrema salsugineum (= Thellungiella salsuginea, Brassicaceae) between Asia and North America." *PLoS One* **10**(5): e0124010.

Wang, X. M. (2000). "Multiple forms of phospholipase D in plants: the gene family, catalytic and regulatory properties, and cellular functions." *Progress in Lipid Research* **39**(2): 109-149.

Wang, Y. G., X. He, W. Y. Ma, X. Q. Zhao, B. Li and Y. P. Tong (2014). "Wheat PROTON GRADIENT REGULATION 5 is Involved in Tolerance to Photoinhibition." *Journal of Integrative Agriculture* **13**(6): 1206-1215.

Wang, Z., M. Gerstein and M. Snyder (2009). "RNA-Seq: a revolutionary tool for transcriptomics." *Nature Reviews Genetics* **10**(1): 57-63.

Wang, Z. I., P. H. Li, M. Fredricksen, Z. H. Gong, C. S. Kim, C. Q. Zhang, H. J. Bohnert, J. K. Zhu, R. A. Bressan, P. M. Hasegawa, Y. X. Zhao and H. Zhang (2004). "Expressed sequence tags from Thellungiella halophila, a new model to study plant salt-tolerance." *Plant Science* **166**(3): 609-616.

Wanner, L. A. and O. Junttila (1999). "Cold-induced freezing tolerance in Arabidopsis." *Plant Physiol* **120**(2): 391-400.

Warnecke, D. and E. Heinz (2003). "Recently discovered functions of glucosylceramides in plants and fungi." *Cellular and Molecular Life Sciences* **60**(5): 919-941.

Wathugala, D. L., S. A. Richards, H. Knight and M. R. Knight (2011). "OsSFR6 is a functional rice orthologue of SENSITIVE TO FREEZING-6 and can act as a regulator of COR gene expression, osmotic stress and freezing tolerance in Arabidopsis." *New Phytologist* **191**(4): 984-995.

Whitlow, T. H., N. L. Bassuk, T. G. Ranney and D. L. Reichert (1992). "An Improved Method for Using Electrolyte Leakage to Assess Membrane Competence in Plant-Tissues." *Plant Physiology* **98**(1): 198-205.

Wilhelm, K. S. and M. F. Thomashow (1993). "Arabidopsis-Thaliana Cor15b, an Apparent Homolog of Cor15a, Is Strongly Responsive to Cold and Aba, but Not Drought." *Plant Molecular Biology* **23**(5): 1073-1077.

Wong, C. E., Y. Li, A. Labbe, D. Guevara, P. Nuin, B. Whitty, C. Diaz, G. B. Golding, G. R. Gray, E. A. Weretilnyk, M. Griffith and B. A. Moffatt (2006). "Transcriptional profiling implicates novel interactions between abiotic stress and hormonal responses in Thellungiella, a close relative of Arabidopsis." *Plant Physiology* **140**(4): 1437-1450.

Wong, C. E., Y. Li, B. R. Whitty, C. Diaz-Camino, S. R. Akhter, J. E. Brandle, G. B. Golding, E. A. Weretilnyk, B. A. Moffatt and M. Griffith (2005). "Expressed sequence tags from the Yukon ecotype of Thellungiella reveal that gene expression in response to cold, drought and salinity shows little overlap." *Plant Molecular Biology* **58**(4): 561-574.

Worrall, D., Y. K. Liang, S. Alvarez, G. H. Holroyd, S. Spiegel, M. Panagopulos, J. E. Gray and A. M. Hetherington (2008). "Involvement of sphingosine kinase in plant cell signalling." *Plant J* **56**(1): 64-72.

Wu, H. J., Z. H. Zhang, J. Y. Wang, D. H. Oh, M. Dassanayake, B. H. Liu, Q. F. Huang, H. X. Sun, R. Xia, Y. R. Wu, Y. N. Wang, Z. Yang, Y. Liu, W. K. Zhang, H. W. Zhang, J. F. Chu, C. Y. Yan, S. Fang, J. S. Zhang, Y. Q. Wang, F. X. Zhang, G. D. Wang, S. Y. Lee, J. M. Cheeseman, B. C. Yang, B. Li, J. M. Min, L. F. Yang, J. Wang, C. C. Chu, S. Y. Chen, H. J. Bohnert, J. K. Zhu, X. J. Wang and Q. Xie (2012). "Insights into salt tolerance from the genome of Thellungiella salsuginea." *Proceedings of the National Academy of Sciences of the United States of America* **109**(30): 12219-12224.

Xie, K. B., B. Minkenberg and Y. N. Yang (2015). "Boosting CRISPR/Cas9 multiplex editing capability with the endogenous tRNA-processing system." *Proceedings of the National Academy of Sciences of the United States of America* **112**(11): 3570-3575.

Xin, Z. and J. Browse (2000). "Cold comfort farm: the acclimation of plants to freezing temperatures." *Plant Cell and Environment* **23**(9): 893-902.

Xing, H. L., L. Dong, Z. P. Wang, H. Y. Zhang, C. Y. Han, B. Liu, X. C. Wang and Q. J. Chen (2014). "A CRISPR/Cas9 toolkit for multiplex genome editing in plants." *Bmc Plant Biology* **14**.

Xiong, L. and J. K. Zhu (2003). "Regulation of abscisic acid biosynthesis." *Plant Physiol* **133**(1): 29-36.

Xiong, L. M., K. S. Schumaker and J. K. Zhu (2002). "Cell signaling during cold, drought, and salt stress." *Plant Cell* **14**: S165-S183.

Xu, C. C., J. L. Fan, A. J. Cornish and C. Benning (2008). "Lipid trafficking between the endoplasmic reticulum and the plastid in Arabidopsis requires the extraplastidic TGD4 protein." *Plant Cell* **20**(8): 2190-2204.

Xu, S. M., X. C. Wang and J. Chen (2007). "Zinc finger protein 1 (ThZF1) from salt cress (Thellungiella halophila) is a Cys-2/His-2-type transcription factor involved in drought and salt stress." *Plant Cell Reports* **26**(4): 497-506.

Xu, X. J., J. C. Feng, S. Y. Lu, G. T. Lohrey, H. L. An, Y. J. Zhou and M. A. Jenks (2014). "Leaf cuticular lipids on the Shandong and Yukon ecotypes of saltwater cress, Eutrema salsugineum, and their response to water deficiency and impact on cuticle permeability." *Physiologia Plantarum* **151**(4): 446-458.

Xu, Y., K. M. P. Caldo, K. Jayawardhane, J. A. Ozga, R. J. Weselake and G. Chen (2019). "A transferase interactome that may facilitate channeling of polyunsaturated fatty acid moieties from phosphatidylcholine to triacylglycerol." *J Biol Chem*.

Xu, Z. Y., X. Zhang, M. Schlappi and Z. Q. Xu (2011). "Cold-inducible expression of AZI1 and its function in improvement of freezing tolerance of Arabidopsis thaliana and Saccharomyces cerevisiae." *J Plant Physiol* **168**(13): 1576-1587.

Xue-Xuan, X., S. Hong-Bo, M. Yuan-Yuan, X. Gang, S. Jun-Na, G. Dong-Gang and R. Cheng-Jiang (2010). "Biotechnological implications from abscisic acid (ABA) roles in cold stress and leaf senescence as an important signal for improving plant sustainable survival under abiotic-stressed conditions." *Crit Rev Biotechnol* **30**(3): 222-230.

Xue, H. W., X. Chen and Y. Me (2009). "Function and regulation of phospholipid signalling in plants." *Biochemical Journal* **421**: 145-156.

Yadav, N. S., A. Wierzbicki, M. Aegerter, C. S. Caster, L. Perezgrau, A. J. Kinney, W. D. Hitz, J. R. Booth, B. Schweiger, K. L. Stecca, S. M. Allen, M. Blackwell, R. S. Reiter, T. J. Carlson, S. H. Russell, K. A. Feldmann, J. Pierce and J. Browse (1993). "Cloning of Higher-Plant Omega-3-Fatty-Acid Desaturases." *Plant Physiology* **103**(2): 467-476.

Yamaguchi-Shinozaki, K. and K. Shinozaki (1994). "A Novel Cis-Acting Element in an Arabidopsis Gene Is Involved in Responsiveness to Drought, Low-Temperature, or High-Salt Stress." *Plant Cell* **6**(2): 251-264.

Yamaguchi-Shinozaki, K. and K. Shinozaki (2006). "Transcriptional regulatory networks in cellular responses and tolerance to dehydration and cold stresses." *Annu Rev Plant Biol* **57**: 781-803.

Yamori, W., N. Sakata, Y. Suzuki, T. Shikanai and A. Makino (2011). "Cyclic electron flow around photosystem I via chloroplast NAD(P)H dehydrogenase (NDH) complex performs a significant physiological role during photosynthesis and plant growth at low temperature in rice." *Plant Journal* **68**(6): 966-976.

Yamori, W. and T. Shikanai (2016). "Physiological Functions of Cyclic Electron Transport Around Photosystem I in Sustaining Photosynthesis and Plant Growth." *Annual Review of Plant Biology, Vol 67* **67**: 81-106.

Yan, L. H., S. W. Wei, Y. R. Wu, R. L. Hu, H. J. Li, W. C. Yang and Q. Xie (2015). "High-Efficiency Genome Editing in Arabidopsis Using YAO Promoter-Driven CRISPR/Cas9 System." *Molecular Plant* **8**(12): 1820-1823.

Yang, R. L., D. E. Jarvis, H. Chen, M. A. Beilstein, J. Grimwood, J. Jenkins, S. Q. Shu, S. Prochnik, M. M. Xin, C. Ma, J. Schmutz, R. A. Wing, T. Mitchell-Olds, K. S. Schumaker and X. F. Wang (2013). "The reference genome of the halophytic plant Eutrema salsugineum." *Frontiers in Plant Science* **4**.

Yang, X. P., H. Y. Zhao, D. K. Kosma, P. Tomasi, J. M. Dyer, R. J. Li, X. L. Liu, Z. Y. Wang, E. P. Parsons, M. A. Jenks and S. Y. Lu (2017). "The Acyl Desaturase CER17 Is Involved in Producing Wax Unsaturated Primary Alcohols and Cutin Monomers." *Plant Physiology* **173**(2): 1109-1124.

Yang, Y., N. Yao, Z. K. Jia, J. Duan, F. J. Chen, Z. Y. Sang and L. Y. Ma (2016). "Effect of exogenous abscisic acid on cold acclimation in two Magnolia species." *Biologia Plantarum* **60**(3): 555-562.

Yoshida, S. and M. Uemura (1986). "Lipid-Composition of Plasma-Membranes and Tonoplasts Isolated from Etiolated Seedlings of Mung Bean (Vigna-Radiata L)." *Plant Physiology* **82**(3): 807-812.

Yoshida, S., K. Washio, J. Kenrick and G. Orr (1988). "Thermotropic Properties of Lipids Extracted from Plasma-Membrane and Tonoplast Isolated from Chilling-Sensitive Mung Bean (Vigna-Radiata [L] Wilczek)." *Plant and Cell Physiology* **29**(8): 1411-1416.

Zhang, H., J. L. Dong, X. H. Zhao, Y. M. Zhang, J. Y. Ren, L. T. Xing, C. J. Jiang, X. G. Wang, J. Wang, S. L. Zhao and H. Q. Yu (2019). "Research Progress in Membrane Lipid Metabolism and Molecular Mechanism in Peanut Cold Tolerance." *Frontiers in Plant Science* **10**.

Zhang, J. Y., X. M. Li, H. X. Lin and K. Chong (2019). "Crop Improvement Through Temperature Resilience." *Annual Review of Plant Biology, Vol 70* **70**: 753-780.

Zhang, Q. Y., L. Y. Wang, F. Y. Kong, Y. S. Deng, B. Li and Q. W. Meng (2012). "Constitutive accumulation of zeaxanthin in tomato alleviates salt stress-induced photoinhibition and photooxidation." *Physiologia Plantarum* **146**(3): 363-373.

Zhang, R. and T. D. Sharkey (2009). "Photosynthetic electron transport and proton flux under moderate heat stress." *Photosynth Res* **100**(1): 29-43.

Zhang, X., S. G. Fowler, H. Cheng, Y. Lou, S. Y. Rhee, E. J. Stockinger and M. F. Thomashow (2004). "Freezing-sensitive tomato has a functional CBF cold response pathway, but a CBF regulon that differs from that of freezing-tolerant Arabidopsis." *Plant J* **39**(6): 905-919.

Zhang, X. D., R. P. Wang, F. J. Zhang, F. Q. Tao and W. Q. Li (2013). "Lipid profiling and tolerance to low-temperature stress in Thellungiella salsuginea in comparison with Arabidopsis thaliana." *Biologia Plantarum* **57**(1): 149-153.

Zhang, Y., S. H. Shi, F. L. Li, C. Z. Zhao, A. Q. Li, L. Hou, H. Xia, B. S. Wang, J. L. Baltazar, X. J. Wang and S. Z. Zhao (2019). "Global transcriptome analysis provides new insights in Thellungiella salsuginea stress response." *Plant Biology* **21**(5): 796-804.

Zhang, Z., L. Hua, A. Gupta, D. Tricoli, K. J. Edwards, B. Yang and W. Li (2019). "Development of an Agrobacterium-delivered CRISPR/Cas9 system for wheat genome editing." *Plant Biotechnol J* **17**(8): 1623-1635.

Zheng, H., O. Rowland and L. Kunst (2005). "Disruptions of the Arabidopsis Enoyl-CoA reductase gene reveal an essential role for very-long-chain fatty acid synthesis in cell expansion during plant morphogenesis." *Plant Cell* **17**(5): 1467-1481.

Zhou, Y., L. T. Zeng, X. M. Fu, X. Mei, S. H. Cheng, Y. Y. Liao, R. F. Deng, X. L. Xu, Y. M. Jiang, X. W. Duan, S. Baldermann and Z. Y. Yang (2016). "The sphingolipid biosynthetic enzyme Sphingolipid delta8 desaturase is important for chilling resistance of tomato." *Scientific Reports* **6**.

Zhu, J. K. (2001). "Cell signaling under salt, water and cold stresses." *Current Opinion in Plant Biology* **4**(5): 401-406.

Zhu, J. K. (2015). "The Next Top Models." *Cell* **163**(1): 18-18.

Zuther, E., K. Buchel, M. Hundertmark, M. Stitt, D. K. Hincha and A. G. Heyer (2004). "The role of raffinose in the cold acclimation response of Arabidopsis thaliana." *FEBS Lett* **576**(1-2): 169-173.

Zuther, E., I. Juszczak, Y. P. Lee, M. Baier and D. K. Hincha (2015). "Time-dependent deacclimation after cold acclimation in Arabidopsis thaliana accessions." *Sci Rep* **5**: 12199.

Zuther, E., Y. P. Lee, A. Erban, J. Kopka and D. K. Hincha (2018). "Natural Variation in Freezing Tolerance and Cold Acclimation Response in Arabidopsis thaliana and Related Species." *Survival Strategies in Extreme Cold and Desiccation: Adaptation Mechanisms and Their Applications* **1081**: 81-98.

Zuther, E., E. Schulz, L. H. Childs and D. K. Hincha (2012). "Clinal variation in the non-acclimated and cold-acclimated freezing tolerance of Arabidopsis thaliana accessions." *Plant Cell Environ* **35**(10): 1860-1878.

Appendices

Appendix 1 NCBI BLAST Results for the Designed gRNAs

To confirm the sequence uniqueness of the four gRNAs selected. gRNA1 and gRNA2 targeted conserved regions in exons 1 and 7, respectively, of *ThFAD7* and *ThFAD8*, gRNA3 targeted exon 1 of *ThFAD7*, and gRNA4 targeted exon 1 of *ThFAD8*. ID, identity; G, Gap; Q. start, Query start; Q. end, Query end; S. start, Subject start; S. end, Subject end.

gRNA	Sequence ID	% ID	Alignment length	Mismatch number	G	Q. start	Q. end	S. start	S. end	E value	Score (bits)	Predicted Definition
1	XM_006398954.2	100	23	0	0	1	23	655	633	6.24e-06	46.1	Eutrema salsugineum temperature-sensitive sn-2 acyl-lipid omega-3 desaturase (ferredoxin), chloroplastic (LOC18018373), mRNA (FAD8)
1	XM_006407405.2	100	23	0	0	1	23	706	684	6.24e-06	46.1	Eutrema salsugineum omega-3 fatty acid desaturase, chloroplastic (LOC18023475), mRNA (FAD7)
1	XM_024154385.1	100	15	0	0	1	15	1748	1762	0.37	30.2	Eutrema salsugineum ELKS/Rab6-interacting/CAST family member 1 (LOC18015239), mRNA
1	XM_006401564.2	100	14	0	0	4	17	809	822	1.5	28.2	Eutrema salsugineum stomatin-like protein 2, mitochondrial (LOC18017567), mRNA
1	XM_024148225.1	94.4	18	1	0	4	21	2778	2795	1.5	28.2	Eutrema salsugineum uncharacterized LOC18027229 (LOC18027229), transcript variant X3, mRNA
1	XM_024148224.1	94.4	18	1	0	4	21	2898	2915	1.5	28.2	Eutrema salsugineum uncharacterized LOC18027229 (LOC18027229), transcript variant X2, mRNA
1	XM_024148223.1	94.4	18	1	0	4	21	2157	2174	1.5	28.2	Eutrema salsugineum uncharacterized LOC18027229 (LOC18027229), transcript variant X1, mRNA

(Continued on the next page)

gRNA	Sequence ID	% ID	Alignment length	Mismatch number	G	Q. start	Q. end	S. start	S. end	E value	Score (bits)	Predicted
1	XM_024151761.1	100	13	0	0	3	15	435	447	5.8	26.3	Eutrema salsugineum ras GTPase-activating protein-binding protein 1 (LOC18012980), mRNA
1	XM_006395647.2	100	13	0	0	1	13	389	401	5.8	26.3	Eutrema salsugineum pentatricopeptide repeat-containing protein At2g03380, mitochondrial (LOC18011545), mRNA
1	XM_006394152.2	100	13	0	0	5	17	735	747	5.8	26.3	Eutrema salsugineum protein trichome birefringence-like 14 (LOC18011673), mRNA
2	XM_006398954.2	100	23	0	0	1	23	1323	1301	6.35e-06	46.1	Eutrema salsugineum temperature-sensitive sn-2 acyl-lipid omega-3 desaturase (ferredoxin), chloroplastic (LOC18018373), mRNA
2	XM_006407405.2	100	23	0	0	1	23	1374	1352	6.35e-06	46.1	Eutrema salsugineum omega-3 fatty acid desaturase, chloroplastic (LOC18023475), mRNA
2	XM_006414910.2	100	14	0	0	10	23	564	577	1.5	28.2	Eutrema salsugineum uncharacterized CRM domain-containing protein At3g25440, chloroplastic (LOC18029980), transcript variant X3, mRNA
2	XM_024149463.1	100	14	0	0	10	23	466	479	1.5	28.2	Eutrema salsugineum uncharacterized CRM domain-containing protein At3g25440, chloroplastic (LOC18029980), transcript variant X2, mRNA
2	XM_024149462.1	100	14	0	0	10	23	564	577	1.5	28.2	Eutrema salsugineum uncharacterized CRM domain-containing protein At3g25440, chloroplastic (LOC18029980), transcript variant X1, mRNA

(Continued on the next page)

gRNA	Sequence ID	% ID	Alignment length	Mismatch number	G	Q. start	Q. end	S. start	S. end	E value	Score (bits)	Predicted
2	XM_024159397.1	100	14	0	0	10	23	1496	1483	1.5	28.2	Eutrema salsugineum DNA mismatch repair protein MSH2 (LOC18023691), mRNA
2	XM_006389858.2	100	13	0	0	4	16	283	271	5.9	26.3	Eutrema salsugineum protein WHAT'S THIS FACTOR 1 homolog (LOC18009219), mRNA
2	XM_006389779.2	100	13	0	0	11	23	2147	2159	5.9	26.3	Eutrema salsugineum putative cyclic nucleotide-gated ion channel 8 (LOC18008625), mRNA
2	XM_006394631.2	100	13	0	0	1	13	4070	4058	5.9	26.3	Eutrema salsugineum MAG2-interacting protein 2 (LOC18012302), transcript variant X3, mRNA
2	XM_024151778.1	100	13	0	0	1	13	4306	4294	5.9	26.3	Eutrema salsugineum MAG2-interacting protein 2 (LOC18012302), transcript variant X2, mRNA
3	XM_006407405.2	100	23	0	0	1	23	515	493	$6.24e^{-06}$	46.1	Eutrema salsugineum omega-3 fatty acid desaturase, chloroplastic (LOC18023475), mRNA
3	XM_006402731.2	100	15	0	0	1	15	362	376	0.37	30.2	Eutrema salsugineum MATH domain and coiled-coil domain-containing protein At3g58280 (LOC18019700), mRNA
3	XM_006395551.2	94.4	18	1	0	1	18	895	878	1.5	28.2	Eutrema salsugineum homocysteine S-methyltransferase 1 (LOC18013142), mRNA
3	XM_006399517.2	100	14	0	0	4	17	434	421	1.5	28.2	Eutrema salsugineum putative methyltransferase DDB_G0268948 (LOC18017792), mRNA
3	XM_024156703.1	100	13	0	0	1	13	1483	1471	5.8	26.3	Eutrema salsugineum serine/threonine-protein kinase AGC1-7 (LOC18008419), mRNA
3	XM_006390785.2	100	13	0	0	1	13	88	76	5.8	26.3	Eutrema salsugineum probable phosphoglucomutase, cytoplasmic 2 (LOC18009113), mRNA
3	XM_006393320.2	100	13	0	0	1	13	164	152	5.8	26.3	Eutrema salsugineum translation initiation factor IF-2 (LOC18011167), mRNA

(Continued on the next page)

gRNA	Sequence ID	% ID	Alignment length	Mismatch number	G	Q. start	Q. end	S. start	S. end	E value	Score (bits)	Predicted
3	XM_006392969.2	100	13	0	0	1	13	1375	1363	5.8	26.3	Eutrema salsugineum KH domain-containing protein HEN4 (LOC18010752), transcript variant X2, mRNA
3	XM_024150240.1	100	13	0	0	1	13	1418	1406	5.8	26.3	Eutrema salsugineum KH domain-containing protein HEN4 (LOC18010752), transcript variant X1, mRNA
3	XM_006395488.2	100	13	0	0	3	15	488	476	5.8	26.3	Eutrema salsugineum uncharacterized LOC18011826 (LOC18011826), mRNA
4	XM_006398954.2	100	23	0	0	1	23	465	443	6.27 e-06	46.1	Eutrema salsugineum temperature-sensitive sn-2 acyl-lipid omega-3 desaturase (ferredoxin), chloroplastic (LOC18018373), mRNA
4	XM_006392559.2	100	12	0	0	2	13	2	13	23	24.3	Eutrema salsugineum L-ascorbate oxidase homolog (LOC18011377), mRNA
4	XM_006400403.2	100	12	0	0	2	13	1352	1363	23	24.3	Eutrema salsugineum basic 7S globulin (LOC18018930), mRNA
4	XM_006407492.2	100	12	0	0	4	15	390	401	23	24.3	Eutrema salsugineum probable U3 small nucleolar RNA-associated protein 7 (LOC18023417), mRNA
4	XM_006409540.2	100	12	0	0	4	15	1036	1047	23	24.3	Eutrema salsugineum uncharacterized LOC18026137 (LOC18026137), mRNA
4	XM_024157021.1	100	12	0	0	4	15	2927	2916	23	24.3	Eutrema salsugineum DNA helicase INO80 (LOC18019967), mRNA
4	XM_006406309.2	100	12	0	0	1	12	81	70	23	24.3	Eutrema salsugineum DNA polymerase I B, chloroplastic/mitochondrial (LOC18024602),
4	XM_024159119.1	93.8	16	1	0	7	22	145	130	23	24.3	Eutrema salsugineum cell wall integrity protein scw1 (LOC18023972), mRNA
4	XM_024147868.1	100	12	0	0	2	13	243	232	23	24.3	Eutrema salsugineum alpha-L-fucosidase 1 (LOC18027421), mRNA
4	XM_024150593.1	100	11	0	0	4	14	593	603	91	22.3	Eutrema salsugineum uncharacterized LOC112082907 (LOC112082907), mRNA

Appendix 2 Guide RNA Promoter Sequences

Nucleotide sequence for the four promoters used to express each of the four guide RNAs, the promoters were chosen based on published work which is referenced below each of the promoters' name.

Name	Promoter Sequence
pU3B (Ma *et al.* 2015, Morineau *et al.* 2016)	TTTACTTTAAATTTTTTCTTATGCAGCCTGTGATGGATAACTGAAT CAAACAAATGGCGTCTGGGTTTAAGAAGATCTGTTTTGGCTATG TTGGACGAAACAAGTGAACTTTTAGGATCAACTTCAGTTTATATA TGGAGCTTATATCGAGCAATAAGATAAGTGGGCTTTTTATGTAAT TTAATGGGCTATCGTCCATAGATTCACTAATACCCATGCCCAGTA CCCATGTATGCGTTTCATATAAGCTCCTAATTTCTCCCACATCGC TCAAATCTAAACAAATCTTGTTGTATATATAACACTGAGGGAGCA ACATTGGTCACGACCTTACTTGAACAGGATCTGTTCTATAGGCT CGTACCTCTGTTTCCTTGATTTCTCAAGAGACAGGCCCTTAACC CTGGTTGATGAACCATGACCGTGCGGCTAGAGCGTGATTGACG GCTACGATCGTCCTCGGACGCATCCAGTGCTGTAGAGGATCGT TACTCGGCTCGGTTTCTACCTTGCCGGGGTGGTCGCACGGCGG TCTGACAGGTCCCTTTCCTTTTTTCTTTTTTTTGCCATAAACTTAA ATTTGTATATCGATCATTGTAGATATTGAAAACCTAGAACAAACC AACATCCATGTGAATGTCTTTCATGACTGATTTAGAGATCATTCT TGAATTTTGGAACTAGAATCTATAATGAGCCC
pU6-29 (Ma *et al.* 2015)	AAATATCAGAGATCTCTTACAGTTAGTTTCGTTCTTAATCCAAACT ACTGCAGCCTGACAGACAAATGAGGATGCAAACAATTTTAAAGT TTATCTAACGCTAGCTGTTTTGTTTCTTCTCTCTGGTGCACCAAC GACGGCGTTTTCTCAATCATAAAGAGGCTTGTTTTACTTAAGGCC AATAATGTTGATGGATCGAAAGAAGAGGGCTTTTAATAAACGAG CCCGTTTAAGCTGTAAACGATGTCAAAAACATCCCACATCGTTCA GTTGAAAATAGAAGCTCTGTTTATATATTGGTAGAGTCGACTAAG AGATTGTCCCTTCGGGGACATCCGATAAAATTGGAACGATACAG AGAAGATTAGCATGGCCCCTGCGCAAGGATGACACGCATAAATC GAGAAATGGTCCAAATTTTTTTGGATAGAATTTCCCAGCTTTTTT GCGTGTTTCAGCTCTCATGATCCTTGGCCAATGGGTGTAGTAAA TTTTCTGCACATTCATTGGATGGAAAAGAATGGTTTTAGCTTTAG GGAATAAGAAAAGTGTATAAGGGGATTTTTGTACAATCACATTTG AATTAGGTCTTTGAAGTGACATGGAATGAGGACATATGATGAAG CTCTGTCCCTTCCAAGAAGTAAGCCGGTGTTCTTGTCTCAGATTT TCGTTTGGCCCTGACATAAACAGAGTCATAACCTTACTAGGAGG GTTAACTTGATTTTGCAGCAAAGAAGAGGCTTTTCCATTATGTAT TCGGTTGCTAATACATAATGGAACGATATATTCGAGATTTATATA GTAAAACTATAATCCAACCATAAACTCATGGGACATTTATATGCC AAGCTT

(Continued on the next page)

Name	Promoter Sequence
pU6-1 (Ma *et al.* 2015)	AGAAATCTCAAAATTCCGGCAGAACAATTTTGAATCTCGATCCGT AGAAACGAGACGGTCATTGTTTTAGTTCCACCACGATTATATTTG AAATTTACGCTGAGTGTGAGTGAGACTTGCATAAGAAAATAAAAT CTTTAGTTGGGAAAAAATTCAATAATATAAATGGGCTTGAGAAGG AAGCGAGGGATAGGCCTTTTTCTAAAATAGGCCCATTTAAGCTA TTAACAATCTTCAAAAGTACCACATCGCTTAGGTAAAGAAAGCAG CTGAGTTTATATATGGTTAGAGACGAAGTAGTGATTGTCCCTTCG GGGACATCCGATAAAATTGGAACGATACAGAGAAGATTAGCATG GCCCCTGCGCAAGGATGACACGCATAAATCGAGAAATGGTCCA AATTTTTTTTGGCAAAAATTTTCAGATTTTTTCTTCATCTGTAGATT TCTGGGTTTTTTTTTCCGTTTCGGTGAATCATAAGTGAAGTTTTG GATGCAAATCTGCGCGAAAAAAGTTGGACCTGCAATGAGCTTAT TTAGATAGCTAAGACAAAGTGATTGGTCCGTTGTTTCAGTTCTGA TTGTCAGAGAGTTTGTTTCGAGACGGCGACACCAATGCGTTTTG TTAACCAGATTTCGGGTAAGAAATGTATCGAGAGTTTGTTTCGAG ACGGCTACATCATTTTCTTATGAAGGGTGAAATTAGATAGACCAA AGATTGAAACACAACATTTCTTTCACAAAAATATAATAAACTTGAT AGCATTTAGGATCAGCTACTCTCACTAATCAGT
pU6-26 (Ma *et al.* 2015, Morineau *et al.* 2016)	AAGCTTCGTTGAACAACGGAAACTCGACTTGCCTTCCGCACAAT ACATCATTTCTTCTTAGCTTTTTTTCTTCTTCTTCGTTCATACAGT TTTTTTTTGTTTATCAGCTTACATTTTCTTGAACCGTAGCTTTCGT TTTCTTCTTTTTAACTTTCCATTCGGAGTTTTTGTATCTTGTTTCAT AGTTTGTCCCAGGATTAGAATGATTAGGCATCGAACCTTCAAGA ATTTGATTGAATAAAACATCTTCATTCTTAAGATATGAAGATAATC TTCAAAAGGCCCCTGGGAATCTGAAAGAAGAGAAGCAGGCCCA TTTATATGGGAAAGAACAATAGTATTTCTTATATAGGCCCATTTAA GTTGAAAACAATCTTCAAAAGTCCCACATCGCTTAGATAAGAAAA CGAAGCTGAGTTTATATACAGCTAGAGTCGAAGTAGTGATTGTC CCTTCGGGGACATCCGATAAAATTGGAACGATACAGAGAAGATT AGCATGGCCCCTGCGCAAGGATGACACGCATAAATCGAGAAAT GGTCCAAATTTTTTTTGCAAAATTTTCCAGATCGATTTCTTCTTCC TCTGTTCTTCGGCGTTCAATTTCTGGGTTTTTCTCTTCGTTTTCT GTAACTGAAACCTAAAATTTGACCTAAAAAAAATCTCAAATAATAT GATTCAGTGGTTTTGTACTTTTCAGTTAGTTGAGTTTTGCAGTTC CGATGAGATAAACCAATAACTTTGCTTAGATCTAATTCATTCCGT TACACCTCTGATGGAGATGGAAGGTTCTTAATAATGATGCCATTT TTTGGGTAATAATTTTGAATTAGAATCAAGGGTATAAGATTCATA ATTAACATCACTTAAGCAAAGTTCGTAATATACGACCACAGGATA TAATTTTTGAATTC

Appendix 3 Arabidopsis and Eutrema RNA-Seq Results

The transcriptomic analysis by RNA-Seq of *Arabidopsis thaliana* (Arabidopsis) under cold stress conditions discussed in Chapter 3 was performed previously by Cristina Barrero-Sicilia, Louise V. Michaelson, and Richard P. Haslam, and the results were kindly shared with Susana Silvestre for analysis and interpretation. In parallel with Arabidopsis, the same analysis was performed in the extremophile *Eutrema salsugineum* (Eutrema). The respective results were not presented in this thesis; however, they were used occasionally for comparison with other gene-candidates studied throughout the thesis. The table below reflects this data.

Species	Gene	Protein	Log2 FC	P value
Eutrema	*ThADS4*	Acyl-CoA Desaturase Like 4	2.121	p<0.01
	ThPES1	Phytyl Esther Synthase	2.261	p<0.001
	ThSLD1	Sphingoid Long-Chain Base Δ^8-Desaturase 1	0.751	p<0.01
	ThFAD7	Fatty Acid Desaturase 7	0.759	p<0.001
	ThFAD8	Fatty Acid Desaturase 8	0.709	p<0.001
Arabidopsis	*AtIPCS1*	Inositol Phosphorylceramide Synthase 1	-1.398	p<0.001
	AtIPCS2	Inositol Phosphorylceramide Synthase 2	-0.940	p<0.001
	AtSLD1	Sphingoid Long-Chain Base Δ^8-Desaturase 1	0.612	p<0.001

Appendix 4. Genotype of the Homozygous T-DNA Lines

Mutant	T-DNA Accession	Wild-type LP/RP		RP/LBa1 of T-DNA	
		WT	Mutant	WT	Mutant
azi1	SALK_085727C				
elip2	GABI_252D03				
elip1	GABI_369A04				
elip1elip2	*elip1*	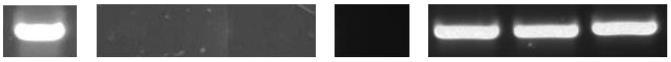			
	elip2				
cor15a	SALK_033954C				
cor15b	SALK_085398C				
ltr	SALK_118610C	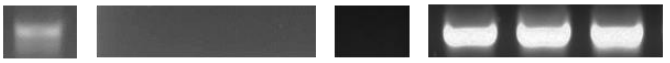			
fabo	SALK_084020C				
gstu17	SALK_139615C				
pes1	SALK_076354C	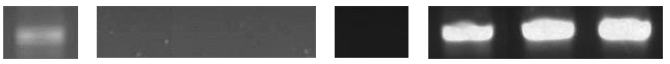			
ltp3	SALK_095248C				
ltp 4	SALK_000561C				
ads4	SALK_043674C				
ipcs3	SALK_152650C				
sfr2	SALK_112965C				
pgr5l1a	SALK_024747C				
pgr5l1b	SALK_059238C	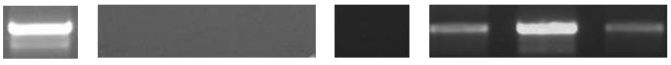			
cyp74b2	SALK_094392C				
csla1	SALK_152629C				

The T-DNA lines analysed in the chlorophyll fluorescence cold stress screen were previously confirmed to be homozygous by PCR using two sets of primer pairs. First, the left (LP) and right (RP) primers tested the absence of the wild-type sequence, followed by the use of the left border of the T-DNA insertion (LBa1) in conjunction with the RP to assess the presence of the T-DNA insertion.

Appendix 5. F_v/F_m of *pes1* and *pgr5l1a* under Control, Cold, and Recovery

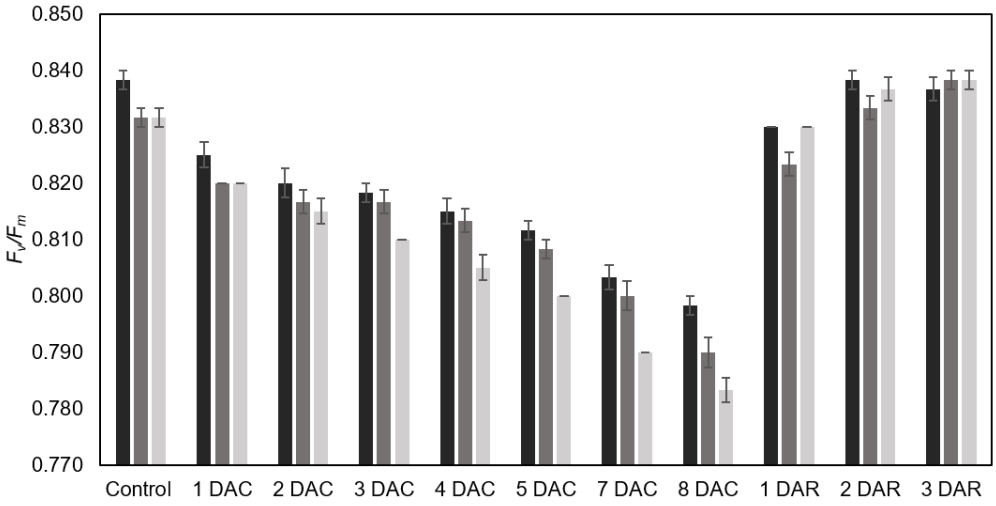

Quantitative assessment of the maximum quantum efficiency of the photosystem II (F_v/F_m) for the Arabidopsis wild-type Col-0 (■), and the T-DNA lines *pes1* (■) and *pgr5l1a* (■) measured at control conditions of 23 °C (Control) and throughout the eight days of cold stress experiment at 5 °C (1 – 8 DAC, days after cold). After which the plants were moved to control 23 °C to recover for three days (1 – 3 DAR, days after recovery). Bars represent mean ± standard error for six replicates per genotype.

Appendix 6 Canonical Multivariate Loadings for Galactolipid Profile

Canonical variates (CV) loadings with respective data variation accounted for (%) for each of the lipid class and molecular species. A CVA was performed per temperature, using “Genotype” as treatment. This data corresponds to the CVAs presented in Figure 4.6, Chapter 4, Section 4.2.4.

Lipid	Molecular Species	Control (23°C)		8 DAC (4°C)	
		CV1 (76.63%)	CV2 (18.76%)	CV1 (92.81%)	CV2 (7.19%)
lipid	ms	Cv1	Cv2	Cv3	Cv4
DGDG	34:1	0.000144	-0.000048	-0.001897	-0.000401
DGDG	34:2	-0.000062	-0.000028	0.000492	0.000102
DGDG	34:3	-0.000319	-0.000111	0.003605	0.000725
DGDG	34:4	-0.000125	-0.000091		
DGDG	34:5	-0.000069	0.000047	-0.000339	-0.000077
DGDG	34:6	-0.000287	0.000027	0.000358	0.000088
DGDG	36:3	0.000035	-0.000022	0.000646	0.000150
DGDG	36:4	-0.000066	-0.000024	0.000129	0.000041
DGDG	36:5	-0.000244	0.000326	-0.000149	-0.000036
DGDG	36:6	0.000028	-0.000161	-0.000840	-0.000230
DGDG	38:6	0.000284	-0.000210		
MGDG	34:3	-0.000089	0.000087	-0.000494	-0.000117
MGDG	34:4	-0.000277	-0.000081	-0.002434	-0.000529
MGDG	34:5	-0.000442	0.000203	-0.001546	-0.000356
MGDG	34:6	-0.000199	-0.000454	0.000723	0.000252
MGDG	36:4	-0.000376	0.000891		
MGDG	36:5	0.000002	-0.000126	0.001292	0.000252
MGDG	36:6	0.000672	0.001250	-0.001966	-0.000514
PG	32:0	0.000467	0.000333	-0.000937	-0.000228
PG	32:1	0.000108	0.000599	-0.000750	-0.000113
PG	34:1	0.000510	-0.001004	0.002440	0.000444
PG	34:2	0.000066	-0.000164	0.001051	0.000092
PG	34:3	0.000515	0.000053	-0.002430	-0.000917
PG	34:4	-0.000687	0.000122	0.002508	0.000294
SQDG	34:1	0.000010	0.000009		
SQDG	34:2	0.000061	0.000078	0.000679	0.000144
SQDG	34:3	-0.000358	0.001005	0.003086	0.000617
SQDG	34:4	0.000023	-0.000016		
SQDG	36:3	-0.000048	0.000050		
SQDG	36:5	0.000088	0.000063	0.000120	0.000022
SQDG	36:6	-0.000082	0.000254	0.000994	0.000194

Appendix 7 Canonical Multivariate Loadings for *pes1* TAG, DAG, FFA, and Phospholipids

Canonical variates (CV) loadings with respective data variation accounted for (%) for each of the lipid class (Class) and molecular species (MS). This data corresponds to the CVA presented in Figure 4.9, Chapter 4, Section 4.2.5.

TAG			DAG			FFA			Phospholipids			
MS	CV1 (91.14%)	CV2 (8.25%)	MS	CV1 (75.28%)	CV2 (22.70%)	MS	CV1 (95.28%)	CV2 (4.32%)	Class	MS	CV1 (88.06%)	CV2 (11.61%)
44:0	0.000270	0.000522	32:0	0.011930	0.012020	14:0	0.003681	0.000836	LPC	16:0	-0.000210	-0.000201
44:1	0.000588	0.001741	34:2	-0.006320	0.021210	16:0	0.001183	-0.000317	LPC	18:1	0.000053	0.000026
44:2	0.000911	-0.000632	34:3	-0.005660	-0.027640	16:1	0.000809	0.000631	LPC	18:2	-0.000394	-0.000351
46:0	-0.000419	0.000149	36:4	0.034000	-0.140920	18:0	-0.000777	0.000605	LPC	18:3	-0.000319	0.000588
46:1	0.001168	0.001158	36:5	-0.065130	0.044930	18:1	-0.000446	0.000050	PC	34:1	0.000171	0.000134
46:2	-0.003122	0.000234	36:6	0.016470	0.059550	18:2	0.000213	0.000420	PC	34:2	0.001834	0.000248
46:7	-0.000738	-0.000667	40:4	0.001200	0.013550	18:3	-0.000352	-0.000147	PC	34:3	-0.000231	-0.000353
48:0	0.000430	0.001211	40:5	0.001260	-0.060170	20:0	-0.001504	-0.000523	PC	34:4	-0.000192	-0.000060
48:1	0.000106	-0.000180				20:1	0.002318	0.000777	PC	36:2	0.000107	-0.001190
48:2	-0.001350	-0.001309				20:2	0.000596	-0.000142	PC	36:3	-0.000251	0.000653
48:3	-0.000457	-0.000533				20:3	-0.000579	-0.000425	PC	36:4	0.000226	-0.000419
48:8	-0.000560	0.000124				22:0	0.001269	0.000705	PC	36:5	0.000304	-0.000768
50:0	0.000018	0.000275				24:0	0.002696	0.000847	PC	36:6	-0.001344	0.001894
50:1	0.000870	0.000533				24:1	0.000241	-0.000092	PE	34:1	0.000059	0.000055
50:2	0.000452	-0.001183				26:0	0.000349	-0.000471	PE	34:2	0.000336	0.001078

(Continued on the next Page)

TAG					Phospholipids			
MS	CV1	CV2			Class	MS	CV1	CV2
50:3	-0.001510	-0.002363			PE	34:3	0.000091	0.000944
50:4	0.000285	-0.000622			PE	36:2	0.000113	0.000087
50:5	0.000346	0.000390			PE	36:3	0.000268	0.000085
50:6	-0.000524	-0.001498			PE	36:4	0.000481	-0.000542
50:7	-0.000886	-0.001717			PE	36:5	0.000423	-0.000320
50:8	-0.000926	0.000116			PE	36:6	0.000125	-0.000550
50:9	-0.001252	0.001520			PE	42:2	-0.000087	-0.000196
52:2	-0.001614	-0.001676			PE	42:3	0.000012	-0.000571
52:3	0.001148	0.001031			PE	42:4	0.000060	-0.000252
52:4	0.001402	0.000747			PG	32:0	0.000067	-0.000209
52:5	0.000464	0.003571			PG	32:1	-0.000476	-0.001944
52:6	0.001438	-0.000765			PG	34:1	0.000809	0.000130
52:7	-0.002757	-0.001428			PG	34:2	0.000697	0.001624
52:8	0.000483	0.000553			PG	34:3	-0.000045	-0.001371
52:9	0.000356	0.000255			PG	34:4	-0.000373	0.000459
54:2	0.000248	-0.000852			PS	34:0	-0.000016	-0.000020
54:3	-0.001383	-0.000848			PS	34:1	0.000142	0.000343
54:4	0.000147	0.001837			PS	34:3	0.000154	0.000454
54:5	-0.000157	0.001539			PS	34:4	-0.000009	0.000025
54:6	-0.000214	0.002822			PS	34:5	-0.000001	-0.000001

(Continued on the next Page)

TAG					Phospholipids			
MS	CV1	CV2			Class	MS	CV1	CV2
54:7	-0.002751	-0.001729			PS	36:1	0.000003	-0.000002
54:8	0.001102	-0.001303			PS	36:2	-0.000014	-0.000116
54:9	0.000932	-0.002641			PS	36:3	-0.000073	0.000215
56:5	-0.000175	0.000516			PS	36:5	0.000015	0.000025
56:6	-0.000537	0.001181			PS	38:2	-0.000021	0.000020
56:7	-0.000060	0.000513			PS	38:3	0.000104	0.000175
56:8	-0.000096	0.000124			PS	38:4	0.000010	-0.000039
58:4	-0.000567	0.002735			PS	38:5	-0.000011	0.000037
60:4	0.000063	0.000123			PS	38:6	-0.000005	-0.000047
60:5	-0.000028	-0.000877			PS	40:2	-0.000015	0.000032
60:6	0.000083	0.000049			PS	40:3	0.000017	0.000176
60:7	0.000391	-0.001253			PS	40:4	-0.000016	0.000028
62:0	-0.000591	-0.000651			PS	42:0	-0.000009	-0.000018
					PS	42:2	-0.000190	0.000127
					PS	42:3	0.000087	0.000012
					PS	42:4	0.000089	-0.000581
					PS	44:1	-0.000041	-0.000011
					PS	44:3	-0.000028	0.000042
					PS	44:4	-0.000010	-0.000059

Appendix 8 Canonical Multivariate Loadings *pgr5l1a* TAG, Phospholipids and FFA

Canonical variates (CV) loadings with respective data variation accounted for (%) for each of the lipid class (Class) and molecular species (MS). This data corresponds to the CVA presented in Figure 4.10, Chapter 4, Section 4.2.6

TAG			Phospholipids				FFA		
MS	CV1 (87.46%)	CV2 (7.28%)	Class	MS	CV1 (92.99%)	CV2 (5.46%)	MS	CV1 (89.67%)	CV2 (7.59%)
44:0	0.000080	0.000101	LPC	16:0	0.000223	0.000247	14:0	-0.000046	0.000215
44:1	-0.000150	0.000695	LPC	18:1	-0.000015	0.000016	16:0	0.000303	0.000413
44:2	0.000218	-0.000229	LPC	18:2	0.000245	0.000566	16:1	-0.000195	0.000156
46:0	0.000254	0.000586	LPC	18:3	0.000454	0.001043	18:0	-0.000330	-0.000350
46:1	-0.000164	0.000631	PC	34:1	0.000268	-0.000206	18:1	-0.000275	0.000765
46:2	0.000837	-0.001190	PC	34:2	0.000013	-0.000617	18:2	-0.000009	-0.000568
46:7	0.000009	0.000088	PC	34:3	0.000230	0.000851	18:3	0.000002	0.000025
48:0	-0.000087	0.000407	PC	34:4	0.000175	-0.000106	20:0	0.000281	0.000611
48:1	0.000001	0.000691	PC	36:2	-0.000083	-0.000403	20:1	0.000077	0.000619
48:2	0.000062	0.000251	PC	36:3	0.000635	-0.000455	20:2	0.000172	0.000552
48:3	0.000018	-0.000038	PC	36:4	0.000381	0.000120	20:3	0.000122	0.000269
48:8	0.000058	0.000540	PC	36:5	-0.000083	-0.000176	22:0	0.000203	-0.000545
50:0	0.000003	0.000130	PC	36:6	-0.001133	-0.000338	24:0	0.000072	0.000595
50:1	0.000313	-0.000015	PE	34:1	-0.000017	0.000033	24:1	0.000220	0.000640
50:2	0.000313	-0.000852	PE	34:2	0.000341	0.000413	26:0	-0.000538	-0.000731
50:3	0.000004	-0.000330	PE	34:3	0.000443	0.000047			

(Continued on the next page)

TAG			Phospholipids			
MS	CV1	CV2	Class	MS	CV1	CV2
50:4	0.000246	-0.000462	PE	36:2	-0.000016	0.000063
50:5	0.000155	-0.000013	PE	36:3	-0.000026	0.000266
50:6	0.000489	-0.000265	PE	36:4	-0.000001	0.000674
50:7	-0.000116	0.000184	PE	36:5	-0.000091	0.000522
50:8	-0.000162	0.000721	PE	36:6	0.000107	0.000284
50:9	0.000618	0.000404	PE	42:2	0.000034	0.000119
52:2	-0.000059	0.000321	PE	42:3	0.000106	0.000369
52:3	0.000107	0.000506	PE	42:4	0.000051	0.000154
52:4	-0.000763	0.001354	PG	32:0	-0.000052	-0.000070
52:5	-0.000795	0.001354	PG	32:1	-0.000056	-0.000391
52:6	0.001121	-0.001292	PG	34:1	-0.000404	0.000529
52:7	0.000746	-0.000386	PG	34:2	0.000004	0.001204
52:8	0.001009	0.000770	PG	34:3	-0.000087	-0.000133
52:9	-0.000069	0.002273	PG	34:4	0.000196	-0.000460
54:2	0.000277	-0.000534	PS	34:0	0.000015	-0.000009
54:3	0.000226	0.000695	PS	34:1	-0.000073	0.000020
54:4	0.000208	0.000008	PS	34:3	-0.000021	-0.000183
54:5	0.000055	-0.001015	PS	34:4	0.000005	-0.000020
54:6	0.000036	-0.000425	PS	34:5	0.000000	-0.000002
54:7	-0.000696	0.000085	PS	36:1	-0.000005	-0.000002

(Continued on the next page)

TAG			Phospholipids			
MS	CV1	CV2	Class	MS	CV1	CV2
54:8	-0.001591	-0.001071	PS	36:2	-0.000026	-0.000018
54:9	-0.000453	-0.001412	PS	36:3	0.000015	0.000018
56:5	0.000193	-0.000992	PS	36:5	-0.000020	0.000028
56:6	-0.000100	0.000022	PS	38:2	-0.000021	0.000021
56:7	0.000047	-0.000031	PS	38:3	-0.000040	0.000046
56:8	0.000078	0.000057	PS	38:4	0.000006	-0.000006
58:4	0.000165	0.000055	PS	38:5	-0.000006	0.000013
60:4	0.000032	-0.000128	PS	38:6	0.000004	0.000002
60:5	0.000058	-0.000232	PS	40:2	0.000015	-0.000025
60:6	0.000024	-0.000016	PS	40:3	-0.000013	-0.000092
60:7	0.000068	-0.000569	PS	40:4	0.000010	-0.000002
62:0	0.000102	-0.000055	PS	42:0	0.000002	-0.000004
			PS	42:2	0.000025	-0.000004
			PS	42:3	0.000046	0.000069
			PS	42:4	0.000046	0.000099
			PS	44:1	0.000000	-0.000017
			PS	44:3	-0.000002	-0.000005
			PS	44:4	0.000001	0.000001

Appendix 9 TAG Profile for *pes1*, *pgr5l1a* under Control and Cold Conditions

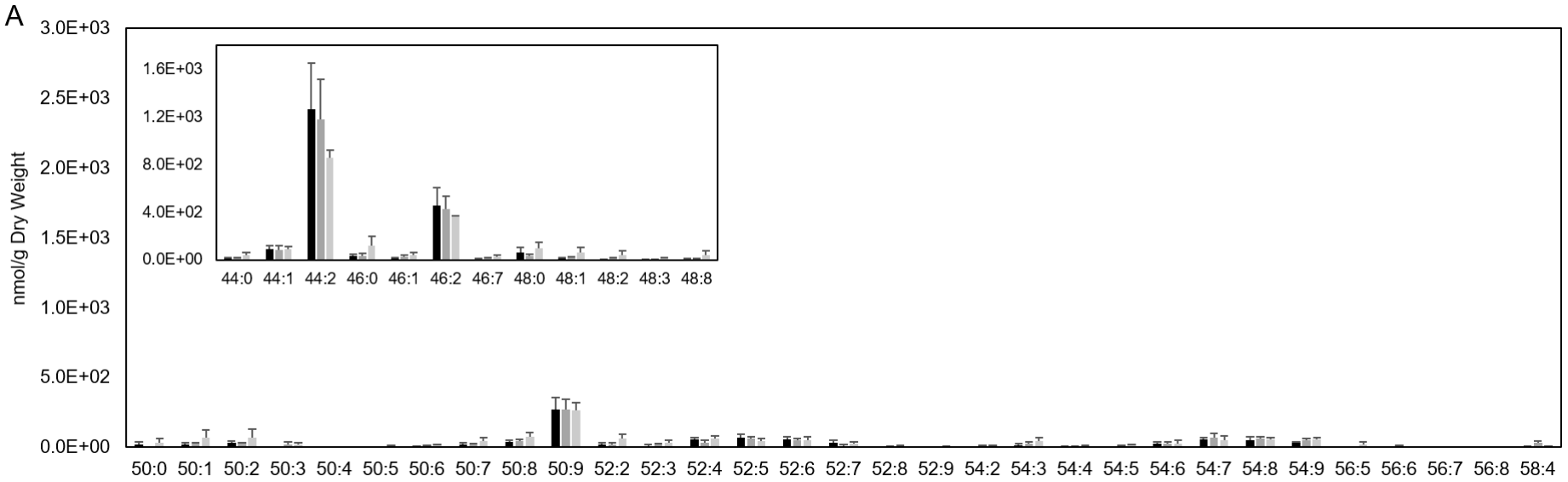

(Continued on the next page)

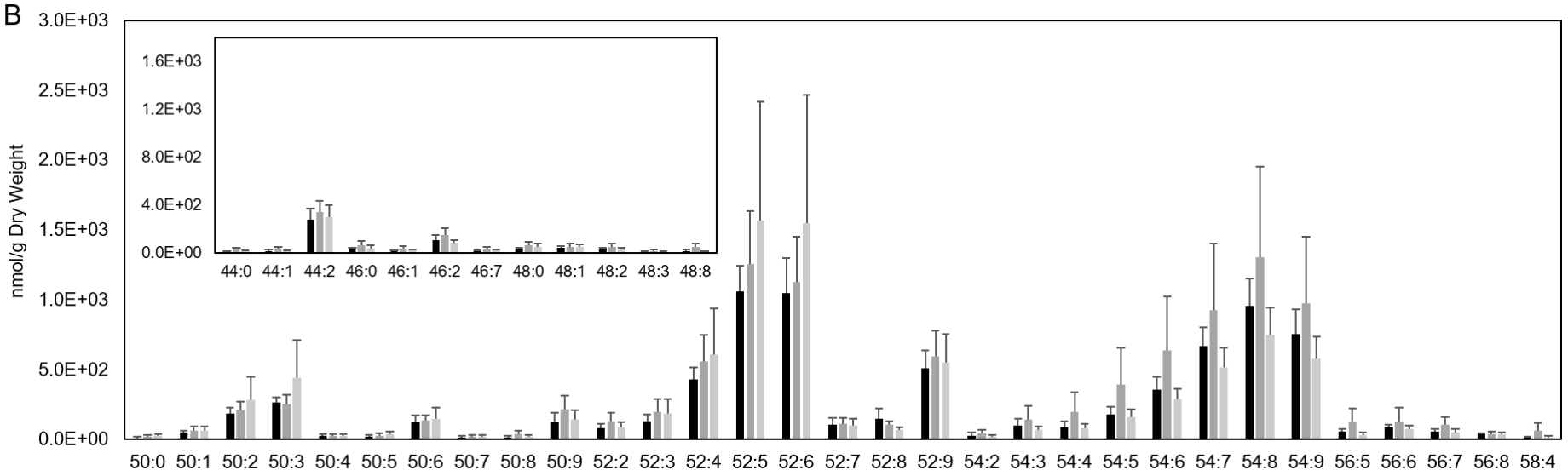

Triacylglycerol (TAG) profile for Col-0 (■), *pes1* (■), and *pgr5l1a* (■) at control 23°C (A) and eight days of cold 4°C (B). Insert shows the profile of the molecular species with a total of 44 to 48 carbon acyl chain molecular species. Bars represent mean + standard error, N=3.

Appendix 10 DAG Profile for *pes1* under Control and Cold Conditions

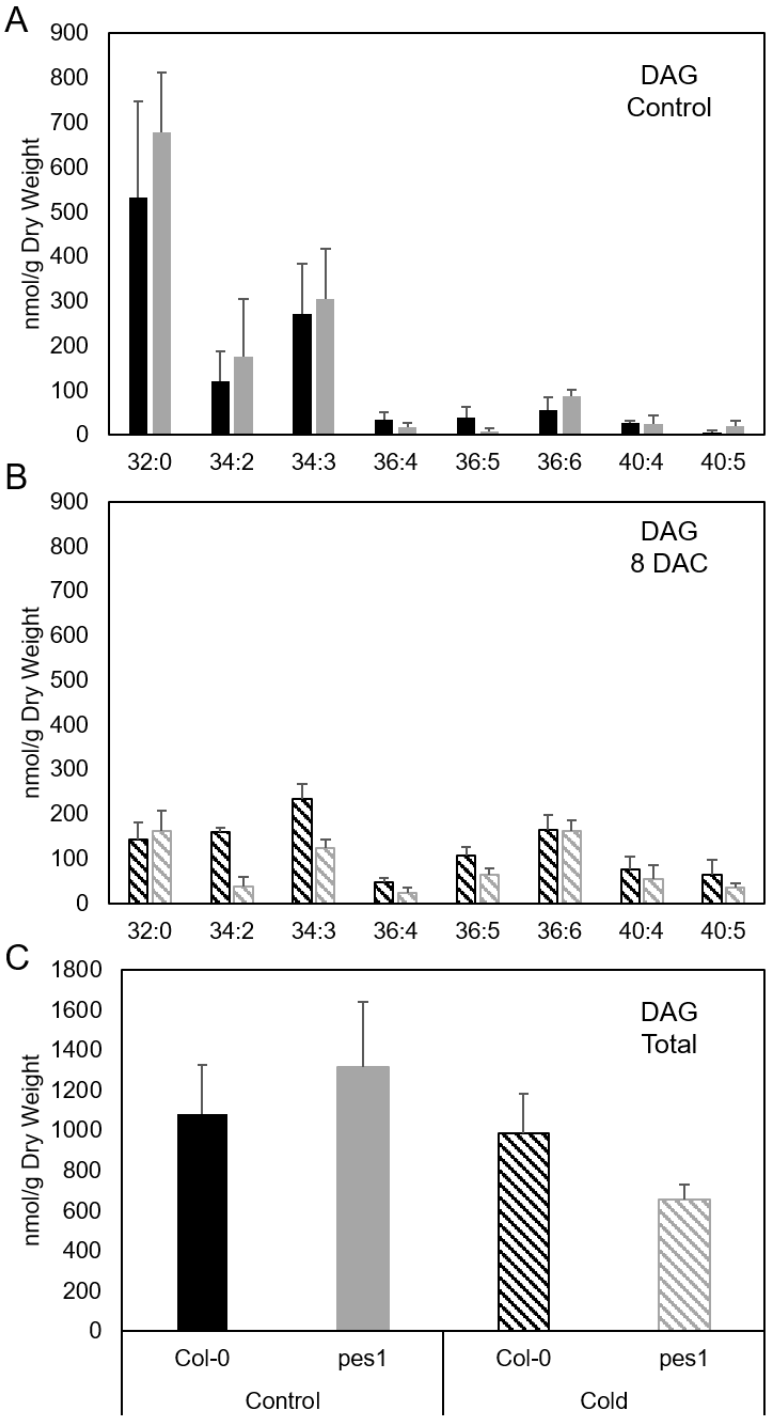

Diacylglycerol (DAG) profile for the genotypes Col-0 (■) and *pes1* (■) at control 23°C (A, block colour) and after eight days of cold 4°C (B, patterned). A canonical multivariate analysis of the profile was discussed in Chapter 4, Section 4.2.5. (C) Total DAG content per genotype (p=0.839) and temperature (p=0.140). Bars represent mean + standard error, N=3.

Appendix 11 Phospholipid Profile for *pes1* and *pgr5l1a* under Control and Cold Conditions

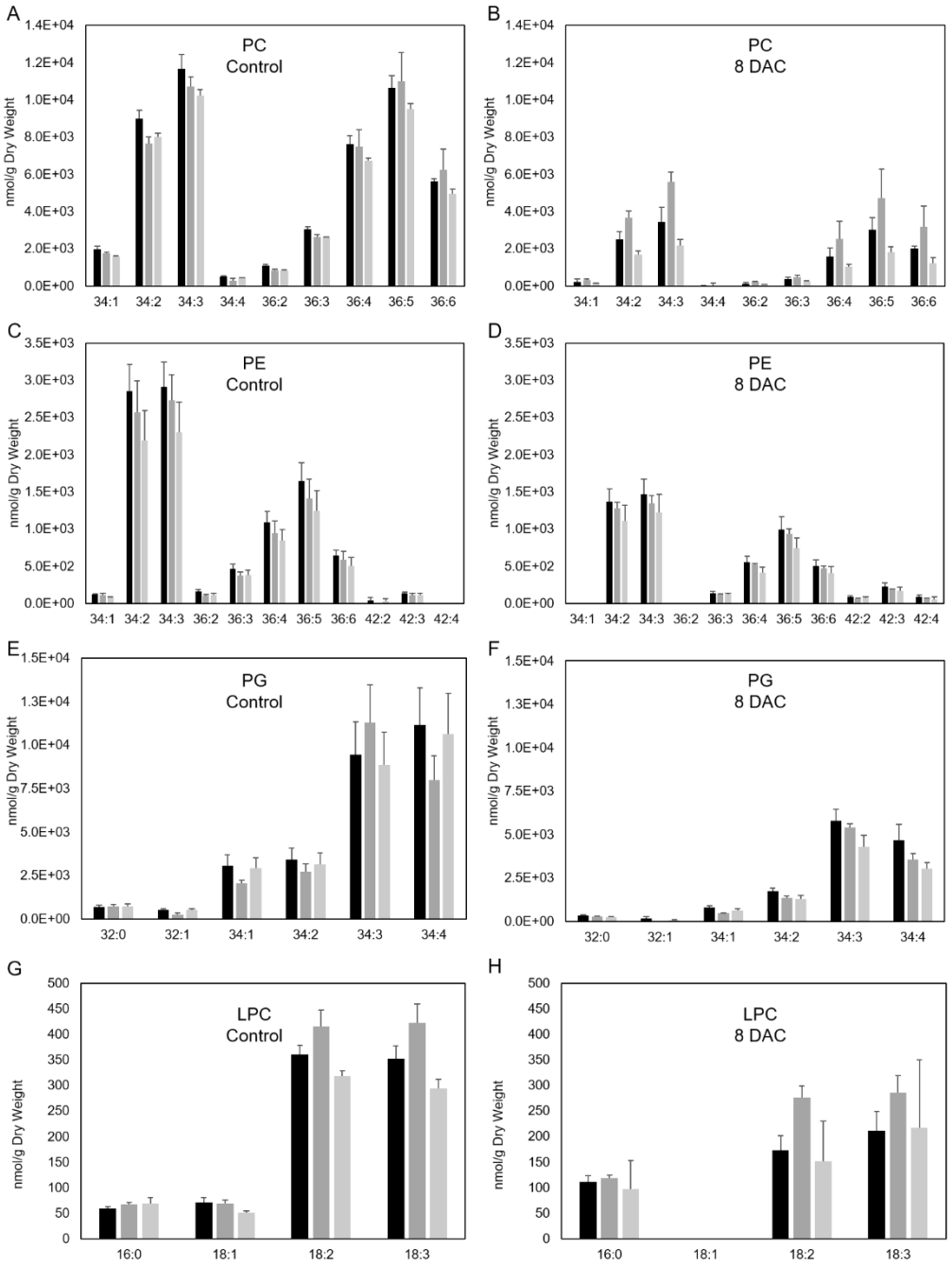

(Continued on the next page)

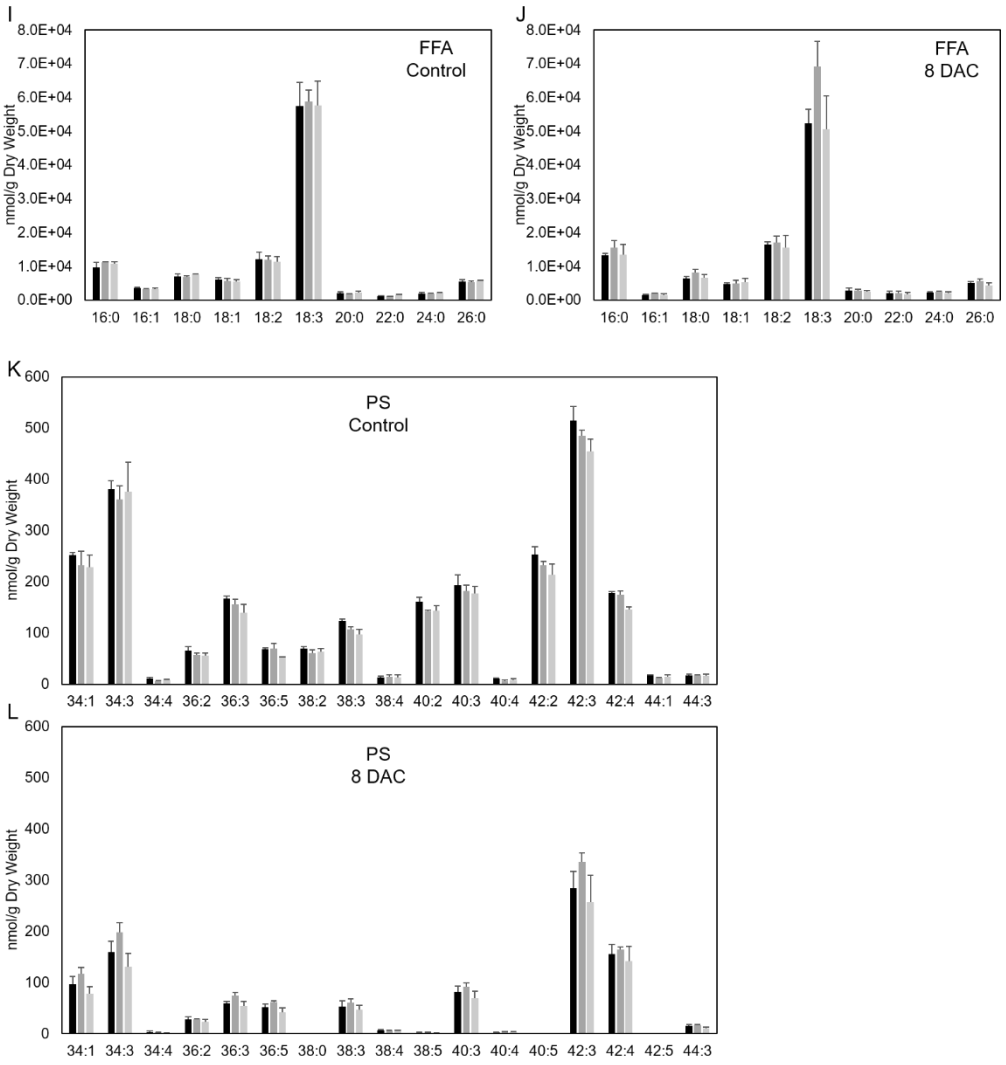

Phospholipid classes PC, phosphotadylcholine (A, B); PE, phosphatidylethanolamine (C, D); PG, phosphatodylglycerol (E, F); LPC lyso phosphotadylcholine (G, H); FFA, free fatty acids (I, J); and PS, phosphatidylserine (K, L) for genotypes Col-0 (■) , *pes1* (■), and *pgr5l1a* (■) at control 23°C (A, C, E, G, I, K) and after eight days of cold (8 DAC) at 4°C (B, D, F, H, J, L). Results discussed in Chapter 4. Bars represent mean + standard error, N=3.

Appendix 12 Principal Components Loadings for *ipcs3* Ceramide and GIPC

Principal components (PC) loadings with respective data variation accounted for (%) for the four LCBs and ten fatty acid (FA) combinations that compose ceramides and glycosylinositolphosphoryl ceramide (GIPC). This data corresponds to the PCAs presented in Figure 4.12, Chapter 4, Section 4.2.7.

LCB	FA	Ceramides			GIPC		
		PC-1 (42.01%)	PC-2 (29.78%)	PC-3 (16.05%)	PC-1 (48.57%)	PC-2 (27.20%)	PC-3 (15.52%)
d18:0	16:0	0.099	-0.071	-0.331	0.165	-0.158	0.150
	18:0	0.232	0.032	0.060	0.179	-0.141	-0.043
	20:0	0.156	-0.132	0.105	0.138	-0.187	0.171
	20:1	0.234	0.019	0.053	0.184	-0.131	0.146
	22:0	0.236	-0.005	0.050	0.177	-0.139	0.155
	22:1	0.193	0.104	0.058	0.207	0.031	0.154
	24:0	-0.016	0.003	0.030	0.187	0.049	-0.207
	24:1	0.144	0.198	0.015	0.125	0.226	0.107
	26:0	-0.032	0.253	0.164	0.135	0.021	-0.325
	26:1	0.202	0.089	-0.011	0.118	0.136	-0.276
d18:1	16:0	0.182	-0.157	-0.128	0.203	-0.093	-0.013
	18:0	0.212	0.008	0.091	0.159	-0.190	0.087
	20:0	0.236	-0.044	0.017	0.184	-0.131	0.146
	20:1	0.239	0.008	0.030	0.117	-0.039	-0.312
	22:0	0.231	-0.082	0.036	0.207	0.031	0.154
	22:1	0.154	-0.028	0.183	0.083	-0.004	0.310
	24:0	0.143	-0.214	0.067	0.125	0.226	0.107
	24:1	0.226	-0.067	0.034	-0.012	0.270	0.089
	26:0	0.236	-0.008	0.027	0.139	0.169	-0.223
	26:1	0.201	0.031	0.094	0.002	0.286	0.098
t18:0	16:0	0.098	-0.176	-0.263	0.158	-0.206	-0.069
	18:0	0.240	0.003	0.020	0.153	-0.098	0.064
	20:0	0.085	-0.025	-0.355	0.195	-0.063	-0.142
	20:1	0.227	0.021	0.054	0.216	-0.052	0.031
	22:0	0.000	0.182	-0.300	0.139	0.138	0.259
	22:1	0.238	0.038	0.008	0.208	0.099	-0.003
	24:0	0.102	0.218	-0.182	0.204	0.048	-0.110
	24:1	-0.044	0.249	-0.179	0.169	0.197	-0.020
	26:0	0.121	0.225	0.008	0.078	-0.016	-0.380
	26:1	0.049	0.253	-0.143	0.082	0.263	-0.014

(Continued on the next page)

LCB	FA	Ceramide			GIPC		
		PC-1 (42.01%)	PC-2 (29.78%)	PC-3 (16.05%)	PC-1 (48.57%)	PC-2 (27.20%)	PC-3 (15.52%)
t18:1	16:0	0.131	-0.098	-0.275	0.182	-0.130	-0.144
	18:0	0.036	0.073	-0.315	0.197	-0.133	-0.042
	20:0	0.052	0.117	-0.322	0.216	-0.052	0.031
	20:1	0.167	0.173	0.104	0.071	-0.142	-0.158
	22:0	0.011	0.246	-0.196	0.208	0.099	-0.003
	22:1	-0.010	0.273	0.068	0.186	0.022	0.087
	24:0	0.000	0.289	-0.003	0.169	0.197	-0.020
	24:1	-0.054	0.250	0.151	0.117	0.232	0.051
	26:0	0.027	0.272	0.083	0.080	0.275	-0.048
	26:1	-0.026	0.254	0.165	0.061	0.279	0.038

Appendix 13 Sphingolipid Profile for *ipcs3* under Control and Cold Conditions

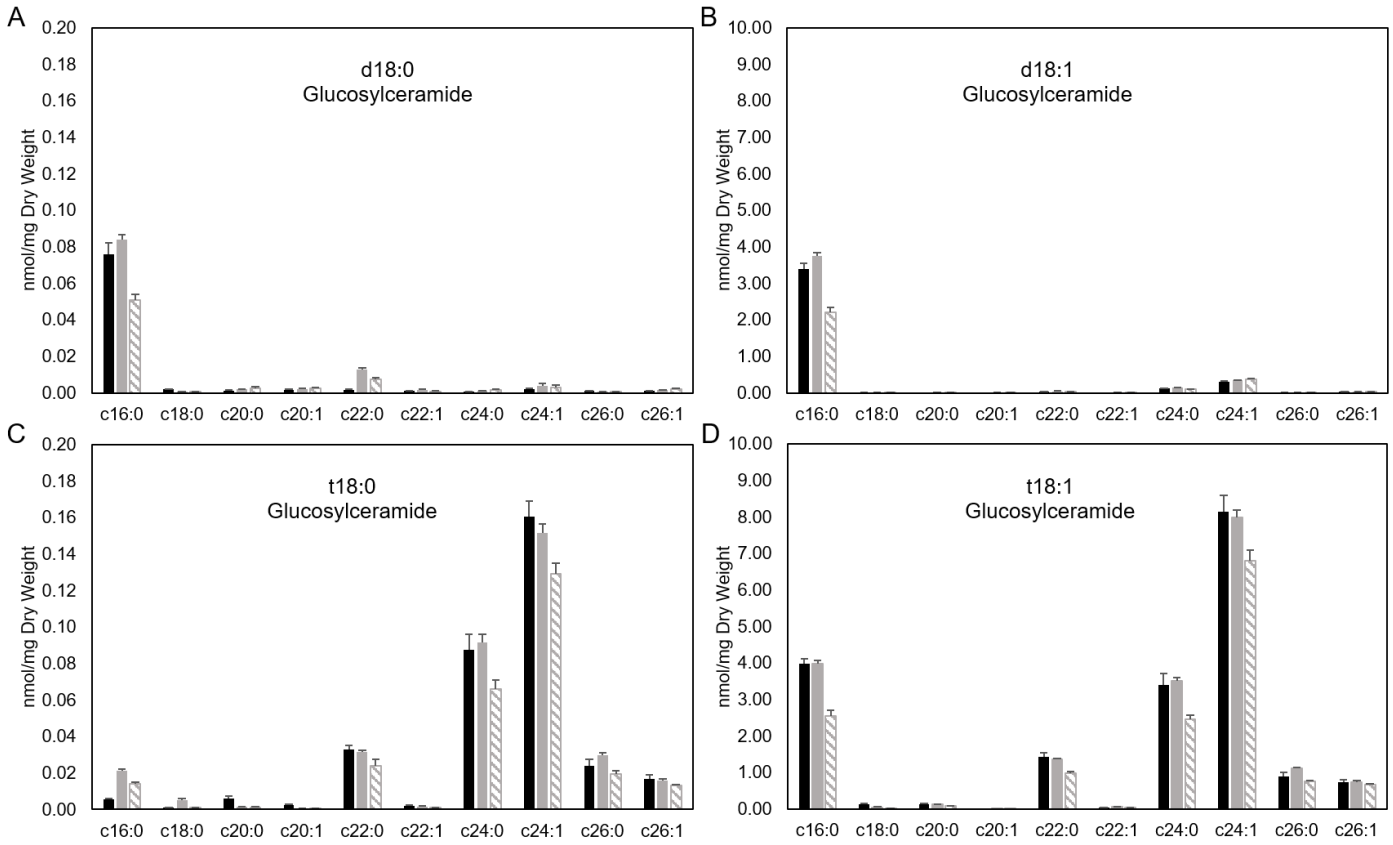

(Continued on the next page)

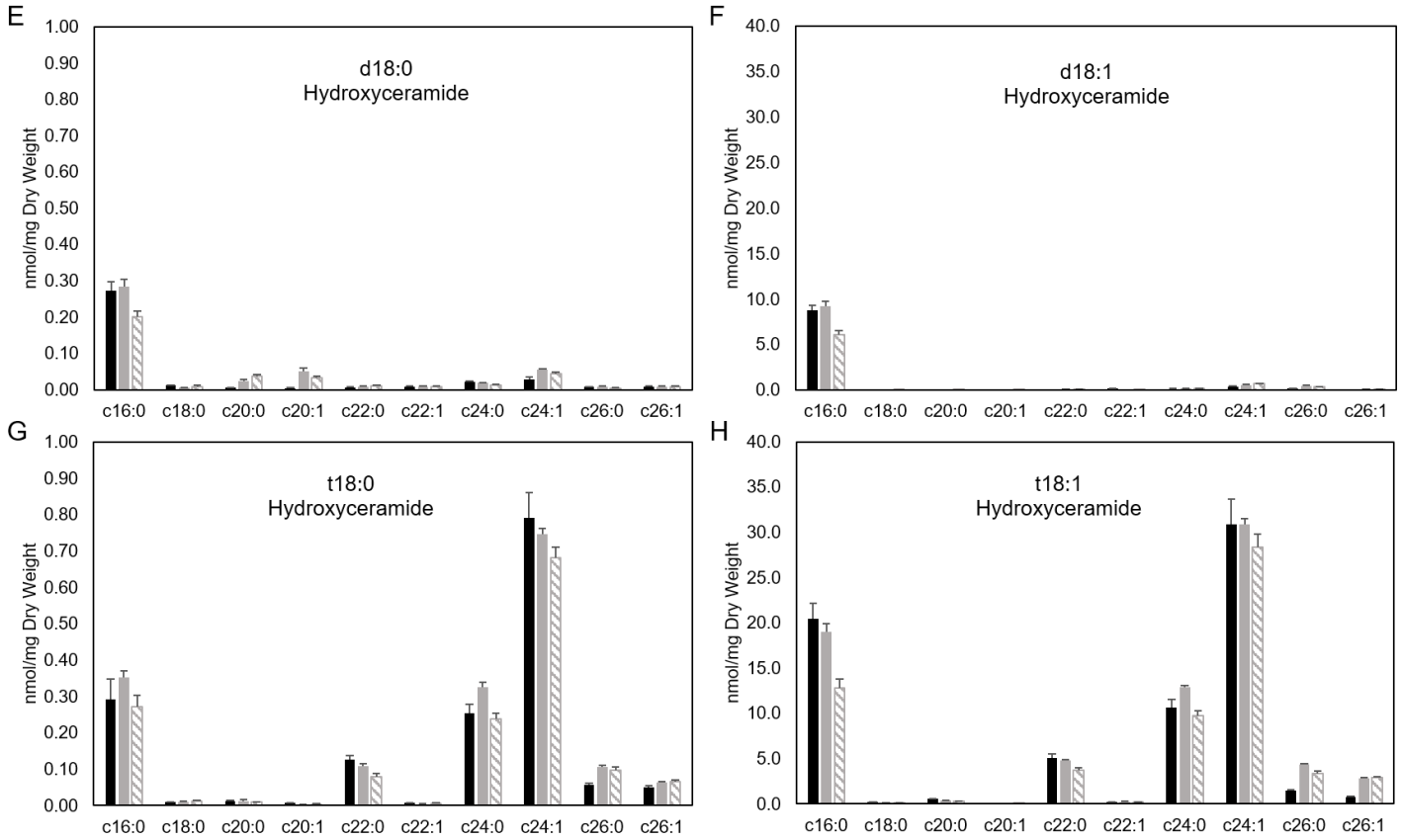

Glucosylceramide (A-D) and hydroxyceramide (E-H) fatty acid profile for the LCBs d18:0 (A, E), d18:1 (B, F), t18:0 (C, G), and t18:1 (D, H) profiles for Col-0 under control (■), *ipcs3* under control 23°C (■) and after eight days of cold 4°C (■ patterned) conditions. Bars represent mean + standard error, N=6.

Appendix 14 Total Sphingolipid Content for *ipcs3*

A

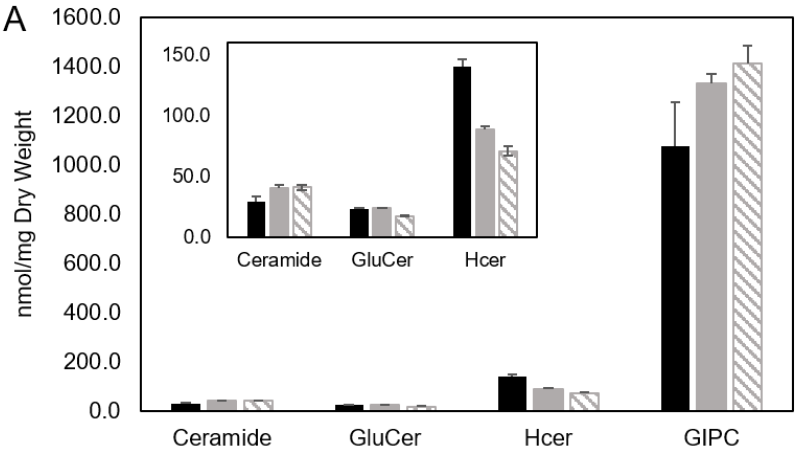

B

Data	Col-0 (23 °C) vs. *ipcs3* (23 °C)	Col-0 (23 °C) vs. *ipcs3* (4 °C)	*ipcs3* (23 °C) vs. *ipcs3* (4 °C)
Ceramide	* (p= 0.037)	* (p= 0.031)	nd p= 0.979
GluCer	nd (p= 0.555)	** (p= 0.002)	*** (p< 0.001)
Hcer	*** (p< 0.001)	*** (p< 0.001)	** (p= 0.003)
GIPC	nd (p=0.220)	nd (p= 0.111)	nd (p= 0.324)

(A) Total content of ceramides, glucosylceramides (GluCer), hydroxyceramides (Hcer), and glycosylinositolphosphoryl ceramides (GIPC) in the wild-type Col-0 under control 23°C (■) and in *ipcs3* (■) under control (block colour) and after eight days of cold 4°C (patterned). Insert detailed data for each of the three first classes. Bars represent mean + standard error, N=6. (B) Unpaired t-test results table for pairwise comparisons showed no differences (nd), or differences with significant levels of p<0.001 (***), p<0.01 (**), and p<0.05 (*), with respective *p* value in parenthesis.

Appendix 15 SLD Amino Acid FASTA Sequences

>AtSLD1

MAEETEKKYITNEDLKKHNKSGDLWIAIQGKVYNVSDWIKTHPGGDTV
ILNLVGQDVTDAFIAFHPGTAWHHLDHLFTGYHIRDFQVSEVSRDYRR
MAAEFRKLGLFENKGHVTLYTLAFVAAMFLGVLYGVLACTSVFAHQIA
AALLGLLWIQSAYIGHDSGHYVIMSNKSYNRFAQLLSGNCLTGISIAW
WKWTHNAHHLACNSLDYDPDLQHIPVFAVSTKFFSSLTSRFYDRKLT
FDPVARFLVSYQHFTYYPVMCFGRINLFIQTFLLLFSKREVPDRALNFA
GILVFWTWFPLLVSCLPNWPERFFFVFTSFTVTALQHIQFTLNHFAAD
VYVGPPTGSDWFEKQAAGTIDISCRSYMDWFFGGLQFQLEHHLFPRL
PRCHLRKVSPVVQELCKKHNLPYRSMSWFEANVLTINTLKTAAYQAR
DVANPVVKNLVWEALNTHG

>AtSLD2

MADQTKKRYVTSEDLKKHNKPGDLWISIQGKVYDVSDWVKSHPGGE
AAILNLAGQDVTDAFIAYHPGTAWHHLEKLHNGYHVRDHHVSDVSRD
YRRLAAEFSKRGLFDKKGHVTLYTLTCVGVMLAAVLYGVLACTSIWAH
LISAVLLGLLWIQSAYVGHDSGHYTVTSTKPCNKLIQLLSGNCLTGISIA
WWKWTHNAHHIACNSLDHDPDLQHIPIFAVSTKFFNSMTSRFYGRKL
TFDPLARFLISYQHWTFYPVMCVGRINLFIQTFLLLFSKRHVPDRALNI
AGILVFWTWFPLLVSFLPNWQERFIFVFVSFAVTAIQHVQFCLNHFAA
DVYTGPPNGNDWFEKQTAGTLDISCRSFMDWFFGGLQFQLEHHLFP
RLPRCHLRTVSPVVKELCKKHNLPYRSLSWWEANVWTIRTLKNAAIQ
ARDATNPVLKNLLWEAVNTHG

>ThSLD1

MADETEKKYITNEDLRKHNKSGDLWIAIQGKVYDVSDWIKSHPGGDT
VILNLVGQDVTDAFIAFHPGTAWNHLGNLFTGYHIRDFEVSEVSRDYR
RMAAEFRKLGLFENKGHVTLYTLAFVAAMFAGVLYGVLACTSVFAHQI
AAALLGLLWIQSAYIGHDSGHYVIMSNKSYNRFAQLLSGNCLTGISIAW
WKWTHNAHHLACNSLDYDPDLQHIPVFAVSTKFFNSITSRFYDRKLTF
DPLARFLVSYQHFTYYPVMCFGRINLFVQTFLLLFSKRHVPDRALNFA
GILVFWTWFPLLVSCLPSWPERFFFVFTSFTVTALQHIQFTLNHFAAD

VYVGPPTGNDWFEKQAAGTLDISCRSYMDWFFGGLQFQLEHHLFPR
LPRCHLRKVAPVVQELCKKHNLPYRSLSWWEANVWTIRTLKKAAFQA
RDAANPVVKNLVWEALNTHG

>ThSLD2

MAEQTKKRYISSEDLKTHNKSGDLWISIQGKVYDVSDWVRSHPGGEA
AILNLAGQDVTDAFIAYHPGTAWHHLEKLHNGYHVRDFHVSDVSRDY
RRLAAEFSKRGLFDKKEHVTLYTLTCVAVMFAAVVYGVLACTSVWAH
LVSAVLLGLLWIQSAYVGHDSGHYNVTSTKPCNKIVQLLSGNCITGISI
AWWKWTHNAHHIACNSLDHDPDLQHIPIFAVSTKFFKSMTSRFYGRK
LTFDPLARFLISYQHWTFYPVMCVGRINLFVQTFLLLFSKRHVPDRAL
NIAGILVFWTWFPLLVSFLPNWPERIIFVFTSFAVTAIQHVQFCLNHFAA
DVYTGPPNGNDWFEKQTAGTLDISCRSYMDWFFGGLQFQLEHHLFP
RLPRCHLRRVSPVVQELCKKHNLPYRSLSWWEANVWTIRTLRNAAV
QARDATNPVLKNLLWEAVNTHG

Appendix 16 Canonical Multivariate Loadings for SLD Sphingolipid Profile

Canonical variates (CV) loadings with respective data variation accounted for (%) for the long-chain base (LCB), and fatty acids (FA) combinations that compose each sphingolipid class. GIPC, glycosylinositolphosphoryl ceramide. CVAs were performed using "Genotype" and "Line" as treatment. This data corresponds to the CVAs presented in Figure 5.6, Chapter 5, Section 5.2.5.

Class	LCB	FA	Genotype		Line	
			CV1 (92.97%)	CV2 (5.60%)	CV1 (90.33%)	CV2 (4.33%)
Ceramides	d18:0	16:0	4.31e-01	8.67e-02	2.83e-02	-3.03e-02
		18:0	-5.70e-02	-3.07e-02	-9.19e-03	-8.36e-03
		20:0	2.18e-02	1.23e-02	1.36e-02	1.18e-02
		20:1	3.70e-02	4.29e-03	4.10e-03	-2.76e-03
		22:0	2.16e-02	5.23e-03	5.02e-03	5.38e-03
		22:1	-8.83e-03	-1.91e-03	-6.50e-04	1.55e-03
		24:0	-9.46e-03	-5.15e-02	-2.74e-02	-7.45e-03
		24:1	2.23e-02	2.97e-03	-2.47e-03	-4.67e-03
		26:0	-1.69e-02	-2.13e-02	-1.39e-02	-1.08e-02
		26:1	-1.11e-02	6.97e-03	-4.80e-04	4.04e-03
	d18:1	16:0	7.42e-02	-1.15e-01	-8.71e-02	-6.05e-02
		18:0	5.23e-02	-2.49e-02	-1.84e-02	-2.55e-02
		20:0	5.82e-03	1.94e-02	1.43e-03	9.80e-03
		20:1	-1.34e-01	2.67e-01	1.06e-01	1.15e-01
		22:0	2.73e-02	5.78e-03	-8.70e-03	-1.20e-02
		22:1	1.77e-02	8.64e-03	4.36e-03	-2.59e-03
		24:0	-3.11e-01	-1.73e-01	2.14e-02	-8.32e-02
		24:1	7.83e-02	3.23e-02	-1.74e-03	4.76e-03
		26:0	2.63e-01	-3.54e-02	-1.12e-02	-5.14e-02
		26:1	1.13e-01	-9.62e-03	-5.45e-03	-2.95e-02
	t18:0	16:0	-6.49e-02	-3.11e-02	-1.33e-01	-6.24e-02
		18:0	-6.19e-02	2.76e-02	9.24e-03	3.40e-02
		20:0	5.02e-02	-1.89e-02	-1.43e-02	-2.50e-02
		20:1	1.08e-02	7.79e-03	-7.00e-04	6.18e-03
		22:0	-1.34e-01	1.65e-02	-6.61e-03	3.68e-02
		22:1	-1.22e-01	1.86e-02	3.59e-03	2.70e-02
		24:0	2.34e-01	-4.36e-02	4.46e-02	9.76e-02
		24:1	-4.32e-01	-2.36e-01	-2.18e-01	-6.90e-02
		26:0	4.04e-02	7.30e-02	-2.82e-02	1.00e-01
		26:1	9.35e-02	-3.64e-02	-2.76e-02	-6.36e-02
	t18:1	16:0	1.68e-01	7.35e-02	-1.26e-01	-9.79e-02
		18:0	3.84e-02	2.87e-02	1.24e-02	9.21e-03
		20:0	-2.19e-01	6.21e-02	-5.90e-04	3.88e-02

(Continued on the next page)

Class	LCB	FA	Genotype		Line	
			CV1	CV2	CV1	CV2
Ceramides	t18:1	20:1	-2.36e-02	-4.93e-02	-1.88e-02	-1.99e-02
		22:0	-5.53e-01	1.56e-01	4.27e-02	1.28e-01
		22:1	-2.01e-01	-2.85e-02	5.99e-03	4.66e-02
		24:0	-4.22e-02	-7.93e-02	-1.39e-01	-6.13e-03
		24:1	3.95e-01	3.73e-01	2.71e-01	1.39e-02
		26:0	-1.87e-01	9.83e-02	1.36e-01	4.17e-01
		26:1	-2.02e-01	-8.36e-02	7.01e-03	4.90e-02
GIPC	d18:0	16:0	-1.31e-01	1.16e-01	8.36e-02	1.69e-01
		18:0	1.19e-01	-1.26e-02	-3.36e-03	-2.10e-02
		20:0	2.90e-01	-1.35e-02	3.31e-02	-1.83e-02
		20:1	-9.66e-02	-6.63e-02	-1.01e-01	-9.81e-03
		22:0	-1.41e-01	-2.72e-01	-2.76e-01	8.71e-03
		22:1	1.64e-01	-4.22e-02	-9.28e-02	-2.24e-02
		24:0	4.02e-01	-1.11e-01	5.53e-02	5.51e-02
		24:1	-6.96e-02	1.67e-01	1.16e-01	1.18e-01
		26:0	-4.67e-01	2.67e-02	-1.14e-03	-8.17e-02
		26:1	-1.09e-01	1.40e-01	-1.80e-01	5.41e-02
	d18:1	16:0	3.69e-01	8.03e-02	6.18e-02	-1.84e-01
		18:0	4.98e-02	5.27e-03	1.64e-02	2.13e-02
		20:0	-9.66e-02	-6.63e-02	-1.01e-01	-9.81e-03
		20:1	4.32e-02	-1.41e-02	5.32e-03	-1.67e-02
		22:0	1.64e-01	-4.22e-02	-9.28e-02	-2.24e-02
		22:1	2.76e-01	9.90e-04	2.29e-02	-4.67e-02
		24:0	-7.26e-02	-4.22e-02	-3.59e-02	-7.73e-03
		24:1	4.65e-02	-2.21e-01	-3.49e-02	-3.12e-01
		26:0	1.73e-01	-1.21e-01	1.13e-01	-9.47e-03
		26:1	-1.86e-01	-9.19e-02	2.92e-02	-1.07e-01
	t18:0	16:0	-1.85e-01	4.64e-02	-1.09e-01	-5.16e-02
		18:0	-1.93e-01	-1.32e-01	-4.80e-02	-1.98e-02
		20:0	-1.64e-01	1.93e-01	-1.65e-02	2.11e-01
		20:1	-2.59e-01	-7.80e-02	1.20e-01	4.10e-02
		22:0	2.06e-01	4.72e-02	1.37e-01	-6.47e-02
		22:1	6.92e-02	-1.99e-01	1.71e-02	4.09e-02
		24:0	7.26e-02	-5.18e-03	3.53e-03	-6.51e-03
		24:1	1.90e-02	-9.82e-03	-3.26e-03	-1.32e-02
		26:0	-9.29e-02	-6.16e-02	1.14e-01	2.05e-01
		26:1	-1.27e-01	6.82e-02	-2.81e-02	1.46e-02
	t18:1	16:0	-1.98e-02	1.92e-02	1.77e-02	7.22e-03
		18:0	9.08e-02	4.75e-02	1.74e-02	1.02e-01
		20:0	-2.63e-01	-6.90e-02	1.18e-01	3.81e-02
		20:1	1.47e-01	-1.40e-01	-4.05e-02	-6.76e-02

(Continued on the next page)

Class	LCB	FA	Genotype		Line	
			CV1	CV2	CV1	CV2
GIPC	t18:1	22:0	-9.24e-02	1.57e-01	-3.94e-02	-5.55e-02
		22:1	-2.14e-02	1.81e-02	-2.45e-01	-3.40e-01
		24:0	-1.77e-02	-5.51e-03	-1.76e-02	-2.85e-02
		24:1	1.96e-03	1.67e-02	1.83e-03	2.02e-02
		26:0	1.24e-01	-9.38e-03	3.11e-02	2.70e-02
		26:1	6.03e-02	-5.22e-02	9.49e-02	1.52e-02
Glucosylceramides	d18:0	16:0	-1.91e-01	1.81e-01	7.21e-02	1.01e-01
		18:0	1.43e-02	-4.50e-04	3.70e-04	-2.17e-03
		20:0	1.25e-02	-1.50e-03	-5.10e-04	-1.11e-03
		20:1	4.40e-03	2.01e-03	5.00e-05	1.09e-03
		22:0	1.36e-03	-9.30e-04	-2.00e-05	2.80e-04
		22:1	-6.60e-04	-2.10e-04	-1.00e-05	-6.90e-04
		24:0	2.88e-03	2.36e-03	1.05e-03	6.30e-04
		24:1	3.45e-03	-1.11e-03	1.29e-03	-6.80e-04
		26:0	-4.98e-03	1.80e-04	-8.90e-04	6.50e-04
		26:1	1.05e-03	-1.10e-04	2.90e-04	-4.00e-05
	d18:1	16:0	-4.13e-01	-2.96e-02	1.04e-01	1.68e-01
		18:0	-1.55e-02	1.09e-02	4.61e-03	8.23e-03
		20:0	-3.90e-04	2.23e-03	4.80e-04	1.75e-03
		20:1	4.13e-03	7.50e-04	-2.40e-04	-1.10e-04
		22:0	4.19e-02	2.80e-03	6.72e-03	-1.22e-03
		22:1	1.54e-03	1.78e-03	1.92e-03	1.70e-03
		24:0	1.99e-02	2.73e-02	1.38e-02	7.95e-03
		24:1	-7.64e-02	3.75e-02	1.61e-02	4.96e-02
		26:0	-3.51e-03	2.02e-03	3.50e-04	2.48e-03
		26:1	4.56e-02	2.27e-03	8.61e-03	-6.59e-03
	t18:0	16:0	-1.85e-01	1.95e-02	1.13e-02	4.05e-02
		18:0	6.82e-03	1.35e-03	3.40e-04	-4.90e-04
		20:0	-3.71e-03	-4.46e-03	1.27e-03	-3.85e-03
		20:1	4.94e-03	-1.08e-03	-2.10e-04	-1.72e-03
		22:0	1.18e-02	2.39e-03	1.83e-02	3.59e-03
		22:1	-7.03e-03	3.92e-03	2.07e-03	4.11e-03
		24:0	-4.43e-02	-1.53e-02	9.03e-03	1.75e-02
		24:1	-7.39e-01	-1.04e-02	2.50e-03	1.31e-01
		26:0	1.34e-02	4.02e-03	7.33e-03	2.26e-03
		26:1	1.87e-02	1.65e-02	-1.85e-03	4.08e-03
	t18:1	16:0	2.86e-01	-1.06e-01	-1.81e-02	2.01e-01
		18:0	1.01e-01	1.44e-02	-7.20e-04	5.34e-03
		20:0	2.77e-02	1.08e-02	4.39e-03	1.93e-02
		20:1	-5.32e-03	3.45e-03	8.50e-04	3.65e-03
		22:0	3.63e-02	1.79e-01	4.32e-02	1.90e-01

(Continued on the next page)

Class	LCB	FA	Genotype		Line	
			CV1	CV2	CV1	CV2
Glucosylceramides	t18:1	22:1	3.74e-03	-1.07e-02	-7.58e-03	-4.04e-03
		24:0	2.69e-01	-9.32e-02	1.68e-01	-6.80e-02
		24:1	-1.16e-01	-7.71e-02	4.01e-02	-1.39e-02
		26:0	1.46e-01	1.10e-02	1.17e-01	-1.76e-02
		26:1	-4.75e-02	-5.12e-02	3.42e-02	2.66e-03
Hydroxyceramides	d18:0	16:0	5.14e-02	-6.13e-02	-3.47e-02	-6.28e-02
		18:0	-1.87e-01	-3.42e-02	-1.21e-02	3.15e-02
		20:0	3.82e-02	2.94e-03	-5.41e-03	-7.44e-03
		20:1	-2.49e-02	-1.86e-03	-7.70e-04	9.88e-03
		22:0	5.10e-04	-3.42e-03	3.76e-03	-7.90e-04
		22:1	-8.14e-02	1.53e-03	5.05e-03	1.76e-02
		24:0	-7.37e-03	3.65e-02	2.32e-02	1.56e-02
		24:1	7.88e-02	3.61e-02	-2.44e-03	1.08e-03
		26:0	7.87e-02	-2.48e-03	4.02e-03	-1.83e-02
		26:1	1.24e-01	-3.43e-03	1.22e-02	-1.98e-02
	d18:1	16:0	-5.68e-01	-2.69e-01	-2.39e-01	-1.37e-01
		18:0	1.30e-01	2.37e-02	2.25e-02	-1.57e-02
		20:0	-6.42e-02	3.76e-02	7.88e-03	4.46e-02
		20:1	3.03e-02	1.40e-02	5.02e-03	-3.98e-02
		22:0	9.33e-03	2.24e-02	1.06e-02	4.12e-02
		22:1	5.57e-02	-1.63e-01	1.52e-02	-1.55e-01
		24:0	-4.38e-01	9.80e-02	7.20e-02	1.64e-01
		24:1	8.11e-02	5.42e-02	-1.77e-02	-5.44e-02
		26:0	5.95e-01	-2.61e-03	-5.84e-02	-1.98e-01
		26:1	2.98e-02	1.40e-03	1.22e-02	-7.80e-04
	t18:0	16:0	-8.75e-03	1.78e-01	1.18e-01	-8.24e-02
		18:0	-2.13e-02	-3.58e-02	-1.95e-02	1.22e-03
		20:0	2.14e-01	6.26e-02	4.44e-02	1.56e-02
		20:1	9.20e-03	5.52e-03	9.31e-03	4.60e-03
		22:0	1.41e-01	8.50e-03	1.32e-02	-1.97e-02
		22:1	-1.62e-02	7.72e-03	-3.73e-03	1.61e-02
		24:0	1.23e-01	5.77e-02	-1.43e-02	6.30e-04
		24:1	-1.47e-01	-2.06e-01	-3.52e-01	1.68e-01
		26:0	1.21e-01	3.91e-02	9.09e-03	-1.67e-02
		26:1	1.19e-01	1.32e-01	4.14e-03	3.76e-02
	t18:1	16:0	2.15e-01	2.41e-02	3.92e-03	1.72e-01
		18:0	1.16e-01	-9.96e-02	-2.70e-02	-8.75e-02
		20:0	3.35e-01	-4.83e-02	1.04e-01	-9.86e-02
		20:1	2.55e-02	0.00e+00	2.48e-03	8.49e-03
		22:0	9.49e-02	3.11e-01	3.21e-02	1.79e-02
		22:1	-4.52e-02	1.82e-01	4.26e-02	7.88e-02

(Continued on the next page)

Class	LCB	FA	Genotype		Line	
			CV1	CV2	CV1	CV2
Hydroxyceramides	t18:1	24:0	-1.86e-01	-7.84e-02	3.26e-03	-2.18e-01
		24:1	2.00e-02	-4.10e-03	3.17e-02	1.86e-02
		26:0	-4.79e-02	-5.82e-02	7.41e-02	2.88e-03
		26:1	5.75e-01	8.70e-02	8.78e-02	1.74e-01

Appendix 17 Canonical Multivariate Loadings for Col-0:*SLD* Sphingolipid Profile

Canonical variates (CV) loadings with respective data variation accounted for (%) for the long-chain base (LCB), and fatty acids (FA) combinations that compose each sphingolipid class. GIPC, glycosylinositolphosphoryl ceramide. CVAs were performed using “Genotype” and “Line” as treatment. This data corresponds to the CVAs presented in Figure 5.7, Chapter 5, Section5.2.5.

Class	LCB	FA	Genotype	
			CV1 (84.10%)	CV2 (13.48%)
Ceramides	d18:0	16:0	-1.23e-03	-4.46e-03
		18:0	6.74e-02	6.39e-02
		20:0	3.38e-04	-2.26e-04
		20:1	3.63e-03	2.22e-03
		22:0	5.26e-04	-2.14e-03
		22:1	-3.91e-03	-2.11e-03
		24:0	6.49e-04	4.10e-05
		24:1	5.92e-04	2.20e-05
		26:0	-2.65e-03	-3.80e-04
		26:1	-1.48e-03	3.88e-04
	d18:1	16:0	4.48e-03	-1.82e-03
		18:0	6.13e-02	1.49e-02
		20:0	6.32e-04	6.56e-04
		20:1	2.05e-04	2.12e-04
		22:0	2.56e-03	1.13e-03
		22:1	-2.32e-03	-1.05e-03
		24:0	4.89e-03	1.98e-03
		24:1	2.75e-03	2.25e-03
		26:0	2.62e-03	1.97e-03
		26:1	1.65e-03	8.63e-04
	t18:0	16:0	-2.74e-03	-1.40e-02
		18:0	-9.38e-04	-2.15e-03
		20:0	6.64e-04	2.00e-06
		20:1	4.40e-04	6.62e-04
		22:0	-1.16e-03	-3.74e-03

(Continued on the next page)

Class	LCB	FA	Genotype	
			CV1	CV2
Ceramides	t18:0	22:1	1.55e-02	4.60e-03
		24:0	1.50e-02	-1.12e-02
		24:1	7.27e-03	1.96e-02
		26:0	3.27e-02	4.93e-03
		26:1	1.45e-02	1.24e-04
	t18:1	16:0	2.39e-02	4.36e-02
		18:0	2.38e-03	1.65e-03
		20:0	3.23e-03	1.69e-03
		20:1	2.37e-03	1.50e-03
		22:0	5.05e-04	2.99e-03
		22:1	-1.63e-02	5.63e-03
		24:0	-3.19e-02	-1.25e-02
		24:1	9.57e-03	-5.32e-03
		26:0	1.02e-03	-1.38e-02
		26:1	-8.54e-03	-3.16e-02
GIPC	d18:0	16:0	5.01e-02	7.06e-02
		18:0	-4.40e-03	-1.12e-03
		20:0	1.61e-03	1.50e-03
		20:1	4.46e-03	7.65e-03
		22:0	-6.96e-04	6.92e-03
		22:1	8.86e-03	3.52e-02
		24:0	-4.79e-02	1.27e-02
		24:1	6.57e-03	3.04e-02
		26:0	-5.45e-02	-5.67e-04
		26:1	1.56e-02	5.58e-02
	d18:1	16:0	-2.59e-02	1.11e-01
		18:0	-3.00e-03	-1.59e-03
		20:0	7.55e-03	1.74e-03
		20:1	1.78e-04	1.22e-03
		22:0	4.32e-03	2.60e-02
		22:1	5.75e-04	2.10e-04
		24:0	-1.48e-03	2.90e-02
		24:1	-1.23e-02	-3.93e-03
		26:0	4.94e-02	9.02e-03
		26:1	5.53e-03	1.31e-02
	t18:0	16:0	2.42e-03	-3.48e-02
		18:0	-1.50e-03	-3.33e-03
		20:0	5.05e-03	2.41e-03
		20:1	1.05e-02	9.09e-03
		22:0	8.91e-03	4.03e-02
		22:1	-2.25e-02	-2.38e-02

(Continued on the next page)

Class	LCB	FA	Genotype	
			CV1	CV2
GIPC	t18:0	24:0	-1.61e-02	-5.82e-03
		24:1	1.69e-02	1.91e-02
		26:0	1.01e-02	1.57e-02
		26:1	-3.06e-02	1.27e-02
	t18:1	16:0	1.86e-02	2.18e-02
		18:0	2.81e-03	4.00e-03
		20:0	7.47e-03	4.30e-04
		20:1	3.63e-03	2.95e-03
		22:0	-5.70e-02	-5.05e-02
		22:1	1.36e-02	3.99e-03
		24:0	7.83e-03	-1.81e-02
		24:1	-5.52e-03	-3.65e-02
		26:0	-4.40e-02	1.70e-02
		26:1	-8.74e-02	1.01e-02
Glucosylceramides	d18:0	16:0	-5.60e-05	7.13e-03
		18:0	3.70e-05	1.20e-05
		20:0	1.05e-04	-9.60e-05
		20:1	-3.80e-05	-1.24e-04
		22:0	3.18e-04	3.67e-04
		22:1	-1.47e-03	-4.30e-05
		24:0	5.50e-05	7.70e-05
		24:1	-1.52e-04	-1.10e-05
		26:0	1.80e-05	-3.20e-05
		26:1	-5.00e-05	3.10e-05
	d18:1	16:0	-1.57e-02	3.85e-02
		18:0	8.50e-05	7.20e-05
		20:0	2.74e-04	3.22e-04
		20:1	-1.74e-04	7.70e-05
		22:0	3.61e-04	9.94e-04
		22:1	2.83e-04	3.84e-04
		24:0	-6.40e-04	3.92e-04
		24:1	1.08e-03	2.91e-03
		26:0	2.78e-04	2.89e-04
		26:1	-2.29e-04	3.21e-04
	t18:0	16:0	2.35e-03	3.63e-03
		18:0	-1.48e-03	-1.41e-03
		20:0	-9.00e-05	3.00e-06
		20:1	-4.30e-05	1.10e-05
		22:0	-9.19e-04	1.68e-03
		22:1	-9.70e-05	8.60e-05
		24:0	-3.03e-03	3.67e-03

(Continued on the next page)

Class	LCB	FA	Genotype	
			CV1	CV2
Glucosylceramides	t18:0	24:1	-1.00e-02	1.04e-02
		26:0	-2.96e-04	-1.49e-04
		26:1	6.05e-04	1.17e-03
	t18:1	16:0	-2.18e-03	-2.24e-03
		18:0	-1.63e-03	-2.57e-04
		20:0	-1.26e-03	4.17e-04
		20:1	-2.99e-04	-1.38e-04
		22:0	2.31e-03	2.92e-03
		22:1	-1.12e-03	-9.26e-04
		24:0	-6.42e-03	-1.44e-02
		24:1	-2.70e-02	-1.71e-02
		26:0	-1.42e-03	-1.80e-03
		26:1	-5.09e-04	-5.94e-04
Hydroxyceramides	d18:0	16:0	4.52e-02	-3.11e-03
		18:0	4.20e-04	9.55e-04
		20:0	2.49e-03	9.95e-04
		20:1	2.34e-03	-4.56e-03
		22:0	-4.86e-04	-7.51e-04
		22:1	2.94e-04	2.84e-04
		24:0	2.82e-03	3.52e-03
		24:1	2.14e-03	9.85e-04
		26:0	-5.85e-04	-2.75e-04
		26:1	-3.11e-04	1.28e-04
	d18:1	16:0	-5.69e-02	-2.29e-02
		18:0	-1.11e-04	7.40e-05
		20:0	-1.28e-03	-2.86e-04
		20:1	8.02e-04	6.56e-04
		22:0	-5.04e-04	-1.82e-03
		22:1	2.80e-05	-1.80e-05
		24:0	-1.42e-02	-5.40e-03
		24:1	2.59e-02	8.89e-03
		26:0	-1.19e-02	-8.32e-03
		26:1	2.65e-03	3.47e-04
	t18:0	16:0	5.95e-02	1.44e-02
		18:0	1.21e-03	2.03e-03
		20:0	-1.63e-03	-1.34e-03
		20:1	1.67e-04	3.56e-04
		22:0	4.55e-03	1.58e-03
		22:1	-1.04e-04	-2.39e-04
		24:0	-3.08e-02	-3.97e-02
		24:1	2.24e-02	7.04e-03

(Continued on the next page)

Class	LCB	FA	Genotype	
			CV1	CV2
Hydroxyceramides	t18:0	26:0	-7.78e-03	-6.97e-03
		26:1	-1.03e-02	-4.88e-03
	t18:1	16:0	3.83e-03	7.13e-04
		18:0	1.81e-03	1.79e-03
		20:0	-3.73e-03	-2.08e-03
		20:1	-2.83e-04	-3.00e-05
		22:0	1.67e-02	1.06e-02
		22:1	-2.77e-03	-5.73e-04
		24:0	-1.12e-02	1.19e-02
		24:1	-1.47e-03	2.05e-02
		26:0	5.98e-03	1.41e-02
		26:1	-2.36e-02	-1.79e-02

Appendix 18 Canonical Variate Loadings for SLD Ceramide Profile

Canonical variates (CV) loadings with respective data variation accounted for (%) for the long-chain base (LCB), and fatty acids (FA) combinations that compose the ceramide. CVAs were performed using “Genotype” as treatment. This data corresponds to the CVAs presented in Figure 5.11Figure 5.7, Chapter 5, Section 5.2.7.

LCB	FA	CV1 (64.53%)	CV2 (28.33%)	CV3 (7.14%)
d18:0	16:0	36.1	80.0	31.0
	18:0	-275.5	-241.1	-36.0
	20:0	18.7	80.1	-64.2
	20:1	-228.0	950.7	-272.7
	22:0	528.8	466.3	86.4
	22:1	-573.8	2114.9	140.2
	24:0	152.0	-153.4	88.3
	24:1	227.3	260.9	-85.3
	26:0	-30.7	198.3	-273.1
	26:1	174.4	-38.0	174.8
d18:1	16:0	-13.1	2.8	-44.3
	18:0	130.1	97.5	16.4
	20:0	-7.8	330.8	60.4
	20:1	12.2	45.2	-13.8
	22:0	58.1	-15.1	23.7
	22:1	8.4	-744.6	-116.0
	24:0	3.7	-12.7	-9.3
	24:1	-158.0	-114.6	-36.4
	26:0	-171.3	94.4	-35.1

(Continued on the next page)

LCB	FA	CV1 (64.53%)	CV2 (28.33%)	CV3 (7.14%)
d18:1	26:1	159.9	-184.7	117.6
t18:0	16:0	0.0	0.7	-0.7
	18:0	56.1	-346.4	67.3
	20:0	30.2	-192.9	16.3
	20:1	-379.4	-571.4	-532.2
	22:0	-37.3	-24.2	-41.4
	22:1	15.0	42.1	-9.9
	24:0	1.1	4.1	5.2
	24:1	9.7	12.6	1.5
	26:0	-1.7	-1.1	-2.4
	26:1	-35.3	-43.4	12.3
t18:1	16:0	0.2	-4.1	2.2
	18:0	-128.6	-183.6	-28.2
	20:0	-77.9	297.0	19.2
	20:1	-92.5	444.7	38.8
	22:0	11.5	-24.2	-5.8
	22:1	7.9	-56.8	9.2
	24:0	2.9	-9.8	3.3
	24:1	0.6	-8.0	2.9
	26:0	2.3	2.7	-1.2
	26:1	-12.6	41.1	-12.2

Appendix 19 Canonical Variate Loadings for SLD Acyl-CoA Profile

Canonical variates (CV) loadings with respective data variation accounted for (%) for the long-chain base (LCB), and fatty acids (FA) combinations that compose the ceramide. CVAs were performed using “Genotype” as treatment. This data corresponds to the CVAs presented in Figure 5.18, Chapter 5, Section 5.2.12.

FA	Genotype (Control)		Line (Control)		Genotype (Cold)		Line (Cold)	
	CV1 (61.43%)	CV2 (27.51%)	CV1 (47.93%)	CV2 (29.35%)	CV1 (55.30%)	CV2 (34.36%).	CV1 (37.16%)	CV2 (23.66%)
14:0	2.31E-01	3.75E-01	2.54E-01	2.96E-02	4.24E-02	-1.44E-01	-6.79E-01	1.99E-01
16:0	-6.22E-02	-2.96E-02	-6.32E-02	6.62E-02	2.98E-02	1.08E-02	-1.94E-02	2.71E-02
16:1	-2.10E+00	-2.03E+00	-1.35E+00	-5.51E+00	1.67E+00	9.54E-01	-3.58E+00	3.31E-01
16:3	1.67E+00	1.69E+00	1.18E+00	1.38E+00	-7.14E-01	-1.75E-01	3.78E+00	7.35E-01
18:0	-2.02E-01	-3.30E-03	-3.24E-01	-1.08E-01	1.82E-01	3.31E-01	-9.66E-01	-1.20E+00
18:1	-6.32E-01	2.01E-01	-5.06E-01	-1.74E-01	-7.59E-01	2.79E-01	2.22E+00	-7.79E-01
18:2	1.30E-01	-2.68E-02	9.88E-02	-7.92E-02	-2.89E-01	-9.37E-02	1.51E-01	-1.77E-01
18:3	5.32E-02	1.08E-01	2.17E-02	3.60E-01	-8.20E-03	-1.87E-02	1.84E-01	-1.12E-01
20:0	-2.21E-01	-3.76E-01	-2.19E-01	4.60E-02	1.39E-01	-6.07E-01	-1.49E+00	9.28E-01
20:1	1.35E-01	-8.60E-01	6.47E-01	9.60E-01	1.79E+00	6.38E-01	-6.85E+00	2.15E-01
22:0	-2.59E-01	8.12E-02	-1.93E-01	-1.57E-01	-1.23E-01	6.22E-02	1.13E+00	-1.75E-01
22:1	1.94E+00	2.60E+00	1.71E+00	3.02E+00	1.94E+00	2.36E-01	2.46E-02	1.33E+00
24:0	5.26E-01	-2.64E-01	4.87E-01	-3.60E-01	-2.78E-01	3.52E-01	5.85E-01	-4.44E-01
24:1	7.97E-01	-5.31E-01	8.38E-01	-4.20E-01	-2.77E-01	3.34E-01	5.89E-01	-2.34E-01
26:0	-5.28E-01	5.17E-01	-3.69E-01	-6.50E-01	6.54E-02	-8.79E-01	1.08E-02	5.23E-01
26:1	-1.21E+00	1.33E+00	-1.21E+00	6.58E-01	1.50E+00	-8.04E-01	-1.79E+00	2.55E+00
28:0	2.14E-01	3.99E-02	1.29E-01	3.88E-01	-1.29E-01	5.31E-01	-2.60E-01	-2.64E-01
28:1	7.88E-02	-2.87E-01	-1.30E-01	1.18E+00	-8.77E-01	-5.62E-02	6.63E-01	-1.18E+00

Appendix 20 PCA Analysis on the SLD Glucosylceramide Profile

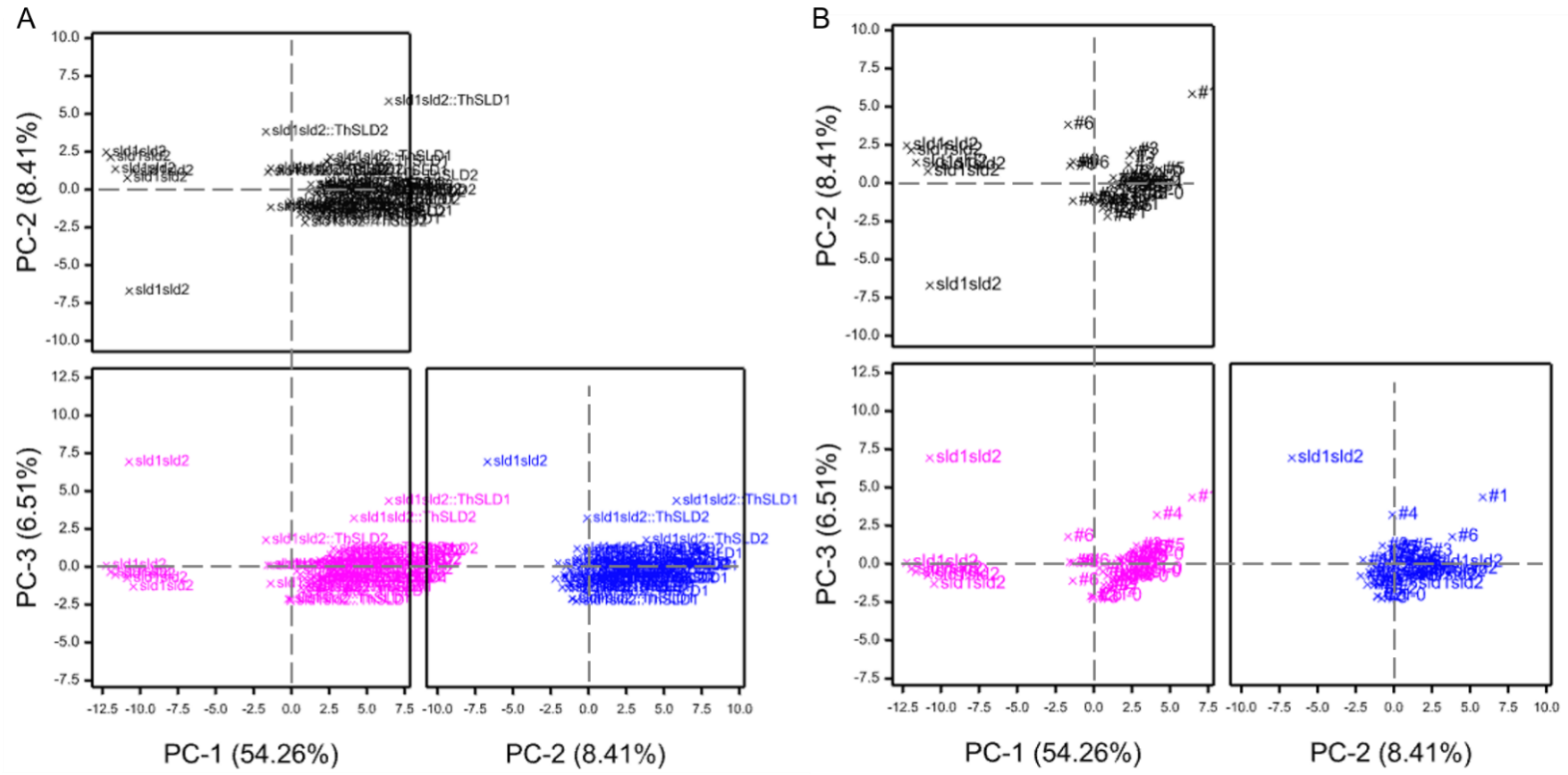

Glucosylceramides principal components (PC) analysis (PCA) of *sld1sld2*, Col-0, *sld1sld2*:*ThSLD1* and *sld1sld2*:*ThSLD2*, genotypes identified in (A) and lines in (B). Three PC explained 69.18% of the variability in the dataset. Individual replicas are represented by "×", N=6, dashed lines represent zero in each axis.

Appendix 21 PCA Analysis on the SLD GIPC Profile

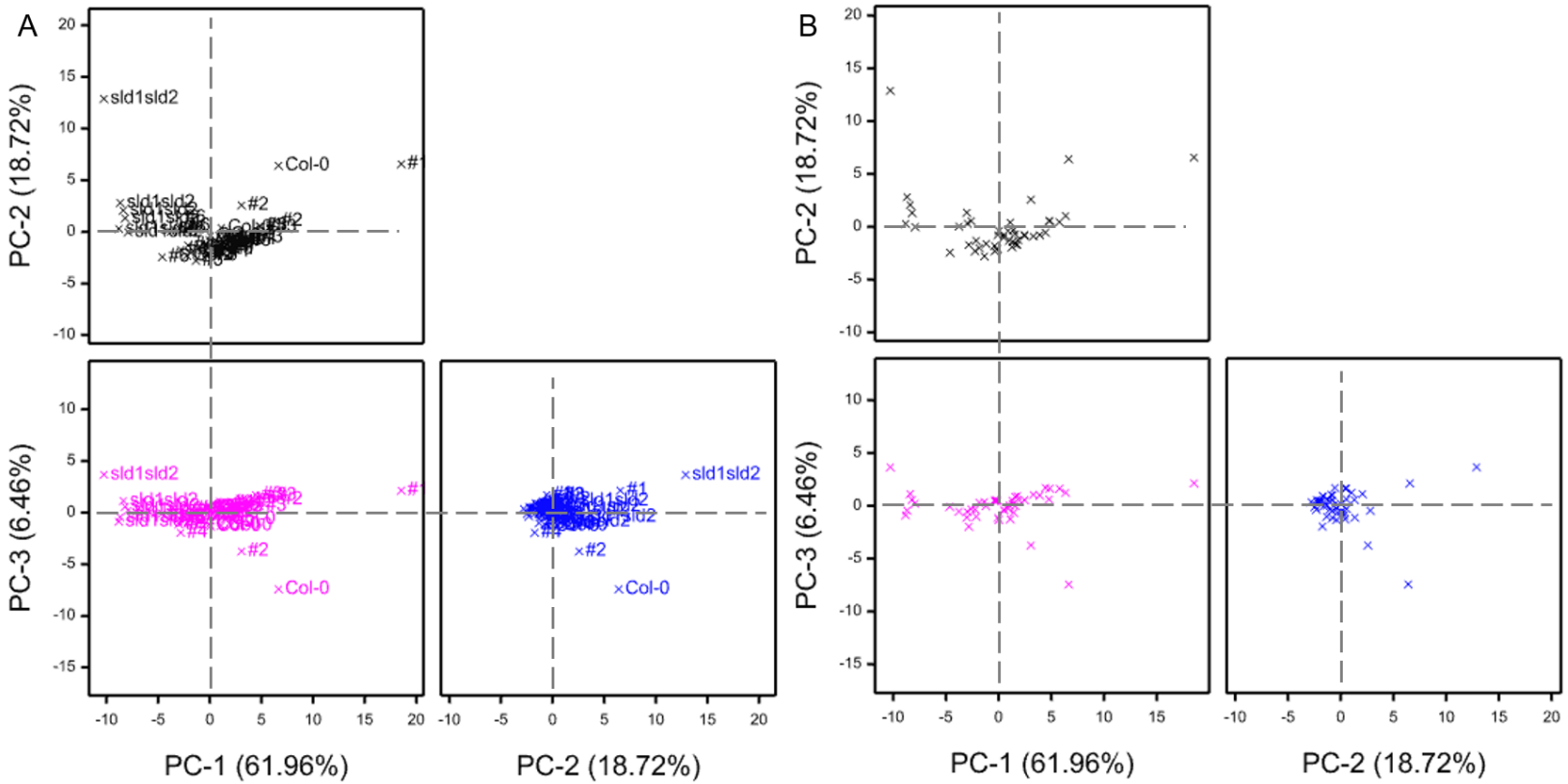

GIPC principal components (PC) analysis (PCA) of *sld1sld2*, Col-0, *sld1sld2*:*ThSLD1* and *sld1sld2*:*ThSLD2*, lines identified in (A) and no labels in (B). Three PCs explained 87.14% of the variability in the dataset. Individual points are represented by "×", dashed lines represent zero.

Appendix 22 Arabidopsis Mutant *fad7fad8* Sequencing

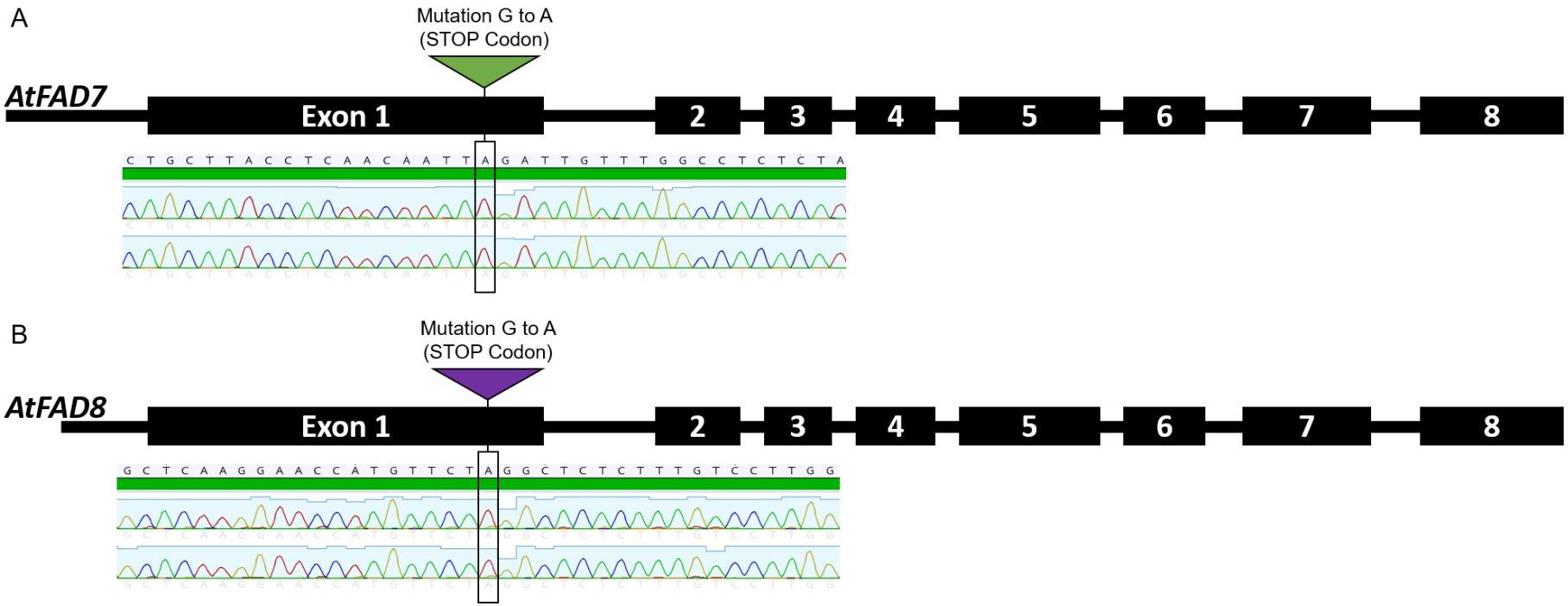

Sequencing results for *AtFAD7* (A) and *AtFAD8* (B) in the double mutant *fad7fad8* showing the substitution mutation of G to A, which originates a premature STOP codon. Sequence alignment performed with Geneious® against the FASTA sequence for *AtFAD7* and *AtFAD8* as represented by the respective gene structures. Green bar (■) represents the sequence identity, traces are adenine (A, —), thymine (T, —), guanine (G, —), and cytosine (C, —).

Appendix 23 T1 CRISPR Lines Sequencing for Targeted *ThFAD7*, Exon 1

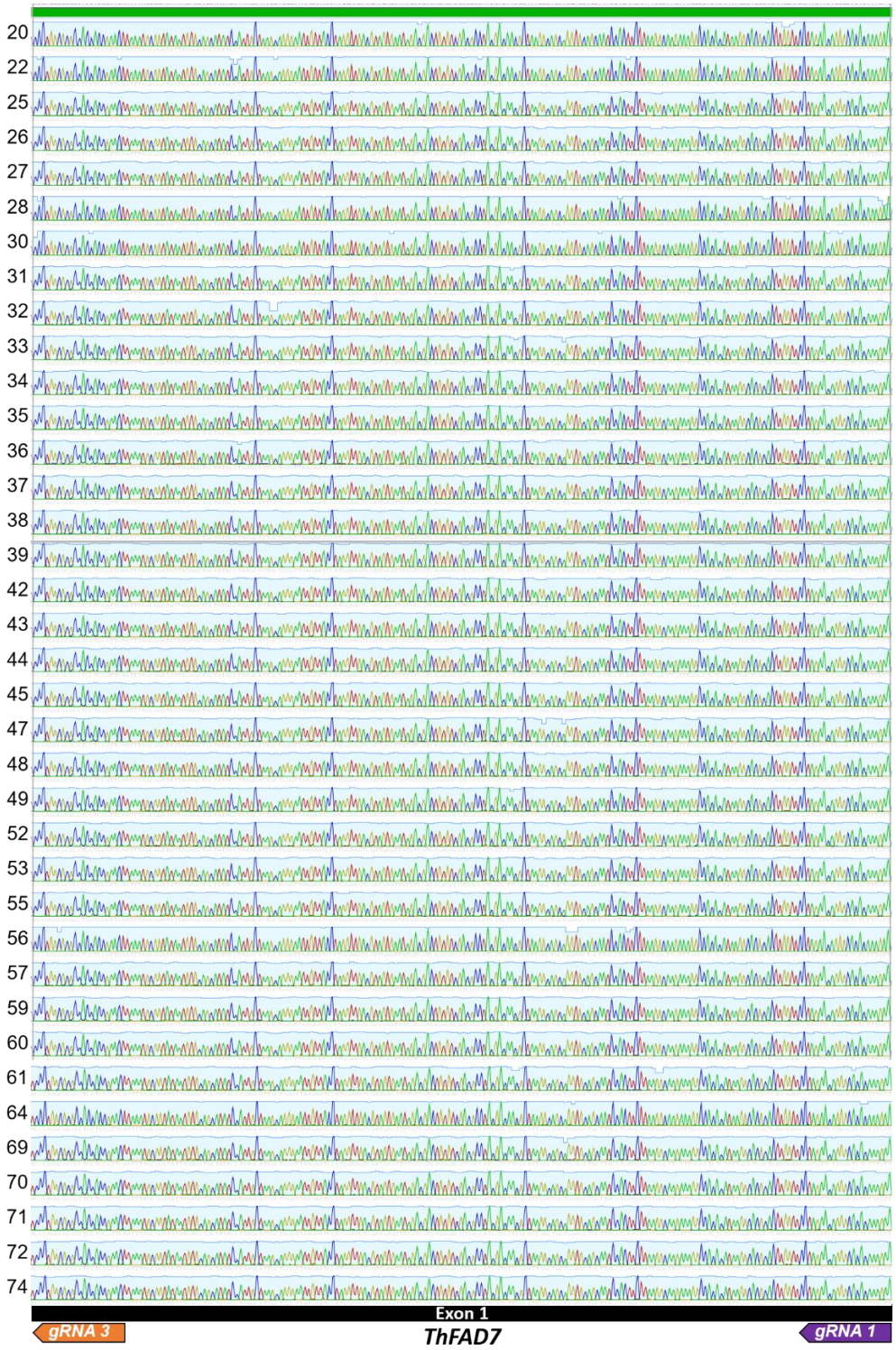

Lines 20 to 74 covering gRNA1 (■) and gRNA3 (■) in exon 1 of *ThFAD7*. Sequence alignment performed with Geneious® against the FASTA sequence for *ThFAD7* and the designed gRNAs (bottom panel). Green bar (■) represents the sequence identity, traces are adenine (A, —), thymine (T, —), guanine (G, —), and cytosine (C, —).

Appendix 24 T1 CRISPR Lines Sequencing for Targeted *ThFAD8*, Exon 1

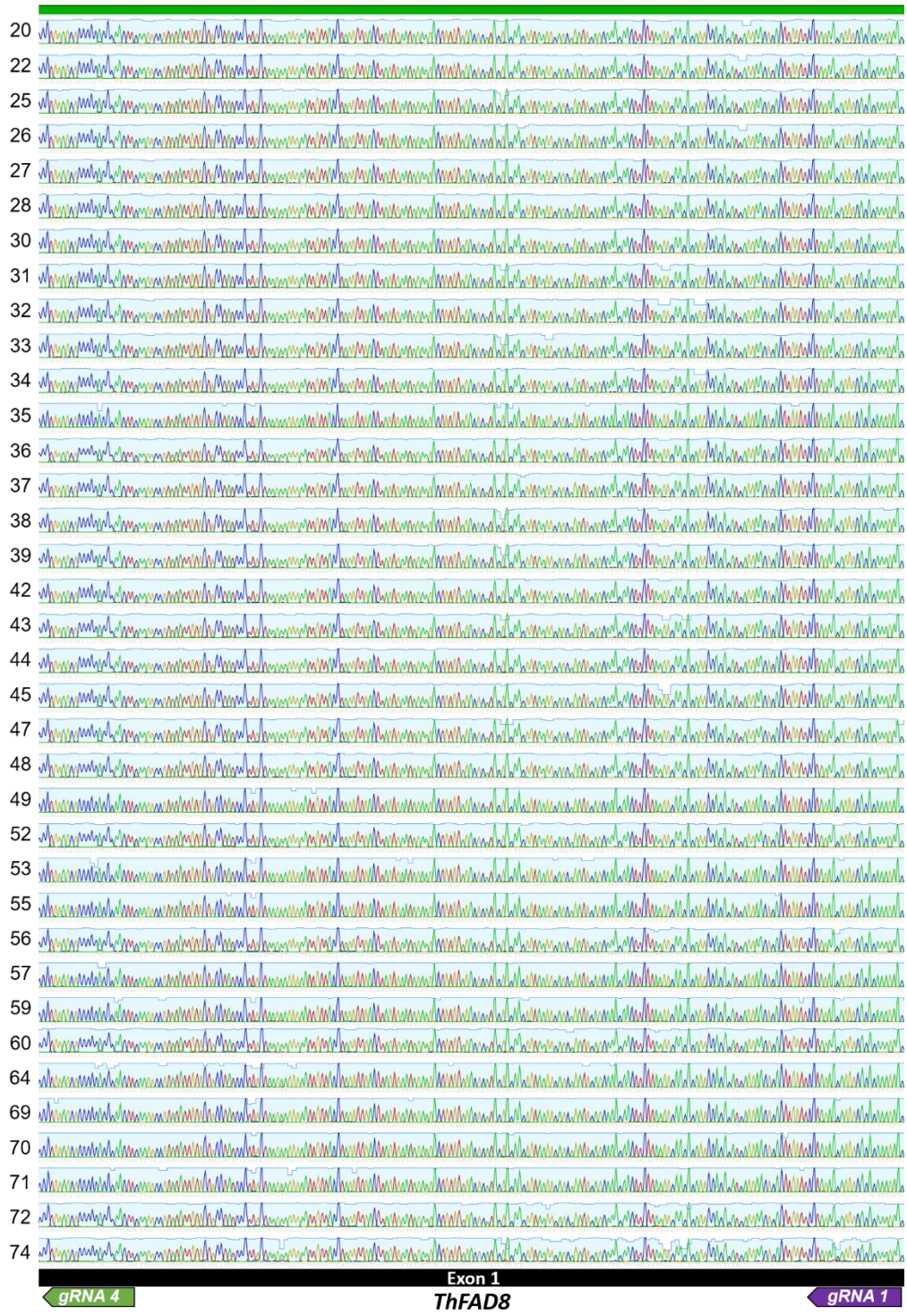

Lines 20 to 74 covering gRNA1 (■) and gRNA4 (■) in exon 1 of *ThFAD8*. Sequence alignment performed with Geneious® against the FASTA sequence for *ThFAD8* and the designed gRNAs (bottom panel). Green bar (■) represents the sequence identity, traces are adenine (A, —), thymine (T, —), guanine (G, —), and cytosine (C, —).

Appendix 25 Microhomology Predicted Deletions

gRNA	Bae-Score	Sequence	Effect
		AATTACCAGTCATGGCCAAGAACAAAGAGAGCCCAGAACATGGTTCCTTGAGCGAGCCAATAGAGAGGCCAAACAAGCCA	(Wild-type sequence)
gRNA1	258.3	AATTACCAGTCATGGCCAAGAACAAAGAGAGCC----------AATAGAGAGGCCAAACAAGCCA	25 bp deleted → framshift
gRNA1	245	AATTACCAGTCATGGCCAAGAACAAAGAGAGC----------GAGCCAATAGAGAGGCCAAACAAGCCA	**21 bp deleted → no framshift**
gRNA1	208.8	AATTACCAGTCATGGCCAAGAACAAAGAGAGCCC----------TTGAGCGAGCCAATAGAGAGGCCAAACAAGCCA	13 bp deleted → framshift
gRNA1	198.8	AATTACCAGTCATGGCCAAGAACAAAGAGAGCC----------TTGAGCGAGCCAATAGAGAGGCCAAACAAGCCA	14 bp deleted → framshift
gRNA1	158.5	AATTACCAGTCATGGCCAAGAACAAAGAG----------CGAGCCAATAGAGAGGCCAAACAAGCCA	23 bp deleted → framshift
gRNA1	150.5	AATTACCAGTCATGGCCAAGAACAAAGAGAGCCCA----------ATAGAGAGGCCAAACAAGCCA	**24 bp deleted → no framshift**
gRNA1	149.1	AATTACCAGTCATGGCCAAGAACAAAGAGAGCCCAGA----------GCGAGCCAATAGAGAGGCCAAACAAGCCA	14 bp deleted → framshift
gRNA1	148.5	AATTACCAGTCATGGCCAAGAACAAAGAGAG----------GCCAAACAAGCCA	**36 bp deleted → no framshift**
gRNA1	134.7	AATTACCAGTCATGGCCAAGAACAAAGAGAGCCCAG----------CGAGCCAATAGAGAGGCCAAACAAGCCA	16 bp deleted → framshift
gRNA1	129.5	AATTACCAGTCATGGCCAAGAACAAAGAG----------CCAATAGAGAGGCCAAACAAGCCA	**27 bp deleted → no framshift**
gRNA1	123.5	AATTACCAGTCATGG----------TTCCTTGAGCGAGCCAATAGAGAGGCCAAACAAGCCA	28 bp deleted → framshift
gRNA1	122.1	AATTACCAGTCATGGCCAAGAACAAAGAGAGCCCAGA----------GCCAATAGAGAGGCCAAACAAGCCA	**18 bp deleted → no framshift**
gRNA1	116.1	AATTACCAGTCATGGCCAAGAACAAAGAGAGCCCAGAACA----------ATAGAGAGGCCAAACAAGCCA	19 bp deleted → framshift
gRNA1	110.4	AATTACCAGTCATGGCCAAGAACAAAGAGAGCCCAG----------CCAATAGAGAGGCCAAACAAGCCA	20 bp deleted → framshift
gRNA1	109.8	AATTACCAGTCATGGCCAAGAACAAAGAGAG----------AGGCCAAACAAGCCA	34 bp deleted → framshift
gRNA1	103.6	AATTACCAGTCATGGCCAAGAACAAAGAGAGCCCAGA----------GAGGCCAAACAAGCCA	**27 bp deleted → no framshift**
gRNA1	103.2	AATTACCAGTCATGGCCAA----------TAGAGAGGCCAAACAAGCCA	41 bp deleted → framshift
gRNA1	94.2	AATTACCAGTCATGGCCAAGAACAAAGAGAGCC----------AAACAAGCCA	37 bp deleted → framshift
gRNA1	94	AATTACCAGTCATGGCCAAGAACAAAGAGAGCCCAGA----------GGCCAAACAAGCCA	29 bp deleted → framshift
gRNA1	90	AATTACCAGTCATGGCCAAGAACAAAGAG----------GCCAAACAAGCCA	38 bp deleted → framshift
gRNA1	89.2	AATTACCAGTCATGGCC----------TTGAGCGAGCCAATAGAGAGGCCAAACAAGCCA	**30 bp deleted → no framshift**
gRNA1	87	AATTACCAGTCATGGCCAAGAACAAAGAGAGCCCAGAACA----------AGCCA	35 bp deleted → framshift
gRNA1	86.1	AATTACCAGTCATGGCCAAGAACAAAG----------CGAGCCAATAGAGAGGCCAAACAAGCCA	25 bp deleted → framshift
gRNA1	82.5	AATTACCAGTCATGGCCAAGAACAAAGAGAGCCCA----------AACAAGCCA	**36 bp deleted → no framshift**
gRNA1	71	AATTACCAGTCATGGCCAA----------ACAAGCCA	53 bp deleted → framshift
gRNA1	70.5	AATTACCAGTCATGGCCAAGAACAAAG----------CCAATAGAGAGGCCAAACAAGCCA	29 bp deleted → framshift
gRNA1	70	AATTACCAGTCATGGCCAAGAACAAAGAGAGCC----------A	46 bp deleted → framshift
gRNA1	69.6	AATTACCAGTCATGGCCAAGAACAA----------TAGAGAGGCCAAACAAGCCA	35 bp deleted → framshift
gRNA1	66.9	AATTACCAGTCATGGCCAAGA----------GCGAGCCAATAGAGAGGCCAAACAAGCCA	**30 bp deleted → no framshift**
gRNA1	66.6	AATTACCAGTCATGGCCAAGAACAAAGAGAGCCCAGAA----------TAGAGAGGCCAAACAAGCCA	22 bp deleted → framshift
gRNA1	63.6	AATTACCAGTCATGGCCAAGAACAAAGAGAGCCCAGAACA----------AACAAGCCA	31 bp deleted → framshift
gRNA1	63.6	AATTACCAGTCATGGCCAAGAACAAAGAGAGCCCAG----------GCCAAACAAGCCA	31 bp deleted → framshift
gRNA1	62.8	AATTACCAGTCATGGC----------GAGCCAATAGAGAGGCCAAACAAGCCA	37 bp deleted → framshift
gRNA1	60.6	AATTACCAGTCATGGCCAAGAACAAAGAGAG----------AGAGGCCAAACAAGCCA	32 bp deleted → framshift
gRNA1	60.6	AATTACCAGTCATGGCCAAG----------CGAGCCAATAGAGAGGCCAAACAAGCCA	32 bp deleted → framshift
gRNA1	54.9	AATTACCAGTCATGGCCAAGA----------GCCAATAGAGAGGCCAAACAAGCCA	34 bp deleted → framshift
gRNA1	54.9	AATTACCAGT----------TCCTTGAGCGAGCCAATAGAGAGGCCAAACAAGCCA	34 bp deleted → framshift
gRNA1	54	AATTACC----------TTGAGCGAGCCAATAGAGAGGCCAAACAAGCCA	40 bp deleted → framshift
gRNA1	52.5	AATTACCAGTCATGGCCAAGAACAAAGAGAGCCCA----------	**45 bp deleted → no framshift**
gRNA1	52.2	AATTACCAGTC----------CTTGAGCGAGCCAATAGAGAGGCCAAACAAGCCA	35 bp deleted → framshift
gRNA1	49.5	AATTACCAGTCATGGCCAAG----------CCAATAGAGAGGCCAAACAAGCCA	**36 bp deleted → no framshift**
gRNA1	49.5	AATTACCAGTCATG----------AGCGAGCCAATAGAGAGGCCAAACAAGCCA	**36 bp deleted → no framshift**
gRNA1	47.5	AATTACCAGTCATGGCCAAGAACAAA----------CAAGCCA	47 bp deleted → framshift
gRNA1	46.8	AATTACCAGTCATGGCCAAGAACAA----------GCCA	**51 bp deleted → no framshift**
gRNA1	46.4	AATTACCAGTCATGGCCAAGA----------GAGGCCAAACAAGCCA	43 bp deleted → framshift
gRNA1	42	AATTACCAGTCATGGCCAAGA----------GGCCAAACAAGCCA	**45 bp deleted → no framshift**
gRNA1	40.5	AATTACCAGTCATGGCCAAGAACAAAGAGAGCCCAGAACA----------	40 bp deleted → framshift
gRNA1	40.5	AATTACCAGTCATGGCCAAGAACAAAGAGAGCCCA----------AGCCA	40 bp deleted → framshift
gRNA1	40.5	AATTACCAGTCATGGCCAAGAACAAAG----------GCCAAACAAGCCA	40 bp deleted → framshift
gRNA1	39	AATTACCA----------ATAGAGAGGCCAAACAAGCCA	**51 bp deleted → no framshift**
gRNA1	38.7	AATTACCAGTCATGGCCAAGAACAAAGAGAGCCCAG----------CCA	41 bp deleted → framshift
gRNA1	36.6	AATTACCAGTCATGGCCAAGAACAAAGAGAGCCCAGAA----------ACAAGCCA	34 bp deleted → framshift
gRNA1	36.6	AATTACCAGTCATGGCCAAGAACAAA----------TAGAGAGGCCAAACAAGCCA	34 bp deleted → framshift
gRNA1	34.8	AATTACCAGTCATGGCCAAG----------CCA	**57 bp deleted → no framshift**
gRNA1	34.8	AATTACCAG----------CGAGCCAATAGAGAGGCCAAACAAGCCA	43 bp deleted → framshift
gRNA1	32.8	AATTACCAGTCATGGCCAAGAACAAAG----------CCA	50 bp deleted → framshift
gRNA1	31.5	AATTACCAGTCATGGCCA----------	62 bp deleted → framshift
gRNA1	30	AATTACCAGTCATGGCCAAGAACAAAGAGAGCCCAGAA----------GCCA	38 bp deleted → framshift
gRNA1	30	AATTACCAGTCATGGCCAAGAA----------TAGAGAGGCCAAACAAGCCA	38 bp deleted → framshift
gRNA1	28.5	AATTACCAGTCATGGCCAAG----------GCCAAACAAGCCA	47 bp deleted → framshift
gRNA1	28.5	AATTACCAGTCA----------ATAGAGAGGCCAAACAAGCCA	47 bp deleted → framshift
gRNA1	28.5	AATTACCAG----------CCAATAGAGAGGCCAAACAAGCCA	47 bp deleted → framshift
gRNA1	27.3	AATTACCAGTCATGGCCAAGAACAAAGAG----------CCA	**48 bp deleted → no framshift**
gRNA1	25.8	AATT----------CCTTGAGCGAGCCAATAGAGAGGCCAAACAAGCCA	41 bp deleted → framshift
gRNA1	21.5	AATTACCA----------AACAAGCCA	**63 bp deleted → no framshift**
gRNA1	21	AATT----------GAGCGAGCCAATAGAGAGGCCAAACAAGCCA	**45 bp deleted → no framshift**
gRNA1	20.1	AATTACCAG----------AGAGGCCAAACAAGCCA	**54 bp deleted → no framshift**
gRNA1	20	AATTACCAGTCATGGCCAAGAACAAA----------ACAAGCCA	46 bp deleted → framshift
gRNA1	18.3	AATTACCAGTCATGGCCAAGAACA----------	56 bp deleted → framshift
gRNA1	18.3	AATTACCAG----------AGGCCAAACAAGCCA	56 bp deleted → framshift
gRNA1	18.2	AATTACCAGTCATGGCCAAGAACAA----------CAAGCCA	**48 bp deleted → no framshift**
gRNA1	18.2	AATTACCAGTCAT----------AGAGAGGCCAAACAAGCCA	**48 bp deleted → no framshift**
gRNA1	16.5	AATTACCAG----------GCCAAACAAGCCA	58 bp deleted → framshift
gRNA1	16.5	AAT----------AGAGAGGCCAAACAAGCCA	58 bp deleted → framshift
gRNA1	16.4	AATTACCAGTCATGGCCAAGAA----------ACAAGCCA	50 bp deleted → framshift
gRNA1	15.6	AATTACCAGTCA----------AACAAGCCA	59 bp deleted → framshift
gRNA1	13.5	AATTACCA----------	**72 bp deleted → no framshift**
gRNA1	13.4	AATTACCAGTCATGGCCAAGAA----------GCCA	**54 bp deleted → no framshift**
gRNA1	13.4	AATTACCAGTCATGGCCAA----------CAAGCCA	**54 bp deleted → no framshift**
gRNA1	12.9	AATTACCAGTCA----------AGCCA	**63 bp deleted → no framshift**
gRNA1	11.6	AATTA----------GAGAGGCCAAACAAGCCA	**57 bp deleted → no framshift**
gRNA1	10.5	AATTACCA----------AGCCA	67 bp deleted → framshift
gRNA1	9.9	AATTACCAGTCA----------	68 bp deleted → framshift
gRNA1	9.9	AATTACCAG----------CCA	68 bp deleted → framshift
gRNA1	9.9	AATTAC----------AAGCCA	68 bp deleted → framshift
gRNA1	6	AA----------ACAAGCCA	70 bp deleted → framshift
gRNA1	5.8	AA----------CAAGCCA	71 bp deleted → framshift
gRNA1	5	AA----------GCCA	74 bp deleted → framshift

(Continued on the next page)

gRNA	Bae-Score	Sequence	Effect
		TTTTGTTTCAATTACTTACTGCTTCTACTAGATGATAATGTGGAATCTGGGGGAAAAGATGATGTATCACATGAGTTCCA	(Wild-type sequence)
gRNA2	271.5	TTTTGTTTCAATTACTTACTGCTTCTACTAGATGATAATG--GAATCTGGGGGAAAAGATGATGTATCACATGAGTTCCA	2 bp deleted → framshift
gRNA2	233.1	TTTTGTTTCAATTACTTACTGCTTCTACTAGATGAT----------GTATCACATGAGTTCCA	27 bp deleted → no framshift
gRNA2	211.5	TTTTGTTTCAATTACTTACTGCTTCTACTAGATGATAAT-------CTGGGGGAAAAGATGATGTATCACATGAGTTCCA	7 bp deleted → framshift
gRNA2	201	TTTTGTTTCAATTACTTACTGCTTCTACTAGATG--------GAATCTGGGGGAAAAGATGATGTATCACATGAGTTCCA	8 bp deleted → framshift
gRNA2	191.4	TTTTGTTTCAATTACTTACTGCTTCTACTAGATGATAATG---------GGGGAAAAGATGATGTATCACATGAGTTCCA	9 bp deleted → no framshift
gRNA2	191.4	TTTTGTTTCAATTACTTACTGCTTCTACTAGATGA---------ATCTGGGGGAAAAGATGATGTATCACATGAGTTCCA	9 bp deleted → no framshift
gRNA2	164.7	TTTTGTTTCAATTACTTACTGCTTCTACTAGA----------ATCTGGGGGAAAAGATGATGTATCACATGAGTTCCA	12 bp deleted → no framshift
gRNA2	141.6	TTTTGTTTCAATTACTTACTGCTTCTACTAGATG----------GGGGAAAAGATGATGTATCACATGAGTTCCA	15 bp deleted → no framshift
gRNA2	140	TTTTGTTTCAATTACTTACTGCTTCTACTAGATGATAATG----------ATGTATCACATGAGTTCCA	21 bp deleted → no framshift
gRNA2	133.8	TTTTGTTTCAATTACTTACTGCTTCTACTAGATG----------TATCACATGAGTTCCA	30 bp deleted → no framshift
gRNA2	133.2	TTTTGTTTCAATTACTTACTGCTTCT----------GGGGGAAAAGATGATGTATCACATGAGTTCCA	22 bp deleted → framshift
gRNA2	123.5	TTTTGTTTCAATTACTTACTG----------GGGGAAAAGATGATGTATCACATGAGTTCCA	28 bp deleted → framshift
gRNA2	121.4	TTTTGTTTCAATTACTTACTGCTTCTACTAGATGAT----------CTGGGGGAAAAGATGATGTATCACATGAGTTCCA	10 bp deleted → framshift
gRNA2	120.4	TTTTGTTTCAATTACTTACTGCTTCTACTAGATGATAATG----------TATCACATGAGTTCCA	24 bp deleted → no framshift
gRNA2	120.4	TTTTGTTTCAATTACTTACTGCTTCTACTAGATGAT----------GATGTATCACATGAGTTCCA	24 bp deleted → no framshift
gRNA2	116.1	TTTTGTTTCAATTACTTACTGCTTCTACTAGATGA----------AAAGATGATGTATCACATGAGTTCCA	19 bp deleted → framshift
gRNA2	116.1	TTTTGTTTCAATTACTTACTGCTTCTACT----------GGGGGAAAAGATGATGTATCACATGAGTTCCA	19 bp deleted → framshift
gRNA2	105	TTTTGTTTCAATTACTTACTG----------GAATCTGGGGGAAAAGATGATGTATCACATGAGTTCCA	21 bp deleted → no framshift
gRNA2	104.4	TTTTGTTTCAATTACTTACTGCTTCTACTAGAT----------CTGGGGGAAAAGATGATGTATCACATGAGTTCCA	13 bp deleted → framshift
gRNA2	99.9	TTTTGTTTCAATTACTTACTGCTTCTACTAGA----------AAAGATGATGTATCACATGAGTTCCA	22 bp deleted → framshift
gRNA2	86.1	TTTTGTTTCAATTACTTACTGCT----------GGGGGAAAAGATGATGTATCACATGAGTTCCA	25 bp deleted → framshift
gRNA2	85.4	TTTTGTTTCAATTACTTACTGCTTCTACTAGATGATAA----------AAGATGATGTATCACATGAGTTCCA	17 bp deleted → framshift
gRNA2	81.4	TTTTGTTTCAATTACTTACTGCTTCTACTAGATGATAA----------AGATGATGTATCACATGAGTTCCA	18 bp deleted → no framshift
gRNA2	77.4	TTTTGTTTCAATTACTTACTGCTTCTACTAGATGATAA----------GATGATGTATCACATGAGTTCCA	19 bp deleted → framshift
gRNA2	76.8	TTTTGTTTCAATTACTTACTGCTTCTACTAGATGATAATG----------AGTTCCA	33 bp deleted → no framshift
gRNA2	71	TTTTGTTTCAATTACTTACTGCTTCTACTAGATGA----------GTTCCA	39 bp deleted → no framshift
gRNA2	60.6	TTTTGTTTCAATTACT----------GGGGGAAAAGATGATGTATCACATGAGTTCCA	32 bp deleted → framshift
gRNA2	54.9	TTTTGTTTCAAT----------CTGGGGGAAAAGATGATGTATCACATGAGTTCCA	34 bp deleted → framshift
gRNA2	49.4	TTTTGTTTCAATTACTTACTGCTTCTACTAGATGATAAT----------CACATGAGTTCCA	28 bp deleted → framshift
gRNA2	47.1	TTTTG----------GAATCTGGGGGAAAAGATGATGTATCACATGAGTTCCA	37 bp deleted → framshift
gRNA2	47	TTTTGTTTCAATTACTTACTGCTTCTACTAGATGATA----------TCACATGAGTTCCA	29 bp deleted → framshift
gRNA2	45	TTTTGTTTC----------TGGGGGAAAAGATGATGTATCACATGAGTTCCA	38 bp deleted → framshift
gRNA2	42.4	TTTTGTTTCAATTACTTACTGCTTCTACTAGATGAT----------CACATGAGTTCCA	31 bp deleted → framshift
gRNA2	40.5	TTTTGTTTCAATTACTTACTG----------ATGTATCACATGAGTTCCA	40 bp deleted → framshift
gRNA2	36.6	TTTTGTTTCAATTACTTACTGCTTCTACTAGAT----------CACATGAGTTCCA	34 bp deleted → framshift
gRNA2	36.6	TTTTGTTTCAATTACTTACTGCTTCTACTAGA----------GTTCCA	42 bp deleted → no framshift
gRNA2	36.6	TTTTGTTTCAATTACTTACTGCTTCTAC----------ATGAGTTCCA	42 bp deleted → no framshift
gRNA2	34.8	TTTTGTTTCAATTACTTACTGCTTC----------ACATGAGTTCCA	43 bp deleted → framshift
gRNA2	34.8	TTTTGTTTCAATTACTTACTG----------TATCACATGAGTTCCA	43 bp deleted → framshift
gRNA2	33.3	TTTTGTTTCAATTACTTACTGCTTCTACTAG----------TTCCA	44 bp deleted → framshift
gRNA2	33.3	TTTTG----------GGGGAAAAGATGATGTATCACATGAGTTCCA	44 bp deleted → framshift
gRNA2	33	TTTTGTTTCAATTACTTACTGCTTCTACTAGATGAT----------GAGTTCCA	36 bp deleted → no framshift
gRNA2	33	TTTTGTTTCAATTACTTACTGCTTCTACTA----------TCACATGAGTTCCA	36 bp deleted → no framshift
gRNA2	28.4	TTTTGTTTCAATTACTTACTGCTTCTA----------TCACATGAGTTCCA	39 bp deleted → no framshift
gRNA2	28.4	TTTTGTTTCAATTACTTACTGCTTC----------CA	53 bp deleted → framshift
gRNA2	23.4	TTTTGTTTCAATTACTTAC----------ATGAGTTCCA	51 bp deleted → no framshift
gRNA2	22.2	TTTTGTTTCAATTACTTACTG----------AGTTCCA	52 bp deleted → framshift
gRNA2	22.2	TTTTGTTTCAA----------AAGATGATGTATCACATGAGTTCCA	44 bp deleted → framshift
gRNA2	21	TTTTGTTTCAA----------AGATGATGTATCACATGAGTTCCA	45 bp deleted → no framshift
gRNA2	20.8	TTTTGTTTCA----------CATGAGTTCCA	59 bp deleted → framshift
gRNA2	20.8	TTTTGT----------ATCACATGAGTTCCA	59 bp deleted → framshift
gRNA2	20	TTTTGTTTCAA----------GATGATGTATCACATGAGTTCCA	46 bp deleted → framshift
gRNA2	19.2	TTTTGTTTCAATTAC----------ATGAGTTCCA	55 bp deleted → framshift
gRNA2	18.3	TTTTG----------ATGTATCACATGAGTTCCA	56 bp deleted → framshift
gRNA2	18.2	TTTTGTTTCAATTACTTA----------TCACATGAGTTCCA	48 bp deleted → no framshift
gRNA2	18.2	TTTTGTTTCAAT----------GATGTATCACATGAGTTCCA	48 bp deleted → no framshift
gRNA2	15.6	TTTTGTTTCAAT----------GTATCACATGAGTTCCA	51 bp deleted → no framshift
gRNA2	14.8	TTTTGTTTCAATTA----------TCACATGAGTTCCA	52 bp deleted → framshift
gRNA2	14.1	TTTTGTTTCA----------TGAGTTCCA	61 bp deleted → framshift
gRNA2	12.8	TTTTGTTTCAAT----------CACATGAGTTCCA	55 bp deleted → framshift
gRNA2	12.8	TTTTGTTTC----------CA	69 bp deleted → no framshift
gRNA2	12	TTTTGTT----------CCA	70 bp deleted → framshift
gRNA2	10	TTTTGTTTCAATTACTT----------CCA	60 bp deleted → no framshift
gRNA2	10	TTTTGTTTCAAT----------GAGTTCCA	60 bp deleted → no framshift
gRNA2	9.9	TTTTG----------AGTTCCA	68 bp deleted → framshift
gRNA2	9	TTTTGTTTCA----------	70 bp deleted → framshift
gRNA2	8.2	TTTTGTTTCAATT----------CCA	64 bp deleted → framshift
gRNA2	5.2	TTTT----------CCA	73 bp deleted → framshift
gRNA2	5	TTT----------CCA	74 bp deleted → framshift
gRNA2	4.8	TT----------CCA	75 bp deleted → no framshift

(Continued on the next page)

gRNA	Bae-Score	Sequence	Effect
		AGCTCTAATATCCGCTAAATTGAACGGAGGAGGCGCGCCTGGGTCGAATCTCTGCGTCTCGTGTTCCTCCTCGATTGGAG	(Wild-type sequence)
gRNA3	255.2	AGCTCTAATATCCGCTAAATTGAACGGAGGAGGCGCG---------AATCTCTGCGTCTCGTGTTCCTCCTCGATTGGAG	9 bp deleted → no frameshift
gRNA3	255.2	AGCTCTAATATCCGCTAAATTGAACGGAGGAGG---------GTCGAATCTCTGCGTCTCGTGTTCCTCCTCGATTGGAG	9 bp deleted → no frameshift
gRNA3	242.8	AGCTCTAATATCCGCTAAATTGAACGGAGGAGG----------TCGAATCTCTGCGTCTCGTGTTCCTCCTCGATTGGAG	10 bp deleted → frameshift
gRNA3	232.2	AGCTCTAATATCCGCTAAATTGAACGGAGGAGGCGCG----------TCTCGTGTTCCTCCTCGATTGGAG	19 bp deleted → frameshift
gRNA3	230.8	AGCTCTAATATCCGCTAAATTGAACGGAGGAGGCG----------AATCTCTGCGTCTCGTGTTCCTCCTCGATTGGAG	11 bp deleted → frameshift
gRNA3	219.6	AGCTCTAATATCCGCTAAATTGAACGGAGG----------GTCGAATCTCTGCGTCTCGTGTTCCTCCTCGATTGGAG	12 bp deleted → no frameshift
gRNA3	210	AGCTCTAATATCCGCTAAATTGAACGGAGGAGGCG----------TCTCGTGTTCCTCCTCGATTGGAG	21 bp deleted → no frameshift
gRNA3	208.8	AGCTCTAATATCCGCTAAATTGAACGGAGG----------TCGAATCTCTGCGTCTCGTGTTCCTCCTCGATTGGAG	13 bp deleted → frameshift
gRNA3	188.8	AGCTCTAATATCCGCTAAATTGAACGG----------GTCGAATCTCTGCGTCTCGTGTTCCTCCTCGATTGGAG	15 bp deleted → no frameshift
gRNA3	179.6	AGCTCTAATATCCGCTAAATTGAACGG----------TCGAATCTCTGCGTCTCGTGTTCCTCCTCGATTGGAG	16 bp deleted → frameshift
gRNA3	173.1	AGCTCTAATATCCGCTAAATTGAACGGAGGAGGCGCGCCT----------CTGCGTCTCGTGTTCCTCCTCGATTGGAG	11 bp deleted → frameshift
gRNA3	170.8	AGCTCTAATATCCGCTAAATTGAACGGAGGAGGCGCGC----------GTCTCGTGTTCCTCCTCGATTGGAG	17 bp deleted → frameshift
gRNA3	156.6	AGCTCTAATATCCGCTAAATTGAACGGAGGAGGCGCGCCT----------GCGTCTCGTGTTCCTCCTCGATTGGAG	13 bp deleted → frameshift
gRNA3	147.2	AGCTCTAATATCCGCTAAATTGAACG----------AATCTCTGCGTCTCGTGTTCCTCCTCGATTGGAG	20 bp deleted → frameshift
gRNA3	134.7	AGCTCTAATATCCGCTAAATTGAACGGAGGA----------ATCTCTGCGTCTCGTGTTCCTCCTCGATTGGAG	16 bp deleted → frameshift
gRNA3	123.5	AGCTCTAATATCCGCTAAATTGAACGGAGGAGGCGCGCCT----------CCTCGATTGGAG	28 bp deleted → frameshift
gRNA3	120.4	AGCTCTAATATCCGCTAAATTGAACGGAGGAGGCGCG----------TGTTCCTCCTCGATTGGAG	24 bp deleted → no frameshift
gRNA3	120.4	AGCTCTAATATCCGCTAAATTGAA----------TCTCTGCGTCTCGTGTTCCTCCTCGATTGGAG	24 bp deleted → no frameshift
gRNA3	116.1	AGCTCTAATATCCGCTAAATTGAACGGAGGAGGCGCGCCT----------CGTGTTCCTCCTCGATTGGAG	19 bp deleted → frameshift
gRNA3	116.1	AGCTCTAATATCCGCTAAATTGAACGGA----------ATCTCTGCGTCTCGTGTTCCTCCTCGATTGGAG	19 bp deleted → frameshift
gRNA3	109.2	AGCTCTAATATCCGCTAAATTGAACGGAGGAGGCG----------TGTTCCTCCTCGATTGGAG	26 bp deleted → frameshift
gRNA3	106	AGCTCTAATATCCGCTAAATTGAACGGAGGAGGCGCGCCT----------CGATTGGAG	31 bp deleted → frameshift
gRNA3	89.2	AGCTCTAATATCCGCTAAATTGAACG----------TCTCGTGTTCCTCCTCGATTGGAG	30 bp deleted → no frameshift
gRNA3	80.8	AGCTCTAATATCCG----------AATCTCTGCGTCTCGTGTTCCTCCTCGATTGGAG	32 bp deleted → frameshift
gRNA3	70.5	AGCTCTAATATCCGCTAAAT----------CTCTGCGTCTCGTGTTCCTCCTCGATTGGAG	29 bp deleted → frameshift
gRNA3	69.6	AGCTCTAATATCCGCTAAATTGAACG----------TGTTCCTCCTCGATTGGAG	35 bp deleted → frameshift
gRNA3	66	AGCTCTAATATCCGCTAAATTGAACGGAGGAGGCGCG----------ATTGGAG	36 bp deleted → no frameshift
gRNA3	63.7	AGCTCTAATATCCGCTAAATTGAACGGAGGAG----------	48 bp deleted → no frameshift
gRNA3	60.6	AGCTCTAATATCCGCTAAATTG----------CGTCTCGTGTTCCTCCTCGATTGGAG	32 bp deleted → frameshift
gRNA3	60	AGCTCTAATATCCGCTAAATTGAACGGAGGAGGCG----------ATTGGAG	38 bp deleted → frameshift
gRNA3	60	AGCTCTAATATC----------TCTGCGTCTCGTGTTCCTCCTCGATTGGAG	38 bp deleted → frameshift
gRNA3	57.6	AGCTCTAATATC----------GAATCTCTGCGTCTCGTGTTCCTCCTCGATTGGAG	33 bp deleted → no frameshift
gRNA3	**57**	**AGCTCT----------GCGTCTCGTGTTCCTCCTCGATTGGAG**	**47 bp deleted → frameshift**
gRNA3	54.6	AGCTCTAATATCCGCTAAATTGAACGGAG----------	51 bp deleted → no frameshift
gRNA3	54	AGCTCTAATATCCGC----------GTCTCGTGTTCCTCCTCGATTGGAG	40 bp deleted → frameshift
gRNA3	52.2	AGCTCTAATATCCGCT----------CTGCGTCTCGTGTTCCTCCTCGATTGGAG	35 bp deleted → frameshift
gRNA3	48.8	AGCTCTAATATCCG----------TCTCGTGTTCCTCCTCGATTGGAG	42 bp deleted → no frameshift
gRNA3	47.1	AGCTCTAATATCCGCT----------GCGTCTCGTGTTCCTCCTCGATTGGAG	37 bp deleted → frameshift
gRNA3	44.6	AGCTCTAATATCCGCTAA----------TCTCTGCGTCTCGTGTTCCTCCTCGATTGGAG	30 bp deleted → no frameshift
gRNA3	42	AGCTCTAATATCCGCTAAATTGAACGGAGGAGG----------	45 bp deleted → no frameshift
gRNA3	42	AGCTCT----------CTGCGTCTCGTGTTCCTCCTCGATTGGAG	45 bp deleted → no frameshift
gRNA3	40.5	AGCTCTAATATC----------TGCGTCTCGTGTTCCTCCTCGATTGGAG	40 bp deleted → frameshift
gRNA3	40.5	AGCTCTAAT----------CTCTGCGTCTCGTGTTCCTCCTCGATTGGAG	40 bp deleted → frameshift
gRNA3	40.5	AGCTC----------GAATCTCTGCGTCTCGTGTTCCTCCTCGATTGGAG	40 bp deleted → frameshift
gRNA3	38.7	AGCTCTAATATCCGCTAAATTG----------TTCCTCCTCGATTGGAG	41 bp deleted → frameshift
gRNA3	38	AGCTCTAATATCCGCTAAATTGAACG----------ATTGGAG	47 bp deleted → frameshift
gRNA3	38	AGCTCTAATATCCG----------TGTTCCTCCTCGATTGGAG	47 bp deleted → frameshift
gRNA3	34.8	AGCTCTAATATCCGCTAAATTGAACGGAGGA----------TTGGAG	43 bp deleted → frameshift
gRNA3	34.8	AGCTCTAATATCCGCT----------CGTGTTCCTCCTCGATTGGAG	43 bp deleted → frameshift
gRNA3	33.5	AGCTCTAATATCC----------TCCTCGATTGGAG	54 bp deleted → no frameshift
gRNA3	32	AGCTCTAATATCCGCTAAATTG----------GAG	55 bp deleted → frameshift
gRNA3	32	AGCTC----------GTGTTCCTCCTCGATTGGAG	55 bp deleted → frameshift
gRNA3	30	AGCTCTAATATCCGCTAAATTGAACGGA----------TTGGAG	46 bp deleted → frameshift
gRNA3	30	AGCTCTAATATC----------TCGTGTTCCTCCTCGATTGGAG	46 bp deleted → frameshift
gRNA3	29.6	AGC----------GTCTCGTGTTCCTCCTCGATTGGAG	52 bp deleted → frameshift
gRNA3	29	AGCTCTAATATCC----------TCGATTGGAG	57 bp deleted → no frameshift
gRNA3	28.4	AGCTCT----------CGTGTTCCTCCTCGATTGGAG	53 bp deleted → frameshift
gRNA3	27.3	AGCTCTAATATC----------GTGTTCCTCCTCGATTGGAG	48 bp deleted → no frameshift
gRNA3	25.8	AGCT----------GCGTCTCGTGTTCCTCCTCGATTGGAG	49 bp deleted → frameshift
gRNA3	23.4	AGCTCTAATATCCGCTAAATTGA----------TTGGAG	51 bp deleted → no frameshift
gRNA3	22.2	AGCTCTAATATCCGCTAAATT----------CCTCCTCGATTGGAG	44 bp deleted → frameshift
gRNA3	22.2	AGCTCTAATATCCGCT----------CCTCGATTGGAG	52 bp deleted → frameshift
gRNA3	20.8	AGCTCTAATATCCG----------ATTGGAG	59 bp deleted → frameshift
gRNA3	20.5	AGCTC----------CTCGATTGGAG	64 bp deleted → frameshift
gRNA3	19.2	AGCTCTAATATCCGCT----------CGATTGGAG	55 bp deleted → frameshift
gRNA3	18.3	AGCTCTAATATCCGCTAAATTGA----------G	56 bp deleted → frameshift
gRNA3	17.5	AGCTC----------GATTGGAG	67 bp deleted → frameshift
gRNA3	15	AGCTCTAATATC----------GATTGGAG	60 bp deleted → no frameshift
gRNA3	14.1	AGCTC----------CTCCTCGATTGGAG	61 bp deleted → frameshift
gRNA3	13.5	AGCTCT----------CCTCGATTGGAG	62 bp deleted → frameshift
gRNA3	11.7	AGCTCT----------CGATTGGAG	65 bp deleted → frameshift
gRNA3	8.2	AGCTCTAATAT----------TGGAG	64 bp deleted → frameshift
gRNA3	7.4	AGCTCTAAT----------TGGAG	66 bp deleted → no frameshift
gRNA3	6	AG----------	78 bp deleted → no frameshift

(Continued on the next page)

gRNA	Bae-Score	Sequence	Effect
		CTGCTCTTATATCGGCCAAGTTGAAGGGAGGGGGCGCACCTGGGTCGAATCTCTTCGTGTGTTCCTCCTCGGACGGAGGC	(Wild-type sequence)
gRNA4	364.2	CTGCTCTTATATCGGCCAAGTTGAAGGGAGGGGG----------TCGAATCTCTTCGTGTGTTCCTCCTCGGACGGAGGC	10 bp deleted → frameshift
gRNA4	346.2	CTGCTCTTATATCGGCCAAGTTGAAGGGAGGGG----------TCGAATCTCTTCGTGTGTTCCTCCTCGGACGGAGGC	11 bp deleted → frameshift
gRNA4	329.4	CTGCTCTTATATCGGCCAAGTTGAAGGGAGGG----------TCGAATCTCTTCGTGTGTTCCTCCTCGGACGGAGGC	12 bp deleted → no frameshift
gRNA4	269.4	CTGCTCTTATATCGGCCAAGTTGAAGGG----------TCGAATCTCTTCGTGTGTTCCTCCTCGGACGGAGGC	16 bp deleted → frameshift
gRNA4	255.2	CTGCTCTTATATCGGCCAAGTTGAAGGGAGGGGG---------GTCGAATCTCTTCGTGTGTTCCTCCTCGGACGGAGGC	9 bp deleted → no frameshift
gRNA4	230.8	CTGCTCTTATATCGGCCAAGTTGAAGGGAGGGGGCG----------AATCTCTTCGTGTGTTCCTCCTCGGACGGAGGC	11 bp deleted → frameshift
gRNA4	208.8	CTGCTCTTATATCGGCCAAGTTGAAGGGAGG----------TCGAATCTCTTCGTGTGTTCCTCCTCGGACGGAGGC	13 bp deleted → frameshift
gRNA4	188.8	CTGCTCTTATATCGGCCAAGTTGAAGGG----------GTCGAATCTCTTCGTGTGTTCCTCCTCGGACGGAGGC	15 bp deleted → no frameshift
gRNA4	170.8	CTGCTCTTATATCGGCCAAGTTGAAGG----------TCGAATCTCTTCGTGTGTTCCTCCTCGGACGGAGGC	17 bp deleted → frameshift
gRNA4	140	CTGCTCTTATATCGGCCAAGTTGAAGGGAGGGGGCG----------TGTGTTCCTCCTCGGACGGAGGC	21 bp deleted → no frameshift
gRNA4	120.4	CTGCTCTTATATCGGCCAAGTTGAA----------TCTCTTCGTGTGTTCCTCCTCGGACGGAGGC	24 bp deleted → no frameshift
gRNA4	116.1	CTGCTCTTATATCGGCCAAGTTGAAGGGA----------ATCTCTTCGTGTGTTCCTCCTCGGACGGAGGC	19 bp deleted → frameshift
gRNA4	116.1	CTGCTCTTATATCGGCCAAGTTG----------GGTCGAATCTCTTCGTGTGTTCCTCCTCGGACGGAGGC	19 bp deleted → frameshift
gRNA4	114.8	CTGCTCTTATATCGGCCAAGTTGAAGGGAGGGGGCGCACC----------TCCTCGGACGGAGGC	25 bp deleted → frameshift
gRNA4	98.8	CTGCTCTTATATCGGCCAAGTTGAAGGGAGGGGGCGCACC----------TCGGACGGAGGC	28 bp deleted → frameshift
gRNA4	98.8	CTGCTCTTATATCGG----------GTCGAATCTCTTCGTGTGTTCCTCCTCGGACGGAGGC	28 bp deleted → frameshift
gRNA4	96	CTGCTCTTATATCG----------AATCTCTTCGTGTGTTCCTCCTCGGACGGAGGC	33 bp deleted → no frameshift
gRNA4	94	CTGCTCTTATATCGG----------TCGAATCTCTTCGTGTGTTCCTCCTCGGACGGAGGC	29 bp deleted → frameshift
gRNA4	90.3	CTGCTCTTATATCGGCCAAGT----------CGAATCTCTTCGTGTGTTCCTCCTCGGACGGAGGC	24 bp deleted → no frameshift
gRNA4	81.9	CTGCTCTTATATCGGCCAAGTTGAAGGGAGG----------C	48 bp deleted → no frameshift
gRNA4	69.6	CTGCTCTTATATCGGCCAAGTTGAAGGGAGGGGGCG----------GACGGAGGC	35 bp deleted → frameshift
gRNA4	66.5	CTGCTCTT----------CGTGTGTTCCTCCTCGGACGGAGGC	47 bp deleted → frameshift
gRNA4	63	CTGCTCTTATATCGGCCAAGTTGAAGGGAGGGGGC----------	45 bp deleted → no frameshift
gRNA4	60	CTGCTCTTATATCGGCCAAGTTGAAGGGAGGGGG----------ACGGAGGC	38 bp deleted → frameshift
gRNA4	60	CTGCTCTTATATC----------TCTTCGTGTGTTCCTCCTCGGACGGAGGC	38 bp deleted → frameshift
gRNA4	58	CTGCTCTTATATCG----------TGTGTTCCTCCTCGGACGGAGGC	43 bp deleted → frameshift
gRNA4	56.8	CTGCTCTTATATCGGCCAAGTTGAAGGGAGGGGGCG----------GAGGC	39 bp deleted → no frameshift
gRNA4	56.8	CTGCTCTTATATCGGCCAAGTTGAAGGGAGGGG----------ACGGAGGC	39 bp deleted → no frameshift
gRNA4	55.5	CTGCTCTTATATCGGCCAAGTTGAAGGGA----------CGGAGGC	44 bp deleted → frameshift
gRNA4	54	CTGCTCTTATATCGGCCAAGTTGAAGGGAGGG----------ACGGAGGC	40 bp deleted → frameshift
gRNA4	52.2	CTGCTCTTATATCGGCCAAGTTGAAGGGAGGGGGCGCAC----------GGAGGC	35 bp deleted → frameshift
gRNA4	51.6	CTGCTCTTATATCGGCCAAGTTGAAGGGAGG----------ACGGAGGC	41 bp deleted → frameshift
gRNA4	51.6	CTGCTCTTATATCGGCCAAGTT----------CCTCCTCGGACGGAGGC	41 bp deleted → frameshift
gRNA4	49.5	CTGCTCTTATATCGGCCAAGTTG----------TGTTCCTCCTCGGACGGAGGC	36 bp deleted → no frameshift
gRNA4	48.8	CTGCTCTTATATCGGCCAAGTTGAAGGGAGGGGG----------AGGC	42 bp deleted → no frameshift
gRNA4	47.1	CTGCTCTTATATCGGCCAAGT----------GTGTTCCTCCTCGGACGGAGGC	37 bp deleted → frameshift
gRNA4	46.4	CTGCTCTTATATCGGCCAAGTTGAAGGGAGGGGGCGC----------	43 bp deleted → frameshift
gRNA4	46.4	CTGCTCTTATATCGGCCAAGTTGAAGGGAGGGG----------AGGC	43 bp deleted → frameshift
gRNA4	45	CTGCTCTTATATCGGCCAAGTTG----------TTCCTCCTCGGACGGAGGC	38 bp deleted → frameshift
gRNA4	44.6	CTGCTCTTATATCGGCCAA----------TCTCTTCGTGTGTTCCTCCTCGGACGGAGGC	30 bp deleted → no frameshift
gRNA4	44.4	CTGCTCTTATATCGGCCAAGTTGAAGGGAGGG----------AGGC	44 bp deleted → frameshift
gRNA4	42.6	CTGCTCTTATATCGGCCAAGT----------GTTCCTCCTCGGACGGAGGC	39 bp deleted → no frameshift
gRNA4	42.6	CTG----------GGTCGAATCTCTTCGTGTGTTCCTCCTCGGACGGAGGC	39 bp deleted → no frameshift
gRNA4	42	CTGCTCTTATATCGGCCAAGTTGAAGGGAGG----------AGGC	45 bp deleted → no frameshift
gRNA4	42	CTGCTCTTATATCGGCCAAGTTGAAGG----------ACGGAGGC	45 bp deleted → no frameshift
gRNA4	42	CTGCTCT----------CTTCGTGTGTTCCTCCTCGGACGGAGGC	45 bp deleted → no frameshift
gRNA4	40.6	CTGCTCTTATATCGG----------ACGGAGGC	57 bp deleted → no frameshift
gRNA4	40.5	CTGCTCTTATATC----------TTCGTGTGTTCCTCCTCGGACGGAGGC	40 bp deleted → frameshift
gRNA4	40.5	CTGCTC----------GAATCTCTTCGTGTGTTCCTCCTCGGACGGAGGC	40 bp deleted → frameshift
gRNA4	40	CTGCTCTTATATCGGCCAAGTTGAAGGGAGGGG----------C	46 bp deleted → frameshift
gRNA4	38.4	CTGCTCTTATATCGGCCAAGTT----------CGTGTGTTCCTCCTCGGACGGAGGC	33 bp deleted → no frameshift
gRNA4	38	CTGCTCTTATATCGGCCAAGTTGAAGGGAGGG----------C	47 bp deleted → frameshift
gRNA4	37	CTGCTCTTATATCGGCCAAGTTGAAGG----------C	52 bp deleted → frameshift
gRNA4	36.4	CTGCTCTTATATCGGCC----------TCCTCGGACGGAGGC	48 bp deleted → no frameshift
gRNA4	34.4	CTGCTCTTATATCGGCCAAGTTGAAGG----------AGGC	49 bp deleted → frameshift
gRNA4	31.2	CTGCTCTTATATCGGCCAAGTTGAAGGG----------C	51 bp deleted → no frameshift
gRNA4	31.2	CTGCTCTTATATCGGCC----------TCGGACGGAGGC	51 bp deleted → no frameshift
gRNA4	28.2	CTGCTCTTATATCGG----------AGGC	61 bp deleted → frameshift
gRNA4	27	CTGCTCTTAT----------CTCTTCGTGTGTTCCTCCTCGGACGGAGGC	40 bp deleted → frameshift
gRNA4	25.8	CTGCTCTTATATCGGCCAAGTTGA----------CGGAGGC	49 bp deleted → frameshift
gRNA4	25.8	CTGCT----------TCGTGTGTTCCTCCTCGGACGGAGGC	49 bp deleted → frameshift
gRNA4	24.6	CTGCTCTTATATCGGC----------	64 bp deleted → frameshift
gRNA4	24.6	CTGCTC----------GTGTGTTCCTCCTCGGACGGAGGC	50 bp deleted → frameshift
gRNA4	24.6	CT----------CTTCGTGTGTTCCTCCTCGGACGGAGGC	50 bp deleted → frameshift
gRNA4	23.5	CTGCTC----------CTCGGACGGAGGC	61 bp deleted → frameshift
gRNA4	23.4	CTGCTCTTATATC----------CTCCTCGGACGGAGGC	51 bp deleted → no frameshift
gRNA4	22.2	CT----------TCGTGTGTTCCTCCTCGGACGGAGGC	52 bp deleted → frameshift
gRNA4	21.3	CTGCTCTTATATCGGCCAAGTTGA----------GGC	53 bp deleted → frameshift
gRNA4	20.5	CTGCTC----------GGACGGAGGC	64 bp deleted → frameshift
gRNA4	20.1	CTGCTCTTATATC----------CTCGGACGGAGGC	54 bp deleted → no frameshift
gRNA4	18.3	CTG----------TGTTCCTCCTCGGACGGAGGC	56 bp deleted → frameshift
gRNA4	16.5	CTGCTCTTATATCGGCCAAG----------GC	58 bp deleted → frameshift
gRNA4	16.5	CTGCTC----------CTCCTCGGACGGAGGC	58 bp deleted → frameshift
gRNA4	16.5	CTG----------TTCCTCCTCGGACGGAGGC	58 bp deleted → frameshift
gRNA4	15.6	CTGCTCT----------CCTCGGACGGAGGC	59 bp deleted → frameshift
gRNA4	13.5	CTGCTCT----------CGGACGGAGGC	62 bp deleted → frameshift
gRNA4	12.8	CTGCTCTT----------CCTCCTCGGACGGAGGC	55 bp deleted → frameshift
gRNA4	12.3	CT----------CCTCGGACGGAGGC	64 bp deleted → frameshift
gRNA4	10.5	CT----------CGGACGGAGGC	67 bp deleted → frameshift
gRNA4	8.8	CTGC----------	76 bp deleted → frameshift

The possible deletions are marked as "-", for each of the four gRNAs according to the method developed by Bae *et al.* (Bae *et al.* 2014) based in the microhomology in the sequence flanking the target site for each of the gRNAs. The respective number of bp deleted and the probability of causing a frameshift or no-frameshift deletion is also showed. This analysis was performed with the online tool CRISPOR.

Appendix 26 Review article published in *Plant Science* by Susana Silvestre as a first co-author

Barrero-Sicilia, C., Silvestre, S., Haslam, R. P., and Michaelson, L. V. (2017). *Lipid remodelling: Unravelling the response to cold stress in Arabidopsis and its extremophile relative Eutrema salsugineum*.

Plant Science, 263: 194-200.

http://dx.doi.org/10.1016/j.plantsci.2017.07.017